MMET 02

Conference Proceedings

2002 International Conference on

MATHEMATICAL METHODS IN ELECTROMAGNETIC THEORY

DISTRIBUTION STATEMENT A
Approved for Public Release
Distribution Unlimited



REPORT DOCUMENTATION PAGE

Form Approved OMB No. 0704-0188

Public reporting burden for this collection of information is estimated to average 1 hour per response, including the time for reviewing instructions, searching existing data sources, gathering and maintaining the data needed, and completing and reviewing the collection of information. Send comments regarding this burden estimate or any other aspect of this collection of information, including suggestions for reducing this burden to Washington Headquarters Services, Directorate for Information Operations and Reports, 1215 Jefferson Davis Highway, Suite 1204, Arlington, VA 22202-4302, and to the Office of Management and Budget, Paperwork Reduction Project (0704-0188), Washington, DC 20503.

1. AGENCY USE ONLY (Leave blank)	2. REPORT DATE	3. REPORT TYPE AND DATES COVERED
	2002	Conference Proceedings, 10-13 September 2002

4. TITLE AND SUBTITLE

2002 International Conference on Mathematical Methods in Electromagnetic Theory (MMET 02), Volume 1

5. FUNDING NUMBERS

N62558-02-M-6003

6. AUTHOR(S)

7. PERFORMING ORGANIZATION NAME(S) AND ADDRESS(ES)

National Academy of Sciences, Ukraine

IEEE catalog no. 02EX554
ISBN 0-7803-7391-X

9. SPONSORING/MONITORING AGENCY NAME(S) AND ADDRESS(ES

USARDSG-UK, Fiscal Office, Edison House, 223 Old Marylebone Road, London NW1 5th, UK

10. SPONSORING/MONITORING AGENCY REPORT NUMBER

R&D 9294-EE-02

11. SUPPLEMENTARY NOTES

Conference Proceedings of the 2002 International Conference on Mathematical Methods in Electromagnetic Theory, Volumes 1 (pages 1-340) and 2 (pages 341-696) based on work supported by the European Office of Aerospace Research and development, Air Force Office of Scientific Research, Air Force Research Laboratory, under contract no. F61775-02-WF065, IEEE Catalog Number 02EX554 , ISBN 0-7803-7391-X, 696 pages total..

12a. DISTRIBUTION/AVAILABILITY STATEMENT

Approved for Public Release.

12b. DISTRIBUTION CODE

A

ABSTRACT (Maximum 200 words)

Table of Contents– Volume 1. See attached with presentation titles of the sessions listed below:

PLENARY SESSIONS
TIME-DOMAIN METHODS
COMPUTATIONAL OPTOELECTRONICS
PRINTED ANTENNAS AND CIRCUITS
GEORADAR AND REMOTE SENSING
WIRE AND WAVEGUIDE ANTENNAS

14. SUBJECT TERMS

US Army Research, Ukraine, Electromagnetic theory, Waveguides, Diffraction gratings, Planar structures, Hallen's equation, Wiener-Hopf factorization method, Printed-circuit transmissions, Time Domain, Optoelectronics, Printed antennas, Georadar, Remote sensing

15. NUMBER OF PAGES

16. PRICE CODE

17. SECURITY CLASSIFICATION OF REPORT	18. SECURITY CLASSIFICATION OF THIS PAGE	19. SECURITY CLASSIFICATION OF ABSTRACT	20. LIMITATION OF ABSTRACT
Unclassified	Unclassified	Unclassified	Unlimited

Table of Contents– Volume 1

PLENARY SESSIONS: Study and microwave applications of artificial periodic substrate PBG planar circuits; Measures for accelerating EM computations; Propagation of electromagnetic waves in open cylindrical waveguides with nonlinear media; Hybrid numerical-asymptotic method for the calculation of the coupling between elements of a conformal microstrip patch array; Application of evolution strategies in optimal design problems involving diffraction gratings; BMIA/AIM formulation for the analysis of large stacked patch antennas; Evolutionary computational techniques in electromagnetics; The use of hierarchy in modeling tools for planar structures; Time-dependent self-action of periodically modulated laser beams in resonant media; On the solvability and application of numerical methods to Hallen's equation; Some classes of nonlinear synthesis problems for radiation systems: theory and methods of solution; The Wiener-Hopf factorization method for the diffraction by wedges having arbitrary aperture angle; Basic properties of leaky modes in printed- circuit transmission lines; Large-scale discretization and generalized mode-matching as a basis for fast electromagnetic solvers; The concept of waves: theory and applications in electronic problems; Analytical study of microwave structures printed on aniso-tropic substrates based on the Wiener-Hopf technique; Complex and real rays in three dimensional Minkowski space; Artificial anisotropy; Homogenization of photonic crystals; Approximated factorizations for kernels involved in the scattering due by a wedge at skew incidence; The transmission-line matrix (TLM) method: an efficient tool for problem segmentation (diakoptics); Spectral properties of the operator describing EM wave propagation in anisotropic dielectric guiding structures with arbitrary transversal inhomogeneity; Infinite-sheet branching of the habitat of the natural-frequencies of open resonators as a result of admission of infinite boundaries; Wiener-Hopf analysis of the RCS of two canonical, parallel-plate waveguide cavities with material loading; Wave transmission trough inhomogeneous chain of transparent obstacles; Adapted grids for the wavelet-based simulation of complex planar circuits; Volume singular integral equation method in electromagnetic theory; Electromagnetics of complex media and metamaterials.

TIME-DOMAIN METHODS: Evolution equation for near-field thermal radio emission; Time-domain electromagnetic fields in a resonator with dispersive medium; Energy transformation of a transient wave on radiating aperture; Excitation of a slotted bicone by an impulse magnetic dipole; A novel dual-polarized Ku-band antenna subarray; Integral equations in time domain for electromagnetic fields of waveguide structurs; Photonic Green's functions calculation by using FDTD method; Calculation of complexity of a pulse transformation in time-varying medium; Investigation of electromagnetic field in a plate-parallel wavegiude with time varying medium; Direct study of fields and radiation patterns of antennas with the account of closely located objects; Electromagnetic signals in a waveguide filled with an inhomogeneous time-variant medium; Accurate "absorbing" conditions for nonsinusoidal problems of diffraction for compact objects; Modeling of videopulse scattering by plane layered dielectric structures in the presence of errors; Terminated two-wire transmission line suspended in air illuminated by electromagnetic field and measurement of differential mode current.

COMPUTATIONAL OPTOELECTRONICS: Single-mode fiber with a reduced non-zero dispersion in wide range of wavelength; Mathematical analysis of the guided modes of an integrated optical guide; Full vectorial analysis of optical fibre facet; Mathematical modelling of unsymmetrical optical mirrors for femtosecond impulse generation; Modelling of radiation field excited on sharp waveguide discontinuities by numerical and semi-analytical methods; Coupled oscillations in the theory of layered dielectric; Stratification method for analysis of the radial inhomogeneous dielectric waveguide: a new approach towards realization.

PRINTED ANTENNAS AND CIRCUITS: Diffraction of electromagnetic wave by an array of complex shape microstrip reflectors; Comparison of CAD formulas, moment method and experiments for rectangular microstrip antennas; A line integral representation of the physical optics far field from plane PEC scatterers illuminated by electric or magnetic Hertzian dipoles; Closed-form Green's function and its using for analysis of microstrip antennas; Accurate analysis of PBG structures for high efficiency power amplifier design; Numerical simulation of the microstrip phased array; The photonic bandgap microstrip class-E amplifier; Diffraction of a plane H-polarized electromagnetic wave by two sequentially included stratified periodic dielectric structures.

GEORADAR AND REMOTE SENSING: Wind flight conditions model; Nonparametric algorithm for a detection of random process disorder in the signals of radar remote sensing; Doppler-polarimetric retrieval of rain rate and turbulence intensity in precipitation; Relationship between an interval of correlation of echo-signal envelope and turbulence intensity in radar reflecting volume of cloud or precipitation; Methods of improving of the subsurface objects images reconstructed by the tomography process; An ART algorithm for imaging of buried cylindrical bodies illuminated by gaussian beams; Estimation of geo metrical parameters of perfectly conducting cylindrical object buried in dielectric half-space by its scattering characteristics; Application of wavelet analysis for detection of cylindrical objects in dielectric layer using characteristic of reflection; Parameters optimization for synthesizing aperture method at practical use of continuous radiation underground radar.

WIRE AND WAVEGUIDE ANTENNAS: Curved-wire antennas solution technique; The properties of the fractal wire antenna; Radiation resistance of an electric dipole having different orientations when changing the position of a plane screen; Analysis of vertical wire antenna above imperfect ground using discrete complex image method; Radiation from a planar waveguide with symmetrical flange; Rigorous theory of rectangular waveguide arrays with finite flush mounted dielectric cover; Solution of three-dimensional electromagnetic problems; Basis functions in the analysis of electrically long slots in rectangular waveguide with the induced magnetomotive forces method; A waveguide-based antenna array exited by a surface wave.

CONFERENCE PROCEEDINGS

2002 International Conference on

MATHEMATICAL METHODS IN ELECTROMAGNETIC THEORY

MMET*02

DISTRIBUTION STATEMENT A
Approved for Public Release
Distribution Unlimited

Volume 1

Kiev, Ukraine

September 10-13, 2002

20030106 031 AQ F03-02-0377

Organized and sponsored by

IEEE AP/MTT/AES/ED/GRS/NPS/EMB Societies East Ukraine Joint Chapter

in cooperation with

Scientific Council of NAS on Radio Physics and Microwave Electronics
Institute of Radio-Physics and Electronics of NAS
National Technical University of Ukraine – Kiev Polytechnic Institute
Ukrainian National URSI Committee

technically co-sponsored by

IEEE AP, MTT and ED Societies
URSI

We wish to thank the following for their contribution to the success of this conference:

IEEE ED, MTT and AP Societies
European Office of Aerospace Research and Development
European Research Office, USARDSG-UK
TICRA

2002 International Conference on Mathematical Methods in Electromagnetic Theory

IEEE Catalog Number: 02EX554
ISBN: 0-7803-7391-X

Library of Congress: 2002100182

This material is based upon work supported by the European Office of Aerospace Research and development, Air Force Office of Scientific Research, Air Force Research Laboratory, under Contract No. F61775-02-WF065.

Copyright and Reprint Permission: Abstracting is permitted with credit to the source. Libraries are permitted to photocopy beyond the limit of U.S. copyright law for private use of patrons those articles in this volume that carry a code in the bottom of the first page, provided the per-copy fee indicated in the code is paid through Copyright Clearance Center, 222 Rosewood Drive, Danvers, MA 01923. For other copying, reprint or republication permission, write to IEEE Copyrights Manager, IEEE Service Center, 445, Hoes Lane, P.O. Box 1331, Piscataway, NJ 08855-1331. All rights reserved. Copyright © 2002 by the IEEE, Inc.

MMET*02 Chairman

Prof. E. I. Veliev, IRE NASU, Kharkov, Ukraine

MMET*02 Organizing Committee

Prof. V. I. Naidenko, NTUU-KPI, Kiev
Local Organization Chairman

Mr. H. A. Borsch, NTUU-KPI, Kiev
Local organization and technical support

Dr. V. G. Drygailo, NTUU-KPI, Kiev
Director of the Science Library

Dr. E. V. Guseva, NTUU-KPI, Kiev
Local organization and technical support

Dr. Y. M. Kuleshov, IRE NASU, Kharkov
IEEE East Ukraine Joint Chapter Chairman

Prof. L. N. Litvinenko, IRA NASU, Kharkov
Ukrainian National URSI Committee Vice-Chairman

Mr. A. A. Nosich, KNU, Kharkov
System administrator and technical support

Prof. V.I. Pravda, NTU-KPI, Kiev
Dean of Dept. Radio Engineering

Dr. A. Shishkova, KNU, Kharkov
Secretary and web designer

Mrs. S. Spivakova, KNPU, Kharkov
Proceedings editor and designer

Mr. A. D. Ustimenko, IRE NAS, Kharkov
Local Organization Manager

Prof. V. M. Yakovenko, IRE NASU, Kharkov
Ukrainian National URSI Committee Vice-Chairman

Prof. F. J. Yanovsky, National Aviation University, Kiev
Local Organization Coordinator

Prof. M. Z. Zgurovsky, NTUU-KPI, Kiev
Rector

MMET*02 CHAIRMAN

Prof. E. I. Veliev, IRE NASU, Kharkov, Ukraine

MMET*02 Technical Program Committee

Co-Chairmen:

Prof. A. I. Nosich, IRE NASU, Kharkov, Ukraine

Dr. W. Ross Stone, IEEE AP-S & URSI, San Diego, USA

Members:

Prof. T. Benson, University of Nottingham, UK
Prof. O. Breinbjerg, TU of Denmark, Lyngby, Denmark
Prof. N. Engheta, University of Pennsylvania, Philadelphia, USA
Prof. Y. V. Gandel, Kharkov National University, Ukraine
Prof. F. Gardiol, Ecole Polytechnique, Lausanne, Switzerland
Prof. M. Hashimoto, Osaka Electro-Commmunication University, Japan
Prof. A. Jacob, Technical University of Braunschweig, Germany
Prof. A. A. Kirilenko, IRE NASU, Kharkov, Ukraine
Prof. K. Kobayashi, Chuo University, Tokyo, Japan
Prof. M. Marciniak, Institute of Telecommunications, Warsaw, Poland
Prof. Z. T. Nazarchuk, PMI NASU, Lviv, Ukraine
Prof. M. Ney, ENSTB, Brest, France
Prof. Y. Okuno, Kumamoto University, Japan
Prof. A. Samokhin, Moscow TU of Radio Electronics, Russia
Prof. H. Shigesawa, Doshisha University, Kioto, Japan
Prof. S. V. Sukhinin, IH SB RAS, Novosibirsk, Russia
Prof. I. Sukhoivanov, Kharkov NU of Radio Electronics, Ukraine
Prof. D. I. Vavriv, IRA NASU, Kharkov, Ukraine
Dr. S. N. Vorobyov, IRA NASU, Kharkov, Ukraine
Prof. T. Yamasaki, Nihon University, Tokyo, Japan
Prof. F. J. Yanovsky, National Aviation University, Kiev, Ukraine
Dr. N. P. Yashina, IRE NASU, Kharkov, Ukraine
Prof. L. P. Yatsuk, Kharkov National University, Ukraine

CHAIRMEN'S WELCOME

Dear Colleagues –

We are happy to open MMET*02 in Kiev, over-a-thousand years old capital of the eleven years old independent Ukraine. The venue of the conference, this time, is the largest technical university of Ukraine, NTUU-KPI, or *Kyivska Politekhnika.*

As with the previous MMET conferences held in 1990-2000, we have tried to follow our several basic traditions. One of them is the idea that a cross-fertilization of mathematicians and microwave engineers is a natural necessity that should be promoted by all means. There are many other meetings covering *only* applied mathematics or computing and *only* microwaves or physics. MMET is a unique combination of the both. Therefore the technical program is a mixture of fundamental mathematical studies into boundary-value problems of wave scattering and studies into applications and implementations of various analysis methods. Another eternal idea is that interaction with the Western science has always been and still is very important for Ukrainians, Russians, Belarussians, Georgians, and other Eastern Europeans. Therefore we intended to attract as many as possible keynote speakers from the West Europe, America and Japan, from one hand, and good contributed papers from the East Europe, from the other hand. At the same time we still believe that having two working languages and massive poster sessions, as done sometimes, is a wrong way of international conference organization in our conditions. Instead, MMET gives one a chance to train in writing and presenting a paper in the major international science language, which is English. Still another traditional idea is to help young scientists from low-income regions come and participate, even if they travel from very far away. Humiliation of a 50-Euro a month salary of a scientist should be neutralized, at least once in two years, by an opportunity to join the holiday of MMET.

This year the Technical Program Committee had invited 28 papers and accepted 148 contributed ones, out of 161 submitted. We enjoyed working with all the members of Local Organizing Committee and Technical Program Committee. We are extremely thankful to the staff and executives of the Department of Radio Engineering and the Scientific Library of NTUU-KPI. All of us should kindly thank the editing group that prepared the conference proceedings and supported the Website of MMET*02. The generosity of the conference sponsors is greatly appreciated.

We thank everybody of participants who have come to Kiev this September despite many other professional commitments. We hope to see you at the future conferences in Ukraine.

Eldar I. Veliev and Alexander I. Nosich

It looks like MMET*02 has quite a nice program. Congratulations! Best wishes with the conference.

W. Ross Stone

MMET*02 PAPERS GEOGRAPHY

•	ENTITY	PAPERS
1	UKRAINE	83
2	RUSSIA	33
3	TURKEY	8
4	JAPAN	6
5	FRANCE	4
6	BELARUS	3
7	DENMARK	3
8	GERMANY	3
9	GREECE	3
10	ITALY	3
11	USA	3
12	BULGARIA	2
13	GEORGIA	2
14	SWITZERLAND+TURKEY	2
15	UKRAINE+FRANCE	2
16	UKRAINE+JAPAN	2
17	AUSTRIA	1
18	BELGIUM	1
19	CROATIA	1
20	CZECH REPUBLIC	1
21	IRAN	1
22	JORDAN	1
23	MEXICO	1
24	The NETHERLANDS	1
25	POLAND	1
26	SWEDEN	1
27	UK	1
28	UKRAINE+DENMARK	1
29	UKRAINE+TURKEY	1
30	UKRAINE+UK	1
	TOTAL	176

TABLE OF CONTENTS

Volume I

PLENARY SESSIONS

01 **A. Andrenko,** Study and microwave applications of artificial periodic substrate PBG planar circuits..... 21

02 **A. Baghai-Wadji,** Measures for accelerating EM computations..... 27

03 **Yu. Smirnov, S. Ivleeva,** Propagation of electromagnetic waves in open cylindrical waveguides with nonlinear media..... 33

04 **F. Molinet,** Hybrid numerical-asymptotic method for the calculation of the coupling between elements of a conformal microstrip patch array..... 38

05 **T. Magath, K. Schuenemann,** Application of evolution strategies in optimal design problems involving diffraction gratings..... 42

06 **A. Freni, P. De Vito, A. Mori,** A BMIA/AIM formulation for the analysis of large stacked patch antennas..... 48

07 **A. Hoorfar,** Evolutionary computational techniques in electromagnetics.... 54

08 **G. Vandenbosch, M. Vrancken, and B. Van Thielen** The use of hierarchy in modeling tools for planar structures..... 61

09 **V. L. Derbov, V. V. Serov, I. L. Plastun, S. V. Shilov,** Time-dependent self-action of periodically modulated laser beams in resonant media..... 67

10 **G. Fikioris,** On the solvability and application of numerical methods to Hallen's equation..... 73

11 **P. O. Savenko, B. M. Podlevskii, M. D. Tkach, M. I. Andriychuk,** Some classes of nonlinear synthesis problems for radiation systems: theory and methods of solution..... 79

12 **V. Daniele,** The Wiener-Hopf factorization method for the diffraction by wedges having arbitrary aperture angle 87

13 **H. Shigesawa, M. Tsuji,** Basic properties of leaky modes in printed- circuit transmission lines..... 93

14 **A. Kirilenko,** Large-scale discretization and generalized mode-matching as a basis for fast electromagnetic solvers..... 99

15 **H. Baudrand, W. Sidina, B. Damienne** The concept of waves: theory and applications in electronic problems..... 100

16 **G. Kyriacou,** Analytical study of microwave structures printed on anisotropic substrates based on the Wiener-Hopf technique..... 105
17 **E. Hasanov,** Complex and real rays in three dimensional Minkowski space 112
18 **F. Zolla, D. Felbacq,** Artificial anisotropy.....118
19 **A. Krokhin, J. Arriaga, P. Halevi,** Homogenization of photonic crystals.....124
20 **V.G. Daniele, R. E. Zich,** Approximated factorizations for kernels involved in the scattering due by a wedge at skew incidence.....130
21 **M. Ney, S. Le Maguer,** The transmission-line matrix (TLM) method: an efficient tool for problem segmentation (diakoptics).....136
22 **T. Jablonskii,** Spectral properties of the operator describing EM wave propagation in anisotropic dielectric guiding structures with arbitrary transversal inhomogeneity.....141
23 **A. Nosich,** Infinite-sheet branching of the habitat of the natural-frequencies of open resonators as a result of admission of infinite boundaries..... 150
24 **S. Koshikawa, K. Kobayashi,** Wiener-Hopf analysis of the RCS of two canonical, parallel-plate waveguide cavities with material loading.....152
25 **S. V. Sukhinin, D. A. Kondratenko,** Wave transmission trough inhomogeneous chain of transparent obstacles..... 157
26 **G. Schneider, A. Jacob,** Adapted grids for the wavelet-based simulation of complex planar circuits..... 163
27 **A. Samokhin,** Volume singular integral equation method in electromagnetic theory.....169
28 **N. Engheta,** Electromagnetics of complex media and metamaterials..... 175

TIME-DOMAIN METHODS

01 **K. P. Gaikovich,** Evolution equation for near-field thermal radio emission... 183
02 **M. S. Antyufeyeva, O. A. Tretyakov,** Time-domain electromagnetic fields in a resonator with dispersive medium..... 186
03 **A. N. Dumin, V. A. Katrich,** Energy transformation of a transient wave on radiating aperture..... 189
04 **V. A. Doroshenko,** Excitation of a slotted bicone by an impulse magnetic dipole..... 192
05 **S. Martynyuk, F. Dubrovka, P. Edenhofer** A novel dual-polarized Ku-band antenna subarray.....195

06 **A. Nerukh, T. Benson,** Integral equations in time domain for electromagnetic fields of waveguide structurs.....198

07 **I. S. Maksymov, G. I. Churyumov,** Photonic Green's functions calculation by using FDTD method.....201

08 **N. N. Ruzhytska, A. G. Nerukh, D. A. Nerukh.**Calculation of complexity of a pulse transformation in time-varying medium.....204

09 **N. Sakhnenko, A. Nerukh,** Investigation of electromagnetic field in a plate-parallel wavegiude with time varying medium.....207

10 **V. A. Ruchenkov, K. N. Klimov, B. V. Sestroretsky , M. A. Drize, Y. P. Bolshakov,** Direct study of fields and radiation patterns of antennas with the account of closely located objects.....210

11 **A. Y. Butrym, O. A. Tretyakov,** Electromagnetic signals in a waveguide filled with an inhomogeneous time-variant medium.....213

12 **A. I. Vyazmitinova,** Accurate "absorbing" conditions for nonsinusoidal problems of diffraction for compact objects.....216

13 **O. Puzanov,** Modeling of videopulse scattering by plane layered dielectric structures in the presence of errors.....219

14 **I. Araz, O. Cerezci, Z. Demir,** Terminated two-wire transmission line suspended in air illuminated by electromagnetic field and measurement of differential mode current.....222

COMPUTATIONAL OPTOELECTRONICS

01 **A. M. Gomilko, A. A.Gourjii, V. B. Katok, V. G. Levandovskyy, Y. D. Shchepkina,** Single-mode fiber with a reduced non-zero dispersion in wide range of wavelength.....227

02 **E. Kartchevski, G. Hanson,** Mathematical analysis of the guided modes of an integrated optical guide.....230

03 **I. Vorgul, A. Vukovic, P. Sewell, T. Benson,** Full vectorial analysis of optical fibre facet.....233

04 **I. A. Sukhoivanov, V. V. Lysak, A. Shulika,** Mathematical modelling of un-symmetrical optical mirrors for femtosecond impulse generation.....236

05 **E. A. Romanova, S. B. Gaal,** Modelling of radiation field excited on sharp waveguide discontinuities by numerical and semi-analytical methods..... 239

06 **M. I. Ayzatsky, K. Y. Kramarenko,** Coupled oscillations in the theory of layered dielectric.....242

07 **V. Katok, M. Kotenko, O. Ometsinska,** Stratification method for analysis of the radial inhomogeneous dielectric waveguide: a new approach towards realization.....245

PRINTED ANTENNAS AND CIRCUITS

01 **A. M. Lerer, G. P. Sinyavsky, D. E. Zelenchuk,** Diffraction of electromagnetic wave by an array of complex shape microstrip reflectors.....251

02 **V. Schejbal, Z. Raida, Z. Novacek,** Comparison of CAD formulas, moment method and experiments for rectangular microstrip antennas..... 254

03 **S. Arslanagic, P. Meincke, E. Jorgensen, O. Breinbjerg,** A line integral representation of the physical optics far field from plane PEC scatterers illuminated by electric or magnetic Hertzian dipoles.....257

04 **L. M. Karpukov, S. N. Romanenko, R. D. Pulov,** Closed-form Green's func-tion and its using for analysis of microstrip antennas..... 260

05 **J. V. Rassokhina, A. N. Rudiakova, V. G. Krizhanovski,** Accurate analysis of PBG structures for high efficiency power amplifier design..... 263

06 **A. O. Kasyanov, V. A. Obukhovets, V. I. Zagorovsky,** Numerical simulation of the microstrip phased array..... 266

07 **A. N. Rudiakova, Ju. V. Rassokhina, V. G. Krizhanovski,** The photonic bandgap microstrip class-E amplifier..... 267

08 **V. Naidenko, E. Guseva,** Diffraction of a plane H-polarised electromagnetic wave by two sequentially included stratified periodic dielectric structures..... 270

GEORADAR AND REMOTE SENSING

01 **Yu. A. Averyanova, A. A. Averyanov, F. J. Yanovsky,** Wind flight conditions model.....275

02 **I. Prokopenko, K. Prokopenko,** Nonparametric algorithm for a detection of random process disorder in the signals of radar remote sensing.....278

03 **F. J. Yanovsky,** Doppler-polarimetric retrieval of rain rate and turbulence intensity in precipitation.....281

04 **Y. S. Khraisat,** Relationship between an interval of correlation of echo-signal envelope and turbulence intensity in radar reflecting volume of cloud or precipitation..... 287

05 **A. Vertiy, S. Gavrilov,** Methods of improving of the subsurface objects images reconstructed by the tomography process.....290

06 **F. Dikmen, A. Alkumru, O. Yildirim,** An ART algorithm for imaging of buried cylindrical bodies illuminated by gaussian beams.....293

07 **A. V. Muzychenko, A. Z. Sazonov, O. I. Sukharevsky,** Estimation of geometrical parameters of perfectly conducting cylindrical object buried in dielectric half-space by its scattering characteristics.....296

08 **M. V. Andreev, O. O. Drobakhin, D. Yu. Saltykov,** Application of wavelet analysis for detection of cylindrical objects in dielectric layer using characteristic of reflection.....299

09 **A. A. Palto,** Parameters optimization for synthesizing aperture method at practical use of continuous radiation underground radar.....302

WIRE AND WAVEGUIDE ANTENNAS

01 **M. B. Protsenko,**Curved-wire antennas solution technique.....307

02 **L. M. Karpukov, V. M. Onufrienko, S. N. Romanenko,** The properties of the fractal wire antenna.....310

03 **N. P. Yeliseyeva, N.N. Gorobets,** Radiation resistance of an electric dipole having different orientations when changing the position of a plane screen.....313

04 **B. A. Arand, M. Hakkak,** Analysis of vertical wire antenna above imperfect ground using discrete complex image method.....316

05 **S. G. Vashtalov,** Radiation from a planar waveguide with symmetrical flange.....319

06 **M. B. Manuilov,** Rigorous theory of rectangular waveguide arrays with finite flush mounted dielectric cover.....322

07 **V. M. Morozov, V. I. Magro, M. Guarab,** Solution of three-dimensional electromagnetic problems.....325

08 **V. A. Katrich, V. I. Kiyko, L. P. Yatsuk, M. N. Nesterenko,** Basis functions in the analysis of electrically long slots in rectangular waveguide with the induced magnetomotive forces method.....328

09 **A. V. Gribovsky,** A waveguide-based antenna array exited by a surface wave.....331

Volume II

WIENER-HOPF AND FUNCTION-THEORETIC METHODS

01 **A.V. Shishkova, S. N. Pivnenko, O. S. Kim, N. N. Gorobets,** Phase radiation characteristics of an open-ended circular waveguide.....361

02 **Z. T .Nazarchuk, Y. P. Kulynych,** Frechet differentiability of a field operator for scattering from an open screen.....364

03 **V. F. Borulko,** Reflection of surface waves and their coupling with wave beams at anisotropically perturbed impedance plane.....367

04 **D. B. Kuryliak, K. Kobayashi, S. Koshikawa, Z. T. Nazarchuk,** Axial symmetric wave diffraction by a circular waveguide cavity.....370

05 **E. A. Gevorkyan,** On the method of solution of the wave equation with periodic coefficients.....373

06 **D. V. Golovin, D. O. Batrakov,** Fractional cylindrical functions implementation for electromagnetic waves scattering analysis.....376

07 **V. M. Lewykin, V. M. Onufriyenko,** Integro-differential potentials for the analysis of a fractal cover properties.....379

08 **V. M. Onufriyenko,** Integro-differential charges and currents distribution on the fractal medium topology.....382

GRATINGS AND FREQUENCY-SELECTIVE SURFACES

01 **G. A. Kalinchenko, A. M. Lerer, A. A. Yachmenov,** Mathematical simulation of impedance diffraction gratings.....387

02 **A. O. Kasyanov, V. A. Obukhovets,** Analysis of frequency selective structures with fractal elements.....390

03 **P. L. Mladyonov,** Electromagnetic wave diffraction by double-layer periodic grating of curvilinear metal strips.....395

04 **G. Elschner, A. Rathsfeld, G. Schmidt,** FEM and its generalization for the diffraction by polygonal profile gratings.....398

05 **N. V. Sidorchuk, V. V. Yachin, S. L. Prosvirnin,** Electromagnetic characteristics of doubly-periodic magnetodielectric layer bounded by two uniform media.....401

06 **T. Yamasaki, T. Hinata, T. Hosono,** Scattering of electromagnetic waves by homogeneous dielectric gratings with perfectly conducting strip.....404

07 **A. Bijamov, R. Zaridze, K. Tavzarashvili, V. Tabatadze,** Simulation of the finite photonic crystal –based adaptive antenna..... 407

08 **Y. Okuno, D. Q. Zhou, K. Yoshimoto, A. Matsushima, and T. Matsuda,** A combination of up- and down-going plane waves used to describe the field inside grooves of a deep grating..... 410

09 **T. L. Zinenko, A. I. Nosich,** Scattering and absorption of light by nano-thickness negative-dielectric strip gratings..... 413

10 **J. Chandezon, A. Poyedinchuk, N. Yashina,** Reconstruction of periodic boundary between dielectric media..... 416

11 **M. U. Sitsko, V. I. Demidtchik,** Reflective properties of grid structures with dielectric coating..... 420

12 **K. Watanabe,** Comparative study of integration schemes used on differential theory of gratings..... 423

13 **S. L. Prosvirnin, D. O. Tyrnov,** Eigenwaves in the layered medium of biperiodic strip arrays..... 426

14 **Y. V. Gandel, V. V. Khoroshun,** Mathematical models of electromagnetic wave scattering by two-element strip grating with perpendicularly magnetized gyrotropic medium..... 429

15 **T. Bugrova,** Dispersive and diffraction analysis of integrated periodic waveguide structure..... 432

ANTENNA ANALYSIS AND SYNTHESIS

01 **S. V. Nechitaylo, A. Z. Sazonov, O. I. Sukharevsky,** Calculation of electromagnetic field in near field zone of reflector antenna with edge radar absorbing coating..... 437

02 **G. V. Yermakov,** Analysis of reflector pattern in different frequency ranges in the backward hemisphere..... 440

03 **S. V. Buharov,** To the problem of analysis of dielectric rod antennas..... 443

04 **V. V. Ovsyanikov,** Statistical analysis of internal parameters of radiating systems with reactance elements..... 446

05 **M. V. Romanenko,** An algorithm of the sidelobe level optimization for the dual shaped symmetric reflector antenna..... 449

06 **S. N. Sorokin, V. V. Savelyev, E. V. Ivanchenko, M. P. Oleynik,** Fitness function calculation technique in the yagi–uda antennas evolutionary design..... 452

07 **B. Turetken, E. San, M. Yazici, I. Araz, A. I. Yurekli, M. Hekim,** Evaluation of uncertainty budget for antenna calibrations..... 455

08 **O. N. Nosenko, N. N. Gorobets,** Antenna arrays synthesis according to the sector pattern by multiparametric method of regularization..... 458

NUMERICAL TECHNIQUES

01 **M. B. Kurt, N. Ari, O. Cerezci,** A study for the fast solution of electromagnetic scattering problems: a wavelet based approach.....463

02 **N. Ari, A. Tesneli, S. S. Seker, O. Cerezci,** Symbolic computation techniques for aperture antennas.....466

03 **T. V. Kamichev, K N. Klimov, B. V. Sestroretsky, S. A. Ivanov,** The 2,5-D electromagnetic analysis in time domain mode..... 469

04 **B. Colak, O. Cerezci, Z. Demir, M. Yazici, B. Turetken, I. Araz,** Calculation of leakage through apertures on coaxial cable braided screens.....473

05 **O. S. Kim, E. Jorgensen, P. Meincke, O. Breinbjerg,** Efficient CFIE-mom analysis of 3-D PEC scatterers in layered media..... 476

06 **T. Trifonov,** The partial region method in 2-D electromagnetic and acoustic problems..... 479

07 **A. Y. Poyedinchuk, A. A. Kirilenko, N. P. Yashina,** Dielectric parameters recognition by using a waveguide cavity and a rigorous processing algorithm..... 482

08 **G. Ghvedashvili , R. Zaridze, K. Tavzarashvili, G. Saparishvili, A. Bijamov,** Drop shaped monopole antenna and its interaction with the user's head..... 485

09 **Y. O. Shlepnev,** Building Treffts finite elements for electromagnetic problems..... 488

SCATTERING AND RADAR CROSS SECTION

01 **N. V. Barkhudaryan, A. Z. Sazonov, O. I. Sukharevsky,** Calculation of near-zone electromagnetic fields scattered by complex shape airborne objects and estimation of their angular coordinates by onboard antenna systems.....493

02 **A. A. Gousenkova,** Mathematical methods in some diffraction problems for domains with defects.....496

03 **M. Karamehmedovic, O. Breinbjerg,** Application of the method of auxiliary sources for the analysis of plane wave scattering by impedance spheres.... 499

04 **Yu. G. Smirnov, A. A. Tsupak,** Volume singular integral equations method for solving of diffraction problem of electromagnetic waves on dielectric body in a box..... 502

05 **H. T. Anastassiu,** Radar cross section of a perfectly conducting, flat, polygonal plate over a dielectric, lossy half-space: a closed form, physical optics expression..... 505

06 **V. N. Kisel, A. I. Fedorenko,** Electromagnetic modeling of the jet aircraft intake with the interior impeller..... 508

07 **A. M. Lebedev,** Finite element analysis of scattering from 2D-objects of arbitrary composition..... 511

08 **V. A. Vasilets, S. A. Gorelyshev, K. I. Tkachuk,** Radioabsorbing material optimal using in the reduction of aircraft radar cross-section..... 514

09 **A. A. Zvyagintsev, A. I. Ivanov,** Minimization of the field diffracted from a convex impedance body to the shadow region..... 517

WAVEGUIDE CIRCUITS

01 **V. V. Khardikov, V. B. Kazanskiy,** Influence of defects on electrodynamic properties of a semi-infinite periodic sequence of the metal-dielectric scatterers..... 523

02 **A. R. Sorkin,** Waveguide filters on the lumped elements..... 526

03 **V. P. Chumachenko, I. V. Petrusenko,** Wave scattering by a cylindrical obstacle in a generalized waveguide..... 529

04 **A. Kirilenko, L. Mospan, V. Tkachenko,** Capacitive iris bandpass filter with spurious harmonic modes suppression..... 532

05 **A. A. Kirilenko, D. Yu. Kulik,** Data preprocessing for generalized mode-matching method..... 535

06 **S. F. Kulishenko, A. A. Kirilenko, S. L. Senkevich,** Mode-matching approach for the calculation of a waveguide tee distorted by semi-plates in the branching region..... 540

07 **L. B. Minakova, L. A. Rud,** The effects of resonance energy absorption in lossy waveguide-dielectric resonators..... 543

08 **I. N. Pleshchinskii, N. B. Pleshchinskii,** Diffraction on the eigenwaves on an inclined medium interface in the waveguides with metallic walls..... 546

COMPOSITE MEDIA AND METAMATERIALS

01 **V. F. Borulko,** The second or the third harmonic generation on a nonlinear film in a Bragg resonator.....551
02 **K. Vytovtov,** Analytical investigation of periodic media with negative parameters.....554
03 **R. V. Kornev, V. I. Demidtchik,** Investigation of composite materials with controllable electrodynamic properties.....557
04 **S. Hrabar, J. Bartolic,** Simplified analysis of split ring resonator used in backward meta-material.....560
05 **K. A. Vytovtov,** The analytical method of investigation of Faraday chiral media.....563
06 **A. V. Malyuskin, D. N. Goryushko, A. A. Shmat'ko, S. N. Shulga,** Scattering of a wave beam by inhomogeneous anisotropic chiral layer.....566
07 **V. Goblyk, Y. Yakovenko,** Modeling of electromagnetic field from mobile phone distributed in the human head phantom.....569
08 **A.A. Cheremisin, Yu .V. Vassilyev,** The mechanisms of gravitophotophoresis for aerosol aggregates in the free-molecular regime.....570

ANALYTICAL REGULARIZATION

01 **A. V. Brovenko, P. N. Melezhik, A. Ye. Poyedinchuk,** The plane H-polarized wave diffraction by a metal grating with a magnetoactive plasma.....573
02 **E. Ozkan, F. Dikmen, Yu. Tuchkin, S. Tarapov,** Wave diffraction by axially symmetrical system of finite soft cylinders.....576
03 **S. B. Panin, A. Ye. Poyedinchuk,** Diffraction by a screened chiral layer with a grating.....579
04 **A.V. Sulima,** Resonant coupling of cavity-backed slots.....582
05 **T. Oguzer, A. Nosich, A. Altintas,** Radiation characteristics of a 2D parabolic reflector antenna excited by the H-polarized complex source.....586
06 **E. K. Semenova, V. A. Doroshenko,** Electromagnetic waves scattering on an unclosed cone with an isotropic one inside.....589
07 **L. N. Illyashenko,** Electromagnetic backscattering from a triangular dielectric cylinder.....592
08 **S. Rondineau, A. I. Nosich, M. Himdi, J.-P. Daniel,** Simulation of a discrete Luneburg lens fed by a conformal printed antenna.....594

PROPAGATION AND SIGNAL PROCESSING

01 **Y.V. Kondratyev, O O. Drobakhin,** The filter for horn antenna multifrequency data processing..... 599

02 **I. Urazghildiiev, C. C. Logothetis, A. Rydberg, K. Wallin,** On unique estimation of azimuth-elevation-carriers by volume arrays..... 602

03 **O. Tveretina, H. Zantema,** Comparing techniques for proving unsatisfiability.....605

04 **A. Bychkov, A. Bychkov,** Modified method of geometric electromagnetics for the analysis of radio field in marine tropospheric waveguides..... 608

05 **V. B. Ivanov, M. V. Tolstikov,** Nonlinear stage of propagation of wave disturbances in the topside ionosphere.....611

06 **A. V. Oinats, V. I. Kurkin, S. N. Ponomarchuk,** The technique for calculating of HF-signals characteristics taking into consideration ionosphere waveguide propagation..... 614

07 **V. V. Khakhinov,** Electrodynamic model of the receiving antenna in terms of a waveguide representation of the HF field..... 617

08 **Y. Goncharenko, F. Kivva,** Evaluation of the atmospheric aerosol particle size in the reflective layer produced by strong solar flares.....620

09 **A. V. Shvets, V. K. Ivanov, A. V. Varavin,** On possibility of Schumann resonance observations within industrial areas..... 623

BEAMS AND PLASMAS

01 **N. N. Beletskii, S. A. Borysenko,** Bistability of nonlinear surface polaritons in conducting antiferromagnets..... 629

02 **Y. V. Bludov,** Propagation of intra-subband plasmons in a weakly disordered array of quantum wires.....632

03 **V. I. Miroshnichenko, V. M. Ostroushko,** Calculation of impedance of a sharp plasma boundary with a mixed-type electron scattering in anomalous skin-effect conditions..... 635

04 **V. V. Ovsyanikov, A. N. Gordienko,** Radiophysical characteristics of a radiator from the gas discharge plasma.....638

05 **A. N. Opanasenko,** Radiation by self-oscillating relativistic charged particle moving along periodic structure.....641

06 **A. F. Rusanov, V. M. Yakovenko,** Interaction of a non-relativistic electron beam with a semiconductor cylinder in an external magnetic field..... 644

07 **K. V. Ilyenko, V. A. Goryashko, T. Yu. Yatsenko, B. P. Yefimov,** An analytical method for construction of single particle electron trajectories in free electron lasers..... 647

08 **I. V. Yakovenko, V. M. Yakovenko,** Collisionless damping of surface plasma oscillations and possibilities of its revers at the interaction with charged particle flows..... 650

09 **Yu. O. Averkov, V. M. Yakovenko,** Peculiarities of nonlinear stabilization of the plasma-beam instability in semiconductor GaAs..... 653

EIGENVALUE PROBLEMS

01 **I. S. Chikichev,** Eigenoscillations near cascade of thin disks between the pair of parallel planes..... 659

02 **Yu. F. Filipov, Yu. V. Prokopenko,** Influence of an elliptical non-uniformity of dielectric sphere on spectral characteristics of resonance oscillations..... 662

03 **V. V. Linnik, N. B. Pleshchinskii,** On perturbation of the spectrum of planar dielectric waveguide by refraction index profile..... 665

04 **A. I. Makarov,** Numerical investigation of eigenoscillations near a honeycomb in a circular channel..... 668

05 **I. B. Yumov,** Existence theorems for eigenoscillations in 3-D rectangular waveguides..... 671

06 **G. Georgiev, M. Georgieva-Grosse,** Some aspects of the slow waves in the circular waveguide with azimuthally magnetized ferrite rod..... 674

07 **V. Bondarev, L. Logacheva,** Dispersion characteristics of a waveguide with periodic impedance of walls..... 677

08 **L. P. Yatsuk, A. A. Komyachko, Yu.V. Zhironkin,** The problem of orthogonality of eigenwaves in a waveguide partially filled with a lossy dielectric..... 680

09 **E. R. Bartuli,** Rotor stator acoustic interaction, death and birth of resonance frequency..... 683

10 **V. I. Naidenko, H. A. Borsch,** Characteristics of spatially-developed square multimode resonators..... 686

PLENARY SESSIONS

STUDY AND MICROWAVE APPLICATIONS OF ARTIFICIAL PERIODIC SUBSTRATE PBG PLANAR CIRCUITS

Andrey S. Andrenko
Fujitsu Laboratories LTD.
YRP R&D Center, 5-5, Hikari-no-Oka, Yokosuka, 239-0847, Japan
andrey@flab.fujitsu.co.jp

ABSTRACT

This paper presents the results of analytical study and numerical simulation as well as discusses various microwave applications of artificial periodic substrate photonic bandgap (PBG) circuits. The configurations considered are planar microstrip and coplanar line circuits on the high-density dielectric substrate containing finite-periodic groups of air blocks underneath the lines. Transmission matrix method has been applied for analyzing the transmission/reflection characteristics of the circuits and obtaining the stopband and passband conditions. Simulation results illustrating applications of PBG circuits as microwave bandpass filters and harmonic tuning elements are presented. The configurations discussed here provide certain advantages and promising solutions in the design of novel integrated antennas and adaptive arrays for the next-generation mobile communication systems.

INTRODUCTION

The 1990's have introduced an additional terminology into the field of electromagnetics and microwave engineering, namely photonic bandgap (PBG). It originally appeared in optics study where the phenomena of optical propagation through periodic structures were considered [1]. PBG is an effect when the propagation of EM waves of certain frequency bands is forbidden along specified direction in a periodic environment. The frequency response of PBG structures is scalable within wide frequency band and, as a result, various PBG configurations have been proposed and investigated Among them are planar patch antennas on periodic substrates to increase radiation efficiency and eliminate surface wave excitation [2], design of broadband power amplifiers [3], and waveguide band pass and low pass filters [4]

In microwave community, PBG is referred to as filter stopband long studied in periodic microwave circuits. Recently, the terminology of electromagnetic bandgap dealing with the same effect of constructive and destructive wave interference within the periodic structure has been used [5]. As confusing as it may seem, the uses of PBG or microwave PBG terminology can be justified taking into account its current vide spread in various microwave and antenna applications. There have been several attempts to utilize PBG structures in planar transmission lines technology, mostly by etching a periodic pattern of circles or holes in the ground plane along the microstrip. In this study, we analyze an alternative PBG periodic substrate for microstrip and coplanar lines, which can be effectively integrated with modern MMIC circuitry and manufactured using micromachining technology. The structure under consideration is a grounded dielectric layer with rectangular periodic air holes underneath the transmission lines as depicted in Fig. 1. The numerical results presented here correspond to the alumina (eps=10.5) high-density dielectric substrate. It has been shown that this configuration is an attractive candidate for integrated antenna filters used in active antenna design for next-generation mobile communication systems [6]. First, transmission matrix method is used to analytically obtain the stopband/passband conditions of the periodic substrate circuits. Next, numerical results of S-parameters illustrating filter characteristics of microstrip and coplanar lines PBG circuits are presented.

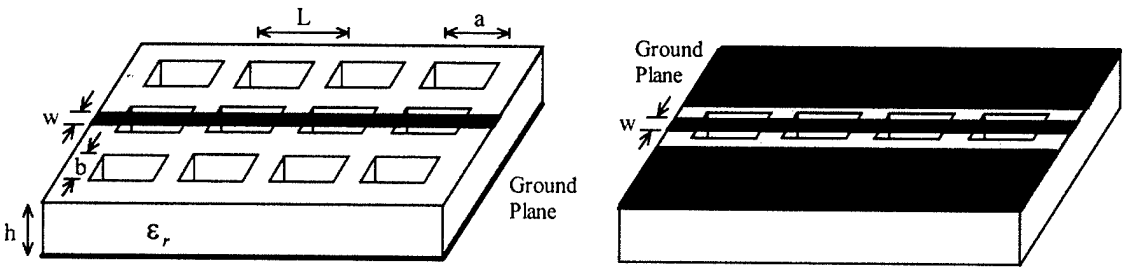


Fig.1. The geometry of microstrip and coplanar lines periodic substrate PBG circuits.

TRANSMISSION MATRIX ANALYSIS OF PBG CIRCUITS

The initial design of PBG circuits can be based on the Bragg condition expressed as

$$\beta L \approx \pi, \tag{1}$$

where β is the phase constant in the direction of periodicity L. Calculation of phase constant yields the formula for the central stopband frequency but it should be noted that the other important design parameters of a PBG substrate structure, such as stopband width and passband frequencies, would only be obtained from full-wave EM simulation of an actual periodic configuration. Transmission matrix method may provide analytical conditions of stopband and passband, which are quite useful in microwave circuit design. In applying transmission matrix approach, scattering parameters of a two-port network can be determined by defining its transmission matrix, also referred to as ABCD matrix, relating the voltages and currents at the input and output

$$[F_t] = \begin{bmatrix} A & B \\ C & D \end{bmatrix} \tag{2}$$

The reflection and transmission coefficients can be calculated through ABCD-parameters by using S-parameter conversions, which are readily available from the literature [7]

$$S_{11} = \frac{A + B - C - D}{A + B + C + D} \tag{3}$$

$$S_{12} = \frac{2(AD - BC)}{A + B + C + D} \tag{4}$$

$$S_{21} = \frac{2}{A+B+C+D} \tag{5}$$

$$S_{22} = \frac{-A+B-C+D}{A+B+C+D} \tag{6}$$

In case of lossless network, the condition of symmetry of a transmission line is

$$|S_{11}| = |S_{22}| \tag{7}$$

and substituting (3), (6) into (7) yields the relation of ABCD-parameters for symmetrical circuit

$$A = D \tag{8}$$

Reciprocity condition in case of equal impedance input and output ports is expressed by

$$|S_{21}| = |S_{12}| \tag{9}$$

which, by using (4), (5), yields reciprocity criterion it terms of transmission matrix parameters

$$AD = 1 + BC \tag{10}$$

Now consider how these formulas can be used in practical applications. In microwave filter design, the condition of passband, equivalent to full transmission, is given by

$$|S_{11}| = 0 \tag{11}$$

Therefore, from (3) we have

$$A + B = C + D \tag{12}$$

while for symmetrical circuits the condition of passband is simplified by (8) as

$$B = C \tag{13}$$

Similarly, the condition of stopband corresponding to total reflection is analytically expressed by

$$|S_{11}| = 1 \tag{14}$$

and from (3) we have

$$C + D = 0 \tag{15}$$

Now let's consider a PBG circuit as a microstrip line on a finite length periodic substrate. The results of 3-D EM simulation of this structure show that in order to realize proper PBG operation the transverse dimension of air blocks b should be a few times that of a microstrip, with optimal value being $(5 \div 6)w$. Therefore, without substantial loss of accuracy, we can approximate actual geometry of the circuit as a periodic set of microstrip line over uniform air-

filled substrate of length a and that on the conventional substrate of length l. Thus, for the structure depicted on Fig.2, the total voltage-current transmission matrix is defined as

$$[F_T]=[F]^N \tag{16}$$

where $[F]$ is the matrix of one period and N is the number of periods. Formula (16) implies that we consider a periodic circuit of length NL made of N two-port elements. For one period of structure shown in Fig.2, its voltage-current transmission matrix is represented as follows

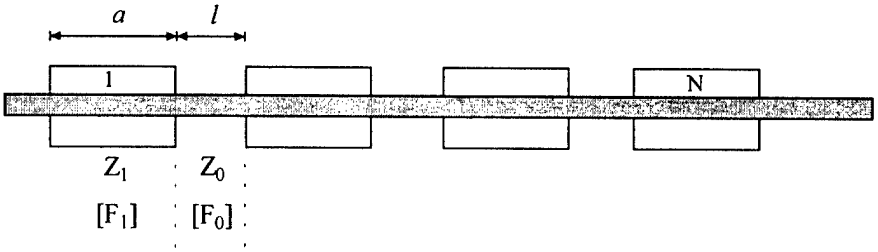


Fig. 2. Transmission matrix representation of artificial periodic substrate microstrip circuit.

$$[F]=[F_1][F_0], \tag{17}$$

where $[F_1]$ is the matrix of microstrip line of length a over air block while $[F_0]$ is that of conventional line of length l on dielectric substrate. As is well known, transmission matrix of a two-port circuit can be defined in terms of line impedance and phase length as follows

$$[F_1]=\begin{bmatrix} \cos\theta_1 & jZ_1\sin\theta_1 \\ jZ_1^{-1}\sin\theta_1 & \cos\theta_1 \end{bmatrix} \tag{18}$$

$$[F_0]=\begin{bmatrix} \cos\theta_0 & jZ_0\sin\theta_0 \\ jZ_0^{-1}\sin\theta_0 & \cos\theta_0 \end{bmatrix} \tag{19}$$

with $\theta_1=\dfrac{2\pi a}{\lambda}$, $\theta_0=\dfrac{2\pi l}{\lambda_\varepsilon}$ and Z_1, Z_0 being the characteristic impedance of the line over air block and substrate, respectively. Therefore, voltage-current transmission matrix (17) becomes

$$[F]=\begin{bmatrix} (\cos\theta_1\cos\theta_0 - C\sin\theta_1\sin\theta_0) & jZ_0(\cos\theta_1\sin\theta_0 + C\sin\theta_1\cos\theta_0) \\ jZ_0^{-1}(\cos\theta_1\sin\theta_0 + C^{-1}\sin\theta_1\cos\theta_0) & (\cos\theta_1\cos\theta_0 - C^{-1}\sin\theta_1\sin\theta_0) \end{bmatrix} \tag{20}$$

where $C=Z_1Z_0^{-1}$. Next, S-parameters of the entire periodic circuit can be defined through A,B,C,D parameters of the total transmission matrix (16) by matrix multiplication. A simple yet interesting illustration of the above analysis can be obtained by considering the microstrip over single air block, i.e. length a circuit. This is a symmetrical two-port structure whose voltage-current transmission matrix is given by (18). Condition (8) is satisfied so that passband condition (13) leads to

$$\sin\frac{2\pi a}{\lambda}=0 \tag{21}$$

which shows that there exist a fundamental solution at zero frequency and the discrete set of solutions for

$$a = n\frac{\lambda}{2},\ n = (1,2,3,...) \tag{22}$$

It means that relatively long, of the order of few centimeters, single air block in the microstrip substrate can cause no reflection for the mode propagating along the line. In attempting to obtain stopband condition of single-element microstrip circuit, one obtains the following equation

$$j\tan\theta_1 = -Z_1 \tag{23}$$

which has no physical solution so that stopband cannot be produced. These results are illustrated on Fig. 3 showing calculated S-parameters of microstrip line over single air block of length 15 mm. Similar results have been obtained for the coplanar line over single air block.

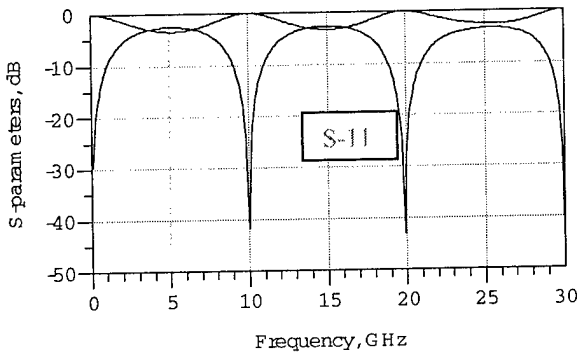


Fig. 3. Calculated S-parameters of microstrip line over single air block of length 15 mm.

NUMERICAL STUDY OF STOPBAND/PASSBAND CHARACTERISTICS

The microstrip and coplanar PBG circuits of various geometries have been numerically investigated towards their filter applications in integrated amplifiers and array antenna systems. Both microstrip and coplanar circuits display similar PBG characteristics with the difference being the stopband and passband frequency shift of about 2 GHz for the same artificial periodic substrates.

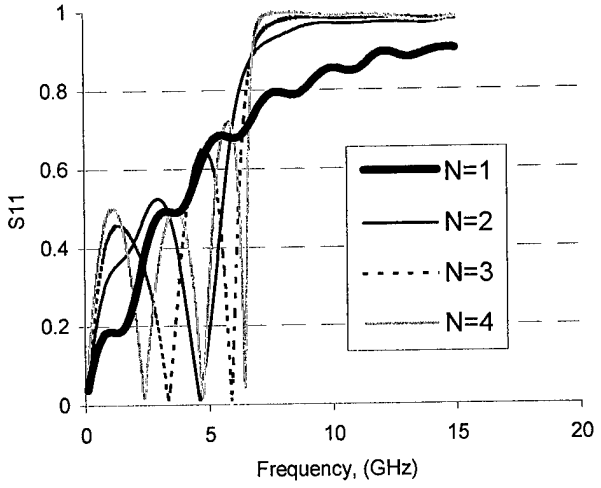


Fig. 4. Reflection coefficients of PBG microstrip circuits with different number of elements

An important result is presented in Fig. 4 showing calculated reflection coefficients of microstrip PBG circuits with varying number of elements with parameters a=6.0mm, b=2.5mm, l =9.5mm. It is seen that the number of passbands equals the number of circuit elements and their locations change as the number of elements increases while the location of stopband remains practically the same. The circuits considered are able to produce extremely wide (of the order of 15-20 GHz) stopband while requiring fewer elements than conventional PBG configurations. Fig. 5 shows simulation results of the 5-element circuit optimized as an output filter of the 5 GHz class-F operation MMIC amplifier. More numerical results on the stopband

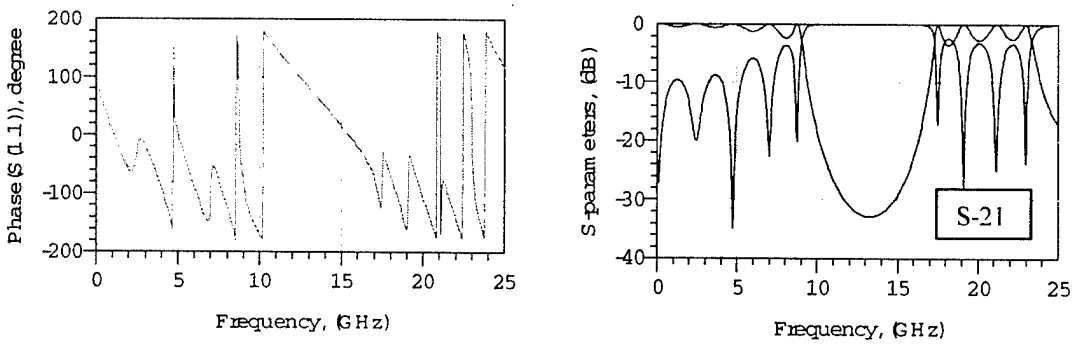


Fig. 5. Reflected wave phase and S-parameters of 5-element microstrip PBG circuit, L=7.0mm, a=4.5mm

harmonics control and phase shifter applications of the circuits considered will be presented at the Conference.

CONCLUSIONS

Detailed study and some numerical results of the planar artificial periodic substrate PBG circuits have been presented. The advantages of the proposed configurations in the design of integrated filters for active antenna systems have been discussed. An ongoing study of novel microwave devices incorporating multi-layer periodic PBG structures is currently being continued.

REFERENCES:

[1]J.D. Joannopoulos, R.D. Meade, and J.N. Winn, *Photonic Crystals: Molding the Flow of Light.* Princeton, NJ: Princeton University Press, 1995.

[2]Y. Qian, R. Coccioli, D. Sievenpiper, V. Radisic, E. Yablonovitch, and T. Itoh, " A microstrip patch antenna using novel photonic band-gap structures," *Microwave Journal*, vol. 42, no. 1, pp. 66-76, Jan. 1999.

[3]V. Radisic, Y. Qian, and T. Itoh, "Broad-band power amplifier using dielectric photonic bandgap structure," *IEEE Microwave Guided Wave Lett.*, vol. 8, no. 1, pp. 13-14, Jan. 1998.

[4]T. Kim and C. Seo, "A novel photonic bandgap structure for low-pass filter of wide stopband," *IEEE Microwave Guided Wave Lett.*, vol. 10, no. 1, pp. 13-15, Jan. 2000..

[5]R. Agi, M. Mojahedi, B. Minhas, E. Schamiloglu, and K. Malloy, "The effects of an electromagnetic crystal substrate on a microstrip patch antenna," *IEEE Trans. Antennas Propagat.*, vol. AP-50, pp. 451-456, April 2002.

[6]A. S. Andrenko, Y. Ikeda, and Osami Ishida, "Application of PBG microstrip circuits for enhancing the performance of high-density substrate patch antennas," *Microw. Opt. Technol. Lett.*, vol. 32, no. 5, pp. 340-344, 2002.

[7]M. W. Medley, Jr., Microwave and RF Circuits: Analysis, Synthesis and Design. Artech House, Boston, London, 1993.

MEASURES FOR ACCELERATING EM COMPUTATIONS

Ali R. Baghai-Wadji[1]

Vienna University of Technology
Gusshausstr. 27-29, A-1040, Vienna, Austria, EU
E-mail: alireza.baghai-wadji@tuwien.ac.at

ABSTRACT

Utilizing Maxwell's equations in diagonalized form we outline a procedure for the construction of universal functions for accelerating the method of moments computations. It is shown that the universal functions are coordinate-free, material-, and frequency independent. The procedure for the construction of universal functions automatically regularizes the involved integrals in the near- as well as the far field.

INTRODUCTION

Recently we formulated a conjecture stating that linear PDEs in mathematical physics are diagonalizable [1]. In particular we demonstrated the existence of diagonalized forms for the Maxwell's equations in isotropic, anisotropic, and general bi-anisotropic media. Diagonalized forms transform into eigenequations using the Fourier transformation. The associated eigenpairs serve as building blocks for the construction of Green's functions in the spectral (k) domain. In [2] we demonstrated that the $k \to \infty$ asymptotics of the eigenpairs can be used to construct real-space near-field asymptotics of the Green's functions simply by inspection. In [3] it is shown that the underlying ideas can be used to construct universal functions for accelerating the method of moments computations [4]. In this contribution, restricting our discussion to the simplest cases possible, our attempt is to communicate the key steps in our procedure for the construction of universal functions.

DERIVATION OF GREEN'S FUNCTIONS IN THE REAL SPACE

Consider a unit point charge in the free space located at the point (x', y', z'): $\vec{\nabla}\cdot\vec{D} = \delta(x-x')\,\delta(y-y')\,\delta(z-z')$. Using $\vec{D} = \varepsilon_0\vec{E}$, which relates the dielectric displacement $\vec{D}$ and the electric field $\vec{E}$, and $\vec{E} = -\vec{\nabla}G$ which defines the scalar potential function $G = G(x, y, z \mid x',\ y',\ z')$ we obtain the Poisson equation for the infinite domain Green's funciton G

$$\vec{\nabla}\cdot\vec{\nabla}G = -\frac{1}{\varepsilon_0}\delta(x-x')\delta(y-y')\delta(z-z'). \tag{1}$$

[1]The author is also affiliated with Arizona State University, Mathematics and Statistics Dept. Arizona, USA, and Helsinki Univesrity of Technology, Materials Physics Lab., Espoo, Finland.

The symmetry of the problem suggests the form $G = C/r$, with r being the distance between the source and the observation point (x, y, z), and C a constant. To determine C integrate both sides of (1) over the volume of a sphere of radius η and the center (x', y', z'), and let η approach zero (see e.g. [5]): $\lim_{\eta\to 0+} \int_{V_\eta} dV \vec{\nabla} \cdot \vec{\nabla} G = -1/\varepsilon_0$. Applying Gauss' divergence theorem to the resulting integral we obtain $\lim_{\eta\to 0+} \oint_{S_\eta} dS\ \vec{n} \cdot \vec{\nabla} G = \lim_{\eta\to 0+} \oint_{S_\eta} dS\ dG/dr = \lim_{\eta\to 0+} 4\pi\eta^2\ C(-1)\ 1/\eta^2 = -C4\pi$, leading to $C = 1/(4\pi\varepsilon_0)$, and thus to $G = 1/(4\pi\varepsilon_0 r)$. This is a **symmetric** representation in terms of $x - x'$, $y - y'$, and $z - z'$ (see (5a)).

3D SPECTRAL DECOMPOSITION

In 3D spectral doamin (1) results in $\overline{G}(k_1, k_2, k_3) = e^{-jk_1x'}\ e^{-jk_2y'}\ e^{-jk_3z'}\ /\ [\varepsilon_0\ (k_1^2 + k_2^2 + k_3^2)]$, from which we obtain the integral representation in (2), which is again **symmetric** in terms of $x - x'$, $y - y'$, and $z - z'$.

$$G(x - x', y - y', z - z') = \int_{-\infty}^{\infty}\int_{-\infty}^{\infty}\int_{-\infty}^{\infty} \frac{dk_1}{2\pi}\frac{dk_2}{2\pi}\frac{dk_3}{2\pi} \frac{e^{jk_1(x-x')}e^{jk_2(y-y')}e^{jk_3(z-z')}}{\varepsilon_0(k_1^2 + k_2^2 + k_3^2)}. \quad (2)$$

DIAGONALIZED FORMS: 2D SPECTRAL DECOMPOSITION

In [1] we have shown that (1) can be diagonalized:

$$\begin{aligned}
&\begin{bmatrix} 0 & -\frac{1}{\varepsilon_0} \\ \varepsilon_0(\frac{\partial^2}{\partial_{xx}} + \frac{\partial^2}{\partial_{yy}}) & 0 \end{bmatrix} \begin{bmatrix} G \\ D_3 \end{bmatrix}^{>} \mathcal{H}(z - z') + \begin{bmatrix} 0 & -\frac{1}{\varepsilon_0} \\ \varepsilon_0(\frac{\partial^2}{\partial_{xx}} + \frac{\partial^2}{\partial_{yy}}) & 0 \end{bmatrix} \begin{bmatrix} G \\ D_3 \end{bmatrix}^{<} \\
&\times \mathcal{H}(z' - z) = \frac{\partial}{\partial z} \begin{bmatrix} G \\ D_3 \end{bmatrix}^{>} \mathcal{H}(z - z') + \frac{\partial}{\partial z} \begin{bmatrix} G \\ D_3 \end{bmatrix}^{<} \mathcal{H}(z' - z) \qquad (3) \\
&+ \begin{bmatrix} G \\ D_3 \end{bmatrix}^{>} \delta(z - z') - \begin{bmatrix} G \\ D_3 \end{bmatrix}^{<} \delta(z' - z) - \begin{bmatrix} 0 \\ \delta(x - x')\delta(y - y') \end{bmatrix} \delta(z - z').
\end{aligned}$$

$\mathcal{H}(\cdot)$ stands for the Heaviside's step function. Here, we arbitrarily have diagonalized with respect to the $z-$ coordiante. The symbols $^>$ and $^<$ signify the regions $z > z'$ and $z < z'$, respectively. Note that the terms associated with $\mathcal{H}(z - z')$ and $\mathcal{H}(z' - z)$ are equivalent to the Laplace equation in the respective regions. The terms associated with the Dirac's delta function constitute the "interface conditions". A 2D Fourier transformation projects (3) onto an algebraic eigenform with the eigenpairs $\pm\sqrt{k_1^2 + k_2^2} \Longleftrightarrow \left(1, \mp\sqrt{k_1^2 + k_2^2}\right)^T$. Using (3), $G^{\gtrless} \propto \overline{G}e^{\mp\sqrt{k_1^2+k_2^2}|z'-z|}$ and $-\varepsilon_0\ \partial G^>/\partial z + \varepsilon_0\ \partial G^</\partial z = \delta(x - x')\ \delta(y - y')$, which satisfy the "interface conditions", we obtain $\overline{G} = 1/\ (2\varepsilon_0\ \sqrt{k_1^2 + k_2^2})$, and thus

$$G(x-x',y-y',z-z') = \int_{-\infty}^{\infty}\int_{-\infty}^{\infty} \frac{dk_1}{2\pi}\frac{dk_2}{2\pi} \frac{e^{jk_1(x-x')}e^{jk_1(y-y')}e^{-\sqrt{k_1^2+k_2^2}|z-z'|}}{2\varepsilon_0\sqrt{k_1^2+k_2^2}}. \quad (4)$$

In conclusion we have established the following equivalent representations:

$$\frac{1}{r} = \frac{1}{\sqrt{(x-x')^2+(y-y')^2+(z-z')^2}} \quad (5a)$$

$$= \frac{1}{2\pi^2}\int_{-\infty}^{\infty}\int_{-\infty}^{\infty}\int_{-\infty}^{\infty} dk_1dk_2dk_3 \frac{e^{jk_1(x-x')}e^{jk_2(y-y')}e^{jk_3(z-z')}}{k_1^2+k_2^2+k_3^2} \quad (5b)$$

$$= \frac{1}{2\pi}\int_{-\infty}^{\infty}\int_{-\infty}^{\infty} dk_1dk_2 \frac{e^{jk_1(x-x')}e^{jk_2(y-y')}e^{-\sqrt{k_1^2+k_2^2}|z-z'|}}{\sqrt{k_1^2+k_2^2}}. \quad (5c)$$

Comments: (i) Obviously, the representation (5c) is **not symmetric** with respect to $x-x'$, $y-y'$, and $z-z'$. There are indeed this type of representations which we will use to construct **universal functions**. The representation (5c) offers great flexibility in designing formula: Consider the points (x',y',x') and (x,y,z) and draw the following picture. Assume a sphere with radius r. Let the center of the sphere coincide with the source point. Then the sphere inhabits the observation point on its surface. So far we have not specified any coordinate system. Obviously there are infinitely many choices for a cartesian coordinate system with the center of the sphere being its origin. Each of these coordiante systems partitions r into the corresponding set of $x-x'$, $y-y'$, and $z-z'$. However, in view of (5c) $x-x'$ and $y-y'$ determine the oscillation rates of our integral, while $z-z'$ dictates its decaying behavior. *By selecting a specific "local" coordinate system we have the flexibility to manipulate the oscillatory- and decaying properties of our integrals.* In particular, we may select a coordinate system such that both the source- and observation points lie either on the $x-$ axis, $y-$axis, or the $z-$axis, resulting in 1D purely oscillating or decaying integrals. The key for these considerations is the diagonalized form in (3). (ii) These ideas are not restricted to the static fields in the free space. Similar integral representations can be obtained for the Green's function associated with the scalar Helmholz equation, i.e. e^{jk_0r}/r. Thereform, integral representations for the dyadic Green's functions in isotropic media can be obtained simply by inspection. (iii) In [1] we have presented a simple recipe for the diagonalization of Maxwell's equations in general bianisotropic media, which allows the construction of similar integrals for the Green's functions in general complex media.

ELECTRODYNAMIC FIELD DISTRIBUTIONS

In the following sections we describe the construction of universal functions by considering a simple example: Let $G_{11}(\vec{r}-\vec{r'})$ be the $x-$ component of the electric

field as the response to an electric current element oriented in the $x-$ direction. Consider the "asymmetric" representation (see e.g. [1])

$$G_{11}(\vec{r}-\vec{r'}) = \int_{-\infty}^{\infty}\int_{-\infty}^{\infty} \frac{dk_1}{2\pi}\frac{dk_2}{2\pi}\frac{j}{2\varepsilon\omega}\frac{k_2^2-\lambda^2}{\lambda}e^{-\lambda|z-z'|}e^{jk_1(x-x')}e^{jk_1(y-y')}, \tag{6}$$

with

$$\lambda = \begin{cases} \sqrt{k_1^2+k_2^2-\varepsilon\mu\omega^2}; & k_1^2+k_2^2-\varepsilon\mu\omega^2>0, \\ -j\sqrt{\varepsilon\mu\omega^2-k_1^2-k_2^2}; & \varepsilon\mu\omega^2-k_1^2-k_2^2>0. \end{cases} \tag{7}$$

UNIVERSAL FUNCTIONS

Assume we already have discretized a continuous boundary value problem of interest. Consider two parallel square-shaped metallic elements (m^{th} and n^{th} elements). We wish to calculate a_{mn}, the interaction of these elements related to G_{11}. To this end we utilize the Method of Moments [4] and consider the basis- $b_n(x,y,z)$ and the testing function $w_m(x,y,z)$. Here, $b_n(x,y,z) = P_n(x,y)\delta(z-z_n)$ with $P_n(x,y)$ being a rectangular window function with its support extending from x_n^b to x_n^e in $x-$direction, and from y_n^b to y_n^e in $y-$direction, and $\delta(z-z_n)$ being a delta function. Similarly we can define $w_m(x,y,z) = P_m(x,y)\delta(z-z_m)$. a_{mn} is then given by

$$\begin{aligned} a_{mn} &= \int\cdots\int dx'dy'dz'dxdydzb_n(x',y',z')w_m(x,y,z)G_{11}(x-x',y-y',z-z') \\ &= \int_{-\infty}^{\infty}\int_{-\infty}^{\infty}\frac{dk_1}{2\pi}\frac{dk_2}{2\pi}\frac{1}{2\varepsilon\omega}\frac{k_2^2-\lambda^2}{k_1^2k_2^2\lambda}e^{-\lambda|z_m-z_n|} \\ &\times\left[e^{jk_1(x_m^e-x_n^e)}-e^{jk_1(x_m^b-x_n^e)}-e^{jk_1(x_m^e-x_n^b)}+e^{jk_1(x_m^b-x_n^b)}\right] \\ &\times\left[e^{jk_2(y_m^e-y_n^e)}-e^{jk_2(y_m^b-y_n^e)}-e^{jk_2(y_m^e-y_n^b)}+e^{jk_2(y_m^b-y_n^b)}\right]. \end{aligned} \tag{8}$$

REGULARIZATION AT $(k_1,k_2)=(0,0)$

The terms in the square brackets in (8) collectively guarantee that the integrand is regular at $(k_1,k_2)=(0,0)$. However, the construction of our universal function requires the separation of these terms, with individual terms being singular at the origin. To remedy this difficulty we realize that the replacement of the exponential functions $e^{jk_{1,2}(\cdot)}$ by $1-e^{jk_{1,2}(\cdot)}$ leaves (8) unchanged. Note also that $(k_2^2-\lambda^2)/(\lambda k_1^2k_2^2)\exp(-\lambda|z_m-z_n|)$ is even in both k_1 and k_2. Therefore, we have

$$a_{mn} = \frac{1}{2\pi^2\varepsilon\omega}\int_0^\infty\int_0^\infty dk_1 dk_2 \frac{k_2^2-\lambda^2}{k_1^2 k_2^2 \lambda} e^{-\lambda|z_m - z_n|}$$
$$\times \{[1-\cos k_1(x_m^e - x_n^e)]\,[1-\cos k_2(y_m^e - y_n^e)] \mp 15 \text{ terms } \} \qquad (9a)$$
$$= \frac{2}{\pi^2\varepsilon\omega}\int_0^\infty\int_0^\infty dk_1 dk_2 \frac{k_2^2-\lambda^2}{\lambda} e^{-\lambda|z_m - z_n|}$$
$$\times \left\{ \frac{\sin^2[k_1(x_m^e - x_n^e)/2]}{k_1^2} \frac{\sin^2[k_2(y_m^e - y_n^e)/2]}{k_2^2} \mp 15 \text{ terms } \right\}. \qquad (9b)$$

(9b) can now be separated into sixteen integrals without any concerns.

SCALING OUT THE FREQUENCY DEPENDENCE

By introducing the "slownesses" $\tilde{k}_1 = k_1/\omega$, $\tilde{k}_2 = k_2/\omega$, and $\tilde{\lambda} = \lambda/\omega$, and the "velocities" $\tilde{x} = \omega x$, and $\tilde{y} = \omega y$, we introduce the function $A(\tilde{x}, \tilde{y}, \tilde{z})$:

$$\frac{\pi^2\varepsilon\omega^2}{2} A(\tilde{x}, \tilde{y}, \tilde{z}) = \int_0^\infty\int_0^\infty d\tilde{k}_1 d\tilde{k}_2 \frac{\tilde{k}_2^2 - \tilde{\lambda}^2}{\tilde{\lambda}} e^{-\tilde{\lambda}|\tilde{z}|} \left[\frac{\sin^2(\tilde{k}_1\tilde{x})}{\tilde{k}_1^2}\right] \left[\frac{\sin^2(\tilde{k}_2\tilde{y})}{\tilde{k}_2^2}\right], \qquad (10)$$

$\tilde{\lambda} = \sqrt{\tilde{k}_1^2 + \tilde{k}_2^2 - \varepsilon\mu}$ for $\tilde{k}_1^2 + \tilde{k}_2^2 - \varepsilon\mu > 0$, and an adequate definition for $\tilde{k}_1^2 + \tilde{k}_2^2 - \varepsilon\mu < 0$. (9b) and (10) show that a_{mn} can be calculated by sampling $A(\tilde{x}, \tilde{y}, \tilde{z})$ at sixteen points, and appropriately adding and subtracting the sampled data.

SCALING OUT THE MATERIAL PAMATERS

Define the characteristic "slowness" s_c by $\varepsilon\mu = 1/v_c^2 = s_c^2$. Introducing $\hat{\tilde{k}}_1 = \tilde{k}_1/s_c$, $\hat{\tilde{k}}_2 = \tilde{k}_2/s_c$, $\hat{\tilde{\lambda}} = \tilde{\lambda}/s_c$, $\hat{\tilde{x}} = s_c\tilde{x}$, and $\hat{\tilde{y}} = s_c\tilde{y}$, we obtain

$$U_{11}(\hat{\tilde{x}}, \hat{\tilde{y}}, \hat{\tilde{z}}) = \int_0^\infty\int_0^\infty d\hat{\tilde{k}}_1 d\hat{\tilde{k}}_2 \frac{1 - \hat{\tilde{k}}_1^2}{\hat{\tilde{\lambda}}} e^{-\hat{\tilde{\lambda}}|\hat{\tilde{z}}|} \left[\frac{\sin^2(\hat{\tilde{k}}_1\hat{\tilde{x}})}{\hat{\tilde{k}}_1^2}\right] \left[\frac{\sin^2(\hat{\tilde{k}}_2\hat{\tilde{y}})}{\hat{\tilde{k}}_2^2}\right] \qquad (11)$$

with $\pi^2\varepsilon\omega^2 s_c/2\ A_{11}(\hat{\tilde{x}}, \hat{\tilde{y}}, \hat{\tilde{z}}) = U_{11}(\hat{\tilde{x}}, \hat{\tilde{y}}, \hat{\tilde{z}})$. Here, $\hat{\tilde{\lambda}} = \sqrt{\hat{\tilde{k}}_1^2 + \hat{\tilde{k}}_2^2 - 1}$ for $\hat{\tilde{k}}_1^2 + \hat{\tilde{k}}_2^2 > 1$, and an adequate definition for $\hat{\tilde{k}}_1^2 + \hat{\tilde{k}}_2^2 < 1$. $U_{11}(\hat{\tilde{x}}, \hat{\tilde{y}}, \hat{\tilde{z}})$ is our **Universal Function**.

REGULARIZATION AT $\hat{\tilde{k}} \to \infty$

In cylindrical coordinates ($\hat{\tilde{k}}_1 = \hat{\tilde{k}}\cos\theta$, $\hat{\tilde{k}}_2 = \hat{\tilde{k}}\sin\theta$) it is easily seen that

$$\lim_{\hat{k}\to\infty}\left\{\begin{matrix}\hat{\hat{k}}\dfrac{1-\hat{\hat{k}}_1^2}{\hat{\hat{k}}_1^2\hat{\hat{k}}_2^2\hat{\hat{\lambda}}}e^{-\hat{\hat{\lambda}}|\hat{\hat{z}}|}\end{matrix}\right\}=\lim_{\hat{k}\to\infty}\underbrace{\left(\frac{1}{\cos^2\theta\sin^2\theta}\frac{\frac{1}{\hat{\hat{k}}^4}}{\sqrt{1-\frac{1}{\hat{\hat{k}}^2}}}-\frac{1}{\sin^2\theta}\frac{\frac{1}{\hat{\hat{k}}^2}}{\sqrt{1-\frac{1}{\hat{\hat{k}}^2}}}\right)e^{\hat{\hat{k}}(1-\sqrt{1-\frac{1}{\hat{\hat{k}}^2}})|\hat{\hat{z}}|}}_{\mathcal{Q}(\hat{\hat{k}},1/\hat{\hat{k}}|\cos^2\theta,\sin^2\theta,|\hat{\hat{z}}|)=\mathcal{Q}(\hat{\hat{k}},1/\hat{\hat{k}})}$$

$$\times e^{-\hat{\hat{k}}|\hat{\hat{z}}|}\quad\Longrightarrow\quad P(1/\hat{\hat{k}}|\cos^2\theta,\sin^2\theta,|\hat{\hat{z}}|)e^{-\hat{\hat{k}}|\hat{\hat{z}}|}=\mathcal{P}(1/\hat{\hat{k}})e^{-\hat{\hat{k}}|\hat{\hat{z}}|}. \tag{12}$$

The asymptotic expansion $\mathcal{P}(1/\hat{\hat{k}})$ is a polynomial in $1/\hat{\hat{k}}$, with coefficients involving integer powers of $\hat{\hat{z}}$ and $\cos^2\theta$ and $\sin^2\theta$. We obtain

$$U_{11}(\hat{\hat{x}},\hat{\hat{y}},\hat{\hat{z}})=\frac{\hat{\hat{x}}^2\hat{\hat{y}}^2}{4}\int_0^{\pi/2}\int_0^1 d\theta d\hat{\hat{k}}\underbrace{\frac{\hat{\hat{k}}(1-\hat{\hat{k}}^2\cos^2\theta)}{\hat{\hat{\lambda}}}\mathrm{sinc}^2\Big(\frac{\hat{\hat{k}}\cos\theta\hat{\hat{x}}}{2}\Big)\mathrm{sinc}^2\Big(\frac{\hat{\hat{k}}\sin\theta\hat{\hat{y}}}{2}\Big)e^{-\hat{\hat{\lambda}}|\hat{\hat{z}}|}}_{\text{regularized at }\hat{\hat{k}}=0}$$

$$+\frac{\hat{\hat{x}}^2\hat{\hat{y}}^2}{4}\int_0^{\pi/2}\int_1^{\infty} d\theta d\hat{\hat{k}}\underbrace{\Big\{\mathcal{Q}(\hat{\hat{k}},1/\hat{\hat{k}})-\mathcal{P}(1/\hat{\hat{k}})\Big\}}_{\text{virtually band limited}}e^{-\hat{\hat{k}}|\hat{\hat{z}}|}\mathrm{sinc}^2\Big(\frac{\hat{\hat{k}}\cos\theta\hat{\hat{x}}}{2}\Big)\mathrm{sinc}^2\Big(\frac{\hat{\hat{k}}\sin\theta\hat{\hat{y}}}{2}\Big)$$

$$+\underbrace{\frac{\hat{\hat{x}}^2\hat{\hat{y}}^2}{4}\int_0^{\pi/2}\int_1^{\infty} d\theta d\hat{\hat{k}}\Big\{\mathcal{P}(1/\hat{\hat{k}})\Big\}e^{-\hat{\hat{k}}|\hat{\hat{z}}|}\mathrm{sinc}^2\Big(\frac{\hat{\hat{k}}\cos\theta\hat{\hat{x}}}{2}\Big)\mathrm{sinc}^2\Big(\frac{\hat{\hat{k}}\sin\theta\hat{\hat{y}}}{2}\Big)}_{\text{can be calculated ``simply-by-inspection''}}. \tag{13}$$

With reference to (13) we have constructed a function associated with the Green's function $G_{11}(x-x',y-y',z-z')$ which possesses the desired properties.

REFERENCES

[1] A. R. Baghai-Wadji, "A Symbolic Procedure for the Diagonalizatioin of Linear PDEs in Accelerated Computational Engineering," a chapter in *the Proc. of SNSC'01*, F. Winckler, and U. Langer (Eds), Springer Verlag, 2002.

[2] —, "Theory and Applications of Green's Functions," a chapter in *Advances in Surface Acoustic Wave Technology, Systems and Applications (Vol. 2)*, C.C.W. Ruppel, and T.A. Fjeldly (Eds), pp. 83-149, World Scientific, 2001.

[3] —, "Fast-MoM: A Method-of-Moments Formulation for Fast Computations," in ACES Journal, pp. 75-80, vol. 12, no. 2, 1997.

[4] R. Harrington, "Field Computation by Moment Methods," New York: Macmillan, 1968.

[5] W. C. Chew, "Waves and Fields in Inhomogeneous Media," Van Nostrand Reinhold, 1990.

PROPAGATION OF ELECTROMAGNETIC WAVES IN OPEN CYLINDRICAL WAVEGUIDES WITH NONLINEAR MEDIA

Yuriy G. Smirnov, Svetlana N. Ivleeva

Penza State University, Penza, Russia
e-mail: smirnov@tl.ru, ivlieva@penza.com.ru

This paper deals with the problem of propagation of electromagnetic waves in cylindrical dielectric waveguide $W := \{x : x_1^2 + x_2^2 < R^2\}$ [1]. The waveguide is regular to z direction. The dielectric permittivity outside of the waveguide is constant, i.e. $\varepsilon_1 = const$. The dielectric permittivity of waveguide has nonlinear dependence on electric fields by Kerr's law [2]:

$$\varepsilon_2 = \varepsilon_f + a_f |E|^2,$$

where E denotes the electric field in waveguide. Assume that a_f and ε_f are real positive constants. Electromagnetic fields E, H satisfies Maxwell equations, transmission conditions of continuity of the tangent components on the jump of medium and radiation conditions on the infinity.

For solving the problem the cylindrical system of coordinates (ρ, φ, z) in used.

The first case (problem P1) assumes that $E = \{0; E_\varphi; 0\}$, $H = \{H_\varphi; 0; H_2\}$. Maxwell's equations are reduced to its specific form:

$$-\frac{\partial E_\varphi}{\partial z} = i\omega\mu H_\rho \tag{1}$$

$$\frac{1}{\rho}\frac{\partial}{\partial_\rho}(\rho E_\varphi) = i\omega\mu H_z \tag{2}$$

$$\frac{1}{\rho}\frac{\partial H_z}{\partial \varphi} = 0 \tag{3}$$

$$\frac{\partial H_\rho}{\partial z} - \frac{\partial H_z}{\partial \rho} = -i\omega\mu E_\varphi \tag{4}$$

$$-\frac{1}{\rho}\frac{\partial H_\rho}{\partial \varphi} = 0 \tag{5}$$

We will find the solutions of the problem with harmonic dependence on z-coordinate: $E_\varphi(\rho, z) = u(\rho)e^{i\gamma z}$. Then we obtain the equation

$$(\frac{1}{\rho}(\rho u)')' + (\omega^2\varepsilon\mu - \gamma^2)u = 0. \tag{6}$$

Taking into account that $\varepsilon = \varepsilon_1$ inside the waveguide, we have:

$$(\frac{1}{\rho}(\rho u)')' + \hat{k}_1^2 u = 0,$$

$$u'' + \frac{1}{\rho}u' - \frac{1}{\rho^2}u + \hat{k}_1^2 u = 0, \tag{7}$$

where

$$\hat{k}_1^2 = \omega^2 \varepsilon_1 \mu - \gamma^2.$$

Outside the waveguide, where $\varepsilon = \varepsilon_2 = \varepsilon_f + a_f |E|^2$, we have:

$$(\frac{1}{\rho}(\rho\mu)')' + \hat{k}_f^2 u + a|u|^2 u = 0,$$

where $a = \omega^2 a_f \mu$, $\hat{k}_f^2 = \omega^2 \varepsilon_f \mu - \gamma^2$, or, in another form,

$$u'' + \frac{1}{\rho}u' - \frac{1}{\rho^2}u + \hat{k}_f^2 u + a|u|^2 u = 0.$$

For real function $u(\rho)$

$$u'' + \frac{1}{\rho}u' - \frac{1}{\rho^2}u + \hat{k}_f^2 u + a|u|^3 = 0. \tag{8}$$

The transmission conditions are $[E_\varphi]_{\rho=R} = 0$, $[H_z]_{\rho=R} = 0$, which leads to conditions $[u]_{\rho=R} = 0$, $[u']_{\rho=R} = 0$. In this case the spectral parameter is γ.

Consider the second case (problem P2): $E = \{0;0;E_z\}$, $H = \{H_\rho; H_\varphi; 0\}$. Maxwell's equations are reduced to ones:

$$\frac{1}{\rho}\frac{\partial E_z}{\partial_\varphi} = i\omega\mu H_\rho \tag{9}$$

$$-\frac{\partial E_z}{\partial \rho} = i\omega\mu H_\varphi \tag{10}$$

$$-\frac{\partial H_\varphi}{\partial z} = 0 \tag{11}$$

$$\frac{\partial H_\rho}{\partial z} = 0 \tag{12}$$

$$\frac{1}{\rho}\frac{\partial}{\partial \rho}(\rho H_\varphi) - \frac{1}{\rho}\frac{\partial H_\rho}{\partial \varphi} = -i\omega\varepsilon E_z. \tag{13}$$

We will find the solutions of the problem in the form $E_z(\rho,\varphi)=e^{in\varphi}\upsilon(\rho)$, where n is real.
We have the equation in outside of the waveguide

$$\upsilon''+\frac{1}{\rho}\upsilon'+(k_1^2-\frac{n^2}{\rho^2})\upsilon=0, \tag{14}$$

$k_1^2=\omega^2\varepsilon_1\mu$.
For real $\upsilon(\rho)$ inside of the waveguide we obtain the equation

$$\upsilon''+\frac{1}{\rho}\upsilon'+(k_f^2-\frac{n^2}{\rho^2})\upsilon+a\upsilon^3=0, \tag{15}$$

$k_f^2=\omega^2\varepsilon_f\mu$, $a=\omega^2 a_f\mu$. The transmission conditions are $[E_z]_{\rho=R}=0$, $[H_\varphi]_{\rho=R}=0$, which leads to conditions $[\upsilon]_{\rho=R}=0$, $[\upsilon']_{\rho=R}=0$. In this case the spectral parameter is n.
Both cases are reduced to the equations of the following type:

$$y''+\frac{y'}{\rho}-\frac{n^2}{\rho^2}y+K^2y=0, \tag{16}$$

$$y''+\frac{y'}{\rho}-\frac{n^2}{\rho^2}y+K^2y+ay^2=0, \tag{17}$$

where $y=u$ or $y=\upsilon$, $K=\hat{k}$ or $K=k$, $n=1$ in first case. The equation (16) is the Bessel's one. Taking into account radiation conditions, it has solution:

$$y=C_1H_1^{(1)}(K\rho), \tag{18}$$

where C_1 is constant and $H_1^{(1)}$ is Hankel function. Note, that if the real part of K is equal to 0 then

$$y=C_1K_1(|K|\rho), \tag{19}$$

where K is real Macdonald function.
The linear equation could be rewritten as

$$Lu=0, L:=\rho\frac{d^2}{d\rho^2}+\frac{d}{d\rho}+(k^2\rho-\frac{n^2}{\rho}). \tag{20}$$

The function

$$G(\rho,\rho_0):=\frac{\pi}{2}\frac{J_n(k\rho)}{J_n'(kR)}(J_n(k\rho_0)N_n'(kR)-J_n'(kR)N_n(k\rho_0)),\ \rho<\rho_0\le R \tag{21}$$

$$G(\rho,\rho_0):=\frac{\pi}{2}\frac{J_n(k\rho_0)}{J_n'(kR)}(J_n(k\rho)N_n'(kR)-J_n'(kR)N_n(k\rho)),\ \rho_0<\rho\le R \tag{22}$$

is Green's function for boundary value problem

$$LG=-\delta(\rho-\rho_0),$$

$$G|_{\rho=0}=G'|_{\rho=R}=0;n>0(0<\rho_0<R).$$

We have second Green's formula:

$$\int_0^R(\upsilon Lu-uL\upsilon)d\rho=\int_0^R(\upsilon(\rho u')'-u(\rho\upsilon')'d\rho=R(u'(R)\upsilon(R)-\upsilon'(R)u(R)) \tag{23}$$

Consider equation

$$Lu+aB(u)=0,B(u)=\rho u^3. \tag{24}$$

Using (23) we have $(\upsilon:=G)$

$$\int_0^R(GLu-uLG)d\rho=R(u'(R-0')G(R,\rho_0)-G'(R,\rho_0)u(R-0))=Ru'(R-0)G(R,\rho_0) \tag{25}$$

or, another,

$$\int_0^R(GLu-uLG)d\rho=-a\int_0^R GB(u)d\rho+u(\rho_0). \tag{26}$$

We obtain

$$u(\rho_0)=a\int_0^R G(\rho,\rho_0)\rho u^3(\rho)dp+Ru'(R-0)G(R,\rho_0),\rho_0<R. \tag{27}$$

Dispersion relations (from $u(R-0)=u(R+0),u'(R-0)=u'(R+0)$)

$$u(R+0)=a\int_0^R G(\rho,R)\rho u^3(\rho)d\rho+Ru'(R+0)G(R,R) \tag{28}$$

Theorem 1.

If for a certain A>0, A does not depend on a,

$$a\le A \tag{29}$$

then (24) has unique solution and this solution is continuous function.

There is iteration procedure in order to find approximate solution u_n :

$$u_0 = 0, u_{n+1} = a\int_0^R G(\rho, \rho_0)\rho u_n^3 d\rho + f, \tag{30}$$

which converges uniformly to solution u of (24).

It follows from (28) and (19) that

$$C_1 K_1(|k|R) = C_1 K_1'(|k|R)|k|RG(R,R) = a\int_0^R G(\rho, R)\rho u^3(\rho)d\rho$$

or

$$f(\gamma) = aF(\gamma),$$

where

$$f(\gamma) = C_1 K_1(|k|R) - C_1 K_1'(|k|R)|k|RG(R,R), \tag{31}$$

$$F(\gamma) = \int_0^R G(\rho, R)\rho u^3(\rho)d\rho.$$

Theorem 2.

There exist $\varepsilon_1, \varepsilon_f (\varepsilon_f > \varepsilon_1), a > 0$ and eigenvalue $\gamma_0, \omega^2\varepsilon_1\mu < \gamma_0^2 > \omega^2\varepsilon_f\mu$ such that problem P1 has non-trivial soliton-type solution.

REFERENCES

[1] Il'inskii A.S., Kravtsov V.V., Sveshnikov A.G., "*Mathematical Models in Electromagnetics*" (in Russian), Moscow, 1991.

[2] Shurmann H.W., " *TE-polarized waves guided by a lossless nonlinear three-layer structure*", Proc. American Physics Society, vol. 58, no 1, 1998.

[3] Zaitsev V.F., Polyanin A.D., "*Handbook on Nonlinear Ordinary Differential Equations*" (in Russian), Factorial, Moscow, 1997.

HYBRID NUMERICAL-ASYMPTOTIC METHOD FOR THE CALCULATION OF THE COUPLING BETWEEN ELEMENTS OF A CONFORMAL MICROSTRIP PATCH ARRAY

Frédéric Molinet
Société MOTHESIM, La Boursidière, RN 186, 92357 Le Plessis-Robinson, France
fredericmolinet@magic.fr

ABSTRACT

Efficient asymptotic solutions have been developed for the calculation of the self and mutual coupling between patches on a curved 2D surface with variable curvature. For the calculation of the mutual coupling the approach is based on a local circular cylindrical approximation of the surface and on an asymptotic evaluation of the exact dyadic Green's function for a substrate on a circular cylinder. For the calculation of the self-coupling of a patch the curvature of the substrate is neglected and the corresponding Green's function is replaced by the Green's function of a planar layer. The Sommerfeld integrals are calculated by using the Discrete Complex Image Method after having extracted the surface wave contributions. The dyadic Green's function based on the two approaches is introduced in the mixed potentials electric field integral equation which is solved by using the RWG (Rao, Wilton, Glisson) triangular basis functions.

INTRODUCTION

We consider a large conformal array of patch elements (several tens to several hundreds of elements) on a two dimensional convex surface with variable curvature R. We suppose that R is large compared to the wavelength ($kR \gg 1$). The substrate is composed of a single layer of dielectric material. The feeding system is a voltage delta-gap on the patch, hence only current elements tangent to the air dielectric interface have to be considered. Owing to the large dimensions of the array, the coupling and radiation problems cannot be solved by the usual numerical techniques. Our approach consists in determining by analytical procedures the dyadic Green's function of the region exterior to the array, verifying the boundary conditions on the air-dielectric interface, and the radiation condition at infinity. In fact it is only necessary to calculate this Green's function along the air-dielectric interface for the coupling between patches and at infinity for the radiation of the elementary patches. A classical procedure consists in applying the Uniform Theory of Diffraction (UTD) for the coupling between patches. However, this method encounters several difficulties. It is not valid when the source and the observation point become close to each other, typically $d < \lambda/5$ and can therefore not be applied for the calculation of the self-coupling terms in the impedance matrix. Moreover, for larger distances between the source and the observation points, the method brakes generally down when the radius of curvature of the geodesic path between these points becomes large. In the paraxial region where the geodesic tends to a generatrix of the cylindrical surface, new asymptotic solutions have to be developed. In order to circonvent these difficulties, we have introduced a new approach for the calculation of the self coupling terms by neglecting the curvature of the substrate. The

corresponding dyadic Green's function is replaced by that of a planar layer and the Sommerfeld integrals are calculated by using the Discrete Complex Image Method (DCIM) after having extracted the quasi-static and the surface wave contributions. The planer layer approximation has been justified by measuring the reflection coefficient of a single patch on cylinders with different radii of curvature and on a flat substrate. A difference of less than 1% has been observed between the resonance values of the reflection coefficient for a flat substrate and a cylindrical substrate of radius R = 200 mm. For the coupling problem between different patches, we have improved the UTD approach by using more accurate asymptotic expansions for the Hankel functions. In the paraxial region, the curvature of the substrate has been neglected and the Green's function for a planar layer has been used.

FORMULATION OF THE PROBLEM

- *Self-coupling of a patch*

We present only shortly the Discrete Complex Image Method which is well documented in ref. [1, 2]. The Sommerfeld integrals are of the form (time dependence $e^{-i\omega t}$) :

$$I = \int_{\infty e^{i\pi}}^{\infty} \frac{H_o^{(1)}(\xi\rho)}{\sqrt{k_o^2 - \xi^2}} F_1(\xi)\,\xi\, d\xi \tag{1}$$

In order to apply the Sommerfeld identity, the main difficulty is the decomposition of the function $F_1(\xi)$ in a sum of exponentials of the type :

$$F_1(\xi) = \sum_{n=1}^{N} a_n\, e^{-b_n\sqrt{k_o^2-\xi^2}} \tag{2}$$

where a_n and b_n are complex numbers. We must therefore regularise $F_1(\xi)$ by removing its poles and then extract the behaviour of the function when $\xi \to \infty$. An efficient method for decomposing the remaining integral in a sum of exponentials is the Matrix of Pencil Method [3]. The complex images are independent of the position of the observation point and hence are calculated only once. The accuracy of the method can be controlled and fixes the number of complex images. About ten images are necessary for getting en accuracy of order 10^{-6}.

- *Mutual coupling between patches*

The field radiated by an electric Hertzian dipole located on a coated circular cylinder, tangent to the air-dielectric interface, is given by formulas (3) where Ψ_{e2} and Ψ_{m2} are the electric and magnetic cylindrical mode potentials. Applying the boundary conditions (4) on the air (medium 2) – dielectric (medium 1) interface, we get the expressions (5) of these potentials where the different terms are defined in (6), (7), (8) and (9). Watson's transformation is then applied in the usual way to the normal modes series, leading to an integral over the continuous complex variable ν. The main difficulty consists in the calculation of this integral together with the Fourier transform integral over the wave number k_z. Different approaches have been applied in the literature for the computation of these integrals [4]. Since we have conciliated accuracy and low PCU time, we have evaluated the Fourier transform integral by the steepest descent

method. However, in order that this procedure applied to the potentials give correct results for the fields which involve second order derivatives of the potentials, the asymptotic evaluation of the ν -integral must be very accurate. We have therefore adapted a residue series integration of the ν -integral despite the difficulties related to the determination of the poles. The latter have been overcome by starting from the values of the poles on a perfectly conducting surface and following the latter by augmenting stepwise the thickness of the layer. At each step, the poles are determined using Davidenko's method [5]. With this procedure, 20 to 30 poles can be easily calculated. However, the method is sensitive to the radius of curvature of the geodesic joining the source to the observation point. For radii of curvature verifying $10 \le kR \le 50$, Watson's asymptotic approximation of the Hankel functions $H_{\nu}^{(2)}(k_{\rho_2} b)$ give good results. For large radii of curvature $kR > 200$ Debye's asymptotic approximation must be used. In this case the search for poles is accelerated by starting with the values corresponding to a flat substrate. For intermediate values of the curvature Olver's uniform asymptotic expansion is adequate. In our algorithm, Olver's uniform asymptotic expansion has been used throughout together with a test giving the appropriate starting values for the searching of the poles.

$$\vec{E}_i = -\nabla\times(\hat{z}\Psi_{ei}) + \frac{1}{j\varpi\varepsilon_i}\nabla\times\nabla\times(\hat{z}\Psi_{mi}) = \hat{z}\times\vec{\nabla}\Psi_{ei} + \frac{1}{j\omega\varepsilon_i}\left(\frac{\vartheta}{\vartheta z}\vec{\nabla}\Psi_{mi} - \hat{z}\Delta\Psi_{mi}\right)$$

$$\vec{H}_i = -\nabla\times(\hat{z}\Psi_{mi}) + \frac{1}{j\varpi\mu_i}\nabla\times\nabla\times(\hat{z}\Psi_{ei}) = -\hat{z}\times\vec{\nabla}\Psi_{mi} + \frac{1}{j\omega\mu_i}\left(\frac{\vartheta}{\vartheta z}\vec{\nabla}\Psi_{ei} - \hat{z}\Delta\Psi_{ei}\right) \qquad (3)$$

$$\left.\begin{array}{l}\hat{\rho}\times\vec{E}_1 = 0,\ \rho = a \quad \hat{\rho}\times(\vec{E}_2 - \vec{E}_1) = 0 \\ \rho\times(\vec{H}_2 - \vec{H}_1) = \vec{J}_s\end{array}\right\}\ \rho = b \qquad (4)$$

$$\Psi_{m2}(\rho,\phi,z) = -\frac{1}{4\pi^2 b}\sum_{-\infty}^{+\infty} e^{jn(\phi-\phi')}\int_{-\infty}^{+\infty} dk_z e^{-jk_z z}\,\frac{H_n^{(2)}(k_{\rho 2}\rho)}{\left[\Gamma_2^e(n)\Gamma_2^h(n) - f_n^c\right]}$$
$$\frac{1}{k_1 k_2 k_{\rho_1}}\left\{J_{s\phi}k_z\left(\frac{n}{b}\right)\left[\frac{k_1 k_2}{k_{\rho_1}k_{\rho_2}}\Gamma_1^e(n)\right] + J_{sz}k_{\rho_1}^2\left[\frac{k_1 k_2}{k_{\rho_1}k_{\rho_2}}\Gamma_2^e(n)\right]\right\} \qquad (5)$$

$$\Psi_{e2}(\rho,\phi,z) = -\frac{jZ_o}{4\pi^2 b}\sum_{-\infty}^{+\infty} e^{jn(\phi-\phi')}\int_{-\infty}^{+\infty} dk_z e^{-jk_z z}\,\frac{H_n^{(2)}(k_{\rho 2}\rho)}{\left[\Gamma_2^e(n)\Gamma_2^h(n) - f_n^c\right]}\frac{1}{k_2}$$
$$\left\{J_{s\phi}\left[k_z^2\left(\frac{n}{b}\right)\frac{k_{\rho_1}^2 - k_{\rho_2}^2}{k_{\rho_1}^4 k_{\rho_2}^2}H_n^{(2)}(k_{\rho_2}b) - \Lambda_2^e(n)\Gamma_2^h(n)\frac{k_2^2}{k_{\rho_2}^2}\right] + J_{sz}\frac{n}{b}k_z\frac{k_{\rho_1}^2 - k_{\rho_2}^2}{k_{\rho_1}^2 k_{\rho_2}^2}H_n^{(2)}(k_{\rho_2}b)\right\}$$

$$\Gamma_1^e(n) = H_n^{(2)'}(k_{\rho_2}b) - \Lambda_1^e(n)H_n^{(2)}(k_{\rho_2}b) \quad , \quad \Gamma_2^e(n) = H_n^{(2)'}(k_{\rho_2}b) - \Lambda_2^e(n)H_n^{(2)}(k_{\rho_2}b)$$
$$\Gamma_2^h(n) = H_n^{(2)'}(k_{\rho_2}b) - \Lambda_2^h(n)H_n^{(2)}(k_{\rho_2}b) \qquad (6)$$

$$\Lambda_2^e(n) = \mu_r\frac{k_{\rho_2}}{k_{\rho_1}^2}\frac{T_e'}{T_e} \quad , \Lambda_2^h(n) = \varepsilon_r\frac{k_{\rho_2}}{k_{\rho_1}^2}\frac{T_m'}{T_m} \quad , \quad \Lambda_1^e(n) = \frac{k_{\rho_1}^2}{k_{\rho_2}^2}\Lambda_2^e(n) \qquad (7)$$

$$f_n^c = \left(\frac{nk_z}{b}\right)^2 \frac{k_{\rho_2}^2}{k_2^2}\left(\frac{1}{k_{\rho_1}^2}-\frac{1}{k_{\rho_2}^2}\right)^2 \left[H_n^{(2)}\left(k_{\rho_2}b\right)\right]^2 \tag{8}$$

$$T_e = H_n^{(1)}\left(k_{\rho_1}b\right)-\alpha_e H_n^{(2)}\left(k_{\rho_1}b\right) \qquad \alpha_e = \frac{H_n^{(1)'}\left(k_{\rho_1}a\right)}{H_n^{(2)'}\left(k_{\rho_1}a\right)} \tag{9}$$

$$T_m = H_n^{(1)}\left(k_{\rho_1}b\right)-\alpha_m H_n^{(2)}\left(k_{\rho_1}b\right) \qquad \alpha_m = \frac{H_n^{(1)}\left(k_{\rho_1}a\right)}{H_n^{(2)}\left(k_{\rho_1}a\right)}$$

On a circular cylinder the poles depend only on one geometrical parameter : the angle between the geodesic and the generatrixes. When the radius of curvature of the substrate is variable, a local cylindrical approximation is used. In this case the poles depend also on the position along the geodesic curve and have therefore to be calculated at a set of points along this curve.

NUMERICAL RESULTS

The accuracy of the method has been tested on a coated circular cylinder by comparing the results for the self and mutual coupling between patches with results available in the literature. In addition the radiation patterns of a single patch and of an array of seven patches have been computed.

CONCLUSION

In its present state of development, the hybrid UTD-DCIM/MoM code can handle an array of about 50 patches on a workstation. For larger conformal arrays, the matrix inversion algorithm in our MoM code has to be replaced by a fast multilevel iterative solver. This will extend the possibilities of the code to several hundreds of elements. Other future developments are : improvement of the formulas for the paraxial region by taking into account the curvature of the substrate, more realistic feeding systems, multilayer substrate and array truncation effects.

REFERENCES

[1] D.G. Fang, J.J. Yang and G.Y. Delisle, IEEE Proceedings, Vol. 135, Pt.H, n° 5, pp. 297-302, Oct. 1988.

[2] Y.L. Chow, J.J. Yang, D.G. Fang and G.E. Howard, IEEE Proceedings on Microwave Theory and Techniques, Vol. MTT-39, n° 3, pp. 588-592, March 1991.

[3] T.H. Sarkar, O. Pereira, IEEE Ant. Prop. Magazine, Vol. 37, n° 1, pp. 48-55, Feb. 1995.

[4] V.S. Ertürk and G.R. Rojas, IEEE ANP, pp. 1507-1516, Oct. 2000.

[5] D.F. Davidenko, Doklady Akad. Nauk S.S.S.R. (N.S.), Vol. 88, pp. 601-602, 1953.

APPLICATION OF EVOLUTION STRATEGIES IN OPTIMAL DESIGN PROBLEMS INVOLVING DIFFRACTION GRATINGS

Thore Magath and Klaus Schünemann

Arbeitsbereich Hochfrequenztechnik
Technische Universität Hamburg-Harburg
D-21073 Hamburg, Germany
E-mail: schuenemann@tuhh.de and magath@tuhh.de

ABSTRACT

Dielectric gratings with a piecewise constant surface profile are designed as beam splitters and star couplers. In each design problem, the diffraction efficiencies are used to formulate a target function, which has to be optimized. A rigorous grating theory is employed to compute the target function efficiently for each real-valued parameter vector comprising the design variables of the grating. Due to the multi-modal behavior of the target functions, an evolution strategy (ES) is applied as optimization technique. The numerical design examples demonstrate the usefulness of the proposed approach.

INTRODUCTION

This work is concerned with the design of dielectric transmission gratings that act as beam splitters and star couplers. The design of gratings, in general, involves finding the values of the relevant parameters, which ensure that the structure performs in accordance with specified design criteria. The particular designs described here, are casted as optimization problems with inequality constraints, in which no gradient information on the target functions is available. Therefore, classical optimization techniques strictly deterministic in nature, e.g. gradient-based and Newton-type methods, seem inappropriate. Further, the target functions are expected to exhibit multi-modal behavior, as this holds true for most optimization problems involving electromagnetic wave phenomena. Following [1], these problems should be tackled by using stochastic optimization techniques. Examples of these techniques are ESs, genetic algorithms, and simulated annealing. On many occasions these techniques have proven to be very useful tools for electromagnetic optimization problems, even if non-differentiable and/or highly nonlinear target functions are involved. Furthermore, these techniques are ideal candidates for global optimization, since, when compared to their deterministic counterparts, stochastic methods are less likely to get stuck in weak local minima.

In this paper, we apply an ES to our optimization problems. Besides the aforementioned, this choice was suggested by the ability of ESs to easily handle inequality constraints and by its favorable convergence properties. The most expensive part during the optimization process are the target function evaluations. Each evaluation requires the solution of the grating diffraction problem, for which we use a modified version of the rigorous differential method described in [2]. Before we start to describe the applied ES, we first outline the analysis method, that is used to solve the diffraction problem. In the last section, we present numerical results for beam splitters and star couplers designed with our code.

ANALYSIS METHOD

In this section, Maxwell's equations will be reformulated as a first-order system of differential equations. First we consider the case of TM-polarization, so that field components E_z, D_z, H_x and H_y are only involved in the diffraction problem. To start with the analysis, the periodic relative permittivity $\varepsilon_r(x)$ of a single layer, e.g. region 2 in Fig. 1 a), is expanded into a Fourier series:

$$\varepsilon_r(x) = \lim_{M\to\infty} \sum_{m=-M}^{M} \epsilon_m e^{-jm\frac{2\pi}{L}x}, \qquad \epsilon_m = \frac{1}{L}\int_0^L \varepsilon_r(x) e^{+jm\frac{2\pi}{L}x}\,\mathrm{d}x. \tag{1}$$

An incident homogeneous plane wave with wave number vector $\mathbf{k} = k_o[-\sin\varphi^i, \cos\varphi^i]^T$, $k_o = \omega_o\sqrt{\mu_o\varepsilon_o} = 2\pi/\lambda_o$, on such a periodic structure generates a total field that is pseudo-periodic, i.e., it satisfies the Floquet theorem. The electric displacement D_z for instance is given through the following modified Fourier expansion:

$$D_z(x,y) = \lim_{M\to\infty} \sum_{m=-M}^{M} D_{z_m}(y) e^{-j\alpha_m x}, \qquad D_{z_m}(y) = \frac{1}{L}\int_0^L D_z(x,y) e^{+j\alpha_m x}\,\mathrm{d}x, \tag{2}$$

where $\alpha_m = m\frac{2\pi}{L} - k_o\sin\varphi^i$. If we substitute the expansions for D_z, E_z, and ε_r from (1) into the constitutive law $D_z = \varepsilon_o\varepsilon_r E_z$, it can be derived, that the multiplication between the permittivity and the electric field leads to a discrete convolution of the corresponding Fourier coefficients, i.e. $D_{z_m}(y) = \epsilon_m * E_{z_m}(y)$. As is usually done in signal processing, we rewrite this convolution equivalently as a Toeplitz-matrix vector product:

$$\mathcal{D}_z = \varepsilon_o \mathcal{N}^2 \mathcal{E}_z, \tag{3}$$

with vectors $(\mathcal{D}_z)_m := D_{z_m}$, $(\mathcal{E}_z)_m := E_{z_m}$ and refraction matrix $(\mathcal{N}^2)_{mn} := \epsilon_{m-n}$.
In the next step, we substitute the field and permittivity expansions into Maxwell's equations, which simplify for TM-polarization, and utilize the property, that the basis functions $\exp(-j\alpha_m x)$ are linearly independent. Defining vectors $\mathcal{H}_x$, $\mathcal{H}_y$ consistent with $\mathcal{E}_z$, $\mathcal{D}_z$ in (3) and a diagonal matrix $[\alpha] := \mathrm{diag}([\ldots, \alpha_{-1}, \alpha_0, \alpha_1, \ldots])$ yields:

$$-j[\alpha]\mathcal{H}_y - \frac{\mathrm{d}}{\mathrm{d}y}\mathcal{H}_x = j\omega_o\mathcal{D}_z, \quad \frac{\mathrm{d}}{\mathrm{d}y}\mathcal{E}_z = -j\omega_o\mu_o\mathcal{H}_x, \quad j[\alpha]\mathcal{E}_z = -j\omega_o\mu_o\mathcal{H}_y. \tag{4}$$

Eliminating vectors $\mathcal{D}_z$ and $\mathcal{H}_y$ in (3) and (4), we obtain a first-order system of differential equations, that bears close resemblance to the differential equations describing the voltages and currents on a multiconductor transmission line. To make this point clearer, we introduce inductance and capacitance matrices $\mathbf{L}$ and $\mathbf{C}$ and voltage and current vectors $\mathbf{U}$ and $\mathbf{I}$:

$$\mathbf{L} = \mu_o\mathbf{1}, \qquad \mathbf{C} = \varepsilon_o\left(\mathcal{N}^2 - ([\alpha]/k_o)^2\right), \qquad \mathbf{U} = \mathcal{E}_z, \qquad \mathbf{I} = \mathcal{H}_x. \tag{5}$$

For TE-polarization, the procedure described above is also applicable [3]. In any case, the following infinite system of differential equations has to be solved:

$$\frac{\mathrm{d}}{\mathrm{d}y}\mathbf{U}(y) = -j\omega_o\mathbf{L}\,\mathbf{I}(y), \qquad \frac{\mathrm{d}}{\mathrm{d}y}\mathbf{I}(y) = -j\omega_o\mathbf{C}\,\mathbf{U}(y). \tag{6}$$

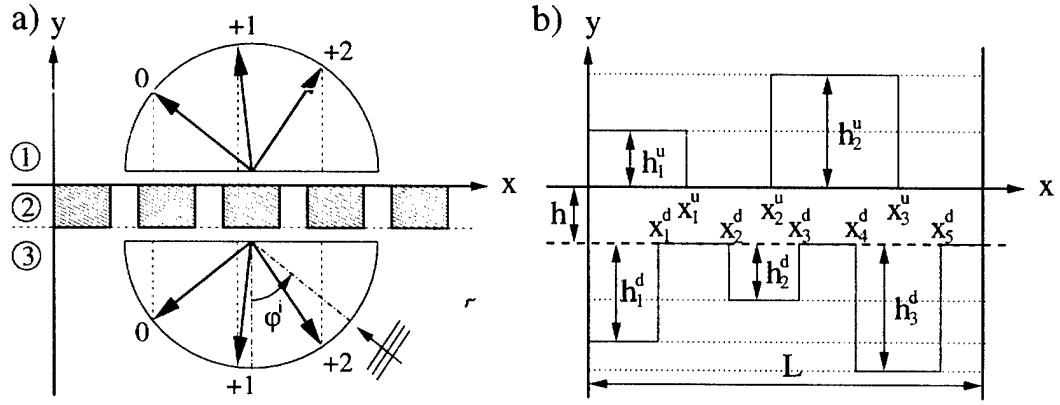


Figure 1: a) Grating with a single periodic layer. Also shown is the geometrical construction of the propagation directions of the spatial harmonics. b) One period of a dielectric grating with a piecewise constant surface profile.

The matrix exponential allows an analytical solution to this system:

$$\mathbf{U}(y) = e^{-[\gamma]y}\mathbf{U}_+ + e^{[\gamma]y}\mathbf{U}_-, \qquad \mathbf{I}(y) = \mathbf{Y}_o\left[e^{-[\gamma]y}\mathbf{U}_+ - e^{[\gamma]y}\mathbf{U}_-\right], \tag{7}$$

where $[\gamma] = j\omega_o\sqrt{\mathbf{LC}}$ and $\mathbf{Y}_o = \mathbf{L}^{-1}\sqrt{\mathbf{LC}}$ are the propagation constant and the characteristic admittance, respectively. Further analogues known from transmission line theory are readily defined, as for instance reflection and transmission coefficients. All these analogues become infinite matrices, which have to be truncated in a numerical implementation.

The solutions in (7) essentially consist of two sets of propagating diffraction orders or spatial harmonics. One set having wave vector components in $+y$-direction, the other in $-y$-direction. In addition to the propagating orders, evanescent waves exist as well.

To solve the diffraction problem of a grating with a piecewise constant surface profile as shown in Fig. 1 b), vectors $\mathbf{U}_+$, $\mathbf{I}_+$, $\mathbf{U}_-$ and $\mathbf{I}_-$ need to be determined uniquely in each layer from the boundary conditions, which require the continuity of the tangential magnetic and electric field components at the discontinuities on one hand, and the outgoing wave conditions in the two semi-infinite regions that surround the grating on the other hand. Substitution of characteristic admittance, reflection and transmission matrices into the system of equations that results from the boundary conditions, leads to a robust R-matrix propagation algorithm, that is applicable to thick gratings.

Finally, we define the efficiencies of the m-th reflected and transmitted waves:

$$(\mathbf{e}_n^r)_m = e_{m,n}^r := \frac{\mathrm{Re}\left\{U_m^r I_m^{r*}\right\}}{\mathrm{Re}\left\{U_n^i I_n^{i*}\right\}}, \qquad (\mathbf{e}_n^t)_m = e_{m,n}^t := \frac{\mathrm{Re}\left\{U_m^t I_m^{t*}\right\}}{\mathrm{Re}\left\{U_n^i I_n^{i*}\right\}}, \tag{8}$$

where U_n^i, I_n^i are the field amplitudes of the n-th incident plane wave. The efficiencies are of significance in grating analysis and will be required to define the target functions in the optimal design problems. Due to energy conservation, the sum of all efficiencies has to equal unity. This property, generally called energy balance criterion [2], provides a test on the soundness of the computer implementation.

OPTIMIZATION METHOD: EVOLUTION STRATEGIES

In the optimal design problems, we applied a multi-membered $(\mu + \lambda)$-ES [4], which basically works as follows. A set of μ arbitrarily chosen individuals $\vec{a}_i$ is grouped together to form an initial population, i.e. $P(0) := \{\vec{a}_1(0), \ldots, \vec{a}_\mu(0)\}$. Each individual of the population is evaluated by assigning some form of fitness value $\Phi(\vec{a}_i(0))$ to it. As a next step, the individuals of population $P(0)$ are manipulated by genetic operators, especially recombination and mutation operators. The λ descendants are evaluated and undergo together with the μ parents a fitness-based selection process afterwards to form the next generation, i.e. population $P(1)$. The cycle of reproduction that has emerged $P(1)$, is now applied to $P(1)$ and generates a population $P(2)$ of higher or at least equal quality. The reproduction cycle is traversed as long until some termination condition $\Omega(P)$ is satisfied. The description given so far can be directly translated into an algorithmic outline, in which t denotes the generation counter.

Algorithm Outline of a $(\mu + \lambda)$-Evolution Strategy

$t := 0$
initialize: $P(0) := \{\vec{a}_1(0), \ldots, \vec{a}_\mu(0)\}$
evaluate: $P(0) : \{\Phi(\vec{a}_1(0)), \ldots, \Phi(\vec{a}_\mu(0))\}$
do
  if $(\Omega(P(t))$==.TRUE.) **then** EXIT
  recombine: $\vec{a}'_k(t) := r(P(t)) \quad \forall k \in \{1, \ldots, \lambda\}$
  mutate: $\vec{a}''_k(t) := m_{\{\tau,\tau_i\}}(\vec{a}'_k(t)) \quad \forall k \in \{1, \ldots, \lambda\}$
  evaluate: $P''(t) := \{\vec{a}''_1(t), \ldots, \vec{a}''_\lambda(t)\} : \{\Phi(\vec{a}''_1(t)), \ldots, \Phi(\vec{a}''_\lambda(t))\}$
  select: $P(t+1) := s_{(\mu+\lambda)}(P(t) \cup P''(t))$
  $t := t + 1$
end do

An individual $\vec{a}$ consists of an object vector $\vec{x}$ comprising all design variables, e.g. :

$$\vec{x} = [\varphi^i, \lambda_o, L, h, h^u_1, h^u_2, \ldots, h^d_1, h^d_2, \ldots, x^u_1, x^u_2, \ldots, x^d_1, x^d_2, \ldots], \tag{9}$$

and a strategic vector $\vec{\sigma}$, i.e. an individual $\vec{a} = (\vec{x}, \vec{\sigma})$. Mutations, denoted by mutation operator $m_{\{\tau,\tau'\}}$, are realized by replacing $\vec{x}$ with $\vec{x}'$, i.e.

$$x'_i = x_i + \sigma'_i N_i(0,1), \qquad \sigma'_i = \sigma_i \exp(\tau' N(0,1) + \tau N_i(0,1)), \tag{10}$$

where $N(0,1)$ denotes a realization of a normally distributed one-dimensional random variable having an expectation of zero and a standard deviation of one, while $N_i(0,1)$ indicates that the random variable is sampled anew for each possible value of the counter i. Parameters τ and τ' are set to $0.71N_x^{-0.25}$ and $0.71N_x^{0.5}$, respectively, when N_x is the number of design variables. The set of inequalities among design variables x^u_i and x^d_u is assumed as a part of the optimization problem. If the offspring $\vec{x}'$ does not satisfy all constraints, it is disqualified and not placed in a new population. If the rate of occurrence of such illegal offspring is high, the ES adjusts its strategy parameters, i.e. the corresponding components of $\vec{\sigma}$ are decreased.

With the help of specified efficiency vectors $\tilde{\mathbf{e}}_n^t$ and $\tilde{\mathbf{e}}_n^t$, we formulate a target function f dependent on the design parameters only. Therefore, it seems advisable to simply define the fitness of an individual as:

$$\Phi(\vec{a}) := f(\vec{x}) = \sum_n \|\tilde{\mathbf{e}}_n^t - \mathbf{e}_n^t(\vec{x})\|_2 + \sum_n \|\tilde{\mathbf{e}}_n^r - \mathbf{e}_n^r(\vec{x})\|_2. \tag{11}$$

Recombination is always used in ESs for the creation of all offspring individuals. Different recombination operators exist. In our implementation, we used an panmictic generalized intermediate recombination operator r defined as follows:

$$a_i' = a_{S,i} + \chi_i(a_{T_i,i} - a_{S_i,i}) \tag{12}$$

The indices S and T denote two parent individuals selected at random from the population. The index i in T_i indicates T to be sampled anew for each value of i. $\chi_i \in [0,1]$ is a uniform random variable, sampled anew for each possible value of the counter i.
Finally, selection operator $s_{(\mu+\lambda)}$ selects the μ best individuals out of the union of parents and offsprings to form the next parent generation.

OPTIMAL DESIGN PROBLEMS

In all optimizations, an (15+100)-ES has been applied with a number of standard deviations equal to the number of design variables, i.e. N_x. The designed transmission gratings were supposed to consist of teflon with a relative permittivity of 2.06 surrounded by air and M was set to 20, so that all truncated matrices had the size 41×41. In each run, the energy balance criterion was satisfied within a tolerance of $\approx 10^{-15}$.

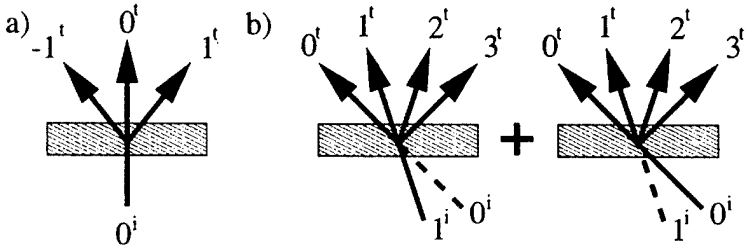


Figure 2: Transmission grating as a) 1-to-3 beam splitter at normal incidence and b) as 4-to-4 star coupler at Bragg incidence. Mirror images of order 0^i and 1^i are omitted.

As design examples, we consider beam splitters and star couplers [5]. The operating principle of these diffractive elements are illustrated in Fig. 2 by means of an 1-to-3 splitter and a 4-to-4 coupler. For the former, we ideally set $\tilde{e}_{m,0}^t = 33.\bar{3}\%$, $m \in \mathcal{W} = \{-1, 0, +1\}$, whereas for the latter, we require that $\tilde{e}_{m,0}^t = \tilde{e}_{m,1}^t = 25\%$, $m \in \mathcal{W} = \{0, 1, 2, 3\}$. All other efficiencies in $\tilde{\mathbf{e}}^t$ and $\tilde{\mathbf{e}}^r$ are set to zero, respectively. Thus fitness function $\Phi(\vec{a})$ in (11) is completely defined.
We exclusively use left-right symmetric profiles, so that the optimization is simplified. The diffraction patterns at the angles of incidence φ_n^i and $-\varphi_n^i$ therefore become mirror images. Hence, if an odd number of signal orders N_s is desired, we choose normal incidence, otherwise, for an even number, we choose Bragg incidence. The period length L was set to $\frac{1+N_s}{2}\lambda_o$. This avoids, that power is lost into unwanted diffraction orders.

To characterize the quality of the designed transmission gratings, the diffraction efficiency $\eta_n := \sum_{m \in \mathcal{W}} e^t_{m,n}$ inside a window $\mathcal{W}$ and the reconstruction error $\delta_n := \|\tilde{\mathbf{e}}^t_n - \mathbf{e}^t_n\|_\infty$ is used. Other figures of interest are the number of grooves on the bottom and upper side of the grating, i.e. $G^{d/u}$, the minimum feature sizes $x^{d/u}_{min} := \min_{i \neq j}\{|x^{d/u}_i - x^{d/u}_j|\}$ and the maximum heights $h^{d/u}_{max} := \max_i\{|h^{d/u}_i|\}$.

Table 1: Numerical results for beam splitters and star couplers.

	Beam Splitter						Star Coupler			
	1/2	1/3	1/4*	1/5	1/6	1/7	3/3	4/4*	5/5*	6/6*
N_x	3	3	4	5	7	7	3	4	6	7
G^d/G^u	1/-	1/-	2/2	1/1	2/2	2/2	1/-	2/2	3/3	4/4
L/λ_o	1.500	2.000	2.500	3.000	3.500	4.000	2.000	2.500	3.000	3.500
h^d_{max}/λ_o	1.642	0.718	1.322	1.103	0.974	0.884	1.394	1.287	1.283	1.328
h/λ_o	1.262	0.403	0.346	0.575	0.728	1.767	1.448	0.364	0.671	1.247
h^u_{max}/λ_o	-	-	1.322	0.456	0.157	0.258	-	1.287	1.283	1.328
Δ^d/λ_o	0.746	0.722	0.214	1.458	0.419	0.548	0.264	0.222	0.113	0.264
Δ^u/λ_o	-	-	0.214	1.277	0.240	0.596	-	0.222	0.113	0.264
$\varphi^i_0(^\circ)$	19.47	0.00	11.54	0.00	8.21	0.00	30.00	36.87	41.81	45.58
$\varphi^i_1(^\circ)$	-	-	-	-	-	-	0.00	11.54	19.47	25.38
$\varphi^i_2(^\circ)$	-	-	-	-	-	-	-	-	0.00	8.21
$\eta_0(\%)$	99.93	99.71	98.65	99.47	98.20	99.64	98.18	98.40	95.45	94.97
$\eta_1(\%)$	-	-	-	-	-	-	99.06	98.58	92.63	96.11
$\eta_2(\%)$	-	-	-	-	-	-	-	-	95.40	94.52
$\delta_0(\%)$	0.03	0.10	0.21	0.12	0.48	0.05	1.20	0.88	1.54	2.59
$\delta_1(\%)$	-	-	-	-	-	-	0.39	0.88	3.06	2.61
$\delta_2(\%)$	-	-	-	-	-	-	-	-	1.21	2.28

* Grating has up-down symmetry.

The optimization results achieved are summarized in Tab. 1 and demonstrate, that ESs are a very powerful tool for designing gratings. The beam splitter and star coupler designs have efficiencies of at least 98.20% and 92.63% with a reconstruction error of less than 0.48% and 3.06%, respectively.

ACKNOWLEDGEMENT

The authors are indebted to the Deutsche Forschungsgesellschaft for financial support.

REFERENCES

[1] A. Boag *et al.*, "Design of Electrically Loaded Wire Antennas Using Genetic Algorithms," *IEEE Trans. Antennas Propagat.*, Vol. 44, pp. 687-695, May 1996.

[2] R. Petit, ed., "Electromagnetic Theory of Gratings," Springer-Verlag, 1980.

[3] M. Shahabadi, "Anwendung der Holographie auf Leistungsaddition bei Millimeterwellen," Dissertation, Hamburg, Germany, 1998.

[4] T. Bäck, "Evolutionary Algorithms in Theory and Practice," Oxford Uni. Press, 1996.

[5] E. Noponen, "Electromagnetic Theory of Diffractive Optics," Dissertation, Espoo, Finland, 1994.

A BMIA/AIM FORMULATION FOR THE ANALYSIS OF LARGE STACKED PATCH ANTENNAS

Angelo Freni, Paolo De Vita, Alessandro Mori

Department of Electronics and Telecommunications
Via di S. Marta 3, I-50139 Florence, Italy
E-mail: freni@unifi.it, devi@unifi.it, mori@ing.unifi.it

ABSTRACT

An efficient technique based on the extension of the Banded Matrix Iterative Approach (BMIA) to a not canonical grid by using the Adaptive Integral Method (AIM) is presented for the analysis of stacked patch antennas of large dimensions. The patches can have arbitrary shape and orientation and are modeled by means of triangular elements.

INTRODUCTION

The analysis of large-scale complex patch antennas by using method of moments (MoM) usually requires large computational resources in terms both of dynamic memory and computation time. Especially for an optimization process, where many slightly different structures have to be analysed, availability of an efficient numerical method is desirable. Similar problems arise in a Monte–Carlo analysis of the scattering from large rough surfaces. In this kind of study the scattered field intensity is averaged over more of one hundred of typical realizations of the assumed scenery built in conformity with its statistical behavior. Obviously, it is very important to minimize the computation time for the analysis of each realization and several techniques have been developed for the fast computation of deterministic profile scattering. These techniques are based on the modification of the classical method of moments (MoM) to allow a fast evaluation of the reaction integral and, when an iterative solver is used, a fast matrix–vector multiplication. Examples include the adaptive integral method (AIM) [1], the fast multipole method (FMM) [2], the matrix decomposition algorithm (MDA) [3], and the banded matrix iterative approach/canonical grid method (BMIA/CAG) [4], [5]. Specifically, the BMIA/CAG method is one of the most efficient when applied to the studying of rough surfaces. As a matter of fact, the statistical description of a rough surface allows the use of a regular grid.

The aim of this paper is to show that the last method, when opportunely modified, can be profitably employed for the analysis of large-scale stacked patch antennas. In particular, the necessity to describe patches of arbitrary shape and size in a regular grid is considered by introducing a set of auxiliary basis functions based on a multipole expansion as in the AIM [1]. Furthermore, special attention has been addressed to the presence of a ground plane, placed below the patches, which

reduces the number of terms we need to evaluate.

In order to simplify the formulation, the antennas analysed in the following are supposed characterized by a substrate of dielectric relative permittivity very close to unity, similar to those usually employed by GSM systems having space and frequency diversity and/or in a GPS system mounted on satellites. This hypothesis allows the analysis of patches in free space by using in the procedure an expansion of the free space Green function. The method, however, can be easily extended to dielectric stratified structure with a little effort when discrete complex image method (DCIM) is employed [6], at least when substrates having low relative permittivity are employed. In fact, the BMIA procedure requires the analytic evaluation of some z–derivatives of the Green's function and this can easily made when, as in DCIM, are used closed–form expressions where only complex coefficients have to be evaluated numerically.

FORMULATION

The general structure sketched in Fig. 1 can be considered a quasi–planar metallic structure located over an infinite ground plane having a height profile $z = f(x, y)$.

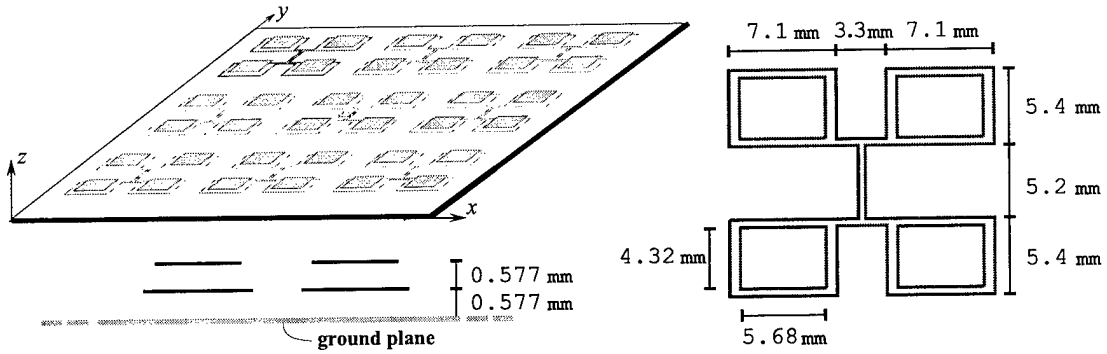


Fig. 1 – Geometry of the problem.

Let $\vec{J}_s$ be the surface current density induced on it by an incident field $\vec{E}^i$ and $\vec{E}^s$ the electric scattered field. The latter can be computed from the surface currents by $\vec{E}^s = -j\omega\vec{A} - \nabla\phi$, with the magnetic vector potential $\vec{A}$ and the scalar potential ϕ defined as

$$\begin{bmatrix} \vec{A}(\vec{r}) \\ \phi(\vec{r}) \end{bmatrix} = \frac{j}{4\pi} \iint_S \begin{bmatrix} -j\mu\vec{J}_s(\vec{r}\,') \\ \nabla \cdot \vec{J}_s(\vec{r}\,')/\omega\varepsilon \end{bmatrix} \cdot G(\vec{r}, \vec{r}\,')\, dS' , \tag{1}$$

where $G(\vec{r}, \vec{r}\,') = \exp(-jkR)/R$, and $R = |\vec{r} - \vec{r}\,'|$. By enforcing the boundary condition $\hat{n} \times \left(\vec{E}^i + \vec{E}^s\right) = 0$ on S, we can derive an integrodifferential equation for $\vec{J}_s$ obtaining

$$\hat{n} \times \vec{E}^i\Big|_S = \hat{n} \times \left(j\omega\vec{A} + \nabla\phi\right)\Big|_S . \tag{2}$$

Equations (1) and (2) represent the so–called electric field integral equation (EFIE). For numerical solution of the pertinent integral equation the surface S is discretized into small triangular patches, and the unknown current $\vec{J}_s$ is expanded using a suitable set of basis functions $\vec{j}_n(\vec{r})$ (e.g., Rao–Wilton–Glisson (RWG) basis functions defined by Rao et al. [7]). That is $\vec{J}_s(\vec{r}) = \sum_{n=1}^{N} I_n \vec{j}_n(\vec{r})$, where I_n are unknown coefficients. Then, a method of moments is applied to obtain a linear system of equations, $\mathbb{Z}\,\mathbf{I} = \mathbf{V}$. In classical BMIA the computational efficiency is achieved defining a distance r_d which separates two regions: a near–interaction region and a weak–interaction region. Then, one can write the matrix $\mathbb{Z}$ as superimposition of a strong matrix $\mathbb{Z}^s$ and a weak–interaction matrix $\mathbb{Z}^w$ (i.e. $\mathbb{Z} = \mathbb{Z}^s + \mathbb{Z}^w$). The elements of $\mathbb{Z}^s$ are related to weighting and base functions having distances $d_{xy} = \sqrt{(x-x')^2 + (y-y')^2} < r_d$. In the weak–interaction region we consider $h = |z - z'| = |f(x,y) - f(x',y')| \ll d_{xy}$. So we can approximate the Green's function by using $\widetilde{M}$ terms of the relevant Taylor series with respect to the height h, resulting

$$G(d_{xy}, h) \simeq \sum_{m=0}^{\tilde{M}} a_m(d_{xy}) \exp(-jkd_{xy})\, h^{2m}\,, \tag{3}$$

where $a_0 = 1/d_{xy}$, $a_1 = -(1 + jkd_{xy})/2d_{xy}^3$, $a_2 = (3 + 3jkd_{xy} - k^2 d_{xy}^2)/8d_{xy}^5$, ... As a consequence, the weak–term of the eq. (1) can be written as

$$\sum_{m=0}^{\tilde{M}} \frac{j}{4\pi} \iint_S \begin{bmatrix} -j\mu \vec{J}_s(x',y',z') \\ \nabla \cdot \vec{J}_s(x',y',z')/\omega\varepsilon \end{bmatrix} a_m(d_{xy}) \exp(-jkd_{xy}) \left[z - z'\right]^{2m} dS'\,. \tag{4}$$

Therefore, by assuming the Galerkin discretization scheme, each element of the weak–interaction matrix $\mathbb{Z}^w$ can be expressed as linear combination of four elements of the form

$$Z_{i,j}^{\alpha} = \sum_{m=0}^{M} \iint_S R_m(z)\ {}_i^{\alpha}(x,y,z) \iint_S A_m(x-x', y-y') Q_m(z')\ {}_j^{\alpha}(x',y',z')\, dS'\, dS\,. \tag{5}$$

where $\alpha = x, y, z, \phi$, ${}_i^{\alpha}$ is the pertinent base or weighting function and $M = (\widetilde{M}+1)^2 - 1$.

When the method is applied for evaluating the backscattering from a rough terrain, since the statistical description of the terrain surface allows the use of a regular grid, it is convenient to project the integration domain on the x, y plane as in [4]. So, each term (5) takes a two–dimensional convolution form and can efficiently be evaluated by means of a two–dimensional FFT. This formulation, however, cannot be directly applied to the analysis of patch antennas structures, either it requires a regular grid for describing the structure or it does not allow the use of basis functions set along the z direction.

One can overcome this problem replacing the original basis and weighting current distribution multiplied by $P_m(z) = Q_m(z)$ or $P_m(z) = R_m(z)$ with an approximately

equivalent set of pointlike currents. The two current distributions are equivalent in the sense that they generate almost identical fields in the weak–interaction region. We choose the pointlike current elements located at nodes of a regular Cartesian two–dimensional grid, parallel to the x, y plane. Both basis and weighting functions are approximated as linear combination of Dirac delta functions, thus

$$P_m(z) \ {}^{\alpha}_{n}(x,y,z) \simeq \sum_{i=0}^{L} \Lambda_{n,i}^{\alpha,m} \, \delta(x-x_i)\delta(y-y_i)\delta(z-z_c)\,, \tag{6}$$

with $(x_i, y_i) \in C_n$, where C_n is the set of $L+1$ grid nodes closest to the center (x_c, y_c, z_c) of the basis or weghting function support.

However, differently from the classical AIM, since we require that pointlike current elements are bound only to be belong to a regular Cartesian two–dimensional grid having N_g nodes, we enforce the equality

$$\iint_S P_m(z) \ {}^{\alpha}_{n}(x,y,z)(x-x_c)^{m_1}(y-y_c)^{m_2} dS = \sum_{i=0}^{L} \Lambda_{n,i}^{\alpha,m} (x_i-x_c)^{m1}(y_i-y_c)^{m2}\,,$$
$$\text{for } 0 \le m_1, m_2 \le L\,. \tag{7}$$

By inserting (6) in eq. (5) we can easily recognize that for the weak–interaction matrix we can write

$$\mathbb{Z}^w \, \boldsymbol{I} = \sum_{m=0}^{M} \sum_{\alpha=x,y,z,\phi} \mathbb{H}_{\alpha}^{T} \, \Lambda_{\alpha,m}^{R} \, \mathbb{A}_m \, \Lambda_{\alpha,m}^{Q} \, \mathbb{H}_{\alpha} \, \boldsymbol{I}\,, \tag{8}$$

where $\mathbb{A}_m = \{A_m(x_i - x_j, y_i - y_j)\}$, $\mathbb{H}_\alpha$ joins the basis (weighting) functions to the unknowns vector $\boldsymbol{I} = \{I_n\}$ and $\Lambda_{\alpha,m}^{R,Q} = \left\{\Lambda_{n,i}^{\alpha,m}\right\}$, where $P_m(z) = Q_m(z)$ or $P_m(z) = R_m(z)$ are considered.

It is worth noting that matrix $\mathbb{A}_m$ is a block Toeplitz matrix, while matrices $\mathbb{H}_\alpha$ and $\Lambda_{\alpha,m}^{R,Q}$ are extremely sparse (few valued elements per row).

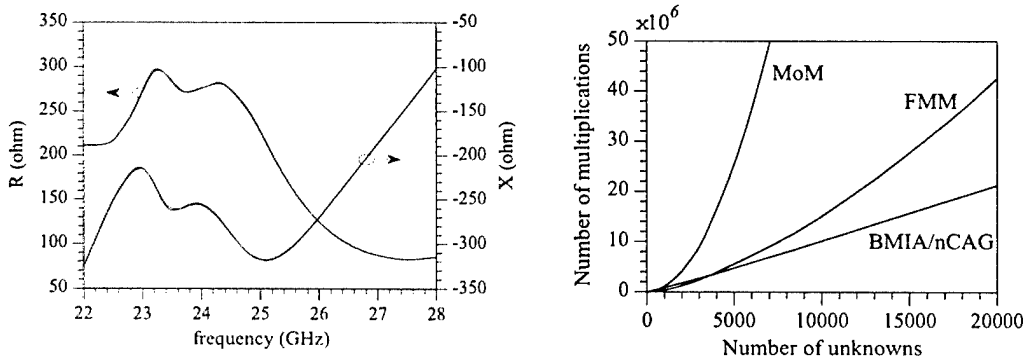
While the $\mathbb{Z}^w$ matrix is a full matrix with $\boldsymbol{O}(N^2)$ elements and usually can not be stored for large–scale problems, we have now to store only $\boldsymbol{O}\,(4N_g)$ elements for each matrix $\mathbb{A}_m$, and some others matrices that need the overall storage of $\boldsymbol{O}\,(4(L+1)N_g)$ elements, where N_g is the number of nodes on the regular two–dimensional grid. Furthermore, when the conjugate gradient (CG) method is used to solve the matrix equation $\mathbb{Z}\,\boldsymbol{I} = \boldsymbol{V}$, the $\mathbb{Z}^w\boldsymbol{I}$ product can be conveniently evaluated by performing, for each term m, first the product $\Lambda_{\alpha,m}^{Q}\mathbb{H}_\alpha\,\boldsymbol{I}$ (pre–multiplication), then the product $\mathbb{A}_m \cdot \left(\Lambda_{\alpha,m}^{Q}\mathbb{H}_\alpha\,\boldsymbol{I}\right)$ by means of two 2D–FFTs, since $\mathbb{A}_m$ is a block Toeplitz matrix. Finally, the product $\mathbb{H}_i^T\mathbb{R}^{(m)} \cdot \left(\mathbb{A}_m\,\Lambda_{\alpha,m}^{Q}\mathbb{H}_\alpha\,\boldsymbol{I}\right)$ can be performed (post–multiplication). The latter scheme allows to evaluate the $\mathbb{Z}^w\boldsymbol{I}$ product by using $\boldsymbol{O}\left(N_g\left[8(2\widetilde{M}+1)\log(4N_g) + 6(\widetilde{M}+1)^2\right]\right)$ operations instead of $\boldsymbol{O}\,(N^2)$.

Furthermore, when we consider the presence in the structure of a ground plane some simplifications arise. As a matter of fact, by applying the image principle we

locate image sources symmetrically with respect to the ground plane, assumed on $z = 0$. This can be taken into account direclty by the H_α matrices. However, since in eq. (5) the term $Q_m(z')$ is proportional to $(z')^{m-1-(\lfloor\sqrt{m-1}\rfloor)^2}$, it is easy to see that when an even power of the source position function z' is considered the presence of an image source leads to annihilate the contribution to the field given by the x and y components of the current density, and by its divergence. In a similar way, contribution given by the z component is annihilated in terms $Q_m(z')$ having an odd power of z'. Therefore, when for example $\widetilde{M} = 2$ (i.e. $M = 8$) one only have to evaluate 18 instead of 40 2D–FFTs for each product $\mathbb{Z}^w \boldsymbol{I}$.

NUMERICAL RESULTS

The convergence of the method has been tested by comparing the results obtained with those given by a standard MoM. First, we have analysed the array sketched in Fig. 1 made up of 6×6 stacked patches. Fig. 2a shows the input impedance at the central element of the array evaluated with both the standard MoM procedure and the proposed one. The curves are almost indistinguishable.



(a) (b)

Fig. 2 – (a) Real and imaginary part of the input impedance of the central element of the array sketched in Fig. 1 (6777 unknowns, $h_{\max}/r_d = 0.082$); (b) Number of multiplications required for each $(\mathbb{Z}^s + \mathbb{Z}^w)\boldsymbol{I}$ product by MoM, FFM and BMIA/AIM method versus the number of unknowns ($\widetilde{M} = 2$).

Fig. 2b shows that the proposed method is profitable, when compared with the FMM, for the analysis of structures that require more than 4000 unknowns. Only first three terms of the Green's function Taylor series (i.e. $\widetilde{M} = 2$) have been considered.

Furthermore, Table I shows the computation time (on a Pentium III 1Ghz) and the dynamic memory required for the analysis of an array of resonant dipoles printed on the PGB structure of the type of that sketched in Fig. 3.

Results relating to more complex structures will also be presented at conference time.

Dimensions	Unknowns	CPU–time per iteration (sec)			Input impedance Ω (frequency= $26\,GHz$)		
		MoM	FMM	BMIA	MoM	FMM	BMIA
$2\lambda \times 2\lambda$	5193	9.4	4.7	1.5	$144.1 + j30.54$	$144.2 + j30.41$	$143.9 + j29.19$
$3\lambda \times 3\lambda$	11765	49.2	15.9	3.9	$99.78 - j25.01$	$99.83 - j25.02$	$99.46 - j25.77$
$4\lambda \times 4\lambda$	17774	—	39.0	6.6	—	$85.97 - j24.51$	$85.89 - j25.07$

Table I

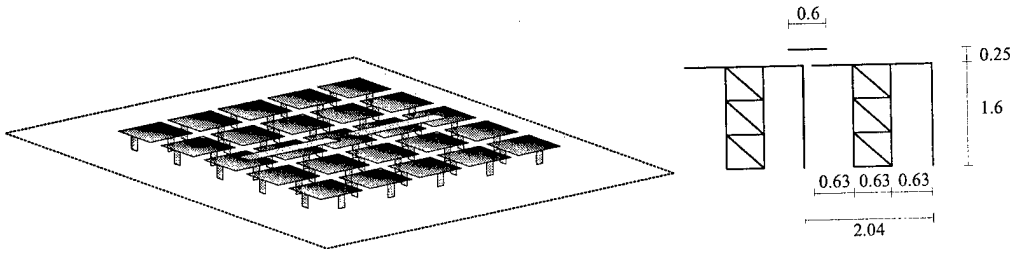


Fig. 3 – Resonant dipole printed on a PGB structure (dimensions are expressed in millimetres).

REFERENCES

[1] E. Bleszynski, M. Bleszynski, T. Jaroszewicz, "AIM: Adaptive integral method for solving large–scale electromagnetic scattering and radiation problems" *Radio Science*, vol. 5, pp. 1225–1251, 1996.

[2] R. Coifman, V. Rohklin, S. Wandzura, "The fast multipole method for the wave equation: a pedestrian prescription," *IEEE Antennas and Propagat.*, vol. AP–35, pp. 7–12, 1993.

[3] A. Boag, E. Michielssen, R. Mittra, "Hybrid multipole beam approach to electromagnetic scattering problems," *J. Appl. Comput. Electromagn. Soc.*, vol. 9, pp. 7–17, 1994.

[4] L. Tsang, C.H. Chan, K. Pak, "Monte–Carlo simulations of two–dimensional random rough surface using the sparse–matrix flat–surface iterative approach," *Electronic Letters*, vol. 29, pp. 1153–1154, 1993.

[5] L. Tsang, C.H.. Chan, K. Pak, H. Sangani, "Monte–Carlo simulations of large–scale problems of random rough surface scattering and application to grazing incidence with BMIA/canonical grid method," *IEEE Trans. Antennas and Propagat.*, vol. AP–43, pp. 851–859, 1995.

[6] Y.L. Chow, J.J. Yang,D.G. Fang, G.E. Howard, "A closed–form spatial Green's function for the thick microstrip substrate," *IEEE Trans. Microwave Theory Tech.*, vol. MTT–39, pp. 588–592, 1991.

[7] S.M. Rao, D.R. Wilton, A.W. Glisson, "Electromagnetic scattering by surfaces of arbitrary shape," *IEEE Trans. Antennas and Propagat.*, vol. AP–30, pp. 409–418, 1982.

EVOLUTIONARY COMPUTATIONAL TECHNIQUES IN ELCTROMAGNETICS

Ahmad Hoorfar

Department of Electrical and Computer Engineering
Villanova University, Villanova, PA 19085, USA
E-mail: hoorfar@ece.vill.edu

ABSTRACT

The three paradigms of the evolutionary algorithms, namely, Genetic Algorithms, Evolution Strategies and Evolutionary Programming, are briefly reviewed, and the applications of the latter to optimizations of continuous as well as mixed parameter electromagnetic problems are discussed in details. Examples presented include optimizations of corrugated horn antennas, array of multi-layered stacked microstrip patch elements, and synthesis of multi-layered dielectric filters.

INTRODUCTION

In optimization and synthesis of antenna and microwave structures, one typically deals with objective functions that are highly non-linear and have a large number of optimization parameters. In addition for many electromagnetic problems, the objective functions manifest epistatic behavior due to strong mutual coupling and other propagation effects, requiring a simultaneous optimization of the design parameters. Also, most complex electromagnetic systems have to be numerically modeled, resulting in objective functions that have no readily available derivatives. For such problems the evolutionary computational techniques can yield robust globally optimized solutions that otherwise are not possible using traditional gradient-based local-search optimization methods. These probabilistic techniques, collectively known as Evolutionary Algorithms (EAs), try to emulate, in one way or the other, the Darwinian model of natural evolution on a computer. Even though there are many branches of EA's, one can in general identify three main trends in the literature: Evolutionary Programming (EP)[1], Evolution Strategies (ES)[2] and Genetic Algorithms (GAs)[3]. All these algorithms are multi-agent stochastic search methods that incorporate random variation and selection. They all operate on a population of candidate solutions and rely on a set of variation operators to generate new offspring population. Selection is then used to probabilistically advance better solutions to the next generation and eliminate less-fit solution according to the objective function being optimized. Of the three paradigms of EAs, GAs are well-known to the electromagnetic community and have been extensively used in optimization of antenna and microwave structures[4-6], whereas the application of EP in electromagnetics appeared more recently [7,8]. The most significant difference among the aforementioned branches of EAs is the choice of variation operator. In GAs the variation operator is a combination of crossover and mutation with the former being the main mechanism of change, whereas in ES both recombination and mutation are used with the latter being the dominant operator. In EP,

however, mutation is the only variation operator used and therefore the evolution process is asexual by nature. In addition, the selection of the crossover and mutation probabilities in GAs is rather arbitrary and they are not adapted during evolution. On the other hand, the selection of the initial values for the so-called strategy parameters for EP and ES are well defined and efficient adaptive and self-adaptive techniques exist for adapting these parameters during evolution. Mutation-based reproduction process in EP can provide a versatile tool in design of the problem specific operators and facilitate easy integration with available apriori knowledge about the problem. It is also noteworthy that unlike conventional GAs, which require the continuous design parameters to be coded and represented as binary strings, EP and ES can both directly work with the continuous, discrete or mixed parameters.

Since the applications of GAs in electromagnetics have been detailed in a recent book [6] as well as in many journal and conference papers (see [6] for a detailed bibliography), in this paper we concentrate on some recent advances in EP and its applications in various constrained antenna and microwave design problems.

META-EP FOR CONTINUOUS PARAMETER OPTIMIZATION

The EP algorithm with self-adaptive mutation operator for global optimization of an n-dimensional objective function $\phi(\bar{x})$, $\bar{x} = [x(1), x(2), \ldots x(n)]$ consists of five basic steps: initialization, fitness evaluation, mutation, tournament and selection. Here we concentrate on the mutation step; the details on the other steps can be found in [1,8]. Design of efficient mutation operators is presently an ongoing topic of research in evolutionary computation. Here we present two algorithms, which use different mutation operators in the evolution process. First let us assume an initial population of μ individuals is formed through a uniform random or a biased distribution. Each individual is taken as a pair of real-valued vectors, $(\bar{x}_i, \bar{\eta}_i)$, $\forall i \in \{1, \ldots \mu\}$, where $\bar{x}_i = [x_i(1), x_i(2), \ldots x_i(n)]$ and $\bar{\eta}_i$ are the n-dimensional solution and its corresponding strategy parameter (variance) vectors, respectively. In EP with Gaussian mutation operator (GMO), each parent $(\bar{x}_i, \bar{\eta}_i)$ creates a single offspring $(\bar{x}_i', \bar{\eta}_i')$ by:

$$x_i'(j) = x_i(j) + \sqrt{\eta_i(j)}\, N_j(0,1) \quad ; \quad \eta_i'(j) = \eta_i(j)\, e^{[\tau' N(0,1) + \tau N_j(0,1)]} \qquad (1)$$

for j = 0,1,2,....n, where *x(j) and η(j)* are the jth components of the solution vector and the variance vector, respectively. N(0,1) denotes a one-dimensional random variable with a Gaussian distribution of mean zero and standard deviation one. Nj(0,1) indicates that the random variable is generated anew for each value of j. The scale factors τ and τ' are commonly set to $\left(\sqrt{2\sqrt{n}}\right)^{-1}$ and $\left(\sqrt{2n}\right)^{-1}$, respectively, where n is the dimension of the search space. Self-adaptive mechanism of the second equation in (1), borrowed from ES, enables the meta-EP to evolve its own variance parameters during the search, exploiting an implicit link between internal model and good fitness values. In EP with Cauchy mutation operator (CMO), the offsprings are still generated according to (1), but with a Cauchy mutation replacing the Gaussian mutation in the first equation, i.e.,

$$x_i'(j) = x_i(j) + \sqrt{\eta_i(j)}\, C_j(0,1) \qquad (2)$$

where C(0,1) is a random variable with a Cauchy distribution operator centered at the origin and with the scale parameter t = 1. After the offspring's population is formed, a tournament/selection process is performed in which a pair-wise comparison with respect to the fitness values over the union of parents and offspring populations is conducted. For each individual $\bar{a}_k$ in the union, $k \in \{1,.... 2\mu\}$, q opponents are chosen at random with equal probability from the total membership 2μ of the union. For each comparison, if the individual fitness is no greater than the opponent's, it receives a "win". The best individual is guaranteed a maximum 'win' score of q and its survival to the next generation. We note that this tournament process differs from the one in conventional GAs and ES and is 'elitist' in nature. The μ individuals out of the union of $(\bar{x}_i, \bar{\eta}_i) \cup (\bar{x}_i', \bar{\eta}_i'), \forall i \in \{1,.... 2\mu\}$, with the most "win" score are then selected to be the parents of the next generation.

For multi-modal functions with many local optima CMO outperforms GMO. To demonstrate this, we consider the n-dimensional Ackley function [2]:

$$f_n(\bar{x}) = -20\exp\left(-0.2\sqrt{\frac{1}{n}\sum_{i=1}^{n} x_i^2}\right) - \exp\left(\frac{1}{n}\sum_{i=1}^{n}\cos(2\pi x_i)\right) + 20 + e \qquad (3)$$

This function has a global minimum at 0 and a total of about $(2a+1)^n$ in the range [-a , a]. We have applied EP algorithms in the range [-5, 5] to the above function when n = 20. The population size and the number of opponents were set to μ = 50 and q = 10, respectively. Figures 1 and 2 show the function-value trajectory of the best population member over 100 trials and the corresponding histogram, respectively. We note that the very large number of local minima, which in this case is about 11^{20}, would trap any gradient-based, hill climbing method.

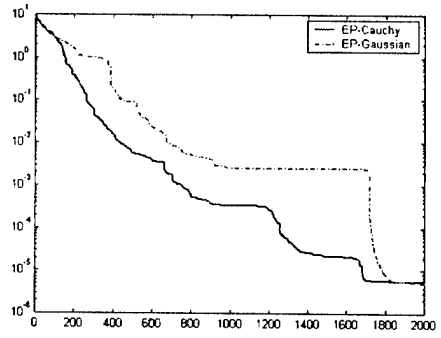


Fig. 1: Convergence rate of the best solution member

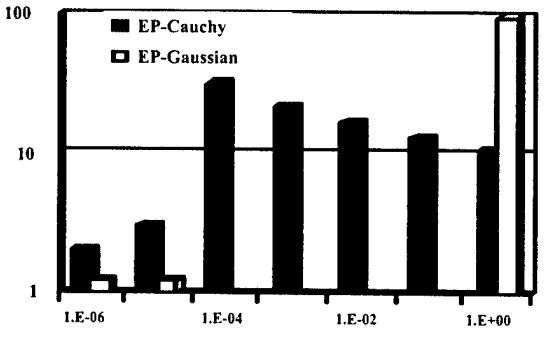


Fig. 2: Histogram for Gaussian and Cauchy mutations

Examples of Continuous Parameter Optimizations using EP

We present two examples on application of EP-GMO to antenna problems. Examples of electromagnetic optimizations using EP-CMO and EP with a hybrid Cauchy-Gaussian mutation are given in [9] and [10], respectively. The first example is that of the pattern optimization of a corrugated conical horn. For optimization purposes the N-section corrugated horn in Figure 1 is mathematically represented as a vector of length n = 2N: $\bar{X} = [r_1, r_2, ... r_N ; d_1, d_2, ..., d_N]^T$ where r_i and d_i are radius and length of the i-th corrugated

segment, respectively. For the minimization of the difference between the E- and the H-plane co-polar patterns, we construct the fitness function as

$$F(\bar{x}) = \frac{1}{M_\theta}\sum_{i=1}^{M_\theta}\left[\left[E(\theta_i,0^\circ) - E(\theta_i,90^\circ)\right]\right] + w(S_{11} - S_{opt}) \qquad (4)$$

where $E(\theta, \phi)$ is the normalized co-polar pattern in dB obtained by using a mode matching technique. M_θ in the first term is the number of elevation angles, θ, sampled in the interval $[0, \theta_{max}]$, in which we require a near circularly symmetric pattern. The last term penalizes, with a weighting factor w, all the solutions that violate the constraint, $S_{11} \le S_{opt}$, on the return loss. As an example, a 45-segment corrugated horn

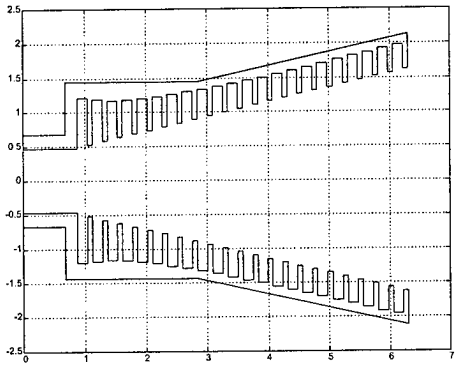


Figure 3. Geometry of corrugated horn before optimization

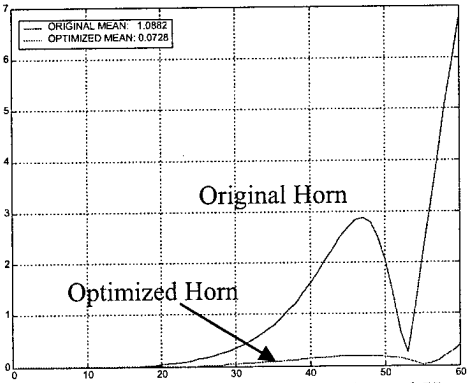


Figure 4: Difference between E- and H-plane Patterns in dB versus Theta.

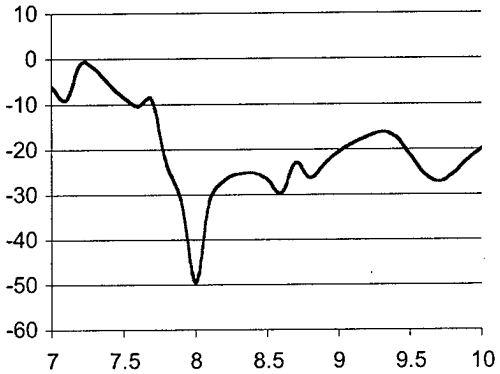


Figure 5. Input S_{11} as a function of frequency for the optimized horn

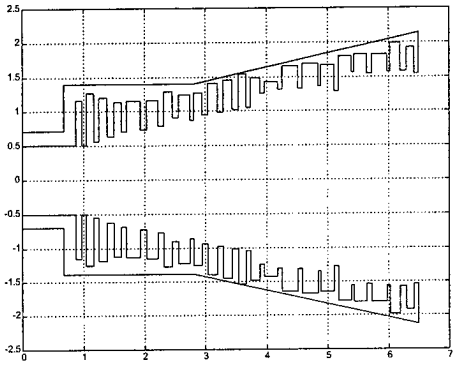


Figure 6. Geometry of corrugated horn after optimization

was optimized with a total of 90 optimization parameters at f = 8GHz [11]. The geometry of the initial structure, before optimization, is shown in Figure 1. The population size and the number of opponents in the tournament selection were set to μ = 10 and q = 4, respectively. The radii and lengths of the sections were randomly initialized around those of the initial structure. The strategy parameters were initialized to $(x_{max}-x_{min})/6$ and kept above a lower bound of 10^{-4} during the self-adaptations in (1). The optimization was performed subject to the constraint on the return loss (< -40 dB), and with M_θ = 60, corresponding to a near circular symmetric pattern up to $\theta = 60^\circ$. Figure 3 show the difference between E- and H-plane patterns after 200 generations of EP. Figure 5 shows the return loss versus frequency for the optimized horn. The

optimization has resulted in a return loss of about –50 dB and an almost perfect circularly symmetric pattern at the design frequency. The geometry of the final optimized structure is shown in Figure 6.

In the second example, a proximity-fed Yagi-like array of stacked patches printed in a multi-layered medium (Figure 7) is optimized for high gain at 31 GHz. The structure is numerically modeled using a mixed potential integral equation [12]. The dielectric constants of layers are set fixed as $\varepsilon_{r1} = \varepsilon_{r2} = 2.2$, $\varepsilon_{r3} = 1$ and $\varepsilon_{r4} = 4.5$ with $d_1 = d_2 = 0.254$ mm. All the remaining design parameters are optimized subject to a VSWR < 2 bandwidth constraint of 1 GHz. Figure 12 shows the gain and return loss for this case. The S_{11} obtained from the commercial code IE3D is also included for comparison. Gain of better than 14 dBi with a radiation efficiency of 93% is obtained. The corresponding best fitness-value trajectory is shown in Figure 9.

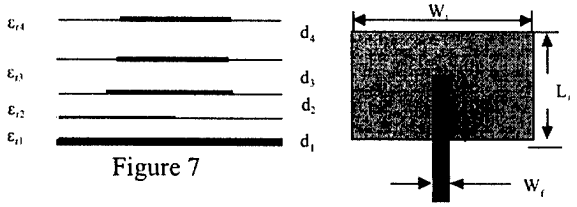


Figure 7

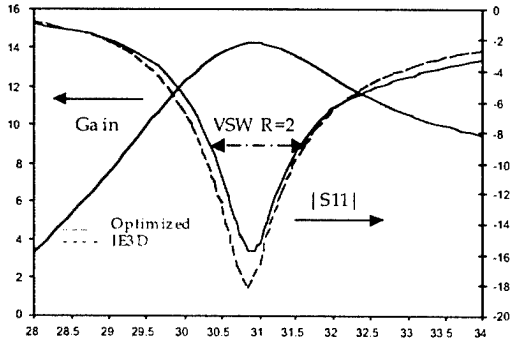


Figure 8. Gain and S11 versus frequency

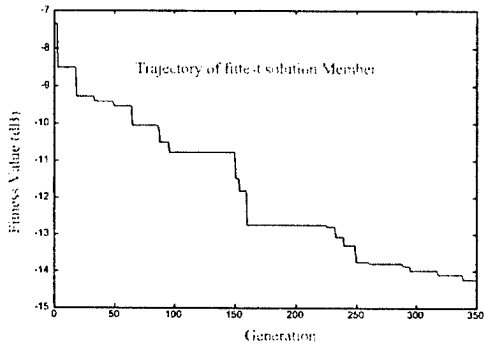


Figure 9. Fitness trajectory of the fittest solution

EP WITH A MIXED-PARAMETER MUTATION OPERATOR

In practical design of many antennas, microwave and electromagnetic systems, one has to deal with objective functions that include both discrete and continuous optimization parameters. For example in frequency response optimization of multilayer filter structure in Figure 10, it is desirable to optimally select from a wide range of commonly available materials with various permittivity, permeability and loss tangent. In such an optimization, the compositions of dielectric layers require a discrete parameter representation, while the thickness of each layer requires a continuous representation. Here we present an implementation of EP with a mixed continuous-discrete parameter representation. The mixed parameter EP (MEP) algorithm differs from the standard implementation of EP only in the mutation step. Let us consider an n-dimensional objective function

$$\phi(\bar{x},\bar{y}),\ \bar{x} = [x(1), x(2), \ldots, x(m)],\ \bar{y} = [y(m+1), y(m+2), \ldots, y(n)] \qquad (5)$$

where x and y are the m continuous and n-m discrete (or integer) optimization parameters. In our implementation of MEP for global optimization of $\phi(\bar{x},\bar{y})$ we first form an initial population of μ individuals, where each individual is considered to be a quartet of vectors, $(\bar{x}_i, \bar{y}_i; \bar{\eta}_i, \bar{\lambda}_i),\ \forall i \in \{1,\ldots,\mu\}$ wherein $\bar{x}_i = [x_i(1), x_i(2), \ldots, x_i(m)]$ and

$\bar{y}_i = [y_i(m+1), y_i(2), \ldots, y_i(n)]$, are the continuous and discrete parameter solution vectors, and $\bar{\eta}_i$ and $\bar{\lambda}_i$ are their corresponding strategy parameter vectors, respectively. The mixed parameter EP in now implemented by generating a single offspring $(\bar{x}_i', \bar{y}_i'; \bar{\eta}_i', \bar{\lambda}_i')$ from each parent $(\bar{x}_i, \bar{y}_i; \bar{\eta}_i, \bar{\lambda}_i)$ according to:

$$\eta_i'(j) = \eta_i(j)\, e^{[\tau' N(0,1) + \tau N_j(0,1)]} \quad ; \quad x_i'(j) = x_i(j) + \eta_i(j) N_j(0,1) \qquad (6)$$

$$\lambda_i'(k) = \lambda_i(k) + \sigma_i'(k)\, N_k(0,1) \quad ; \quad y_i'(k) = \mathrm{Ps}[\lambda_i'(k)] \qquad (7)$$

for j = 0,1,2,...,m and k = m+1,m+2,...,n ; $x_i(j)$,*and* $\eta_i(j)$ are the j-th components of the $\bar{x}_i$ and $\bar{\eta}_i$ vectors, and $y_i(k)$,*and* $\lambda_i(k)$ are the k-th components of the $\bar{y}_i$ and $\bar{\lambda}_i$ vectors respectively. Ps(λ) is a discrete random number with a Poisson distribution operator with a mean of λ. The standard deviation σ_i in (7) can be either set to a constant or log-normally regenerated similar to that of η_i in the first equation in (6).

Application of MEP to Optimization of Dielectric Filters

Figure 10 shows a filter structure consisting of N dielectric layers. The objective is to synthesize the filter for a given frequency response at a given incident angle, by optimizing the thickness of each layer and at the same time optimally selecting its dielectric constant from a given pool of M commonly available materials. To apply the mixed-parameter EP we first index each dielectric constant with a discrete value from 1 to M. The structure is then represented as a vector consisting of the thickness of each layer, d(i), and an integer variable, γ(i) representing the dielectric constant of each layer, $\bar{X} = [d(1), d(2), \ldots, d(N), \gamma(1), \gamma(2), \ldots, \gamma(N)]^T$. For a band-pass filter we construct the fitness function as,

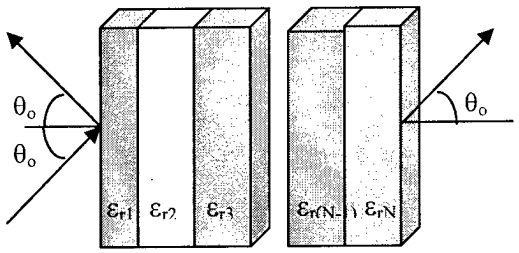


Figure 10

$$F(\bar{X}) = \alpha \sum_p \left[\left| R_{TE}(\bar{X}, f_p) \right|^2 + \left| R_{TM}(\bar{X}, f_p) \right|^2 \right] + \beta \sum_s \left[T_{TE}(\bar{X}, f_s) + T_{TM}(\bar{X}, f_s) \right] + \sum_m P_m(\bar{x}) \qquad (8)$$

where $T_{TE,TM} = |1 - |R_{TE,TM}|^2|$, and R_{TE} and R_{TM} are the reflection coefficients corresponding to *TE* and *TM* waves, respectively, obtained from an equivalent multi-section transmission line of the filter structure. The first and second sums in (5) correspond to the band-pass and band-stop frequencies, respectively; α are β are weight factors chosen to shape response of the filter. P_m , m = 1,2,.. are the penalty criteria for violating a set of constraints, e.g. maximum allowable thickness of the structure, dielectric loss efficiency, etc. A similar fitness function can also be constructed for other filter types, i.e., low-pass filter, high-pass filter, etc. To demonstrate the MEP technique, two filters, a 7-layer band-pass and a 5-layer low-pass, were optimized at an incident angle of 45° for millimeter-wave frequency responses. A database of M=15 dielectric constants, ε_r, were formed from those commercially available with values ranging from 1.01 to 10.2. Order of these values was randomly shuffled before indexing them with

discrete values from 1 to 15 as was outlined above. The MEP parameters were set to $\mu = 50$ and $q = 10$. Standard deviations σ_i in (7) were not adapted and set a constant value of 0.5. For the band-pass case, the optimization was performed subject to the constraints of: i) R_{TE} and R_{TM} less than –15 dB in the band-pass region, and ii) total thickness of the structure less than 3 cm. Desired cutoff frequencies for these designs were 31GHz for the low-pass case, and 27 and 32 GHz for the band-pass case. The reflection coefficients as functions of frequency, after 250 generations of MEP, are shown in Fig. 11 and 12. Figure 13 shows the fitness trajectory of best population member averaged over 45 trials for the low-pass filter. Optimization using the MEP algorithm without the Poisson operator in (7), but with a uniform random mutation for the discrete parameters, is included for comparison.

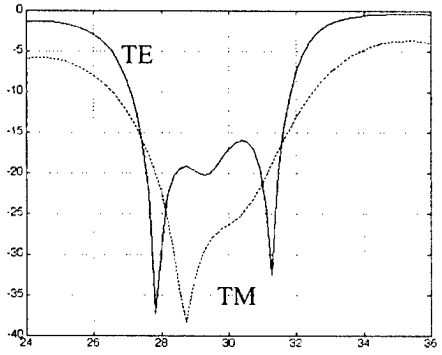


Figure 11: Band pass filter

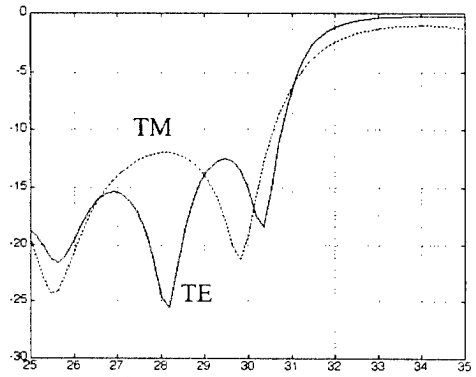


Figure 12: Low pass filter

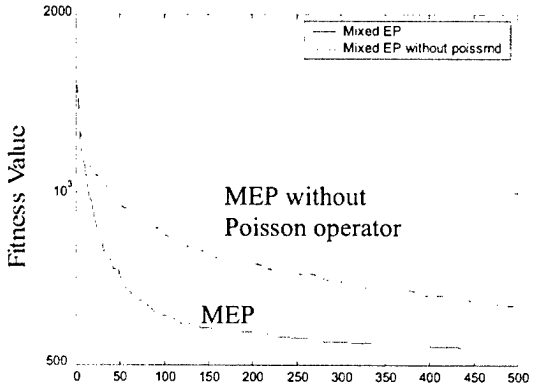


Figure 13: Fittest member averaged over 45 trials

REFERENCES

[1] D. B. Fogel, Evolutionary Computation: Toward a New Philosophy of Machine Intelligence, 1994.
[2] T. Bäck, Evolutionary Algorithms in Theory and Practice, Oxford Univ. Press, 1996.
[3] D. E. Goldberg, Genetic Algorithms in Search, Optimization and Machine Learning, 1989.
[4] D.S.Weile and E. Michielssen, "Genetic algorithm optimization applied to electromagnetics: A review," *IEEE Trans. Antennas Propagat.*, March 1997.
[5] J. M. Johnson and Y. Rahmat-Samii, "Genetic algorithms in engineering electromagnetics," *AP-S Magazine* , August 1997.
[6] Electromagnetic Optimization by Genetic Algorithms, edited by Y. Ramat-Samii and E. Michielssen, 1999.
[7] A. Hoorfar and K. Chellapilla "Gain optimization of a multi-layer printed dipole array using evolutionary programming," *Proc. IEEE AP-S International Symp.*, pp. 46-49, June 1998.
[8] A. Hoorfar, "Mutation-based evolutionary algorithms and their applications to optimization of antennas in layered media," *Proc. IEEE AP-S International Symp* pp. 2876-2879,, July 1999.
[9] A. Hoorfar and Yuan Liu, "A study of Cauchy and Gaussian mutation operators in the evolutionary programming optimization of antenna structures," *16th Annual Review of Applied Computational Electromagnetics*, pp. 63-69, Monterey, California, March 2000.
[10] A. Hoorfar and Yuan Liu, "Antenna Optimization using an Evolutionary Programming Algorithm with a Hybrid Mutation Operator," *Proc. IEEE AP-S Inter. Symp*,, July 2000.
[11] V. Jamnejad, A. Hoorfar and F. Manshadi, "Evolutionary optimization of a Corrugated Horn Antenna," accepted for the *2002 JINA symposium*, Nice, France, November 2002.
[12] A. Hoorfar, "Analysis of a 'Yagi-like' printed stacked dipole array for high gain applications," *Microwave Opt.. Technol. Lett.*, pp. 317-321, April 1998.

THE USE OF HIERARCHY IN MODELING TOOLS FOR PLANAR STRUCTURES

Guy A. E. Vandenbosch, M. Vrancken, and B. Van Thielen
K.U.Leuven, ESAT-TELEMIC, Kasteelpark Arenberg 10, 3001 Leuven, Belgium
guy.vandenbosch@esat.kuleuven.ac.be

ABSTRACT.

Since 1985, the K.U.Leuven has been involved in the analysis of general planar antennas. In 1993, a strategy was developed in order to incorporate the work done in a framework called MAGMAS (Model for the Analysis of General Multilayered Antenna Structures). Essential is the fact that MAGMAS uses a multi-level approach. In our view this is crucial in order to reach the ultimate goal: an accurate, interactive, one-pass CAD tool to design planar and quasi-planar antennas. Antenna examples are given, illustrating the physical structures that can be analyzed with the framework.

INTRODUCTION

In recent years, the EM (ElectroMagnetic) analysis and design of devices (antennas, circuits, boards, ...) is performed more and more in a "rigorous" manner. The basic line of reasoning is always the same. Maxwell's equations are manipulated into matrix equations, using a differential or an integral equation approach. The solution of this set of matrix equations yields an approximation of the solution of the original problem. In most practical devices, the number of unknowns rapidly becomes too large to be solved in an acceptable time. In this paper, it is discussed how the framework developed at K.U.Leuven tries to cope with the problem. The core techniques used are examined in relation to their position within the framework. One of them is the Expansion Wave Concept (EWC). This concept was first developed to reduce the number of unknowns in problems involving layer structures. The direct goal of this paper is not to explain in full detail the working mechanism of each numerical technique. This can be found in the references given. The direct goal is to illustrate the use of hierarchy and modularity.

MODULARITY AND HIERARCHY

A study of the range of commercial CAD packages for the analysis and design of electromagnetic structures (HP-momentum, Ensemble, IE3D, SAPHIR, HP-HFSS, Ansoft HFSS, EMPIRE, MAFIA, Sonnet em, ...) points out that most of these packages are based on a single numerical technique (Method of Moments (MoM), Finite Elements (FE), Finite Difference Time Domain (FDTD), ...). The consequence is that they can handle only "small" structures. The size of "small" strongly depends on the computer power being used. In practice, one can say that with the workstations or PCs of today these software packages are able to handle a single component or an assembly of a few components. They are by no means ready to handle complete systems or "large" structures. However, due to the accuracy of designing using a full-wave approach, there is a clear trend towards the use of EM CAD software for sub-assemblies. Industry already is looking at the future and a lot of requests for EM software able to handle complete systems are being investigated. The steady increase of computer power is certainly a factor. However, in my view the current trend in the EM modeling community, using modularity and hierarchy, will prove to be a crucial factor

in order to reach the ultimate goal: the full-wave analysis of complete systems.
The only way to reach the goal of analyzing and designing complete systems is to use modularity and hierarchy. A scheme to analyze a 2.5D system in a multi-layer environment is illustrated in Fig. 1. Devices like planar antenna arrays, planar circuits, PCBs, etc. can be described in this way. Although designers indeed tend to follow this modular scheme while thinking about the structure, a look at the analysis engines of most of the commercial CAD packages today reveals that they treat the complete system as a single physical entity, using the same numerical technique throughout. In a large planar antenna array for example, the coupling between two elements far apart is described with the same number of unknowns as the coupling within the elements themselves. This is a waste of computer power. The coupling between two elements far apart can be described with much less unknowns. How to implement this in a practical procedure?

3-LEVEL FRAMEWORK BASED ON THE EXPANSION WAVE CONCEPT

This model was developed to analyze medium-sized and large arrays of antenna elements. The key idea is to use the characteristic waves of the layer structure (surface and space wave) to describe mutual coupling. First, coupling between the components is solved at the element type level with a MoM. This means that each so-called "element type" is solved in ca. the same way as done in commercial software. The calculation time is depending on size and complexity of the element type. Note that only the element types have to be solved, and not each element separately. Coupling between the elements is described with expansion waves. Each element has a number of "outgoing waves" generated by the element, and a number of "incoming waves", incident on the element and generated by the rest of the structure. The number of waves per element depends on the layer structure and the lateral size of the element type under consideration, not on its internal complexity. It is typically at least an order of magnitude smaller than the number of unknowns in the MoM used to solve the internal coupling. The concept also allows to describe interactions with the edge of the layer structure (finite layer structures can be solved) and periodic interactions in infinite arrays. As example an 11x11 array of a complex aperture type radiating element, embedded within a layer structure involving 7 layers is considered. The number of unknowns used to solve the internal element coupling is 720. This means that the commercial software packages would have to solve a system of 87120 unknowns (= 121 elements x 720 unknowns per element), involving a full matrix. The expansion wave concept only uses in total 48 unknowns per element. The calculation time was about 3 hours per frequency point on an HP 9000/780 160 MHz 512 MB RAM workstation. The inversion at the array level took 1.5 hours. Extrapolation yields an inversion time at the array level 15^3 times larger for traditional techniques.

3-LEVEL FRAMEWORK BASED ON TRANSMISSION LINES AND EQUIVALENT DIPOLES

This method was developed to analyze coupling, for example in antenna feeding circuits, in reasonable calculation times. This is not possible with traditional circuit simulators, where coupling is not modeled. Using traditional full wave solvers, coupling is included, but calculation times rapidly become prohibitive.

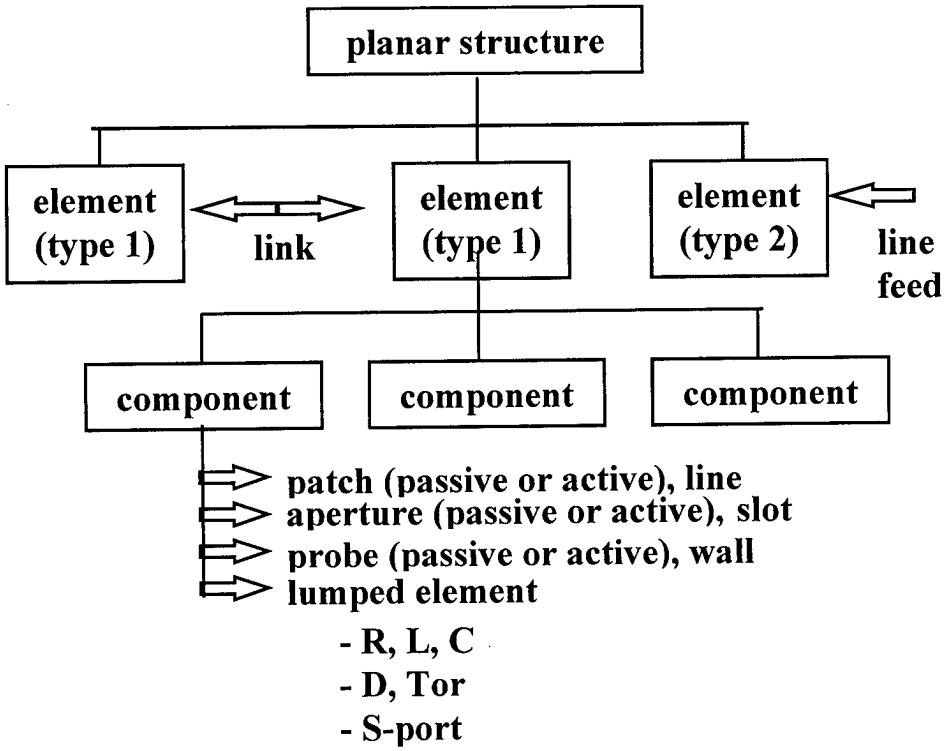


Fig. 1. Hierarchical scheme for 2.5D antenna in multilayer. The planar structure consists of elements of several types, each consisting of several components. Elements may be connected through transmission lines (microstrip or strip line, coplanar waveguide, ...). The structure is solved at three levels. First the internal coupling within the element types is described by solving the component integral equations. Second coupling between the elements is described using Expansion Waves. Third the elements are linked through the transmission lines (= links), assuming the fundamental modes only on these links. This means that no mutual coupling with these links is taken into account. The calculation time is far less than with commercial CAD packages.

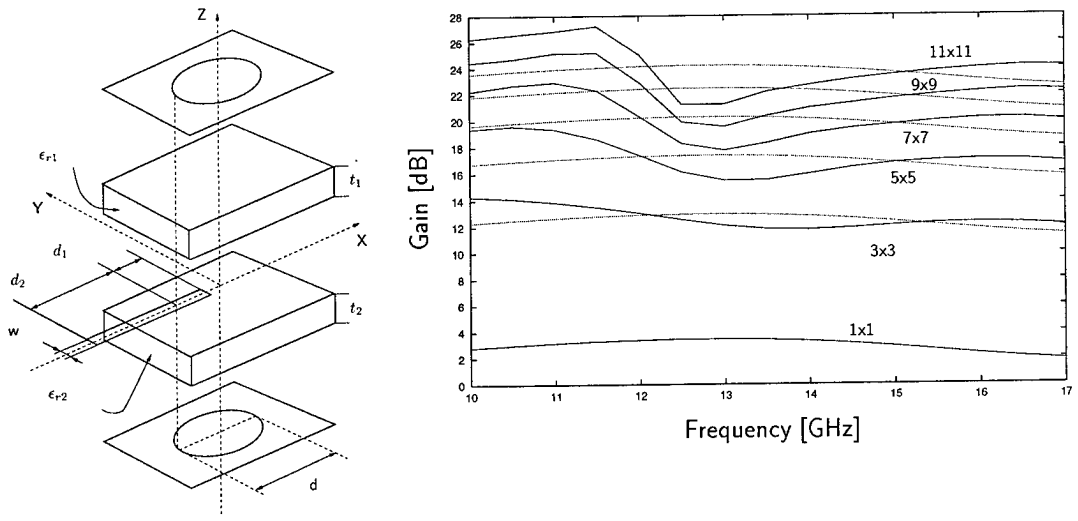


Fig. 2. Left: two stacked circular apertures in two conducting plates fed by strip line. Right: calculated gain of a 1x1, 3x3, 5x5, 7x7, 9x9, 11x11 array of this element type. Gain calculated without mutual coupling is given as a reference. The oscillation is at the frequency where the distance between elements is one wavelength.

analyzed with techniques developed especially for the interaction considered.
The module for the calculation of mutual coupling between transmission lines ([3] and [4]) is developed starting from the general MoM. Only first order coupling is taken into account: the radiation effect of the induced currents is neglected. The calculations are speeded up for coupling between lines by assuming that all lines are terminated in their characteristic impedances and using the travelling current waves on these matched lines. The current on the observation line can then be calculated by convolving the incident field on this line with its "impulse response". The impulse response is the current on an infinitely long line when a spatial Dirac impulse is applied in the middle. This results in a much faster method because no matrix inversion has to be performed. Full details can be found in [3] and [4].
For the calculation of mutual coupling between discontinuities [5], the discontinuities must be small compared to the wavelength and compared to the distance between them. For most circuits these assumptions are valid. Under these circumstances the discontinuity radiation behavior can be accurately modeled by using adequately placed dipoles. This method uses far less unknowns than the MoM. If the distances between the discontinuities become smaller or they become bigger, then the accuracy can be improved by using more dipoles. The position of the dipoles and their excitation are determined by an optimization procedure that matches the combined radiation pattern of the dipoles to that of the discontinuity. The data about the discontinuity's S-parameters, dipole excitations and positions are stored in a library file. These files are used when the circuit itself is calculated. This module also only takes first order coupling into account (scattering of EM fields at the dipoles is ignored). Full details can be found in [5].
Larger structures are treated using the MoM. This works with currents and fields. For circuits, where one is interested in the relations between incoming and outgoing waves on the feeding lines, deembedding (such as in [7]) is therefore required. In [6], the MoM is altered in such a way that incoming and outgoing waves at the structure's ports are extra unknowns in the coupling matrix. This makes it possible to insert the MoM coupling matrix directly into the circuit simulation (along with lines and discontinuities), thereby providing a close integration between the classical MoM, the new modules and the S-parameter circuit simulator. The excitations of the structure's feeding lines are chosen in such a way that they generate incident waves on these lines. The feeding line's self-coupling matrix is modified so that the line appears to be matched. These modifications make it possible to get S-parameters immediately after inverting the structure's Z-matrix, without needing deembedding [6]. The example is a 2 x 2 edge-fed, dual polarisation, patch array that is shown in figure 3. The patches resonate at 7.2 GHz and have an impedance of about 100 Ohm there. The characteristic impedance of all lines is 100 Ohm. This results in an input impedance of 50 Ohms at the inputs (the line sections between port and T-junctions are a multiple of a half wavelength at 7.2 GHz). The substrate has a thickness of 1.575 mm and a relative permitivity of 2.2. The port 2 T-junction should be offset by ¼ wavelength up or down (see figure 3) for normal operation (horizontal polarisation when fed at port 1 and vertical when fed at port 2) to avoid the vertically polarised patches being fed 180 degrees out of phase. This offset is not present here in order to increase coupling between both ports, because we want to demonstrate the validity of the new analysis method for large rather tightly coupled structures. The patches of the structure are

meshed with 24 x 31 segments. The dense mesh is needed to accurately model the incisions. The lines have 3 segments across their width.
The structure was calculated using the MoM (needing 663 MByte and 41 minutes and 26 seconds per frequency point on a Hp J-5000, 445 MHz workstation). This result was compared to the result of the new method, using 32 dipoles on the patch (many dipoles needed here because the patches are not small compared to the wavelength and very close to lines and bent) and 6 dipoles for the bent. The new method only needs about 100 KByte and 8 seconds. The calculation times given do not include the time needed to calculate the Green's functions. The structure is calculated for L=6.43 mm (as shown in figure 3, results in figure 4 at the left) and for L=4.43 mm (figure 4 at the right).

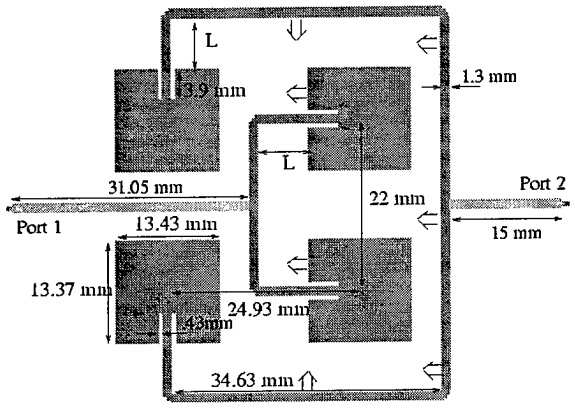


Fig. 3. 2 x 2, dual polarization, edge-fed array of patch antennas. In the position shown above L = 6.43 mm. Arrows indicate parts movement when L is made smaller.

CONCLUSIONS

In this paper the modular approach followed within MAGMAS has been explained, illustrating how to use modularity and hierarchy in analysis engines. Modularity and hierarchy will prove to be essential in the search for engines able to cope with larger and larger problems. The key feature is to address each problem at its own level of complexity. The expansion wave concept and the dipole model are examples of this.

REFERENCES

[1] F. J. Demuynck, G. A. E. Vandenbosch, and A. R. Van de Capelle, "The expansion wave concept – part I", IEEE-AP, vol. 46, no.3, pp. 397-406, March 1998
[2] G. A. E. Vandenbosch and F. J. Demuynck, "The expansion wave concept – part II", IEEE-AP, vol. 46, no.3, pp. 407-413, March 1998
[3] B. L. A. Van Thielen and G. A. E. Vandenbosch, "Method for the acceleration of transmission-line coupling calculations," IEEE Trans. Microwave Theory Tech., vol. 48, No. 9, pp. 1531-1536, Sept 2000
[4] B. L. A. Van Thielen and G. A. E. Vandenbosch, "Fast transmission line coupling calculation using a convolution technique," IEEE Trans. Electromagn. Compat., vol. 43, no. 1, pp. 11-17, Feb 2001
[5] B. L. A. Van Thielen and G. A. E. Vandenbosch, "Method for the calculation of mutual coupling between discontinuities in planar circuits," IEEE-MTT, vol. , no. ,pp., January 2002
[6] B. L. A. Van Thielen and G. A. E. Vandenbosch, "Fast S-parameter extraction method for the analysis of planar structures using the method of moments," International Journal of Microwave and Millimeter-Wave Computer-Aided Engineering, vol. 11, no. 6, pp. 404-415, Nov 2001
[7] J. Sercu, N. Fache and D. De Zutter, "Characterisation of TEM and non-TEM Planar Transmission Lines with a Full-Wave 3D Field Analysis Technique", Proc. 23rd European Microwave Conf., pp. 328-329, 1993.

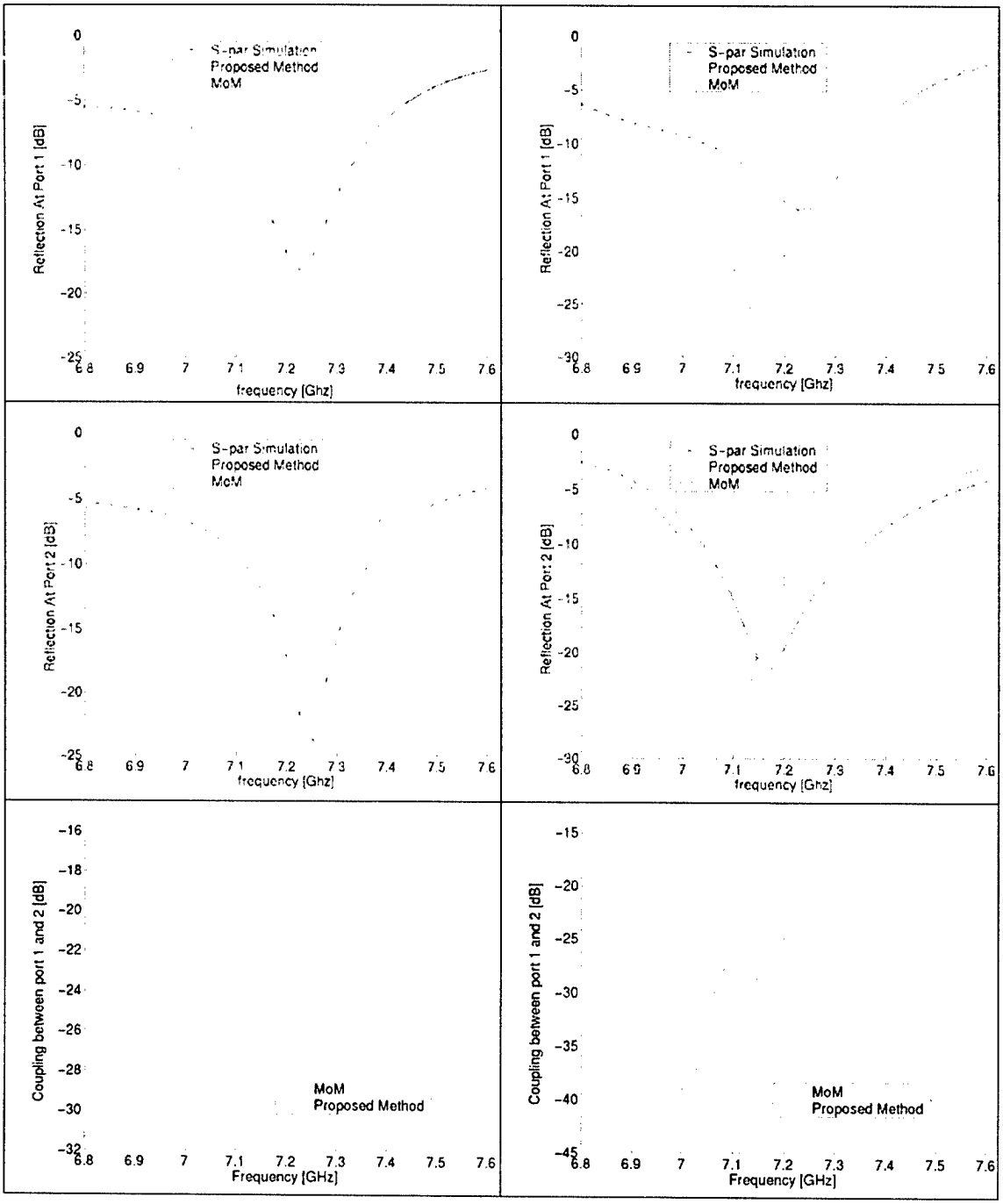


Fig. 4. Results for the structure of figure 3. Left figures: L=6.43 mm, Right figures L=4.43 mm. Continuous line is result of MoM, '+' line is result using new method. All S-parameters are referenced to 50 Ohm.

TIME-DEPENDENT SELF-ACTION OF PERIODICALLY MODULATED LASER BEAMS IN RESONANT MEDIA

Vladimir L. Derbov, Vladislav V. Serov,
Inna L. Plastun[1], and Sergey V. Shilov[1]
Saratov State University, 155, Moskovskaya st., Saratov 410026, Russia,
e-mail:derbov@sgu.ru
[1]-Saratov State Technical University, 77, Politekhnicheskaya st., Saratov 410054, Russia

ABSTRACT

We study the self-action of an amplitude-modulated beam in a two-level saturable absorbing medium. We also consider the radial quadratic dependence of the linear refraction index to apply the results to doped waveguides. As the modulation period approaches the relaxation times, the medium response is no more instantaneous, so that one should solve the full set of Maxwell-Bloch equations. We propose a second-order scheme with the Gauss-Laguerre transformation of the transverse field pattern. A simplified approach based on the synchronous interaction approximation is used for thin layers. We analyze the transient behavior of the medium response and its manifestation in the modulation of the beam diffracting after a thin saturable absorber. Nonlinear distortions of the modulation signal passed through a doped waveguide appeared to be unexpectedly small compared with those of the local polarization and population difference.

INTRODUCTION

Near-resonance self-focusing and self-aperturing of a CW laser beam in saturable absorbing medium has been a subject of a number of theoretical and experimental studies [1-4]. In laser spectroscopy CW beams are typically modulated in amplitude or frequency. If the period of modulation is large compared with the atomic relaxation times, the medium response, obviously, follows the variation of the field adiabatically, so that at each instant of time the CW saturation theory holds. In this case the medium may be described by means of a nonlinear susceptibility [2,3]. When the period of modulation approaches the relaxation times, one can expect transient behavior of the medium. Experimental manifestations of non-stationary near resonant self-focusing of frequency-modulated beams have been reported [5] for inhomogeneously broadened absorption lines in molecular gases. Obviously, in homogeneously broadened systems the non-stationary response of the medium should affect the transmitted beam in a similar way. To describe fast modulation the simple nonlinear susceptibility approach is no more valid, and the time-dependent Maxwell-Bloch equations should be solved simultaneously. The schemes developed for short pulses (see, e.g., [6-8]) and based on the field limitation both in space and in time are not convenient for periodically modulated fields.

The goal of the present paper is to develop appropriate computational schemes and to study numerically the influence of the transient response of the medium on the transmission of modulated beam through an initially homogeneous saturable absorbing medium or a gradient waveguide doped with saturable absorbers. We start from formulating the general equations and the scheme of their numerical solution. For thin

layers the approximation of simultaneous interaction is presented. The numerical study starts from a simplified model, in which the initially Gaussian beam is passed through a thin layer of the absorbing medium and then propagates through free space. The thickness of the absorber is considered to be small compared to the diffraction length, so that the diffraction in the medium is negligible. It takes place in free space leading to redistribution of the light intensity across the beam. Moreover, in case when both the diffraction length and the medium thickness are small compared to the wavelength of modulation, the variations of the field envelope function may be considered as simultaneous in the whole volume under study. Our estimates show the possibility of such conditions in real experiments with atomic vapor absorbing cells.

The full numerical scheme is applied to the model of a doped gradient waveguide, namely, an ensemble of two-level absorbers embedded in a transparent medium having a parabolic profile of the refraction index. The distribution of absorbing centers is homogeneous. We account for the saturation effect in the two-level absorbers, while the refraction in the transparent medium is linear. We study the output field at different modulation frequencies. Most of attention is paid to the transmission of the modulation signal. It is demonstrated that the nonlinear distortions of the output field are much smaller than those in the local response. The amplitude of transmitted modulation is minimal at frequencies close to the relaxation rate of the absorbers.

THEORY

Within the framework of scalar paraxial optics the system is described by normalized Maxwell-Bloch equations

$$2i\left(\frac{\partial E}{\partial z}+\frac{1}{c}\frac{\partial E}{\partial t}\right)+\nabla_{\perp}^{2}E-\nu^{2}r_{\perp}{}^{2}E=gP \tag{1}$$

$$\frac{\partial D}{\partial t}=-\gamma\left[D-1+i\left(E^{*}\,P-E\,P^{*}\right)\right] \tag{2}$$

$$\frac{\partial P}{\partial t}=-\left(\Gamma+i\Delta\right)-\frac{i}{2}\Gamma DE, \tag{3}$$

where g is the unit length absorption, γ,Γ are the population and polarization decay rates, respectively, $D(z,\vec{r}_{\perp},t)$ is the population difference normalized to its non-saturated value, $P(z,\vec{r}_{\perp},t)$ is the slow-varying amplitude of the polarization, Δ is the detuning of the carrier frequency of the field from the atomic transition frequency, ν is the parameter of the waveguide. For non-waveguide medium it is zero. The unit field amplitude corresponds to CW saturation with $D=0.5$. Eqs. (1)-(3) should be solved under the initial conditions

$$E(z=0,\vec{r}_{\perp},t)=E^{0}(\vec{r}_{\perp},t);\quad E(z,\vec{r}_{\perp},t=0)=0;\quad D(z,\vec{r}_{\perp},t=0)=1;\quad P(z,\vec{r}_{\perp},t=0)=0.$$

To solve Eqs. (1)-(3) we propose a second-order scheme making use of the decomposition of the transverse field pattern in terms of Gauss-Laguerre modes [8]. These modes are taken to be the eigenmodes of the empty linear waveguide when $\nu\neq 0$. Otherwise the mode beam parameter should be related to that of the initial beam. We introduce the discrete grid with the nodes $t_n=nh/c$, $z_k=kh$, ρ_i is the i-th radial

node, i=0,…,L, $\varphi_j = \dfrac{2\pi j}{2M+1}$ is the j-th azimuthal node, $j = 0,...,2M$; $l = 0,..,L$ is the number of radial nodes of the Gauss-Laguerre mode, $m = -M,...,M$ is the number of azimuthal nodes. In these notations the numerical algorithm may be presented as follows.

$$E_{n,k,i,j} \to C_{n,k,l,m}; \tag{4}$$

$$P_{n,k,i,j} \to F_{n,k,l,m}. \tag{5}$$

$$i\frac{C_{n+1,k+1,l,m} - C_{n,k,l,m}}{h} = b_{l,m}\frac{C_{n+1,k+1,l,m} + C_{n,k,l,m}}{2} + g\frac{F_{n,k+1,l,m} + F_{n,k,l,m}}{4} \tag{6}$$

$$C_{n+1,k,l,m} \to E_{n+1,k,i,j}; \tag{7}$$

$$c\frac{D_{n+2,k,i,j} - D_{n,k,i,j}}{2h} = -\gamma\left[\frac{D_{n+2,k,i,j} + D_{n,k,i,j}}{2} - 1 - 2\,\mathrm{Im}\left(E^*_{n+1,k,i,j}\frac{P_{n+2,k,i,j} + P_{n,k,i,j}}{4}\right)\right]; \tag{8}$$

$$c\frac{P_{n+2,k,i,j} - P_{n,k,i,j}}{2h} = -(\Gamma + i\Delta)\frac{P_{n+2,k,i,j} + P_{n,k,i,j}}{2} - i\frac{\Gamma}{2}E_{n+1,k,i,j}\frac{D_{n+2,k,i,j} + D_{n,k,i,j}}{2};$$

$$P_{n+2,k,i,j} \to F_{n+2,k,l,m}; \tag{9}$$

$$i\frac{C_{n+2,k+1,l,m} - C_{n+1,k,l,m}}{h} = b_{l,m}\frac{C_{n+2,k+1,l,m} + C_{n+1,k,l,m}}{2} + g\frac{F_{n+2,k+1,l,m} + F_{n+2,k,l,m}}{4} \tag{10}$$

$$C_{n+2,k,l,m} \to E_{n+2,k,i,j}. \tag{11}$$

The steps (4) and (5) are the direct Gauss-Laguerre transformations. The steps (7), (9) and (11) are the inverse Gauss-Laguerre transformations. The step (8) yields a set of two linear equations with respect to the pair of variables $\{D_{n+2,k,i,j}, P_{n+2,k,i,j}.\}$.

For propagation distances small compared with the modulation wavelength we use the approximation in which the field changes in time synchronously at any z. Then the Bloch equations (2), (3) can be solved separately in each layer Δz. For rough estimations at short traces one may also omit the diffraction terms in Eq. (1). We apply this model to non-waveguide media, so that $\nu = 0$. This yields the following scheme

$$E(z_{n+1}, \vec{r}_\perp, t) = E(z_n, \vec{r}_\perp, t) - i\frac{g}{2}P(z_n, \vec{r}_\perp, t)\Delta z \tag{12}$$

This approximation is, particularly, helpful to distinguish between the contributions to the output field from the local transient behavior of the medium and from the essentially wave nonlinear phenomena.

NUMERICAL SIMULATIONS

3.1. Thin nonlinear absorber. Local response is expected to manifest itself in almost unchanged way in a thin nonlinear absorber. Consider an initially Gaussian beam whose amplitude is harmonically modulated in time

$$E(0, r, t) = (E_0 - E_1\cos\Omega t)\exp(-r^2/w) \quad , \tag{13}$$

where E_0, E_1 are real constants, Ω is the modulation frequency, $r = |\vec{r}_\perp|$ in the axially symmetric system. We start from the numerical solution of the Bloch equations (2), (3). We take here =Γ=1, ν=0 , w=1 . When the frequency of modulation is much smaller than 1, the medium response follows the variations of the field amplitude adiabatically.

Considerable changes arise when Ω approaches 1. At very high frequencies the inertial medium is smoothing the fast oscillations of the field. Fig. 1 illustrates the effect of strong saturating field (curve 1) at Ω=2 and Δ=0. The medium response demonstrates transient behavior followed by periodic oscillations. The population difference oscillations (curve 2) are significantly delayed with respect to the field modulation. The population inversion $D<0$ takes place in the vicinity of each maximal value of the field amplitude. Note that in the adiabatic regime the minimal value of D is zero. The imaginary part of P demonstrates strongly anharmonic periodic oscillations, which is typical for high amplitudes of modulation $E_1 \sim E_0$. These oscillations are also shifted with respect to the modulation.

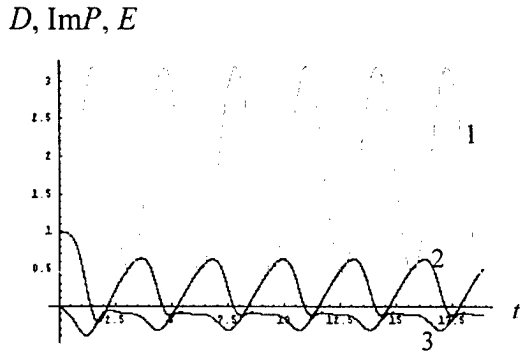


Fig. 1. Time dependence of the field amplitude E (1), the difference of populations D (2), and the imaginary part of the polarization P (3) for the case of exact resonance Δ=0. E_0=4., E_1=3., Ω=2., r=0.5.

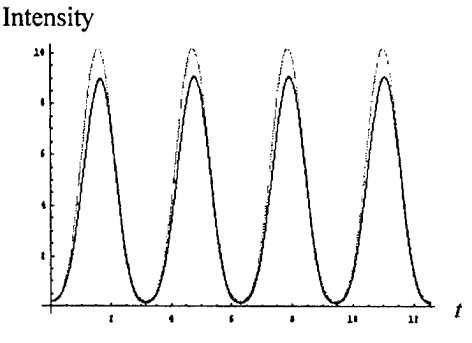


Fig. 2. The dependence of input (grey curve) and output (black curve) field intensity on time at r =0.5; Δ=0, E_0=4., E_1=3., Ω =2., Γ=1.5.

In the simplest case when the medium is optically thin, so that the difference between the input and output field is small enough, one can make use of the single-step scheme (4). Obviously, in this case the manifestations of the non-stationary response of the medium in the output field intensity are expected to be small, however they are detectable, as seen in Fig. 2. The output field intensity oscillation (black curve) is anharmonic and slightly delayed with respect to the harmonic modulation of the input field (grey curve).

Note that we consider the exact resonance self-action for which the real part of the polarization and thus the lens effect is zero in the purely absorbing layer. However, the absorption in the case considered is strongly nonlinear, since the maximal amplitude of the field in the beam is four times the saturation value. Therefore, the output intensity distribution is different from Gaussian; namely, the absorption is very small in the middle of the beam and very large in the off-axis region, where the field is weak. This is expected to cause the diffraction "self-focusing" [1,2] in the far zone. Consider the free propagation of the beam passed through the absorbing layer. The beam transverse profile is no more self-similar when moving along z-axis, and it is of interest to study the time modulation of the intensity depending on the position of a detector. It is remarkable that at different points this dependence may be very different, although in

the input field the law of the amplitude modulation is the same all over the beam cross section.

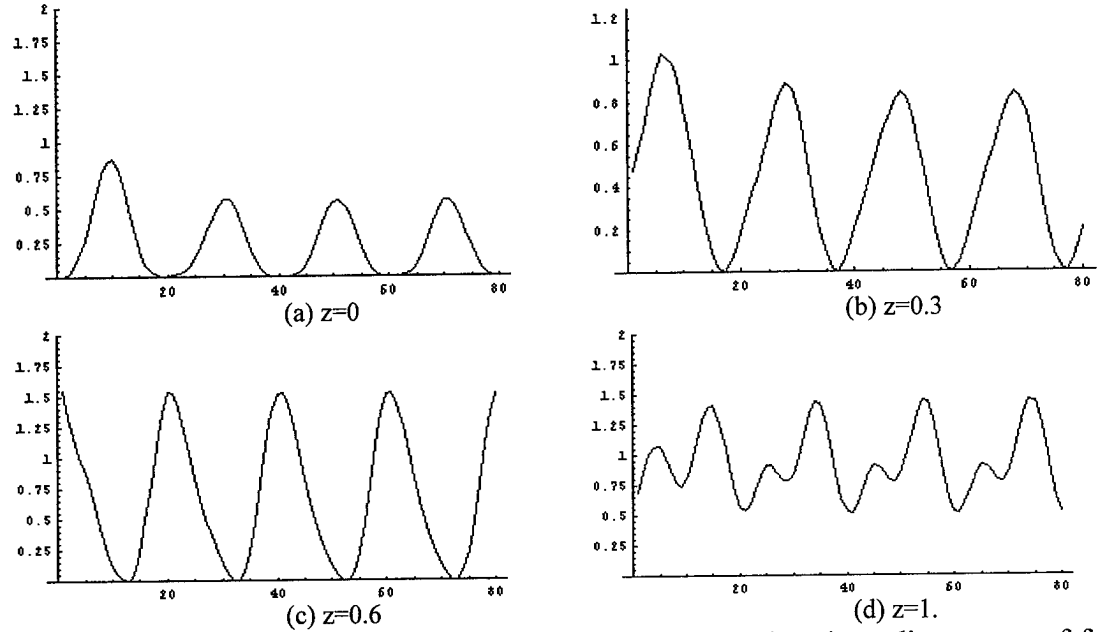


Fig. 3. Time dependence of the field intensity at r=0.5 and various distances z of free propagation after passing the thin nonlinear absorber. Δ=0, E_0=4., E_1=3., Ω =2., Γ=1.5.

3.2. Doped waveguide: full calculation: Now we remove the thin layer limitation and consider a doped waveguide, $\nu \neq 0$, by means of the general scheme (4)-(11). The incident field (13) is taken to be the linear waveguide fundamental mode with the beam radius w fitting the parameter ν in Eq. (1). We calculated the output field distribution at a given length $z=d$ as a function of time. At moderate levels of saturation the variations of the beam spot size and wave front curvature due to the resonant self-action in the waveguide appeared to be small. Here we focus our attention at the intensity modulation transmission to the output field. As follows from the preliminary calculations of the local response, one may expect significant distortion of the output field modulation under strong saturation conditions. It is an integral effect to which both the local delayed saturation and the non-stationary wave beam self-action contribute. To estimate this integral effect we calculated the output-to-input ratio of maximal intensities characterizing the transmission of the modulation signal versus the frequency of modulation (Fig. 4).

Fig. 5 illustrates the mechanism of the frequency dependence of the modulation transmission ratio. The time behavior of the field and the medium response are shown under the same conditions as in Fig. 4 at three different modulation frequencies. It is clearly seen that the time behavior of the medium response is drastically sensitive to the modulation frequency variations in the vicinity of the typical relaxation rate values. In this connection one might expect strong distortions of the modulation signal carried by a self-acting beam passing through a saturable absorber. However, even for high saturation our simulations revealed only a slight time delay of the output intensity with respect to the input one. The anharmonicity of the output signal remains negligible and the amplitude ratio varies between 80 and 90%.

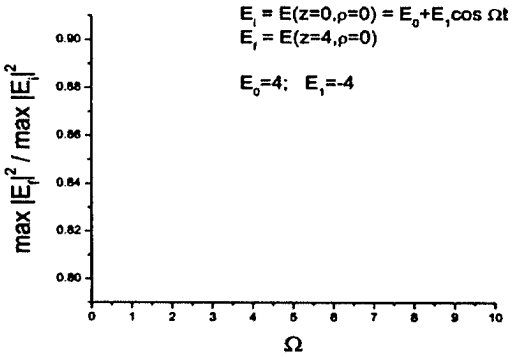


Figure 4. The output-to-input intensity amplitude ratio versus the modulation frequency. The input field is $E(0,0,t) = 4(1-\cos\Omega t)$, $\Delta = 0$, $z = 4$, $\gamma = \Gamma = 1$, $g = 1$.

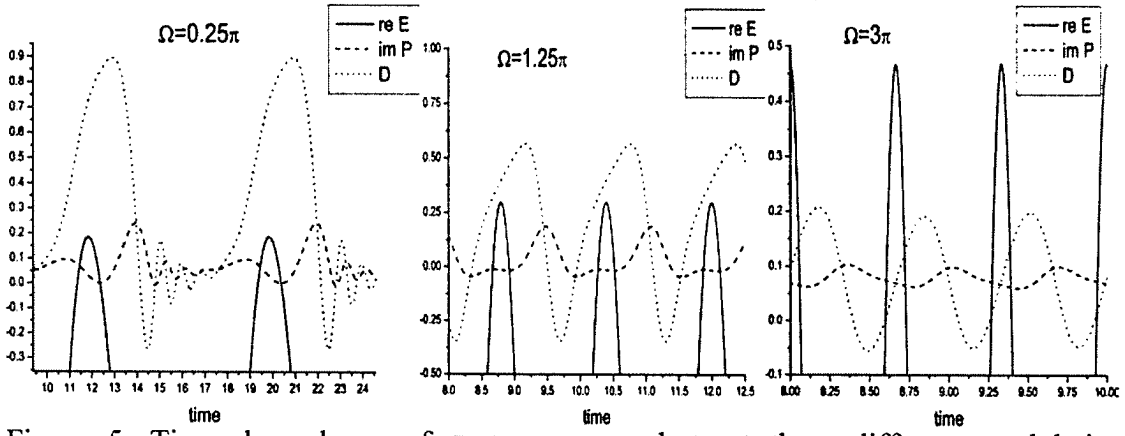


Figure 5. Time dependence of $\mathrm{Re}\,E$, $\mathrm{Im}\,P$, and D at three different modulation frequencies Ω .

ACKNOWLEDGMENTS

This work was supported in part by Award No. REC-006 of the U.S. Civilian Research & Development Foundation for the Independent States of the Former Soviet Union (CRDF).

REFERENCES

[1] M. LeBerre, E. Ressayre, A. Tallet, *Coherence and Quantum Opt. 5: Proc.5 Rochester Conf., 1983*, p. 331, 1984.

[2] K. Tai, H.M.Gibbs, et al., *Opt. Letters.*, **9**, 243 (1984).

[3] V.L. Derbov, L.A. Melnikov, A.D. Novikov, S.K. Potapov, *J. Opt. Soc. Amer. B*, **7**, 1076 (1990).

[4] M.L. Dowell., R.C. Hart, A. Gallagher, J. Cooper, *Phys. Rev. A.*, **53**, 1775 (1996).

[5] E.N. Bazarov, G.A. Gerasimov, V.P. Gubin, *Sov. J. Quant. Electron.*, **20**, 161 (1990).

[6] F.P. Mattar, M. Newstein, *Opt. Communs.*, **18**, 70 (1976).

[7] A.I. Konukhov, L.A. Melnikov, *Proc. SPIE*, **4243**, 12 (2000).

[8] L.A. Melnikov., V.L. Derbov, I.V. Veshneva., A.I. Konukhov. *Computers Math. Applic.*, **34**, 881 (1997).

ON THE SOLVABILITY AND APPLICATION OF NUMERICAL METHODS TO HALLEN'S EQUATION

George Fikioris

Department of Electrical and Computer Engineering
National Technical University of Athens, Greece
Email: gfiki@cc.ece.ntua.gr

ABSTRACT

Certain fundamental mathematical properties of Hallen's equation with the approximate kernel are discussed. Three cases are considered: **(1)** The delta-function generator, **(2)** the case of plane-wave incidence, and **(3)** the case of the frill generator. For a particular moment-method procedure (Galerkin's method with pulse functions), the consequences to the numerical solutions are examined. Generalizations to other numerical methods with subsectional basis functions are mentioned. Many of the results in this paper come from studying the simpler problem of the antenna of infinite length analytically and applying the understanding thus obtained to the case of the finite antenna.

INTRODUCTION

The simplest type of wire antenna or scatterer is the straight cylindrical dipole of length $2h$ and radius a. The integral equation satisfied by the current distribution on this antenna is usually referred to as Hallen's equation (HE). There are two choices of kernel, the exact and the approximate or reduced kernel. The approximate kernel is the focus of this paper.

Extensions of HE, or of the corresponding integro-differential equation of the Pocklington type (PE), apply to complicated, "real-life" structures such as curved wire antennas and arrays of wire antennas. Such equations are usually dealt with by moment methods. Therefore, it is important to thoroughly understand the difficulties associated with the application of moment methods to HE/PE. (It is true that blind application of numerical methods can often give good results; at the very least, a thorough understanding of the difficulties helps one trust—or distrust—one's results). It is especially important to know the types of error that can occur, as well as the reason for the errors.

Both HE and PE have been around for many, many years; they have been dealt with by moment methods since the mid-sixties. Nonetheless, for the case of the approximate kernel, and for subsectional basis functions, an in-depth study of the difficulties was only performed recently [1]. In [1], the antenna is center-driven by a delta-function generator. The underlying reason for the most important difficulties is the fact that, with the delta-function generator, neither HE nor PE has a solution, something which is frequently not mentioned in recent textbooks. In [2], the case of plane-wave incidence (receiving antenna) is considered. It is shown in [2] that HE/PE are, once again,

nonsolvable when the approximate kernel is used, and the difficulties resulting from this nonsolvability are discussed.

In the present paper, the results of [1] and [2] are summarized, and some new extensions to the case of the frill generator (which is generally considered to be a more precise feed than the delta-function generator) are outlined. The study of the finite-length antenna is helped by an analytical study of the antenna of infinite length.

INTEGRAL EQUATION AND NUMERICAL METHOD

Hallen's equation (HE) for the current $I(z)$ on an antenna of length $2h$ is

$$\int_{-h}^{h} K_{ap}(z-z')I(z')dz' = r(z), \qquad -h < z < h. \tag{1}$$

The RHS is **(1)** $r(z) = r_d(z) = [iV/(2\varsigma_0)]\sin k|z| + C\cos kz$, for the case of the delta-function generator; **(2)** $r(z) = r_r(z) = [iV/(2\varsigma_0)] + C\cos kz$, for the case of the receiving antenna, **(3)** $r(z) = r_f(z) = (1/k)\int_0^z g_f(t)\sin k(z-t) + C\cos kz$, where

$$g_f(z) = \frac{ikV}{2\varsigma_0 \ln(b/a)}\left[\frac{\exp(ik\sqrt{z^2+a^2})}{\sqrt{z^2+a^2}} - \frac{\exp(ik\sqrt{z^2+b^2})}{\sqrt{z^2+b^2}}\right], \tag{2}$$

for the case of the frill generator. V is the driving voltage, $\varsigma_0 = 376.73$ Ohms, C is a constant to be determined from the condition $I(\pm h) = 0$, and k is the free-space wavenumber. For the case **(3)** of the frill-generator, the above HE can be deduced from the PE provided in [3, pg. 394]; the RHS of PE is $g_f(z)$. In (2), *a (b)* is the inner (outer) radius of the feeding coaxial transmission line.

The approximate kernel $K_{ap}(z)$ given by

$$K_{ap}(z) = \frac{1}{4\pi}\frac{\exp(ik\sqrt{z^2+a^2})}{\sqrt{z^2+a^2}}, \tag{3}$$

where a is the antenna radius. As opposed to $K_{ap}(z)$, the so-called exact kernel $K_{ex}(z)$ [1] is logarithmically singular at $z=0$.

Our numerical method is Galerkin's method with pulse functions, as described in detail in [1]. There are $2N+1$ pulse basis functions $u_n(z)$, each of width z_0, so that $(2N+1)z_0 = 2h$. For $n=0$, the basis function $u_0(z)$ is centered at the driving point $z=0$.

DELTA-FUNCTION GENERATOR: NONSOLVABILITY

Suppose that the delta-function generator is used together with the approximate kernel. Under mild admissibility conditions on $I(z)$, one can pass a derivative inside the integral on the LHS of (1), and then set $z = 0$. Therefore, the LHS of (1) is differentiable at $z = 0$. On the other hand, because of the absolute value sign, the RHS $r_d(z)$ is not differentiable at $z = 0$. This argument shows that, for the delta-function generator, the

integral equation does not have a solution when the approximate kernel is used. Physically, this equation requires a line current located on the z-axis to maintain a field with a delta-function behavior at $\rho = a, z = 0$, and this is not possible.

This nonsolvability was known as far back as 1952 [4], but is frequently not mentioned in recent textbooks. The nonsolvability naturally gives rise to the following two questions: (1) What does one obtain if one applies a numerical method involving a large number of basis functions? (2) Under what conditions are numerical solutions obtained with the two kernels similar, and in what sense? We address these questions in what follows.

DELTA-FUNCTION GENERATOR: INFINITE ANTENNA

We refer, still, to the case of the delta-function generator. Much understanding is obtained if the numerical method is applied to the antenna of **infinite** length, in which $h = \infty$. Here, we are dividing the entire real axis into segments of length z_0, where kz_0 is small. The full procedure is described in [1]. Briefly, the method yields a (doubly) infinite Toeplitz system of algebraic equations in which z_0 appears as a parameter. The infinite system is solved exactly for nonzero z_0. Then, the exact solution is developed asymptotically for the case where z_0 is small or, more precisely, when z_0 is much smaller than the radius a. The final asymptotic formula for the "numerical solution" I_n turns out to be

$$I_n \approx \frac{-iV}{\varsigma_0}\frac{\pi^3}{32\sqrt{2}}kz_0\sqrt{\frac{z_0}{a}}(-1)^n \exp\left(\frac{a\pi}{\varsigma_0}\right)\frac{1}{\cosh\left(\frac{\pi}{2}\frac{z_0}{a}n\right)}, \quad z_0 << a. \tag{4}$$

This formula reveals that, for sufficiently small pulse width, the numerical method yields an exponentially large, purely imaginary "driving-point admittance" and a large, purely imaginary, rapidly oscillating "current," at least for points on the antenna not too far from the driving point.

On the other hand, the numerical method yields a finite real part $\mathrm{Re}\{I_n/V\}$ of the current. Furthermore, this real part is close to the corresponding quantity when the exact kernel is used. These facts are shown analytically in [1].

DELTA-FUNCTION GENERATOR: FINITE ANTENNA

Let us now return to the antenna of **finite** length, still driven by a delta-function generator. We assume that the approximate kernel is used with $z_0 << a$. Here, this condition is the same as $N >> h/a$. In light of the analytical results for the infinite antenna, it is logical to expect that the real part $\mathrm{Re}\{I_n/\mathrm{V}\}$ of the numerical solution is close to that obtained with the exact kernel. On the other hand, near the driving point, the values $\mathrm{Im}\{I_n/\mathrm{V}\}$ are large and oscillate rapidly. In fact, the values $\mathrm{Im}\{I_n/\mathrm{V}\}$ are very closely approximated by the corresponding values for the case of the infinite antenna and the asymptotic formula (4).

The above assertions have been verified by extensive numerical calculations. An interesting corollary is that the initial values of $\mathrm{Im}\{I_n/\mathrm{V}\}$ are independent of the length h of the antenna, they depend only on a and z_0. Numerical calculations also reveal another feature when $z_0 << a$, an oscillatory behavior near the endpoints $z=\pm h$ (or $n=\pm N$). These last oscillations occur both in $\mathrm{Re}\{I_n/\mathrm{V}\}$ and in $\mathrm{Im}\{I_n/\mathrm{V}\}$.

The oscillations near the driving point/endpoints are the main consequences of the nonsolvability of the integral equation; the important parameter is h/a. The analytical study is useful because analytical predictions are free of roundoff errors, to which—as is typical in Fredholm integral equations of the first kind—the numerical solutions are highly susceptible. Roundoff error/matrix ill-conditioning is a separate but also important effect.

We have extended [1] the above conclusions to a number of other numerical methods, as well as to numerical methods applied to Pocklington's equation.

FINITE RECEIVING ANTENNA

We now turn to the case of the finite receiving antenna. It is natural to inquire whether the integral equation has a solution. The nonsolvability argument given above does not apply because $r_r(z)$ is differentiable at $z=0$. Nonetheless, the integral equation is once again nonsolvable. The relevant argument of [2] proceeds, in summary, as follows.

Assume that a *continuous* function $I(z')$ satisfies the integral equation (1). Both the LHS and the RHS are initially defined for real z between $-h$ and h, and are equal for those values of z. Now think of z as a complex variable and consider values of z not lying on the line segment $-h<z<h$. Obviously, the RHS $r_r(z)$ is an analytic function of z. As a consequence of the continuity of $I(z)$ and the analyticity of the approximate kernel $K_{ap}(z)$, we have shown [2] that the LHS is also an analytic function of z. We are thus considering the analytic continuations (to complex values of z) of the two sides of the equation.

Take, in particular z to be large. For any $I(z')$, the LHS of (1) oscillates and decays like $1/z$ for large z (or faster, if the coefficient of $1/z$ happens to vanish). For any choice of C, however, the RHS of (1) cannot decay like $1/z$. Since the two functions defined for real z between $-h$ and h have analytic continuations which are not the same, they themselves cannot be the same. This is because analytic continuation is unique. This contradiction shows that the integral equation for the finite receiving antenna has no (continuous, at least) solution. It is stressed that this nonsolvability argument does not apply when the exact kernel is used because that kernel is singular.

Numerical calculations show that the main consequence of this nonsolvability is the appearance of oscillations near the endpoints $z=\pm h$ (or $n=\pm N$). These oscillations occur, once again, when $N>>h/a$. This time, there are no oscillations near the center $z=0$ of the antenna.

THE CASE OF THE FRILL GENERATOR

When the antenna is center-driven by a frill generator, the situation turns out to be quite different from the case of the delta-function generator. For the case of the frill generator and for the approximate kernel, we have shown that

1. For the **infinite** antenna, both HE and PE are solvable. (In contrast to the delta-function generator case, where HE and PE are nonsolvable). In fact, the solution can be determined explicitly by applying a spatial (in z) Fourier transformation. This works because the integral on the LHS is a convolution: One easily ends up with an integral representation of the solution. The key point is that one ends up with a convergent integral. (This should be contrasted to the case [1] of the delta-function generator, where the corresponding integral diverges).

2. For the **infinite** antenna, we can apply Galerkin's method with pulse basis functions to HE. We have shown analytically that the numerical solution thus obtained converges to the true solution in the limit of pulse basis functions of zero width.

3. For the **finite** antenna, in contrast to the case of infinite length, HE and PE are nonsolvable. The argument here proceeds from PE as follows: As in the case of the receiving antenna, the LHS of the integral equation is an analytic function of z. However, the RHS $g_f(z)$ is nonanalytic when $z=\pm ib$. (Specifically, these two points of non-analyticity are branch points). This contradiction demonstrates nonsolvability of PE, and nonsolvability of HE follows immediately.

With the approximate kernel, the LHS of the PE is (apart from a multiplicative constant) the z-component of the electric field on the cylindrical surface $\rho=a$, $|z|<h$; the source maintaining this field is a *line source I(z)*, located on the z-axis between $-h$ and h. Our nonsolvability result states that no line source $I(z)$ can maintain a field equal to the specific $g_f(z)$. This result is by no means peculiar because, on a cylindrical observation surface, a line source cannot maintain an arbitrary field. To clarify this point further, we briefly discuss some similarities to the classical synthesis problem (SP) in which one seeks a line source maintaining a prescribed radiation field: This SP is governed by an integral equation [5], but the observation surface is a spherical surface at infinity, not a cylindrical surface at finite distance. In order to have a solvable SP, one cannot arbitrarily specify the radiation field and in fact, the class of "realizable" radiation patterns is a rather narrow one [5]. (A given pattern—function of the complex variable $\sin\theta$, where θ is the observation angle—is realizable if and only if it is an "entire function of exponential type" [5,6]). Like the nonsolvability result of the present paper, the above result for the SP: (1) is based on the theory of functions of a complex variable; (2) has as a key hypothesis the *finite extent* of the line source. Therefore, the integral equation of an arbitrary SP is likely to be nonsolvable, as are the integral equations herein.

In the literature, one finds many integral equations that use the approximate kernel. By now, it should be clear that "most" of them are nonsolvable. The aforementioned

solvable integral equations for an **infinite** antenna driven by a frill generator are therefore exceptional.

4. If we apply Galerkin's method with pulse basis functions to the **finite** antenna, it is logical to expect that, near the driving point, the numerical solutions should resemble those of the infinite antenna. In particular, one should not expect oscillations near the driving point. We have verified this by extensive numerical calculations.

5. In contrast, one should expect that the numerical solutions oscillate near the endpoints of the antenna. We have verified this numerically. The oscillating values occur, once again, when $z_0 << a$; furthermore, these oscillating values are numerically close to the corresponding values for the case of the delta-function generator.

CONCLUSION

In summary, the solvability/nonsolvability of some fundamental integral equations for straight wire antennas with the approximate kernel were discussed. It was found that "most" such integral equations are nonsolvable. (The integral equation for an **infinite** antenna center-driven by a frill generator is an instructive exception to this rule.) When subsectional basis functions are used in moment methods for **finite** antennas, the main consequence of this nonsolvability is the appearance of rapid oscillations, both in the real and the imaginary parts of the solution, near the endpoints of the antenna. For the case of the delta-function generator, the imaginary part also oscillates rapidly near the driving-point (center) of the antenna. Numerically, these last oscillating values are very close to those for the case of the infinite antenna; these are (perhaps surprisingly) *exponentially* large in N. All oscillations occur when $z_0 << a$, or $N >> h/a$.

We stress that all oscillations discussed herein are not due to roundoff error. As a consequence, they do not depend on the particular hardware and software used, and they cannot be overcome by using more powerful computers. Roundoff error is also important; but it is a separate and in a sense secondary effect (Even in the case of roundoff error, the important parameter is h/a.)

REFERENCES

[1] G. Fikioris and T. T. Wu, "On the application of numerical methods to Hallen's equation," IEEE Trans. Antennas Propagat., vol. 49, pp. 383—392, March 2001.
[2] G. Fikioris, "The approximate integral equation for a cylindrical scatterer has no solution," J. of Electromagn. Waves and Appl., vol. 15, pp. 1153—1159, 2001.
[3] C. A. Balanis, *Antenna Theory: Analysis and Design,* 2nd ed. New York: John Wiley & Sons, 1997.
[4] S. A. Schelkunoff, *Advanced Antenna Theory.* New York, John Wiley & Sons, 1952.
[5] D. S. Jones, *Methods in Electromagnetic Wave Propagation,* 2nd ed. New York: IEEE Press, 1995, pp. 605—608.
[6] N. I. Achieser, *Theory of Approximation.* New York: Dover Publications, Inc., 1992, pp. 130—137.

SOME CLASSES OF NONLINEAR SYNTHESIS PROBLEMS FOR RADIATION SYSTEMS: THEORY AND METHODS OF SOLUTION

P. O. Savenko, B. M. Podlevskii, M. D. Tkach, M. I. Andriychuk

Pidstryhach Institute of Applied Problems of Mechanics & Mathematics, NASU
3b Naukova St., 79601, Lviv, Ukraine
Phone: +380 322 651944, E-mail: andr@iapmm.lviv.ua, savenko@iapmm.lviv.ua

ABSTRACT

The theory and methods to solve some classes of the nonlinear inverse problems arising in the process of synthesis of the radiating systems are stated. The requirements to the amplitude radiation pattern and restrictions on the distribution of the extrinsic electromagnetic fields excitation sources in the variational statements of problems are prescribed. Investigation of the structure and properties of solutions for the nonlinear integral equations, which are the Euler equations of the corresponding functionals, is based on the methods of nonlinear analysis. The iterative processes for the numerical determination of solutions are constructed and substantiated. The results of analytical and numerical investigations of the synthesis problems for various types of the antenna arrays, as well as the synthesis problem of the hybrid antenna systems are presented.

INTRODUCTION

In the first part of paper, the problems of the amplitude-phase and phase synthesis of the antenna arrays (AAs) according to the prescribed amplitude radiation pattern (RP) with due regard for the mutual coupling of radiators are considered. The absence of requirements to the phase RP is used as an additional possibility to improve the approximation quality of modules of the given and synthesized RP, but the incompleteness of initial data in the condition of problem generates a class of nonlinear essentially ill-posed problems. In this connection, the AAs mathematical models of the various degree of accuracy, allowing to take into account the mutual coupling of radiators, are used. The theorems of existence of the quasi-solutions in the appropriate spaces are proved.

It is shown that the non-uniqueness and branching of the solutions appear for the considered problems. This branching depends on properties of the prescribed amplitude RP, geometry and basic parameters of the considered array. The methods of nonlinear functional analysis allowing to locate the branching solutions are applied for investigation of solutions and determination of their number and qualitative characteristics. Such approach to considerable extent simplifies determination of the optimal solutions using the numerical methods. The iterative processes for the numerical solving the corresponding non-linear equations are constructed. The theorems of convergence and relaxation are proved.

In the second part of paper, the nonlinear synthesis problems of the hybrid mirror and lens antennas, as well as the synthesis on their basis of the contour RPs of the fixed and

changeable form are considered. The idea of synthesis of the partial beams having in a cross section the rectangular or triangular form is offered as a basis of approach to synthesize the RP of the changeable form. It allows to synthesize the contour RP without the critical zones.

SYNTHESIS OF ANTENNA ARRAYS ACCORDING TO THE PRESCRIBED AMPLITUDE RP WITH DUE REGARD FOR THE MUTUAL COUPLING OF RADIATORS

The asymptotic of solution of the electromagnetic (EM) field excitation problem in the unlimited homogeneous isotropic space (with dielectric permittivity ε and magnetic permeability μ) by the extrinsic EM sources, that are localized in some area $\overline{V} \subset \mathbb{R}^3$ and have the time-harmonic dependence $e^{i\omega t}$ (ω is the circular frequency), in the spherical coordinate system at $r \to \infty$, is given in [7, 8]

$$\boldsymbol{E}(r,\vartheta,\varphi) = -i\omega\mu \frac{e^{-ikr}}{4\pi r}\{0, f_\vartheta(\vartheta,\varphi), f_\varphi(\vartheta,\varphi)\},$$
$$\boldsymbol{H}(r,\vartheta,\varphi) = ik \frac{e^{-ikr}}{4\pi r}\{0, f_\varphi(\vartheta,\varphi), -f_\vartheta(\vartheta,\varphi)\}, \qquad (1)$$

where $\boldsymbol{E}$, and $\boldsymbol{H}$ are the vectors of complex amplitudes of intensity of the electrical and magnetic fields, f_ϑ , f_φ are the components of the vector RP.

Abstracting from specific type of radiating system, we present the functions f_ϑ and f_φ in the formulas (1) using the linear operator $A = \{A_\vartheta, A_\varphi\}$:

$$\boldsymbol{f} = A\boldsymbol{I}, \quad (f_\nu = A_\nu \boldsymbol{I}, \quad \nu = \vartheta,\varphi). \qquad (2)$$

This operator acts from some complex Hilbertian space H_I, to which the functions of distribution of currents (fields) $\boldsymbol{I}$ belong, into the complex space $C_f^{(2)} = C[\Omega] \oplus C[\Omega]$ of vector-valued continuous functions on the compact $\overline{\Omega} \in \mathbb{R}^2$ (or $\overline{\Omega} \in \mathbb{R}^1$). This space has the scalar product and norm, and it includes a set of the realized RPs. The form and properties of the operators A_ν depend on a type and geometry of radiating system. In particular, one notes that the operator A for the considered types of the radiating systems is the fully continuous one.

In the simplest case, the synthesis problem of radiating system according to the prescribed amplitude RP can be formulated as a problem to determine the solution of nonlinear operator equation [1]

$$|A\boldsymbol{I}| \equiv (|A_\vartheta \boldsymbol{I}|^2 + |A_\varphi \boldsymbol{I}|^2)^{1/2} = F, \qquad (3)$$

where $F = \left(F_\vartheta^2 + F_\varphi^2\right)^{1/2}$ is the amplitude RP given in the area $\overline{\Omega} \in \mathbb{R}^2$ (or $\overline{\Omega} \in \mathbb{R}^1$). If F does not belong to area of values of the operator $|A\boldsymbol{I}|$, the problem (3) is essentially incorrect [35]. In this case, all three classical conditions of correctness by Adhamar, namely existence and uniqueness of solution, as well as the continuous dependence of

solution on change of the initial data, cannot satisfy. Therefore the problems of search of the quasi-solutions that satisfy the certain criteria are considered for the equation (3).
A key role in the process of solution of the synthesis problems represents the solution of the analysis problem. The mathematical models of arrays of the various rigor and accordingly exactness are used to solve the analysis problems of array [5, 36].
General methods of solution of the synthesis problems are developed most fully for the case, when the RP of array satisfies the theorem of multiplication of the RPs. Such mathematical model of array allows to take into account the mutual coupling of radiators only in the first approximation. The more exact mathematical models of arrays are based on the strong electrodynamic statements of the analysis problems, which are reduced to the solution of the electrodynamic boundary problems. For such problems the number of boundary surfaces coincides with the radiator number of array [6, 17].
As a rule, the type and configuration of radiators, their number, the geometry of array, as well as the character of an environment are taken into account in the process of statement and solution of the analysis problems.
The method of the integral equations is one of the most universal and adequate for the practical analysis problems of arrays. In particular, the integral equations with respect to the electrical currents $\boldsymbol{J}_n^e(P)$ on $2N+1$ surfaces S_n of ideally conducting radiators which are placed in homogeneous isotropic space, can be written by the reason of the boundary condition $\boldsymbol{E}_\tau = 0$ as [5]

$$[[\boldsymbol{n}_m \times (\text{grad div} + k^2) \sum_{n=-N}^{N} \int_{S_n} \boldsymbol{J}_n^e(P) G(Q,P) ds_n] \times \boldsymbol{n}_m] = -i\omega\varepsilon[[\boldsymbol{n}_m \times \boldsymbol{E}_m^{cm}(P_m)] \times \boldsymbol{n}_m],$$
$$(m = -N \div N) \tag{4}$$

where $\boldsymbol{n}_m$ is the normal vector to the surface of the m-th radiator, $G(Q,P)$ is the Green function, $\boldsymbol{E}_m^{cm}(P_m)$ is the extrinsic electrical field. The equation system (4) can be written as system of the linear integral equations of first kind

$$\sum_{n=-N}^{N} \int_{S_n} \boldsymbol{J}_n^e(Q_n') K_{nm}(Q_n, Q_m') ds_n = \boldsymbol{E}_{\tau m}^{cm}(Q_m) \quad (m = -N \div N), \tag{5}$$

where $K_{nm}(Q_n, Q_m')$ is matrix kernel, $\boldsymbol{E}_{\tau m}^{cm}(Q_m)$ is the tangential component of a vector $\boldsymbol{E}_m^{cm}(Q_m)$ on a surface of m-th radiator. It is known [35], that the integral equations of first kind have an unstable solution. However, the kernel of the Green function type, having singularity at $Q_n \to Q_m'$, allows to construct stable algorithms for the numerical search of solutions of the integral equation (5)[1] using the regularization methods [35].
We write system (5) in the operator form as

$$B\boldsymbol{J}^e = \boldsymbol{E}^{cm}. \tag{6}$$

Here B is the linear matrix-integral operator carrying out a continuous one-to-one transformation from the metric space H_J into the metric space H_E.

[1] Note that the self-regularization method for solving the integral equation systems, that have the logarithmic singularity in the kernel, was proposed by Tikhonov and Dmitriev in [36]

If in space H_J is allocated a compact class of the solutions $\omega_J \subset H_J$, on which the problem $B\boldsymbol{J}^e = \boldsymbol{E}^{cm}$ is correct, that is the operator B^{-1} is continuous on an image $B(\omega_J) \subset H_E$, then the solution of system (6) can be presented by $\boldsymbol{J}^e = B^{-1}\boldsymbol{E}^{cm}$.

Using this expression and the equality (2), we receive obvious dependence of the RP of array on the extrinsic sources [29, 30]

$$\boldsymbol{f} = AB^{-1}\boldsymbol{E}^{cm}, \quad (f_\nu = A_\nu \boldsymbol{Z}^{-1}\boldsymbol{U} \qquad \nu = \vartheta, \varphi), \tag{7}$$

which allows to consider the synthesis problems of arrays taking into account the mutual coupling of their elements, in the case when $\boldsymbol{E}^{cm} \in B(\omega_J) \subset H_E$.

We assume that prescribed amplitude RP is given as a finite function $F \in C_f^{(2)}$ with the compact carrier $\overline{\Omega} \in \mathbb{R}^2$ (or $\overline{\Omega} \in \mathbb{R}^1$). The synthesis problem of arrays we formulate as a problem of search of such distribution of the extrinsic electrical field on surfaces of radiators $\boldsymbol{E}^{cm} = \{\boldsymbol{E}^{cm}_{-N}, \boldsymbol{E}^{cm}_{-N+1}, \ldots, \boldsymbol{E}^{cm}_{N}\}$, which would minimize the smoothing functional

$$\sigma_{F_a}(\boldsymbol{U}) = \| F_\vartheta - | A_\vartheta \boldsymbol{Z}^{-1}\boldsymbol{E}^{cm} | \|^2_{C^{(2)}_{(\overline{G})}} + \| F_\varphi - | A_\varphi \boldsymbol{Z}^{-1}\boldsymbol{E}^{cm} | \|^2_{C^{(2)}_{(\overline{G})}} + \alpha \| \boldsymbol{E}^{cm} \|^2_{H_E} \tag{8}$$

in the Hilbertian space $H_E = L_2(V) \oplus L_2(V) \oplus \ldots \oplus L_2(V)$.

Differentiating the functional (8) by Gateaux and using the condition of the functional extremum, we receive the equation concerning the vector $\boldsymbol{E}^{cm}$

$$\begin{aligned} \alpha \cdot \boldsymbol{E}^{cm} &= -\widetilde{B}^{*^{-1}} A^*_\vartheta A_\vartheta \widetilde{B}^{-1}\boldsymbol{E}^{cm} - \widetilde{B}^{*^{-1}} A^*_\varphi A_\varphi \widetilde{B}^{-1}\boldsymbol{E}^{cm} + \\ &+ \widetilde{B}^{*^{-1}} A^*_\vartheta \left(F_\vartheta e^{i \arg A_\vartheta \widetilde{B}^{-1}\boldsymbol{E}^{cm}} \right) + \widetilde{B}^{*^{-1}} A^*_\varphi \left(F_\varphi e^{i \arg A_\varphi \widetilde{B}^{-1}\boldsymbol{E}^{cm}} \right) \end{aligned} \tag{9}$$

on the basis of necessary condition of the functional extremum. In (9), $\widetilde{B}$ is the operator obtained from B by means of regularization.

If the zero set of the operator $A\widetilde{B}^{-1}$ consists only of a zero element, then assuming in (9) $f_{\vartheta,\varphi} = A_{\vartheta,\varphi}\widetilde{B}^{-1}\boldsymbol{E}^{cm}$ and acting on both parts of equality (9) by the operators $A_\vartheta \widetilde{B}^{-1}$, and $A_\varphi \widetilde{B}^{-1}$, we receive equivalent to (9) equations

$$\begin{aligned} \alpha \cdot \begin{pmatrix} f_\vartheta \\ f_\vartheta \end{pmatrix} &= - \begin{pmatrix} A_\vartheta \widetilde{B}^{-1}\widetilde{B}^{*^{-1}} A^*_\vartheta & A_\vartheta \widetilde{B}^{-1}\widetilde{B}^{*^{-1}} A^*_\varphi \\ A_\varphi \widetilde{B}^{-1}\widetilde{B}^{*^{-1}} A^*_\vartheta & A_\varphi \widetilde{B}^{-1}\widetilde{B}^{*^{-1}} A^*_\varphi \end{pmatrix} \begin{pmatrix} f_\vartheta \\ f_\vartheta \end{pmatrix} + \\ &+ \begin{pmatrix} A_\vartheta \widetilde{B}^{-1}\widetilde{B}^{*^{-1}} A^*_\vartheta & A_\vartheta \widetilde{B}^{-1}\widetilde{B}^{*^{-1}} A^*_\varphi \\ A_\varphi \widetilde{B}^{-1}\widetilde{B}^{*^{-1}} A^*_\vartheta & A_\varphi \widetilde{B}^{-1}\widetilde{B}^{*^{-1}} A^*_\varphi \end{pmatrix} \begin{pmatrix} F_\vartheta e^{i \arg f_\vartheta} \\ F_\varphi e^{i \arg f_\varphi} \end{pmatrix} \end{aligned} \tag{10}$$

with respect to the components of the synthesized RP. The equation (9) and (10) are the nonlinear operator equations of the Hammerstein type.

The theorems of existence of at least one points of an absolute minimum of the functional (8) in the Hilbertian space H_E are proved in [3, 20, 24, 34]. Since the functional (8) is growing and has m – property, then it follows from the existence

theorem that the equation (9) in the space H_E, and equation (10) in the space $\boldsymbol{C}^{(2)}_{(\bar{\Omega})}$ accordingly have at least one solution.

The equation (9) and (10) are the basic equations of synthesis for various types of radiating systems according to the prescribed amplitude RP. Their expanded form depends on the type of radiators and geometry of array [2, 9, 29, 30, 32].

The methods of the solutions branching theory of the nonlinear equations [37] are used for investigation of the number of the equation (10) solutions and qualitative characteristics of them.

The use of methods of the nonlinear analysis allows to determine the number and qualitative characteristics of the solution of (10) for a series of specific types of the antenna arrays. These characteristics depend on the prescribed amplitude RP and geometry of array [11, 12, 19, 21, 22, 23]. The general structure of the investigated solutions is established. It allows to locate the existing solutions and thus to a considerable extent to simplify their numerical determination.

The properties of solutions of the equation (10) for linear array consisting of thin cylindrical radiators [10], linear array consisting of conic spiral radiators [30], microstrip array consisting of rectangular radiators [32, 33], and waveguide array [2] (two-dimensional problem) are investigated.

The iterative processes for numerical determination of solutions are constructed. The implicit scheme of the method of successive approximation is used in such processes [1, 24, 25]. In particular, the iterative process to solve the equation system (10) has the form

$$\alpha\cdot\begin{pmatrix} f_\vartheta^{(n+1)} \\ f_\varphi^{(n+1)} \end{pmatrix}+\begin{pmatrix} A_\vartheta\widetilde{B}^{-1}\widetilde{B}^{*^{-1}}A_\vartheta^* & A_\vartheta\widetilde{B}^{-1}\widetilde{B}^{*^{-1}}A_\varphi^* \\ A_\varphi\widetilde{B}^{-1}\widetilde{B}^{*^{-1}}A_\vartheta^* & A_\varphi\widetilde{B}^{-1}\widetilde{B}^{*^{-1}}A_\varphi^* \end{pmatrix}\begin{pmatrix} f_\vartheta^{(n+1)} \\ f_\varphi^{(n+1)} \end{pmatrix}=$$

$$=\begin{pmatrix} A_\vartheta\widetilde{B}^{-1}\widetilde{B}^{*^{-1}}A_\vartheta^* & A_\vartheta\widetilde{B}^{-1}\widetilde{B}^{*^{-1}}A_\varphi^* \\ A_\varphi\widetilde{B}^{-1}\widetilde{B}^{*^{-1}}A_\vartheta^* & A_\varphi\widetilde{B}^{-1}\widetilde{B}^{*^{-1}}A_\varphi^* \end{pmatrix}\begin{pmatrix} F_\vartheta e^{i\arg f_\vartheta^{(n)}} \\ F_\varphi e^{i\arg f_\varphi^{(n)}} \end{pmatrix}, \qquad (11)$$

where n is the number of iteration. In essence, the corresponding to (10) linear system of equations is solved in each step of iteration. The results of investigation of the solution properties of (10) by the methods of branching theory are used in the process of choice of the initial approximation. The theorems of convergence and relaxation properties of (11) relatively of the functional (8) are proved.

The phase synthesis problems of arrays are considered with due regard for the mutual coupling of radiators, which are excited by the concentrated electromotive power [10]. The amplitude RP and amplitude distribution of extrinsic potentials are prescribed in this case; the phase distribution of extrinsic potentials is sought for. The synthesis results of microstrip array and array consisting of linear half-wave vibrators are presented.

The computing experiments show that freedom of choice of the phase RP allows (at the certain values of geometrical parameters of array) to decrease on 40 % the value of functional σ_{F_α} in comparison with the solutions belonging to a class of the in-phase RPs [9]. As a result of calculations, it is established that the relative error of mathematical models of arrays, which do not take into account the mutual coupling of

radiators, in comparison with mathematical models of arrays taking into account such coupling, is approximately 10% in the region of sidelobes.

SYNTHESIS OF THE MULTI-BEAM AND CONTOUR RADIATION PATTERNS USING THE HYBRID ANTENNA SYSTEMS

The use of approach proposed above for the synthesis problems of the hybrid antenna systems is considered. At the beginning, a generalized problem of synthesis of one-reflector antenna consisting of some radiator and a cut of the ideally conducting reflector of the parabolic form is proposed. In this case we find such RP of the radiating element and such form of the reflector cut, which form the amplitude RP which would be maximally close (in the mean-square approximation) to the required one. The functional like (8) with the account of the additional restrictions on the electromagnetic field in the reflector surface and on the form of cut from it is used as the optimization criterion of the form of reflector cut and the induced currents on it. The minimization problem of the constructed functional is reduced to solving the appropriate set of the Euler equations. If the amplitude RP should have a special form (quadrate, triangle etc.), the optimization of the form of cut is an additional possibility, which can improve the effectiveness of synthesis in ranges 50 % in a comparison with the non-optimized antenna [4, 26, 27].

The synthesis problem of the hybrid reflector antenna consisting of non-symmetric ideally conducting reflector and radiating array is considered too. The synthesis problem is solved as the problem of determination of such amplitude-phase distribution $\boldsymbol{J} = \{J_1, J_2, \ldots J_N\}$, ($N$ is the quantity of radiators) in the radiating array, which minimizes the functional (8). As the result, we obtain a set of equations with respect to the optimal currents or nonlinear equation for the synthesized RP. Such approach can be applied to a wide class of antennas of this type, and the numerical algorithm of solving the problem does not superimpose any restrictions on the placement of elements of the radiating array. It can be both the flat and the conformal arrays. In particular, their phase centers can be taken out from the focal plane of reflector [13, 28].

The hybrid lens antenna consisting of TEM-lens of the Rotman type and radiating array [18] is investigated. The synthesis problem of multi-beam system is considered in various statements, in particular, the synthesis problem of not only the summary RP, but also the partial one is considered. In the last case, we obtain an optimal partial RP, which has in its cross-section the rectangular or triangular form. It allows to obtain a contour RP without critical zones in the region of upkeep. We also note that using the obtained partial RP of the special form, we can form some contour RP by simple inclusion-expelling of active elements of the radiating array [4, 31].

The synthesis problems of contour RP on the basis of hybrid mirror antenna with a flat radiating array, which radiates some area of a terrestrial surface (region of upkeep) [14, 15, 16] is considered too.

CONCLUSION

1. The stated on the operator basic the methods of solution of the non-linear inverse problems allow to solve the synthesis problem for antenna systems using the various on accuracy mathematical models of the radiating systems. To solve the synthesis problem of the specific antenna or antenna array, it is necessary to determine the operators A and A^* accordingly, and to obtain extended form of the equations (9) and (10).

2. The existence of various structure solutions of the synthesis problem, that form the same amplitude RPs (or close amplitude RPs), presents the possibility to choose such solution which has more simple technical realization for the practical applications.

3. The stated synthesis problems of the considered arrays with due regard for the mutual coupling of radiators can be simply generalized for the synthesis problem of arrays of other types. Thus, the presence of the stable and effective methods to solve the direct (analysis) problem, that is determination of the operator A, plays a key role.

4. Optimization of the aperture form (form of the mirror cut) gives an additional possibility to improve the quality of approximation of the modulus of the prescribed and synthesized RPs. The use of this approach allows to synthesize the contour RPs of the fixed and variable form without a critical zone.

REFERENCES

1. Andriychuk M. I., Voitovich N. N., Savenko P. A., Tkachuk V. P. *The antenna synthesis according to amplitude radiation pattern: numerical methods and algorithms.* Kiev, Nauk. Dumka, 1993. – 256 p. (In Russian).
2. Andriychuk M. I., Savenko P. O. Proc. of Int. Seminar/Workshop DIPED-2001. Lviv, Ukraine, 2001. – P. 151-155.
3. Andriychuk M. I., Savenko P. O., Topolyuk Yu. P. Proc. of URSI Int. Symp. on Electromagn. Theory. St. Petersburg, Russia, 1995. - P. 197- 199.
4. Anokhin V. J., Golub V. M., Podlevskyi B. M., Romanenko V. Ya, Savenko P. A., Tkach M. D. Proc. of XXVIIth Int. Conf. on Antenna Theory and Technique. Moscow, 1994. – P. 214-217.
5. Chaplin A. F. *Analysis and synthesis of the antenna arrays.* Lviv, Vyshcha shkola, 1987. – 179 p. (In Russian).
6. Dmitriev V. I., Berezina N. I. *Numerical methods of solution of the synthesis problems of the radiating systems.* Moscow, MGU, 1986. – 112 p. (In Russian).
7. Markov G. T., Petrov B. M., Grudinskaya G. P. *Electrodynamics and propagation of the radiowaves.* Moscow, Sov. Radio, 1979. – 374 p. (In Russian).
8. Markov G. T., Sazonov D. N. *Antennas.* Moscow, Energia, 1975. – 528 p. (In Russian).
1. Pasnak L. M., Savenko P. O. Radiotechnika i electronika. – 1997. – **42**, № 5. – P. 567-572.
10. Pasnak L. M., Savenko P. A. Izv. VUZ'ov. Radioelectronics. – 1997. – **40**, No 9. – P. 50-62.
11. Pasnak L. M., Savenko P. O. Proc. of Int. Conf. AP-2000. Davos, Switzerland, 2000. – Vol. I. – P. 201.
12. Podlevskyi B. M. Math. Methods and Phys.-Mech. Fields. – 2001. – **44**, No 2. – P. 34-38.
13. Podlevskyi B., Savenko P. Proc. of VIth Int. Conf. on Math. Methods in Electromagn. Theory. Lviv, Ukraine, 1996. – P. 521-524.
14. Podlevskyi B., Savenko P. Electromagnetics. – 1998. – **18**, No 5. – P. 507-527.

15. Podlevskyi B .M., Savenko P. O., Tkach M. D. Proc. of IInd Int. Conf. on Antenna Theory and Techniques. Kyiv, Ukraine, 1997. - P. 370-372.
16. Podlevskyi B. M., Savenko P .O. Proc. of IIIrd Int. Conf. on Antenna Theory and Techniques. Sevastopil, Ukraine, 1999. - P. 187-189.
17. Prosvirnin S. L., Nechaev Yu. B., Seleznev D. G. Kharkov, 1992. – 56 p. (Prepr. /AS of Ukraine, Inst. of Radioastronomy, 92-60).
18. Rotman W. IEEE Trans. on Antennas and Propag. – 1963. – **11**, No. 6. – P. 623.
19. Savenko P. A. Izv. VUZ'ov. Radiophysics. – 1986. – **29,** No 3. – P. 339-345.
1. Savenko P. O. Dop. AN Ukrainy. – 1994. – № 8. – P. 48-52.
21. Savenko P .A. Izv. VUZ'ov. Radioelectronics. – 1996. - **39,** No 2. – P. 35-50.
22. Savenko P. O. Math. Methods and Phys.-Mech. Fields. – 1997. – **40**, № 1. – P. 146-150.
23. Savenko P. A. Radiophysics and Radioastronomy. – 2000. – **5**, No. 4. – P. 405-415.
24. Savenko P. A. Comput. Math. and Math. Physics. – 2000. – **40,** No. 6. – P. 889-899.
25. Savenko P. O. Math. Methods and Phys.-Mech. Fields. – 2000. – **43**, No. 2. – P. 105-111.
26. Savenko P. O., Anokhin V. J. Theoretical electrotechniques. Lviv, Edit. of LSU. – 1996. – **53**. – P. 118-126.
27. Savenko P. O., Anokhin V. J. IEEE Trans. on Antennas and Propag. – 1997. – **45**, No. 4. – P. 744-747.
28. Savenko P. A., Novakivskyi I. I. Antennas. Moscow, Radio i Svyaz'. – 1990. – **37**. – P. 28-32.
29. Savenko P. A., Pasnak L. M. Izv. VUZ'ov. Radioelectronics. – 1997. – **40,** No 12. – P. 11-25.
30. Savenko P. A., Pasnak L. M. Izv. VUZ'ov. Radioelectronics. – 2000. – **43,** No 8. – P. 1-15.
31. Savenko P. A., Podlevskyi B. M., Tkach M. D. Golub V. M., Romanenko V. Ya. Radiotechnika i electronika. – 1995. – **40**, No 10. – P. 1496-1505.
32. Savenko P. A., Tkach M. D. Izv. VUZ'ov. Radioelectronics. – 2001. – **44,** No 6. – P. 19-32.
33. Savenko P. A., Tkach M. D. Radiotechnika i electronika. – 2001. – **46,** No 1. – P. 58-65.
34. Savenko P. O., Topolyuk Yu. P., Voitovich N. N. Proc. of Int. Seminar/Workshop DIPED-2000. Lviv-Tbilisi, 2000. – P. 57-59.
35. Tikhonov A. N., Arsenin V. Ya. *Methods of solution of the ill-posed problems*. Moscow, Nauka, 1986. – 288 p. (In Russian).
36. Tikhonov A. N., Dmitriev V .I. Comput. Math. and Programming. Moscow, MGU, 1968. – Vol. 10. – P. 3-8.
37. Vainberg M. M., Trenogin V. A. *The branching theory of solutions of the nonlinear equations*. Moscow, Nauka, 1969. – 528 p. (In Russian).

THE WIENER-HOPF FACTORIZATION METHOD FOR THE DIFFRACTION BY WEDGES HAVING ARBITRARY APERTURE ANGLE

V. G. Daniele

Dipartimento di Elettronica, Politecnico di Torino
C.so Duca degli Abruzzi 24, 10129 Torino (Italy)
E-mail:daniele@polito.it

ABSTRACT

The Wiener-Hopf technique for studying diffraction problems involving wedge shaped region is here addressed.

INTRODUCTION

Fifty years ago Malyuzhinets solved the diffraction by a wedge, of known surface impedances, problem, by using an original and very important method based on a Sommerfeld representation of the involved fields [1]. This method is very popular since it is usually preferred to the more effective Wiener-Hopf technique for studying fields and waves in wedge shaped regions. The main reason of this preference is the common belief that the Wiener-Hopf technique do apply only for some values of the wedge aperture angle. This author always felt not satisfied for this limited use of the W-H technique dealing with wedge problems. In fact, in some recent works [2-4] he started showing that the diffraction due to an impenetrable wedge having arbitrary aperture angle always leads to a standard Wiener-Hopf matrix factorization. The aim of this paper is to report some of these results in order to deeply investigate this problem.

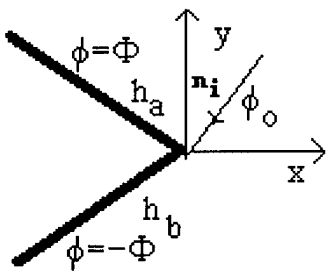


fig la impenetrable wedge with arbitrary aperture angle

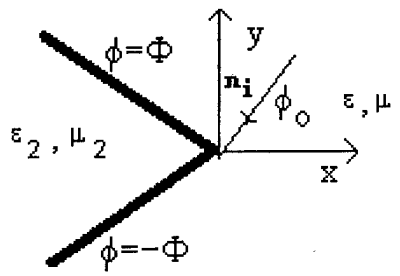


fig. 1b
penetrable wedge with arbitrary aperture angle
Isorefractive case: $\varepsilon\mu = \varepsilon_2\mu_2$

The Wiener-Hopf technique for wedge problems stands on the introduction of the following Laplace transforms of the tangential to the wedge surface field components E_z, E_ρ, H_z, H_ρ:

$$V_{z+}(\eta,\varphi)=\int_0^\infty E_z(\rho,\varphi)e^{j\eta\rho}d\rho\ ,\ I_{z+}(\eta,\varphi)=\int_0^\infty H_z(\rho,\varphi)e^{j\eta\rho}d\rho \tag{1}$$

$$V_{\rho+}(\eta,\varphi)=\int_0^\infty E_\rho(\rho,\varphi)e^{j\eta\rho}d\rho\ ,\ I_{\rho+}(\eta,\varphi)=\int_0^\infty H_\rho(\rho,\varphi)e^{j\eta\rho}d\rho \tag{2}$$

Without loosing generality we assume the z dependency, specified by the $e^{j\alpha_o z}$ factor, here omitted. As it has been showed in [3], the following eight equations hold:

$$\xi\, V_{z+}(\eta,0)\mp\frac{\tau_o^2}{\omega\varepsilon}I_{\rho+}(\eta,0)\mp\frac{\alpha_o\eta}{\omega\varepsilon}I_{z+}(\eta,0)=-n\ V_{z+}(-m,\pm\Phi)\mp\frac{\tau_o^2}{\omega\varepsilon}I_{\rho+}(-m,\pm\Phi)\pm\frac{\alpha_o m}{\omega\varepsilon}I_{z+}(-m,\pm\Phi) \tag{3a}$$

$$\xi\, I_{z+}(\eta,0)\pm\frac{\tau_o^2}{\omega\mu}V_{\rho+}(-\eta,0)\pm\frac{\alpha_o\eta}{\omega\mu}V_{z+}(\eta,0)=-n\,I_{z+}(-m,\pm\Phi)\pm\frac{\tau_o^2}{\omega\mu}V_{\rho+}(-m,\pm\Phi)\mp\frac{\alpha_o m}{\omega\mu}V_{z+}(-m,\pm\Phi)$$

$$\pm\xi\ \ V_{z+}(-\eta,\pm\pi)+\frac{\tau^2}{\omega\varepsilon}I_{\rho+}(-\eta,\pm\pi)-\frac{\alpha\eta}{\omega\varepsilon}I_{z+}(-\eta,\pm\pi)=n\ V_{z+}(-m,\pm\Phi)+\frac{\tau^2}{\omega\varepsilon}I_{\rho+}(-m,\pm\Phi)-\frac{\alpha m}{\omega\varepsilon}I_{z+}(-m,\pm\Phi) \tag{3b}$$

$$\pm\xi\, I_{z+}(-\eta,\pm\pi)-\frac{\tau^2}{\omega\mu}V_{\rho+}(-\eta,\pm\pi)+\frac{\alpha\eta}{\omega\mu}V_{z+}(-\eta,\pm\pi)=\pm n\,I_{z+}(-m,\pm\Phi)-\frac{\tau^2}{\omega\mu}V_{\rho+}(-m,\pm\Phi)+\frac{\alpha m}{\omega\mu}V_{z+}(-m,\pm\Phi)$$

where: $\tau_o=\sqrt{k^2-\alpha_o^2}$, $\mathrm{Im}[\tau_o]\le 0$, $\xi=\xi(\eta)=\sqrt{\tau_o^2-\eta^2}$ with the branch $\xi(0)=\tau_o$,

$m=m(\eta)=-\eta\cos\Phi+\xi\sin\Phi$, $n=n(\eta)=-\xi\cos\Phi-\eta\sin\Phi$ (4)

The functional equations (3) show the connection between the Laplace transforms of the tangential components of **E** and **H** evaluated on the four particular directions $\varphi=0$, $\varphi=\pm\pi$, $\varphi=\Phi$ and $\varphi=-\Phi$. They have been obtained by the use of a complex procedure [3], based on the introduction of oblique Cartesian coordinates. These equations are the necessary starting point for the deduction of the W-H equations for wedge shaped regions.

GENERALIZED WIENER-HOPF EQUATIONS FOR IMPENETRABLE WEDGES

Fig.1 shows the considered problem. A plane wave with skew incidence $\hat{\mathbf{n}}_i$ excites an impenetrable wedge where, on the boundaries $\varphi=\Phi$ and $\varphi=-\Phi$, linear conditions are defined on the tangential components of the electromagnetic field. The longitudinal field components of the plane wave are so defined by:

$$E_z^i=E_o e^{j\tau_o\rho\cos(\varphi-\varphi_o)}e^{-j\alpha_o z}\qquad H_z^i=H_o e^{j\tau_o\rho\cos(\varphi-\varphi_o)}e^{-j\alpha_o z} \tag{5}$$

where E_o and H_o are known quantities, ϑ_o is the angle between the $\hat{\mathbf{n}}_i$ and $\hat{\mathbf{z}}$ and $\tau_o=k\sin\vartheta_o$, $\alpha_o=k\cos\vartheta_o$.

In order to give an example of how the factorization method works dealing with wedge problems, let us consider the Malyuzhinets problem, where the incident plane wave is not oblique ($\alpha_o=0$) and isotropic impedances Z_a and Z_b are defined on the two wedge surfaces $\varphi=\Phi$ and $\varphi=-\Phi$. In this particular case the four equations (3a) reduce to two decoupled systems of order two. By considering, just as an example, the E-polarization case, we have:

$$G_\Phi(\eta)F_+(\eta) = Y_+(-m) \tag{6}$$

where $G_\Phi(\eta) = \begin{bmatrix} e(\eta) & -e(\eta)\dfrac{\omega\mu}{\xi} \\ -h(\eta) & -h(\eta)\dfrac{\omega\mu}{\xi} \end{bmatrix}$, $F_+(\eta) = \begin{vmatrix} V_{z+}(\eta,0) \\ I_{\rho+}(\eta,0) \end{vmatrix}$, $Y_+(-m) = \begin{vmatrix} I_{\rho+}(-m,\Phi) \\ I_{\rho+}(-m,-\Phi) \end{vmatrix}$,

$$e(\eta) = -\frac{\xi}{Z_a(n+n_a)}, h(\eta) = -\frac{\xi}{Z_b(n+n_b)}, \quad n_{a,b} = \frac{\omega\mu}{Z_{a,b}} \ .$$

It is important to observe that the mapping $\eta = \eta(\overline{\eta}) = -\tau_o \cos[\frac{\Phi}{\pi}[\arccos[-\frac{\overline{\eta}}{\tau_o}]]$ yields: $m = -\eta(-\overline{\eta})$. This reduces the equations (6) to the following classical Wiener-Hopf system in the $\overline{\eta}$ – *plane* [3,4]:

$$\overline{G}_\Phi(\overline{\eta}))\overline{F}_+(\overline{\eta}) = \overline{Y}_+(-\overline{\eta}) \tag{7}$$

where the notation $\overline{X}(\overline{\eta}) = X(\eta(\overline{\eta}))$ have been used for all the involved functions. Introducing $\overline{F}_-(\overline{\eta}) = \overline{F}_-^d(\overline{\eta}) + \overline{F}_-^g(\overline{\eta})$, where $\overline{F}_-^g(\overline{\eta}) = \dfrac{R_o}{\overline{\eta} - \overline{\eta}_o}$, $(\overline{\eta}_o = -k\cos(\frac{\pi}{\Phi}\varphi_o)$, R_o depends on the faces that are illuminated) is the known geometrical optics contribution, the W-H technique provides the solution:

$$\overline{F}_+(\overline{\eta})) = \overline{G}_{\Phi+}^{-1}(\overline{\eta}))\overline{G}_{\Phi-}^{-1}(\overline{\eta}_o)\frac{R_o}{\overline{\eta} - \overline{\eta}_o} \tag{8}$$

where $\overline{G}_{\Phi+}(\overline{\eta}))$ and $\overline{G}_{\Phi-}(\overline{\eta})$ are the factorized matrices of $\overline{G}_\Phi(\overline{\eta})) = \overline{G}_{\Phi-}(\overline{\eta})\overline{G}_{\Phi+}(\overline{\eta}))$.

If $Z_a = Z_b = 0$ (PEC wedge case) we only need the scalar factorization, that can be accomplished by using standard techniques [3,4]. For example, dealing with the functions $\xi = \sqrt{\tau_o^2 - \eta^2}$ and $n = -\xi\cos\Phi - \eta\sin\Phi$ defined in (4), we obtained:

$$\overline{\xi}_-(\overline{\eta}) = \sqrt{\frac{\tau_o + \overline{\eta}}{2}}, \ \overline{\xi}_+(\overline{\eta}) = \frac{\xi(\eta(\overline{\eta}))}{\overline{\xi}_-(\overline{\eta})}, \ \overline{n}_+(\overline{\eta}) = \sqrt{\frac{\tau_o - \overline{\eta}}{2}} \quad \overline{n}_-(\overline{\eta}) = \frac{n(\eta(\overline{\eta}))}{\overline{n}_+(\overline{\eta})} \tag{9}$$

On the contrary, if Z_a *and* Z_b are not vanishing, the kernel $\overline{G}_\Phi(\overline{\eta})$ is a matrix of order two. Even though the two-order matrices generally cannot be factorized in a closed form, nevertheless for the Malhiuzinets problem we obtained an explicit factorization by the use of the following procedure. First we rewrite $\overline{G}_\Phi(\overline{\eta})$ in the form:

$$\overline{G}_\Phi(\overline{\eta}) = \frac{(Z_a - Z_b)\xi\, n}{2Z_aZ_b(n+n_a)(n+n_b)}\begin{bmatrix}1 & 1\\ 1 & -1\end{bmatrix}\begin{bmatrix}1 & 0\\ 0 & \dfrac{\sqrt{\omega\,\mu}}{\overline{\xi}_-(\overline{\eta})}\end{bmatrix}\begin{bmatrix}1 & a\\ b & 1\end{bmatrix}\begin{bmatrix}1 & 0\\ 0 & \dfrac{\sqrt{\omega\,\mu}}{\overline{\xi}_+(\overline{\eta})}\end{bmatrix}\begin{bmatrix}1 & 0\\ 0 & -1\end{bmatrix} \tag{10}$$

where: $a = f(\eta)\frac{\sqrt{\omega\,\mu}}{\bar{\xi}_-(\bar{\eta})}$, $b = f(\eta)\frac{\bar{\xi}_-(\bar{\eta})}{\sqrt{\omega\,\mu}}$, $f(\eta) = \frac{e(\eta)+h(\eta)}{e(\eta)-h(\eta)}$.

Eq. (10) reduces the matrix factorization of $\bar{G}_\Phi(\bar{\eta})$ to that of the central matrix $\begin{bmatrix} 1 & a \\ b & 1 \end{bmatrix}$. Since $\bar{\xi}_-^2(\bar{\eta}) = \frac{1}{2}(k+\bar{\eta})$, the ratio $\frac{a}{b} = \frac{\omega\mu}{\bar{\xi}_-^2(\bar{\eta})}$ is a rational function of $\bar{\eta}$. It follows that the matrix $\begin{bmatrix} 1 & a \\ b & 1 \end{bmatrix}$ is a Daniele-Khrapkov matrix that can be factorized by a well known method [5,7]. It yields:

$$\begin{bmatrix} 1 & a \\ b & 1 \end{bmatrix} = \begin{bmatrix} 1 & a \\ b & 1 \end{bmatrix}_- \bullet \begin{bmatrix} 1 & a \\ b & 1 \end{bmatrix}_+$$ where the minus and plus factorized matrices are given by:

$$\begin{bmatrix} 1 & a \\ b & 1 \end{bmatrix}_- = \sqrt{\bar{g}_-(\bar{\eta})} \begin{vmatrix} \cosh\left[\frac{1}{2}\log[\frac{-Z_b}{Z_a}]\right] & \frac{\sqrt{\omega\,\mu}}{\bar{\xi}_-(\bar{\eta})}\sinh\left[\frac{1}{2}\log[\frac{-Z_b}{Z_a}]\right] \\ \frac{\bar{\xi}_-(\bar{\eta})}{\sqrt{\omega\,\mu}}\sinh\left[\frac{1}{2}\log[\frac{-Z_b}{Z_a}]\right] & \cosh\left[\frac{1}{2}\log[\frac{-Z_b}{Z_a}]\right] \end{vmatrix} \bullet$$

$$\bullet \begin{vmatrix} \cosh\left[\frac{\sqrt{\omega\,\mu}}{2}\bar{t}_-(\bar{\eta})\bar{\xi}_-(\bar{\eta})\right] & \frac{\sqrt{\omega\,\mu}}{\bar{\xi}_-(\bar{\eta})}\sinh\left[\frac{\sqrt{\omega\,\mu}}{2}\bar{t}_-(\bar{\eta})\bar{\xi}_-(\bar{\eta})\right] \\ \frac{\bar{\xi}_-(\bar{\eta})}{\sqrt{\omega\,\mu}}\sinh\left[\frac{\sqrt{\omega\,\mu}}{2}\bar{t}_-(\bar{\eta})\bar{\xi}_-(\bar{\eta})\right] & \cosh\left[\frac{\sqrt{\omega\,\mu}}{2}\bar{t}_-(\bar{\eta})\bar{\xi}_-(\bar{\eta})\right] \end{vmatrix} \tag{11}$$

$$\begin{bmatrix} 1 & a \\ b & 1 \end{bmatrix}_+ = \sqrt{\bar{g}_+(\bar{\eta})} \begin{vmatrix} \cosh\left[\frac{\sqrt{\omega\,\mu}}{2}\bar{t}_+(\bar{\eta})\bar{\xi}_-(\bar{\eta})\right] & \frac{\sqrt{\omega\,\mu}}{\bar{\xi}_-(\bar{\eta})}\sinh\left[\frac{\sqrt{\omega\,\mu}}{2}\bar{t}_+(\bar{\eta})\bar{\xi}_-(\bar{\eta})\right] \\ \frac{\bar{\xi}_-(\bar{\eta})}{\sqrt{\omega\,\mu}}\sinh\left[\frac{\sqrt{\omega\,\mu}}{2}\bar{t}_+(\bar{\eta})\bar{\xi}_-(\bar{\eta})\right] & \cosh\left[\frac{\sqrt{\omega\,\mu}}{2}\bar{t}_+(\bar{\eta})\bar{\xi}_-(\bar{\eta})\right] \end{vmatrix}$$

The factorization of the scalar function:

$$g(\eta) = 1 - f^2(\eta) = -\frac{4Z_aZ_b}{(Z_a-Z_b)^2}\frac{n+n_a}{n}\frac{n+n_b}{n} = \bar{g}_-(\bar{\eta})\bar{g}_+(\bar{\eta}),$$

and the decomposition of the scalar function:

$$t(\eta) = \frac{1}{\sqrt{\omega\,\mu}\,\bar{\xi}(\bar{\eta})}\log[\frac{1+f(\eta)}{1-f(\eta)}] - \frac{1}{\sqrt{\omega\,\mu}\,\bar{\xi}(\bar{\eta})}\log[-\frac{Z_b}{Z_a}] = \frac{1}{\sqrt{\omega\,\mu}\,\bar{\xi}(\bar{\eta})}\log[\frac{n+n_b}{n+n_a}] = \bar{t}_-(\bar{\eta}) + \bar{t}_+(\bar{\eta})$$

can be accomplished without any difficulty through the Cauchy decomposition. In order to achieve this purpose it is convenient to introduce the $\bar{w}-plane$ defined by $\bar{\eta} = -\tau_o\cos\bar{w}$.

In this plane we obtained [3]:

$$\left[\frac{n+n_{a,b}}{n}\right]_+\Big|_{\overline{\eta}=-k\cos\overline{w}} = \frac{1}{\pi}\int_0^\infty \arctan\left[\frac{\sin\vartheta_{a,b}}{\sinh[\frac{\Phi}{\pi}u]}\right]\frac{\sinh u}{\cosh u-\cos\overline{w}}du \tag{12a}$$

$$\left\{\frac{1}{\overline{\xi}_-(\overline{\eta})}\log\left[\frac{n+n_b}{n+n_a}\right]\right\}_+\Big|_{\overline{\eta}=-k\cos\overline{w}} = \frac{2}{\pi}\int_0^\infty\left[\arctan\left[\frac{\sin\vartheta_b}{\sinh[\frac{\Phi}{\pi}u]}\right]-\arctan\left[\frac{\sin\vartheta_a}{\sinh[\frac{\Phi}{\pi}u]}\right]\right]\frac{\sinh\frac{u}{2}}{\cosh u-\cos\overline{w}}du \tag{12b}$$

with $n_{a,b}=k\sin\vartheta_{a,b}=k\cos\widetilde{\vartheta}_{a,b}$, $\widetilde{\vartheta}_{a,b}=\frac{\pi}{2}-\vartheta_{a,b}$.

Note that $\overline{g}_-(\overline{\eta})$ and $\overline{g}_+(\overline{\eta})$ behave as constants for $\overline{\eta}\to\infty$. In addition, taking into account that $\eta\approx\overline{\eta}^{\Phi/\pi}$, it follows that $\overline{t}_\pm(\overline{\eta})=O\left[\frac{1}{\overline{\eta}^{1/2}\overline{\eta}^{\Phi/\pi}}\right]$. Since the argument of the hyperbolic functions in eq. (11) is constant, or vanishing for $\overline{\eta}\to\infty$, it yields the algebraic behavior of both the factorized matrices. The factorization of $\overline{G}_\Phi(\overline{\eta})$ is completed since ξ and n have been factorized by the use of eq. (9).

It is worth to observe that the integrals in eq. (12) involve the Malyuzhinets function $\Psi_\Phi(w)$. In fact a cumbersome evaluation procedure shows that [3]:

$$\left[\frac{n+n_{a,b}}{n}\right]_+\Big|_{\eta=-k\cos w} = \Psi_\Phi(w+\Phi+\widetilde{\vartheta}_{a,b})\Psi_\Phi(w+\Phi-\widetilde{\vartheta}_{a,b})\Psi_\Phi(w-\Phi+\widetilde{\vartheta}_{a,b})\Psi_\Phi(w-\Phi-\widetilde{\vartheta}_{a,b})$$

$$\left\{\frac{\sqrt{k}}{\overline{\xi}_-(\overline{\eta})}\log\left[\frac{n+n_b}{n+n_a}\right]\right\}_+\Big|_{\eta=-k\cos w} = \frac{1}{\sin[\frac{\pi w}{2\Phi}]}\log\left[\frac{\Psi_\Phi(w-\Phi-\widetilde{\vartheta}_b)\Psi_\Phi(w-\Phi+\widetilde{\vartheta}_b)\Psi_\Phi(w+\Phi-\widetilde{\vartheta}_a)\Psi_\Phi(w+\Phi+\widetilde{\vartheta}_a)}{\Psi_\Phi(w+\Phi-\widetilde{\vartheta}_b)\Psi_\Phi(w+\Phi+\widetilde{\vartheta}_b)\Psi_\Phi(w-\Phi-\widetilde{\vartheta}_a)\Psi_\Phi(w-\Phi+\widetilde{\vartheta}_a)}\right]$$

where $\eta=-\tau_o\cos w$, $w=\frac{\Phi}{\pi}\overline{w}$. These expressions allow to verify that the obtained Wiener-Hopf solution agrees completely with the Malyuzhinets solution [1].

CONCLUSIONS

This paper shows that the wedge problems solved by the Sommerfeld-Malyuzhintes method can be successfully solved also by the classical Wiener-Hopf technique. However there are practical and theoretical differences between the two methods. For instance the Sommerfeld- Maliuyzhinets approach requires the solution of a set of difference equations, whereas the Wiener-Hopf technique involves decomposition-factorization problems. Even though it seems that the two methods have the same capability for solving wedge problems, it should be observed however that the extension of the W-H technique even to arbitrary angular regions definitively establishes this last method as the most general and effective method for solving field problems involving geometrical discontinuities. The young researchers interested to diffraction problems should invest major time for studying this fascinating technique. To this author's

opinion the superiority of Wiener-Hopf approach with respect to the Sommerfeld-Malhyuzinets one is more evident when no closed form solutions are possible, and approximated techniques become necessary. In fact, approximated factorizations face these problems better than approximated difference equations solutions [6].
Even though some penetrable wedges (fig.1b), as the isorefractive ones for example, can be solved with the factorization method [3], an important question is if there is the possibility to face with the Wiener-Hopf technique arbitrary penetrable wedge diffraction problems. Using different media in the different angular regions, it yields a set of functional equations that can be classified as modified generalized W-H equations [8]. The same occurs when we are dealing with anisotropic or general linear media in angular regions. Up to now this author was not able to obtain a closed form solutions for these fundamental problems. However effective approximated solutions seem to be possible. These will be discussed in another work.

ACKNOWLEDGEMENT

This work was supported by the Italian Ministry of University and Scientific Research (MURST) under grant MM093227718

REFERENCES

[1] A.V.Osipov and A.N. Norris (1999), The Malyuzhinets theory for scattering from wedge boundaries: a Review, Wave motion, .29, pp.313-340.
[2] V.Daniele: "Generalized Wiener-Hopf technique for wedge shaped regions of arbitrary angles", 2000 International Conference on Mathematical Methods in electromagnetic theory (MMET 2000).Kharkov. Ukraine, September 12-15, 2000. pp.432-434.
[3] V.Daniele, "Generalized Wiener-Hopf technique for wedge shaped regions of arbitrary angles", Rapporto Interno ELT-2000-1. Dipartimento di Elettronica-Politecnico di Torino. Settembre 2000
[4] V.Daniele: "New analytical Methods for wedge problems", ". 2001 International Conference on Electromagnetics in Advanced Applications (ICEAA01), September 10-14 2001, Torino (Italy), pp.385- 393
[5] V.Daniele: "On the factorization of W-H Matrices in problems solvable with Hurd's methods, IEEE Trans. on Antennas and Propag., AP-26, July 1978, p.614-616
[6] V.Daniele-R.Zich: An approximate factorization for the kernel involved in the scattering by a wedge at skew incidence, invited for 2002 International Conference on Mathematical Methods in Electromagnetic theory (MMET 2002).Kiev. Ukraine, September 2002
[7] A.Büyükaksoy and A.H Serbest (1993), *Matrix Wiener-Hopf Factorization Methods and Applications to Some Diffraction Problems*, ch.6 in "Analytical and Numerical Methods in Electromagnetic Wave Theory", M. Hashimoto, M.Idemen and O.A. Tretyakov Editors, Science House Co.,Ltd., Tokio,
[8] V.Daniele, "Recent advancements on the Wiener-Hopf technique. Rapporto Interno ELT-2002-1. Dipartimento di Elettronica-Politecnico di Torino. gennaio 2002

BASICS PROPERTIES OF LEAKY MODES IN PRINTED-CIRCUIT TRANSMISSION LINES

Hiroshi Shigesawa and Mikio Tsuji*

Department of Electronics, Doshisha University
Kyotanabe, Kyoto 610-0321, Japan
E-mail: hshigesa@mail.doshisha.ac.jp

* Department of Electronics, Doshisha University
Kyotanabe, Kyoto 610-0321, Japan
E-mail: mtsuji@mail.doshisha.ac.jp

ABSTRACT

Printed-circuit transmission lines used in microwave and millimeter-wave integrated circuits can exhibit several new propagation phenomena. They have relevance to leaky modes in integrated circuits that leak power in the form of the surface wave and/or the space wave, and they influence significantly the circuit behavior. In this paper, we will explain first why and when these transmission lines can become leaky, and then present some important phenomena discovered recently.

INTRODUCTION

Leakage phenomena in printed-circuit transmission lines have been recognized only for the last 10 or 12 years [1][2]. Many people do not understand the nature of leaky waves because they have mathematically improper one that their fields increase transversely away from the leaky guiding structure. So these people wonder if leaky waves are actually physical and measurable. It may be easily shown, however, that the leaky wave is defined only within a sector of space at a finite distance from the source, and that the wave never reaches transverse infinity. As a result, the leaky wave is certainly physical and measurable within its region of validity, and in fact its near-field properties really ruin the circuit performance [3] in the form of power loss, crosstalk between neighboring portions of the circuit, and various undesired package effects. So we must know when leakage can occurs and how to avoid it, or, in applications based on leakage, how to control it.

In this paper, we present the dispersion behaviors of two types of leaky modes: one is the surface-wave leaky mode that leaks power in the form of a surface wave on the surrounding substrate, and the other is the space-wave leaky mode that leaks power in the form of a space wave radiating into space as well as a surface wave. Then we will explain why and when these transmission lines can become leaky, and summarize the principal properties of these leaky modes. After that, some of new propagation phenomena relevant to leaky waves are briefly explained.

LEAKY MODE IN SURFACE-WAVE FORM

The basic cause of the leakage can be understood quite simply and is explained. In Fig. 1 we see the bird-eye view of a metal strip on air-dielectric interface, where this strip can represent the strip of microstrip line, or one of a pair of coplanar strips, or whatever. Let us assume that leakage power is leaking away at an angle θ with respect to the transmission-line axis z, as seen in figure. The dominant mode has the phase constant β, and the wavenumber of the surface wave on surrounding substrate relevant to power leakage is k_s. From the figure, we can find an approximate relation between the wavenumbers and the leakage angle θ as follows.

$$\cos\theta \cong \beta/k_s \qquad (1)$$

This simple expression is a very good approximation, and is helpful in understanding the basic physics of leakage. From (1) we can see that, for real-power leakage at an angle θ, we must have the relation $\beta<k_s$ or, dividing by k_0

$$\beta/k_s < k_s/k_0 \ . \qquad (2)$$

This relation (2) is the simple condition that must be satisfied for leakage to occur [2]. If this condition is satisfied for two surface waves on surrounding substrate, the leaky mode, of course, leaks power in the form of two surface waves at the same time, though at different angles.

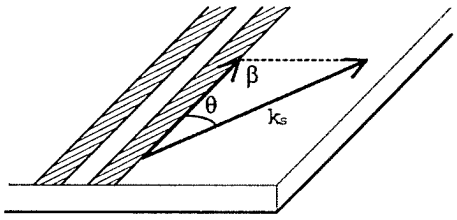


Fig. 1. Metal strip and the wavenumbers' relation.

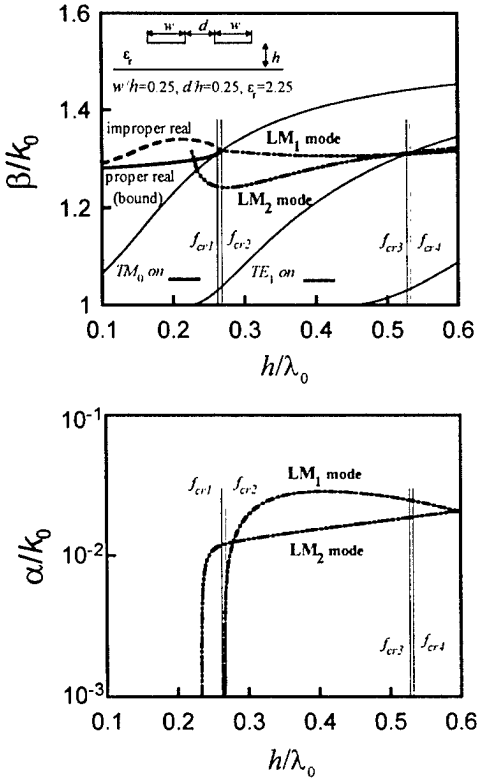


Fig. 2. Normalized phase and leakage constants for the conductor-backed coplanar strips for w/h = 0.25 and d/h = 0.25.

A typical example of the dispersion behavior for conductor backed coplanar strips (CPS) is shown in Fig.2, which is obtained by the spectral domain method. The structure is shown in the inset of that figure. The dispersion behavior of the normalized phase constant β/k_0 and leakage constant α/k_0 as a function of normalized frequency h/λ_0 is shown in Fig. 2, where h is the substrate thickness and $w/h = d/h = 0.25$, $\varepsilon_r = 2.25$ are selected. The plot indicated as proper real in Fig. 2 means the bound mode that ends at frequency f_{cr1}. This bound-mode solution is obtained by selecting the integration path along the real axis as shown in Fig. 3. The spectral gap appears between the frequencies f_{cr1} and f_{cr2} as seen, and the nonphysical improper-real solution is continuously connected to the bound solution, and then turns back to low frequencies.

The plots indicated by LM_1 and LM_2 show the surface-wave leaky modes that leak power by the TM_0 surface wave and by both TM_0 and TE_1 surface waves, respectively. For the calculation of LM_1 mode, we should select the path of integration so that it surrounds only the TM_0 surface-wave pole as shown in Fig. 4(*a*). For LM_2 mode, we should select the integration path as shown in Fig. 4(*b*), where it surrounds both the TM_0 and TE_1 surface-wave poles. As the frequency is increased from the critical frequency f_{cr2}, the dispersion curve for LM_1 eventually crosses the dispersion curve for the TE_1 surface wave at the frequency f_{cr3}, and then above this frequency the LM_1 mode is nonphysical. While the LM_2 leaky mode is physical above the frequency f_{cr4} at which the dispersion curve for LM_2 crosses the dispersion one for the TE_1 surface wave, so that the LM_2 leaky mode is nonphysical below the frequency f_{cr4}. The transition between these two leaky solutions results in a new type of the spectral gap.

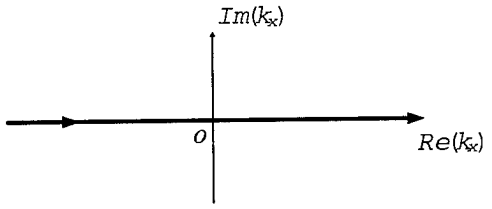
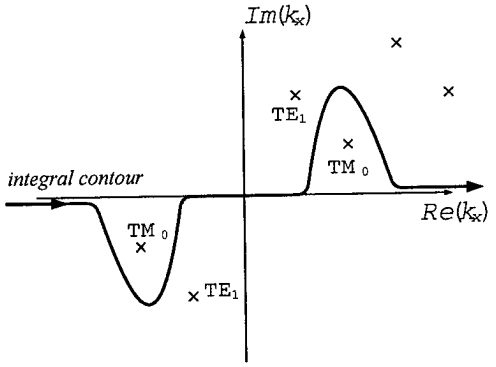
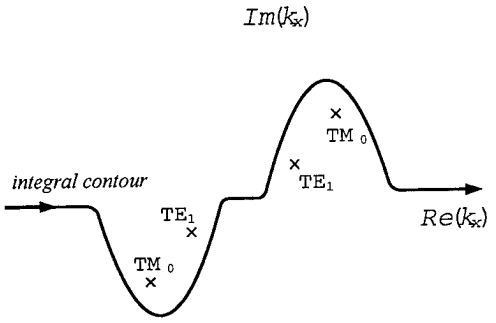


Fig. 3. The path of integration in SDM for the bound mode (proper-real solution).



(a) LM_1 mode



(b) LM_2 mode

Fig. 4. The paths of integration for LM_1 (a) and LM_2 (b) leaky modes.

Until recently, everyone thought that when the relative dimensions of the cross section of transmission lines are changed, the only effects are to modify the behaviors of the propagation wavenumber. We now know that this assumption is incorrect. It was found that, when the strip widths of conductor-backed coplanar strips are changed, there can exist a frequency range within which the bound and leaky modes can propagate simultaneously, and that the spectral gap then disappears. This effect is found to be quite general, applying to many different lines. A typical example for conductor-backed coplanar strips is shown in Fig. 5, when the strip width is changed from w/h = 0.25 of Fig. 2 to 0.60. The dispersion behavior is now seen to be dramatically different from that in Fig. 2, with the bound and leaky modes propagating simultaneously over a very wide frequency range. Since the bound and leaky modes have very similar current distributions on the strips, a circuit designer may need to keep this point in mind. In this case, the dispersion curve of the LM_2 mode is omitted because it does not change so much for the strip widths. Instead, another leaky mode that is obtained from the same integral path for the LM_1 mode is indicated in Fig. 5. This leaky mode that has been called "leaky surface-wave-

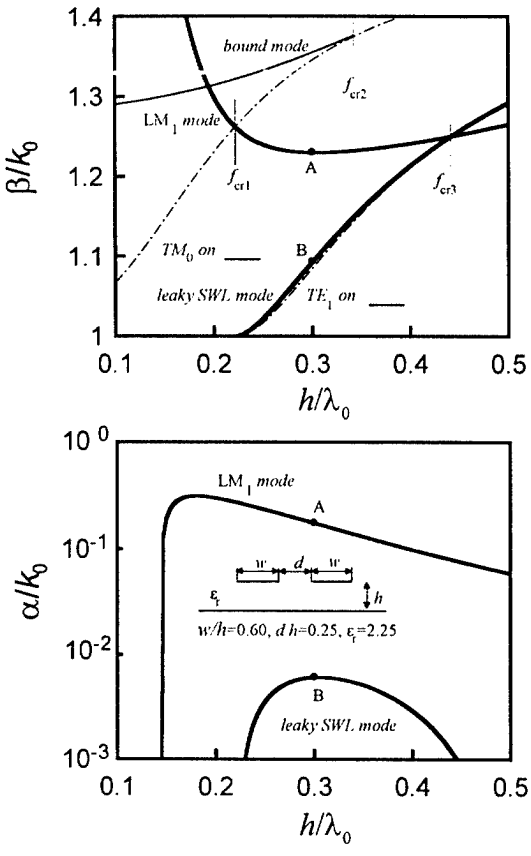


Fig. 5. Normalized phase and leakage constants as a function of the normalized frequency h/λ_0, when w/h is selected as 0.6.

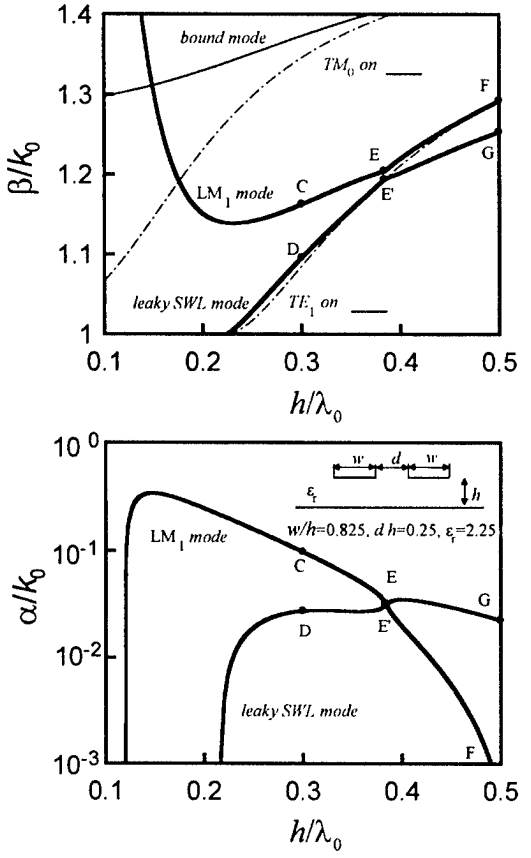


Fig. 6. Normalized phase and leakage constants as a function of the normalized frequency h/λ_0, when w/h is selected as 0.825.

like (SWL) mode." appears just above the TE_1 surface-wave curve shown by the dot-broken curve, and its feature resembles, in the field structure, the TE_1 surface wave on a grounded-dielectric layer, but the power leakage occurs in the form of the TM_0 surface wave. Fig. 6 shows the dispersion behaviors when the strip width w/h is changed from 0.60 to 0.825, keeping the slot width d/h = 0.25. Then the mode coupling occurs between the standard LM_1 leaky mode and the leaky SWL mode as shown in Fig. 6, accordingly, the conversion of the dispersion curves occurs. The coupling effect shown in Fig. 6 is seen to be sharp and the behavior is of the classical "directional coupler" co-flow type.

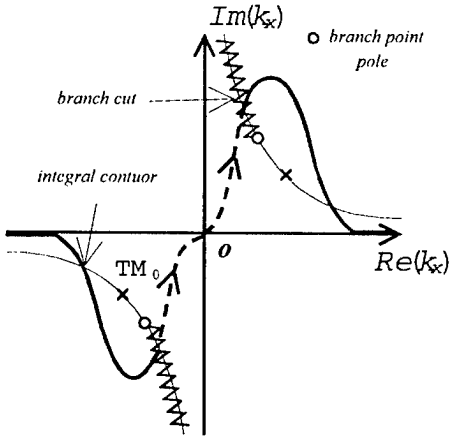


Fig. 7. The paths of integration for LM_1 leaky mode and for LM_2 leaky mode.

LEAKY MODE IN SPACE-WAVE FORM

Recently, the space-wave leaky mode becomes a tempting subject in printed-circuit technology

in connection with leaky-wave planar antennas. The space-wave leaky mode becomes physical in the region in which radiation of the space wave and leakage of the surface wave occur simultaneously, so that its complex-propagation constant is obtained by taking the path of integration shown in Fig. 7, where a part in the path of integration shown by the broken curve runs on the improper Riemann sheet, on which the imaginary part of the complex wavenumber normal to the dielectric-air interface is positive.

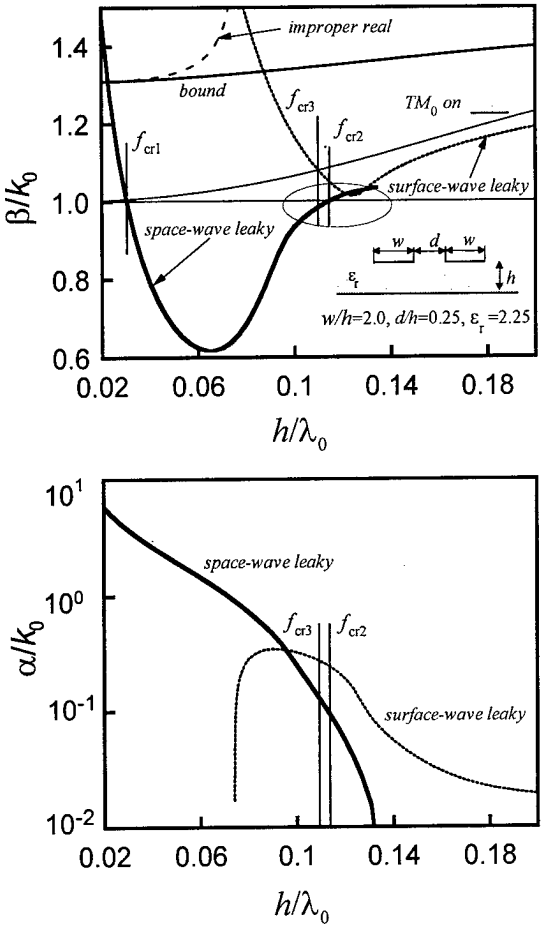
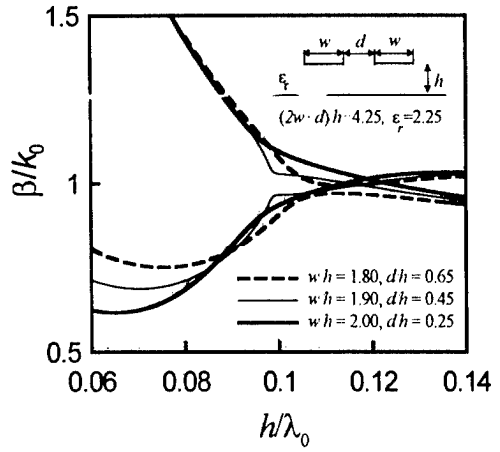


Fig. 8. Normalized phase and leakage constants as a function of the normalized frequency h/λ_0, when w/h is selected as 2.0.

The radiation condition into space wave is given, in good approximation, by $k_0 > \beta$. On the other hand, the relation $k_s > k_0$ is always held, so that the leakage condition into surface wave $k_s > \beta$ is always satisfied by the space-wave leaky mode. Fig. 8 shows the normalized phase and leakage constants for the strip width w/h= 2.0. The other dimensions and ε_r are shown in the figure. The solid curve indicated as "*bound*" is the bound dominant mode, while the bold-solid curve indicated as "*space-wave leaky*" means the space-wave leaky mode. For this strip width, the space-wave leaky mode takes the β/k_0 value smaller than unity between the critical frequencies f_{cr1} and f_{cr2}, so this leaky mode is physical only in this limited frequency range. Thus we notice that the physical-space-wave leaky mode can propagate simultaneously with the bound dominant mode that is, of course, physical. Also, we have one more leaky-mode solution at rather high frequencies in Fig. 8. It is the surface-wave-leaky-mode solution shown by the dot-broken curve indicated as "surface-wave leaky." Since it is physical only above a critical frequency f_{cr3}, the surface-wave leaky mode propagate simultaneously with the bound dominant mode in the frequency range $f > f_{cr3}$. In this case, two different kinds of the simultaneous-propagation range overlap between $f_{cr3} < f < f_{cr2}$, though the overlap width is narrow as shown in Fig. 8. Then, in this overlap range, we can see the simultaneous-propagation effect of the different three kinds of the physical mode, the bound dominant mode, the surface-wave leaky mode and the space-wave leaky mode.

We have the circle area in Fig. 8. In this area, there is some fine structure of the dispersion behavior, and the space-wave leaky mode is not shown correctly there. Such fine structure is caused by the mode coupling between the space-wave leaky modes discussed above. Fig. 9 shows one example of the results obtained for w/h = 1.80, 1.90



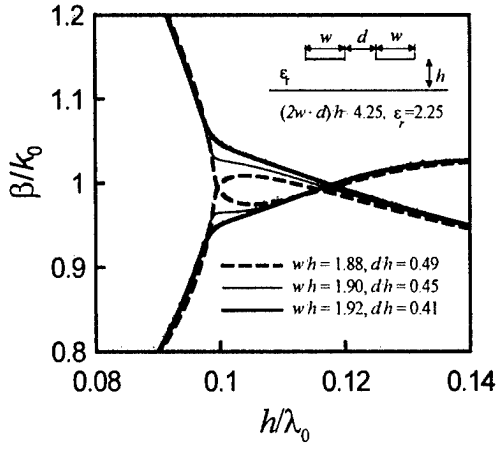
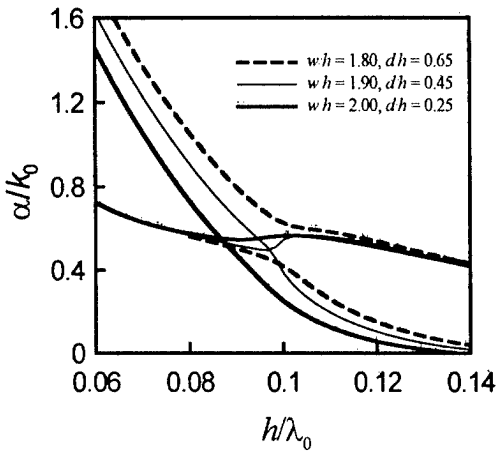


Fig. 9. Fine structures of the dispersion behavior in the circle area of Fig. 8.



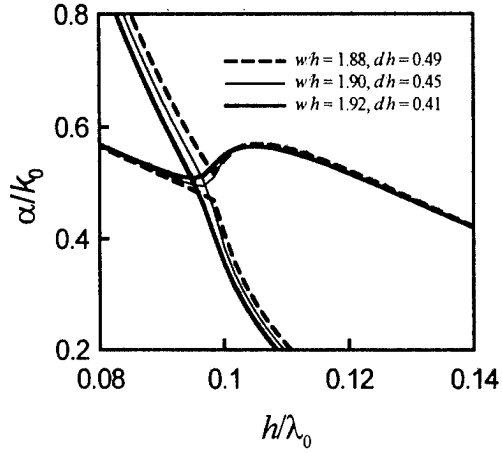


Fig. 10. Mode-coupling effect between two space-wave leaky modes.

and 2.00, keeping $(2w + d)/h = 4.25$. The mode-coupling effect between two leaky modes (complex modes) occurs only when both β/k_0 and α/k_0 values become identical or mutually take close values, and the curve of $w/h = 1.90$ in Fig. 9 seems to be the situation immediately before the mode coupling. So, we further calculated for the $w/h = 1.88$, 1.90 and 1.92, and the results are shown in Fig. 10, in which the coupling effect does not occur for the case of $w/h = 1.88$, but it occurs for $w/h = 1.90$ and 1.92. Such a coupling effect makes the dispersion behavior of the new leaky mode very difficult.

REFERENCES

[1] H. Shigesawa, M. Tsuji and A. A. Oliner, "Conductor-backed slot line and coplanar waveguide: Danger and full-wave analyses," *IEEE/MTT-S IMS Digest*, pp. 199-202, New York, May 1988.

[2] H. Shigesawa, M. Tsuji and A. A. Oliner, "Dominant mode power leakage from printed-circuit waveguides," *Radio Science*, vol. 26, pp. 559-564, Mar./Apr. 1991.

[3] A. A. Oliner, "Leaky wave in microwave and millimeter-wave integrated circuits: Basic properties and applications," Workshop at 1998 APMC at Yokohama, WS8, pp.5-22, 1998.

LARGE-SCALE DISCRETIZATION AND GENERALIZED MODE-MATCHING AS A BASIS FOR FAST ELECTROMAGNETIC SOLVERS

Anatoly Kirilenko

IRE NANU, ul. Proskury 12, Kharkov, 61085, Ukraine. E-Mail: kirilenko@ire.kharkov.ua

The mode-matching technique (MMT) was and still is the most powerful tool for the analysis, design and optimization of microwave devices - among other methods of computational electromagnetics. Simple and clear, it was devised in the early period of microwave research and provided solutions of many boundary value problems in the analysis of waveguides and gratings. MMT is credited for three important features: relative versatility (within a wide class of geometries), good convergence, and high accuracy. MMT does not loose its positions even now with a wide expansion of the grid methods, being superior in the calculation speed and accuracy and providing fast solutions of very complicated minimax problems. Perhaps a single demerit of MMT is necessity of an individual consideration of each new problem. Moreover, certain experience of designer is needed in analytical treatment of the boundary-value problems. So far there were no MMT-based tools good for arbitrary geometries at least in a certain class. Therefore solving a realistic problem requires not only computer time but also much greater human time for development of MMT algorithm and corresponding code.

In this paper, we present milestones of GMMT - a new generalized approach to implementation of MMT. *Firstly*, generalization consists in consideration of problems with "unpredetermined" topology and geometry. We imply arbitrary configurations within certain wide class of coordinate boundaries. *Secondly,* generalization implies automatic generation of all required structural data for building a corresponding set of the MMT matrix operators. *Thirdly*, fine structure of any specified geometry is taken into account: longitudinal and transversal symmetry of device; symmetry of excitation; symmetry of separate complicated waveguide sections and their parts arising at dividing into the domains with perfectly electric (magnetic) walls in the planes of symmetry; connectivity of the waveguide cross-sections, symmetry of the plane junctions of separate waveguides, etc. Finally, implementation of a unified criterion for the accuracy control both in algorithms of full modal bases building and in procedures of automatic electromagnetic assembling by S-matrix technique can be considered as a generalization. Within the framework of a general idea of MMT one can distinguish two ways of analytical treatment. The widespread one is simple, conventional and has been used starting from the 60's. It is based on intermediate matching of the fields of separate subdomains on common apertures. Besides of a necessity to support required ratios between the numbers of the field space harmonics (Mittra's rule), this way requires sometimes implementation of a zero-length virtual subdomain if a common boundary cannot not be treated as a "small" subdomain aperture within a "large" one. Another way of field matching is based on introduction of unknown electrical fields on subdomain common apertures. Here, besides of reduction of the number of unknowns there is an essential advantage of using special expansion bases. They can take into account all types of the field behavior near the rims of coupling apertures: rectangular or sharp edges, electrical or magnetic walls, etc. These algorithms have shown very good convergence on a range of particular configurations in the 80's and are popular again.

We have used GMMT approach to develop an automatic electromagnetic solver used in several practical designs of ridged waveguide evanescent mode filters, combined bandpass filters, lowpass waffle-iron filters, magic-tee based on double-ridged waveguides, low-pass-filters on the multilayer circuits, etc. GMMT solver is the main part of the AutoCAD based commercial solver (*MWD*) for analysis and design of complicated microwave circuits.

THE CONCEPT OF WAVES : THEORY AND APPLICATIONS IN ELECTRONIC PROBLEMS

BAUDRAND Henri *, WANE Sidina *, BAJON Damienne**

* ENSEEIHT 2 Rue C.Camichel 31000 Toulouse France
** SUPAERO 10 Av. E. Belin 31400 Toulouse France

INTRODUCTION

The fundamental quantities which describe the electronic -low or high frequencies- devices are electric and magnetic fields, or after integration, currents and voltages when their definition are possible pertinent.
The introduction of waves amplitude (or more simply, waves) replied firstly to the necessity of finding eigenvectors in propagation phenomena - in TEM-lines or waveguides - (see for instance [1]). This change of basis permitted to define a scattering matrix. The scattering matrix presents two important advantages : First, the scattering matrix of an arbitrary device does always exist (it is not the case for impedance or admittance matrix). Second, for passive devices, the scattering matrix is bounded and unitary in the case of lossless devices).
This first point is well known, however, its consequences in numerical methods are not yet entirely exploited: The relations between electric and magnetic fields give Finite elements method (F.E.M.), Finite difference in time domain (F.D.T.D), Electric Field Integral Equation (E.F.I.E.), Magnetic Field Integral Equation (M.F.I.E.) etc. What is now the position of wave-based formulations in numerical methods and why may it be interesting to investigate on how to take advantage of them ? In the following an overview on wave-based formulation approach is presented. Recent implementations of the Wave Concept Iterative Procedure (W.C.P.I [2]) in an integral form is presented through different applications. The wave concept based formulation, here presented, in circumventing the inversion of an integral operator, required in the moment (MoM) approach to compute the scattering parameters, uses an iterative procedure involving planar exciting sources. Since potentially the S-parameters can be directly obtained from the incident and reflected waves, the computation of the impedance (or admittance) matrix responsible of singularities in the MoM.

DEFINITION OF WAVES. FINITE DIFFERENCE FORMULATION AND ITERATIVE PROCEDURE.

Since the waves in a line are defined as a linear combination of longitudinal current and voltage existing on a transverse section of the line, in a non -TEM mode, the amplitude of the waves may be defined at each point of the transverse section by an adequate combination of electric and magnetic fields.
In the general case of non-guided waves, the transverse section will be replaced by an arbitrary surface S, which will divide the space into two parts, the waves being defined in a half-space characterised with an unitary vector $\bar{n}$ orthogonal to S. For evident reasons of mathematical coherence (Electric and Magnetic Fields don't have the same tensorial character) the waves are defined as :

$$\vec{A}(x,y) = \frac{1}{2\sqrt{Z_0}}(\vec{E}_T(x,y) + Z_0\vec{H}(x,y) \wedge \vec{n})$$
$$\vec{B}(x,y) = \frac{1}{2\sqrt{Z_0}}(\vec{E}_T(x,y) - Z_0\vec{H}(x,y) \wedge \vec{n}) \quad (1)$$

x,y are coordinates running on S, $\vec{E}_T$ is the tangential electric field and $\vec{H}$ is the Magnetic field. A, B are two components functions of x,y. Z_o is an arbitrary normalizing impedance.

The use of tangential fields on a surface and their relations, as the concept of half-space is common in Spectral Domain Approach (S.D.A.) [3] and in the equivalent schemes for the resolution of electromagnetic problems by integral Methods [4].
The formulation of TLM Method with waves was shown by P.Russer [5] : the condensed node is nothing else than the scattering matrix of a little cube, treated by a finite difference scheme. The Integral Method applied to a wave formulation has the following properties :

- there is no need of trial functions on sub-domain (as in S.D.A.) because of the existence of scattering operator for any obstacles.
- the quality of the scattering operator, which is bounded, permits the use of an iterative procedure that always converges [2].

Let's consider a circuit defined on a surface S. At each point of this circuit, one can define boundary conditions in term of waves as:

$$B = \hat{S}A + B_0 \quad (2)$$

where $\hat{S}$ represents a Scattering Operator Matrix.
The External relations are written as:

$$A = \hat{\Gamma}B \quad (3)$$

B_0 being localised source on S.
These two relations give a natural iterative procedure : relation (2) is firstly used with $B = B_0$ in the spectral domain whereas equation (2) allows, in spatial domain, to determine B, relation (2) being recalled for a second iteration, and so on. This approach is quite similar to the one used in the Harmonic Balance method [6] which splits a circuit into linear and non-linear parts while W.C.I.P splits, in the integral equation surface conditions (2) and homogeneous embedding half-spaces conditions (3). In this last method the time domain is the counterpart of the spatial domain, and the harmonic domain stands for the spectral (or modal) domain. It has to be noticed that the reflection operator in (3) has a diagonal representation in the spectral domain when homogeneous spaces are considered .

APPLICATIONS

From some years ago numerous applications of W.C.I.P. have been developed: Planar active circuits [7], antennas [8], and filters [9]. The use of spherical geometry was also applied to radiating elements [10]. In addition to their flexibility to handle complex geometry, the integral operators take advantage of both the spectral and spatial domain, the toggling between the two domains using an optimized Fast Mode Transform (FMT). On the other hand, inhomogeneous buried diffusions with arbitrary patterned doping profiles inserted to reduce substrate-epitaxial coupling noise [11] in BiCMOS

structures (Fig.1), have been investigated from a full-wave analysis based on a new original hybrid method combining the integral wave concept based formulation to a local space finite-difference approach applied to the transverse operator . The boundary conditions at the level of the inhomogeneous layers are expressed in terms of incident and reflected waves via the Transverse Operator Method (T.O.M) in a differential form. To improve the time delay computations with the wave concept based formulation, a multiscale approach, can allow an optimum number of iterations to be chosen in reference to the discretising cells size considered for the description of a given circuit. Fig.2 shows the Convergence of the input admittance imaginary part against the number of iterations in the case of a simple interconnect circuit for different values of the scale parameter $k_o a$ (a being the circuit dimension, and k_o the vacuum wave-number) . As the number of iterations increases when the scale parameter grows, a change in the describing cell size resulting in refined meshing gives the possibility to reduce the number of iterations.

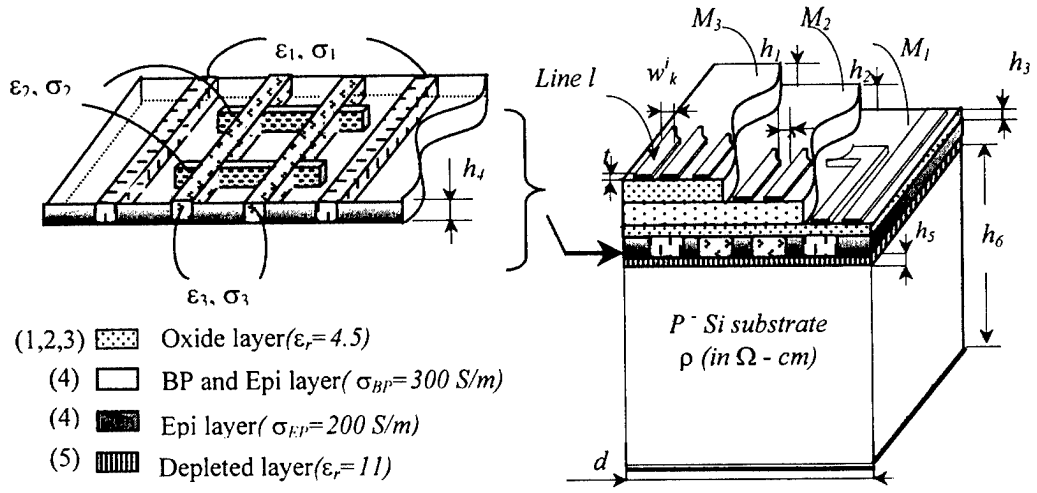


Fig.1. *Typical BiCMOS structure with buried diffusions (b) – Overview of the buried diffusions with different doping profiles (a) .*

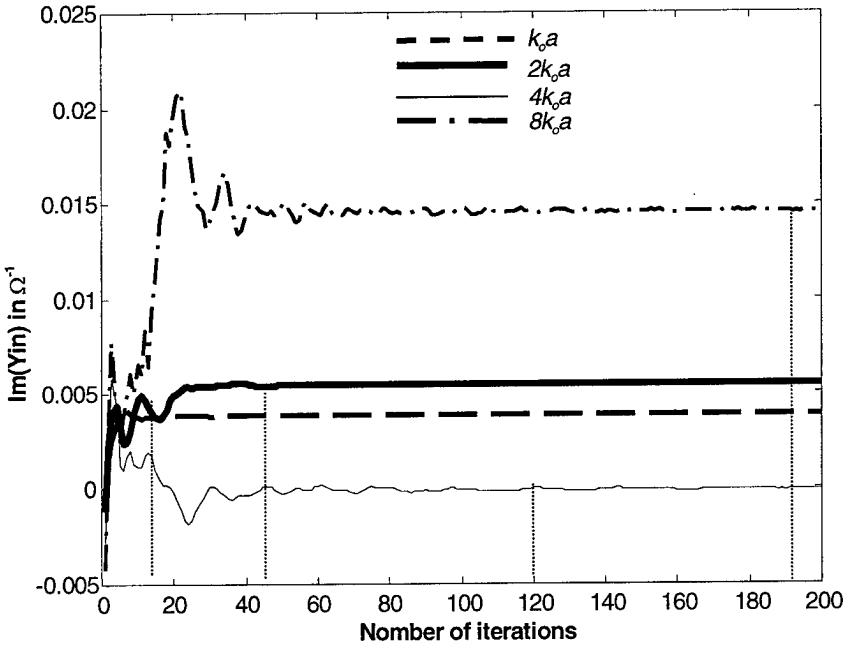


Fig.2 - *Convergence of the input admittance imaginary part against the number of iterations in the case of a simple interconnect circuit for different values of the scale parameter (koa= 0.6*

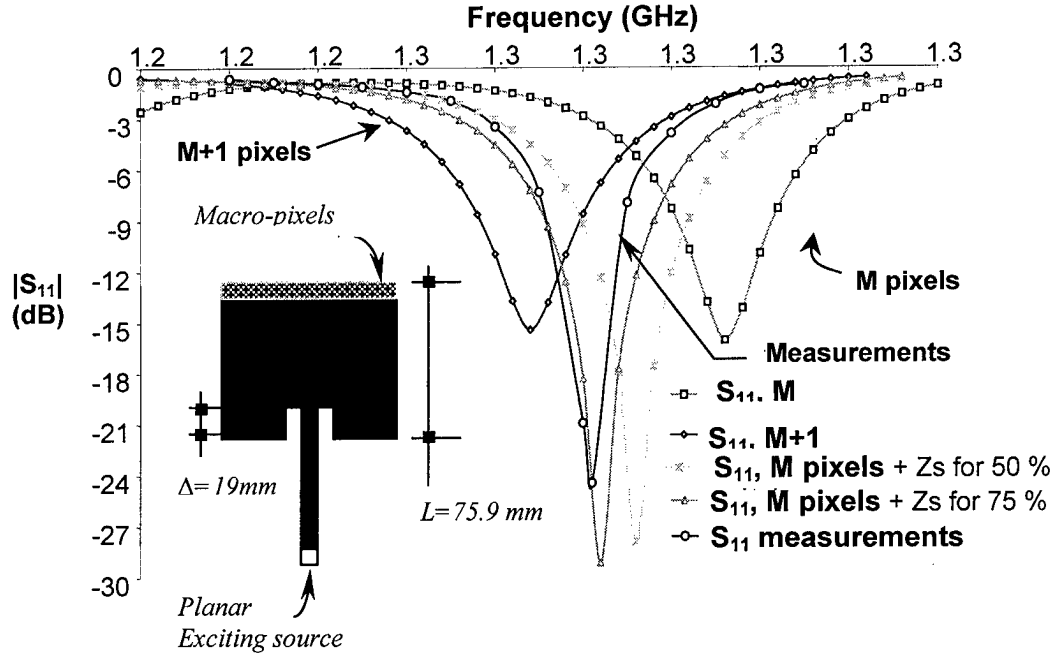


Fig.3 - *Application of non uniform meshing to planar antenna. Confrontation of the simulated insertion parameter and the measured one with and without macro-pixels against frequency.*

CONCLUSION

It has been shown that, beyond any numerical analysis considerations, integral equations in terms of waves have natural capabitilies to be solved using an iterative procedure. The wave based formulation handles scattering and reflection operators which are always bounded for physical reasons. In multi-layered structures, the limitation to homogeneous layers stack is overcomed owing to the wave-based formulation. To improve the computation time for the analysis of complex circuits, a non uniform meshing has been introduced (use of macro-pixels, Fig.3). Future investigations concerning multi-scale approaches are understudy.

REFERENCES

[1] COLLIN *"Field Theory of Guided Waves"* New York I.E.E. E. Press

[2] R.S. N'GONGO, H. BAUDRAND *"Application of wave concept iterative procedure in planar circuits"* Transword Research Network. cchglm2002 Wiley, vol. 15, pp.23-57

[5] M. KRUMPHOLZ, P. RUSSER *"A field theoretical derivation of T.L.M."* 9/1994 I.E.E.E. Trans on M.T.T. Vol. 42, n°9, pp.1661-1668.

[6] A.R. KERR *"A technique for determining the local oscillator. Wave forms in a microwave mixer"* 10/1975 I.E.E.E. Trans. on M.T.T. pp. 828-831

[7] T.P. VUONG, R. GARCIA, N. RAVEU, A. ZEID, H. BAUDRAND, J.C. PEUCH *"F.W.C.I.P. Method for P.G.B. planar structures"* Int. Journal of R.F. Microwave Computer-Aided Engineering Issue 3, pp. 236-246

[8] R.S. N, GONGO, H. BAUDRAND *"A new approach for microstrip active antennas using MODAL F.F.T. Algorithm"* 7/1999 I.E.E.E AP-S International Symposium Orlando

[9] A. GHARSALLAH, R. GARCIA, A. GHARBI, H. BAUDRAND. *W.C.I.P. merges with modal F.F.T. to analyse microstrip filters.* 3/2001 Applied Computational Electromagnetic Society Journal

[10] E. RICHALOT, M.F. WONG, H. BAUDRAND, V. FOUAD HANNA *" An iterative method for modelling of antennas"* 6/2001 R.F.and Microwave Computer Engineering ,vol 11, pp 194-201

[11] D. BAJON, S. WANE, H. BAUDRAND, P. GAMAND *"Full wave Analysis of Isolated Pockets to Improve Isolation Performances in Silicon based Technology", IEEE MTT-S ,* Seattle June *2002.*

ANALYTICAL STUDY OF MICROWAVE STRUCTURES PRINTED ON ANISOTROPIC SUBSTRATES BASED ON THE WIENER-HOPF TECHNIQUE

George A. Kyriacou

Department of Electrical and Computer Engineering
Demokritos University of Thrace, GR-67100, Xanthi, Greece
Tel.:+30-541-79593, Fax:+30-541-27264, E-mail: gkyriac@ee.duth.gr

ABSTRACT

An analytical approach for the study of microwave devices and antennas printed on anisotropic substrates is presented. This is based on the geometrical optics approach in conjunction with a reflection coefficient established through a Wiener-Hopf solution of the corresponding canonical problem. A parallel plane waveguide with a semi-infinite upper conductor and loaded with a plasma magnetized parallel to the edge of the truncated plane conductor is considered. The scattering problem of the dominant extra-ordinary TEM wave normally incident up on the edge of the truncated conductor is formulated in the Fourier transformed domain and solved using a Wiener-Hopf technique.

INTRODUCTION

The introduction of anisotropic substrates constitutes a research challenge in the electromagnetic field, particularly when an analytical approach is employed. Even when numerical techniques are used, the study of microwave structures printed on substrates with a generalized anisotropy still constitutes a difficult problem with a lot of unresolved issues. However, the anisotropy could be an important parameter either in the case when this is an inherent property of the material (e.g. sapphire and quartz) or an artificially caused (e.g. Epsilam-10) during the fabrication process. The most general anisotropy occurs when ferrite or plasma materials are subject to constant magnetic field of an arbitrary direction, which are then described by full tensor permeability $(\overline{\overline{\mu}}_r)$ and permittivity $(\overline{\overline{\varepsilon}}_r)$ respectively. These tensor constitutive parameters depend on the biasing magnetic field and the operating frequency. This dependence enables their dynamic control through the DC current of an electromagnet used to generate the biasing magnetic field. Recently, the exploitation of the exceptional features offered by magnetized ferrites in printed microwave devices and antennas has received a considerable effort. Wideband electronic tuning, beam steering and possible surface wave and RCS reduction are some of the widely known features. Magnetized plasmas behave as the dual of magnetized ferrites but still offering the same features, it could thus be more suitable for some geometries. However, there was only a minor effort in the exploitation of its properties in printed antennas and microwave circuits, while there was a considerable effort in the study of antennas embedded in a magnetized plasma in their operating environment (mostly for satellite and nuclear fusion applications). This lack may due to the difficulties in generating and controlling ionized gas plasma. However, the evolution in the electronic solid state technology (currently at cryogenic temperatures) may stimulate its introduction in printed microwave structures and antennas. Some recent publications based on numerical techniques [1-3] are directed toward these applications.

Analytical studies and especially the Wiener-Hopf technique offer a clear physical insight into the problem enabling an integral exploitation of the structure properties. This is of primary importance, even though its application concerns only simple geometrical structures. Since, the

extracted properties can be extended to more complicated structures of practical use which can then be simulated numerical.

Concerning the uniaxially anisotropic substrate, El-Sherbiny [4, 5] has directly applied the Wiener-Hopf technique for the study of microstrip-lines and fin-lines. In our previous works, e.g. [6-8] we have indirectly applied the Wiener-Hopf for the study of wide microstrip lines as well as rectangular and triangular patch antennas printed on uniaxial dielectric substrate. This is based on the solution of the canonical problem of the scattering of a TEM wave obliquely incident upon the edge of a semi-infinite plane conductor printed on a grounded uniaxial substrate (this structure can be considered as a dielectric loaded parallel plane waveguide with a truncated upper conductor). A reflection coefficient is established from this analysis which is in turn combined with a geometrical optics approach and a transverse resonance condition in order to study the printed lines or antennas. Moreover, the physical insight offered by the solution of the canonical problem is by itself of particular significance.

Our present research effort is directed toward the study of wide microstrip lines and patch antennas printed on magnetized ferrite or magnetized plasma substrates. The first step again concerns the solution of the corresponding canonical problem, as described above. Unfortunately, when an obliquely incident TEM wave is considered, the formulation yields two Wiener-Hopf equations coupled in a very complicated manner. Up to now we were not able to decouple or solve this system, even though we have studied all the available literature on the coupled Wiener-Hopf equations. However, we found out that there are certain simpler cases of specific orientations of DC magnetization for which the Wiener-Hopf equations for the electric and magnetic field are inherently decoupled. This is exactly the subject on which our present research effort is focused. A case of particular practical importance is the infinitely extending parallel plane waveguide loaded with a ferrite or plasma layer which is magnetized parallel to the edge of its truncated upper conductor. Considering a normally incident TEM wave on this edge and formulating the scattering field yields two decoupled Wiener-Hopf equations. This was first observed by Johansen [9], who studied the scattering, by the end of a semi-infinite parallel plane waveguide loaded with magnetized plasma. Furthermore, the normal incidence is very useful in the study of rectangular patch antennas. Considering the patch to be probe-fed and studying any arbitrary TEM wave emanating from the probe, it can be proved (e.g. [6]) that at the antenna resonance (the desired operating condition) the dominant TEM mode incidents almost normally at the patch radiating edge.

Furthermore, it must be noted that in a parallel plane waveguide loaded with ferrite the dominant TEM mode is the ordinary one, since the extraordinary TEM mode has an electric field component parallel to the two metallic planes. In contrary, in the magnetized plasma case this occurs vice-versa and the extra-ordinary TEM mode becomes dominant. From this observation one may conclude that is more convenient to exploit the dynamic $\bar{\bar{\varepsilon}}_r$ control in patch antennas printed-placed on magnetized (solid state) plasma. Summarizing, this presentation will first review our established procedure for the Wiener-Hopf analysis of structures printed on uniaxial substrate, while we will then focus on our recent work on the study of the canonical problem in the magnetized plasma case.

GEOMETRICAL OPTICS TECHNIQUE

In order to explain the need for the solution of the canonical problem described below; consider the probe-fed microstrip line shown in Fig.1. According to the geometrical optics technique the field emanating from the probe can be expressed as a sum (or integral in general) of rays (TEM-waves) propagating at any possible direction around the probe. These rays are successively reflected at the two edges (apertures) defined by the ends of the microstrip line, becoming parallel after two reflections. Only those rays having an angle of incidence (propagation constant) such that the parallel ones are in phase, thus interacting in a constructive manner, are

propagating. All the other rays interact in a destructive manner and they vanish at a small distance from the probe. In other words the propagation constant of the line is defined based on a transverse resonance condition. The rectangular patch antenna as well as some triangular ones (the 45^0-45^0-90^0, 60^0-60^0-60^0 and 30^0-60^0-90^0) can be analyzed in a quite similar way. In any one of these cases the complex reflection coefficient of an obliquely incident ray at the aperture formed by the edge of a printed line or antenna must be known.

If this edge could be considered "isolated", namely by ignoring the mutual coupling between the different edges of the printed structure, then the desired reflection coefficient could be obtained from the solution of the corresponding canonical problem. This approximation seems to be reasonable for wide microstrip lines and any patch antenna that could be analyzed using the geometrical optics technique. This is based on the fact that printed antennas are operating around their resonance, thus they have fairly large resonant dimensions (comparable to $\lambda_g/2$). Obviously, this technique cannot be used for the study of printed dipoles, due to their small transverse dimension. It is worth to recall here that strong coupling between printed components occurs only when their distance is comparable to the substrates thickness (d), while at a distance greater than 3 to 4 times d the coupling can be practically ignored. It is that expected that the geometrical optics technique is best suited for relatively thin dielectric substrates (this is the usual practice) and in any case its thickness must be well below a quarter wavelength.

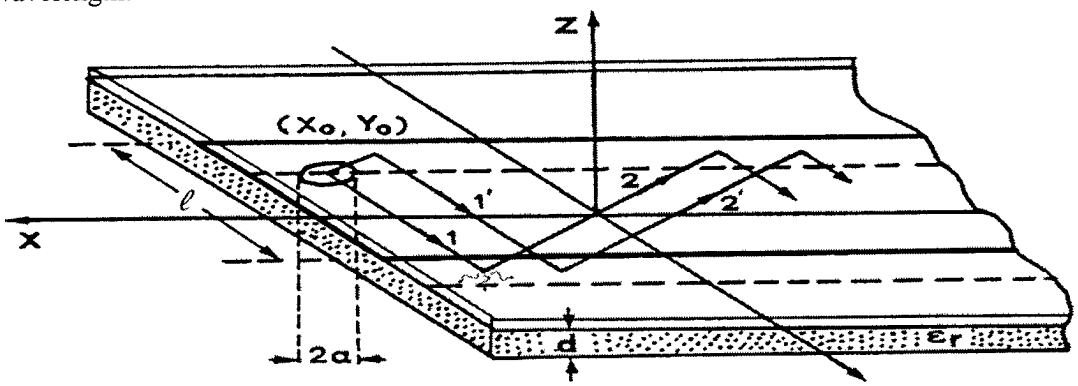


Fig.1. Ray analysis under a probe fed microstrip line with a superstrate.

Details concerning the evaluation of the field under the patch for both the propagating and the evanescent modes as well as the establishment of the transverse resonance technique can be found in our previous works, [6-8].

Starting from the probe-fed microstrip line of width-ℓ, as in Fig.1, a rectangular patch antenna can be obtained by cutting the line at two edges at a distance-h between them. The reflection coefficient established by the Wiener-Hopf technique is used in any one of the occurring reflections. The propagation constant and the excited modes are defined in exactly the same manner as for the microstrip line. The resulting field propagating along the line is reflected back and forth between the two edges at $x=\pm h/2$. Once again when the parallel rays between these successive reflections are in-phase or have phase difference $q.2\pi$, with $q=1,2,\ldots$, then the field under the patch becomes maximum

It is important to note that at the antenna resonant condition the dominant mode field (ray) incidents almost normally at the radiating edge. Moreover, the above technique applies with an acceptable accuracy when any one (or more) of the patch antenna edge is short-circuited to the ground plane. At this edge a perfect reflection is approximately assumed.

The remaining of this article will be focused on the canonical problem when a magnetized plasma substrate is considered.

FORMULATION OF THE CANONICAL PROBLEM

The geometry to be studied is shown in Fig.2. Basically it consists of a parallel plane waveguide loaded with magnetized plasma, where the lower conductors (ground plane) and the plasma substrate are assumed extending to infinity while a semi-infinite (truncated z<0) upper conductor is considered. The biasing constant magnetic field ($\overline{H}_{dc}$) is assumed parallel to the two planes and parallel to the edge ($\hat{y}$-axis, $\overline{H}_{dc} = H_o \hat{y}$). The extra-ordinary TEM wave (possibly emanating from a probe feed) propagating along the $\hat{z}$-axis (transverse to $\overline{H}_{dc}$) is considered to be incident normally on the edge defined by the truncated upper conductor. Time harmonic fields ($e^{j\omega t}$) and a λ-space spectrum Fourier transform pair in the z-direction are considered (in the form $e^{jk_o\lambda z}$).

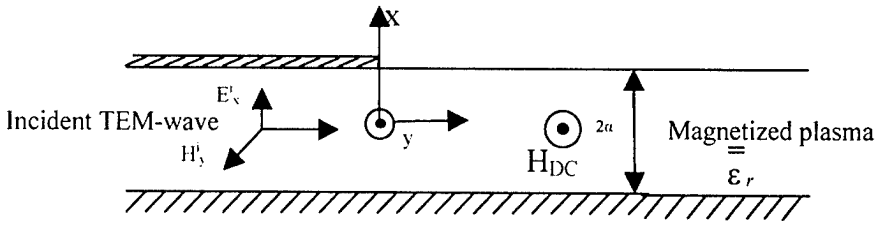


Fig.2. A TEM wave incident upon the edge defined by the truncate upper conductor of a parallel plane waveguide loaded with magnetic plasma.

This assumption results in a simplification of the wave equation by substituting $\partial/\partial y = -jk_0\lambda$. Since the excited extra-ordinary TEM wave propagating in the parallel plane region (z<0) is assumed to be incident normally on the edge z=0, there will be no variation of the scattered field in the also infinitely extending y-direction. This in turn results to a further simplification of $\partial/\partial y = 0$. Moreover, the magnetized plasma ($\overline{H}_{DC} = H_o \hat{y}$) relative permeability tensor is given in [9] as:

$$\overline{\overline{\varepsilon}}_r = \begin{bmatrix} \varepsilon_{r1} & 0 & j\varepsilon_{r2} \\ 0 & \varepsilon_{r3} & 0 \\ -j\varepsilon_{r2} & 0 & \varepsilon_{r1} \end{bmatrix} \tag{1}$$

Where $$\varepsilon_{r1} = \frac{\Omega^2 - R^2 - 1}{\Omega^2 - R^2},\ \varepsilon_{r2} = \frac{R}{\Omega(\Omega^2 - R^2)},\ \varepsilon_{r3} = 1 - \frac{1}{\Omega^2}$$

and $\Omega = \omega/\omega_p$, $R = \omega_c/\omega_p$, $\omega_p^2 = Ne^2/m\varepsilon_o$, $\omega_c = -e\mu_o H_o/m$.

The plasma frequency is symbolized as ω_p and its gyromagnetic frequency as ω_c also, e and m are the charge and the mass of an electron and ε_o, μ_o are the free space permittivity and permeability. With the above considerations, the wave equation for the scattered magnetic field in the λ-domain ($\tilde{H}^s_y$) for the plasma region can be written as:

$$\{\frac{\vartheta^2}{\vartheta x^2} + k_o^2(\frac{\varepsilon_{rq}}{\varepsilon_{r1}} - \lambda^2)\}\tilde{H}^s_y = 0 \tag{2}$$

Where $k_o = \omega\sqrt{\mu_o\varepsilon_o}$ the free space wavenumber and $\varepsilon_{rq} = \varepsilon_{r1}^2 - \varepsilon_{r2}^2$.

The general solution of (2) in the plasma region $-a \le x \le a$ takes the form:

$$\tilde{H}^s_y = B_p(\lambda)\cosh(k_o u_p x) + C_p(\lambda)\sinh(k_o u_p x) \tag{3}$$

where $u_p = \sqrt{\lambda^2 - \varepsilon_{rq}/\varepsilon_{r1}}$ and $\mathrm{Re}(u_p) \geq 0$.

The transverse field components can also be expressed in the transformed domain as:

$$\tilde{E}_x^s = \frac{\zeta_o}{\varepsilon_{rq}}\{\lambda\varepsilon_{r1}\tilde{H}_y^s - \frac{\varepsilon_{r2}}{k_o}\cdot\frac{\partial\tilde{H}_y^s}{\partial x}\} \qquad \tilde{E}_z^s = j\frac{\zeta_o}{\varepsilon_{rq}}\{\lambda\varepsilon_{r2}\tilde{H}_y^s - \frac{\varepsilon_{r1}}{k_o}\cdot\frac{\partial\tilde{H}_y^s}{\partial x}\} \tag{4}$$

where $\zeta_o = \sqrt{\mu_o/\varepsilon_o} = (120\pi)\Omega$ the free space characteristic impedance.

The remaining field components vanish ($\tilde{E}_y^s = \tilde{H}_x^s = \tilde{H}_z^s = 0$) due to the assumption $\partial/\partial y = 0$. The general solution for the air region can be obtained by substituting in equations (2)-(4) its characteristics ($\varepsilon_{r1} = \varepsilon_{r3} = 1, \varepsilon_{r2} = 0$). However, this solution must also obey the radiation condition at infinity, so for the air region $x \geq a$, we have:

$$\tilde{H}_z^s = A_p(\lambda)\cdot e^{-k_o u_o (x-a)} \quad \text{with } u_o = \sqrt{\lambda^2 - 1} \text{ and } \mathrm{Re}(u_o) \geq 0 \tag{5a}$$

and

$$\tilde{E}_x^s = \zeta_o \lambda \cdot \tilde{H}_y^s \qquad \tilde{E}_x^s = \frac{1}{j\omega\varepsilon_o}\cdot\frac{\partial\tilde{H}_y^s}{\partial x} \tag{5b}$$

The quantities $A_p(\lambda)$, $B_p(\lambda)$ *and* $C_p(\lambda)$ involved in the above equations are arbitrary spectral functions to be estimated from the application of the boundary conditions. The incident extra-ordinary TEM wave propagating in the parallel-plane region toward the positive z-direction is given by Johansen, [9] as:

$$H_y^i = \exp\{k_o\varepsilon_{r1}x/\sqrt{\varepsilon_{r1}} - jk_o\sqrt{\varepsilon_{r1}}z\} \quad \text{and} \quad E_x^i = (\zeta_o/\sqrt{\varepsilon_{r1}})\cdot H_y^i \tag{6}$$

where a unit amplitude is assumed for H_y^i just for convenience. The scattering on the edge will excite a reflected TEM wave along with higher order modes, which will in turn vanish at a relatively small distance from the edge, provided that the plasma-substrate thickness is small enough (in order for these modes to be below cut-off). The reflected TEM wave propagating in the negative z-direction can be expressed as:

$$H_y^r = \Gamma_{TEM}\cdot\exp\{-k_o\varepsilon_{r2}\cdot x/\sqrt{\varepsilon_{r1}} + jk_o\sqrt{\varepsilon_{r1}}z\} \quad \text{and} \quad E_x^r = (-\zeta_o/\sqrt{\varepsilon_{r1}})\cdot H_y^r \tag{7}$$

Where Γ_{TEM} is the complex reflection coefficient to be sought from the study of the scattering at the edge, using Wiener-Hopf technique. The Jone's method is employed for convenience reasons, [10-11], namely the wave equation solution and the application of the boundary conditions are carried out in the transformed λ-domain. Specifically, the scattered tangential electric field $\tilde{E}_z^s$ must vanish on the metallic ground plane (x=-a) and preserve its continuity at the plasma-air interface at $x = a$. Note that the corresponding tangential component of the incident field is identically zero $\left(E_z^i = E_z^r = 0\right)$. Also the tangential electric field must vanish on the truncated upper conductor $\left(x = a, z < 0\right)$:

$$E_z^s\left(x = a^+, z < 0\right) = f_+(z) = j\zeta_o\int_{C_+} u_o A_p(\lambda) e^{-jk_o\lambda z} = 0 \tag{8}$$

In order to satisfy (8), we are looking for a function which must be identically zero for z<0 and with α-value $f_+(z) \neq 0$ to be defined for $z > 0$. This may result from the inverse Fourier transform of a "positive" spectral function $R_+(\lambda) = u_o A_p(\lambda)$ analytic in the upper λ half-plane. Using the two previously described boundary conditions the two spectral functions $B_p(\lambda)$ and $C_p(\lambda)$ are also expressed in terms of $R_+(\lambda)$. The dependence of the scattered field from the incident extra-ordinary TEM wave (excitation) can be obtained either by applying

the continuity of the total normal electric flux density $D_{x,tot}$, or the continuity of the total tangential magnetic field $H_{y,tot}$ at the plasma-air interface $(x=a, z>0)$. At this point we assume that the incident field propagates un-attenuated in the region $z>0$, or that it exists in the area $(|x|\le a, -\infty<z<+\infty)$. This is a usual assumption of the Wiener-Hopf technique, e.g. [11, p.126], since it simplifies the problem while its contribution can be evaluated and subtracted latter from the corresponding residue of the propagating field. Imposing in turn the latter boundary condition for $\tilde{H}_{y,tot}=\tilde{H}_y^s+\tilde{H}_y^i$, yields:

$$\tilde{L}_-(\lambda)=\tilde{H}_y^s\left(x=a^+,\lambda\right)-\tilde{H}_y^s\left(x=a^-,\lambda\right)-\tilde{H}_y^i\left(x=a^-,\lambda\right)=0 \quad \text{valid for } z>0 \tag{9}$$

Taking the inverse Fourier transform and requiring the integral to be identically zero for $z>0$ and to have a non-zero value for $z<0$, we may define the spectral function $\tilde{L}_-(\lambda)$ as a "negative" one. Namely, a function analytic in the lower λ-half-plane. The combination of the above expressions yields a Wiener-Hopf equation of the form:

$$Q(\lambda)\tilde{R}_+(\lambda)=\tilde{L}_-(\lambda)-\tilde{j}_+(\lambda) \tag{10}$$

Where

$$Q(\lambda)=\frac{1}{u_o}+\frac{\lambda\varepsilon_{r2}+\varepsilon_{r1}\cdot u_p\cdot coth\left(k_o u_p a\right)}{\left(\lambda^2-\varepsilon_{r1}\right)} \tag{11}$$

and

$$\tilde{j}_+(\lambda)=-j\,exp\left(k_o\varepsilon_{r2}a/\sqrt{\varepsilon_{r1}}\right)/\left\{2\pi\left(\lambda-\sqrt{\varepsilon_{r1}}\right)\right\} \tag{12}$$

The spectral function $\tilde{j}_+(\lambda)$ represents the Fourier transform of a fictitious current density that could be induced on $(x=a, z>0)$ if a conductor would be placed there. The remaining of the analysis involves the factorization of the kernel $Q(\lambda)$ into a product of "positive" and "negative" function $Q(\lambda)=Q_+(\lambda)\cdot Q_-(\lambda)$ and in turn the evaluation of $\tilde{R}_+(\lambda)$. This enables the evaluation of the scattered field, the TEM wave reflection coefficient and in extension the radiated sky-wave field. The Kernel Q(λ) involves a branch cut at $u_0=0$ or at $\lambda=\pm1$, thus the factorization cannot be carried out in a closed form. An appropriate factorization formula is given by Mittra and Lee, [11, p.116-119] and this is the one employed herein. In order to get purely analytical results an equivalent closed geometry is considered. For this purpose an infinitely extending plane conductor placed parallel to the structure of Fig.2 and at a distance (d) is assumed. the above analysis is then repeated for this closed (shielded) geometry to yield a meromorphic Kernel function $Q_c(\lambda)$ of the form :

$$Q_c(\lambda)=\frac{1}{u_0\tanh[k_0u_0(d-a)]}+\frac{\lambda\varepsilon_{r2}+\varepsilon_{r1}u_p\coth(2k_0u_p\alpha)}{\lambda^2-\varepsilon_{r1}} \tag{13}$$

This was then factorized in the form of highly convergent infinite products according to Noble [10] and Mittra and Lee [11]. These expressions are similar to those of Janaswamy, [12]. In order to get the factorized expressions for the actual grounded geometry we take the limit when the distance of the shield tends to infinity ($d\to\infty$). We are currently evaluating-comparing the results of the two factorization approaches. More details along with the further process will be presented during the symposium. It must also be noted that following a similar approach and exploiting the remaining boundary conditions a Wiener-Hopf equation involving the induced change density, can be obtained.

CONCLUSIONS

An analytical study of microwave devices and antennas printed on anisotropic substrates is first reviewed. Its establishment based on the geometrical optics and a Wiener-Hopf type analysis is then summarized. In particular a geometry of a parallel plane waveguide, loaded with a magnetized plasma with a semi-infinite upper conductor is considered. The scattering of the dominant extra-ordinary TEM-wave normally incident upon the edge defined by the truncated upper conductor is treated analytically. A Wiener-Hopf equation is obtained factorized and solved. The equivalent shielded geometry is also treated in order to get the final expressions in closed form.

REFERENCES

[1] F. Hunsberger, R. Luebbers and K. Kunz, "Finite-Difference Time-Domain analysis of gyrotropic media-I: Magnetized plasma", IEEE Trans. vol. AP-40, pp. 1489-1495, Dec. 1992.

[2] T. Kashiwa, N. Yoshida and I. Fukai, "Transient analysis of a magnetized plasma in three-dimensional space", IEEE Trans., vol. AP-36, pp. 1096-1105, Aug. 1988.

[3] T. Kashiwa, N. Yoshida and I. Fukai, "Time domain analysis of patch antennas in a magnetized plasma by a spatial network method", IEEE Trans., vol. AP-39, pp. 147-150, Feb. 1991.

[4] A.M. El-Sherbiny, "Hybrid mode analysis of microstrip lines on anisotropic substrates", IEEE Trans. Microwave Theory Tech., vol.29, pp.1261-1265, Dec. 1981.

[5] A.M. El-Sherbiny, "Exact analysis of shielded microstrip lines and bilateral fin lines", IEEE Trans. Microwave Theory Tech., vol.29, pp.669-675, July 1981.

[6] G.A. Kyriacou and J.N. Sahalos, "The edge admittance model for the study of microstrips on uniaxial substrate", Archiv. für Elektrotech., vol.76, pp.169-179, 1993.

[7] G.A. Kyriacou and J.N. Sahalos, "A Wiener-Hopf type analysis of Microstrips printed on uniaxial substrates : Effect of the substrate thickness", IEEE Trans. Microwave Theory Tech., vol.43, pp.1967-1977, Aug. 1995.

[8] G.A. Kyriacou and J.N. Sahalos, "A Wiener-Hopf type analysis of uniaxial substrates-superstrate microstrip structures", IEEE Trans. Microwave Theory Tech., vol.45, pp.616-629, May 1997.

[9] E.L. Johansen, "The radiation properties of a parallel-plane waveguide in a transversely magnetized homogeneous plasma", IEEE Trans., vol. MTT-13, pp. 77-89, Jan 1965.

[10] B. Noble, "Methods based on the Wiener-Hopf Technique", Pergamon Press, 1958.

[11] R. Mittra and S.W. Lee, "Analytical techniques in the theory of guided waves", McMillan, New York, 1971.

[12] R. Janaswamy, "Wiener-Hopf analysis of the asymmetric slotline", Radio Science, vol.25, no.5, pp.699-706, 1990.

COMPLEX AND REAL RAYS IN THREE DIMENSIONAL MINKOWSKI SPACE

Elman Hasanov
Isik University, College of Arts and Science, Mathematics Department
Istanbul,Turkey
E-mail: elman@isikun.edu.tr

ABSTRACT

A new approach to the theory of complex rays is proposed. It is shown that the Minkowski space is more appropriate for describing these rays than the usual Euclidian spaces. Some illustrative examples are represented.

INTRODUCTION

Despite remarkable progress in computitional technics and numerical methods used in electromagnetic theory, the ray method remains one of the powerful methods of the applied and theoretical electromagnetic theory due to its simplicity and informativity. In this approximation wave field is written in the form of locally plane wave

$$u = Ae^{ikS} \tag{1}$$

where $A = A(r)$ is amplitude and $S = S(r)$ is eikonal which determines the phase structure of the field. These functions usually are slowly variable functions of their arguments. k is a large number, so function $kS(r)$ can take large values. (1) usually is considered as a leading term in the asymtotic expansion called ray expansion or WKB ansatz of the solution $u(r)$ to the Helmholtz equation. In homogenious medium function $S(r)$ satisfies eikonal equation (4). In our days there exist many excellent books and articles describing fundaments of the ray theory and their various applications. If for real rays (i.e. real solutions of the eikonal equations) the geometry of the problem is very clear and character of arising problems are mainly analitical, in the case of complex rays (i.e. complex solutions of the eikonal equations) many difficulties are connected with the geometrical representation of complex rays, since it is not possible geometrically to draw complex rays in two or three dimensional spaces. Usually complex rays are thought as an analytical continuation of the real rays ([1,2]). However, this procedure requires analyticity of initial functions for Helmholtz equation and other involved ray parametres and immediately fails if the boundary or the boundary datas are not analytic. We think instead of the complexfication of the coordinates (i.e. instead of the theory of the functions of complex variables) it will be more reasonable to complexficate the distances, i.e. consider the rays in the pseudeuclidian spaces. The aim of this paper is to describe a new approach to the real and complex rays. We will show that the three dimensional Minkowski space is more appropriate for geometrization both real and complex rays than usual Euclidian spaces and visually there is no difference between real and complex rays in this space: complex

rays are rays inside the light cone and real rays are rays outside of the light cone. At each point real and complex are orthogonal in the sense of the Minkowski metrics. For example a Gaussian beam of the "waist" R simple is a bundle of paraxial normals to the pseudesphere with center at origin and radius iR in R^3_2

MAPPINGS BETWEEN INITIAL AND TERMINAL PLANES GENERATED BY OPTICAL FIELDS

Consider standard Helmholtz equation

$$\Delta u + k^2 u = 0 \tag{2}$$

Assume that we are seeking solution (2) under rapidly oscillating initial condition which is given on the some domain D of the plane $z = 0$ as

$$u(x, y, 0) = A_0(x, y) e^{ik\varphi(x,y)} \tag{3}$$

where $A_0(x, y)$ is amplitude, $\varphi(x, y) = S(x, y, 0)$ and $S(x, y, z)$ the solution of the eikonal equation

$$\nabla^2 S = 1 \tag{4}$$

Can easily be shown that the corresponding ray solution is

$$\xi = x + \sigma\varphi_x, \qquad \eta = y + \sigma\varphi_y, \qquad \sigma = \frac{z}{\sqrt{1 - \varphi_x{}^2 - \varphi_y{}^2}} \tag{5}$$

Eqs. (5) represent rays that start at (x, y) and end at (ξ, η), so (5) can be considered as a mapping between (x, y) and (ξ, η) planes (for fixed z).

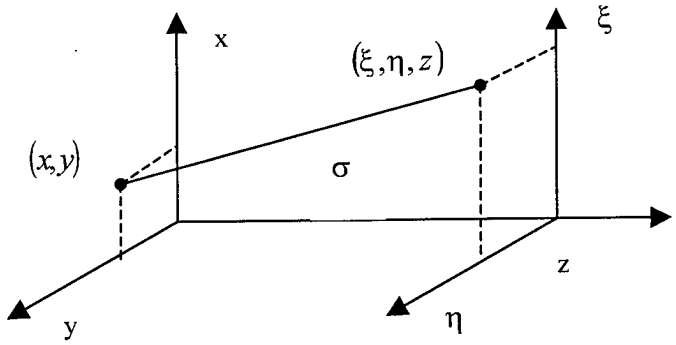


Fig.1. Mapping between initial and end planes

To each point on the ray described by (5) we can assign at least three triple coordinates: cartesian coordinates (ξ, η, z), ray coordinates (x, y, σ) (or (ξ, η, σ)) and coordinates (x, y, z) geometrical meaning which we will indicate below. Excluding σ from (5) we get mapping $\xi = \xi(x, y), \eta = \eta = \eta(x, y)$ between (ξ, η) and (x, y) planes:

$$\xi = x + \frac{z\varphi_x}{\sqrt{1-\varphi_x{}^2-\varphi_y{}^2}} \qquad \eta = y + \frac{z\varphi_y}{\sqrt{1-\varphi^2{}_x-\varphi_y{}^2}} \tag{6}$$

In the terms of mapping (6) the energy conversation law in a small tube can be written as

$$\frac{\partial\xi}{\partial x}\frac{\partial\eta}{\partial y}-\frac{\partial\xi}{\partial y}\frac{\partial\eta}{\partial x}=\pm\frac{A^2{}_0(x,y)}{A^2(\xi,\eta,z)} \tag{7}$$

where $A(\xi,\eta,z)$ is the amplitude of the field on the plane (ξ,η,z)

CAUSTICS AND GEOMETRICAL MEANING OF (5)

Since on caustics ray tube vanishes then left side hand of (7) also vanishes:

$$\frac{\partial\xi}{\partial x}\frac{\partial\eta}{\partial y}-\frac{\partial\xi}{\partial y}\frac{\partial\eta}{\partial x}=0 \tag{8}$$

Calculating partial derivatives in (6) and substituting into (8) provides

$$1+z\frac{\left(1-\varphi_y{}^2\right)\varphi_{xx}+2\varphi_x\varphi_y\varphi_{xy}+\left(1-\varphi_x{}^2\right)\varphi_{yy}}{\left(1-\varphi^2{}_x-\varphi^2{}_y\right)\sqrt{1-\varphi^2{}_x-\varphi^2{}_y}}+z^2\frac{\varphi_{xx}\varphi_{yy}-\varphi^2{}_{xy}}{\left(1-\varphi^2{}_x-\varphi^2{}_y\right)^2}=0 \tag{9}$$

Eq. (10) can be interpreted in two ways. First, for given $\varphi(x,y)$ we can solve (9) for z to find two sheets $z_{1,2}=z_{1,2}(x,y)$ of the caustic surfaces in the coordinates (x,y,z). Substituting $z_i(x,y)$ into (6) we get parametrical equations of the caustics in the (ξ,η,z) coordinates. Second, if $z=z(x,y)$ is known, then substituting it into Eq. (9) we obtain a differential equation for determining $\varphi(x,y)$, for which caustic is $z=z(x,y)$

In order to understand the geometric nature of Eq. (9) we introduce the three dimensional pseudoeuclidian space $R^3{}_2$, which is the three-dimensional analog of the well known four-dimensional Minkowski space of the special theory of relativity. In this space the length of a vector $|\vec{u}|=(\xi,\eta,\zeta)$ is defined as

$$|\vec{u}|^2=\zeta^2-\xi^2-\eta^2 \tag{10}$$

The geometrical place of the points where (10) vanishes is a, so called, "light cone". Vectors inside of the light cone have positive length, and vectors outside of the light cone have imaginary length. The unit normal to the surface $\zeta=\varphi(\xi,\eta)$ in $R^3{}_2$ is

$$\vec{n}=\left(\frac{\varphi_\xi}{\sqrt{1-\varphi^2{}_\xi-\varphi^2{}_\eta}},\frac{\varphi_\eta}{\sqrt{1-\varphi^2{}_\xi-\varphi^2{}_\eta}},\frac{1}{\sqrt{1-\varphi^2{}_\xi-\varphi^2{}_\eta}}\right) \tag{11}$$

For the "space-like" surfaces, $1-\varphi^2{}_\xi-\varphi^2{}_\eta>0$, $\vec{n}$ has positive length and for "time-like" surfaces , $1-\varphi^2{}_\xi-\varphi^2{}_\eta<0$, $\vec{n}$ has imaginary length. Now let us rewrite Eqs. (5) in the form

$$\xi = x + \frac{z\varphi_x}{\sqrt{1-\varphi_x{}^2-\varphi_y{}^2}} \qquad \eta = y + \frac{z\varphi_y}{\sqrt{1-\varphi^2{}_x-\varphi_y{}^2}}$$

$$\zeta = \sigma + \varphi(x,y) = \varphi(x,y) + \frac{z}{\sqrt{1-\varphi^2{}_\xi - \varphi^2{}_\eta}} \tag{12}$$

where $\zeta = \sigma + \varphi(x,y)$ is total phase, or

$$(\xi,\eta,\zeta) = (x,y,\varphi(x,y)) + z\left(\frac{\varphi_x}{\sqrt{1-\varphi^2{}_x - \varphi^2{}_y}}, \frac{\varphi_y}{\sqrt{1-\varphi_x{}^2 - \varphi^2{}_y}}, \frac{1}{\sqrt{1-\varphi^2{}_x - \varphi^2{}_y}}\right) \tag{13}$$

Eq. (13) persists to assume that $\varphi(x,y)$ is a wave front in $R^3{}_2$ and (13) (or the same (5)) is no other than normal mapping for the surface $\varphi(x,y)$ in $R^3{}_2$, that is rays for the problem (2)–(3) exactly are normals to $\varphi(x,y)$ in $R^3{}_2$, that is the ray is real if it lies inside the light cone $(1-\varphi^2{}_\xi - \varphi^2{}_\eta > 0)$ and it is complex if it lies outside the light cone $(1-\varphi^2{}_\xi - \varphi^2{}_\eta < 0)$. The case $1-\varphi^2{}_x - \varphi_{\ y} = 0$ requires a special study. The set of points in (x,y) plane, where $1-\varphi^2{}_x - \varphi_{\ y} = 0$ we call Stokes line of the problem (2)-(3). Note that according to (13) the coordinates (x,y,z) mentioned above, are ray coordinates for wave front $\varphi(x,y)$ in $R^3{}_2$. At the focal points of $\varphi(x,y)$ the jacobian of (13) vanishes:

$$\frac{\partial(\xi,\eta,\zeta)}{\partial(x,y,z)} = 0 \tag{14}$$

or after calculating partial derivatives in (12)

$$1 + z\frac{\left(1-\varphi_y{}^2\right)\varphi_{xx} + 2\varphi_x\varphi_y\varphi_{xy} + \left(1-\varphi_x{}^2\right)\varphi_{yy}}{\left(1-\varphi^2{}_x - \varphi^2{}_y\right)\sqrt{1-\varphi^2{}_x - \varphi^2{}_y}} + z^2\frac{\varphi_{xx}\varphi_{yy} - \varphi^2{}_{xy}}{\left(1-\varphi^2{}_x - \varphi^2{}_y\right)^2} = 0 \tag{15}$$

which exactly is Eq. (9). This persists to assume that (15) is a characteristic equation for $\varphi(x,y)$ in $R^3{}_2$ and its roots $z_i = \frac{1}{R_i(x,y)}$ are radii of curvature of $\varphi(x,y)$ in the metrics (10). Eq. (9) can be written also as

$$1 + z\frac{\left(1-\varphi_y{}^2\right)\varphi_{xx} + 2\varphi_x\varphi_y\varphi_{xy} + \left(1-\varphi_x{}^2\right)\varphi_{yy}}{\left(1-\varphi^2{}_x - \varphi^2{}_y\right)\sqrt{1-\varphi^2{}_x - \varphi^2{}_y}} + z^2\frac{\varphi_{xx}\varphi_{yy} - \varphi^2{}_{xy}}{\left(1-\varphi^2{}_x - \varphi^2{}_y\right)^2} = \frac{(R_1 z - 1)(R_2 z - 1)}{R_1 R_2} \tag{16}$$

which is an analog of the formula for wave fronts in Euclidian space.

GAUSSIAN BEAMS

The Gaussian beam is usually thought of as a beam with a complex source. In such an interpretation the ray structure of Gaussian beams remains unclear. We show that in the above proposed approach the Gaussian beam possesses a simple ray structure. Consider problem (2)-(3) taking

$$\varphi(x,y) = -\sqrt{x^2 + y^2 - R^2} \tag{17}$$

Then

$$\sqrt{1-\varphi^2{}_x - \varphi^2{}_y} = \frac{iR}{\sqrt{x^2 + y^2 - R^2}} \tag{18}$$

that is $\varphi(x,y)$ is a time-like surface and normals lie outside of the light cone, that is the corresponding rays are complex. The mapping (12) takes form

$$\xi = x\left(1-\frac{z}{iR}\right), \quad \eta = y\left(1-\frac{z}{iR}\right), \quad \zeta = -\sqrt{x^2+y^2-R^2}+\frac{z\sqrt{x^2+y^2-R^2}}{iR} \tag{19}$$

Excluding x and y in (19) we get phase function in the form

$$\zeta = \zeta(\xi,\eta,z) = \sqrt{\xi^2+\eta^2+(z-iR)^2} \tag{20}$$

Rewritteng (17) in the form

$$\zeta^2 - x^2 - y^2 = -R^2 \tag{21}$$

we see that initial phase function is no other than a sphere with an imaginary radius iR in the space $R^3{}_2$. Since normals are orthogonal to this surface (in the sense of metrics (10)) then rays under question are simple radii of the sphere (21). For paraxial rays

$$\zeta = \sqrt{\xi^2+\eta^2+(z-iR)^2} \approx z-iR+\frac{1}{2}\frac{\xi^2+\eta^2}{z-iR}, \tag{22}$$

Substituting (22) into the fundamental solution of the Helmholtz equation $e^{ik\zeta}/\zeta$ we get

$$u \approx \frac{e^{ik(z-iR)}}{z-iR}\exp\left(\frac{ik}{2}\frac{\xi^2+\eta^2}{z-iR}\right) \tag{23}$$

since for paraxial rays and sufficiently large z,ζ can be replaced by $z-iR$. In (23) we recognize the standard Gaussian beam with "waist" R

FIELDS BEYOND CAUSTICS

Since caustics are envelopes of real ray families and since complex rays are orthogonal to real rays (in $R^2{}_3$ sense) then complex rays also are orthogonal to caustics , that is they are normals to caustic surfaces. So it might be expected that complex rays penetrate into the region beyond caustics and possess definite directions. We illustrate this on the standard example of circular caustics throughly studied before [2-4]. For simplicity we consider the two dimesional case. Setting

$$\varphi(x) = \cos^{-1}\left(\frac{1}{x}\right)-\sqrt{x^2-1} \qquad (x>1) \tag{24}$$

in (2)-(3), and having

$$1-\varphi'^2 = \frac{1}{x^2} > 0 \tag{25}$$

we see that (24) is a space-like. Mapping (12) becomes as

$$\xi = x - z\sqrt{x^2-1}, \qquad \zeta = \cos^{-1}\left(\frac{1}{x}\right)-\sqrt{x^2-1}+zx \tag{26}$$

Excluding x we get phase function in the form

$$\zeta(\xi,z)=\tan^{-1}\left(\frac{z}{\xi}\right)+\cos^{-1}\left(\frac{1}{\sqrt{z^2+\xi^2}}\right)-\sqrt{\xi^2+z^2-1} \tag{27}$$

Equation for caustics are: in (x,z)coordinates $z=x^{-1}\sqrt{x^2-1}$, in (ξ,z) coordinates $\xi^2+z^2=1$ and $\zeta=\cos^{-1}\xi$ in (ξ,ζ) coordinates. Since real rays are tangent to caustics then the complex phase is pure imaginary on the caustics. The value of the complex phase on the caustics is

$$\varphi(x)=i\left(\cosh^{-1}\left(\frac{1}{x}\right)-\sqrt{1-x^2}\right) \qquad (x<1) \tag{28}$$

The unite normal to this surface is $\left(-i\sqrt{1-x^2},x\right)$, then the corresponding mapping is determined as

$$\xi=x-zi\sqrt{1-x^2}, \qquad \zeta=i\left(\cosh^{-1}\left(\frac{1}{x}\right)-\sqrt{1-x^2}\right)+zx \tag{29}$$

Excluding x again as above for complex phase function beyond caaustics we get

$$\zeta(\xi,z)=\tan^{-1}\left(\frac{z}{\xi}\right)+i\left(\cosh^{-1}\left(\frac{1}{\sqrt{z^2+\xi^2}}\right)-\sqrt{1-\xi^2-z^2}\right) \tag{30}$$

LINEAR PHASE

Now let $\varphi(x,y)=ax+by+c$ where a,b,c are constant or depend on some outer parameter. Then $1-\varphi^2{}_x-\varphi^2{}_y=1-a^2-b^2$ and mapping (12) becomes as

$$\xi=x+\frac{za}{\sqrt{1-a^2-b^2}}, \quad \eta=y+\frac{zb}{\sqrt{1-a^2-b}}, \quad \zeta=ax+by+c+\frac{z}{\sqrt{1-a^2-b^2}} \tag{31}$$

Excluding x,y we get

$$\zeta(\xi,\eta,z)=a\xi+b\eta+c+z\sqrt{1-a^2-b^2} \tag{32}$$

REFERENCES

[1] Keller J.B. Streifer W. Complex rays with an application to Gaussian beams, J. Opt. Soc. Am. **61**(1), 40-43.

[2] Chapman S.J. and etc. On the theory of complex rays, SIAM Review, **41** (4), 417-509.

[3] Keller J.B. A geometrical theory of diffraction, in: Calculus of Variation and its Applications, Proc. Symp. Appl. Math. **8**, 27-38.

[4] Kravtsov Yu.A. and etc. Theory and applications of complex rays, E. Wolf, Progress in Optics XXXIX, 1999,1-62.

ARTIFICIAL ANISOTROPY

† Frédéric Zolla , ‡ Didier Felbacq

† Institut Fresnel, U.M.R. 6133,
Faculté de Saint Jérôme Case 161, 13397 Marseille Cedex 20
email : frederic.zolla@fresnel.fr
‡ LASMEA, U.M.R. 6602, Complexe des Cézeaux
63177 Aubière Cedex, France

June 11, 2002

ABSTRACT

This paper is intended to propose an efficient numerical method called Method of fictitious charges for solving a large class of annex problems which appear in the theory of homogenization of dielectric (lossless or not) materials. In the second step, we prove rigorously the convergence of the proposed algorithm. Finally, we give some examples in order to show the capabilities of our method.

INTRODUCTION

At an atomic scale, matter behaves as if it were essentially heterogeneous, but daily experiments show it rather homogeneous. This property is one of salient feature of matter : microscopic heterogeneity can lead to mesoscopic homogeneity. At first sight, one can say that there are two kinds of inhomogeneities : the first ones of a periodic type (such as crystals) and the others of a random type (such as amorphous glass). In this paper, we only deal with periodic structures namely photonic crystals (P.C.). We address the problem of the low-frequency behavior of these structures, i.e. the homogenization theory of the Maxwell system. In the rigorous approach [1, 2, 3] to homogenization, which is currently used in Mechanics, Electrostatics or Magnetostatics [4], one performs an asymptotic analysis in which the period over wavelength ratio tends to zero, and hence the number of scatterers tends to infinity. The domain containing the scatterers and the wavelength are kept fixed. The effective permittivity tensor is then defined in terms of solutions of partial differential equations (the annex problems). The aim of this work is to propose a new numerical method for solving these so-called annex problems

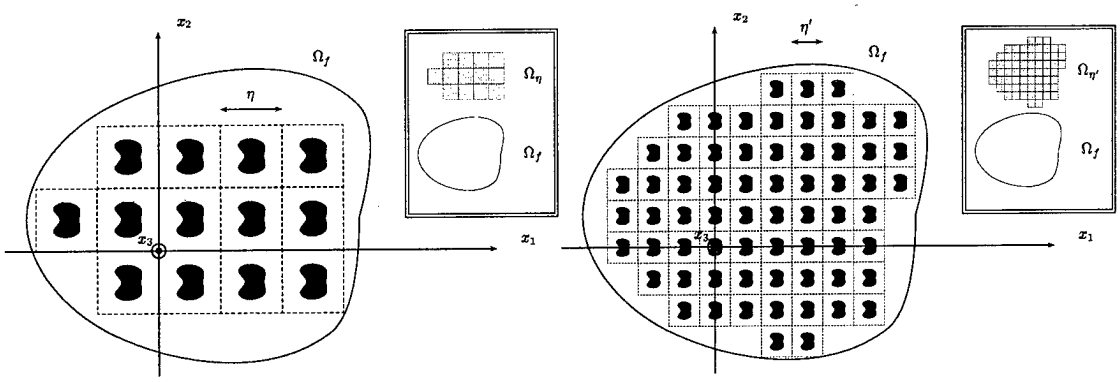


Figure 1: For the sake of simplicity, we only draw the homogenized process in the 2-D case. The fixed set Ω_f with two "scaffolding" $\Omega_{\eta'}$ and Ω_η (with $\eta < \eta'$) are plotted.

SET UP OF THE PROBLEM

From now on, assuming a time dependence in $e^{-i\omega t}$, we will deal with time harmonic Maxwell equations. We consider a cartesian coordinates system of axes (O, x_1, x_1, x_3) with origin O. We consider a collection of identical scatterers which are displayed at the center of a square mesh of a grid covering a fixed area Ω_f. The side of mesh C_η is equal to η. We define a "scaffolding" Ω_η of Ω_f in the following manner : Ω_η is defined as the greatest (in the set theoretical meaning) union of boxes of size η which are entirely contained in Ω_f and whose fineness in controlled by η. More precisely, the finer the scaffolding (the smaller the η), the better the imitation (cf. figure 1). Obviously, as we wish to "build up" Ω_f, the number N_η of cells depends upon η, since it corresponds to the following equivalence.

$$N_\eta = \frac{\text{meas}(\Omega_\eta)}{\eta^d} \simeq \frac{\text{meas}(\Omega_f)}{\eta^d} \tag{1}$$

where d corresponds to the dimension of our problem and $\text{meas}(\Omega)$ denotes the measure of Ω (namely $\text{meas}(\Omega)$ denotes the volume of Ω when $d = 3$ and denotes the area of Ω when $d = 2$).

For each grid (i.e. for each η) it is possible to define an electromagnetic field $\mathbf{F}_\eta = (\mathbf{E}_\eta, \mathbf{H}_\eta)$ corresponding to the field diffracted by N_η scatterers when they are illuminated by the field $\mathbf{F}_i = (\mathbf{E}_i, \mathbf{H}_i)$. In [1] the authors demonstrated that the field $\mathbf{F}_\eta$ does converge (in a sense defined in the quoted article) to a field $\mathbf{F}_{hom}$ (*homogenized field*) when η tends to zero. This field $\mathbf{F}_{hom}$ is the field diffracted by a homogeneous material filling entirely the set Ω_f. The characterization of the electromagnetic properties of the homogeneous material depends strongly on the dimension of the problem and the polarization of the incident field as is schown in the following section.

THEORETICAL RESULTS

3.1 2D-case (T.E.)

When η tends to zero, the collection of cylindrical scatterers can be replaced by a homogeneous isotropic cylinder of section Ω_f with a permittivity ε_{hom} equal to: $\varepsilon_{hom} = \langle\varepsilon\rangle_Y$, where $\langle\varepsilon\rangle_Y$ denotes the average of ε in the cell Y with $Y =]0,1]^2$ (i.e. $\int_Y \varepsilon(y_1, y_2)\, dy_1 dy_2$).

3.2 2D-case (T.M.)

Let us denote $H^1_{0,\sharp}(Y)$ the first Sobolev space of functions on $Y =]0,1]^2$ which have the same trace on the opposite side on Y of null mean value. When η tends to zero, the collection of cylindrical scatterers can be replaced by a homogeneous anisotropic cylinder of section Ω_f with a permittivity ε_{hom} equals to:

$$\varepsilon^{-1}_{hom} = \langle\varepsilon^{-1}(Id - \nabla\mathbf{V}')\rangle_Y \quad , \tag{2}$$

where $\mathbf{V}' = (V'_1, V'_2)$, and V'_j is the unique solution with null mean of the following electrostatic problem (K'_j):

$$(K'_j): \quad \mathrm{div}(\varepsilon_r^{-1}(\nabla(V'_j - y_j))) = 0\ ,\ j \in \{1,2\} \tag{3}$$

and where $\nabla\mathbf{V}'$ denotes the jacobian matrix of $\mathbf{V}'$.

3.3 3D-case

In this section, we denote $Y =]0,1]^3$. When η tends to zero, the collection of scatterers can be replaced by a homogeneous anisotropic material filling the set Ω_f with a permittivity matrix ε_{hom} equals to:

$$\varepsilon_{hom} = \langle\varepsilon(Id - \nabla\mathbf{V})\rangle_Y \tag{4}$$

where $\mathbf{V} = (V_1, V_2, V_3)$ is the unique solution in $H^1_{0,\sharp}(Y)$ of the following electrostatic problem (K_j) :

$$(K_j): \quad \mathrm{div}(\varepsilon_r(\nabla(V_j - y_j))) = 0\ ,\ j \in \{1,2,3\} \tag{5}$$

PRACTICAL APPLICATIONS

In most applications, one has just to consider a two valued piecewise constant permittivity in the unit cell Y and more precisely, the relative permittivity yields ε_2 in what one usually calls the scatterer S and ε_1 elsewhere. Consequently, the problem we are dealing with is only defined by two complex numbers ε_1 and ε_2 and the shape of the scatterers Γ(in other words, the scatterers lie in the volume area, support of the above function). It is therefore easy to show [5] that, in this case, the resolution of the annex problems K_j introduced

in the fundamental theorem amounts to find the functions V_i solutions of the following system where derivatives are taken in the usual sense :

$$\left\{ \begin{array}{lcl} \triangle V_i & = & 0 \quad , \text{in } Y \setminus \Gamma \\ [\varepsilon D_n V_i]_\Gamma & = & -[\varepsilon]_\Gamma \, n_i \\ [V_i]_\Gamma & = & 0 \end{array} \right. \tag{6}$$

with

$$\varepsilon = \left\{ \begin{array}{ll} \varepsilon_{1,r} & , \text{in } \Omega_1 \\ \varepsilon_{2,r} & , \text{in } \Omega_2 \end{array} \right. \tag{7}$$

and where $[f]_\Gamma$ denotes the jump of f across the boundary Γ i.e. the difference between the outer and the inner trace of f in Γ , and n_i, $i \in \{1,2,3\}$, denotes the projection on the axis $\hat{\mathbf{x}}_i$ of the outer normal of Γ ($n_i = \mathbf{n} \cdot \hat{\mathbf{x}}_i$).

THE METHOD OF FICTITIOUS CHARGES AS APPLIED TO THE ANNEX PROBLEM

For the sake of simplicity, we are only dealing with the $2D-$case. But it is worth noting that the methodology described below can be easily extended to the $3D-$case.

5.1 The spaces $\mathcal{V}$, $\mathcal{V}_1$ and $\mathcal{V}_2$

It is convenient to introduce the following notations:

$$W_1 = \begin{pmatrix} -V_{1|\Gamma} \\ -\varepsilon_1 \, D_n V_{1|\Gamma} \end{pmatrix} , W_2 = \begin{pmatrix} V_{2|\Gamma} \\ \varepsilon_2 \, D_n V_{2|\Gamma} \end{pmatrix} \text{ and } W_0 = \begin{pmatrix} 0 \\ [\varepsilon] \, n_i \end{pmatrix} . \tag{8}$$

With this notations our problem is reduced to find the columns W_1 or W_2, the column W_0 being known, such that: $W_0 = W_1 + W_2$.

We thus consider the space $\mathcal{V} = L^2(\Gamma) \times L^2(\Gamma)$ of pairs of functions $\Phi = \begin{pmatrix} \phi \\ \psi \end{pmatrix}$ defined on Γ. The space $\mathcal{V}$ is a Hilbert space for the following inner product:

$$(\Phi_1, \Phi_2)_\mathcal{V} = \int_\Gamma \phi_1 \overline{\phi_2} \, dl + \int_\Gamma \psi_1 \overline{\psi_2} \, dl \tag{9}$$

We will now define two subspaces of $\mathcal{V}$, the spaces $\mathcal{V}_1$ and $\mathcal{V}_2$. The space $\mathcal{V}_j$ is defined as the subspace of $\mathcal{V}$ of columns Φ verifying the following property :

> The functions ϕ and ψ are such that there is a regular $Y-$periodic harmonic function f defined on Ω_j (i.e. $\triangle f = 0$) such that $\phi = f_{|\Gamma}$ and $\psi = \varepsilon_j D_n f_{|\Gamma}$.

Consequently, $\mathcal{V}_1$ can be said to be associated with the field in Ω_1 whereas $\mathcal{V}_2$ is associated with the field in Ω_2. Returning now to the columns W_0, W_1 and W_2, it is clear that W_0 is in $\mathcal{V}$, W_1 is in $\mathcal{V}_1$ and W_2 is in $\mathcal{V}_2$. Besides W_0 being given in $H^1_{0,\sharp}(Y)$, W_1 and W_2 are unique (the solution of system (6) is unique !) and therefore the decomposition $W_0 = W_1 + W_2$ is unique.

5.2 The solution of the annex problem

The problem is now to find the column W_1 (or the column W_2) such as $W_0 = W_1 + W_2$, with a known column W_0. In order to find this column W_1 there is a general procedure based on looking for total families in $\mathcal{V}_1$ and $\mathcal{V}_2$ and on the use of least squares method [7, 8, 9]. Let us assume that we know, in each vector space $\mathcal{V}_j$ ($j \in \{1,2\}$) a total family $\{W_{j,n}\}$. This means that each vector W_j in $\mathcal{V}_j$ is the limit of a linear combination of the $W_{j,n}$. Then, if the complex numbers $\{c_{j,n}\}$ are so that

$$\lim_{N \longrightarrow +\infty} ||W_0 - (W_1^N + W_2^N)||_{\mathcal{V}} = 0 \ , \quad \text{with} \quad W_j^N = \sum_{n=1}^{N} c_{j,n}(N) W_{j,n} \tag{10}$$

then

$$\lim_{N \longrightarrow +\infty} ||W_j^N - W_j)||_{\mathcal{V}} = 0 \ . \tag{11}$$

In practice, for evident reasons linked with numerical calculation, we consider spaces $\mathcal{V}_j^N$ of finite dimension N instead of spaces $\mathcal{V}_j$. The spaces $\mathcal{V}_j^N$ are generated by N columns W_j^N. By and large, there are no column W_j^N which belongs to $\mathcal{V}_j^N$ such that the norm $||W_0 - (W_1^N + W_2^N)||_{\mathcal{V}}$ is null. The problem is therefore for fixed N to find the coefficients $c_{j,n}(N)$ which minimize the positive real Δ_N defined as follows:

$$\Delta_N = ||W_0 - (W_1^N + W_2^N)||_{\mathcal{V}} \ . \tag{12}$$

Having found the coefficients $\tilde{c}_{j,n}(N)$ which minimize Δ_N, we obtain the approximation $\tilde{W}_j^N$ of W_j with:

$$\tilde{W}_j^N = \sum_{n=1}^{N} \tilde{c}_{j,n}(N) W_{j,n} \ . \tag{13}$$

The method which has just been described converges in the following sense:

- $\lim_{N \longrightarrow +\infty} \tilde{\Delta}_N = 0 \quad , \quad \text{with} \quad \tilde{\Delta}_N = ||W_0 - (\tilde{W}_1^N + \tilde{W}_2^N)||_{\mathcal{V}}$
- $\lim_{N \longrightarrow +\infty} \tilde{\Delta}_N^j = 0 \quad , \quad \text{with} \quad \tilde{\Delta}_N^j = ||W_j - \tilde{W}_j^N||_{\mathcal{V}} \quad .$

In summary, we have shown that $\tilde{W}_j^N$ is a good approximation of W_j.

5.3 One example of total family in $\mathcal{V}_1$ and $\mathcal{V}_2$

We consider two sufficient regular curves (curves of class $C^\infty(\mathbb{R})$ γ_1 and γ_2). The curve γ_1 (resp. γ_2) must be in Ω_2 (resp. Ω_1) so that they lie on either side and "all along" the boundary Γ. We can prove the following theorem :

Theorem 5.1 *Let us consider a dense and countable set of points $P_{j,k}$ of coordinates $\mathbf{x}_{j,k} = (x_{j,k}, y_{j,k})$ on γ_j. Denoting $V_{j,k}^\sharp$ the unique solution in $H^1_{0,\sharp}(Y)$ of the equation:*

$$\triangle V_{j,k}^\sharp(\mathbf{x}) = \sum_{\mathbf{m} \in \mathbb{Z}^2} \delta(\mathbf{x} - \mathbf{x}_{j,k} - \mathbf{m}) - 1 \quad , \textit{with } \mathbf{x} = (x,y) \textit{ and } \mathbf{m} = (m_1, m_2) \tag{14}$$

and denoting by $W_{j,k}$ the column defined on Γ (Class C^2), as follows

$$W_{j,k} = \begin{pmatrix} V^{\sharp}_{j,k|\Gamma} \\ \varepsilon_j \, D_n V^{\sharp}_{j,k|\Gamma} \end{pmatrix} \tag{15}$$

then the family $\{W_{j,k}\}_{k\in\mathbb{N}}$ is a total family in $\mathcal{V}_j$.

REFERENCES

[1] S. Guenneau and F. Zolla. Homogenization of three-dimensional finite photonic crystals. *PIER*, 27:91–127, 2000.

[2] G. Bouchitté D. Felbacq. Homogenization of a set of parallel fibers. *Waves in Random Media*, 7:245–256, 1997.

[3] G. Bouchitté D. Felbacq. Anomalous behaviour of metallic photonic crystals. *J. Phys. A: Math. Gen.*, 33:815–821, 2000.

[4] G. Papanicolaou A. Bensoussan, J.L. Lions. *Asymptotic analysis for a periodic structures*. North-Holland, Amsterdam, 1978.

[5] S. Guenneau and F. Zolla. Homogenization of three-dimensional finite photonic crystals. *JEWA*, 14:529–530, 2000.

[6] M. Cessenat. *Mathematical method in electromagnetism*. World scientific, 1996.

[7] R. Petit and F. Zolla. The method of fictitious sources as applied to the conical diffraction by a homogeneous rod. *Journal of Electromagnetic Waves and Applications*, 8:1–18, 1994.

[8] F. Zolla, R. Petit, and M. Cadilhac. Electromagnetic theory of diffraction by a system of parallel rods : the method of fictitious sources. *J. Opt. Soc. Am A*, 11(3), March 1994.

[9] F. Zolla and R. Petit. Method of fictitious sources as applied to the electromagnetic diffraction of a plane wave by a grating in conical mounts. *J. Opt. Soc. Am A*, 13(4), April 1996.

[10] I.E. Stegun M. Abramowitz. *Handbook of mathematical functions*, volume 55. National Bureau of Standards Applied Mathematics, 1972.

HOMOGENIZATION OF PHOTONIC CRYSTALS

Arkady Krokhin, Jesús Arriaga*, and Peter Halevi**

Instituto de Física, Universidad Autónoma de Puebla, Apartado Postal J-48, Pue., 72570, Mexico
E-mail: arkady@sirio.ifuap.buap.mx

Instituto de Física, Universidad Autónoma de Puebla, Apartado Postal J-48, Pue., 72570, Mexico
E-mail: arriaga@sirio.ifuap.buap.mx

Instituto Nacional de Astrofísica, Optica y Electrónica, Apartado Postal 51, Puebla, 72000, Mexico and Dept. of Chemical Physics, Weizmann Institute of Science, Rehovot, 76100, Israel
E-mail: halevi@inaoep.mx

ABSTRACT

We consider the long-wavelength limit for two-dimensional photonic crystals – periodic arrangement of dielectric rods with dielectric constant ε_a embedded in a dielectric background (ε_b). Using the Fourier expansion method in the low-frequency limit we develop an effective medium theory and give a rigorous proof that, in this limit, a periodic medium behaves like a homogeneous one. We derive compact analytical formulas for the effective dielectric constants of a 2D photonic crystal. These formulas are very general, namely the Bravais lattice, the cross-sectional form of cylinders, their filling fractions and the dielectric constants are all arbitrary. So is the direction of propagation of the Bloch wave -- out-of-plane in general, with special attention paid to the limiting case of high dielectric contrast between the constituents of the photonic crystal.

INTRODUCTION

Photonic crystals (PC) are artificial semiconductor structures widely used in low-power micro-lasers, fiber optics communications, near-infrared devices and other optoelectronic applications [1]. Fabricated from two different dielectrics, arranged periodically in space, PC may possess a band-gap, i.e. a region of frequencies where electromagnetic signal cannot propagate due to destructive interference. Electromagnetic modes with frequencies above and below the band gap in a PC behave similar to electrons and holes in a semiconductor. This allows to manipulate the optical signal in a way comparable to that of the carriers of current into sophisticated electronic devices. The materials of the PC are high-quality dielectrics [1] possibly with a metallic fraction [2]. It is clear that these artificial periodic composites can be also employed in the region of linear dispersion, i.e. for the frequencies well below the gap. Here the PC's can be used as traditional optical elements, like prisms, lenses, and polarizers [3]. The

advantage of the PC's in comparison to natural optical materials (e.g. quartz) is that the properties of the artificial structure may be specially designed and possess such properties (e.g. large optical anisotropy) that do not exist for natural crystals.

In this paper we develop an effective medium theory for 2D photonic crystals. We have found that in the long-wavelength limit, when the wavelength of the propagating wave is much larger than the lattice constant of the PC, the periodic structure can be replaced by a homogeneous medium. We also calculate explicitly the dielectric characteristics of this effective medium. This homogenization procedure can be applied to a 2D PC with arbitrary Bravias lattice, cross-section of the rods, and constituent materials.

Photon transport through a PC is characterized by dispersion law, $\omega = \omega_n(\vec{k})$, where ω is the frequency, $\vec{k}$ is the Bloch vector of photon, and $n = 1,2,\ldots$ is the band index. Calculation of the band structure requires application of different numerical methods, however the most popular and universal one is the method of plane waves [4]. In what follows we apply the method of plane waves to calculate the limit

$$\varepsilon_{eff} = \lim_{k\to\infty}\left(\frac{kc}{\omega}\right)^2, \tag{1}$$

which by its definition gives the effective dielectric constant of a PC.

WAVE EQUATION

The 2D periodic structure of dielectric cylinders supports propagation of two uncoupled modes with either *E*-polarization (vector **E** is parallel to the rods) or *H*-polarization (vector **H** is parallel to the rods). The electric field of the *E*-mode is tangential to the cylinders. Due to the boundary conditions it is continuous across the structure. In this geometry the effective dielectric constant is known to be the space-average dielectric constant [5]

$$\varepsilon_{eff}^{E} = \bar{\varepsilon} = f\varepsilon_a + (1-f)\varepsilon_b . \tag{2}$$

Here f is the filling fraction of the component a. This result is valid not only for periodic systems, but also for any inhomogeneous dielectrics with dielectric constant that is independent of the coordinate parallel to the cylinders (coordinate z).

The wave equation for the monochromatic wave with vector **H** = (*0, 0, H*$_z$) oriented along the cylinders has the following form,

$$\nabla_t \cdot \left(\eta(\vec{r})\nabla_t H_z\right) + \frac{\omega^2}{c^2} H_z = 0 . \tag{3}$$

Here ∇_t is the two-dimensional gradient in the $x-y$ plane and $\eta(\vec{r})=1/\varepsilon(\vec{r})$ is the inverse dielectric constant. Being a periodic function it can be expanded in a Fourier series

$$\eta(\vec{r})=\frac{1}{\varepsilon(\vec{r})}=\sum_{\vec{G}}\eta\ (\vec{G})\exp(i\vec{G}\cdot\vec{r}) \tag{4}$$

over the reciprocal lattice vectors **G**. In a periodic system the solution of the wave equation is represented in a form of a Bloch wave,

$$H_z(\vec{r})=\sum_{\vec{G}}h_k(\vec{G})\exp[i(\vec{k}+\vec{G})\cdot r]\,. \tag{5}$$

Substituting Eqs. (4) and (5) into (3) we obtain a standard eigenvalue problem,

$$\sum_{\vec{G}'}\eta\ (\vec{G}-\vec{G}')\left(\vec{k}+\vec{G}\right)\cdot\left(\vec{k}+\vec{G}'\right)h_k(\vec{G}')=\frac{\omega^2}{c^2}h_k(\vec{G})\,. \tag{6}$$

HOMOGENIZED SOLUTION OF THE WAVE EQUATION

In the long-wavelength limit the Bloch wave (5) approaches the solution for homogeneous media, i.e. a plane wave. In the Fourier series (5) the plane-wave solution is given by the term with $\vec{G}=0$. All other terms vanish when $k\to 0$. To calculate the limit (1) we expand Eq. (6) in powers of k taking into account that $h_k(\vec{G})\underset{k\to 0}{\to}0$ and $h_k(0)=h_0=const$. In the zero approximation, substituting $\omega=k=0$ in Eq. (6), we obtain a set of homogeneous equations $\sum_{\vec{G}'\neq 0}\eta\ (\vec{G}-\vec{G}')\vec{G}\cdot\vec{G}'h_k(\vec{G}')=0$. It has only a trivial solution, $h_k(\vec{G}\neq 0)=0$, that can be considered as a proof of the conjecture $h_{k=0}(\vec{G}\neq 0)=0$. To calculate the term h_0 we consider Eq. (6) for $\vec{G}=0$ and keep the k^2-terms in both parts. This gives

$$(\varepsilon_{eff}^{-1}-\overline{\eta})^{-1}\sum_{\vec{G}'\neq 0}\eta\ (-\vec{G}')\frac{\vec{k}\cdot\vec{G}'}{k^2}h_k(\vec{G}')=h_0\,. \tag{7}$$

Since h_0 is finite when $k\to 0$, the non-zero harmonics vanish linearly with k. For these harmonics (with $\vec{G}\neq 0$) we keep the linear terms in Eq. (6) and obtain

$$\sum_{\vec{G}'\neq 0}\eta\ (\vec{G}-\vec{G}')\vec{G}\cdot\vec{G}'h_k(\vec{G}')+\vec{k}\cdot\vec{G}\eta(\vec{G})h_0=0\,. \tag{8}$$

Substituting h_0 from Eq. (7) into Eq. (8) we get a homogenized set of equations for $h_k(\vec{G}\neq 0)$

$$\sum_{\vec{G}'\neq 0}\left\{\Lambda\eta\ (\vec{G}-\vec{G}')\vec{G}\cdot\vec{G}'+\vec{n}\cdot\vec{G}\,\vec{n}\cdot\vec{G}'\eta(\vec{G})\eta(-\vec{G}')\right\}h_k(\vec{G}')=0, \tag{9}$$

where $\vec{n}=\vec{k}/k$ is the unit vector in the direction of propagation and $\Lambda=\varepsilon_{eff}^{-1}-\overline{\eta}$. The effective dielectric constant is calculated from the condition that a homogeneous set (9) has a non-trivial solution. Although the corresponding determinant is of the infinite order, it is easy to demonstrate that the solution for ε_{eff} is unique. By multiplying Eq. (9) from the right by the matrix $\left[\eta\ (\vec{G}-\vec{G}')\vec{G}\cdot\vec{G}'\right]^{-1}$, we got a standard eigenvalue problem

$$\sum_{\vec{G}'\neq 0}B\left(\vec{G},\vec{G}'\right)h_k(\vec{G}')=\Lambda\,h_k(\vec{G}), \tag{10}$$

$$B\left(\vec{G},\vec{G}'\right)=-\vec{n}\cdot\vec{G}\eta(\vec{G})\sum_{\vec{G}''\neq 0}\vec{n}\cdot\vec{G}''\eta(-\vec{G}'')\left[\eta\ (\vec{G}''-\vec{G}')\vec{G}''\cdot\vec{G}'\right]^{-1}.$$

The matrix $B\left(\vec{G},\vec{G}'\right)$ is written in a multiplicative form, $B\left(\vec{G},\vec{G}'\right)=a(\vec{G})b(\vec{G}')$, i.e. it is a projection operator. It has a single eigenvalue. Due to the multiplicative property of the matrix $B\left(\vec{G},\vec{G}'\right)$ all the eigenvectors may be represented in the form $h_k(\vec{G})=Ca(\vec{G})$, where $C=const$. Substituting these eigenvectors into Eq. (10) we get the eigenvalue

$$\Lambda=\sum_{\vec{G}'\neq 0}a(\vec{G})b(\vec{G})=\mathrm{Tr}B\left(\vec{G},\vec{G}'\right). \tag{11}$$

Now the effective dielectric constant $\varepsilon_{eff}=1/(\Lambda+\overline{\eta})$ is written as follows [6,7],

$$\varepsilon_{eff}(\vec{n})=1\Big/\left\{\overline{\eta}-\sum_{\vec{G},\vec{G}'\neq 0}\vec{n}\cdot\vec{G}\,\vec{n}\cdot\vec{G}'\eta(\vec{G})\eta(-\vec{G}')\left[\eta\ (\vec{G}'-\vec{G})\vec{G}\cdot\vec{G}'\right]^{-1}\right\}. \tag{12}$$

It depends on the direction of the wave vector and on the microstructure of the unit cell. It is worth to note that the theory of homogenization of periodic composites has been developed in many mathematical papers (see, e.g. [8]), however, to the best of our knowledge, no explicit formulas for the effective parameters have been obtained. The effective dielectric constant for 3D photonic crystals was calculated in Ref. [9], but since the polarization of the eigenmodes cannot be calculated analytically, the final formula for ε_{eff} does not have such a compact and explicit form as Eq. (12).

SYMMETRY

The angular dependence of $\varepsilon_{eff}(\vec{n})$ in the $x-y$ plane is given by a quadratic form

$$\frac{1}{\varepsilon_{eff}(\vec{n})}=\left(\overline{\eta}-A_{xx}\right)\cos^2\varphi+\left(\overline{\eta}-A_{yyx}\right)\sin^2\varphi-A_{xy}\sin 2\varphi, \tag{13}$$

$$A_{ik} = \frac{1}{2}\sum_{\vec{G},\vec{G}'\neq 0}\left(G_i G_k' + G_k G_i'\right)\eta(\vec{G})\eta(-\vec{G}')\left[\eta\,(\vec{G}-\vec{G}')\vec{G}\cdot\vec{G}'\right]^{-1}, \quad i,k = x,y,$$

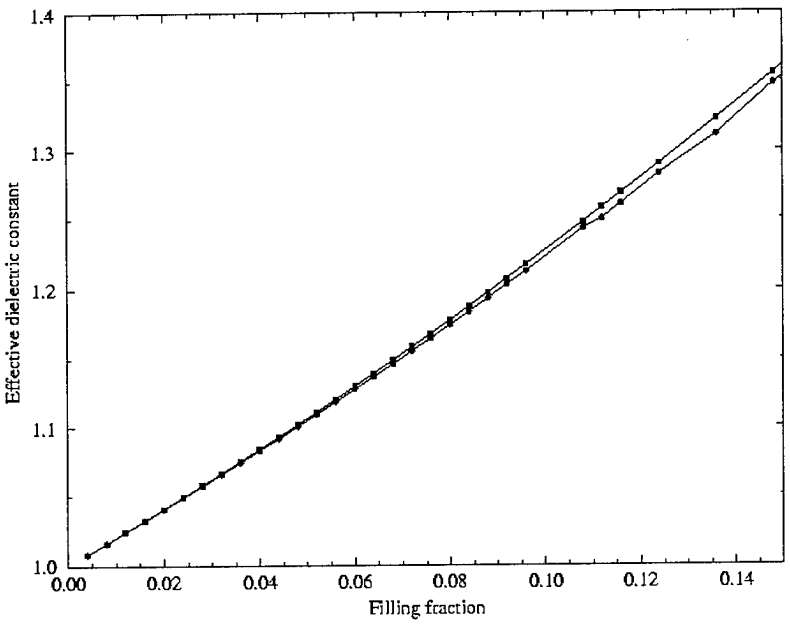
which is obtained from Eq. (12) by substitution $\vec{n} = (\cos\varphi, \sin\varphi)$. Eq. (13) is the equation of an ellipse in polar coordinates $\left(\varepsilon_{eff}^{-1/2}(\varphi),\varphi\right)$. The semiaxes of the ellipse give two principal values $(\varepsilon_1,\varepsilon_2)$ of the dielectric tensor ε_{ik} of a 2D photonic crystal. The third principal value $\varepsilon_3 = \bar{\varepsilon}$ corresponds to the axis of the index ellipsoid the z-direction. In the general cases 2D photonic crystal is biaxial, $\varepsilon_1 \neq \varepsilon_2$. If the unit cell possesses a third- or higher-order rotational symmetry with respect to axis z, then the PC is uniaxial, $\varepsilon_1 = \varepsilon_2$. Unlike 3D crystals, a 2D PC cannot be isotropic due to its uniformity along the axis z.

PHOTONIC CRYSTAL WITH PERFECTLY CONDUCTING CYLINDERS

Eq. (12) is very useful for numerical calculations. It gives high accuracy with moderate numerical efforts. Examples of calculations for uniaxial and biaxial PC's can be found in Refs. [6,7]. The accuracy of the results is checked with Keller's theorem [10]. It is valid for conjugate structures, where the materials a and b are interchanged, and it states that

$$\varepsilon_1(\varepsilon_a,\varepsilon_b)\varepsilon_2(\varepsilon_b,\varepsilon_a) = \varepsilon_2(\varepsilon_a,\varepsilon_b)\varepsilon_1(\varepsilon_b,\varepsilon_a) = \varepsilon_a\varepsilon_b\ . \qquad (14)$$

There is a limiting case of perfectly conducting cylinders ($\varepsilon_a = \infty$) when Keller's theorem cannot be used. Although this case can be hardly realized experimentally, it is frequently used in theoretical studies. It turns out that this case allows to obtain rigorous mathematical results for the band structure for some particular lattices [11]. The effective dielectric constant for a square lattice with circular cylinders was calculated in Ref. [12] using a pure electrostatic approach and in Ref. [13] by taking numerically the long-wavelength limit (1). The results obtained are in disagreement with each other. The band-structure calculations give the result that is $\sqrt{1-f}$ times less than the electrostatics result. Later on this factor was justified analytically in Ref. [14]. In Refs. [13,14] the disagreement between the electrostatics and electrodynamics has been attributed to the fact that the limits $k \to 0$ and $\varepsilon_a \to \infty$ do not commute. However Eq. (12) gives for $\varepsilon_a = \infty$ numerical results that are in a complete agreement with electrostatics [15]. Thus we may conclude that Electrostatics is still the long-wavelength limit of Electrodynamics even for the case of ideal conductors. Apparently, the approach [13,14] based on the boundary-condition method fails for infinite periodic 2D structures. In our approach the boundary conditions are not used explicitly and the medium is considered as a continuous one. It is not clear yet why the boundary-conditions method fails for PC with perfectly conducting inclusions. This problem requires further study.



We have checked Eq. (12) for a PC of perfectly conducting cylinders in the case $f << 1$. This limit was thoroughly studied [16] using electrostatics and the ε_{eff} was calculated in quadratic approximation, $\varepsilon_{eff} \approx 1 + 2f + 2.744989676 f^2$.

In figure we plot this parabolic dependence (upper line) together with the data obtained from Eq. (12) for $\varepsilon_a \to \infty$ (lower line). Again one can see very good agreement between our exact results and the perturbative ones of Ref. [16].

This work was supported by CONACyT (Mexico), grants Nos. 32191-E and 33808-E.

REFERENCES

[1] E. Yablonovich, Scientific American, December 2001, p. 47.
[2] J.G. Flemming, S.Y. Lin, I. El-Kady, R. Biswas, and K.M. Ho, Nature **417**, 52 (2002).
[3] P. Halevi, A.A. Krokhin, and J. Arriaga, Appl. Phys. Lett. **75**, 2725 (1999).
[4] J. D. Joannopoulos, R.D. Meade, and J.N. Winn, *Photonic Crystals: Molding the Flow of Light*, (Princeton University Press, New Jersey, 1995).
[5] R. Fuchs, Phys. Rev. B **11**, 1732 (1975).
[6] P. Halevi, A.A. Krokhin, and J. Arriaga, Phys. Rev. Lett. **82**, 719 (1999).
[7] A.A. Krokhin, P. Halevi, and J. Arriaga, Phys. Rev. B **65,** 115208 (2002).
[8] M. Birman and T. Suslina, Operator Theory: Adv. and Appl. **129**, 72 (2001).
[9] S. Datta, C.T. Chan, K.M. Ho, and C.M. Soukoulis, Phys. Rev. B **48**, 14936 (1993).
[10] J. B. Keller, J. Math. Phys. **5**, 548 (1964).
[11] P. Kuchment, The Mathematics of Photonic Crystals, in *Mathematical Modeling in Optical Science*, ed. by G. Bao, L. Cowsar, and Wen Masters, series Frontiers in Applied Mathematics, v. 22, SIAM, pp. 207-272, 2001.
[12] W. Perrins, D. McKenzie, and R.C. McPhedran, Proc. R. Soc. Ser. A **369**, 207 (1979).
[13] N.A. Nicorovici, R.C. McPhedran, and L.C. Botten, Phys. Rev. Lett. **75**, 1507 (1995).
[14] D. Felbacq, J. Math. Phys. **43**, 52 (2002).
[15] P. Halevi, A.A. Krokhin, and J. Arriaga, Phys. Rev. Lett. **86**, 3211 (2001).
[16] B.R. Djordjević, J.H. Hetherington, and M.F. Thorpe, Phys. Rev. B **53**, 14862 (1996).

APPROXIMATED FACTORIZATIONS FOR KERNELS INVOLVED IN THE SCATTERING DUE BY A WEDGE AT SKEW INCIDENCE

Vito G. Daniele, Riccardo E. Zich*
Dipartimento di Elettronica, Politecnico di Torino
C.so Duca degli Abruzzi 24, 10129 Torino (Italy)
E-mail:daniele@polito.it

* Dipartimento. di Elettrotecnica, Politecnico di Milano,
Piazza Leonardo da Vinci 32, 20133 Milano
E-mail:riccardo.zich@etec.polimi.it

ABSTRACT

Some approximated factorization techniques related to wedge problems have here addressed.

INTRODUCTION

In some previous works [1-3] the Wiener-Hopf technique has been extended so far in order to effectively deal with wedge problems and it has been compared with the popular Sommerfeld- Maliuyzhinets method [4]. The two different approaches turn the diffraction problems, due to the presence of a wedge, into the solution of a set of difference equations (Sommerfeld- Maliuyzhinets) or into decomposition-factorization problems (Wiener-Hopf technique) respectively.
The matrix factorization and the solution of a difference equations set of general order are two very difficult mathematical problems that appear definitively far one from the other. On the contrary, according to the authors opinion, the theoretical difficulties that one has to face in order to solve these problems are exactly the same, and they arise from the necessity of decoupling, on one side, the systems of generalized W-H equations and, on the other, the systems of difference finite equation of first order.
For what concerns the latter, even if they are ambiguous, the difference equations may be solved apparently by simpler technique with respect to those required for factorize or decompose matrix functions. However, the theory of the factorization is better mathematically founded in comparison of the theory of the difference equations. This aspect is particularly important when no closed form solutions of the difference equations are available or even possible, and approximated techniques become necessary to overcome the problem. According to the opinion of the authors, approximated factorizations face these problems in a more suitable and effective way. The aim of this paper is to investigate this class of approximated techniques.

GENERALIZED WIENER-HOPF EQUATIONS FOR IMPENETRABLE WEDGES

By applying the arbitrary linear impedance conditions on the two faces of the wedge $\varphi = \Phi$ and $\varphi = -\Phi$, and by using the same notations of the companion paper [5], algebraic manipulations on the equations (3a) yield the generalized Wiener-Hopf equation [1]:

$$G_\Phi(\eta)F_+(\eta) = F_-(m) \tag{1}$$

where: $n = \sqrt{\tau_o^2 - m^2}$, $\xi = \sqrt{\tau_o^2 - \eta^2}$, $R_1(m) = \begin{vmatrix} 1 - n^2 \dfrac{P_a^2(m)}{\Delta_a^2(m)} & 0 \\ 0 & 1 - n^2 \dfrac{P_b^2(m)}{\Delta_b^2(m)} \end{vmatrix}$

$$G_\Phi(\eta) = R_1(m)^{-1} \begin{vmatrix} U - n\dfrac{P_a(m)}{\Delta_a(m)} & 0 \\ 0 & U - n\dfrac{P_b(m)}{\Delta_b(m)} \end{vmatrix} \begin{vmatrix} \xi U & U \\ \xi U & -U \end{vmatrix}, \tag{2}$$

$$F_+(\eta) = \begin{vmatrix} V_{z+}(\eta,0) \\ I_{z+}(\eta,0) \\ -\dfrac{\tau_o^2}{\omega\varepsilon} I_{\rho+}(\eta,0) - \dfrac{\alpha_o \eta}{\omega\varepsilon} I_{z+}(\eta,0) \\ \dfrac{\tau_o^2}{\omega\mu} V_{\rho+}(-\eta,0) + \dfrac{\alpha_o \eta}{\omega\mu} V_{z+}(\eta,0) \end{vmatrix}, \quad F_-(m) = \begin{vmatrix} -\dfrac{\tau_o^2}{\omega\varepsilon} I_{\rho+}(-m,\Phi) + \dfrac{\alpha_o m}{\omega\varepsilon} I_{z+}(-m,\Phi) \\ \dfrac{\tau_o^2}{\omega\mu} V_{\rho+}(-m,\Phi) - \dfrac{\alpha m}{\omega\mu} V_{z+}(-m,\Phi) \\ \dfrac{\tau_o^2}{\omega\varepsilon} I_{\rho+}(-m,-\Phi) - \dfrac{\alpha_o m}{\omega\varepsilon} I_{z+}(-m,-\Phi) \\ -\dfrac{\tau_o^2}{\omega\mu} V_{\rho+}(-m,-\Phi) + \dfrac{\alpha_o m}{\omega\mu} V_{z+}(-m,-\Phi) \end{vmatrix} \tag{3}$$

U is the identity matrix of order two and $P_{a,b}$ and $\Delta_{a,b}$ are the matrix and scalar polynomials of m, not reported here, respectively. In the following some exact factorization and a general technique of approximated factorization will be considered.

SOME EXACT FACTORIZATIONS

Equations (1) remarkably simplify dealing with the half-plane case $\Phi = \pi$, the two half-plane junction ($\Phi = \dfrac{\pi}{2}$), and when right wedges are present. In fact, in these cases, we are concerning with classical W-H equations [1], where the matrix kernels does commute with a polynomial matrix. These matrices can be explicitly factorized by using the procedure reported in [4]. However, the plane wave with at skew incidence ($\alpha_o \neq 0$) excitation is very cumbersome to deal with and it still constitutes matter of mathematical further analysis [5]. This specific topic is beyond the scope of this work, and it will not be pursued on in this context.

It is remarkable that even in presence of wedges having an arbitrary aperture angle equations (1) can be reduced to a classical W-H equations in the $\overline{\eta}$ – *plane* by using the

mapping [1,3] $\eta = \eta(\overline{\eta}) = -\tau_o \cos[\frac{\Phi}{\pi}[\arccos[-\frac{\overline{\eta}}{\tau_o}]]]$. In particular, the explicit factorization for $G_\Phi(\eta)$ have been provided for the PEC case and for and the Malyuzhinets problem [1-3].

In order to investigate the real possibility to obtain closed form exact solutions dealing with plane waves and skew incidence ($\alpha_o \neq 0$), algebraic manipulations allow to rewrite the generalized W-H equation in the following form:

$$\begin{vmatrix} \xi_- n_- & 0 \\ 0 & n_- \end{vmatrix} \begin{vmatrix} U & \frac{1}{\xi_-} f \\ \xi_- f & U \end{vmatrix} \begin{vmatrix} \xi_+ n_+ & 0 \\ 0 & n_+ \end{vmatrix} F_+(\eta) = R(m) F_-(m) \tag{4}$$

where $\xi_\pm$ and $n_\pm$ are given by eq.s (9) of [3] and:

$$f = \frac{1}{n}\left[\frac{P_b(m)}{\Delta_b(m)} - \frac{P_a(m)}{\Delta_a(m)}\right]^{-1}\left[2U - n(\frac{P_a(m)}{\Delta_a(m)} + \frac{P_b(m)}{\Delta_b(m)})\right],\ R(m) = r(m)\begin{vmatrix} U & -U \\ U & U \end{vmatrix} R_1(m). \tag{5}$$

Being $R(m)$ a rational matrix, for what concerns m, the factorization problem has been reduced to that of the central matrix $M = \begin{vmatrix} U & \frac{1}{\xi_-} f \\ \xi_- f & U \end{vmatrix}$. Furthermore, since $\frac{1}{\xi_-} f\left[\xi_- f\right]^{-1} = \xi_-^{-2}(\overline{\eta}) = \left[\frac{1}{2}(\tau_o + \overline{\eta})\right]^{-1}$ is a rational function of $\overline{\eta}$, M differs from Daniele-Khrapkov matrices [8] only for the fact that f is not a scalar but a matrix of order two. Unfortunately, the factorization of this class of matrices can be accomplished in a closed form only when f has some particular forms. For instance when $f = d$ is a diagonal matrix (or more generally a Jordan matrix), we obtain:

$$M_\mp = [\sqrt{U - d^2}]_\mp \exp[\left\{\frac{1}{2\xi_-}\log\left(\frac{U+d}{U-d}\right)\right\}_\mp \otimes \begin{vmatrix} 0 & 1 \\ \xi_-^2 & 0 \end{vmatrix}] \tag{10}$$

where $[...]_\mp$ means multiplicative decomposition and $\{...\}_\mp$ additive decomposition in the $\overline{\eta}$ – *plane*. The decomposition equations can be obtained by the Cauchy formula. In order to achieve this result, it is convenient to introduce the angular complex planes w *and* $\overline{w}$ so suitably defined:

$$\eta = -\tau_o \cos w,\ \overline{\eta} = -\tau_o \cos \overline{w},\quad w = \frac{\Phi}{\pi}\overline{w}. \tag{11}$$

that yield: $\xi = -\tau_o \sin w$, $m = \tau_o \cos(w + \Phi)$, $n = \tau_o \sin(w + \Phi)$.

With these new variables w *and* $\overline{w}$, and the known function $X(\eta) = \overline{X}(\overline{\eta}) = X_+(\eta) + X_-(m) = \overline{X}_+(\overline{\eta}) + \overline{X}_-(\overline{\eta})$, an algebraic manipulation of the

Cauchy formula yields the following expression of the decomposed plus $\overline{X}_+(\overline{\eta}) = X_+(\eta)$ [3] :

$$\overline{X}_+(\overline{\eta}) = -\frac{1}{\pi\ j}\int_{-\infty}^{\infty}[\hat{X}(-\pi + ju) - \hat{X}(-\pi - ju)]\frac{\sinh u}{\cosh u - \cos\overline{w}}du + \sum_i \frac{R_i}{\overline{\eta} - \overline{\eta}_i} \qquad (12)$$

or:
$$X_+(\eta) = -\frac{1}{\pi\ j}\int_{-\infty}^{\infty}[\hat{X}(-\pi + ju) - \hat{X}(-\pi - ju)]\frac{\sinh u}{\cosh u - \cos\frac{\pi}{\Phi}w}du + \sum_i \frac{R_i}{\overline{\eta} - \overline{\eta}_i}$$

(13)

where $\hat{X}(\overline{w}) = \overline{X}(-\tau_o \cos\overline{w})$ and R_i represent the residue of $\overline{X}(\overline{\eta})$ in the poles $\overline{\eta}_i$ in the half plane $\mathrm{Im}[\overline{\eta}] \le 0$ located.

APPROXIMATE FACTORIZATION

In general, the f matrix of order two previously defined, presents a skew diagonal part that prevents the use of exact factorization formulae. In these cases an efficient approximated factorization can be obtained by using the rational (or Pade) approximants for the entries of the involved matrices. In general, we can approximate the matrix M with the rational matrices $\tilde{M}$ by introducing Pade approximants of their entries. Let us introduce $\varepsilon = M - \tilde{M}$ as the approximation error. By introducing then the rational factorized matrices $\tilde{M}_+$ and $\tilde{M}_-$ of $\tilde{M} = \tilde{M}_-\tilde{M}_+$, the question is:

"Do the rational matrices $\tilde{M}_+$ and $\tilde{M}_-$ approximate the exact factorized matrices M_+ and M_- of $M = M_-M_+$?"

In order to answer to this question let us introduce the matrices $\Delta_\pm$ suitably defined as the differences: $\Delta_- = M_- - \tilde{M}_-$, $\Delta_+ = M_+ - \tilde{M}_+$. From: $M = (\tilde{M}_- + \Delta_-)(\tilde{M}_+ + \Delta_+)$ we have: $\tilde{M}_-\Delta_+ + \Delta_-\tilde{M}_+ + \Delta_-\Delta_+ = \varepsilon$. Now it is possible to see that the pseudo Wiener-Hopf equation: $\tilde{M}_-\Delta_+ + \Delta_-\tilde{M}_+ + \Delta_-\Delta_+ = 0$ presents only the solution $\Delta_- = 0$ and $\Delta_+ = 0$. In fact, this equation can be rewritten: $(\Delta_-)^{-1}\tilde{Y}_-\Delta_+(\Delta_+)^{-1} + (\Delta_-)^{-1}\Delta_-\tilde{Y}_+(\Delta_+)^{-1} + 1 = 0$ or

$(\Delta_-)^{-1}\tilde{Y}_- + \tilde{Y}_+(\Delta_+)^{-1} + 1 = 0$

Looking at the first term, that is a plus (bounded) function, and at the second term, that is a minus (bounded) function, this equation cannot be satisfied for not vanishing $\Delta_\pm$ since $\tilde{Y}_-$ and $\tilde{Y}_+$ are rational and $\Delta_\pm$ is not rational. If the error ε in the Pade approximants $\tilde{M}$ is vanishing, it means that actually $\tilde{M}_+$ and $\tilde{M}_-$ approximate the exact factorized matrices M_+ and M_-.

There are many possibilities to approximate arbitrary matrices with rational matrices. For instance impenetrable wedges require the factorization of matrices having the following form:

$$M = \begin{vmatrix} 1 & \frac{1}{\xi_-} f \\ \xi_- f & 1 \end{vmatrix} \tag{14}$$

Since every matrix is similar to a Jordan matrix d: $f = S\,d\,S^{-1}$, we can rewrite:

$$m = \begin{vmatrix} S & 0 \\ 0 & S \end{vmatrix} \begin{vmatrix} 1 & \frac{1}{\xi_-} d \\ \xi_- d & 1 \end{vmatrix} \begin{vmatrix} S^{-1} & 0 \\ 0 & S^{-1} \end{vmatrix} \tag{15}$$

As we showed in the previous section, the central matrix can be factorized in a closed form. A Pade approximant of the matrix S in the $\overline{\eta}$ – *plane*

$$S = \frac{P}{\Delta} + \varepsilon \tag{16}$$

where P and Δ are rational, yields the following approximate equation

$$W_+(\overline{\eta}) F_+(\eta) = W_-(\overline{\eta}) R(m) F_-(m) \tag{17}$$

where the $W_-(\overline{\eta})$ and $W_+(\overline{\eta})$ matrices, regular in the half planes $\mathrm{Im}[\overline{\eta}] \le 0$ and $\mathrm{Im}[\overline{\eta}] \ge 0$ respectively, are given by:

$$W_+(\overline{\eta}) = \left[\begin{vmatrix} 1 & \frac{1}{\xi_-} f \\ \xi_- f & 1 \end{vmatrix} \right]_+ \begin{vmatrix} P_a & 0 \\ 0 & P_a \end{vmatrix} \begin{vmatrix} \xi_+ n_+ & 0 \\ 0 & n_+ \end{vmatrix}, \tag{18}$$

$$W_-(\overline{\eta}) = \left[\begin{vmatrix} 1 & \frac{1}{\xi_-} f \\ \xi_- f & 1 \end{vmatrix} \right]_-^{-1} \begin{vmatrix} P_a & 0 \\ 0 & P_a \end{vmatrix} \begin{vmatrix} \frac{1}{\xi_- n_-} & 0 \\ 0 & \frac{1}{n_-} \end{vmatrix} R(m) \tag{19}$$

with P_a being the adjoint matrix of P .

We take into account the plane wave source by introducing: $\overline{F}_-(\overline{\eta}) = \overline{F}_-^{\,d}(\overline{\eta}) + \overline{F}_-^{\,g}(\overline{\eta})$, where $\overline{F}_-^{\,g}(\overline{\eta}) = \frac{R_o}{\overline{\eta} - \overline{\eta}_o}$, $(\overline{\eta}_o = -k\cos(\frac{\pi}{\Phi}\varphi_o))$ is the known geometrical optics contribution. In addition, the rational function $R(m)$ induces poles in the half plane $\mathrm{Im}[\overline{\eta}] \le 0$. Let's indicate them with $\overline{\eta}_i$, $i = 1,..,N_m$. We can rewrite (17) in the following form:

$$W_+(\overline{\eta})\overline{F}_+(\overline{\eta}) - W_-(\overline{\eta}_o)\frac{R(m_o)R_o}{\overline{\eta} - \overline{\eta}_o} - \sum_{i=1}^{N_m} \frac{C_i}{\overline{\eta} - \overline{\eta}_i} = W_-(\overline{\eta}) R(m) \overline{F}_-(\overline{\eta})) - W_-(\overline{\eta}_o) R(m_o) \frac{R_o}{\overline{\eta} - \overline{\eta}_o} - \sum_{i=1}^{N_m} \frac{C_i}{\overline{\eta} - \overline{\eta}_i} = w(\overline{\eta})$$

where C_i is the residue of $W_-(\overline{\eta}) R(m) F_-(m)$ in $\overline{\eta} = \overline{\eta}_i$.

Taking into account that $m, \eta \approx \overline{\eta}^{\Phi/\pi}$ as $\overline{\eta} \to \infty$, we can ascertain that the vector $w(\overline{\eta})$ is an entire function having algebraic behavior as $\overline{\eta} \to \infty$: it means that it is a

polynomial of the $\overline{\eta}$ variable. The degree of the entries of $w(\overline{\eta})$ depends on the degree of the entries of P_a and $R(m)$. The coefficients of the polynomial $w(\overline{\eta})$ must be evaluated by imposing the regularity of $\overline{F}_-(\overline{\eta})$ and $\overline{F}_+(\overline{\eta})$ in the half planes $\mathrm{Im}[\overline{\eta}] \leq 0$ and $\mathrm{Im}[\overline{\eta}] \geq 0$ respectively.

REFERENCES

[1] V.Daniele, "Generalized Wiener-Hopf technique for wedge shaped regions of arbitrary angles", Rapporto Interno ELT-2000-1. Dipartimento di Elettronica-Politecnico di Torino, Settembre 2000.

[2] V.Daniele: "New analytical Methods for wedge problems", 2001 International Conference on Electromagnetics Advanced Applications (ICEAA01), September 10-14 2001, Torino (Italy), pp.385- 393.

[3] V.Daniele: "The Wiener-Hopf factorization method for the diffraction by wedges having arbitrary aperture angle, invited paper for the 2002 International Conference on Mathematical Methods in Electromagnetic theory (MMET 2002), Kiev, Ukraine, September 2002

[4] V.Daniele: "On the solution of vector Wiener-Hopf equations occurring in scattering problems", RADIO SCIENCE, vol.19, pp.1173-1178, 1984.

[5] E.Luneburg and A.H. Serbest (2000), Diffraction of a obliquely incident plane wave by a two-face impedance half plane: Wiener-Hopf approach, Radio Science, 35, pp.1361-1374.

[6] A.Büyükaksoy and A.H Serbest (1993), *Matrix Wiener-Hopf Factorization Methods and Applications to Some Diffraction Problems*, ch.6 in "Analytical and Numerical Methods in Electromagnetic Wave Theory", M. Hashimoto, M.Idemen and O.A. Tretyakov Editors, Science House Co.,Ltd., Tokio.

[7] V.Daniele: "On the factorization of W-H Matrices in problems solvable with Hurd's methods, IEEE Trans. on Antennas and Propag., AP-26, July 1978, p.614-61

THE TRANSMISSION-LINE MATRIX (TLM) METHOD: AN EFFICIENT TOOL FOR PROBLEM SEGMENTATION (DIAKOPTICS)

M. M. Ney, and S. Le Maguer

Laboratory of Electronics and Systems for Telecommunication Systems
(LEST, CNRS)
BP 832, 29285 Brest Cedex, FRANCE
michel.ney@enst-bretagne.fr

ABSTRACT

The paper describes a numerical procedure, called diakoptics, that allows one to solve for sub-domains of a large structure in a rigorous manner. Hence, one can optimize such a sub-domain during subsequent simulations without meshing the whole structure. In addition, the technique is naturally well suited for Transmission-Line Matrix (TLM) computations. Although diakoptics is very demanding in terms of computer cost for three-dimensional (3D) cases, various accelerating procedure can substantially reduce the memory and CPU time requirement. Some of these techniques are briefly described and discussed. Finally, examples of applications will be presented at the conference.

INTRODUCTION

In many applications for which radiation and coupling phenomena cannot be neglected, solutions require the solution of Maxwell's field equations. Numerous numerical methods have been proposed to solve these equations in a most rigorous way. They all have their advantages and drawbacks and the choice of one of them depends mainly on the application. For instance, the Finite Difference Time Domain (FDTD) [1] or Transmission-Line Matrix (TLM) [2] methods are well suited for complex geometry and their efficiency for analyzing antenna systems, guiding structures and even indoor propagation. In addition, these methods, which are typically time-domain methods, allow a wideband characterization and can easily handle non-linear problems. However, these methods (called volumic methods) are costly in terms of memory and CPU requirement. In particular, they cannot sustain the analysis of large (multi-wavelength) structures as other volumic approaches (e.g. Finite Element Method). Furthermore, in many applications electromagnetic modeling is the only approach to design and optimize a structure. Even if the structure is relatively small, optimization or Computer Aided Design (CAD) procedures cannot be directly applied using full-wave analyses. Therefore, much effort has been done to decrease their computer cost. When geometric or electromagnetic parameters of a small portion of a large problem are supposed to be modified several times (e.g. for optimization), subsequent simulations constitute a lengthy process. As a result, it may not be possible to reach an optimized solution over a reasonable period of time. However, if one can solve only for the subvolume under investigation without meshing the rest of the structure, then an optimization procedure becomes feasible.

BASIC ALGORITHM

The basic (unloaded) cubic SCN-TLM cell illustrated in fig. 1, can be seen as a six-arm device, each consisting of two orthogonal transmission-line with voltage that can be associated to local plane wave.

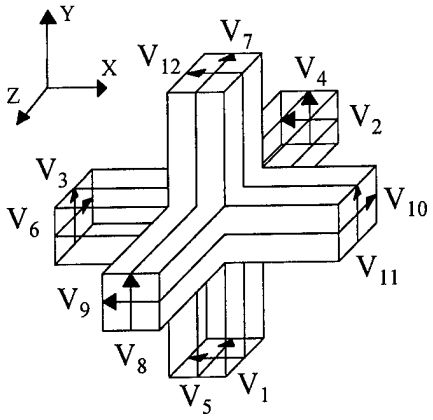


Fig. 1. SCN-TLM after

Fields at the center of the cell can be shown as a linear combination of the incident voltages on the arms. Suppose that some incident voltage (due to some source) impinges on the node. A scattering process will then occur, producing reflected voltage at all arms. Hence, the TLM cell corresponds to a 12-port device with scattering matrix defined by:

$$[V]^{r}_{k+1} = [S] \circ [V]^{i}_{k} \qquad (1)$$

where $[V]^{i}_{k}$ and $[V]^{r}_{k+1}$ is the vector of incident and reflected voltages at all node arms, respectively, and k the time index. The next step is to transfer reflected voltages to the neighboring cells at time $(k+1)\Delta t$. Thus, they become new incident voltages for the next time iteration. Note that unlike FDTD, the TLM scheme does not explicitly solve Maxwell's equations but simulate propagation mechanism by means of local waves. Thus, the TLM process can be seen as a discretized version of Huygens' principle [3].

The presence of material and/or parallelepiped cell is accounted for by adding stubs to the basic twelve-port illustrated in Fig. 1. Thus, a completely loaded SCN includes eighteen ports, losses being included in the matrix [S] components. Unlike FDTD, the connection between nodes in different media or size (irregular mesh) is trivial for SCN-TLM. The scattering matrix for the general case can be rigorously established by using Maxwell's equations in integral form [4]. New TLM nodes have been proposed to remove stub requirement and, thus, reducing the number of voltages. This is done by setting arm impedances at values different from Z_0 (vacuum intrinsic impedance). Different combinations lead to the Hybrid (HSCN) [5] and Super (SSCN) [6] condensed node that uses only fifteen and twelve voltages in the general case, respectively. It

should be stressed that the TLM algorithm provides some more information as compared to Yee's: The six field components at the same time and location (center of the cell) are computed from the incident voltages.

DIAKOPTICS

Diakoptics was first used by Kron [7] for solving power networks. Johns transposed the procedure for TLM computations [8]. The diakoptiks procedure consists of splittig a structure into sub-domains and solving for sub-domains only, yet in a rigourous way. The procedure is illustrated in Fig. 2. Domains are separated by adjacent boundaries called "Johns' boundary". Thus, every time and space response of subdomains "seen" through John's boundary are stored in a three-dimensional matrix called "Johns' matrix" (Fig. 3). This matrix is generated in the following manner: To every arm (which includes two orthogonal lines) adjacent to this boundary, one successively injects a Dirac function (say at line n). Then, one stores the corresponding response at all arm

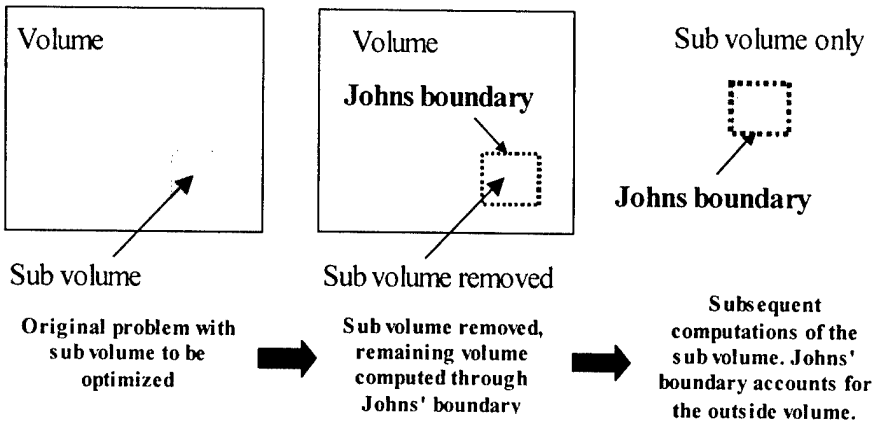


Fig 2. Illustration of the diakoptic principle.

lines (say line m) including the one to which the impulse is injected (m = n). Note that a Johns' boundary consists of a line and surface in the 2D and 3D case, respectively. The process has, generally, to be repeated N times where N is the number of adjacent lines to the boundary. Note that the reflected voltages should not be reflected back to the TLM grid. This requires an absorbing condition on the boundary. However, this type of ABC is trivial in TLM as it consists of terminating the TLM lines by Z_0 (the free-space intrinsic impedance) which is straightforward in TLM simulations.

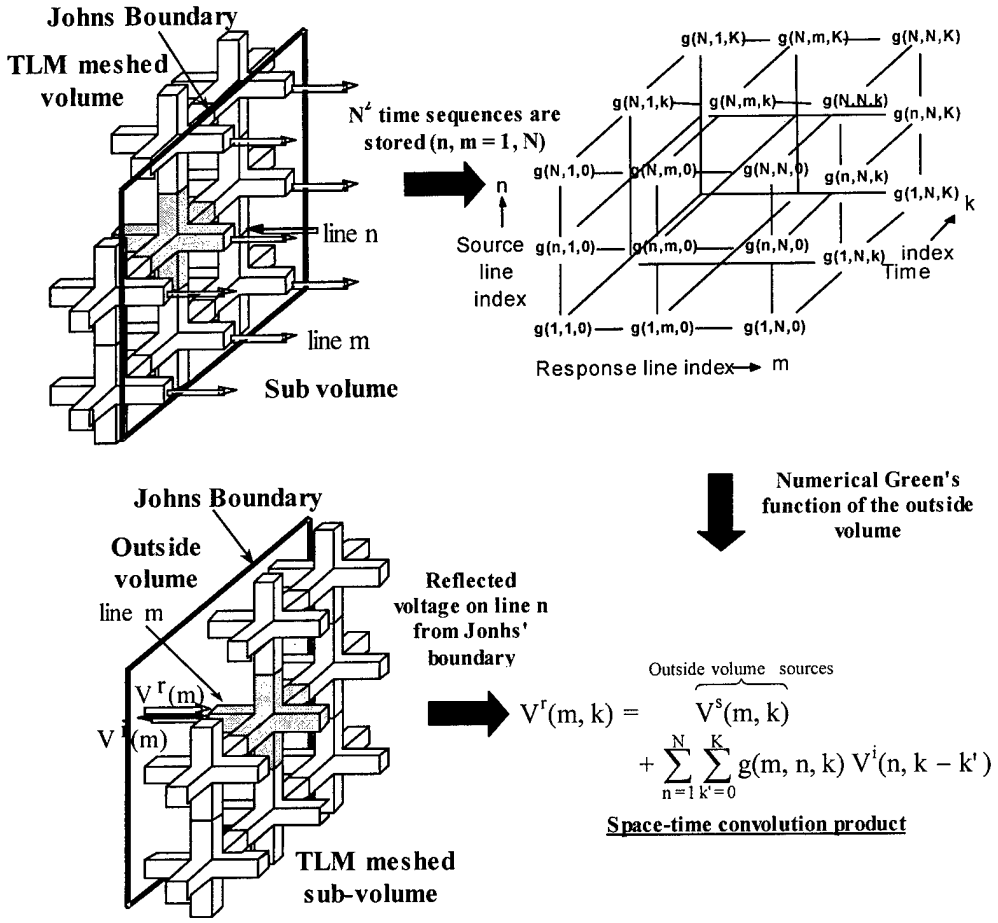
For subsequent simulations of the fixed sub domain illustrated in fig. 2, the TLM network is terminated by the Johns' boundary (fig. 3). Any impulse coming from adjacent arm line and impinging on that boundary will trigger the relevant response (reflected voltage sample g(m,n,k)) at each adjacent line, which was previously stored in the Johns' matrix. Thus, the reflected voltage at line m and time $k\Delta t$ is given by the following space-time discrete convolution:

$$V^r(m,k) = V^s(m,k) + \sum_{n=1}^{N} \sum_{k'=0}^{K} g(m,n,k)\, V^i(n, k-k') \qquad (2)$$

Note, that the contribution from sources V^s that may be contained in the fixed structure are included in (2).

ACCELERATING PROCEDURES

At this stage, one can notice that the initial step of diakoptics is generally heavy in terms of computational cost, as it requires the storage of N^2K samples. As a result, diakoptics can easily exhaust the computational resources. Even if the Johns' boundary involves a relatively small number of branches, the number of time samples can be large in presence of resonances. However, when the fixed substructure has losses (e.g. radiation) responses decay rapidly. Consequently, even with a larger number of nodes adjacent to the boundary, diakoptics is still feasible if an accelerating procedure can be used for the convolution products.



$$V^r(m,k) = \overbrace{V^s(m,k)}^{\text{Outside volume sources}} + \sum_{n=1}^{N}\sum_{k'=0}^{K} g(m,n,k)\, V^i(n,k-k')$$

Fig. 3. TLM procedure for diakoptics.

- Laguerre polynomials

The idea is to approximate impulse responses to be stored in the Johns matrix by a series of basis functions. For instance, one can write the sequences stored in the Johns' matrix as

$$g(m, n, k) = \sum_{p=1}^{\infty} \alpha_p^{m,n} L_p(m, n, k) \tag{3}$$

where $L_p(m,n,k)$ are Laguerre polynomials of order p and $\alpha_p^{m,n}$ the attached series coefficients. One can show that (3) can be transformed in the following recursive expression [9]:

$$V^r(m, k) = V^s(m, k) + \sum_{n=1}^{N} \sum_{p=1}^{P} \alpha_p^{m,n} y_p(m, n, k) \tag{4}$$

in which:

$$y_1(m, n, k) = \xi^{m,n} y_1(m, n, k - 1) + \sqrt{1 - \left(\xi^{m,n}\right)^2}\, V^i(n, k) \tag{5}$$

$$y_p(m, n, k) = x_p(k) - \xi^{m,n} x_p(m, n, k + 1) \tag{6}$$

where p = 2, 3...P and $\xi^{m,n}$ is an optimization parameter that minimizes the required number of polynomials for the approximation of the sequence stored with index (m,n) in the Johns matrix. Thus, instead of storing N^2K samples in the Johns matrix, one has to store only 2NP coefficients. In addition, the recursive form (4) accelerates the convolution computation that normally requires N^2K^2 operations. As a result, a drastic storage reduction and one order of magnitude CPU time reduction can be obtained [9]. This gain in computer efficiency depends on the problem but can be much higher.

- Matrix Pencil

Unfortunately, Laguerre polynomial approximation yields a very poor convergence when Johns matrix responses have some strong oscillatory behavior (resonance effects). A more efficient approach is to approximate the impulse responses by complex exponential whose parameters are computed by the "matrix pencil" (MP) method [10]. The technique consists in finding the best estimate of g(m, n, k) from a sequence y(k) affected by some noise n(k):

$$y(k) = g(m, n, k) + n(k) = \sum_{p=1}^{P} R_p e^{s_p k} + n(k) \tag{7}$$

where R_p are the complex amplitudes (residues), $s_p = -\alpha_p + j\omega_p$ the complex frequency and P the decomposition order. Unlike Laguerre decomposition, MP technique allows a very good approximation for most type of response behaviour. Some prediction can be also achieved with MP technique as from few samples, excellent signal prediction can be obtained [10]. In addition, MP allows recursive form of convolutions, therefore, keeping the same advantage as for Laguerre decomposition. For instance, (2) can be written as [10]:

$$V^r(m, k + 1) = V^s(m, k + 1) + C_k + \sum_{n=1}^{N} \sum_{p=1}^{P} \left[R_p\, e^{s_p (k+1)} V^i(n, k + 1) \right] \tag{8}$$

where

$$C_k = \sum_{n=1}^{N} \sum_{p=1}^{P} \sum_{k'=0}^{k} R_p \, e^{s_p k} \, V^i(n, k-k')$$

CONCLUSION AND FUTURE WORK

The basic principle of the TLM method was presented. The salient feature of the technique is its natural match for segmentation procedure namely, diakoptics. It was shown that TLM via diakoptic procedure can be t a potential tool for direct optimisation of structures in a most rigorous way. However, the basic procedure is a lengthy process and may not be suitable for CAD tools. Consequently, accelerating procedures such as Laguerre polynomials and Matrix Pencil ware presented to drastically decrease the computer cost in terms of both memory storage and CPU time.

However, the process to generate the Johns matrix which has to be performed once before optimisation still takes some exhaustive CPU time. Some work on filtering techniques, such as Moment Expansion [10, 11] is currently carried on. Also, some predicting property of the MP method is being investigated.

REFERENCES

[1] A. Taflove, "Computational Electrodynamics. The Finite Difference Time-Domain Method", Artech House, Norwood, 1995.
[2] P.B. Johns, "A symmetrical condensed node for the TLM method," IEEE Trans. on Mic. Th. and Tech., 35, 370-377, (1987).
[3] P.B. Johns, "A new mathematical model to describe the physics of propagation", The Radio and Electronic Eng., vol. 44, no. 12, 1974, pp. 657-666.
[4] N. Peña and M. M. Ney, "A General Formulation of a Three - dimensional TLM Condensed Node with the Modeling of Electric and Magnetic Losses and Current Sources," 12th Annual Review of Progress in Applied Computational Electromagnetics, Monterey, CA, March 18-22, 1996, pp. 262-269.
[5] R.A. Scaramuzza and A.J. Lowery, "A hybrid symmetrical condensed node for the TLM method," Electron. Letts., vol. 26, 1990, pp. 1947-1949.
[6] V. Trenkic, C. Christopoulos, and T.M. Benson, "New symmetrical super-condensed node for the TLM method," Electron. Lett., vol. 30, pp. 329-330, 1994.
[7] G. Kron, Diakoptics, MacDonald, London, 1963.
[8] P.B. Johns and K. Akhtarzad, "Time-domain approximation in the solution of fields by time-domain diakoptics," Int. Jour. Numer. Methods Eng., vol. 18, 1982, pp. 1361-1373.
[9] M.M. Ney and S. Le Maguer, "Diakoptics: an efficient technique for EMC applications", Proc. EMC Zurich, pp. 339-342, Feb. 1999.
[10] M.M. Ney and S. Le Maguer "acceleration de la methode de segmentation dans le domaine temporel par la methode "matrix pencil" pour l'optimisation de blindage en cem", Proc. 11th CEM conf., Grenoble, France, mars 2002 (*in French*).
[11] G. Marocco and F. Bardati, "Time-Domain Macromodel of Planar Microwave Devices by FDTD and Moment Expansion" IEEE Trans. Microwave Theory Tech., vol. MTT-49, n° 7, 2001, pp. 1321-1328.

SPECTRAL PROPERTIES OF THE OPERATOR DESCRIBING EM WAVE PROPAGATION IN ANISOTROPIC DIELECTRIC GUIDING STRUCTURES WITH ARBITRARY TRANSVERSAL INHOMOGENEITY

Tomasz F. Jabłoński

Applied Mathematics Dept.
Wyższa Szkoła Biznesu - National Louis University
Zielona 27, 33-300 Nowy Sącz, Poland
e-mail: *tjablon@wsb-nlu.edu.pl*

ABSTRACT

A brief mathematical characterization and resulting physical interpretation of EM waves propagation in anisotropic waveguides is presented. It is based on spectral and functional analysis of the operator acting in a suitably chosen Hilbert space. Analytical form of this operator is derived from Maxwell's equations reduced to the eigenproblem for unknown transversal magnetic field components of the guided mode and its propagation constant. Numerical examples demonstrating analyzed features of the guided modes will be shown. A new convenient normalization of physical parameters of anisotropic waveguides with nonaligned optical axes is also proposed.

INTRODUCTION

Anisotropic dielectric waveguides possess several interesting propagation properties and are of great practical interest. Their potential role in various optical and microwave devices cannot be overrated. For example, strong selectivity to linearly polarized light makes anisotropic waveguides very useful as components of coherent optical fiber systems, fiber gyroscopes, birefringent directional couplers and fiber sensors.

Yet, theoretical analysis of anisotropic waveguides encounters substantial mathematical difficulties because of the complicated form of the equations involved. Exact analytical solution is known only for the case of uniaxial circular step-index fiber [1]. Among available approximate methods, those described in [2]–[6] are worth noticing, despite of their often strongly restricted range of application.

In this paper, rigorously formulating the propagation problem for transversally inhomogeneous structure and harmonic time dependence we arrive at a set of two coupled second order partial differential equations of elliptic type that form the eigenproblem with the transversal magnetic field components of the mode field and the propagation constant being unknown. The eigensolutions are then evaluated numerically by the Iterative Spectral Decomposition Method[1] providing demonstrative numerical examples of anisotropic waveguides.

[1]The ISDM is a highly effective method [7], which has been successfully employed to the analysis of isotropic open dielectric waveguides [8]–[13] and of microwave shielded inhomogeneously filled dielectric structures [14].

FORMULATION OF THE PROBLEM

In this section we formulate the propagation eigenproblem with the eigenvalue being the square of the propagation constant and with the eigenvector being the transverse magnetic field of the mode in an anisotropic open dielectric waveguide. This eigenproblem is equivalent to the set of Maxwell's equations under the following assumptions: harmonic time-dependence is $e^{-i\omega t}$, the guiding structure is source-free, homogeneous along the direction of propagation X_3 and it is electrically anisotropic, meaning that

$$\mu = \mu_0, \qquad D = \epsilon_0 \, \mathcal{E} \, E,$$

where μ_0, ϵ_0 — permeability and permittivity of vacuum, respectively, D — electric displacement, E — electric field, $\mathcal{E}$ — relative permittivity tensor.

From the above assumptions it follows that

$$\begin{aligned} \mathcal{E} &= \{\epsilon_{ij}\}_{i,j=1,2,3} \\ \epsilon_{ij} &: \mathbb{R}^2 \ni x = (x_1, x_2) \longrightarrow \mathbb{C} \end{aligned} \tag{1}$$

is a positive definite hermitian matrix with the elements $\epsilon_{ij} = \epsilon_{ij}(x_1, x_2)$ being complex functions of the cross-sectional plane of the waveguide.

In this paper we restrict ourselves to the case of anisotropic waveguides in which one of the principal axes, let us say axis o_3, coincides with the direction of propagation X_3. Then, the permittivity tensor (1) takes the form:

$$\mathcal{E}(x) = \begin{bmatrix} \epsilon_{11} & \epsilon_{12} & 0 \\ \overline{\epsilon_{12}} & \epsilon_{22} & 0 \\ 0 & 0 & \epsilon_{33} \end{bmatrix} \qquad x = (x_1, x_2) \in \mathbb{R}^2 \tag{2}$$

It is possible (and it appears to be advantageous) to formulate the propagation eigenproblem in terms of the transversal magnetic field $h_\perp$ components only:

$$h_\perp = [\, h_1(x_1, x_2), h_2(x_1, x_2) \,]$$

where the total magnetic field has the form:

$$H(x_1, x_2, x_3) = [\, h_1(x_1, x_2), h_2(x_1, x_2), h_3(x_1, x_2) \,] \, e^{i(\beta x_3 - \omega t)},$$

and β is the propagation constant of the mode. Using $h_\perp$ we reduce Maxwell's equations to the following equivalent eigenproblem:

$$(\boldsymbol{T} - \beta^2) \, h_\perp = 0, \tag{3}$$

with the operator $\boldsymbol{T}$ of the form:

$$\begin{aligned}\boldsymbol{T}h_\perp = \; & \nabla_\perp^2 h_\perp + k^2 \begin{bmatrix} \epsilon_{22} & -\overline{\epsilon_{12}} \\ -\epsilon_{12} & \epsilon_{11} \end{bmatrix} h_\perp \\ & + \frac{1}{\epsilon_{33}^2} \begin{bmatrix} \epsilon_{22} & -\overline{\epsilon_{12}} \\ -\epsilon_{12} & \epsilon_{11} \end{bmatrix} \{\nabla_\perp \epsilon_{33} \times (\nabla_\perp \times h_\perp)\} \\ & + \frac{1}{\epsilon_{33}} \begin{bmatrix} \epsilon_{33} - \epsilon_{22} & \overline{\epsilon_{12}} \\ \epsilon_{12} & \epsilon_{33} - \epsilon_{11} \end{bmatrix} \{\nabla_\perp \times (\nabla_\perp \times h_\perp)\} \\ = \; & \boldsymbol{T}_1 h_\perp + \boldsymbol{T}_2 h_\perp + \boldsymbol{T}_3 h_\perp + \boldsymbol{T}_4 h_\perp \end{aligned} \tag{4}$$

Here $k^2 = \omega^2 \mu_0 \epsilon_0$ and the operator $\nabla_\perp = [\frac{\partial}{\partial x_1}, \frac{\partial}{\partial x_2}]$.

It is worth noticing that, since the region is source free and $\mu = \text{const}$, the mode field $h_\perp$ is a vector function that is continuous in the cross-sectional plane of the waveguide regardless of the discontinuities of the permittivity tensor elements $\epsilon_{ij}(x)$. In general, regularity of the solution $h_\perp$ depends strongly on the smoothness of the permittivity tensor $\mathcal{E}$.

PHYSICAL INTERPRETATION OF THE OPERATOR T

The components of the operator $\boldsymbol{T}$ can readily be interpreted physically. The first term $\boldsymbol{T}_1$ in (4) represents plane waves in the isotropic homogeneous medium (the cladding of the waveguide). The second term $\boldsymbol{T}_2$ encodes the way in which the transversal magnetic field components h_1 and h_2 see particular refractive index profiles and determines the guiding properties of the structure. The third term $\boldsymbol{T}_3$ corresponds to electrodynamical coupling[2] of the mode transversal fields in that part of the waveguide cross-section, in which $\nabla\epsilon_{33} \neq 0$. The fourth term $\boldsymbol{T}_4$ describes the influence of relative differences of the permittivity in the directions of principal axes.

The matrices in (4) can be diagonalized, provided that the directions of the principal axes are fixed in the whole cross-sectional plane of the waveguide and that $\epsilon_{ij}(x) \in \mathbb{R}$. Then, in the structures possessing the two mutually orthogonal axes of symmetry X_1, X_2 coinciding with the transversal principal axes o_1, o_2, the modes can be conveniently classified without loss of their polarization properties by making use of so called SA classification [15]. The modes in the structures with rectangular symmetry split into four operator $\boldsymbol{T}$–invariant subgroups denoted as: SA, AS, SS and AA. The first letter encodes the symmetry (or antisymmetry) of the mode vector field $h_\perp$ with respect to the axis X_1, while the second letter — with respect to the axis X_2.

If the structure is isotropic ($\epsilon_{11} = \epsilon_{22} = \epsilon_{33} = \varepsilon$), then the fourth term in (4) vanishes $\boldsymbol{T}_4 \equiv 0$, and the two first matrices trivialize to the form εI, where I is

[2]This can be explained thoroughly after examining the form of the adjoint operator $\boldsymbol{T}^*$ (c.f. [10], [11]).

the identity matrix. However, the problem still remains an essentially vectorial one, because of the third term $\boldsymbol{T}_3$ in (4).

Under the weak anisotropy and the weak guidance assumptions the eigenproblem (3) can be uncoupled into two scalar wave equations with different refractive index profiles by neglecting the third and the fourth terms in (4).

NORMALIZATION OF THE PHYSICAL PARAMETERS

The directions of the principal axes o_1, o_2 in the anisotropic dielectric waveguides met in practice are often the functions of the waveguide cross-section. However, in this short paper, in order to simplify subsequent formulas, we assume in (2) that $\epsilon_{ij}(x) \in \mathbb{R}$, that principal axes are fixed and coincide with the Cartesian coordinate system axes. The tensor (2) reduces then to a diagonal matrix $\mathcal{E}(x) = \mathrm{diag}\,\{\epsilon_1(x), \epsilon_2(x), \epsilon_3(x)\}$ with $\epsilon_i(x)$ being the permittivity profiles along the principal axes.

Without loss of generality of the guiding structures used in practice we can assume that the anisotropy is local in the sense that

$$\exists\, R_A > 0 \quad \forall\, x : |x| = (x_1^2 + x_2^2)^{1/2} > R_A \qquad \epsilon_i(x) = \epsilon_{cl,3} = \mathrm{const} \tag{5}$$

for $i = 1, 2, 3$. Condition (5) means that the structure is isotropic outside a suitably chosen circle with the radius R_A. Thus, each of the three relative permittivity functions ϵ_i can be written in the following form:

$$\epsilon_i(x) = \epsilon_{cl,3} + \{\, (\epsilon_{co,i} - \epsilon_{cl,i})\, s_i(x) \;+\; (\epsilon_{cl,i} - \epsilon_{cl,3}) \,\}\; \chi_{\{x:|x|<R_A\}} \tag{6}$$

with the constants $\epsilon_{co,i}, \epsilon_{cl,i} \in \mathbb{R}$ such that $\epsilon_{co,i} > \epsilon_{cl,i} > 0$ for $i = 1, 2, 3$, where $\epsilon_{co,i}$ — maximal value of the i–th permittivity function attained in the cores of the waveguide, $\epsilon_{cl,i}$ — the i–th permittivity of the cladding, χ — characteristic function of the circle with the radius R_A, and $s_i(x)$ — the i–th normalized refractive index profile defined on the cross-section S of the cores of the waveguide such that:

$$\begin{gathered} \mathrm{supp}(s_i) = S \subset \{x : |x| < R_A\} \\ \sup_{x\in\mathbb{R}^2} s_i(x) = 1, \qquad \inf_{x\in\mathbb{R}^2} s_3(x) > -\frac{\epsilon_{cl,3}}{\epsilon_{co,3} - \epsilon_{cl,3}} \end{gathered} \tag{7}$$

Here $\mathrm{supp}(s_i)$ denotes the support of the function s_i.

We express nondimensional standard parameters V, δ, $\mathcal{B}$, used in the theory of dielectric waveguides, by the longitudinal permittivity ϵ_3:

— normalized frequency V

$$V = k\, r\, (\epsilon_{co,3} - \epsilon_{cl,3})^{1/2} \tag{8}$$

— profile height δ

$$\delta = \frac{\epsilon_{co,3} - \epsilon_{cl,3}}{2\epsilon_{cl,3}} \tag{9}$$

— normalized propagation constant $\mathcal{B}$

$$\mathcal{B} = \frac{\beta^2 - k^2\epsilon_{cl,3}}{k^2(\epsilon_{co,3} - \epsilon_{cl,3})} \tag{10}$$

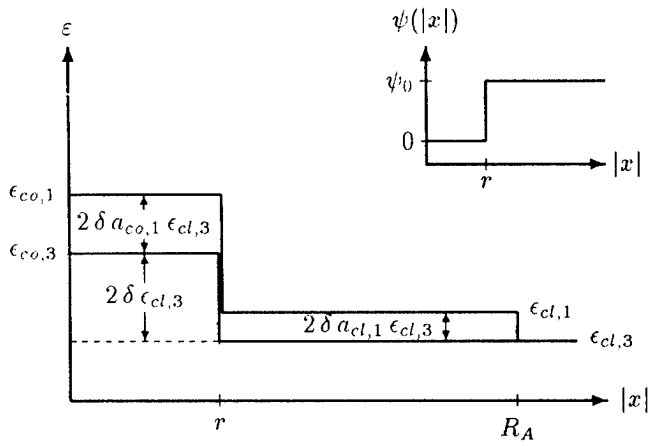


Figure 1: Illustration of the parameters introduced; the refractive index profiles of a uniaxial circular waveguide with the core radius r and with the anisotropy radius R_A. The profiles are such that: $\epsilon_1(x) > \epsilon_2(x) = \epsilon_3(x)$.

where r is a characteristic dimension of the waveguide. For example, in the circular waveguide we set $r = 1/2\ \mathrm{diam}(\mathrm{supp}(s_i)) = \{\text{the core radius}\}$.

We introduce the anisotropy coefficients $a_{co,i}$, $a_{cl,i}$ of the cores and of the cladding, respectively, defined as:

$$a_{co,i} = \frac{c_{co,i} - c_{co,3}}{c_{co,3} - c_{cl,3}} \qquad a_{cl,i} = \frac{c_{cl,i} - c_{cl,3}}{c_{co,3} - c_{cl,3}} \qquad i = 1,2. \tag{11}$$

These coefficients are normalized with respect to the profile height δ. By defining the functions:

$$A_i(x) = \{\,(1 + a_{co,i} - a_{cl,i})\, s_i(x) \;+\; a_{cl,i}\,\}\, \chi_{\{x:|x|<R_A\}} \qquad i = 1,2 \tag{12}$$

we can express c_i from (6) in the following form:

$$c_i(x) = c_{cl,3} \;+\; (c_{co,3} - c_{cl,3})\, A_i(x) \qquad i = 1,2 \tag{13}$$

The physical parameters just introduced are illustrated in the Fig. 1.

In terms of the parameters defined above our eigenproblem (3) takes the form (in the coordinate system X_1X_2 with the unit distance equal r from (8)):

$$\begin{aligned}
&\Delta h_1 \;+\; V^2 A_2\, h_1 \;+\; \frac{\frac{1}{2\delta} + A_2}{(\frac{1}{2\delta} + s_3)^2} \frac{\partial s_3}{\partial x_2} \boldsymbol{G}(h_1, h_2) \\
&+ \left(1 - \frac{\frac{1}{2\delta} + A_2}{\frac{1}{2\delta} + s_3}\right) \frac{\partial}{\partial x_2} \boldsymbol{G}(h_1, h_2) \;-\; V^2 \mathcal{B}\, h_1 = 0 \\
&\Delta h_2 \;+\; V^2 A_1\, h_2 \;-\; \frac{\frac{1}{2\delta} + A_1}{(\frac{1}{2\delta} + s_3)^2} \frac{\partial s_3}{\partial x_1} \boldsymbol{G}(h_1, h_2) \\
&- \left(1 - \frac{\frac{1}{2\delta} + A_1}{\frac{1}{2\delta} + s_3}\right) \frac{\partial}{\partial x_1} \boldsymbol{G}(h_1, h_2) \;-\; V^2 \mathcal{B}\, h_2 = 0
\end{aligned} \tag{14}$$

where

$$\Delta = \frac{\partial^2}{\partial x_1^2} + \frac{\partial^2}{\partial x_2^2}, \qquad \boldsymbol{G}(h_1, h_2) = \frac{\partial h_2}{\partial x_1} - \frac{\partial h_1}{\partial x_2}$$

MATHEMATICAL PROPERTIES OF THE OPERATOR $\boldsymbol{T}$

Spectral properties of the propagation operator strongly depend not only on the formulation of its analytical form, but also on the choice of its domain of definition. Since we are interested in guided modes that decay exponentially as $|x| \to \infty$, we analyze the operator $\boldsymbol{T}$ corresponding to the propagation eigenproblem (3) in the Hilbert space $\mathcal{H} = L^2(\mathbb{R}^2) \otimes \mathbb{C}^2$ of square integrable complex valued vector functions defined on the cross-sectional plane $\mathbb{R}^2$ of the waveguide. Space $\mathcal{H}$ is equipped with the scalar product:

$$(u\ ,\ w)_{\mathcal{H}} \equiv (u_{x_1}\ ,\ w_{x_1})_2 + (u_{x_2}\ ,\ w_{x_2})_2$$

$$u = [u_{x_1}, u_{x_2}], \quad w = [w_{x_1}, w_{x_2}], \qquad \left(u_{x_j}\ ,\ w_{x_j}\right)_2 = \int_{\mathbb{R}^2} u_{x_j}\, \overline{w}_{x_j}\, dx$$

where $j = 1, 2$, and $\overline{\ }$ denotes a complex conjugate.

The operator $\boldsymbol{T}$ has the analytical form (4) with the assumptions about the permittivity tensor and the other parameters further specified in the preceding section (c.f. (5)–(7)). We define the domain of $\boldsymbol{T}$ as:

$$D(\boldsymbol{T}) = D(\boldsymbol{l}) \otimes \mathbb{C}^2, \tag{15}$$

where $D(\boldsymbol{l})$ is the domain of Laplacian in $\mathbb{R}^2$:

$$D(\boldsymbol{l}) = \left\{u \in L^2(\mathbb{R}^2) : \quad \Delta u \in L^2(\mathbb{R}^2) \text{ in the distribution sense}\right\} \tag{16}$$

In fact, $D(\boldsymbol{l}) = H^2(\mathbb{R}^2)$ – the second Sobolev space. With this domain the Laplace operator $\boldsymbol{l}u = \Delta u$ is selfadjoint in $L^2(\mathbb{R}^2)$.

We have proved in [10] that the operator $\boldsymbol{T}$ with the domain $D(\boldsymbol{T})$ defined in (15) is a densely defined and closed operator in $\mathcal{H}$, provided that the permittivity profile functions s_i from (6), (7) are such that $s_i \in H^2(\mathbb{R}^2)$ for $i = 1, 2, 3$. This assumption permits us to analyze the problem in the Hilbert space $\mathcal{H}$ of square integrable vector functions and to assimilate the conditions on the core-cladding boundary into the field equations.

Now we briefly characterize properties of $\boldsymbol{T}$ using the decomposition defined in (4). From (16) it follows that operator $\boldsymbol{T}_1 + k^2\epsilon_{cl,3}$ with the domain $D(\boldsymbol{T})$ defined in (15) is selfadjoint in $\mathcal{H}$. Moreover it is semibounded, with the upper bound $k^2\epsilon_{cl,3}$. Its spectrum is purely continuous and consists of the negative real semiaxis (the spectrum of Laplacian) shifted by $k^2\epsilon_{cl,3}$. It corresponds to the plane waves in an isotropic homogeneous medium with permittivity $\epsilon_{cl,3}$.

Considering the operator $\boldsymbol{T}$ defined in (4), (15) as the $\boldsymbol{T}_2 + \boldsymbol{T}_3 + \boldsymbol{T}_4$ perturbation of selfadjoint $\boldsymbol{T}_1$ appeared to be very useful in determining spectral properties of $\boldsymbol{T}$. The crucial observations here proved so far by the author [9], [10] are the following. Operators $\boldsymbol{T}_2$ and $\boldsymbol{T}_3$ are $\boldsymbol{T}_1$–compact, meaning that for $i = 2, 3$, $D(\boldsymbol{T}_i) \supseteq D(\boldsymbol{T}_1)$ and $\boldsymbol{T}_i(\boldsymbol{T}_1 - \rho)^{-1}$ is a compact operator for all ρ outside the spectrum $\sigma(\boldsymbol{T}_1)$ of

the operator $\boldsymbol{T_1}$. $\boldsymbol{T}_1$–compactness of the operator $\boldsymbol{T}_4$ defined in $L^2(\mathbb{R}^2) \otimes \mathbb{C}^2$ (case of an anisotropic open waveguide) remains an open problem. So far, the author succeeded to prove that $\boldsymbol{T}_4$ is $\boldsymbol{T}_1$– bounded with the relative bound $b = 1$. The methods used in the proofs of $\boldsymbol{T}_1$ compactness of $\boldsymbol{T}_2$ and $\boldsymbol{T}_3$ cannot be directly applied, since the terms with second derivatives occur in $\boldsymbol{T}_4$. However, author proved $\boldsymbol{T}_1$–compactness of $\boldsymbol{T}_4$ in $L^2(P) \otimes \mathbb{C}^2$ where P is a large circle containing the support S of the permittivity profiles (case of an anisotropic shielded waveguide).

Many important spectral properties of $\boldsymbol{T}$ can be inferred from the above facts. In particular, When $\boldsymbol{T}_1$ is perturbed by $\boldsymbol{T}_2 + \boldsymbol{T}_3 + \boldsymbol{T}_4$, only the discrete part of $\sigma(\boldsymbol{T}_1)$ can be modified, since the essential spectrum of the operator does not change under a relatively compact (bounded) perturbation. Hence eigenvalues may appear in $\sigma(\boldsymbol{T})$. They correspond to the modes of the waveguide. In fact, there is always at least one eigenvalue $\beta^2 \in [k^2\epsilon_{cl,3}, \max_{i=1,2,3}(k^2\epsilon_{co,i})]$ (that of the fundamental HE_{11} mode), which can be concluded from the assumptions (6), (7) imposed on the permittivity functions. In particular, these assumptions imply that $\boldsymbol{T}_2$ is bounded and positively defined. The operators $\boldsymbol{T}_3$ and $\boldsymbol{T}_4$ are neither bounded nor symmetric. Hence $\boldsymbol{T}$ is not selfadjoint. Thus, complex modes with fields decaying exponentially outside the waveguide cores may exist. Moreover, both $\boldsymbol{T}_3$ and $\boldsymbol{T}_4$ couple (each in a different way) transversal components of the mode field making the eigenproblem truly vectorial one. Multiplicity of the spectrum $\sigma(\boldsymbol{T})$ essentially depends on the properties of $\boldsymbol{T}_3$ and $\boldsymbol{T}_4$. Namely the shape asymmetry of the permittivity profile supports and the magnitude of the anisotropy introduced are responsible for removing the degeneracy of the eigenvalues of $\boldsymbol{T}$ for circular waveguide. Hence, the design of an anisotropic waveguide strongly selective to linearly polarized light is possible. Several numerical examples of such guiding structures will be presented on the lecture.

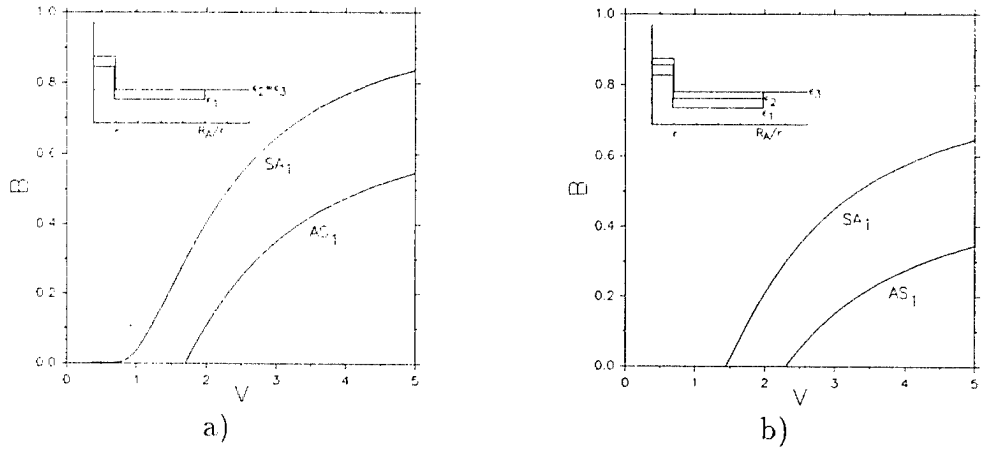


Figure 2: Dispersion curves of fundamental modes in circular uniaxial a) and biaxial b) fibers with parameters: $\delta = 0.001$, $R_A = 5r$ and:
a) $a_{co,1} = -0.3$, $a_{cl,1} = -0.3$, $a_{co,2} = a_{cl,2} = 0$,
b) $a_{co,1} = -0.5$, $a_{cl,1} = -0.5$, $a_{co,2} = -0.2$, $a_{cl,2} = -0.2$.
The dominant component of $h_\perp$ is h_1 for the mode SA_1 (X_1-symmetric, X_2-antisymmetric) and h_2 for the mode AS_1 (X_1-antisymmetric, X_2-symmetric).

References

[1] D. K. Paul and R. K. Shevgaonkar, "Multimode propagation in anisotropic optical waveguides," *Radio Sci.*, vol. 16, pp. 525–533, jul–aug 1981.

[2] A. W. Snyder and F. Rühl, "Single-mode, single-polarization fibers made of birefringent material," *J. Opt. Soc. Am.*, vol. 73, pp. 1165–1174, Sept. 1983.

[3] A. W. Snyder and A. Ankiewicz, "Anisotropic fibers with nonaligned optical (stress) axes," *J. Opt. Soc. Am. A*, vol. 3, pp. 856–863, June 1986.

[4] S. F. Kawalko and P. L. E. Uslenghi, "A method for the analysis of biaxial graded-index optical fibers," *IEEE Trans. Microwave Theory Tech.*, vol. 39, pp. 961–968, June 1991.

[5] I. Bardi and O. Biro, "An efficient finite-element formulation without spurious modes for anisotropic waveguides," *IEEE Trans. Microwave Theory Tech.*, vol. 39, pp. 1133–1139, July 1991.

[6] M. Lu and M. M. Fejer, "Anisotropic dielectric waveguides," *J. Opt. Soc. Am. A*, vol. 10, pp. 246–261, Feb. 1993.

[7] T. F. Jabłoński, "Iterative eigenfunction expansion method for monomode gradient index fibers with arbitrary cross-section," in *Proc. URSI Int. Symp. E. M. Theory, part B*, pp. 415–417, 1986.

[8] T. F. Jabłoński and M. J. Sowiński, "Analysis of dielectric guiding structures by the iterative eigenfunction expansion method," *IEEE Trans. Microwave Theory Tech.*, vol. MTT-37, pp. 63–70, Jan. 1989.

[9] T. F. Jabłoński, "Iterative eigenfunction expansion method for cylindrical fibers," *IFTR Reports*, 3/1986. (in Polish).

[10] T. F. Jabłoński, *Iterative Spectral Decomposition Method and Its Application to the Analysis of Dielectric Guiding Structures.* PhD thesis, Polish Academy of Sciences, Institute of Fundamental Technological Research, Warsaw, Poland, 1991.

[11] T. F. Jabłoński, "Complex modes in open lossless dielectric waveguides," *J. Opt. Soc. Amer. A*, vol. 11, pp. 1272–1282, Apr. 1994.

[12] T. F. Jabłoński, "An efficient iterative scheme for solving eigenproblems in the theory of electromagnetic waves," in *Proc. of 7-th International Conference on Mathematical Methods in Electromagnetic Theory*, (Kharkov, Ukraine), June 1–6 1998.

[13] T. F. Jabłoński, "Monomode fiber coupler with a separating layer of arbitrary refractive index," *J. Lightwave Technol.*, (to appear).

[14] M. Mrozowski, T. F. Jabłoński, and J. Mazur, "Application of the iterative eigenfunction expansion method to the analysis of rectangular dielectric waveguide structures," in *Proc. MIOP'90 Conference*, (Stuttgart), 1990.

[15] T. F. Jabłoński and M. J. Sowiński, "Propagation properties of doublecore optical fibers," *Proc. SPIE, Optical Fibers and Their Applications IV*, vol. 670, pp. 30–38, 1986.

INFINITE-SHEET BRANCHING OF THE HABITAT OF THE NATURAL FREQUENCIES OF OPEN RESONATORS AS A RESULT OF ADMISSION OF INFINITE BOUNDARIES

Alexander I. Nosich

IRE NASU, Ul. Proskury 12, Kharkov 61085, Ukraine. E-mail: alex@emt.kharkov.ua

We consider several eigenvalue problems for the Helmholtz and Maxwell equations, where the fields are assumed time-harmonic, i.e. $\sim e^{-ikct}$, and the normalized frequency k is eigenparameter: localized 2D and 3D dielectric resonators (DR) in free space (1), in PEC-wall waveguide (2), and in stratified dielectric medium (3), localized 3D DR in free space (4), in PEC-wall waveguide or stratified medium (5), and near a fiber (6).

These problems are about the time-harmonic electromagnetic fields in and out of bounded penetrable objects placed in unbounded host medium. Their correct statement needs certain condition imposed on the field behavior at infinity. Such a condition, in each case, follows from the behavior of the corresponding Green's function analytically continued from the real values of k to the complex domain. Here, the real-k Green's function satisfies, each time, the Principle of Radiation in the form of corresponding *radiation condition.* Thus, in (1) this is the Sommerfeld condition [1], in (2) this is the Sveshnikov condition [2], and in (3) this is the condition established in [3]. Different arrangement of "infinity", in each 2D case, entails different shape of the Green's function. As a result, the domains of their analytic continuation to complex k are also different. In (1) this is the Riemann surface (RS) of $Ln\ k$, in (2) this is RS of $\Sigma_{n=0}^{\infty}(k^2-(\pi n/d)^2)^{1/2}$, where d is the waveguide-wall separation, and in (3) this is RS of $Lnk+\Sigma_{n=0}^{\infty}(k^2-k_n^2)^{1/2}$, where k_n are the real-valued critical frequencies of the guided-wave modes of the stratified medium - if they exist. The complex-k conditions at infinity that inherit all the features of real-k radiation conditions and reduce to them at the real axis of the principal sheet of corresponding RS, are called Reichard's conditions [4]. In each case, as one can show by using the Poynting theorem, if dielectric permittivity ε has zero or positive imaginary part (i.e., the object is *passive*), then the k-eigenvalues can be only complex-valued and have negative imaginary parts. The corresponding eigenfunctions, or modal fields, are destined to decay in time but grow up in space away from DR. Therefore these problems are the *generalized eigenvalue problems*, to distinguish them from classical eigenvalue problems. For the 3D problems, instead of Sommerfeld's condition, the real-k case of (4) needs so-called Silber-Muller radiation condition [5,6] that eliminates radial components far from DR. In the case of (5) and (6), the real-k radiation conditions are vector analogies of the 2D ones; for (6) it was established in [3]. Important is that the fiber modes may carry the power in backward direction that must be accounted for in the radiation condition [3]. The domain of analytic continuation of the Green's function in k in the case (4) is just a complex plane. However, as soon as the host medium contains infinite regular boundaries, e.g. a stratification or a fiber, then this domain turns to a composition of logarithmic sheets of the $Ln(k^2-k_n^2)$ type, with the branch points of RS located at the critical frequencies of the guided modes.

Realistic objects are always 3D and finite, hence the habitat of their k_s is just the complex plane (good). Infinite-sheet branching of the domain of continuation of the field function in k is always the price paid for introducing some geometrical infinity. Firstly, neglecting the finite length when switching from the free-space 3-D to the free-space 2-D models leads to the Lnk branching (bad). Secondly, admission of infinite boundaries in the host medium, either PEC ones or penetrable flat and curved ones, leads to additional $\Sigma_{n=0}^{\infty}(k^2-k_n^2)^{1/2}$ or $\Sigma_{n=0}^{\infty}Ln(k^2-k_n^2)$ branching in the 2-D and 3-D models, respectively (ugly). All the eigenvalues, k_s, "live" on a

corresponding RS – this is their natural habitat. Based on the theory of integral equations and operator-valued functions [7], one can verify that each of k_s is a piece-wise analytic function of geometry and material parameters. Analyticity can be violated only if two eigenvalues coalesce. They are only of finite multiplicity and may appear or disappear only at branching points and at infinity on RS. In the real-k scattering problems, the field characteristics display the frequency dependences, which are sharply broken at the critical frequencies k_n (at branch points). This is because their derivatives in frequency contain square-root singularities there. An old example of this effect is the Wood's anomalies in the scattering from infinite-periodic diffraction gratings. Here, elementary cell of the grating can be viewed as a discontinuity in so-called Floquet virtual waveguide with PEC walls, therefore the branching in k has the same features as in the waveguide scattering.

Finally, we discuss the effect of lasing. From the viewpoint of mathematical modeling based on the so-called *cold model* of VCSEL, the lasing is the existence of at least one real-valued natural frequency of an inhomogeneous open DR. This may happen provided that there is a sub-domain, inside DR, that is filled in with an *active material* characterized by gain (equivalently, negative imaginary part of ε). As we have seen, each complex-valued natural frequency k_s of a passive open DR is analytic function of ε, and hence a continuous function of its imaginary part, γ. If the latter is varied, each natural frequency migrates on the corresponding RS, and if it takes negative values, the frequencies are allowed to migrate across the real axis of the principal sheet of RS into the upper halfplane. Purely real value of every k_s may take place only at a specific value of the gain, γ_s. Therefore, the *Lasing Eigenvalue Problem* can be formulated as a homogeneous boundary-value problem with appropriate boundary and radiation conditions adapted to the host medium. It is necessary to find eigenpairs of real-valued normalized frequency k_s and gain γ_s that generate non-zero solutions, i.e. vector (in 3-D) or scalar (in 2-D) field functions of the lasing modes.

Here, as we have seen above, admission of infinite boundaries in the host medium brings infinite number of branch points located at the real k-axis of the principal sheet of RS. The natural frequencies may appear or disappear only at the boundary of the domain of solution analyticity in k, i.e. at the infinity and at the branch points k_n. Therefore, searching for eigenvalues and tracing their trajectories with the loss/gain variation may potentially hit a situation that k_s coalesces with k_n and then either migrates further on the principal sheet (good) or goes to the other, "non-physical", sheet of RS (bad) or even disappears at all (ugly). Such a "swallowing up by the earth" of a lasing mode is of course an exotic thing and tells only about the defect of the model used.

[1] A. Sommerfeld, Die Greensche funktion der schwingungsgleichung, *Jber. Deutsch. Math. Verein*, vol. 21, pp. 309-353, 1912.

[2] A.G. Sveshnikov, The principle of radiation, *Doklady Akademii Nauk SSSR*, vol. 73, no 5, pp. 917-920, 1950 (in Russian).

[3] A.I. Nosich, Radiation conditions, limiting absorption principle, and general relations in open waveguide scattering, *J. EM Waves and Applications*, vol. 8, no 3, pp. 329-353, 1994.

[4] H. Reichardt, Ausstarhlungsbedingungen fur die wellengleichung, *Abh. Mathem. Seminar*, University of Hamburg, vol. 24, pp. 41-53, 1960.

[5] S. Silver, *Microwave Antenna Theory and Design*, MIT Radiation Lab Series, vol. 12, New York: McGraw-Hill, 1949.

[6] C. Muller, Uber die beugung elektromagnetischer schwingungen an endlichen homogenen korpern, *Math. Ann.*, vol. 123, pp. 345-378, 1951.

[7] S. Steinberg, Meromorphic families of compact operators, *Arch. Rational Mech.*, vol. 31, no 5, pp. 372-379, 1968.

WIENER-HOPF ANALYSIS OF THE RCS OF TWO, CANONICAL PARALLEL-PLATE WAVEGUIDE CAVITIES WITH MATERIAL LOADING

Shoichi Koshikawa [1] and Kazuya Kobayashi [2]

[1] Laboratory, Antenna Giken Co., Ltd., 4-72 Miyagayato, Saitama 330-0011, Japan
Tel: +81-48-684-0712, Fax: +81-48-684-9960, E-mail: koshikawa@antenna-giken.co.jp
[2] Department of Electrical, Electronic, and Communication Engineering, Chuo University
1-13-27 Kasuga, Bunkyo-ku, Tokyo 112-8551, Japan
Tel: +81-3-3817-1869, Fax: +81-3-3817-1847, E-mail: kazuya@kazuya.elect.chuo-u.ac.jp

ABSTRACT

Two diffraction problems involving two-dimensional cavities formed by a semi-infinite parallel-plate waveguide and by a finite parallel-plate waveguide are rigorously analyzed for the plane wave incidence using the Wiener-Hopf technique. It is shown that the solution for the semi-infinite case is valid for arbitrary cavity dimensions, whereas the solution for the finite case is valid for the cavity depth large compared with the wavelength. Illustrative numerical examples on the radar cross section (RCS) are presented, and the far field backscattering characteristics are compared between these two cavities.

INTRODUCTION

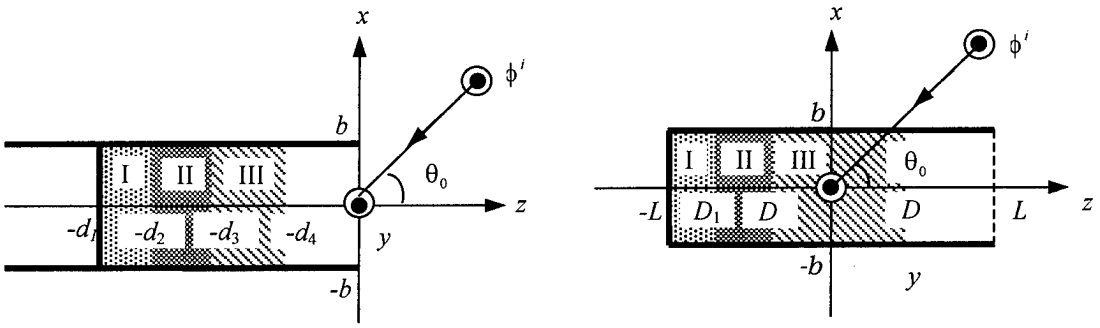
The analysis of electromagnetic scattering from open-ended metallic waveguide cavities has received much attention recently in connection with the prediction and reduction of the radar cross section (RCS) of a target [1-3]. This problem serves as a simple model of duct structures such as jet engine intakes of aircrafts and cracks occurring on surfaces of general complicated bodies. There have been a number of investigations on the scattering by two-dimensional (2-D) and three-dimensional (3-D) cavities of various shapes based on high-frequency techniques and numerical methods. It appears, however, that the solutions obtained by these methods are not uniformly valid for arbitrary cavity dimensions.

The Wiener-Hopf technique is known as a powerful, rigorous approach for solving diffraction problems associated with canonical geometries. In the previous papers [4-7], we have considered two different parallel-plate waveguide cavities with material loading, and carried out a rigorous RCS analysis using the Wiener-Hopf technique. As a result, it has been shown that our final solutions provide accurate, reliable results over a broad frequency range. We have also verified that, for large cavities, the absorbing layer loading inside the cavities results in significant RCS reduction. The results of our recent studies on the cavity RCS are summarized in detail in [8].

This paper is in continuation with our recent research on the cavity RCS. We shall consider two canonical, 2-D parallel-plate waveguide cavities with material loading, and carry out a comparative RCS study of these cavities. The first geometry (referred to as Cavity I) is a cavity formed by a semi-infinite parallel-plate waveguide with an interior planar termination, where three different material layers are coated on the surface of the terminated plate. The second geometry (referred to as Cavity II) is a cavity formed by a finite parallel-plate waveguide with a planar termination at the aperture of the waveguide, where the same material layers as in Cavity I are coated on the surface of the terminated plate. It is noted that geometries of interior regions of the two cavities are

exactly the same as each other. The exterior features are, however, totally different since Cavity I has two parallel semi-infinite plates, being joined to its outer right-angled corners. The analysis of the diffraction problems involving Cavity I and Cavity II has been carried out using the Wiener-Hopf technique in [6, 7] and [4, 5], respectively. The purpose of this paper is to compare the solutions for Cavity I and Cavity II and investigate the effect of geometrical differences of the two cavities on the far field scattering characteristics. Both *E* and *H* polarizations are treated.

The time factor is assumed to be $\exp(-i\omega t)$ and suppressed throughout this paper.



(a) Cavity I.

(b)Cavity II.

Fig.1. Geometry of the cavities.

SUMMARY OF THE WIENER-HOPF ANALYSIS

Cavity I: Cavity Formed by a Semi-Infinite Parallel-Plate Waveguide [6, 7]

We first consider the plane wave diffraction by Cavity I. As mentioned above, Cavity I is formed by a semi-infinite parallel-plate waveguide with an interior planar termination. The problem geometry is shown in Fig. 1(a), where $-\infty < -d_1 < -d_2 < -d_3 < -d_4 < 0$, and the upper and lower plates at $x = \pm b$ and the endplate at $z = -d_1$ are infinitely thin and perfectly conducting. The material layers I $(-d_1 < z < -d_2)$, II $(-d_2 < z < -d_3)$, and III $(-d_3 < z < -d_4)$ inside the waveguide are characterized by the relative permittivity and permeability $(\varepsilon_{rm}, \mu_{rm})$ for $m = 1$, 2, and 3, respectively. Let the total field ϕ' be defined by $\phi'(x,z) = \phi^i(x,z) + \phi(x,z)$, where $\phi^i(x,z) = \exp[-ik(x\sin\theta_0 + z\cos\theta_0)]$ is the incident field of *E* or *H* polarization for $0 < \theta_0 < \pi/2$ with $k[\equiv \omega(\mu_0\varepsilon_0)^{1/2}]$ being the free-space wavenumber. The term $\phi(x,z)$ is the unknown scattered field and satisfies the 2-D Helmholtz equation. As usual in the Wiener-Hopf analysis, we assume that the vacuum is slightly lossy as in $k = k_1 + ik_2$ with $0 < k_2 < k_1$. The solution for real *k* is obtained by letting $k_2 \to +0$ at the end of analysis. Referring to the geometrical classification proposed in [9], Cavity I belongs to a class of the modified Wiener-Hopf geometry of the second kind.

Introducing the Fourier transform for the scattered field and applying boundary conditions in the transform domain, the problem is formulated in terms of the modified Wiener-Hopf equations of the second kind [9], which are solved exactly in a formal sense via the factorization and decomposition procedure. It should be noted, however, that the formal solution involves infinite series with unknown coefficients. Applying a rigorous asymptotics with the aid of the edge condition, approximate expressions of the infinite series are derived leading to an efficient approximate solution of the Wiener-Hopf equations. The approximate solution involves numerical inversion of matrix equations. The results are uniformly valid for arbitrary cavity dimensions. The scattered filed in the real space is evaluated asymptotically by taking the inverse Fourier

transform and applying the saddle point method.

Cavity II: Cavity Formed by a Finite Parallel-Plate Waveguide [4, 5]

We now consider the diffraction problem for Cavity II, which is formed by a finite parallel-plate waveguide with a planar termination at the aperture. The geometry of the cavity is shown in Fig. 1(b), where ϕ' is the incident field of E or H polarization, where $-L < D_1 < D_2 < D_3 < L$, and the cavity plates are perfectly conducting and of zero thickness. The material layers I ($-L < z < D_1$), II ($D_1 < z < D_2$), and III ($D_2 < z < D_3$) inside the cavity are characterized by the relative permittivity/permeability $(\varepsilon_{rm}, \mu_{rm})$ for m = 1, 2, and 3, respectively. Comparing Cavity I and Cavity II, it is seen that the interior cavity geometries are exactly the same as each other.

Taking the Fourier transform of the Helmloltz equation and solving the resultant transformed wave equations, we may derive a scattered field expression in the Fourier transform domain. We apply boundary conditions to the scattered field representation in the transform domain. It should be noted that the cavity is now formed by a finite parallel-plate waveguide and hence, the problem is formulated in terms of the modified Wiener-Hopf equations of the third kind [9]. This is the essential difference in the structure of the Wiener-Hopf equations. The Wiener-Hopf equations are solved exactly in a formal sense via the factorization and decomposition procedure as in the case of Cavity I leading to a formal solution. Due to the geometrical differences between Cavity I and Cavity II, the structure of the formal solution for Cavity II is totally different from that for Cavity I. The solution now involves branch-cut integrals with unknown integrands as well as infinite series with unknown coefficients. Assuming that the cavity depth $2L$ is large compared with the wavelength, we can derive high-frequency asymptotic expansions of the branch-cut integrals. As for the infinite series contained in the formal solution, we apply the edge condition to obtain their approximate expressions. This procedure leads to an approximate solution of the Wiener-Hopf equations, which is valid for the cavity depth large compared with wavelength. As in Cavity I, the solution involves numerical inversion of matrix equations. The scattered field in the real space is derived by taking the Fourier inverse and applying the saddle point method.

NUMERICAL RESULTS AND DISCUSSION

We shall now show representative numerical examples of the RCS for both E and H polarizations to discuss the far field backscattering characteristics of the cavities. In particular, the effect of geometrical differences of the two cavities on the scattered far field is investigated. The RCS per unit length is defined by $\sigma = \lim_{\rho\to\infty}(2\pi\rho\,|\phi/\phi'|^2)$, where the cylindrical coordinate (ρ,θ) has been introduced as in $x = \rho\sin\theta$, $z = \rho\cos\theta$ for $-\pi < \theta < \pi$.

Figures 2(a-c) and 2(d-f) show numerical results of the normalized monostatic RCS σ/λ [dB] as a function of incidence angle θ_0 for E and H polarizations, respectively, where λ is the free-space wavelength. In numerical computation, cavity dimensions have been taken as kb = 3.14, 15.7, 31.4 with $d_1/2b = L/b = 1.0$. As an example of existing three-layer materials, we have chosen Emerson & Cuming AN-73 [1], where the material constants are $\varepsilon_{r1} = 3.4 + i10.0$, $\varepsilon_{r2} = 1.6 + i0.9$, $\varepsilon_{r3} = 1.4 + i0.35$, $\mu_{r1} = \mu_{r2} = \mu_{r3} = 1.0$, and the thickness of each layer is such that $d_1 - d_2 = d_2 - d_3 = d_3 - d_4 = D_1 + L = D_2 - D_1 = D_3 - D_2 (= t/3)$ (see Fig. 1). The total thickness of the three-layer material is taken as kt = 2.08.

It is seen from the figure that, the RCS curves for Cavity I and Cavity II with kb =

3.14 and *E* polarization (Fig. 2(a)) show close features for $0° < \theta_0 < 55°$, whereas in all the other examples, there are some differences on the backscattering characteristics between the two cavities. These differences are clearly observed in the *H*-polarized case, since the RCS curves for Cavity II oscillate rapidly in comparison to those for Cavity I. This oscillation for Cavity II is due to the fact that the multiple diffraction occurs between the leading edges at the aperture and the outer edges of the right-angled back corners.

CONCLUSIONS

In this paper, we have carried out a rigorous Wiener-Hopf analysis of the plane wave diffraction by two different cavities with three-layer material loading, formed by a semi-infinite parallel-plate waveguide (Cavity I) and by a finite parallel-plate waveguide (Cavity II). We have presented numerical examples of the monostatic RCS to discuss the far field backscattering characteristics of the cavities. Comparing the RCS results between Cavity I and Cavity II, some differences on the backscattering characteristics have been observed. It is therefore confirmed that the backscattering from these cavities is affected not only by the interior irradiation but also by the diffraction by the outer edges.

ACKNOWLEDGMENTS

This work was supported in part by Chuo University as one of the 2000 Research Projects for Promotion of Advanced Research at Graduate School and by the Institute of Science and Engineering, Chuo University.

REFERENCES

[1] S.-W. Lee and H. Ling, "Data book for cavity RCS: Version 1," *Tech. Rep.*, no. SWL 89-1, Univ. Illinois, Urbana, January 1989.

[2] W. R. Stone, Ed., *Radar Cross Sections of Complex Objects*, IEEE Press, New York, 1990.

[3] Special Issue on 'Radar Cross Section of Complex Objects', *Annals of Telecommunications*, vol. 50, no. 5-6, May-June 1995.

[4] S. Koshikawa, T. Momose, and K. Kobayashi, "RCS of a parallel-plate waveguide cavity with three-layer material loading," *IEICE Trans. Electron.*, vol. E77-C, no. 9, pp. 1514–1521, September 1994.

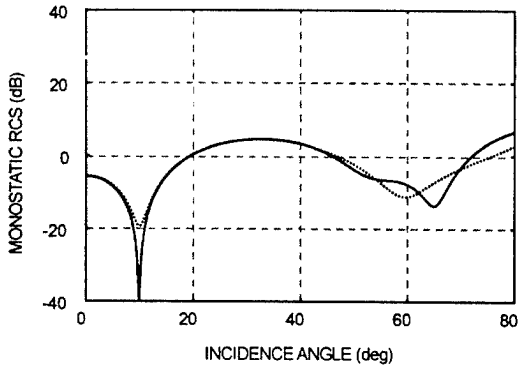
[5] S. Koshikawa and K. Kobayashi, "RCS analysis of a parallel-plate waveguide cavity with three-layer material loading," in *Direct and Inverse Electromagnetic Scattering*, A. H. Serbest and S. R. Cloude, Eds., pp. 142–157, Addison Wesley Longman, Essex, 1996.

[6] S. Koshikawa and K. Kobayashi, "Diffraction by a terminated, semi-infinite parallel-plate waveguide with three-layer material loading," *IEEE Trans. Antennas Propagat.*, vol. AP-45, no. 6, pp. 949–959, June 1997.

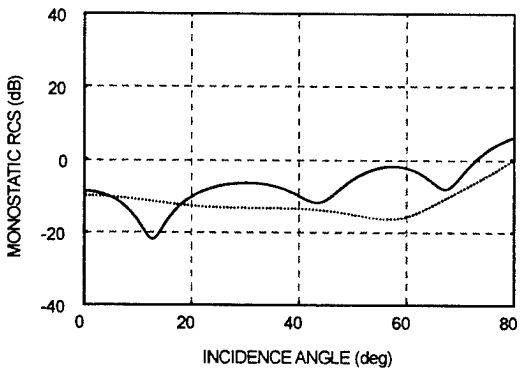
[7] S. Koshikawa and K. Kobayashi, "Diffraction by a terminated, semi-infinite parallel-plate waveguide with three-layer material loading: the case of *H* polarization," *Electromagnetic Waves & Electronic Systems*, vol. 5, no. 1, pp. 13–23, 2000.

[8] K. Kobayashi and S. Koshikawa, "Wiener-Hopf analysis of the radar cross section of parallel-plate waveguide cavitites," *Tech Rep.*, no. KK96-3-8, Chuo Univ., Tokyo, March 1996.

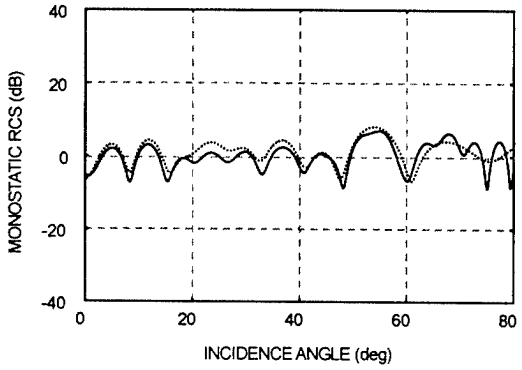
[9] K. Kobayashi, "Some diffraction problems involving modified Wiener-Hopf geometries," in *Analytical and Numerical Methods in Electromagnetic Wave Theory*, M. Hashimoto, M. Idemen, and O. A. Tretyakov, Eds., Chap. 4, Science House, Tokyo, 1993.



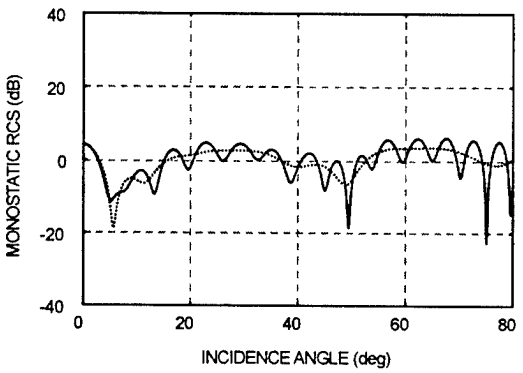
(a) E polarization, $kb = 3.14$.



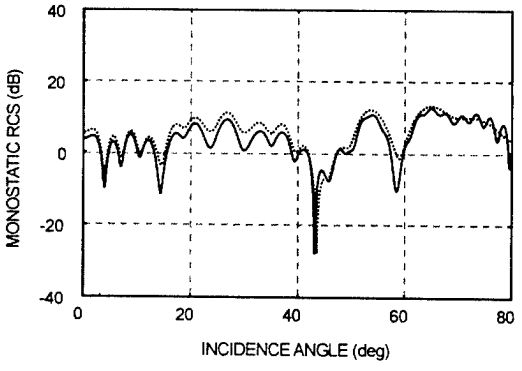
(d) H polarization, $kb = 3.14$.



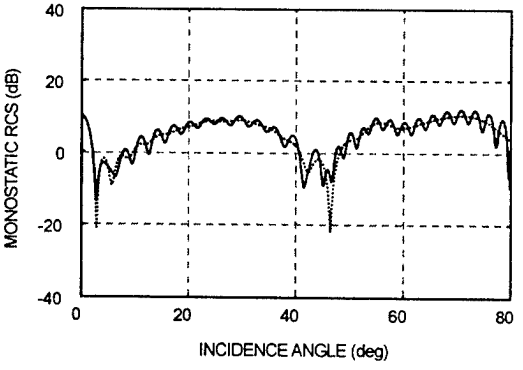
(b) E polarization, $kb = 15.7$.



(e) H polarization, $kb = 15.7$.



(c) E polarization, $kb = 31.4$.



(f) H polarization, $kb = 31.4$.

Fig. 2. Monostatic RCS versus incidence angle for $d_1 / 2b = L/b = 1.0$. ····· : Cavity I, ——— :Cavity II. The three-layer material inside the two cavities is Emerson & Cuming AN-73 with $kt = 2.08$.

WAVE TRANSMISSION TROUGH INHOMOGENEOUS CHAIN OF TRANSPARENT OBSTACLES

S. V. Sukhinin, D. A. Kondratenko.

M. Lavrentyev Institute of Hydrodynamics, Siberian Division of RAS
630090, Novosibirsk, Russia, E-mail: sukhinin@hydro.nsc.ru

ABSTRACT

We investigate the resonance and guiding properties of a chain of inhomogeneous transparent obstacles. Pass and stop bands are studied. Approximate expressions for the first wave-guiding frequencies and phase velocities of the wave-guiding modes in a transparent periodic structure consisting of two different media (chain of transparent obstacles) are found. It is shown that the length of a guided wave in a chain of transparent obstacles can exceed considerably the transparent obstacle sizes. The phase velocity of a guided wave can be smaller than wave velocities in both media in the event that the interaction between neighbouring transparent obstacles is taken into account. The influence of inhomogeneity of transparent obstacle sizes on the first wave-guiding frequencies of a chain of transparent obstacles is investigated. The resonance phenomena in periodical non-homogeneous chains of transparent obstacles for sources localized or distributed in space are investigated. As a result of the analysis, new physical phenomena are reported: 1. Resonance growth of amplitude in the neighbourhood of a source, and 2. Travelling wave resonance. Conditions of realization of the mentioned phenomena are obtained. It is shown that resonance growth of the oscillation amplitude in the neighbourhood of a source takes place for a discrete set of frequencies for which group velocity of waves is equal to zero. The travelling-wave resonance growth of amplitude takes place in the case of the sources of oscillations periodically distributed in space and has the same phase shift in time and space as a guided eigenwave. Similar phenomena are used for acceleration of particles in synchrophasotrons. This study has numerous applications in various areas of mechanics, physics and engineering.

INTRODUCTION

In [1-2] and [3] the propagation of waves in a non-homogeneous medium with a periodic structure was investigated. Suppose that periodic structure consists of two materials: $M1 = \{p^{(1)}, c_1, \rho_1\}$ and $M2 = \{p^{(2)}, c_2, \rho_2\}$. Let in the medium $M1$ a layer of the medium $M2$ with the width D (single obstacle,) is embedded. Everywhere in this paper a spatial variable is non-dimensional due to normalization to some characteristic length. These relations look like

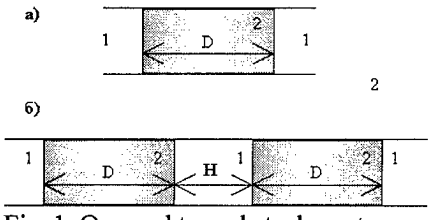


Fig. 1. One and two obstacle systems.

$$p_{xx}^{(1)} + \lambda^2 p^{(1)} = 0, |x| > D/2; \qquad p_{xx}^{(2)} + \lambda^2 \kappa^2 p^{(2)} = 0, |x| < D/2;$$
$$p^{(1)} = p^{(2)}, \tau p_x^{(1)} = p_x^{(2)} |x| = D/2; \qquad (1)$$
$$p^{(1)} = a_1 \exp(i\lambda x), x > D/2; \qquad p^{(2)} = a_2 \exp(-i\lambda x), x < D/2.$$

The notations $\lambda = \omega/c_1$, $\kappa = c_1/c_2$ are hereinafter used. The free obstacle oscillations are determined by a set $\Lambda^* = \{\lambda_k^*, k = 0,1,2,\ldots\}$ of complex values of parameter λ for which there exist nontrivial solutions of the problem (1). Further λ_k^* will be named a scattering frequency of corresponding problem. With the aid of straightforward derivations it is possible to verify that the scattering frequencies of the problem (1) look like

$$\lambda_k^* = \frac{1}{\kappa D}\left\{k\pi + i\ln\left[\frac{(\kappa+\tau)}{(\kappa-\tau)}\right]\right\}, \quad k = 0,1,2,\ldots \tag{2}$$

It is necessary to note that the scattering frequencies of problem (1) continuously depend on parameter τ in the intervals $0 < \tau < \kappa$, $\kappa < \tau < \infty$. The physical sense of real and imaginary parts of the scattering frequencies is obvious enough [1], $c_1 \mathrm{Re}(\lambda_k^*)$ being the eigenfrequency. The damping in time at a fixed point of space is given by the expression $p(x,t) = \mathrm{const}(x)\exp[-tc_1 \mathrm{Im}(\lambda_k^*)]$ for the corresponding mode of scattering oscillations. Scattering frequencies of problem (1) at $\tau \to 0$ tend to the eigenvalues of the Neumann problem in the domain $-D/2 < x < D/2$. This property is similar to the scattering frequencies of a Helmholtz resonator with the radius of the "throat" being a small parameter [1]. Singularity of the Helmholtz resonators is the existence of the scattering frequencies and corresponding scattering oscillations with wavelengths considerably exceeding geometrical size of the resonator, or so-called Helmholtz modes [2]. Such a mode has the scattering frequency $\lambda_0^*(\tau)$, so that $\lim_{\tau\to 0}[\lambda_0^*(\tau)] = 0$ and $\mathrm{Re}[\lambda_0^*(\tau)] = 0$. This entails the existence of eigenoscillation, which corresponds to $\lambda_1^*(\tau)$. From (2), for the scattering frequencies of the problem (1) it follows that in the case of a single obstacle there are no eigenoscillations of the Helmholtz mode type, at least within the framework of one-dimensional theory.

Essentially different property has the structure consisting of two transparent obstacles of gas (, a). As a result of transparent obstacles interaction there exist oscillations of the Helmholtz mode type. Free acoustic oscillations near transparent obstacles are charactrerized by the relations similar to (1). With the aid of representation of solution as a travelling wave, determination of the scattering frequencies is reduced to a search for zeros of certain analytic function. Evaluation of the scattering frequency, $\lambda_0^*(\tau, D, H)$, that is close to 0 as $\tau \to 0$ allows to find eigenoscillation near the two transparent obstacles of the Helmholtz mode type:

$$\lambda_0^*(\tau, D, H) = \frac{\sqrt{\tau}}{D\tau(\kappa^2+1)+\kappa^2 H}\left\{\sqrt{\tau(2\kappa^2+1)+2\kappa^2\frac{H}{D}} + i\sqrt{\tau}\right\}$$

Here, D is the transparent obstacle diameter and H is the distance between transparent obstacles. This estimation allows to state that the frequency characteristic of oscillations of an ensemble of transparent obstacles essentially differs from the performance of one-obstacle oscillations. The presence of neighbouring transparent obstacles causes appearance of low-frequency eigenoscillations of ensemble, the wavelength of these oscillations can exceed linear size of ensemble.

MONO-DISPERSIBLE CHAIN OF TRANSPARENT OBSTACLES

Suppose now that the length (linear concentration) of a layer of material M1 is equal to k_1, and the length of a layer of material M2 (linear concentration of material M2) is equal to k_2 (dimensionless transparent obstacle diameter), so that $k_1 + k_2 = 1$ is the dimensionless spatial period of the chain (Fig. 2). The oscillations in the fundamental cell of chain are described with relations

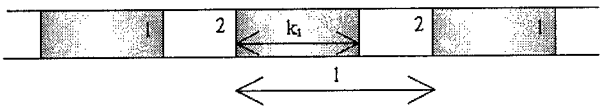


Fig. 2. Chain of mono-dispersible bubbles.

$$p_{xx}^{(1)} + \lambda^2 p^{(1)} = 0, for |x| < k_1/2; p_{xx}^{(2)} + \lambda^2 \kappa^2 p^{(2)} = 0, for k_1/2 < x < 1 - k_1/2;$$
$$p^{(1)}(k_1/2) = p^{(2)}(k_1/2); \tau p_x^{(1)}(k_1/2) = p_x^{(2)}(k_1/2); \quad (3)$$
$$p^{(1)}(-k_1/2)\exp(i\xi) = p^{(2)}(1-k_1/2); \tau p_x^{(1)}(-k_1/2) = p_x^{(2)}(1-k_1/2).$$

Further problem (3) will be called problem $MBC(\xi)$ about a chain of homogeneous (mono-dispersible) transparent obstacles. The general solution of the wave equation in the fundamental cell is $p_1 = a_1 \exp(i\lambda x) + b_1 \exp(-i\lambda x), p_2 = a_2 \exp(i\lambda\kappa x) + b_2 \exp(-i\lambda\kappa x)$. In view of this, expressions (3) are equivalent to a set of equations $\mathbf{A}(\lambda)Y = 0$ for the unknown vector $(a_1, b_1, a_2, b_2) = Y$. The matrix $\mathbf{A}(\lambda)$ has the following form:

$\exp(i\lambda k_1/2)$	$\exp(-i\lambda k_1/2)$	$-\exp(i\lambda\kappa k_1/2)$	$-\exp(-i\lambda\kappa k_1/2)$
$\tau\exp(i\lambda k_1/2)$	$-\tau\exp(-i\lambda k_1/2)$	$-\kappa\exp(i\lambda\kappa k_1/2)$	$\kappa\exp(-i\lambda\kappa k_1/2)$
$\exp[i(-\lambda k_1/2+\xi)]$	$\exp[i(\lambda k_1/2+\xi)]$	$-\exp[i\lambda\kappa(1-k_1/2)]$	$-\exp[-i\lambda\kappa(1-k_1/2)]$
$\tau\exp[i(-\lambda k_1/2+\xi)]$	$-\tau\exp[i(\lambda k_1/2+\xi)]$	$-\kappa\exp[i\lambda\kappa(1-k_1/2)]$	$\kappa\exp[-i\lambda\kappa(1-k_1/2)]$

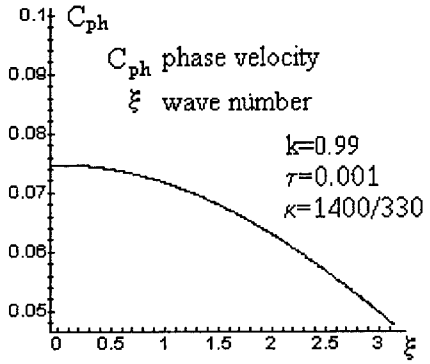


Fig. 3. The phase velocity of the creeping mode C_{ph} as a function of the wavenumber ξ for an air/water mixture (air bubbles in water). Linear concentration of water is k=0.99.

Nontrivial solution of the set of equations (3) exists if $\det[\mathbf{A}(\lambda)] = 0$.

Creeping mode. As wave-guiding frequencies of the problem $MBC(\xi)$ continuously depend on τ, and $\lambda_0 = 0$ is an eigenfrequency of the limiting problem (3) at $\tau = 0$, for small τ there exists an eigenfrequency $\lambda_0^*(\tau)$ of problem $MBC(\xi)$ such that $\lambda_0^*(\tau) \xrightarrow{\tau \to 0} 0$.

This eigenvalue corresponds to the lowest wave-guiding frequency of a mono-dispersible chain of transparent obstacles. Further a wave-guiding mode corresponding to the lowest wave-guiding frequency will be called a creeping mode. It is necessary to note that the length of this wave considerably exceeds the size of transparent obstacles. It is possible to derive the following approximate expression for the wave-guiding frequency of the creeping mode:

$$\lambda_0(\tau,\xi)=\sqrt{\frac{2\tau[1-\cos(\xi)]}{[(1+\kappa^2)\tau-\tau^2-\kappa^2]k_1^2+(\kappa^2-2\tau\kappa^2+\tau^2)k_1+\tau\kappa^2}} \qquad (4)$$

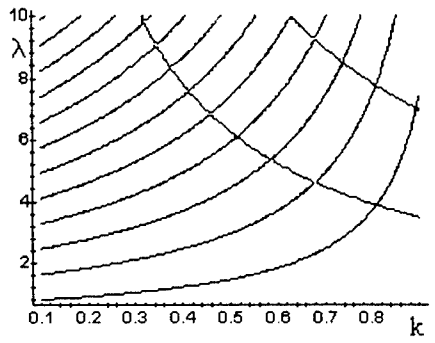


Fig. 4. Wave-guiding frequencies as a function of linear concentration k of water with air bubbles.

For small values of τ, a simplified formula $\lambda_0(\tau,\xi)=\sqrt{2\tau[1-\cos(\xi)]/\kappa^2 k_1(1-k_1)}$ is valid.

It is necessary to note that the wave-guiding frequency of a creeping mode essentially depends on the linear concentration $k = k_1$. It is also necessary to note that for $k = 0.5$ there exists a global minimum of wave-guiding frequency as a function of linear concentration. The phase shift condition allows presenting any solution of the $MBC(\xi)$ problem as $p(x)=w(x)\exp(i\xi x)$, where $w(x)=w(x+1)$ is a periodic function. This representation allows considering ξ as the wavenumber of a guided mode.

The curves characterizing phase velocity of a guided mode of a mono-dispersible transparent obstacle chain (air obstacles in water with linear water concentration $k = 0.99$) corresponding to a creeping mode are shown in Fig. 3. It is necessary to make a note that the phase velocity of a wave-guiding mode in a chain of transparent obstacles can be smaller than velocities of waves in the transparent obstacle medium and in the background medium.

As it is possible to see from Fig. 3 and to calculate with the aid of (4), phase velocity of a creeping mode is 40 times smaller than velocity of wave in air. This example confirms a necessity of registration of non-homogeneities (even with small concentration) when studying the propagation of waves in inhomogeneous regular media.

Acoustical and optical modes. Alongside with a creeping mode a chain of transparent obstacles has higher order wave-guiding modes. The number of these modes is infinite. As the wave-guiding frequencies continuously depend on τ, for small values of this parameter it is possible to find that wave-guiding frequencies are localized in the neighbourhoods of corresponding eigenfrequencies of the Dirichlet problem in the domain M1 and the Neumann one in the domain M2. (in view of wave velocities).

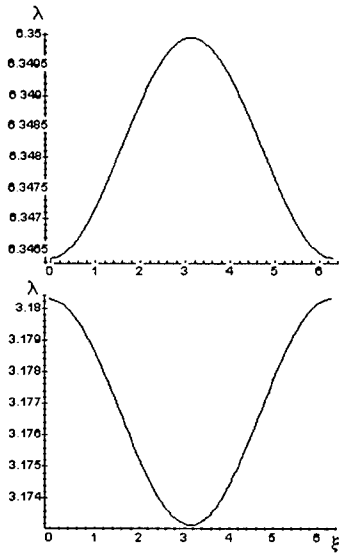


Fig. 5. Dispersion curves for the 2nd and 3d wave-guiding modes, k =0.99, in water/air.

The wave-guiding frequencies of problem $MBC(\pi)$, as a function of linear concentration of water, are shown in Fig. 4. The calculations were carried out for water and air: $\kappa = 1400/330$, $\tau = 0.001$, $k = k_1$, $c_1 = 1400, c_2 = 330$, and $\xi = \pi$. In the dispersion curves for the 2nd (acoustical) and the 3d (optical) wave-guiding modes are shown (the creeping mode is considered as the first one) in a chain of transparent obstacles in water of the same parameters as before. As dimensionless length of obstacle is equal to 0.01 that first wave-guiding frequency will be close to an eigenfrequency of the

Dirichlet problem for the Laplacian in the interval [0, 0.99], which is close to one of the numbers $n\pi$, $n = 0,1,\ldots$. This is also confirmed by computations. The intervals of the variation of dispersion curve on the ordinate axis determine frequency passbands for the chains of transparent obstacles.

CHAIN OF POLY-DISPERSIBLE TRANSPARENT OBSTACLES

In natural conditions, mono-dispersible structures are met seldom enough, therefore it is interesting to investigate propagation of acoustic waves in the chains of poly-dispersible transparent obstacles. The elementary example is a periodic chain with two different transparent obstacles in the fundamental cell. Suppose that the fundamental cell of an inhomogeneous chain of transparent obstacles has the length 1 (in dimensionless variables) and contains two layers of medium 1 (water) with the sizes k_1 and k_3, $k_1 + k_3 = k$, and distances between them (air transparent obstacles) k_2 and k_4 (Fig. 6). In the fundamental cell of the chain, guided modes of the chain are characterized with the same relations as (3), which are equivalent to a system of eight equations for eight unknowns, $\mathbf{A}(\lambda)\mathbf{X} = 0$. The matrix $\mathbf{A}(\lambda)$ is built in the same manner as for a chain of mono-dispersible transparent obstacles with the necessary modifications. The lowest wave-guiding frequency of a chain of poly-dispersible transparent obstacles (creeping mode), for small τ, is given by

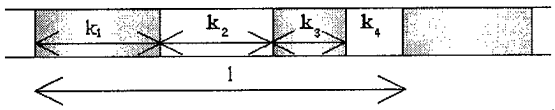


Fig. 6. Fundamental cell of the chain of poly-dispersible bubbles (inhomogeneous chain of bubbles). Water is shown by grey.

$$\lambda_0(\xi, k, \tau) = \sqrt{\frac{2\tau\left[1-\cos(\xi)\right]}{k(1-k)(\tau^2+\kappa^2)+\left[(1-k)^2\kappa^2+k^2\right]\tau}} \qquad (5)$$

One can see that there is a minimum of frequency as a function of concentration k, achieved at $k = 0.5$. It is necessary to make very useful and important

Note. The lowest wave-guiding frequency of a chain of poly-dispersible transparent obstacles, for small τ, does not depend on their sizes and is determined only by the average concentration. It means that the poly-dispersibility of the transparent obstacles in a chain is not essential for a creeping mode. Phase velocity of the creeping mode can be smaller than velocities of waves in the transparent obstacle medium and in the background medium.

Long wave approximation. It is useful to consider asymptotic behaviour of wave-guiding frequency and phase velocity of a creeping mode provided that the wavelength is much greater than the spatial period of a chain of transparent obstacles. For the length L of an acoustic wave of the wave-guiding mode (creeping mode), the expression $L = 2\pi/\xi$ is valid. For large wavelength values (if $\xi \approx 0$), expression (5) will reduce to $\lambda_0(\xi, k, \tau) = \xi\sqrt{\tau}\Big/\sqrt{k(1-k)(\tau^2+\kappa^2)+\left[(1-k)^2\kappa^2+k^2\right]\tau}$. The phase velocity, $C_{ph}^{(0)}(\xi, k, \tau)$, of the propagation of a long wave of the creeping mode, for small τ, is given by the expression $C_{ph}^{(0)}(\xi, k, \tau) = \sqrt{\tau}\Big/\left|\kappa\sqrt{k(1-k)}\right| = (c_2/c_1)\sqrt{\tau/k(1-k)}$

RESONANCE PHENOMENA

In spite of the fact that the domain of oscillations is unbounded, resonance phenomena for localized and periodically distributed sources of oscillations can occur.

Localized resonance phenomenon. If the group velocity for a wave-guiding frequency λ_* and some wave number ξ_* is equal to zero, then the velocity of energy propagation through the chain of transparent obstacles from a source with frequency λ_* is also equal to zero. It means that the resonance phenomena caused by the energy localisation in the oscillation source neighbourhood can arise.

Travelling resonance phenomena. Assume that every fundamental cell of the transparent obstacle chain contains an oscillation source and the space period of the sources distribution is the same as for the chain (equal to 1 in dimensionless variables). Assume also that the sources of oscillations have the same space phase shift ξ as the wavenumber of some guided wave and also have the frequency of oscillations equal to the corresponding guiding frequency $\lambda_*(\xi)$. In this case a resonance growth of amplitude of forced oscillations will move through the chain of transparent obstacles with the phase velocity of the wave-guiding mode. Similar phenomenon is used for acceleration of particles in a synchrophasotron.

SUMMARY

The interaction of oscillations of neighbouring transparent obstacles essentially changes their wave-guiding and resonance properties and causes a series of low-frequency wave-guiding modes of the chains of transparent obstacles. One must take into account the low-frequency eigenoscillations due to interaction of the neighbouring transparent obstacles in the chain when studying the propagation of initial perturbation and the response of the chain to the forced oscillations. It has been shown that the poly-dispersibility of the transparent obstacles does not render essential influence on low-frequency wave-guiding oscillation of the chain. It has been proven that the lowest wave-guiding frequency of oscillations is determined by linear concentration of transparent obstacles.

REFERENCES

1) S.V. Sukhinin, Eigenwaves of one-dimensional transparent periodic chain, *Dynamics of Continuous Medium*, Institute of Hydrodynamics Press, 1992, no 106, pp. 234-243 (in Russian).
2) S.V. Sukhinin, Wave propagation in periodical chains of bubbles, *Advances in Computational Methods in Fluid Dynamics*, ASME Fluid Eng. Div. Summer Meeting, Lake Tahoe, 1994, p. 8.
3) S.V. Sukhinin, Wave propagation and resonance phenomena in non-homogeneous media, *Applied Mechanics and Technical Physics*, 2001, vol. 42, no 3, pp. 32-42 (in Russian).
4) S.V. Sukhinin, Waveguiding, anomalous and whispering properties of a periodic chain of obstacles, *Siberian J. of Industrial Mathematics*, 1998, vol. 1, no 2, pp. 175 – 198 (in Russian).
5) Lord Rayleigh, *Theory of Waves,* vol.2.

ADAPTED GRIDS FOR THE WAVELET-BASED SIMULATION OF COMPLEX PLANAR CIRCUITS

Guido Schneider and Arne F. Jacob

Institut für Hochfrequenztechnik, Technische Universität Braunschweig
P. O. Box 33 29, 38023 Braunschweig, Germany, E-mail: G.Schneider@tu-bs.de

ABSTRACT

Wavelets are well-known to accelerate the simulation of planar microwave circuits. In this paper computational savings in both CPU time and memory are discussed that can be achieved by properly implementing a Wavelet base for the analysis of complex microstrip circuits. The choice of a suitable grid is discussed for two examples.

INTRODUCTION

Method of Moments Galerkin schemes [1] take advantage of Wavelets as basis and testing functions. This is because Wavelets lead to sparsely populated system matrices. This advantage is particularly pronounced for structures of medium size and complex shape [2, 3]. On the other hand, adapted grids allow to alleviate the computational burden because the number of cells can be substantially reduced [4]. So far, only generic examples were considered. It is the purpose of this paper to extend these investigations to circuits of complex topology, better suited for the implementation of Wavelets. Typical structures that meet the requirements are filters. Both a hairpin and an edge coupled filter, emphasizing different aspects in terms of grid definition, will thus be investigated in the following. The computational savings due to the properties of Wavelets are pointed out. Some aspects regarding the implementation of the grids are discussed.

MOMENT METHOD WAVELET GALERKIN SCHEME

The Method of Moments (MoM) is a well known technique to solve the electric field integral equations (EFIE) commonly used to describe planar microwave circuits. The unknown current distribution is expanded in a series of basis functions. After introducing a set of testing functions and an inner product, the EFIE can be transformed into a system of linear equations. An entry g_{ij} of the system matrix is calculated from

$$g_{ij} = -j\,\omega\,\mu \iint_S \iint_{S'} b_{i,u}(x,y)\, G^a_{uv}(x,y,x',y')\, t_{i,v}(x',y')\, dx'\, dy'\, dx\, dy + \tag{1}$$

$$\frac{j}{\omega\varepsilon} \iint_S \iint_{S'} \frac{\partial b_{j,u}(x,y)}{\partial u}\, G^a_{uv}(x,y,x',y')\, \frac{\partial t_{i,v}(x',y')}{\partial v'}\, dx'\, dy'\, dx\, dy$$

$\underline{\underline{G^a}}$ and G^v are the Greens functions of the magnetic vector and the scalar potential, respectively, and ε and μ are the material properties of the substrate material. The j-th basis and i-th testing function directed in $(u/v) \in (x,y)$ direction is represented by $b_{i,u}(x,y)$ and $t_{i,v}(x',y')$, respectively. In contrast to the observation point the coordinates of the source point are primed. The Galerkin scheme implemented here implies $t_i = b_i$.

The basis functions within this work are Wavelets. In the direction of current flow they are Chui-Wang-Wavelets [5] constructed from piecewise linear cardinal B-splines (2nd order). On bounded intervals additional boundary functions are needed [6]. In the perpendicular direction piecewise constant (Haar-)Wavelets are used [7]. These two types of functions build the two dimensional basis functions shown in Fig. 1.

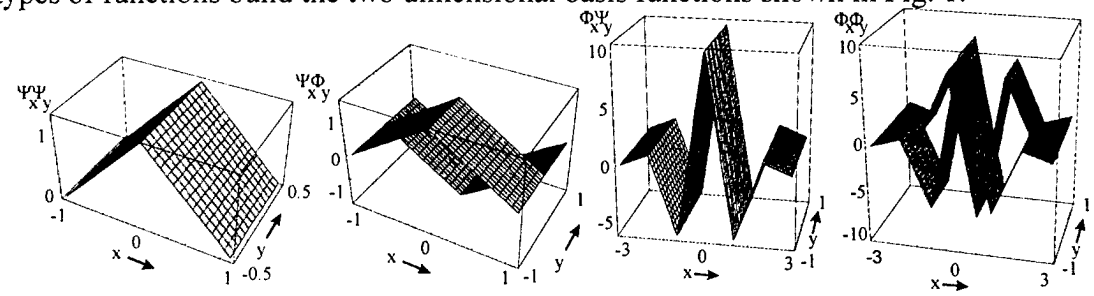


Fig. 1. Set of Wavelet Basis functions.

Wavelets set up a multiresolutional basis defined across increasingly fine grids. The rooftop function in Fig. 1(a) exists only on the coarsest level and is called scaling function. On all finer levels the basis functions comprise Wavelets in one (Fig. 1(b), (c)) or in both directions (Fig. 1(d)). Wavelets $\Phi(x)$ constructed from cardinal B-splines of order n have n vanishing moments, an essential property in the MoM:

$$\int_{-\infty}^{\infty} \Phi(x)\, x^p\, dx = 0, \quad 0 \le p \le n-1. \tag{2}$$

When regarding a Wavelet basis function as an abstract current element its far field is very low. It is thus a poor radiator [8] and, because of reciprocity, a poor receiver as well. Thus, the far field coupling of two Wavelet basis functions on the circuit is very low. The entries of the system matrix g_{ij} (cf. Eq. (1)) describe the coupling between the basis functions. Wavelets being far enough apart have low coupling corresponding to a negligibly small g_{ij}. The system matrix is thus sparsely populated showing a typical band structure. For these band matrices suitable solvers exist, such as the conjugate residues in its stabilized form [9], that allow a fast solution of the thinned matrix. An important aspect when using Wavelets within a Galerkin scheme is that the matrix structure can be predicted before being calculated. This is because the integral operator in eq. (1) is of Calderón-Zygmund-type for which an upper limit can easily be estimated [10]. A simple thresholding procedure yields the relevant matrix entries. The number of time-consuming four-fold integrals (Eq. (1)) is thus reduced, leading to considerable savings in CPU time. In addition, the matrix sparsity saves substantial memory.

NUMERICAL EXAMPLES

To be implemented Wavelets require a given number of knots, i. e. a minimum circuit size. At the coarsest level the scaling functions still have to fulfil the Nyquist rate when sampling the Greens functions, thus setting an upper useful limit to circuit dimension. Hence, Wavelet schemes are best suited for complex structures of medium size [2]. Two suitable examples shown in Fig. 2 are investigated in the following.

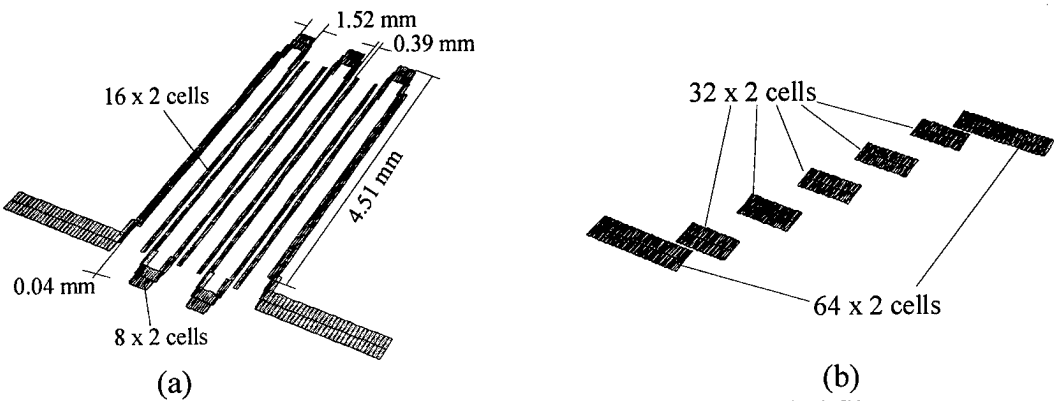


Fig. 2. Geometry of the (a) hairpin and (b) edge coupled filter.

Hairpin Filter Fig. 2(a) depicts the geometry of a microstrip hairpin filter. It consists of six coupled lines connected by uniform lines and mitered bends. Various grid configurations were investigated. In a first step grids adapted to the estimated current distribution on the circuit, e. g. the typical bathtub function for the transverse distribution of the longitudinal current on a uniform microstrip line [4], were tested. In transverse direction four cells were used and compared to the simpler case with only two cells. The latter represents a significantly lower computational burden and turns out to be sufficiently accurate. In particular, it is still able to describe the expected asymmetrical current distribution on the coupled lines. In principle one Haar-Wavelet level can be set-up although this was not done in the present context for sake of algorithm simplicity.

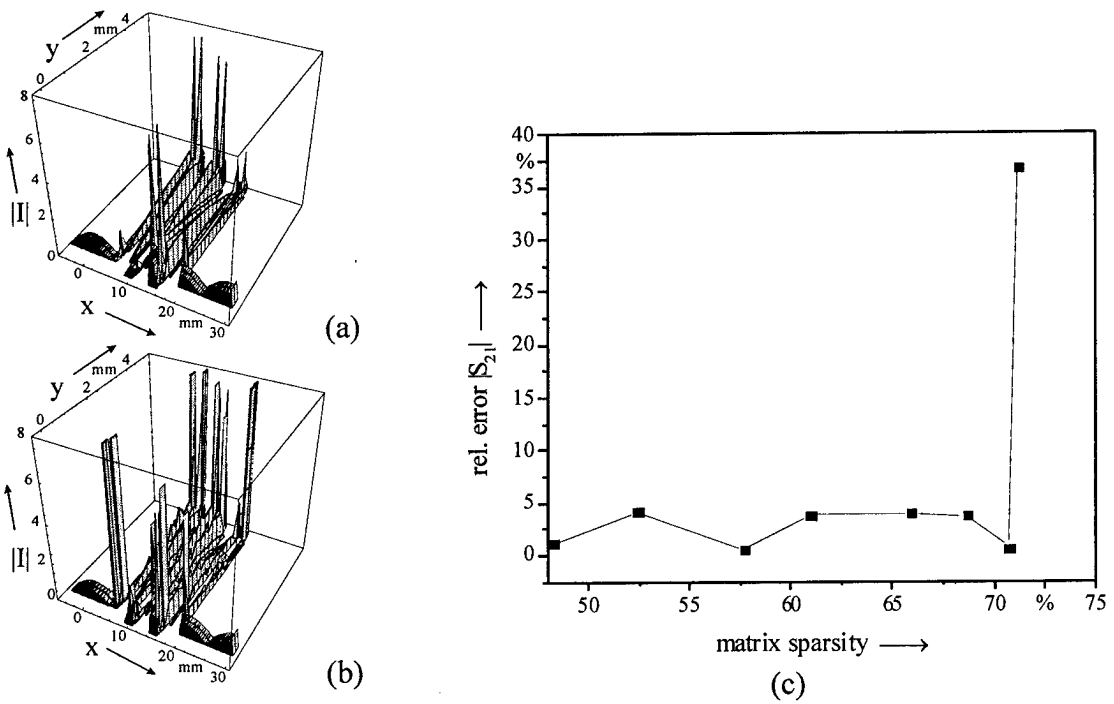
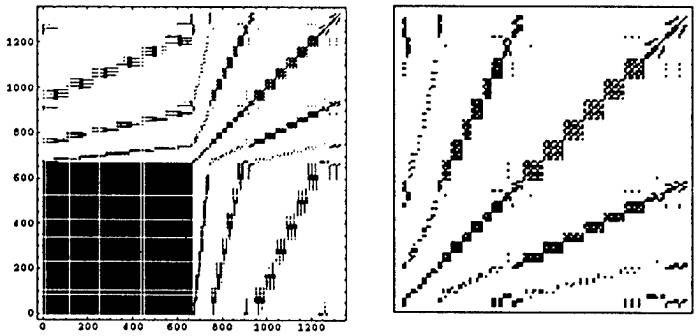


Fig. 3. Current distribution on the hairpin filter (a) with and (b) without compression; (c) relative error in $|S_{21}|$ versus matrix sparsity.

The coupled (uniform) lines were discretized using 16 x 2 (8 x 2) uniform cells. In longitudinal direction, two (one) finer Wavelet levels besides the scaling function level were implemented, here. The bends in Fig. 2(a) are discretized by 4 x 4 cells. This is sufficient to render the change of direction of current flow. However, the grids are refined at the edges of the connecting lines to accomodate the current singularity at the inner corner of the bend. This discretization yields a total number of 1,330 unknown current coefficients.

The calculated current distribution on the hairpin filter with no Wavelet compression applied is depicted in Fig. 3(a). The peaks appearing at the inner corners of the bends result from the field singularity there. The apparent discontinuity of the current here is due to the mismatch between the different coarse grids. Nevertheless, the integrated current is continuous. Fig. 3(c) shows the relative error in $|S_{21}|$ versus matrix sparsity. This graph was calculated by successively increasing the a priori threshold. Up to a sparsity of approximately 70.7 % the error remains below 4.2 %, above that value it increases rapidly. This is illustrated by the corresponding current distributions without and at maximum allowable compression in Figs. 3(a) and (b), respectively. The distortion is clearly seen. Still, the extraction of the scattering parameters from the fundamental mode current distribution yields satisfactory results even at this high sparsity.



(a) (b)

Fig. 4. Complete system matrix and zoom into upper right corner.

The corresponding sparse system matrix is depicted in Fig. 4(a). The completely filled partial matrix in the lower left corner contains all reactions involving two scaling functions. Its relative size can be reduced by implementing all possible Wavelet levels (see above). The remainder of the matrix is very sparsely populated. Only a few bands, such as around the main diagonal, contribute. These reactions involve overlapping and neighboring basis functions. The latter can be located on different parts of the filter, e. g. on coupled lines. The lower right and upper left corner of the matrix contain reactions of a Wavelet and a scaling function. Their sparsity demonstrates the good decorrelation properties of the Wavelets. This is even more pronounced in the upper right corner shown in more detail in Fig. 4(b). Only Wavelets react here. Subcircuits within the filter, for instance individual lines or bends, are represented by submatrices. For illustration, some of these are delimited by gray lines in the Figure. Their emptiness demonstrates the very low coupling at Wavelet level.

Tab. 1. Time required to fill and invert the system matrix.

Filling ratio	Filling of matrix	Solution of system
100 %	3517 s	3.66 s (conj. res., stab.) 9.32 s (Gauß)
29.2 %	2121 s	0.72 s

The computational performance obtained on a *Compaq ES 45* computer is shown in Tab. 1. The time required to fill the system matrix can be reduced by 39.7 %. The inversion of the system matrix can be accelerated from 3.66 s to 0.72 s. For comparison the table includes the inversion time for a Gaussian algorithm which would be needed in conjunction with classical basis functions.

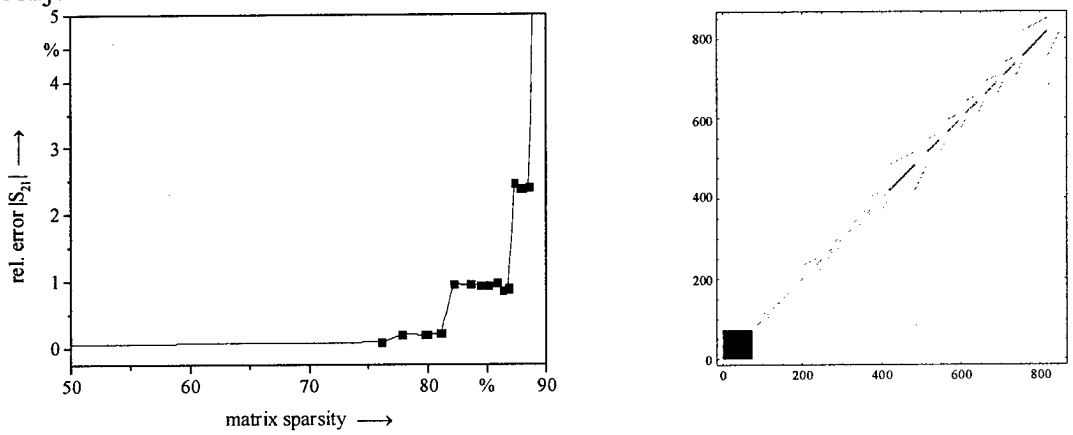


Fig. 5. (a) Relative error in $|S_{21}|$ and (b) matrix structure for the edge coupled filter.

Edge Coupled Filter The second example shown in Fig. 2(b) is similar to the hairpin filter except that it has only straight sections, i. e. no bends. The number of lines and their dimensions are, thus, unchanged. This essentially holds for the discretization, as well. However, as all lines have the same width and there are no discontinuities, such as bends or steps, a completely uniform grid can be set-up, here. The resulting high symmetry significantly accelerates matrix filling. The connecting (inner coupled) lines are discretized by 64 x 2 (32 x 2) cells. On the 64 (32) cells in direction of current flow four (three) Wavelet-levels and the scaling function level are set-up. The total number of unknowns is 850, including 98 scaling functions. Hence, 9,604 reactions involve only scaling functions which corresponds to 1.3 % of the matrix entries. This limits the matrix sparsity to a theoretical value of 98.7 %. Thus, with nearly the same number of unknowns as in the previous example the system matrix of the edge coupled filter should be much more compressible. This is confirmed by Fig. 5(a) which shows that the relative error of $|S_{21}|$ remains below 2.5 % for a matrix sparsity of up to 88.5 %. The corresponding matrix structure is depicted in Fig. 5(b). The significant matrix entries are strongly localized in the lower left corner of the matrix. Again, the coupling of the different microstrip lines mainly takes place at scaling function level. Apart from the main diagonal of the matrix only few significant elements appear. They are within a narrow band and describe reactions of Wavelets located on adjacent microstrip lines. These reactions are located in the upper right corner of the matrix. The sparsity in conjunction with the distinct symmetry of the filter leads to low CPU time: 68 s for

filling and 0.12 s for inversion instead of 132 s and 1.4 s, respectively, without sparsification. One reason for the high compressibility is the increased number of Wavelet levels. The second one is the larger average distance between two basis functions and the resulting low coupling. The high achievable compression justifies the choice of the grid in this more generic case.

CONCLUSION

A hairpin filter and an edge coupled filter were investigated via a Wavelet Galerkin scheme. The size and complexity of these structures are well suited for a Wavelet analysis. Matrix sparsities of 70.7 % and 88.5 %, respectively, could be achieved by properly selecting the grids. The presented results confirm the typical coupling behavior of Wavelet basis functions.

ACKNOWLEDGEMENT

The authors would like to thank the Deutsche Forschungsgemeinschaft (DFG) for financial support.

REFERENCES

[1] R. F. Harrington: *Field Computation by Moment Methods*, Robert E. Krieger Publishing Company, Malabar, Florida, 1968.

[2] G. Oberschmidt, G. Schneider, and A. F. Jacob: *A Priori Estimation of Wavelet-Based Galerkin Matrices*, Proc. 25th International Conference on Infrared and Millimeter Waves, Peking, pp. 241 – 242, Sep. 2000.

[3] G. Schneider, J. Heyen, and A. F. Jacob: *On the Wavelet-Analysis of Small Subcircuits*, Proc. MIKON 2002, pp. 545 – 548, Gdansk, May 2002.

[4] G. Oberschmidt and A. F. Jacob: *Non-Uniform Wavelets on Adapted Grids for Modelling Edge Singularities*, Proc. 27th EuMC, Jerusalem, vol. 2, pp. 1258 – 1263, Sep. 1997.

[5] J. C. Goswami, A. K. Chan, and C. K. Chui: *On Solving First-Kind Integral Equations Using Wavelets on a Bounded Interval*, IEEE Trans. Antennas Propagat., vol. 43, no. 6, pp. 614 – 622, June 1995.

[6] G. Oberschmidt and A. F. Jacob: *Modelling of Coplanar Waveguides with Second Order Chui-Wang Wavelets*, Proc. 9th Conf. on Microwaves and Optronics MIOP '97, Sindelfingen, pp. 365 – 369, April 1997.

[7] A. Haar: *Zur Theorie der orthogonalen Funktionensysteme*, Mathematische Analen, vol. 69, pp. 331 – 371, 1910.

[8] W. C. Chew, J.-M. Jin, C.-C. Lu, E. Michielssen, and J. Song: *Fast Solution Methods in Electromagnetics*, IEEE Trans. Antennas Propagat., vol. 45, no. 3, pp. 533 – 543, June 1995.

[9] W. Hackbusch: *Iterative Lösung großer schwachbesetzter Gleichungssysteme*, Teubner Studienbücher Mathematik, B. G. Teubner, Stuttgart, Germany, 1993.

[10] G. Oberschmidt and A. F. Jacob: *Accelerated Simulation of Planar Circuits by Means of Wavelets*, Proc. 28th EuMC, Amsterdam, pp. 305 – 310, Oct. 1998.

VOLUME SINGULAR INTEGRAL EQUATION METHOD IN ELECTROMAGNETIC THEORY

A.B. Samokhin

Moscow Institute of Radiotechnics, Electronics and Automatics,
78, Vernadsky av., 117454, Moscow, Russia; E-mail: alesam@chat.ru

ABSTRACT

We consider volume singular integral equations which describe the problems of electromagnetic scattering from three-dimensional anisotropic media characterized by permittivity and permeability. We performed a detailed analysis of these equations and corresponding scattering problems, including nonclassical ones. We consider the equivalence of the boundary value problems for the Maxwell equations and the singular integral equations and formulate the corresponding theorem. We obtain the necessary and sufficient conditions that provide the fulfillment of the Noether property of the operator and sufficient conditions for the Fredholm property. We prove the existence and uniqueness theorems for a very wide family scattering problems.

INTRODUCTION

In this paper we consider the scattering of electromagnetic waves from three-dimensional anisotropic media characterized by complex permittivity and permeability. Such problems are great importance in many theoretical and applied fields of science and technology. From the mathematical viewpoint, correct formulations of the problem and analysis of its solvability and uniqueness of solution constitute the most significant topics. For many scattering problems, the existence and uniqueness of solution are proved by reducing to Fredholm integral equations of the second kind. The most complete analysis of such problems is presented in classical monograph [1] where two families of problems are considered: the scatterer is characterized by (i) a scalar permittivity function which is differentiable everywhere, including the interfaces or (ii) the medium has a constant scalar permittivity (the boundary of the scatterer is a smooth surface). Many important scattering problems do not belong to these families,for example, in the case of anisotropic structures, media with variable permittivity and permeability that are discontinuous on the boundary, and so on. However, in the general formulation, a reduction of the scattering problems to Fredholm integral equations was unsuccessful, and during a long period this circumstance hampered their detailed study. Today, the most complete description of the considered family of scattering problems are performed in terms of volume singular integral equations with respect to the electromagnetic field vectors in the domain occupied by the inhomogeneity. These equations enable one to simulate inhomogeneous and anisotropic media in a rather simple manner. In addition, they can be used for investigating various practically important scattering problems when the classical setting (a boundary value problem for the Maxwell equations) is either impossible or very difficult. Note, in particular, the

scattering in structures with sharp edges, for example, when the body has the form of a homogeneous dielectric parallelepiped. However, these equations do not belong to the classical Fredholm equations, which may explain the delay in their studies. Using the theory of multidimensional singular integral equations [2] we performed a detailed analysis of these equations and corresponding scattering problems, including nonclassical ones [4-9]. In this paper we present basic results of the constructed theory.

INTEGRAL EQUATIONS AND SCATTERING PROBLEMS

Consider the following family of problems of electromagnetics. Assume that a medium filling a domain Q bounded by surface S is characterized by the permittivity, $\hat{\varepsilon}$, and permeability, $\hat{\mu}$ dyads, and their components are functions of coordinates. Outside domain Q, the parameters of the medium are constant and the medium is isotropic, i.e., $\varepsilon = \varepsilon_0 = \text{const}$ and $\mu = \mu_0 = \text{const}$. It is necessary to determine the electromagnetic field excited in the medium by an external field with the time dependence $\exp(-i\omega t)$; the field may be excited both by a plane wave and extraneous currents $\vec{J}_E^0$ and $\vec{J}_H^0$. Let us present the corresponding mathematical formulation: find vector–functions $\vec{E}$ and $\vec{H}$ that satisfy the Maxwell equations

$$\operatorname{rot}\vec{H} = -i\omega\hat{\varepsilon}\vec{E} + \vec{J}_E^0,$$

$$\operatorname{rot}\vec{E} = i\omega\hat{\mu}\vec{H} - \vec{J}_H^0 \tag{1}$$

everywhere except maybe S, the continuity of the tangential field components on S, and the radiation condition at infinity

$$\lim_{r\to\infty} r\left(\frac{\partial\psi}{\partial r} - ik_0\psi\right) = 0, \quad k_0 = \omega\sqrt{\varepsilon_0\mu_0}. \tag{2}$$

Here $\operatorname{Im}\varepsilon_0 \geq 0$, $\operatorname{Im}\mu_0 \geq 0$, and $\operatorname{Im}k_0 \geq 0$.

If the electromagnetic field is excited by plane wave $(\vec{E}^0, \vec{H}^0)$, then scattered field $(\vec{E}^S, \vec{H}^S)$, where $\vec{E}^S = \vec{E} - \vec{E}^0$ and $\vec{H}^S = \vec{H} - \vec{H}^0$, must satisfy radiation conditions (2). Using the polarizattion currents and known formulas for the vector potentials, one can obtain two coupled volume singular integral equations with respect to fields $\vec{E}$ and $\vec{H}$

$$\vec{E}(x) = \vec{E}^0(x) - \frac{1}{3}\left[\frac{\hat{\varepsilon}(x)}{\varepsilon_0} - \hat{I}\right]\vec{E}(x) + k_0^2\int_Q\left[\frac{\hat{\varepsilon}(y)}{\varepsilon_0} - \hat{I}\right]\vec{E}(y)G(r)\,dy +$$

$$+v.p.\int_Q\left(\left[\frac{\hat{\varepsilon}(y)}{\varepsilon_0} - \hat{I}\right]\vec{E}(y), grad\right)grad\,G(r)\,dy + +i\omega\mu_0\int_Q\left[\left[\frac{\hat{\mu}(y)}{\mu_0} - \hat{I}\right]\vec{H}(y), grad\right]G(r)\,dy, \tag{3}$$

$$\vec{H}(x) = \vec{H}^0(x) - \frac{1}{3}\left[\frac{\hat{\mu}(x)}{\mu_0} - \hat{I}\right]\vec{H}(x) + k_0^2\int_Q\left[\frac{\hat{\mu}(y)}{\mu_0} - \hat{I}\right]\vec{H}(y)G(r)\,dy +$$

$$+v.p.\int_Q \left([\frac{\hat{\varepsilon}(y)}{\mu_0} - \hat{I}]\vec{H}(y), grad \right) grad\, G(r)\, dy - -i\omega\varepsilon_0 \int_Q \left[[\frac{\hat{\varepsilon}(y)}{\varepsilon_0} - \hat{I}]\vec{E}(y), grad \right] G(r)\, dy, \quad (4)$$

Here $\vec{E}^0(x)$, $\vec{H}^0(x)$ is either the field of the incident plane wave or the field generated by extraneous currents $\vec{J}_E^0$ and $\vec{J}_H^0$ in the homogeneous space with parameters ε_0 and μ_0; $v.p.\int$ denotes a singular integral, for which an infinietly small ball occupying the vicinity of the point $x=y$ is extracted from the domain of integration; $(*,*)$ and $[*,*]$ denote the inner and vector products of three-dimensional vectors; G is the Green function of the Helmholtz equation,

$$G = \frac{\exp(ik_0 r)}{4\pi r},$$

and $r = |x - y|$ is the distance between points x and y.

We will consider equations (3) and (4) as a system of integral equations with respect to functions $\vec{E}$ and $\vec{H}$ in a domain Q. The electromagnetic field outside Q is represented through the values of $\vec{E}$ and $\vec{H}$ in this domain by formulas (3) and (4), where, obviously, singular integrals should be considered as proper ones.

Consider the equivalence of Maxwell equations (1) and system of integral equations (3)–(4). We will assume that the electromagnetic field satisfies the Maxwell equations in the usual sense, i.e., pointwise, except maybe surface S on which the conditions of continuity of the tangential field components are imposed. Such solutions of the initial problem will be called *classical solutions*. Let us specify first the minimum possible smoothness of the electromagnetic field. Inside domain Q, $rot\,\vec{E}$ and $rot\,\vec{H}$ are well-defined operations for vector-functions $\vec{E}$ and $\vec{H}$. Therefore, one may assume that $\vec{E}$ and $\vec{H}$ are at least differentiable functions of coordinates. However, this is not exactly true. Using the definition of rotation based on the Stokes formula, one can show that vector-function $\vec{A}(x)$ for which $rot\,\vec{A}$ is a well-defined operation can be represented as

$$\vec{A}(x) = \vec{A}_0(x) + grad\varphi(x),$$

where $\vec{A}_0(x)$ и $\varphi(x)$ are differentiable functions of coordinatrs. Thus, the set of vector-functions that meet the conditions of existance of the classical solution to the scattering problem is wider than the set of differentiable functions. We have proved the following equivalence theorem.

Theorem 1. *Assume that the given permittivity and permeability dyads $\hat{\varepsilon}$ and $\hat{\mu}$ differ from constant dyads $\varepsilon_0\hat{I}$ and $\mu_0\hat{I}$ only in a finite domain Q bounded by regular surface S. In Q, the components of $\hat{\varepsilon}$ and $\hat{\mu}$ are Hölder-continuous functions. Then any solution of system of integral equations (3) and (4) which is Hölder-continuous in Q is a classical solution of the initial problem; i.e., it satisfies the Maxwell equations, the condition of continuity of the tangential field components on S, and the radiation condition. Conversely, any solution satisfying (1), (2) and the condition of continuity of the tangential field components on S is a solution of (3) and (4).*

Let us consider the properties of system singular integral equations (3) and (4). First, we have to specify appropriate functional spaces. Generally speaking, one can choose different spaces, and the choice governs the results of analysis. It is reasonable to apply the following criterion: functional spaces must be sufficiently wide, providing the consideration of all physically admissible solutions; however, the space should not be too wide, because in this case the uniqueness may be violated due to the presence of solutions that have no physical meaning. The Poynting theorem, which is one of the most general statements in electromagnetics, guarantess the conservation of energy. This theorem employs integrals involving squared magnitudes of fields. Therefore, one may assume that the space of square integrable vector–functions $\vec{L}_2(Q)$ is the most appropriate from the physical viewpoint as applied to the analysis of system of integral equations (3) and (4).

Equations (3) and (4) can be classified as multidimensional singular integral equations, they are studied insufficiently as compared with Fredholm equations. Therefore, below, we impose several restrictions caused by this circumstance. We have constructed explicitely the matrix symbol of the singular operator produced by (3) and (4) and proved the following statement.

Theorem 2. *Assume that given dyads* $\hat{\varepsilon}(x)$ *and* $\hat{\mu}(x)$ *are continuous everywhere in* R^3. *Then the operator of system (3) and (4) is a Noether operator in* $\vec{L}_2(Q)$ *if and only if the condition*

$$(\hat{\varepsilon}(x)\vec{n},\vec{n}) \neq 0, \quad (\hat{\mu}(x)\vec{n},\vec{n}) \neq 0, \tag{5}$$

is satisfied, where $\vec{n}$ *is an arbitrary nonzero vector with real components and* $x \in Q$.

Note that when the scattering from an isotropic medium is considered, conditions (5) take the form

$$\varepsilon(x) \neq 0, \quad \mu(x) \neq 0.$$

Theorem 2 shows that when conditions (5) are violated, the considered operators fail to be the Noether operators; in this case, the domain of images is not closed and the corresponding operator equations are not correctly solvable. In an isotropic medium, plasma resonances may occur when the permittivity vanishes. For anisotropic plasma, one can show that when condition (5) is not valid, plasma resonances also exist. Naturally, the question arises why the physical problem fails to be correct when conditions (5) are violated. One may assume that in these cases a transition from the nonstationary Maxwell equations to stationary equations cannot be justified because the medium contains the points at which the onset of time-harmonic oscillations substantially depends on initial conditions.

One may consider the singular integral operator of system (3) and (4) as a pseudodifferential operator. The condition that the matrix symbol is invertible means that the operator is elliptic. Consider the agreement of this condition with the local ellipticity of Maxwell equations (1). It can be shown that if dyads $\hat{\varepsilon}(x)$ and $\hat{\mu}(x)$ are twice differentiable functions of coordinates in the whole space and conditions (5) are valid, then the Maxwell equations are transformed to a system of differential equations with an elliptic operator. Note that conditions that provide the ellipticity of the Maxwell equations and the singular integral operator in (3) and (4) coincide; however, for the

case of differential equations, a greater smoothness of material parameters is required. Using the Fredholm conditions for system of singular integral equations [2] and properties of the matrix symbol of operator produced by (3) and (4), we prove the following statement.

Theorem 3. *The operator of system of (3) and (4) is a Fredholm operator in* $\vec{L}_2(Q)$ *if the conditions of Theorem 2 are satisfied and*

$$\begin{aligned} &\mathrm{Im}\,(\hat{\varepsilon}(x)\vec{n},\vec{n}) \geq 0, \\ &\mathrm{Im}\,(\hat{\mu}(x)\vec{n},\vec{n}) \geq 0, \end{aligned} \tag{6}$$

where $\vec{n}$ *is an arbitrary nonzero vector and* $x \in Q$.

For an isotropic medium, conditions (6) reduce to

$$\mathrm{Im}\,\varepsilon(x) \geq 0, \quad \mathrm{Im}\,\mu(x) \geq 0.$$

Conditions (6) are satisfied for the overwhelming majority of actual physical media. The physical meaning of these conditions can be formulated as follows: the matter in domain Q cannot generate electromagnetic energy.

The following assertion was proved with the use of the theorem on the smoothness of singular integrals [2].

Theorem 4. *Let the components of given dyads* $\hat{\varepsilon}(x)$ *and* $\hat{\mu}(x)$ *be Hölder-continuous functions everywhere in* R^3 *and satisfy conditions (5). Assume that the electromagnetic field is excited either by a plane wave or by Hölder-continuous currents* $\vec{J}_E^0$ *and* $\vec{J}_H^0$ *localized in a finite spatial domain. Then any solution to (4) and (5) belonging to* $\vec{L}_2(Q)$ *satisfies the Maxwell equations (1) and the radiation condition (2).*

Using Theorems 2–4, integral relationships of the Poynting theorem, and the results of the theory of pseudodifferentional operators [3], one can prove the existence and uniqueness of the classical solution to the scattering problem.

Theorem 5. *Let dyads* $\hat{\varepsilon}(x)$ *and* $\hat{\mu}(x)$ *be Hölder-continuous functions everywhere in* R^3 *satisfying conditions (5) and (6) and the source of electromagnetic field obey the conditions of Theorem 4. Assume that one of the two conditions is met: (i) at least one of the inequalities in (6) is strict; (ii)* $\hat{\varepsilon}(x)$ *and* $\hat{\mu}(x)$ *are three times continuously differentiable functions of coordinates in* R^3. *Then there exists the unique solution to the Maxwell equations (1) that satisfies the radiation condition (2).*

According to the physical meaning of condition (i), the medium in domain Q is lossy; however, loss may be arbitrarily small. Condition (ii) can be satisfied for a lossless medium; in that case, the smoothness of dyads $\hat{\varepsilon}(x)$ and $\hat{\mu}(x)$ should be increased.

Now, let us formulate the theorem concerning the existence and uniqueness of the solution to singular integral equations (3) and (4).

Theorem 6. *Let dyads* $\hat{\varepsilon}(x)$ *and* $\hat{\mu}(x)$ *satisfy the conditions of Theorem 5. Then there exists the unique solution of singular integral equations (3) and (4) in* $\vec{L}_2(Q)$ *for arbitrary* $(\vec{E}^0, \vec{H}^0) \in \vec{L}_2(Q)$. *If the source of the electromagnetic field obeys the conditions of Theorem 4, then this solution is the classical solution to the scattering*

problem; i.e., it satisfies Maxwell equations pointwise.

Consider system of integral equations (3) and (4) imposing minimal restrictions on dyads $\hat{\varepsilon}(x)$ and $\hat{\mu}(x)$; namely, assume that their components are bounded functions of coordinates in domain Q. Using the conditions that ensure the convergence of the minimal residual method, we have proved the following statement.

Theorem 7. *Assume that dyads* $\hat{\varepsilon}(x)$ *and* $\hat{\mu}(x)$ *are bounded functions in domain* Q *and Hermitian dyads* $(\hat{\varepsilon}-\hat{\varepsilon}^*-2i\operatorname{Im}\varepsilon_0\hat{I})/(2i)$ *and* $(\hat{\mu}-\hat{\mu}^*-2i\operatorname{Im}\mu_0\hat{I})/(2i)$ *are positive definite at each point of* Q. *Then there exists the unique solution to (3) and (4) in* $\overline{L}_2(Q)$.

In the isotropic case, the conditions of the theorem mean that

$$\operatorname{Im}\varepsilon(x)>\operatorname{Im}\varepsilon_0,\quad \operatorname{Im}\mu(x)>\operatorname{Im}\mu_0$$

Theorem 7 does not require the smoothness of $\hat{\varepsilon}(x)$ and $\hat{\mu}(x)$. Obviously, it is assumed that in this case, the solutions satisfy the Maxwell equations in Q in the sence of distributions. This theorem specifies the conditions that guarantee the unique solvability for a very wide family of scattering problems, including the classical scattering problems (see the beginning of this paper) and nonclassical scattering problems when material parameters have discontinuities on surfaces with breaks (for example, when the body has the form of a homogeneous dielectric parallelepiped) or are continuous functions of coordinates that do not possess any smoothness.

REFERENCES

[1] C. Müller, *Foundation of the mathematical theory of electromagnetic waves,* Berlin: Springer–Verlag, 1969.

[2] S.G. Michlin, S. Prösdorf, *Singular integral equations,* New York: Akademie–Verlag, 1986.

[3] L. Hörmander, *The analysis of linear partial differential operators,* Berlin: Springer–Verlag, 1985.

[4] A.B.Samokhin, *Integral equations and iteration methods in electromagnetic scattering,* Utrecht: VSP, 2001.

[5] A.B. Samokhin, "Investigation of problems of the diffraction of electromagnetic waves in locally non–uniform media", *Comput. Maths. Math. Phys.* vol. 30, pp. 80–90, 1990.

[6] A.B. Samokhin, "Diffraction of electromagnetic waves by a locally non–homogeneous body and singular integral equations", *Comput. Maths. Math. Phys.,* vol. 32, pp. 673–686, 1992.

[7] A.B. Samokhin, "Integral equations of electrodynamics for three–dimensional structures and iteration method of solving them (A Review)", *J. of Comm. Techn. and Electronics*, vol. 38, pp. 15–34, 1993.

[8] A.B. Samokhin, "An iterative method for the solution of integral equations applied to a scattering problem on a three–dimensional transparent body", *Differential Equations,* vol. 30, pp. 1987–1997, 1994.

[9] A.B. Samokhin, "Integral equations in the problems of scattering from magnetodielectric structures", *J. of Comm. Techn. and Electronics*, vol. 45, suppl. 2, pp. 160–163, 2000.

ELECTROMAGNETICS OF COMPLEX MEDIA AND METAMATERIALS

Nader Engheta

University of Pennsylvania
Department of Electrical and Systems Engineering
Philadelphia, Pennsylvania 19104-6390, U.S.A.
E-mail: engheta@ee.upenn.edu
URL: http://www.ee.upenn.edu/~engheta/

ABSTRACT

An overview of the electromagnetic properties of complex media and metamaterials, particularly metamaterials with negative real permittivity and permeability, will be given and various ideas for potential applications of these materials will be presented.

MOTIVATION AND CONCEPT

The trends in the use of wireless PCS and mobile services, multimedia wireless networking, distributed sensing, and the Internet have increased the needs and challenges in innovation of multifunctional antennas and apertures, specialized materials, smart skins and devices, and other novel elements and components in transmission and reception of information, and signal transduction over various bands of electromagnetic spectrum. Among many elements contributing to performance enhancement of these subsystems, electromagnetic materials play a particularly important role. Study of complex and novel electromagnetic materials and surfaces has now gained considerable interest in part due to the possibility for micro- and nanofabrication of *engineered* materials, known also as metamaterials, exhibiting new, physically realizable properties not readily available in natural materials, especially in regards to scattering, radiation, and guidance of EM waves. These *engineered* metamaterials will offer creative solutions in the design of future EM devices such as multifunctional antennas and embedded sensors suitable for various applications in wireless, RF and optical systems.

In the past two decades, we have been conducting research on theoretical analysis and electromagnetic modelling of wave interaction with complex "unusual" EM materials. (For a sample of our work, see [1]-[13]) These media, which can in principle be conceptualized by embedding constituents/inclusions with novel geometrical shapes and forms in some host media or host surfaces, possess exciting electromagnetic properties and response functions with new applications in the design of devices and components. In our theoretical work, we have introduced and studied novel ideas for some exotic complex electromagnetic media, such as chiral media for microwave regimes (see e.g., [1]-[9]), local and non-local omega media [10], [11], wire media [12], [13], and some concepts for high-impedance ground planes (HIGP). We have also been interested in

exploring exciting potential applications of metamaterials with negative refractive index, in wireless components and elements.

The study of electromagnetic properties of complex media has been the subject of research interests for many research groups in the past several decades [13]-[27]. Various types of electromagnetic complex media, such as chiral materials, omega media, bianisotropic media, local and nonlocal media to name a few, have been studied. Recently, the idea of complex materials in which both permittivity and permeability possess negative real values at certain frequencies has received considerable attention [28]-[43]. In 1968, Veselago theoretically investigated plane wave propagation in a material whose permittivity and permeability were assumed to be simultaneously negative [33]. His theoretical study showed that for a monochromatic uniform plane wave in such a medium the direction of the Poynting vector is antiparallel to the direction of phase velocity, contrary to the case of plane wave propagation in conventional simple media. Recently, Smith *et al.* constructed such a composite medium for the microwave regime, and demonstrated experimentally the presence of anomalous refraction in this medium [28], [29], [31], [32]. It is also worth noting that previous theoretical study of electromagnetic wave interaction with omega media reveals the possibility of having negative permittivity and permeability in omega media for certain range of frequencies [11]. For metamaterials with negative permittivity and permeability, several names and terminologies have been suggested, such as "left-handed" media [28]-[33], media with negative refractive index [28]-[32], "backward media" (BW media) [34], "double negative (DNG)" metamaterials [35], "negative-index media (NIM) [42], to name a few.

The anomalous refraction at the boundary between such a medium and a conventional medium, and the fact that for a time-harmonic monochromatic plane wave the direction of the Poynting vector is antiparallel to the direction of phase velocity, can lead to exciting features that can be advantageous in design of novel devices and components. For instance, we have shown theoretically that a slab of metamaterial having negative permittivity and permeability can function as a phase compensator/conjugator [38]. Such a conceptual structure is sketched in Fig. 1. A two-layer structure formed by a lossless metamaterial with negative permittivity and permeability (a "double-negative (DNG) medium) and a conventional lossless dielectric material with positive permittitvity and permeability (which can be termed as a "double-positive (DPS)" medium) is shown in Fig. 1. In the DPS layer, the direction of Poynting vector ($\boldsymbol{S}_1$) is parallel with the direction of phase velocity or wave vector ($\boldsymbol{k}_1$), whereas in the DNG layer these two directions are antiparallel. The DNG layer can play the role of a phase compensator. With proper choice of the *ratio* of d_1 and d_2, not the *sum* of of d_1 and d_2, one can have the phase of the wave at the left (entrance) interface to be the same as the phase at the right (exit) interface, essentially with no constraint on the total thickness of the structure [38].

As another potential application of this material, we recently introduced the idea of compact subwavelength cavity resonators in which a combination of a slab of conventional material and a slab of metamaterial with negative permittivity and

permeability is inserted [38]. Figure 2 shows the geometry of the problem for such a one-dimensional (1-D) cavity resonator. Our analysis, described in [38], has shown that when the cavity is filled with two layers of materials; the first layer assumed to be a lossless conventional material, and the second layer is taken to be the metamaterial with negative permittivity and permeability, the non-trivial one-dimensional solutions for such a cavity, in principle, depend on the ratio of thicknesses of the two layers, not the

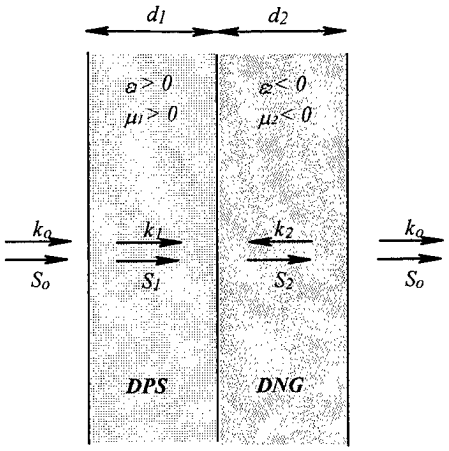


Fig. 1. Sketch of a two-layer structure as a phase compensator. This paired structure is conceptually formed by a lossless metamaterial with negative permittivity and permeability (a "double-negative (DNG) medium) and a conventional lossless dielectric material with positive permittitvity and permeability (a "double-positive (DPS)" medium).

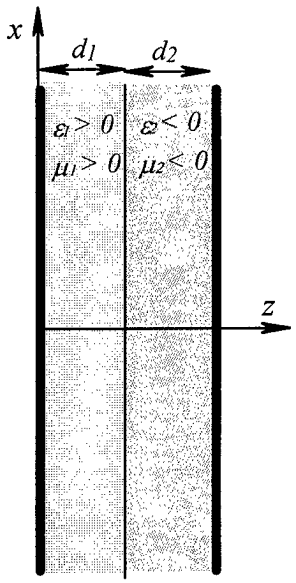


Fig. 2. An idea for a compact, sub-wavelength, thin cavity resonator using a paired DPS-DNG layers shown in Fig. 1. The two-layer structure is sandwiched between the two reflectors. Our analysis in [38] shows that with the proper choice of ratio of d_1 over d_2, one can have a resonant cavity in which the ratio of d_1 and d_2 is the main constraint, *not the sum of thicknesses,* d_1+d_2

sum of thicknesses. In other words, the cavity can conceptually be thin and can still be resonant, as long as the ratio of thicknesses is satisfied the special dispersion relation. This can, in principle, provide possibility for having sub-wavelength, thin, compact cavity resonators. Such sub-wavelength cavity resonators can lead to very interesting designs for various compact, sub-wavelength devices and components.

The problems of radiation, scattering, and guidance of electromagnetic waves in metamaterials with negative permittivity and permeability, and in media in which the combined paired layers of such media together with the conventional media are present, can possess very interesting features leading to various ideas for future potential applications. We have introduced various conceptual ideas for applications of these materials. In this talk, we will first present a brief overview of electromagnetic properties of complex media and metamaterials, particularly the media with negative permittivity and permeability, and we will then discuss some of our ideas for potential applications of these interesting materials.

REFERENCES

[1] N. Engheta and A. R. Mickelson, "Transition Radiation Caused by a Chiral Plate," *IEEE Transactions on Antennas and Propagation, Vol. AP-30, No. 6*, pp. 1213-1216, November 1982.

[2] S. Bassiri, N. Engheta and C. H. Papas, "Dyadic Green's Function and Dipole Radiation in Chiral Media," *Alta Frequenza, Vol. LV-2, No. 2*, pp. 83-88, March-April 1986.

[3] P. Pelet and N. Engheta, "The Theory of Chirowaveguides," *IEEE Transactions on Antennas and Propagation, Vol. AP-38, No. 1*, pp. 90-98, January 1990.

[4] N. Engheta and M. W. Kowarz, "Antenna Radiation in The Presence of A Chiral Sphere," *Journal of Applied Physics, Vol. 67, No. 2*, pp. 639-647, January 15, 1990.

[5] M. W. Kowarz and N. Engheta, "Spherical Chirolenses," *Optics Letters, Vol. 15, No. 6*, pp. 299-301, March 15, 1990.

[6] P. Pelet and N. Engheta, "Coupled-Mode Theory for Chirowaveguides," *Journal of Applied Physics, Vol. 67, No. 6*, pp. 2742-2745, March 1990.

[7] P. Pelet and N. Engheta, "Chirsotrip Antennas: Line Source Problem," *Journal of Electromagnetic Waves and Applications (JEWA)*, Special Issue on *Wave Interaction with Chiral and Complex Media*, Vol. 6, No. 5/6, pp. 771-793, May-June 1992.

[8] N. Engheta, D. L. Jaggard and M. W. Kowarz, "Electromagnetic Waves in Faraday Chiral Media," *IEEE Trans. on Antennas & Propagation*, Vol. 40, No. 4, pp. 367-374, April 1992.

[9] P. G. Zablocky and N. Engheta, "Transients in Chiral Media with Single-Resonance Dispersion," *Journal of Optical Society of America A.*, Vol. 10, No. 4, pp. 740-758, 1993.

[10] M. M. I. Saadoun and N. Engheta, "A Reciprocal Phase Shifter Using Novel Pseudochiral or Ω medium," *Microwave and Optical Technology Letters, Vol. 5, No. 4*, pp. 184-188, April 1992.

[11] M. M. I. Saadoun and N. Engheta, "Theoretical Study of Electromagnetic Properties of Non-Local Ω Media" a chapter in *Progress in Electromagnetics Research (PIER)* Monograph Series, *Vol. 9* on Bianisotropic and Bi-Isotropic Media and Applications, Alain Priou (ed.), December 1994, ch. 15, pp. 351-397.

[12] C. A. Moses and N. Engheta, "An idea for electromagnetic 'feedforward-feedbackward' media," *IEEE Transactions on Antennas and Propagation*, vol. 47, no. 5, pp. 918-928, 1999.

[13] C. A. Moses and N. Engheta, "Electromagnetic Wave Propagation in the Wire Medium: A Complex Medium with Long Thin Inclusions," in the Special Issue of *Wave Motion* on the topic of "Electrodynamics in Complex Environments", Vol. 34, No. 3, pp. 301-318, September 2001.

[14] W. E. Kock, "Metallic delay lenses," *Bell Systems Technical Journal*, vol. 27, pp. 58-82, 1948.

[15] J. Brown, "Artificial dielectrics," in *Progress in Dielectrics*, vol. 2, J. B. Birks and J. H. Schulman, Eds., London: Heywood, 1960, pp. 193-225.

[16] D. L. Jaggard, A. R. Mickelson, and C. H. Papas, "On electromagnetic waves in chiral media," *Journal of Applied Physics*, vol. 18, pp. 211-216, 1979.

[17] I. P. Theron and J. H. Cloete, "The optical activity of an artificial non-magnetic uniaxial chiral crystal at microwave frequencies," *Journal of Electromagnetic Waves and Applications*, vol. 10, pp. 539-561, 1996.

[18] I. V. Lindell, A. H. Sihvola, S. A. Tretyakov, and A. J. Viitanen, *Electromagnetic Waves in Chiral and Bi-Isotropic Media*, Boston, MA: Artech House, 1994.

[19] K. W. Whites, "Full-wave computation of constitutive parameters for lossless composite chiral materials," *IEEE Transactions on Antennas and Propagation*, vol. 43, pp. 376-384, 1995.

[20] A. L. Topa, C. R. Paiva, and A. M. Barbosa, "Radiation Control on a Step Discontinuity of a Grounded Chiral Slab," in *Proceedings of Bianisotropics'2000*, Lisbon, Portugal, 27-29 September 2000, pp. 325-328.

[21] L. R. Arnaut, "Interaction between bianisotropic particles," *Journal of Electromagnetic Waves and Applications*, vol. 11, pp. 133-137, 1997.

[22] A. Lakhtakia, "Isotropic Maxwell-Garnett model for biisotropic-in-biisotropic mixtures," *International J. of Infrared and Millimeter Waves*, vol. 13, no. 4, pp. 551-558, 1992.

[23] W. S. Weiglhofer, A. Lakhtakia, and C. J. Monzon, "Maxwell-Garnett model for composites of electrically small uniaxial objects, " *Microwave and Optical Technology Letters*, vol. 6, no. 12, pp. 681-684, 1993.

[24] A. H. Sihvola, *Electromagnetic Mixing Formulas and Applications*, London: The Institution of Electrical Engineers, 1999.

[25] G. Kristensson, S. Rikte and A. H. Sihvola, "Mixing formulas in the time domain," *J. Opt. Soc. Am. A.*, vol. 15, no. 5, pp. 1411-1422, 1998.

[26] I. V. Lindell and F. Olyslager, "Potentials in bi-anisotropic media," *Journal of Electromagnetic Waves and Applications*, vol. 15, no. 1, pp. 3-18, 2001.

[27] F. Auzanneau and R. W. Ziolkowski, "Theoretical study of synthetic bianisotropic materials, " *Journal of Electromagnetic Waves and Applications*, vol. 12, p. 353, 1998.

[28] D. R. Smith, W. J. Padilla, D. C. Vier, S. C. Nemat-Nasser, and S. Schultz, "Composite medium with simultaneously negative permeability and permittivity," *Phys. Rev. Lett.*, vol. 84, no. 18, pp. 4184-4187, 1 May 2000.

[29] D. R. Smith and N. Kroll, "Negative refractive index in left-handed materials," *Phys. Rev. Lett.*, vol. 85, no. 14, pp. 2933-2936, 2 October 2000.

[30] J. B. Pendry, "Negative refraction makes a perfect lens," *Phys. Rev. Lett.*, vol. 85, no. 18, pp. 3966-3969, 30 October 2000.

[31] R. A. Shelby, D. R. Smith, S. C. Nemat-Nasser, and S. Schultz, "Microwave transmission through a two-dimensional, isotropic, left-handed metamaterial," *Applied Physics Lett.*, vol. 78, no. 4, pp. 489-491, 22 January 2001.

[32] R. A. Shelby, D. R. Smith, S. Schultz, "Experimental verification of a negative index of refraction," *Science*, vol. 292, no. 5514, pp. 77-79, 6 April 2001.

[33] V. G. Veselago, "The electrodynamics of substances with simultaneously negative values of ε and μ," *Soviet Physics Uspekhi*, vol. 10, no. 4, pp. 509-514, 1968. [*Usp. Fiz. Nauk*, vol. 92, pp. 517-526, 1967.]

[34] I. V. Lindell, S. A. Tretyakov, K. I. Nikoskinen, and S. Ilvonen, "BW media – Media with negative parameters, capable of supporting backward waves," *Microwave and Optical Technology Letters*, Vol. 31, No. 2, pp. 129-133, October 2001.

[35] R. W. Ziolkowski, and E. Heyman, "Wave propagation in media having negative permittivity and permeability," *Physical Review E.*, Vol. 64, No. 5, 056625, 2001.

[36] R. W. Ziolkowski, "Superluminal transmission of information through electromagnetic metamaterials," *Phys. Rev. E.*, vol. 63, no. 4, April 2001.

[37] M. W. McCall, A. Lakhtakia, and W. S. Weiglhofer, "The negative index of refraction demystified," *European Journal of Physics*, vol. 23, pp. 353-359, 2002.

[38] N. Engheta, "An idea for thin subwavelength cavity resonators using metamaterials with negative permittivity and permeability," *IEEE Antennas and Wireless Propagation Letters*, Vol. 1, No. 1, 2002 to appear on line soon.

[39] N. Garcia and M. Nieto-Vesperinas, "Left-handed materials do not make a perfect lens," *Physical Review Letters*, Vol. 88, No. 20, 207403, 2002.

[40] R. Marques, F. Medina, and R. Rafii-El-Idrissi, "Role of bianisotropy in genative permeability and left-handed metamaterials," *Physical Review B*, Vol. 65, No. 14, 144440, 2002.

[41] P. M. Valanju, R. M. Walser, and A. P. Valanju, "Wave refraction in negative-index media: Always positive and very inhomogeneous," *Physical Review Letters*, Vol. 88, No. 18, 012220, 2002.

[42] J. A. Kong, B.-I. Wu, and Y. Zhang, "A unique lateral displacement of a Gaussian beam transmitted through a slab with negative permittivity and permeability," *Microwave and Optical Technology Letters*, Vol. 33, No. 2, pp. 136-139, 2002.

[43] R. A. Silin and I. P. Chepurnykh, "On media with negative dispersion," *Journal of Communication Technology and Electronics*, Vol. 46, No. 10, pp. 1121-1125, 2001. (translated from Radiotekhnika, Vol. 46, No. 10, pp. 1212-1217, 2001.)

TIME-DOMAIN METHODS

EVOLUTION EQUATION FOR NEAR-FIELD THERMAL RADIO EMISSION[1]

Gaikovich K.P.
Institute for Physics of Microstructures RAS, GSP-105, Nizhny Novgorod, Russia, 603950
Phone: 8312 327920, Fax: 8312 675553, E-mail: gai@ipm.sci-nnov.ru

ABSTRACT

The simultaneous solution of the equations of near-field thermal emission formation and thermal conductivity has been obtained and the expression related the temperature profile of half-space with the measured thermal radio emission (effective brightness temperature) have been obtained. Example of its application in the process of water surface heating the water is presented.

EVOLUTION EQUATION AND RELATED INVERSE PROBLEMS

In the paper [1], on the basis of the simultaneous solution of the equations of radiation transfer and thermal conductivity, the expressions connecting the temperature profile and heat flux dynamics of half-space with the brightness temperature of its thermal radio emission have been obtained. Using these expressions, various methods of radiometry monitoring of the temperature and heat dynamics of water, soils and atmosphere have been developed.

In the case of measurements of the thermal radio emission in the near-field range the formation of the received emission is different. This difference is related to a specific character of the distribution of the quasistationary field component near a radiating surface. The effective depth of the received emission formation appears to be less than the skin-layer depth and depends on the size of the receiver antenna D and its height above the medium surface, h. This dependence has been obtained from measurements of the emission of a temperature stratified water medium using a specially developed electrically small antenna [2]. It could be considered as a new source of information about the depth temperature distribution [3]. According to [2], the effective brightness temperature T_B of the emission received at $h \geq 0$ above the homogeneous half-space $z \leq 0$ can be written as:

$$T_B(D,h) = \int_{-\infty}^{0} T(z)\left[\iint d^2\kappa F(\kappa,D,h)e^{\gamma(\kappa)z}\right] = \\ = \int_{-\infty}^{0} T(z)\left[\iint_{\kappa\le k_0} d^2\kappa F_1(\kappa,D)e^{\gamma(\kappa)z} + \iint_{\kappa>k_0} d^2\kappa F_2(\kappa,D,h)e^{\gamma(\kappa)z}\right]dz \qquad (1)$$

where $T(z)$ is the temperature depth profile, F, F_1, F_2, γ_1, γ_2 are functions determined in [3]. One can see that the received signal can be expressed in (1) as a sum of the wave (the first term) and the quasistationary (the second term) components. The temperature

[1] This work is supported by Russian Foundation for Basic Research, grant No. 01-02-16432.

profile $T(z,t)$ in a medium can be also expressed as the solution of the thermal conductivity equation. In the absence of sources at the boundary condition $T(0,t) = T_0(t)$ the temperature profile is determined as

$$T(z,t) = \int_{-\infty} T_0(\tau) \frac{-z}{\sqrt{4\pi a^2 (t-\tau)^3}} \exp(-\frac{z^2}{4a^2(t-\tau)}) d\tau, \quad (2)$$

where a^2 is the thermal diffusivity coefficient. At the boundary condition $dT(0,t)/dz = -(1/k)J_0(t)$ the corresponding solution is

$$T(z,t) = \int_{-\infty} J_0(\tau) \frac{-1}{k\sqrt{\pi(t-\tau)}} \exp(-\frac{z^2}{4a^2(t-\tau)}) d\tau. \quad (3)$$

where J_0(t) is the heat flux through surface $z = 0$ and k is the thermal conductivity coefficient. Substituting (2) and (3) into (1) in the same way as it was done in [1] for far-field measurements and carrying out the necessary transformations, we have the evolution equations for measured effective radiobrightness:

$$T_B(t) = \int_{-\infty} d\tau T_0(\tau) \iint d^2\kappa \{F(\kappa, D)[\frac{\gamma a}{\pi(t-\tau)} - (\gamma a)^2 erfc(\gamma a\sqrt{t-\tau}) e^{(\gamma a)^2 (t-\tau)}]\}, \quad (4)$$

$$T_B(t) = -\int_{-\infty} d\tau J_0(\tau) \iint d^2\kappa [F(\kappa, D)(\gamma a^2 / k) erfc(\gamma a\sqrt{t-\tau}) e^{(\gamma a)^2 (t-\tau)}] \quad (5)$$

These equations can be used to solve correspondence inverse problems, i.e. to obtain boundary conditions $T_0(t)$ and $J_0(t)$ using measurements of $T_B(t)$. It is possible to obtain an exact solution of (4) and (5), and, hence, an exact solution of the problem of temperature profile retrieval as it was done for the case of far-field measurements [1]. However, there is a more straightforward way to solve this inverse problem. It is possible to use the mean value theorem and the condition of the unity normalization of the kernel to obtain from (1) the same equation as for far-field measurements:

$$T_B(D,h) = \int_{-\infty}^{0} T(z) \tilde{\gamma}(D,h) e^{\tilde{\gamma}(D,h) z} dz, \quad (6)$$

where $\tilde{\gamma}(D,h)$ is related with the value of the effective depth of the received near-field thermal emission introduced in [2,3] as $d_{eff}(D,h) = 1/\tilde{\gamma}$. So, using the result obtained in [1], we have the expression for the subsurface temperature profile:

$$T(z,t) = \int_{-\infty} T_B(\tau) e^{-[z^2/4a^2(t-\tau)]} \left[\frac{1}{\tilde{\gamma}} (\frac{z^2}{2a^2(t-\tau)} - 1) - z\right] \frac{d\tau}{\sqrt{4\pi a^2 (t-\tau)^3}}. \quad (7)$$

NEAR-FIELD RADIOMETRY OF WATER TEMPERATURE DYNAMICS

In this study we present our results on retrieval of a water subsurface temperature profile using the contact (h = 0) measured dependence $T_B(t)$ at the antenna size D = 1 cm in (7) in the process of water surface heating (with the help of a wire heater) described in [3]. The results of radiobrightness measurements (for two different antennas with the sizes D = 1 cm and D = 4 cm) are shown in Fig.1 along with contact measured temperature dynamics at the five different depth levels. In Fig.4 one can see that the results of the temperature profiles retrieval are in a good agreement with the contact measured profiles. It is possible to see in Fig.1 the dependence of the radiobrightness on the size of antenna, which is related to the near-field effect, and this dependence is also used [2,3] for temperature profile retrieval. It should be mentioned that the value of D in (1) is determined in practice by the measured value of d_{eff}, so the more simple equation (6) could be used instead of (1) in any of possible applications.

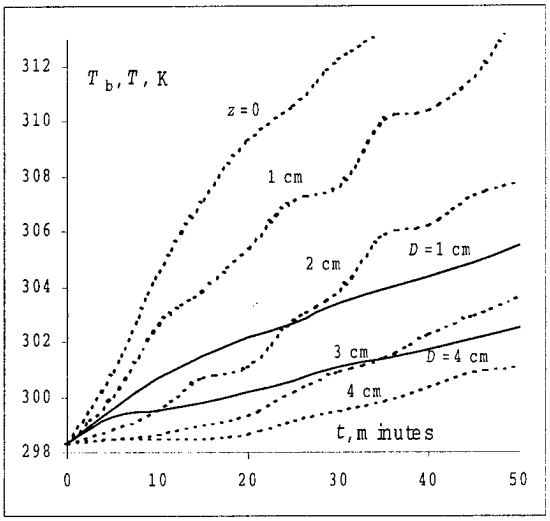


Fig.1. Measurements of the brightness temperature dynamics – solid lines; contact measurements temperature dynamics at different levels inside the water – dashed lines.

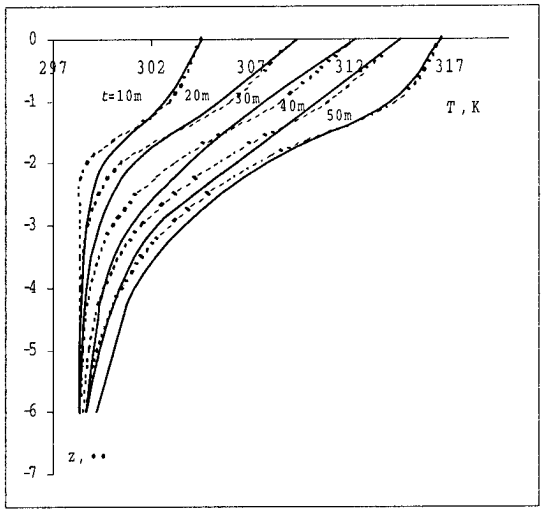


Fig.2. Profiles $T(z)$ retrieved in time interval 10 minutes by measurements of $T_b(t, D$=1 cm) – dashed lines; profiles $T(z)$ measured by contact thermometer.

CONCLUSION

Expressions are derived that relate the half-space temperature profile and the heat flux with the brightness temperature evolution for the case of near-field measurements. This approach gives a possibility to retrieve subsurface temperature profiles by measured dynamics of the radiobrightness in the same way as by the far-field radiometry measurements.

REFERENCES

[1]K.P.Gaikovich, IEEE Trans. Geosci. Remote Sensing, 1994, v.32, *No.*4, p.885.
[2]K.P.Gaikovich, A.N.Reznik, JETP Letters, 2000, v.72, *No.*11, p.546.
[3]K.P.Gaikovich, A.N.Reznik, V.L.Vaks, N.V.Yurasova. Physical Review Letters, 2002, v.88, *No.*10, p.4302.

TIME-DOMAIN ELECTROMAGNETIC FIELDS IN A RESONATOR WITH DISPERSIVE MEDIUM.

M. S. Antyufeyeva, O. A. Tretyakov.

Kharkov National University, 4 Svobody sq., Kharkov, 61077, Ukraine.
E-mail: Maria.S.Antyufeyeva@univer.kharkov.ua.

ABSTRACT

The time domain electromagnetic field evolution in the cavity filled with a homogeneous stationary but dispersive medium is investigated using the *Evolutionary Approach to Electromagnetics*. The kernel of the constitutive relation integral part is chosen as the double-exponential function for dispersive medium description. The solutions for the free and forced oscillations are obtained in analytical form.

INTRODUCTION

Recently, great attention has been paid to the questions which are concerned with nonstationary, dispersive, heterogeneous nonlinear, media. One of the approaches, allowing to consider such problems, is *Evolutionary Approach to Electromagnetics* which is proposed in [1], [2]. Its advantage lies in the separation of spatial and temporary parts of the problem. In the frames of the evolutionary approach, the electromagnetic field strengths are presented in the form of expansions on eigen vectors of the self-adjoint operator, which is separated from Maxwell equations and includes corresponding boundary conditions. For the cavity with singly connected closed surface, decompositions of electromagnetic field strength are as follows

$$\vec{E}(\mathbf{r},t)=\sum_{n=1}^{\infty}e_n(t)\mathbf{E}_n(\mathbf{r})-\sum_{a=1}^{\infty}a_\alpha(t)\nabla\Phi_\alpha(\mathbf{r}),\ \vec{H}(\mathbf{r},t)=\sum_{n=1}^{\infty}h_n(t)\mathbf{H}_n(\mathbf{r})-\sum_{\beta=1}^{\infty}b_\beta(t)\nabla\Psi_\beta(\mathbf{r}). \quad (1)$$

Eigen vectors for the solenoidal part of the problem $\mathbf{E}_n(\mathbf{r})$, $\mathbf{H}_n(\mathbf{r})$ and the irrotational part of the problem $\Phi_\alpha(\mathbf{r})$, $\Psi_\beta(\mathbf{r})$ satisfy corresponding boundary eigenvalue problem for Laplasian

$$\begin{cases} rot\mathbf{H}_n(\mathbf{r})=-ik_n\varepsilon_0\mathbf{E}_n(\mathbf{r}), & (\mathbf{n}_0\cdot\mathbf{H}_n(\mathbf{r}))\big|_S=0 \\ rot\mathbf{E}_n(\mathbf{r})=ik_n\mu_0\mathbf{H}_n(\mathbf{r}), & [\mathbf{n}_0\times\mathbf{E}_n(\mathbf{r})]_S=0 \end{cases},$$

$$(\Delta+\eta_\alpha^2)\Phi_\alpha(\mathbf{r}),\quad \Phi_\alpha(\mathbf{r})\big|_S=0;\qquad (\Delta+\nu_\beta^2)\Psi_\beta(\mathbf{r}),\quad \frac{\partial}{\partial\mathbf{n}_0}\Psi_\beta(\mathbf{r})\Big|_S=0.$$

Evolution equations for electromagnetic field oscillations in the cavity filled with a dispersive medium.

Evolution equations with initial conditions for arbitrary medium are obtained by projection Maxwell equations onto the sets of eigen vectors

$$\frac{d}{dt}e_n(t)+ik_nh_n(t)=-j_n^e(t)-\frac{1}{V}\int_V\left(\frac{d}{dt}\vec{P}(\vec{E})+J(\vec{E},\vec{H})\right)\cdot\mathbf{E}_n^*(\mathbf{r})dV,\quad e_n(t)\big|_{t=0}=e_n^0; \quad (2)$$

$$\frac{d}{dt}h_n(t)+ik_n e_n(t)=-j_n^h(t)-\frac{1}{V}\int_V\left(\frac{d}{dt}\vec{M}(\vec{H})\right)\cdot\mathbf{H}_n^*(\mathbf{r})dV, \qquad h_n(t)\big|_{t=0}=h_n^0; \quad (3)$$

$$\frac{d}{dt}a_\alpha(t)=-i_\alpha^e(t)-\frac{1}{V}\int_V\left(\frac{d}{dt}\vec{P}(\vec{E})+\vec{J}(\vec{E},\vec{H})\right)\cdot\nabla\Phi_\alpha^*(\mathbf{r})dV, \qquad a_\alpha(t)\big|_{t=0}=a_a^0; \quad (4)$$

$$\frac{d}{dt}b_\beta(t)=-i_\beta^h(t)-\frac{1}{V}\int_V\left(\frac{d}{dt}\vec{M}(\vec{H})\right)\cdot\nabla\Psi_\beta^*(\mathbf{r})dV, \qquad b_\beta(t)\big|_{t=0}=b_\beta^0. \quad (5)$$

The cavity filling is the nonmagnetic (μ=1) dispersive medium with dissipation, which is specified by the following material constitutive relations

$$\vec{P}(\vec{E})=\varepsilon_0\chi_0\int_0^\infty\chi_e(\tau)\vec{E}(\mathbf{r},t-\tau)d\tau, \quad \vec{M}(\vec{H})=\vec{H}(\mathbf{r},t), \quad \vec{J}(\vec{E},\vec{H})=\sigma\vec{E}(\mathbf{r},t).$$

$\chi_e(\tau)$ is the susceptibility function, which is defined by the double-exponential function $\chi_e(\tau)=\gamma\left(e^{-p\gamma\tau}-e^{-q\gamma\tau}\right)$ and satisfies δ-function properties when $p=\frac{q}{q+1}$ and $\gamma\to\infty$. With this determination of medium conditions, evolutionary equations are transformed into the following form

$$\frac{d}{dt}e_n(t)+\frac{\sigma}{\varepsilon_0}e_n(t)+ik_n h_n(t)=-j_n^e(t)-\chi_0\int_0^\infty\chi_e(\tau)\frac{de_n(t-\tau)}{dt}d\tau, \qquad e_n(t)\big|_{t=0}=e_n^0; \quad (6)$$

$$\frac{d}{dt}h_n(t)+ik_n e_n(t)=-j_n^h(t), \qquad h_n(t)\big|_{t=0}=h_n^0; \quad (7)$$

$$\frac{d}{dt}a_\alpha(t)=-i_\alpha^e(t)-\chi_0\int_0^\infty\chi_e(\tau)\frac{da_\alpha(t-\tau)}{dt}d\tau, \qquad a_\alpha(t)\big|_{t=0}=a_a^0; \quad (8)$$

$$\frac{d}{dt}b_\beta(t)=-i_\beta^h(t), \qquad b_\beta(t)\big|_{t=0}=b_\beta^0. \quad (9)$$

The evolutionary equation system has analytical solutions, which are obtained by the successive approximations method.

ANALYTICAL SOLUTIONS FOR FREE AND FORCED OSCILLATIONS IN A CAVITY

If the impressed forces for irrotational modes are absent, then corresponding expansion coefficients are easily found as

$$b_\beta(t)=b_\beta^0\equiv const,$$

and

$$a_\alpha(t)=a_\alpha^0\exp\left[-\frac{\sigma}{\varepsilon_0}\left(1-\chi_0\frac{\gamma^2(q-p)}{(p\gamma-\sigma/\varepsilon_0)(q\gamma-\sigma/\varepsilon_0)}\right)t\right].$$

For finding the solenoidal part of the field the evolutionary equations (6), (7) have been solved simultaneously in the following form

$$\begin{pmatrix}e_n(t)\\ h_n(t)\end{pmatrix}=e^{-\rho t}\begin{pmatrix}e_n^0\cos\omega t-ih_n^0\sin\omega t\\ h_n^0\cos\omega t-ie_n^0\sin\omega t\end{pmatrix}-\int_0^t e^{-\rho(t-t')}\begin{pmatrix}j_n^e(t')\cos\omega(t-t')-ij_n^h(t')\sin\omega(t-t')\\ j_n^h(t')\cos\omega(t-t')-ij_n^e(t')\sin\omega(t-t')\end{pmatrix}dt'-$$

$$-\int_0^t e^{\rho(t'-t)}\begin{pmatrix}\chi_0\cos\omega(t-t')\int_0^\infty \chi_e(\tau)\dfrac{de_n(t'-\tau)}{dt'}d\tau\\ -i\chi_0\sin\omega(t-t')\int_0^\infty \chi_e(\tau)\dfrac{de_n(t'-\tau)}{dt'}d\tau\end{pmatrix}dt',$$

where $\rho=\dfrac{\sigma}{2\varepsilon_0}$, $\omega=\sqrt{k_n^2-\rho^2}$.

For the free oscillations with nonzero initial condition e_n^0, unknown time coefficients are found in terms of elementary functions

$$e_n(t)=e_n^0\exp[-(\rho+\delta_1\omega\sin\xi)t]\cos[(1-\delta_1\cos\xi)\omega t]$$

$$h_n(t)=-ie_n^0e^{-\rho t}\left[\sin\omega t+\frac{F}{G}(1-\delta_1\cos\xi)\left\{e^{-\delta_1\omega t\sin\xi}\sin[(1-\delta_1\cos\xi)\omega t-\xi-\zeta]-\sin[\omega t-\xi-\zeta]\right\}\right].$$

For forced field determination, functions of impressed forces are chosen as $j_n^h(t)\equiv 0$, but $j_n^e(t)=J_n\cos\Omega t$, and $\omega-\Omega=\Delta\omega$ is much less then ω or Ω. The expansion time coefficients in this case can be written in the following form

$$e_n(t)=\frac{J_n}{2R}\frac{\sin(\Omega t-\varphi-\psi)}{\sqrt{1-\delta_2\cos(\varphi+\theta)+\delta_2^2}}-$$

$$-\frac{J_n}{2R}e^{-(\rho+\delta_1\omega\sin\xi)t}\{\sin[(1-\delta_1\cos\xi)\omega t-\varphi]+\delta_2\sin[(1-\delta_1\cos\xi)\omega t-2\varphi-\theta]\},$$

$$h_n(t)=\frac{iJ_n}{2R}\left[\cos(\Omega t-\varphi)-e^{-\rho t}\cos(\omega t-\varphi)-\frac{\delta_2\left(\cos(\Omega t-2\varphi-\psi-\theta)-e^{-\rho t}\cos(\omega t-2\varphi-\psi-\theta)\right)}{\sqrt{1-\delta_2\cos(\varphi+\theta)+\delta_2^2}}\right]$$

$$+\frac{iJ_n}{2R}\frac{F}{G}e^{-\rho t}(1-\delta_1\cos\xi)\left\{e^{-\delta_1\omega t\sin\xi}\left(\cos[(1-\delta_1\cos\xi)\omega t-\varphi-\xi-\zeta]+\right.\right.$$

$$\left.\left.+\delta_2\cos[(1-\delta_1\cos\xi)\omega t-2\varphi-\theta-\xi-\zeta]\right)-\cos(\omega t-\varphi-\xi-\zeta)-\delta_2\cos(\omega t-2\varphi-\theta-\xi-\zeta)\right\},$$

where the coefficients F, G, δ_1, δ_2, ξ, θ, ζ depend on parameter γ.

In the course of decision the value ranges of χ_0 and γ are determined, for which the obtained solutions are valid.

REFERENCES.

[1]. O.A. Tretyakov "The method of modal basis.", Radiotechnika i Elektronika, vol. 31,No. 6, 1986 (in Russian). English translation in Soviet J. on Communication Technology and Electronics, 1986.

[2]. O.A. Tretyakov "Essentials of nonstationary and nonlinear electromagnetic field theory", in M. Hashimoto, M.Idemen, O.A. Tretyakov, Eds., "Analytical and numerical methods in electromagnetic wave theory", Science House Co., Ltd., Tokyo, 1993

ENERGY TRANSFORMATION OF A TRANSIENT WAVE ON RADIATING APERTURE

Alexander N. Dumin, Victor A. Katrich
Kharkov National University, Svobody Sq.4., Kharkov, 61077, Ukraine,
e-mail: Alexander.N.Dumin@univer.kharkov.ua

ABSTRACT

Energy transformation of a transient TEM-wave in coaxial waveguide into energy of reflected and radiated waves on coaxial aperture is investigated. The radiation problem is solved by means of Modal Basis Method in time domain. The analytical expressions for amplitudes of fields radiated into free space and reflected inside the waveguide are obtained for step-wise time dependence of amplitude of exciting TEM-wave.

Time dependencies of instant power of the electromagnetic waves in waveguide and free space are obtained. The analysis of the influence of the problem geometry and exciting signal parameters on effectiveness of radiation is carried out.

INTRODUCTION

The Modal Basis Method is a variety of Method of Incomplete Separation of Variables. It permits to transform the transient three-dimensional electromagnetic radiation problem into one-dimensional problem for two independent evolutionary equations of Klein-Gordon type describing propagation TE- and TM-waves in free space [1]. Utilizing the separation of variables method for Klein-Gordon equation on the base of group theory [2], one can get a general solution of these equations without employing Fourier transform.

The purpose of this work is to investigate the transformation of the energy of the incident wave of arbitrary time dependence on the radiating aperture on the base of the solution of the problem for stepwise time dependence of the incident wave [3].

THE STATEMENT OF THE PROBLEM

Incident TEM-wave with step-wise time dependence and unit stream of power density propagates in the semi-infinite coaxial waveguide with inner radius b and outer radius a. On the open end of the waveguide with infinite flange in $z = 0$ the wave will be partially reflected, radiated and converted into the other modes of the coaxial waveguide (see Figure 1).

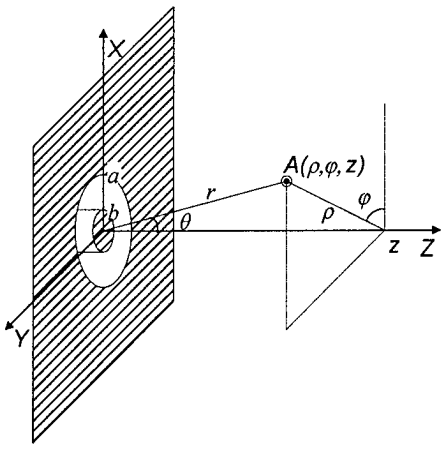


Fig.1. Problem geometry.

The electromagnetic field in the waveguide can be represented as an infinite sum of modes. Also the field in free halfspace is presented in terms of the Modal Basis [1]. Using general solution of Klein-Gordon equation [2] and mode matching technique analytical expressions for the radiated field and the field of reflected TEM-wave in the coaxial waveguide are obtained. The solution of the problem for the case of arbitrary time dependence one can receive by Duhamel's integral because of the problem linearity.

ANALYTICAL SOLUTION.

Modal representation of the E-field in free halfspace gives the following general expressions [1]:

$$\vec{H} = \int_0^{\infty} d\xi \left[\vec{z}_0 \times \nabla\phi^s(\rho,\varphi;\xi)\right]\varepsilon_0 \frac{\partial}{\partial t} B(z,t;\xi); \qquad \vec{E} = -\int_0^{\infty} d\xi \nabla\phi^s(\rho,\varphi;\xi)\frac{\partial}{\partial z} B(z,t;\xi);$$

$E_z = -\int_0^{\infty} \xi^2 d\xi \phi^s(\rho,\varphi;\xi) B(z,t;\xi)$, where $\phi^s = J_0(\xi\rho)/\sqrt{\xi}$ because of the axial symmetry of the problem, $J_m(\cdot)$ – Bessel function of the first kind, $B(z,t;\xi)$ is the evolutionary coefficient, which has the form [3]

$$B = D\frac{[J_0(\xi b) - J_0(\xi a)]}{\xi^{3/2}}\left(\frac{ct-z}{ct+z}\right)^{1/2}\left\{J_1\left(\xi\sqrt{c^2t^2-z^2}\right) + 2\sum_{m=1}^{\infty}\left(\frac{ct-z}{ct+z}\right)^m J_{2m+1}\left(\xi\sqrt{c^2t^2-z^2}\right)\right\},$$

$D = c\mu_0\sqrt{2(a^2-b^2)}/\ln(a/b)$. Thus using mode matching technique one can derive the time dependence of reflected TEM-wave

$$A(ct) = \frac{1}{\ln a/b}\int_0^{\infty} d\xi \frac{[J_0(\xi a) - J_0(\xi b)]^2}{\xi}\{1 - J_0(\xi ct) - J_2(\xi ct)\}.$$

The amplitudes of all components of radiated field and field inside waveguide and, consequently, energy parameters of field for arbitrary time dependence of exciting TEM-wave can be calculated by Duhamel's integral.

NUMERICAL SIMULATION

For the numerical simulation we use the same size of aperture as in [3], namely, $a = 33.5\,\text{mm}$.

a) Step signal simulation. The duration of the transient process on aperture is equal to $2a/c$ because we do not take into account currents on flange. So the power of reflected TEM-wave must be equal to the power of incident wave after $2a/c$. It is clearly seen from Figure 2 where the time dependence of reflected TEM-wave power is depicted.

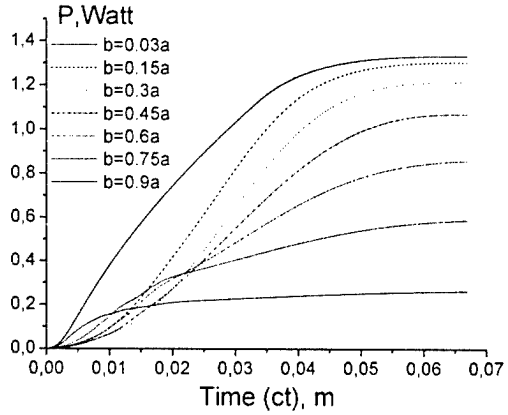


Fig.2. Power of reflected TEM-wave.

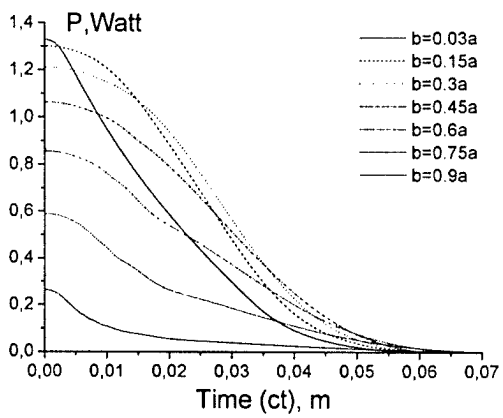


Fig.3. Power of E-waves in waveguide and in free halfspace.

Other part of the incident wave power is transformed into the power of E-waves in

waveguide and free halfspace that is shown in Fig.3. Time dependence of the power of first seven E-modes in waveguide is depicted in Fig. 4 for $b = 0.03a$. To check the law of energy conservation we calculate the radiated energy and energy of electrostatic field in free halfspace and obtain, that 11% of pulse energy is converted into propagating E-wave in free halfspace, 16% is transformed in E-wave in waveguide and 73% of the energy is in electrostatic field in free halfspace. The spatial distribution of electrostatic field energy density is shown in Fig.5. It is seen that electrostatic field and its energy are concentrated near internal conductor and outer waveguide wall.

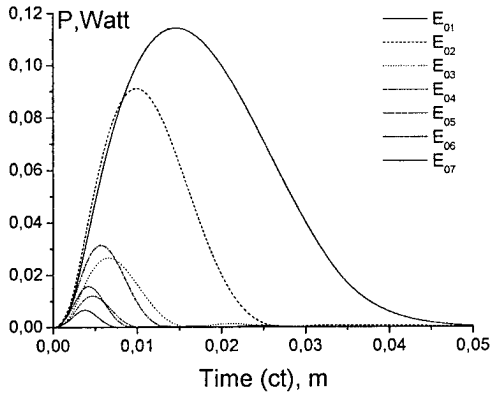


Fig.4. Power of first seven E-modes in waveguide ($b = 0.03a$).

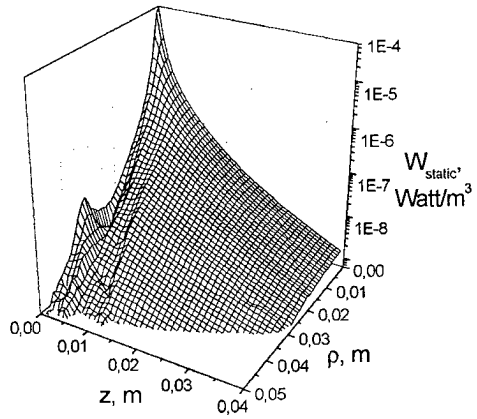


Fig. 5. Spatial distribution of electrostatic field energy density.

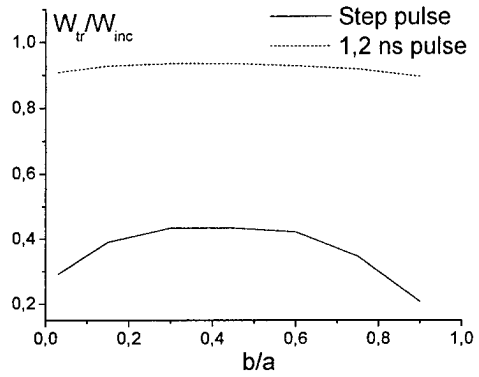


Fig.6. Relation between transformed into E-waves energy and energy of incident pulse for step-wise pulse and arbitrary 1.2 ns pulse.

b) Arbitrary signal simulation.

The same energy characteristics are calculated for typical form of exciting pulse [3]. For this case the transformation of incident wave energy in E-waves in waveguide and free halfspace is more effective that is shown in Fig.6. where the relation between transformed into E-waves energy and energy of incident pulse for step-wise pulse and arbitrary 1.2 ns pulse as well as different b/a is depicted.

CONCLUSIONS

The energy transformation of transient TEM-wave on an open end of coaxial waveguide has been studied. The law of energy conservation for this problem has been verified.

REFERENCES

[1] A.N. Dumin, O.A. Tretyakov, "Radiation of Arbitrary Signals by Plane Disk", Conf. Proc. MMET'96, Lviv, Ukraine, pp. 248-251.

[2] W. Miller. Symmetry and Separation of Variables. London, Addison-Wesley Publishing Company, 1977.

[3] A.N. Dumin, V.A. Katrich, S.N. Pivnenko, O.A. Tretyakov, " Comparative Analysis of Approximate and Exact Solutions of Transient Wave Radiation Problem ", Conf. Proc. MMET'2000, Kharkov, Ukraine, pp. 125-127.

EXCITATION OF A SLOTTED BICONE BY AN IMPULSE MAGNETIC DIPOLE

Vladimir A. Doroshenko,

Kharkov National University of Radioelectronics
14, Lenin av., Kharkov, 61166, Ukraine

ABSTRACT

An analytical-numerical method for solving three-dimensional electrodynamics boundary problems with unclosed perfectly conducting bicone geometries is proposed. The method is based on using the Laplace transform, the Kontorovich- Lebedev transforms and the dual series regularization approach. For the alone slotted cone excited by an impulse dipole the analytical solution is derived.

INTRODUCTION

Modern practical systems those use pulses require wideband or ultrawideband antennas those can radiate and receive temporally specific wideband or ultrawideband pulses. Cones and bicones are models of wideband or ultrawideband antennas. For successful theoretical studying any physical process one should find it's appropriate mathematical model and solve the corresponding mathematical problem. The present paper is devoted to investigation of the model problem of exciting the bicone with periodical longitudinal slots by a magnetic radial dipole provided that the dipole field varies arbitrarily in time.

STATEMENT OF THE PROBLEM AND SOLUTION METHOD

The bicone structure Σ under consideration consists of two semi-infinite circular perfectly conducting thin cones Σ_1 and Σ_2 with N periodical longitudinal slots($\Sigma = \Sigma_1 \cup \Sigma_2$). Cones have the common vertex (the center of the bicone surface) and axis that coincides with the OZ-axis of the Cartesian coordinate system (Fig.1). We introduce a spherical coordinate system r,θ,φ with the origin at the bicone center. In this coordinate system the cones Σ_1 and Σ_2 are defined by the equations $\theta = \gamma_1$ and $\theta = \gamma_2$. Furthermore, we use the following notation: d_κ is the slot width of the cone Σ_κ, $\kappa = 1,2$, $l = 2\pi/N$ is the structure period. The bicone is excited by the magnetic radial dipole that is placed at the point $M_0(r_0,\theta_0,\varphi_0)$ with the moment $\vec{m}_d(\vec{r},t)$:

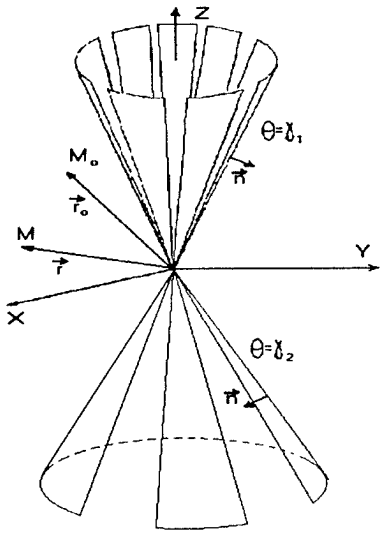


Fig.1. Bicone structure

$\vec{m}_d(\vec{r},t) = \vec{e}_r M_d \cdot \delta(\vec{r}-\vec{r}_0)\cdot f(t-t_0)$, $|\vec{e}_r| = 1$,

$\delta(t)$-delta-function; M_d, $f(t)$ are given and

$$f(t-t_0) = 0, t < t_0.$$

The vectors $\vec{E}(\vec{r},t)$ and $\vec{H}(\vec{r},t)$ of the desired electromagnetic field satisfy the Maxwell equations system with the initial conditions, the boundary conditions on the bicone Σ (the tangent component of the electric field vector vanishes on Σ), the condition of finite stored energy. The above mentioned conditions guarantee the uniqueness of the time-domain problem solution. The interaction of the incident field (the dipole field) with Σ results in a surface current, which in turn generates a scattered electromagnetic fields those are fully characterized by the scalar Debbie potential $v_1(\vec{r},t)$. This one satisfies the wave equation with conditions those guarantee the uniqueness of the second boundary problem of mathematical physics [1]. By virtue of the Laplace transform

$$v_1^s = v_1^s(\vec{r},\vec{r}_0,t_0) = \int_0^{+\infty} v_1(\vec{r},\vec{r}_0,t,t_0)e^{-st}dt \tag{1}$$

one can reduce the time–domain problem to the frequency-domain boundary problem for v_1^s. The algorithm for solving the last one with cone geometry employs the Kontorovich-Lebedev transform with respect to the coordinate r [2]

$$\hat{v}_1^s(\tau,\theta,\varphi) = \int_0^{+\infty} v_1^s(r,\theta,\varphi)\frac{K_{i\tau}(qr)}{\sqrt{r}}dr, \tag{2}$$

$$v_1^s(r,\theta,\varphi) = \frac{2}{\pi^2}\int_0^{+\infty} \tau sh\pi\tau\hat{v}_1^s\frac{K_{i\tau}(qr)}{\sqrt{r}}d\tau, \tag{3}$$

and the dual series regularization approach [3,2], $K_{i\tau}(qr)$ is the Macdonald function. Converting v_1^s (1)-(3) [4,2] leads to the following representation for $v_1(\vec{r},t)$

$$v_1(\vec{r},t) = -\frac{ab}{4rr_0^2}\sum_{m=-\infty}^{+\infty}(-1)^m e^{im\varphi_0}\int_0^{+\infty}\tau th\pi\tau\frac{\Gamma(1/2-m+i\tau)}{\Gamma(1/2+m+i\tau)}\frac{d}{d\gamma_2}P^m_{-1/2+i\tau}(\cos\gamma_2)\times$$
$$\times P^m_{-1/2+i\tau}(-\cos\theta_0)U_{m\tau}(\theta,\varphi)\cdot\Phi_{i\tau}(t-t_0)d\tau,$$

$$U_{m\tau} = \begin{cases} \sum_{n=-\infty}^{+\infty}\alpha_{mn}P^{m+nN}_{-1/2+i\tau}(\cos\theta)e^{i(m+nN)\varphi}, 0<\theta<\gamma_1 \\ \sum_{n=-\infty}^{+\infty}\left[\beta_{mn}P^{m+nN}_{-1/2+i\tau}(\cos\theta)+\xi_{mn}P^{m+nN}_{-1/2+i\tau}(-\cos\theta)\right]e^{i(m+nN)\varphi}, \gamma_1<\theta<\gamma_2 \\ \sum_{n=-\infty}^{+\infty}\zeta_{mn}P^{m+nN}_{-1/2+i\tau}(-\cos\theta)e^{i(m+nN)\varphi}, \gamma_2<\theta<\pi. \end{cases}$$

$$\Phi_{i\tau}(t-t_0) = \int_{\frac{r+r_0}{2}}^{t-t_0} f(t-t_0-z)P_{-1/2+i\tau}(ch\chi(z))dz,\ ch\chi(z) = \frac{a^2z^2-r^2-r_0^2}{2rr_0},\ a = 1/\sqrt{\varepsilon\mu},$$

where $\Gamma(z)$ is gamma-function, $P^m_{-1/2+i\tau}(y)$ is the Legendre function, $\eta(x)$ is the Heaviside function, ε and μ are electric and magnetic permittivity of the media respectively, unknown coefficients $\alpha_{mn},\beta_{mn},\xi_{mn},\zeta_{mn}$ satisfy two coupled linear algebraic equations systems, b is given.

ANALYTICAL SOLUTION

Let the source be the δ – impulse magnetic radial dipole, i.e. $f(t-t_0)=\delta(t-t_0)$. Then

$$\Phi_{i\tau}(t-t_0)=\eta\left(t-t_0-\frac{r+r_0}{2}\right)P_{-1/2+i\tau}\left(ch\chi(t-t_0)\right)$$

and

$$v_1(\vec{r},t)=-\frac{ab}{4rr_0^2}\eta\left(t-t_0-\frac{r+r_0}{2}\right)\sum_{m=-\infty}^{+\infty}(-1)^m e^{im\varphi_0}\int_0^{+\infty}\tau th\pi\tau\frac{\Gamma(1/2-m+i\tau)}{\Gamma(1/2+m+i\tau)}\times$$

$$\times\frac{d}{d\gamma_2}P^m_{-1/2+i\tau}(\cos\gamma_2)U_{m\tau}(\theta,\varphi)P^m_{-1/2+i\tau}(-\cos\theta_0)P_{-1/2+i\tau}\left(ch\chi(t-t_0)\right)d\tau\,.$$

For alone semi-transparent cone Σ_1 (the bicone Σ becomes the cone Σ_1), when the limit

$$\lim_{\substack{N\to+\infty\\ d_1/l\to 0}}\left[-\frac{1}{N}\ln\sin\frac{\pi d_1}{2l}\right]=Q>0$$

exists, the potential $v_1(\vec{r},t)$ has the following form

$$v_1(\vec{r},t)=-\frac{abQ}{2rr_0^2}\eta\left(t-t_0-\frac{r+r_0}{2}\right)\sum_{m=-\infty}^{+\infty}(-1)^m e^{im\varphi_0}\int_0^{+\infty}\tau th\pi\tau\frac{\Gamma(1/2-m+i\tau)}{\Gamma(1/2+m+i\tau)}\frac{\frac{d}{d\gamma_1}P^m_{-1/2+i\tau}(\cos\gamma_1)}{\frac{d}{d\gamma_1}P^m_{-1/2+i\tau}(-\cos\gamma_1)}\times$$

$$\times P^m_{-1/2+i\tau}(-\cos\theta_0)\frac{P^m_{-1/2+i\tau}(-\cos\theta)}{2Q+\Delta^{(m)}_{i\tau}}\cdot P_{-1/2+i\tau}\left(ch\chi(t-t_0)\right)d\tau\,,\qquad \gamma_1<\theta<\pi$$

$$\Delta^{(m)}_{i\tau}=(-1)^{m+1}\frac{ch\pi\tau}{\pi\sin^2\gamma_1}\frac{\Gamma(1/2+i\tau+m)}{\Gamma(1/2+i\tau-m)}\cdot\frac{1}{\frac{d}{d\gamma_1}P^m_{-1/2+i\tau}(\cos\gamma_1)\cdot\frac{d}{d\gamma_1}P^m_{-1/2+i\tau}(-\cos\gamma_1)}\,.$$

CONCLUSIONS

The method for solving the time-domain electrodynamics boundary problem with the unclosed bicone geometry is proposed. The main idea of it is to reduce the original problem to the frequency-time problem and to convert the solution of the last one. The analytical solution is obtained for alone slotted cone that is excited by the δ - pulse magnetic radial dipole.

REFERENCES

[1] *O.A. Ladizshenskaya.* Boundary Problems of Mathematical Physics. Moscow: Nauka, 1973, 408p.(in Russian).

[2] *V.A. Doroshenko and V.F. Kravchenko.* Unsteady Diffraction by a Nonclosed Cone// Doklady Physics. Vol. 46, No.5. 2001. P.331-335 (Engl. Transl.).

[3] *V.P. Shestopalov.* Summary Equations in Modern diffraction Theory. Kiev: Naukova Dumka Public., 1983, 252p. (in Russian).

[4] *Chan K.-K., Felsen L.B.* Transient and time harmonic diffraction by a semi-infinite cone // IEEE Trans. Antennas and Propagat. Vol.25, No.6. 1977. P.802-806.

A NOVEL DUAL-POLARIZED KU-BAND ANTENNA SUBARRAY

S. Martynyuk [1], F. Dubrovka[1], P. Edenhofer[2]

[1] National Technical University of Ukraine ("Kiev Polytechnic Institute"), Radio-Engineering Department, Politechnichna 12, Kiev, Ukraine
E-mail: mart_1974@yahoo.com
[2] Ruhr University of Bochum, Institute for High-Frequency Technique, 44780 Bochum, Germany
E-mail: edh@hf.ruhr-uni-bochum.de

ABSTRACT

The paper presents a novel design of a Ku-band (10,95...14,5 GHz) planar multilayered microstrip antenna using aperture-coupled stacked patch radiating elements with dual polarization capability. Frequency bandwidth of up to 26% (VSWR<2:1) and level of cross-polarization better than -30 dB have been achieved in both E- and H-planes of radiation pattern for the two orthogonal linear polarizations. Numerical results obtained by FDTD computer simulations are compared with experimentally determined characteristics of a manufactured antenna.

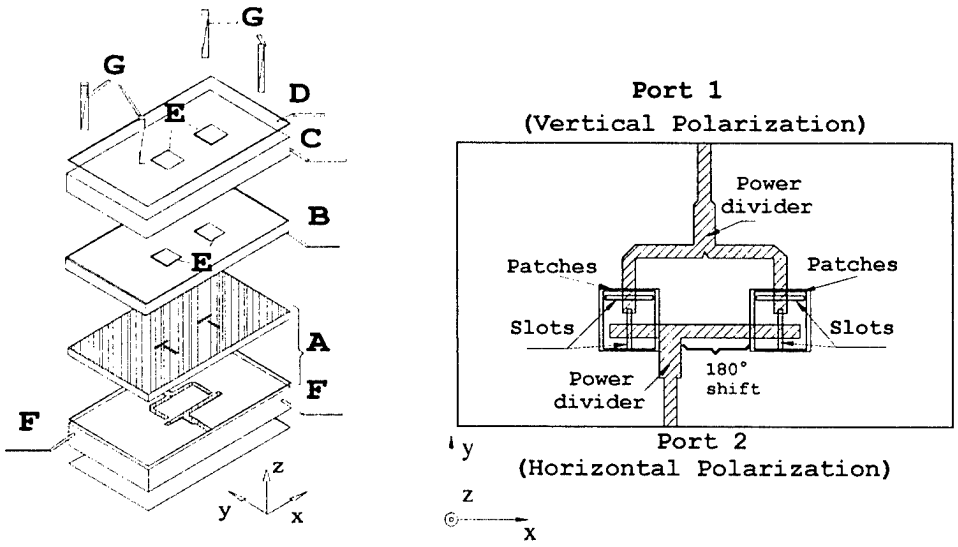
INTRODUCTION

Future mobile satellite telecommunication systems are expected to require wide-band planar phased antenna arrays with dual polarization capability. The challenging trend is to increase the potential data rate of communication links due to both fully using a broadband frequency range and polarization diversity. Many efforts have been dedicated by researchers to the creation of broadband low profile antenna arrays during the last two decades. However, at present it is considered to be very difficult to realize both requirements of wide frequency band and dual linear polarization capability with a bandwidth of above 10% and a level of cross-polarization below -30 dB in planar arrays.

DESIGN OF ANTENNA SUBARRAY

The basic design of the proposed novel multilayered dual-polarized antenna is explained according to Fig. 1. The integrated antenna system consists of two stacked aperture-coupled radiating elements and a microstrip feeding network, combining this radiators in terms of a two-element antenna subarray. The spacing between elements was chosen to be equal of 0,8 of wavelength at the center of the frequency range (12,7 GHz). The stacked antenna structure is manufactured by using four low-loss dielectric layers with different thicknesses and dielectric constants. Each layer was separately manufactured, parameters of them are given in Table. 1.

The composite sandwich structure assembly is situated quarter of a wavelength above the metallic screen at bottom side to suppress backward radiation. This distance is provided by special plastic holders that additionally contain rectangular plastic frames for making the whole assembly mechanically strong.



a) b)

Fig. 1. Geometry of proposed dual-liearly polarized multilayer microstrip antenna. a) Perspective view. b) Top schematic view.

Table 1. Parameters of Layers

Layer	Substrate	Thickness	ε_r	Loss tangent
A	Duroid 5880	0,508 mm	2,2	0,0009
B	Duroid 5880	0,765 mm	2,2	0,0009
C	Rohacell 51 IG	2,5 mm	1,07	0.001
D	Duroid 5880	0,25 mm	2,2	0,0009

PREDICTED AND MEASURED CHARACTERISTICS

For the numerical analysis of the multilayered microstrip planar structure we choose the FDTD method, originally proposed in [1]. This method was also used for the multi-parameter numerical optimization of the antenna structure geometry and its feeding network. Theoretical and experimental (measured using a network analyzer HP8722C) results of VSWR for horizontal and vertical polarization channels in the frequency range 10,5...15,5 GHz are represented in Fig. 2. In Fig. 3, 4 measured and simulated far-zone radiation patterns for both polarization channels at the center frequency (12,7 GHz) are presented, proving good dual linearly polarized performance with level of cross-polar radiation better than -30dB.

REFERENCES

[1]. K.S. Yee, „Numerical solution of initial boundary value problems involving Maxwellrs equations in isotropic media", *IEEE Trans. Antenn. Propagat.*, vol. AP-14, pp.302-307, Mar. 1966.

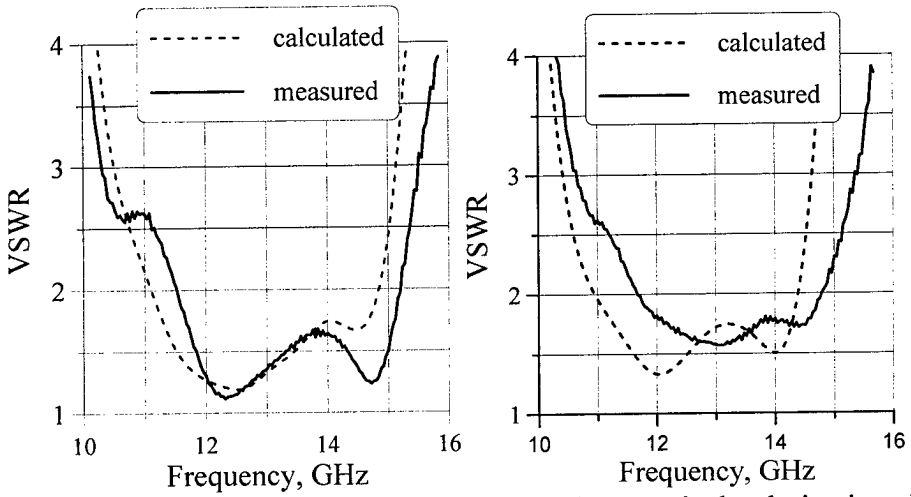


Fig. 2. VSWR for: left – horizontal polarizationl; right – vertical polarization channel.

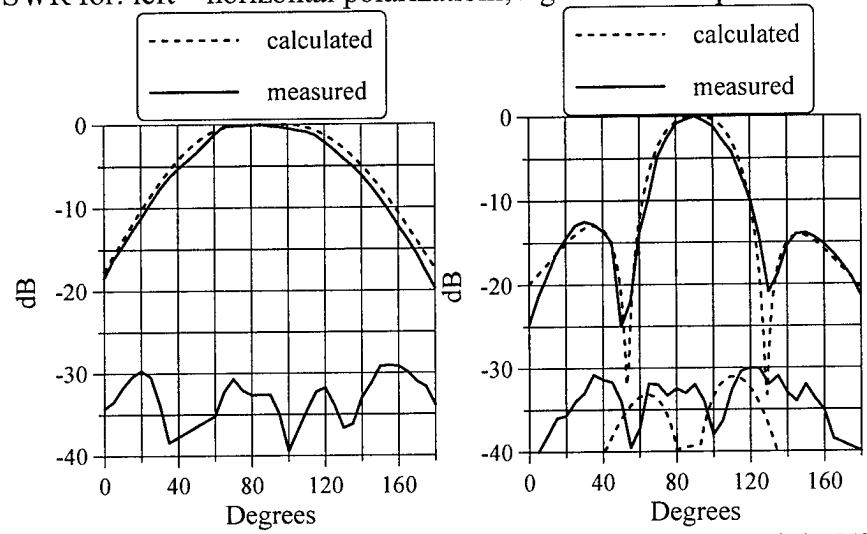


Fig. 3. horizontal polarization channel at 12,7 GHz: left YZ-plane; right XZ-plane.

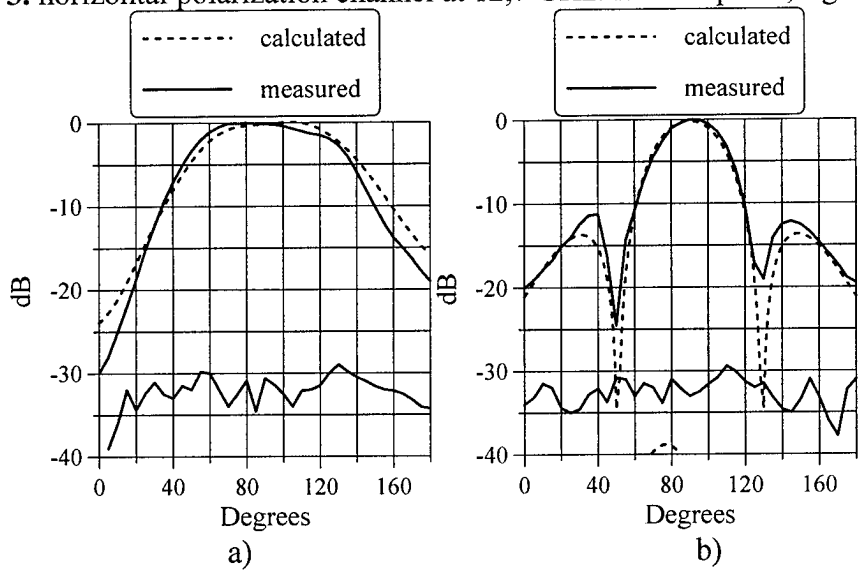


Fig. 4. vertical polarization channel at 12,7 GHz: left YZ-plane; right XZ-plane.

INTEGRAL EQUATIONS IN TIME DOMAIN FOR ELECTROMAGNETIC FIELDS OF WAVEGUIDE STRUCTURES

A. Nerukh

Kharkov National University of Radio Electronics
14 Lenin Ave., Kharkov, 61166, UKRAINE. E-mail: nerukh@ddan.kharkov.ua

T. Benson

School of Electrical & Electronic Engineering, University of Nottingham
University Park, Nottingham, NG7 2RD, UK. E-mail:
Trevor.Benson@nottingham.ac.uk

ABSTRACT

Volterra integral equations in time domain for electromagnetic fields in longitudinal uniform dielectric waveguides with time-varying media in a core are obtained. For a time jump of the core permittivity resolvent operators are constructed and appearing new features in the transients in comparison with an unbounded space is shown.

INTRODUCTION

A problem of solving the Maxwell's equations becomes especially complex when a medium is not only inhomogeneous but a time-varying one also. Such a situation can be met with a propagation of electromagnetic signals in dielectric or semiconductor waveguides. For solving such electromagnetic problems time-domain techniques are in demand and some kind of it have received increased attention in the literature. But most of these techniques are oriented onto numerical calculations only that make difficult an analysis of the phenomena. In this paper an integral equations techniques in time domain is elaborated that allows to take into account in one manner a complex combination of boundary and initial conditions with medium parameters changing in time.

INTEGRAL EQUATIONS

We consider a longitudinal uniform waveguide formed by a core medium and a background cladding medium. If $\hat{\varepsilon}_r$, $\hat{\sigma}_r$ are the operators for the medium inside the waveguide, ε is the relative permittivity and σ is the conductivity of the medium outside the waveguide then integral equations for the lateral components of the magnetic field satisfy the Volterra integral equation

$$\mathbf{B}_\perp = \mathbf{F}_B - \frac{v}{2}\int\limits_{-\infty}^{t} dt' \int\limits_{x-v(t-t')}^{x+v(t-t')} I_0\left(\frac{\alpha}{v}\sqrt{v^2(t-t')^2-(x-x')^2}\right)e^{-\alpha(t-t')} \times\left\{\frac{1}{c^2}\partial_{t'}\chi(\hat{\varepsilon}_r-\varepsilon)\partial_{t'}+\mu_0\chi(\hat{\sigma}_r-\sigma)\partial_{t'}\right\}\mathbf{B}_\perp dx' \tag{1}$$

where the characteristic function χ equals unity inside the waveguide and zero outside of it, c is the light velocity in vacuum, $v=c/\sqrt{\varepsilon}$ is the wave phase velocity in the

cladding (background), I_0 is the modified Bessel function, $\alpha = \frac{v^2 \mu_0 \sigma}{2}$ takes into account the dissipation of the cladding and x is a longitudinal coordinate. Similar form has the equation for the electric field

$$\mathbf{E}_\perp = \mathbf{F}_E - \frac{v}{2} \int_{-\infty}^{t} dt' \int_{x-v(t-t')}^{x+v(t-t')} I_0\left(\frac{\alpha}{v}\sqrt{v^2(t-t')^2-(x-x')^2}\right) e^{-\alpha(t-t')} \times \left\{ \frac{1}{c^2}\partial^2_{t't'}\chi(\hat{\varepsilon}_r - \varepsilon) + \mu_0 \chi \partial_{t'}(\hat{\sigma}_r - \sigma) \right\} \mathbf{E}_\perp dx' \quad (2)$$

The free terms of these equations

$$\mathbf{F}_B = -\frac{v}{2} \int_{-\infty}^{t} dt' \int_{x-v(t-t')}^{x+v(t-t')} dx' I_0\left(\frac{\alpha}{v}\sqrt{v^2(t-t')^2-(x-x')^2}\right) \times e^{-\alpha(t-t')} \left\{ \partial_{1'}\nabla_\perp B_1 - \left[\mathbf{e}_1, \left(\frac{1}{c^2}\partial_{t'}\hat{\varepsilon} + \mu_0(\hat{\sigma} - \sigma) \right) \nabla_\perp E_1 \right] \right\}, \quad (3)$$

$$\mathbf{F}_E = -\frac{v}{2} \int_{-\infty}^{t} dt' \int_{x-v(t-t')}^{x+v(t-t')} I_0\left(\frac{\alpha}{v}\sqrt{v^2(t-t')^2-(x-x')^2}\right) \times e^{-\alpha(t-t')} \left\{ \partial_{1'}\nabla_\perp E_1 + \left[\mathbf{e}_1, \partial_{t'}\nabla_\perp B_1 \right] \right\} dx' \quad (4)$$

are defined in the region of the core of the waveguide as well as out of it and they are known if the longitudinal components of the fields are known. It is worth noting that the expressions (1), (2) are the integral equations for the lateral components only inside the waveguide, where $\chi = 1$. Outside of the waveguide, the lateral components are simply equal to the free terms, $\mathbf{B}_\perp = \mathbf{F}_B$, $\mathbf{E}_\perp = \mathbf{F}_E$. In both cases the problem is a vector 1D one in the time domain.

To obtain the integral equations for the longitudinal components we will consider further a planar waveguide that allows in further comparatively simply to reveal the main features of the transient phenomena. In this case the problem can be made the 2D one and the Volterra integral equations for the longitudinal components take the self-consistent form:

$$B_1 = B_1^{(0)} - \frac{v}{2\pi} \int_{-\infty}^{\infty} dt' \int_{-\infty}^{\infty} dx' \int_0^b dy' e^{\alpha(t-t')} \frac{\cosh\left(a\sqrt{v^2(t-t')^2 - |\mathbf{r}_\perp - \mathbf{r}_\perp'|^2}\right)}{\sqrt{v^2(t-t')^2 - |\mathbf{r}_\perp - \mathbf{r}_\perp'|^2}} \times \theta\left(t-t' - \frac{|\mathbf{r}_\perp - \mathbf{r}_\perp'|}{v}\right) \left\{ \frac{1}{v^2}\partial_{t'}\left(\frac{\hat{\varepsilon}_r}{\varepsilon} - 1\right) + \mu_0(\hat{\sigma}_r - \sigma) \right\} \partial_{t'} B_1(t', \mathbf{r}') \quad (5)$$

$$E_1 = E_1^{(0)} - \frac{v}{2\pi}\int_{-\infty}^{\infty} dt' \int_{-\infty}^{\infty} dx' \int_0^b dy' e^{\alpha(t-t')} \frac{\cosh(a\sqrt{v^2(t-t')^2 - |\mathbf{r}_\perp - \mathbf{r}_\perp'|^2})}{\sqrt{v^2(t-t')^2 - |\mathbf{r}_\perp - \mathbf{r}_\perp'|^2}} \times$$
$$\times\theta(t-t' - \frac{|\mathbf{r}_\perp - \mathbf{r}_\perp'|}{v})\left\{\frac{1}{v^2}\partial_{t't'}^2(\frac{\tilde{\varepsilon}_r}{\varepsilon} - 1) + \mu_0\partial_{t'}(\tilde{\sigma}_r - \sigma)\right\} E_1(t', \mathbf{r}') \quad (6)$$

where θ is the Heaviside unit function and $\mathbf{r}_\perp = (x, y)$. The functions $B_1^{(0)}$ and $E_1^{(0)}$ are the solutions to the homogeneous equation, that is the field that can exist in the background in the absence of the core (the primary or initial fields). The problem for the longitudinal components is a scalar 2D or 3D one in time domain.

The equations (5), (6), as well as the correspondent ones for the lateral components (1), (2), are proper integral equations only with respect to unknown fields in the core. Outside the core these expressions are quadrature formulas for calculation of the field in the cladding via the field in the core.

The initial problem for the field in the waveguide can be solved exactly in the case of the 2D model of the waveguide when the core medium permittivity changes abruptly in time. In this case the expression for the resolvent of the integral equation for the longitudinal field is determined by the expression

$$\left\langle \mathbf{x}\left|\hat{R}_{mn}\right|\mathbf{x}'\right\rangle = \frac{\varepsilon_2 - \varepsilon}{\varepsilon_2}\frac{\theta(y)\theta(b-y)}{2v_2}\theta(y')\theta(b-y')\left\{-\bar{W}_0(t-t', |y-y'|) + \right.$$
$$\left. + \sum_{k=1}^{m}\bar{W}_k(t-t', (k-j_k)b + y - (-1)^{j_k}y') + \sum_{k=1}^{n}\bar{W}_k(t-t', (k+j_k)b - y + (-1)^{j_k}y')\right\} \quad (7)$$

Here, two indexes denote regions of various influences of the waveguide walls on the field after the medium parameters change, the symbol $j_k = \left(1-(-1)^k\right)/2$ is introduced and the operator-functions are determined by the formulae

$$\bar{W}_k(t,y) = \int_{\eta-i\infty}^{\eta+i\infty}\frac{dp}{2\pi i}p^2\frac{R(p)^k}{\varphi_2(p)}e^{pt-\frac{\varphi_2(p)}{v_2}y}, R(p) = \frac{v_2\varphi(p) - v\varphi_2(p)}{v_2\varphi(p) + v\varphi_2(p)}, \quad (8)$$

where $\varphi_i(p) = \sqrt{p^2 + \Omega_i^2}$, $\Omega_i = v_i\Gamma$, $v_2 = c/\sqrt{\varepsilon_2}$.

The constructed resolvent allows calculation of the transformation of the initial eigenwave $B_1^{(-)} = e^{i(\omega t - \Gamma x)}\cos\kappa_1(y - b/2)$ that existed in the waveguide until the moment when the permittivity in the waveguide core jumped. The field on the early stage of the transient when there is no influence of the waveguide walls consists of two waves with a new frequency $v_2\omega/v_1$ but the remained spatial structure. Later, two new kinds of the waves appear. The waves with a frequency of the initial field but the new lateral wavenumber κ_2 and the waves with the new frequency but the lateral wavenumber the same as the initial wave had. The both pairs of the frequency and the wavenumber satisfy the same dispersion equation. Besides of these waves there is a continuous spectrum of waves.

PHOTONIC GREEN'S FUNCTIONS CALCULATION BY USING FDTD METHOD

I. S. Maksymov, G. I. Churyumov

Kharkov National University of Radio Electronics

14 Lenin Ave., 61166 Kharkov, UKRAINE
E-mail: i.maksimov@ieee.org

ABSTRACT

The procedure of calculation of photonic Green's functions by using the finite-difference time-domain method is presented. The main steps of this procedure are considered and basic expressions are derived. By using these expressions the discrete forms of Green's functions can be derived and applied to solve the problems of electromagnetic wave scattering and propagation in periodical structures like photonic crystals. The discrete Green's functions can be also used to act as absorbing and dispersive boundary conditions. All these features are shown by the example of electromagnetic field propagation in the two-dimensional photonic crystal with defects.

INTRODUCTION

At present, Green's functions play a central role in the theoretical investigations of photonic crystal (PC) structures. Apart from the fact that Green's functions represent the power mathematical tool, they are the most useful for PC calculations in the view of description of local densities of states (DOS). They are also easily to apply within the main body of all time-domain methods.

In this paper we present the finite-difference time-domain (FDTD) method for photonic Green's functions for light propagation in periodical structures like PC's. This method is based on the classical FDTD method, proposed by Yee [1]. We choose just this method because of its popularity among the methods for PC's calculation [2].

We apply this FDTD method and present results of calculation for a number of PC structures. These structures are one-dimensional metal-dielectric multilayer and two-dimensional periodical structures of dielectric (metal) rods, which have applications to the design of waveguides, antennas, splitters and cavities (especially PC laser cavities).

FOURIER TRANSFORM

In order to convert results of the FDTD calculation into frequency domain we use the fast Fourier transform FDTD (FFT FDTD) method [3]. But firstly, we have to make some preliminary steps. It is desirable to eliminate the zero frequency. It may be done by subtracting off the static part from the time depended fields. We also must guarantee the accuracy of solution of Maxwell's equations when we replace the Fourier transform integral to discrete sum. It may be done by adding a small positive, imaginary part δ to the frequency. Mathematically, the result of these preliminary steps can be written as:

$$\int_{-\infty}^{\infty} f(t)\exp(i\omega t)dt \Rightarrow \sum_{n=1}^{N} f(n\delta t)\exp\left[i(\omega+i\delta)\left(n\pm\frac{1}{2}\right)\delta t\right] \qquad (1)$$

The size of imaginary part δ is determined by the total time interval over which the fields are integrated. And the final term in the sum must tend to zero. The latest fact is not important in the case of the simple FDTD method, but it is very important for accurate Green's functions FDTD method.
In addition, because of the choices we have to make a correction in (1): it is necessary to include a half time step offset, minus for the E-field and plus for H.

THE GREEN'S FUNCTIONS ON THE FDTD MESH

Without going into the fundamentals of the FDTD method on account of its prevalence, we shall begin from the Green's functions on the FDTD mesh. As is well known [4] the Green's function $G(r,r')$ is generally a two-point function, which depends on r and But taking into account that the FDTD method operates on space coordinates and time (or frequency - in the case of finite-difference frequency-domain (FDFD) method) this function will be three-point. In order to obtain the one-dimensional Green's function on the FDTD mesh (we purposely do not enter subscripts in our calculation for this case) we shall write the Maxwell's equations as (2).

$$M\begin{bmatrix} E \\ H \end{bmatrix} = \omega P \begin{bmatrix} E \\ H \end{bmatrix} \tag{2}$$

where $M = \begin{bmatrix} 0 & i\nabla\times \\ -i\nabla\times & 0 \end{bmatrix}$ and $P = \begin{bmatrix} \varepsilon\varepsilon_0 & 0 \\ 0 & \mu\mu_0 \end{bmatrix}$. Generally, ε and μ depend on r and therefore they can be written as $\varepsilon(r)$ and $\mu(r)$ correspondingly to more fully describe the nonlinear nature of effects, which are modeled.
From equations (2) and (3) we can now define the six vectors, which are the main elements of the FDTD algorithm (their final values are the primitive integrals). They are:

$$F_n = \begin{bmatrix} E_n \\ H_n \end{bmatrix} \tag{3}$$

By using equation (3), we can write down the expression for a Green's function in the frequency domain on the finite-difference mesh. So we derive equation (4).

$$G(\omega,r,r') = \frac{\delta(r-r')}{\left(\omega - P^{-1}M\right)} \tag{4}$$

In order to pass on into time-domain and obtain the Green's function we can use the Fourier transform.

$$G(t,r,r') = \frac{1}{2\pi}\int_{-\infty}^{+\infty} G(\omega,r,r')\exp(-i\omega t)d\omega \tag{5}$$

Then we can make the final step in our operations and obtain the expression for the discrete one-dimensional Green's function.

$$G(t,r,r') = \frac{\delta(t)\delta(r-r')}{\left(i\frac{\partial}{\partial t} - P^{-1}M\right)} \tag{6}$$

Similar procedures must be implemented to obtain the two- and the three-dimensional expressions to use in the full numerical modeling.

RESULTS

In order to demonstrate the FDTD method with discrete Green's functions we have modeled the process of the light propagation through the two-dimensional periodical structure of dielectric rods (two-dimensional PC). The results of this modeling after 1000 steps in time are presented in Fig. 1. The periodical structure is excited by a simple harmonic point source, which is situated at the left in Fig. 1 (white point). The discrete Green's functions here act both as the tool to define the characteristics of electromagnetic wave and as the absorbing boundary conditions (like Berenger's PML [5]) to limit the calculation space for the algorithm of the FDTD method. In addition, using the Green's functions we can obtain more accurate numerical results and test these results analytically [4].

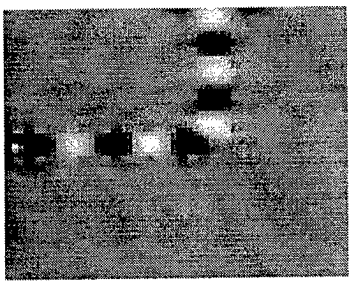


Fig.1

CONCLUSION

Thus, we have applied the FDTD method to calculate the Green's functions in a simple and straightforward way. From the Green's functions a whole range of other physical quantities can be found such as local DOS and electromagnetic field distribution in the PC's. In addition, the Green's functions can be act as the well absorbent boundary conditions for the FDTD method.

REFERENCES

[1] K. S. Yee, "Numerical Solution of Initial Boundary Value Problems Involving Maxwell's Equations," *IEEE Transactions Antennas and Propagation*, vol. AP-14, pp. 302-307, May 1966.

[2] K. Sakoda, *Optical Properties of Photonic Crystals*, Springer, 2001.

[3] W. H. Press et al., *Numerical Recipes in C. The Art of Scientific Computing.* Cambridge University Press, 1992.

[4] G. A. Korn, T. M. Korn, "Mathematical Handbook for Scientists and Engineers," McGraw-Hill, 1961.

[5] J. P. Berenger, "A perfectly matched layer for the absorption of electromagnetic waves," *J. Comput. Phys.*, vol. 114, pp. 185–200, Aug. 1994.

CALCULATION OF COMPLEXITY OF A PULSE TRANSFORMATION IN TIME-VARYING MEDIUM

N.N. Ruzhytska, A.G. Nerukh
Kharkiv National University of RadioElectronics,
14 Lenin Avenue, Kharkov, 61166, Ukraine. E-mail: rzhtsk@ums.kharkov.ua

D.A. Nerukh
Unilever Centre for Molecular Informatics, Department of Chemistry,
University of Cambridge, Lensfield Road, Cambridge, CB2 1EW, UK. E-mail:
dn232@cam.ac.uk

ABSTRACT

A complexity of electromagnetic signals transformed by a short sequence of cycles of medium parameters time changing is investigated. Dependence of the complexity on the modulation parameters is considered and a difference between forward and backward waves that are inevitable result of the medium time changing is shown.

INTRODUCTION

Interactions between electromagnetic pulses and semiconductor active media in waveguides are of significant importance in optical communication technology and time-domain techniques for solving such electromagnetic problems have received increased attention in the literature recently. Parametric phenomena in active media are especially important in optoelectronic systems as they allow controlling of electromagnetic signals by the temporal adjustment of the medium parameters. It is known that a single abrupt change of medium parameters leads to changing of a pulse shape [1-3]. The complexity of the phenomenon arises when only a few cycles of the modulation are considered that happens in ultrafast optics. In this paper a change of the complexity of the initial electromagnetic pulse $E_0(t,x)$ with a number of modulation cycles is considered. In the modulation cycles the permittivity receives constant magnitude ε_1 on the disturbance intervals of the cycles $(n-1)T < t < T_1 + (n-1)T$, $n = 1,...,N$ and the permittivity has constant magnitude ε on the quiescence intervals of the cycles $T_1 + (n-1)T < t < nT$, $n = 1,...,N$. Here, T is the duration of the cycle of the parame-ters change, T_1 is the duration of the disturbance interval of each cycle.

TRANSFORMATION OF THE PULSE AND ITS COMPLEXITY

Investigation of the pulse transformation is based on the Volterra integral equation method, which allows considering problems with arbitrary primary signal [4]. If the initial field has the form $E_0(t,x) = f(x - vt)$ then the transformed field is described by the following expressions: on the disturbance interval of the n-th cycle, $n > 1$ - $E_n(t,x) = E_n^{(+)}(t - x/v_1) + E_n^{(-)}(t + x/v_1)$, where

$$E_n^{(+)}(t-x/v_1)=$$
$$=\frac{a}{2}\left[(a+1)F_{n-1}^{(+)}(\frac{t-x/v_1}{a}-(a-1)(n-1)T)+(a-1)F_{n-1}^{(-)}(-\frac{t-x/v_1}{a}-(a+1)(n-1)T)\right] \tag{9}$$

$$E_n^{(-)}(t+x/v_1)=$$
$$=\frac{a}{2}\left[(a-1)F_{n-1}^{(+)}(-\frac{t+x/v_1}{a}-(a+1)(n-1)T)+(a+1)F_{n-1}^{(-)}(\frac{t+x/v_1}{a}+(a-1)(n-1)T)\right]$$

on the quiescent interval of the n-th cycle $F_n(t,x)=F_n^{(+)}(t-x/v)+F_n^{(-)}(t+x/v)$, where

$$F_n^{(+)}(t-x/v)=F_0(t-x/v)-$$
$$-\frac{1}{2a^2}\sum_{k=0}^{n-1}\left[(a+1)\left\{E_{k+1}^{(+)}(\frac{t-x/v}{a}+\frac{a-1}{a}(kT+T_1))-E_{k+1}^{(+)}(\frac{t-x/v}{a}+\frac{a-1}{a}kT)\right\}-\right.$$
$$\left.-(a-1)\left\{E_{k+1}^{(-)}(-\frac{t-x/v}{a}+\frac{a+1}{a}(kT+T_1))-E_{k+1}^{(-)}(-\frac{t-x/v}{a}+\frac{a+1}{a}kT)\right\}\right], \tag{10}$$

$$F_n^{(+)}(t+x/v)=$$
$$=\frac{-1}{2a^2}\sum_{k=0}^{n-1}\left[(a-1)\left\{E_{k+1}^{(+)}(-\frac{t+x/v}{a}+\frac{a+1}{a}(kT+T_1))-E_{k+1}^{(+)}(-\frac{t+x/v}{a}+\frac{a+1}{a}kT)\right\}-\right.$$
$$\left.-(a+1)\left\{E_{k+1}^{(-)}(\frac{t+x/v}{a}+\frac{a-1}{a}(kT+T_1))-E_{k+1}^{(-)}(\frac{t+x/v}{a}+\frac{a-1}{a}kT)\right\}\right]$$

In order to estimate how complex the transformed signals are we calculated the 'finite statistical complexity' measure of the signals [5, 6]. This approach of estimating the complexity of dynamical process rests on such well-known theories as Kolmogorov-Chaitin algorithmic complexity and Shannon entropy. This measure of complexity

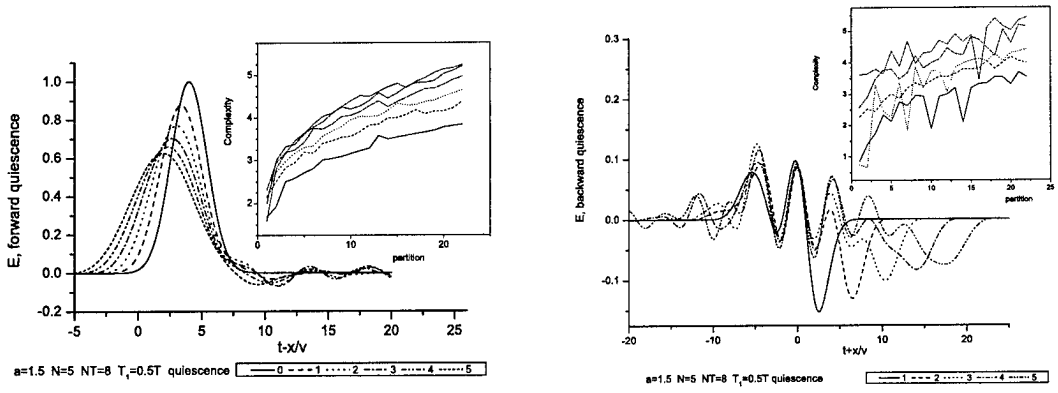


Fig. 1. Transformation of the pulse on the quiescent interval when the medium change beginning coincides with the beginning of the pulse, $a=\sqrt{\varepsilon/\varepsilon_1}$.

shows how much information is stored in the signal. It also indicates how much information is needed to predict the next value of the signal if we know all the values up

to some moment in time. The algorithm of computing the finite statistical complexity follows the method described in [7].

Dependence a signal shape and its complexity on the number of modulation cycled is shown in Fig. 1, 2. The complexity increases with the number of partitions and asymptotical behaviour at infinite number of partitions has a binary logarithm character [8].

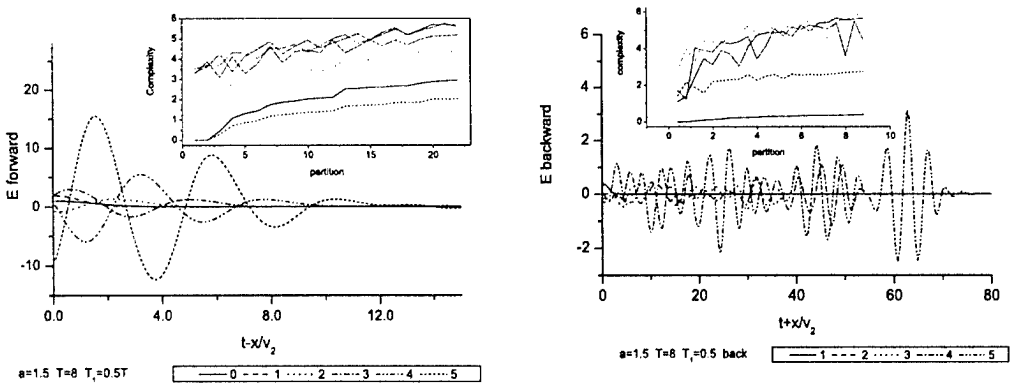


Fig. 2. Transformation of the pulse on the disturbed interval when the medium change beginning coincides with the pulse maximum.

CONCLUSION

Investigations show a strong transformation of the electromagnetic signal by only a short sequence of modulation cycles. Overall the complexity of the signals increases with the number of cycles. However, in those cases when the signals get narrower keeping their shape the complexity may decrease. The backward signals can be either more complex than the forward ones or less complex.

In many cases the calculated complexity allows to quantitatively estimate the relative informational contents of the signals. This is especially true in the situations when it is impossible to judge by eye either when the signals have simple and very similar shape or they are too complex to compare.

REFERENCES

[1] Morgenthaler F.R., *IRE Transactions MTT-6,* p. 167, 1958

[2] Ostrovsky L. A. and N.S. Stepanov, *Radiophysics Quantum Electronics (English transl.)*, **14**, pp. 489-529, 1971.

[3] Harfoush F.A. and A.Taflove, *IEEE Trans. On Antennas and Propag.*, **39**, pp. 898-906, 1991.

[4] Nerukh A.G., *J. of Physics D: Applied Physics*, **32**, pp. 2006-2013, 1999.

[5] Crutchfield J. P. and K. Young, *Phys. Rev. Lett.*, **63**, 105-108,. 1989.

[6] Crutchfield J. P., *Physica D*, **75**, 11, 1994.

[7] Perry N. and P.-M. Binder, *Phys. Rev. E*, **60**, 459, 1999.

[8] Cover T. M. and J.A. Thomas, *Elements of information theory*, John Wiley & Sons, Inc., 1991.

INVESTIGATION OF ELECTROMAGNETIC FIELD IN A PLATE-PARALLEL WAVEGIUDE WITH TIME VARYING MEDIUM

Nataliya Sakhnenko, Alexander Nerukh

Kharkov National University of Radio Electronics
14 Lenin Ave., Kharkov 61166, Ukraine

E-mail: nataliya_sakhnenko@rambler.ru

ABSTRACT

Investigations of an electromagnetic field in plasma resonator that appears in a waveguide at some moment of time is implemented using the Volterra integral equation approach .

INTRODUCTION

Time domain techniques for solving the electromagnetic problems have attracted increased attention in recent years. Some differential methods as well as integral ones for solving time domain problems are used. Here we use the Volterra integral equation approach for revealing physical features of electromagnetic oscillations in time varying plasma resonator. We consider a plate-parallel waveguide with perfectly conducting plates. At zero moment of time, homogeneous time-varying cold plasma appears inside a cylinder of some finite radius. The cylinder is perpendicular to waveguide walls and is co-axial with the source current that may have an arbitrary time dependence. The schematic diagram of the phenomenon is presented in Fig.1.

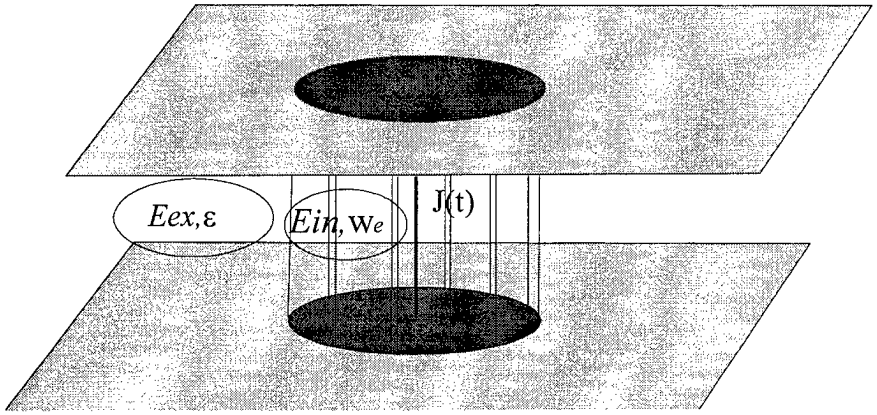


Fig.1

The electromagnetic field in time domain inside the cylinder as well as outside of it is determined by the integral equation that can be represented in an operator form in cylindrical coordinates

$$\vec{E} = \vec{E}_0 + \hat{K}\vec{E} \ , \ \hat{K} = \hat{\Phi}^{-1}\int_0^t dt' \int_0^{\rho_0} \rho' d\rho' \int_0^{2\pi} d\varphi' \int_0^b dz' \cdot \hat{G} \cdot \omega_e^2 \int_0^{t'} dt''(t'-t'')\hat{\Phi}E'(t'',\rho') \qquad (1)$$

where $\vec{E}_0$ is the initial field of the line emitter before plasma appearance, $\vec{E}$ is the transformed field caused by a medium time change. The integral operator $\hat{K}$ contains of

the Green's function that satisfies the boundary conditions on the waveguide walls [2] and medium operator that corresponds to the case of a plasma density ω_e changing from zero moment of time, ρ_0 is the radius of cylinder, matrix $\hat{\Phi}$ takes into account transformation of Cartesian vector components into the cylindrical system of coordinates.

Let us consider the excitation of the waveguide by step-harmonic current $\vec{j} = \frac{\delta(\rho)}{\rho} e^{i\omega_c t}\Theta(t-t_0)\vec{e}_z$, where t_0 is the moment of switching on the emitter. The initial field created by this source is a lowest-order transient waveguide mode, whose field does not depend on lateral coordinate z [3]. The frequency representation of the initial field has a form

$$F(\vec{E}_0) = \frac{2\pi b}{c^2}\vec{e}_z \cdot e^{-i\omega t_0} \cdot K_0(v\rho)\left\{-\omega_c \frac{\omega_c \cdot \cos(\omega_c t_0) + i\omega \sin(\omega_c t_0)}{\omega_c^2 - \omega^2} + \cos(\omega_c t_0)\right\},$$

where $v = \frac{i\omega}{c}$, c is a light velocity in vacuum, b is a distance between the waveguide plates, K_0 is modified Bessel function. It is the running wave that has the frequency ω_c and the spectrum is shown in Fig.2 by dash line. Notation $F(E) = \int_{-\infty}^{\infty} E(t)e^{-i\omega t}dt$ means the Fourier transform.

THE TRASFORMED FIELD INSIDE A PLASMA RESONATOR.

To obtain the transformed field inside the resonator it is necessary to find the solution of the integral equation (1). In time domain, it is the Volterra integral equation of the second kind and its solution can be built by the resolvent method [1]

$$\vec{E}_{in} = \vec{E}_0 + \hat{R}\vec{E}_0 \qquad (2)$$

The resolvent must satisfy the operator equation

$$\hat{R} - \hat{K}\hat{R} = \hat{K}, \qquad (3)$$

where K is the integral operator of (1). It is convenient to solve this equation in form of Fourier-Hankel-Laplace transform. The exact and explicit expression for the resolvent operator of the integral equation has been derived for the case when the plasma density changes in time abruptly [4].

The resolvent operator can be cast into sum of two terms. One of them corresponds to the problem, when the whole waveguide ($\rho_0 = \infty$) is filled with homogeneous plasma at zero moment of time. The second term takes a place only in the case of the finite radius of plasma cylinder and is caused by the presence of the cylinder boundary. The plasma appearance in the whole waveguide yields the composition of fields with frequencies of the current ω_c and of the plasma ω_e. The frequency representation of this field has a form

$$F(\vec{E}) = \frac{2\pi b}{c^2}\vec{e}_z \cdot e^{-i\omega t_0} \cdot K_0(\rho u)\left\{-\omega_c \frac{\omega_c \cdot \cos(\omega_c t_0) + i\omega \sin(\omega_c t_0)}{\omega_c^2 - \omega^2} + \cos(\omega_c t_0)\right\},$$

where $u = \frac{\sqrt{\omega_e^2 - \omega^2}}{c}$. The spectrum is shown in Fig.2 by solid line.

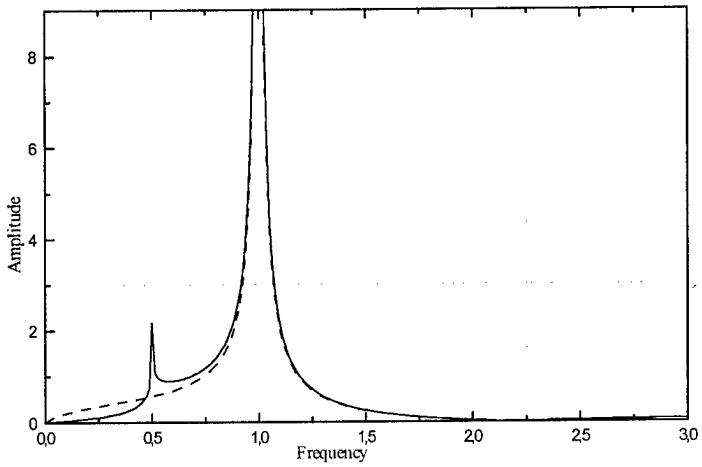


Fig.2

The frequency spectrum of the initial field (dash line), and the transformed field (plasma waveguide).

Here we used the dimensionless values: $\frac{\omega}{\omega_c}$ is dimensionless frequency (horizontal axis), $\frac{\omega_e}{\omega_c} = \frac{1}{2}$.

If the plasma appears only inside a cylinder of a finite radius then the frequency representation is described by the expression

$$F(\vec{E}_{in}) = \frac{2\pi b}{c^2}\vec{e}_z \cdot e^{-i\omega t_0} \cdot \left\{ -\omega_c \frac{\omega_c \cdot \cos(\omega_c t_0) + i\omega \sin(\omega_c t_0)}{\omega_e^2 - \omega^2} + \cos(\omega_c t_0) \right\} \times$$

$$\times \left\{ \frac{uK_1(u\rho_0)K_0(v\rho_0) - vK_0(u\rho_0)K_1(v\rho_0)}{uI_1(u\rho_0)K_0(v\rho_0) + vK_1(v\rho_0)I_0(u\rho_0)} I_0(\rho u) + K_0(\rho u) \right\}.$$

The lateral walls add new frequencies determined by the radius of the cylinder.

REFERENCES

[1] A.G. Nerukh, I. V. Scherbatko, M. Marciniak. Electromagnetics of Modulated Media with Applications to Photonics. Warsaw 2001.

[2] N. Sakhnenko, A. Nerukh, "Transient Axially Symmetric Radiation of Source in a Plane Waveguide", *Kharkov National University Digest*, special issue on Radio-Physics & Electronics, KNU Press, № 467, 2000, pp. 144-147 (in Russian).

[3] N. Sakhnenko, A. Nerukh, "Electromagnetic field transformation caused by plasma creation in flat waveguide", *Proc. Int. Symp. MSMW-01*, Kharkov, 2001.

[4] N. Sakhnenko, A. Nerukh "Transformation of radiation by appearance of a cylindrical plasma inclusion in a waveguide"Proc. Int. Conf. ICTON 2002, Warsaw 2002.

DIRECT STUDY OF FIELDS AND RADIATION PATTERNS OF ANTENNAS WITH THE ACCOUNT OF CLOSELY LOCATED OBJECTS

Vasiliy A. Ruchenkov, Constantin N. Klimov, Boris V. Sestroretsky *, Maria A. Drize* and Yuriy P. Bolshakov **

Moscow State Institute of Electronics and Mathematics, Bolshoy Trechsvytitelsky lane 3/12, Moscow 109028, Russia, ph. (095)-916-88-17, E-mail: const0@online.ru
* Lavochkin Association, Leningradskay st. 24, Chimki-2 Moscow Area 141400, Russia, ph. (095)-575-50-69, E-mail: const0@online.ru
** KB LIRA, Dmitrovskay hw. 110, Moscow 127411, Russia, ph. (095)-777-75-98, E-mail: lira@tsr.ru

ABSTRACT

Gain-phase distributions of an electromagnetic field and the radiation patterns horn antenna for planar tasks, horn antenna in a combination to the various close located objects are submitted. The problem was solved in time area, then by means of Fourier transformation was translated in frequency. The task solution in time area allows to analyze objects with the sizes 500x500 wave-length with step of digitization of 1/20 wave-length (100 million units of a grid) on the personal computer with operative memory 2Gb. The example of the analysis of distortions of the radiation patterns by the phased array obstacles and objects is given.

INTRODUCTION

For 2D the electromagnetic analysis of tasks of dispersion in time area effective procedures and programs were developed [1,2]. At research of antennas and objects the classical characteristics describing their properties, radiation patterns or the scattering graph are. Such characteristics describe objects in stationary modes, i.e. in frequency areas. Therefore it is necessary, preliminary having solved a task in time area, then, using Fourier transformation to translate it in frequency area and to find gain-phase distribution of fields from which by means of the equivalence theorem and Grin's function it is possible to calculate the radiation patterns of all system as a whole..

WAVEGUIDE HORN

The similar research was by us carried out with the help of a program complex Tamic Planar Rt-H Analyzer [3] for 2D of a task waveguide of a horn represented on fig.1 on frequency 10 GHz.
In a fig. 2, 3 the designed amplitude distributions of an electrical field, perpendicular planes of figure and diagrams, appropriate to them, of an orientation are represented at the following meanings of permittivity of the cylinder: $\varepsilon = 0$ (Fig.2), $\varepsilon = -1$ (Fig.3).

ANTENNAS ARRAY

Similarly with use of a program complex Tamic Planar Rt-H Analyzer the influence on the radiation patterns by the antennas array close located metal and dielectric of objects was investigated. Considered antennas array consists of 5 elements, with amplitude

distribution cosines on a pedestal, and the phase distribution is those, that the main maximum is directed under 18 degrees. Length of a array makes 2.5 lengths of a wave. The radiation patterns by the antennas array is shown by a continuous line on fig.5.

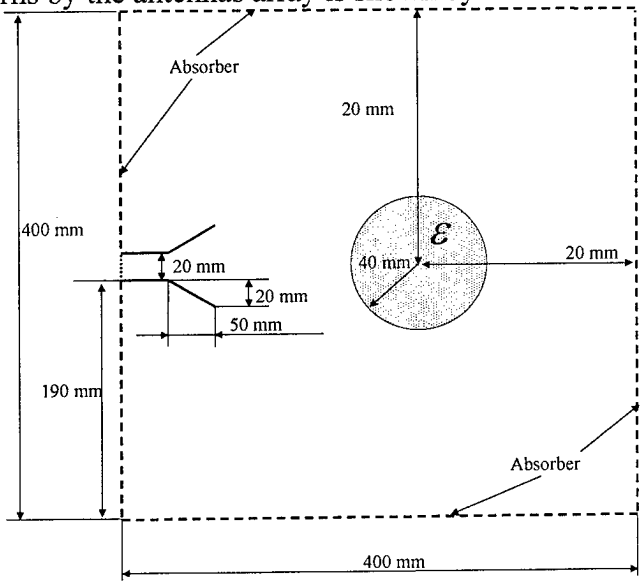


Fig.1 Geometry of H – plane waveguide horn with the dielectric cylinder.

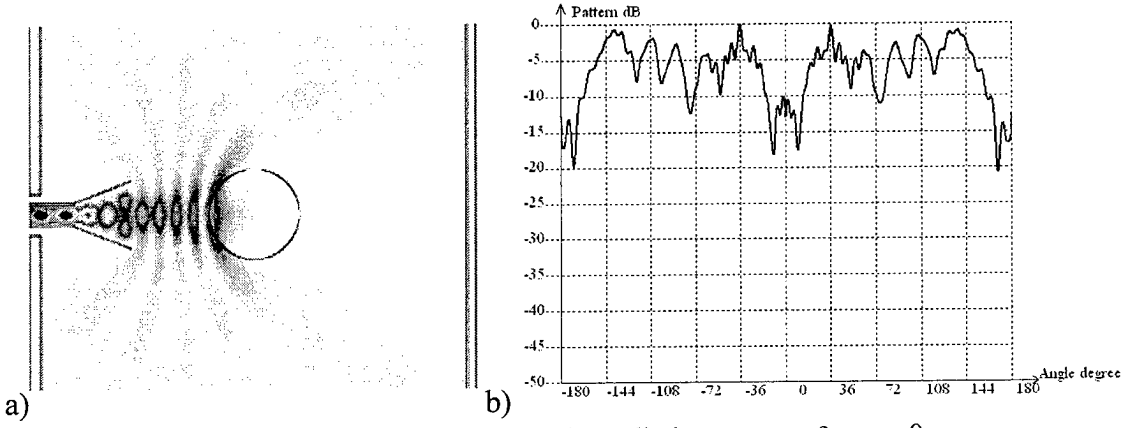


Fig.2 a)-amplitude distribution, b)–radiation patterns for $\varepsilon = 0$.

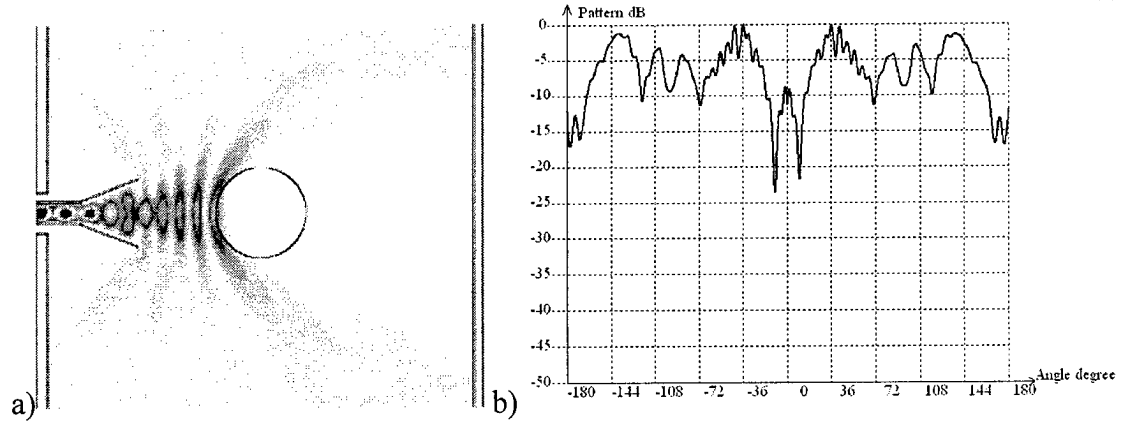
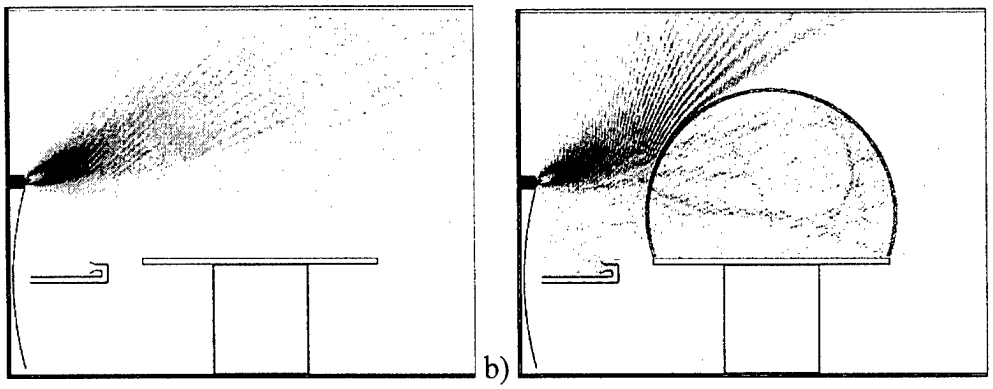
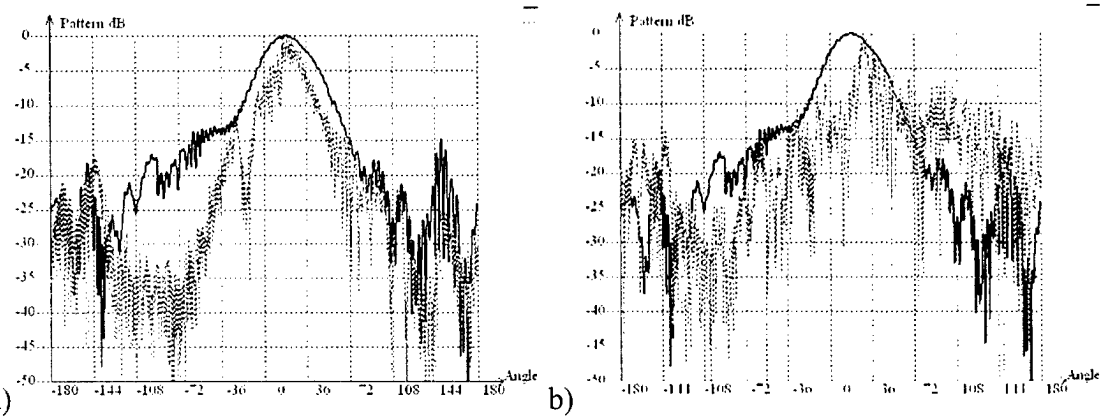


Fig.3 a)-amplitude distribution, b)–radiation patterns for $\varepsilon = -1$.



a) b)

Fig.4 amplitude distribution a) antennas array with metal body's, b) antennas array with metal and dielectric body's.



a) b)

Fig.5 Change radiation patterns of antennas array for geometry with a) metal body's b) metal and dielectric body's.

On fig.4 a) the distribution of amplitude of an electrical field is shown, if near to the antennas array locates metal objects. The metal objects are a cut of the mirror antennas with tracts and support for other antennas. The size of analyzed area makes 98.735 on 76.52 of lengths of waves. The analysis was carried out with a step of a grid of 1/16.2 lengths of a wave. The grid is consisting of 1'989'684 of nodes. On fig.5 a) the radiation patterns by the antennas array with metal objects by a dashed line is represented. On fig.4 b) the distribution of amplitude of an electrical field is shown, if on a metal support is present in addition dielectric protection. On fig.5 b) the radiation patterns by the antennas array with dielectric protection by a dashed line is represented.

REFERENCES

[1]. *Klimov C.N., Sestroretzkiy B.V.* // Journal of communications technology and electronics. Vol. 46, 2001, N 1, p. 24.

[2]. *Klimov C.N., Sestroretzkiy B.V.* // Journal of communications technology and electronics. Vol. 46, 2001, N 4, p.359.

[3]. *Klimov C.N., Sestroretzkiy B.V.* // Journal of communications technology and electronics. Vol. 46, 2001, N 3, p.247.

ELECTROMAGNETIC SIGNALS IN A WAVEGUIDE FILLED WITH AN INHOMOGENEOUS TIME-VARIANT MEDIUM

A.Yu. Butrym, O.A. Tretyakov

Karazin Kharkov National University, 4 Svobody sq., Kharkov, Ukraine
e-mail: Alexander.Yu.Butrym@univer.kharkov.ua

The problem of arbitrary signal propagation in inhomogeneously filled waveguides (with factorized permittivity and permeability $\varepsilon = \varepsilon_\perp(x,y)\cdot\varepsilon_\parallel(z,t)$) is solved by partial separation of variables in the Time Domain (the Evolutionary Waveguide Equations Approach [1-2]). We introduce two self-adjoined operators containing $\varepsilon_\perp, \mu_\perp$ and transversal derivatives and then the electromagnetic field is expanded into series on eigenmodes of these operators with dependent on z and t modal coefficients sought for. Such an approach allows to consider time-variant and nonlinear media as well. Assuming time-harmonic signal one can use this technique to find dispersion characteristic of the waveguide without any need to solve the boundary problem for every frequency [3-4] (lossy media can be treated in this way without extra difficulties). After some generalization this approach can be applied to fiber optics (dielectric waveguides).

PROBLEM STATEMENT

We consider a waveguide with closed singly connected cross-section of PEC surface and loaded with a medium for which $\varepsilon = \varepsilon_\perp(x,y)\cdot\varepsilon_\parallel(z,t)$, $\mu = \mu_\perp(x,y)\cdot\mu_\parallel(z,t)$, $\sigma = \sigma(r,t)$. After expressing H_z and E_z in terms of transverse components $\boldsymbol{H}$ and $\boldsymbol{E}$:

$$\begin{aligned} &\partial_z(\mu H_z) = -\nabla_t\cdot\mu\boldsymbol{H} \qquad \partial_t(\mu_0\mu H_z) = [\nabla_t\times\mathbf{z}_0]\cdot\boldsymbol{E} \\ &\partial_z(\varepsilon E_z) = -\nabla_t\cdot\varepsilon\boldsymbol{E} + \tfrac{1}{\epsilon_0}\rho \quad \partial_t(\varepsilon_0\varepsilon E_z) = [\mathbf{z}_0\times\nabla_t]\cdot\boldsymbol{H} - j_z \end{aligned} \tag{1}$$

we can exclude them from the Maxwell's equations. It yields (in operator form):

$$\begin{aligned} W_H X &= \begin{pmatrix} \frac{1}{\mu_\parallel}\partial_z\mu_\parallel\left\{\partial_t\varepsilon_\parallel\boldsymbol{E} + \partial_z\frac{1}{\varepsilon_\perp}[\boldsymbol{H}\times\mathbf{z}_0]\right\} + \frac{1}{\varepsilon_\perp\mu_\parallel}\partial_z\mu_\parallel\boldsymbol{j} \\ -\partial_t\mu_\parallel\left\{\partial_t\varepsilon_\parallel\varepsilon_\perp[\mathbf{z}_0\times\boldsymbol{E}] + \partial_z\boldsymbol{H}\right\} - \partial_t\mu_\parallel[\mathbf{z}_0\times\boldsymbol{j}] \end{pmatrix} \\ W_E X &= \begin{pmatrix} -\partial_t\varepsilon_\parallel\left\{\partial_z\boldsymbol{E} + \partial_t\mu_\parallel\mu_\perp[\boldsymbol{H}\times\mathbf{z}_0]\right\} - \nabla_t\frac{1}{\varepsilon_\perp}j_z \\ \frac{1}{\varepsilon_\parallel}\partial_z\varepsilon_\parallel\left\{\partial_z\frac{1}{\varepsilon_\perp}[\mathbf{z}_0\times\boldsymbol{E}] + \partial_t\mu_\parallel\boldsymbol{H}\right\} + \frac{1}{\mu_\perp}[\nabla_t\frac{1}{\varepsilon}\rho\times\mathbf{z}_0] \end{pmatrix} \end{aligned}, \tag{2}$$

where $X = \mathrm{col}(\boldsymbol{E},\boldsymbol{H})$ is a 4-dimensinal vector sought, $\boldsymbol{j} = \boldsymbol{j}_0 + \boldsymbol{j}_\sigma$ is a sum of given currents and conductivity currents. We have introduced here the following operators:

$$\begin{aligned} W_H X &= \begin{pmatrix} 0 & [\mathbf{z}_0\times\frac{1}{\varepsilon_\perp}\nabla_t\frac{1}{\mu_\perp}]\nabla_t\cdot\mu_\perp \\ \nabla_t\frac{1}{\mu_\perp}[\mathbf{z}_0\times\nabla_t]\cdot & 0 \end{pmatrix}\begin{pmatrix}\boldsymbol{E}\\ \boldsymbol{H}\end{pmatrix} = \begin{pmatrix} [\mathbf{z}_0\times\frac{1}{\varepsilon_\perp}\nabla_t\frac{1}{\mu_\perp}]\nabla_t\cdot\mu_\perp\boldsymbol{H} \\ \nabla_t\frac{1}{\mu_\perp}[\mathbf{z}_0\times\nabla_t]\cdot\boldsymbol{E} \end{pmatrix} \\ W_E X &= \begin{pmatrix} 0 & \nabla_t\frac{1}{\varepsilon_\perp}[\nabla_t\times\mathbf{z}_0]\cdot \\ [\frac{1}{\mu_\perp}\nabla_t\frac{1}{\varepsilon_\perp}\times\mathbf{z}_0]\nabla_t\cdot\varepsilon_\perp & 0 \end{pmatrix}\begin{pmatrix}\boldsymbol{E}\\ \boldsymbol{H}\end{pmatrix} = \begin{pmatrix} \nabla_t\frac{1}{\varepsilon_\perp}[\nabla_t\times\mathbf{z}_0]\cdot\boldsymbol{H} \\ [\frac{1}{\mu_\perp}\nabla_t\frac{1}{\varepsilon_\perp}\times\mathbf{z}_0]\nabla_t\cdot\varepsilon_\perp\boldsymbol{E} \end{pmatrix} \end{aligned} \tag{3}$$

These operators are self-adjoined in the Hilbert space $L_2^4(S,q)$ with an inner product:

$$\begin{aligned} &\langle X_1, X_2\rangle = \tfrac{1}{2S}\int_S(\varepsilon_\perp\boldsymbol{E}_1\cdot\boldsymbol{E}_2 + \mu_\perp\boldsymbol{H}_1\cdot\boldsymbol{H}_2)\,dS; \qquad 2\langle X_1, X_2\rangle = \langle\boldsymbol{E}_1,\boldsymbol{E}_2\rangle_e + \langle\boldsymbol{H}_1,\boldsymbol{H}_2\rangle_h \\ &\langle\boldsymbol{E}_1,\boldsymbol{E}_2\rangle_e = \tfrac{1}{S}\int_S\varepsilon_\perp\boldsymbol{E}_1\cdot\boldsymbol{E}_2\,dS, \qquad \langle\boldsymbol{H}_1,\boldsymbol{H}_2\rangle_h = \tfrac{1}{S}\int_S\mu_\perp\boldsymbol{H}_1\cdot\boldsymbol{H}_2\,dS. \end{aligned} \tag{4}$$

MODAL BASIS

Due to the self-adjointness of the introduced operators we can set the eigenvalue boundary problems for these operators and state that the eigenvectors obtained are orthogonal:

$$\begin{aligned} &W_H Y_m = p_m Y_m, \quad Y_m = \mathrm{col}\left(\boldsymbol{E}'_m, \boldsymbol{H}'_m\right); \quad \left\langle Y_m, Y_{m'}\right\rangle = \delta_{mm'}; \\ &W_E Z_n = q_n Z_n, \quad Z_n = \mathrm{col}\left(\boldsymbol{E}''_n, \boldsymbol{H}''_n\right), \quad \left\langle Z_n, Z_{n'}\right\rangle = \delta_{nn'}. \end{aligned} \tag{5}$$

It can be proved that $W_H Z_n = 0 = W_E Y_m$,i.e. $\{Z_n\} \subset \ker W_H$, $\{Y_m\} \subset \ker W_E$, $\left\langle Y_m, Z_n\right\rangle = 0$. Let us denote the value space of W_E by $= \{Z_n\}$ (it corresponds to TM or E-waves for the case of hollow waveguide) and similarly we denote the value space of W_H by $= \{Y_n\}$ (it corresponds to TE or H-waves for the case of hollow waveguide). It turned out that for the singly-connected cross-section these two eigenmodes sets originate a basis in the solution space: $L_2^4(S,q) = \quad \oplus \quad = \{Y_m\} \cup \{Z_n\}$. Therefore we can expand the fields sought in series on this basis, it yields:

$$X = \sum_{\substack{m=-\infty \\ m\neq 0}}^{\infty} A'_m(z,t) Y_m + \sum_{\substack{n=-\infty \\ n\neq 0}}^{\infty} A''_n(z,t) Z_n, \quad \text{or} \quad \begin{aligned} \boldsymbol{E} &= \sum_{m=1}^{\infty} e'_m(z,t)\boldsymbol{E}'_m + \sum_{n=1}^{\infty} e''_n(z,t)\boldsymbol{E}''_n, \\ \boldsymbol{H} &= \sum_{m=1}^{\infty} h'_m(z,t)\boldsymbol{H}'_m + \sum_{n=1}^{\infty} h''_n(z,t)\boldsymbol{H}''_n. \end{aligned} \tag{6}$$

The boundary eigenvalue problems (5) can be rewritten in a vector form:

$$\begin{cases} [\mathbf{z}_0 \times \frac{1}{\varepsilon_\perp}\nabla_t \frac{1}{\mu_\perp}]\nabla_t \cdot \mu_\perp \boldsymbol{H}'_m = p_m \boldsymbol{E}'_m, \\ \nabla_t \frac{1}{\mu_\perp}[\mathbf{z}_0 \times \nabla_t] \cdot \boldsymbol{E}'_m = p_m \boldsymbol{H}'_m, \end{cases} \quad \begin{cases} \nabla_t \frac{1}{\varepsilon_\perp}[\nabla_t \times \mathbf{z}_0] \cdot \boldsymbol{H}''_n = q_n \boldsymbol{E}''_n, \\ [\frac{1}{\mu_\perp}\nabla_t \frac{1}{\varepsilon_\perp} \times \mathbf{z}_0]\nabla_t \cdot \varepsilon_\perp \boldsymbol{E}''_n = q_n \boldsymbol{H}''_n, \end{cases} \quad \begin{cases} \cdot \boldsymbol{E}\big|_L, \\ \mathbf{n} \cdot \boldsymbol{H}\big|_L. \end{cases} \tag{7}$$

It admits introducing scalar potentials in the following way:

$$\begin{aligned} \boldsymbol{H}'_m &= \nabla_t \Psi'_m \\ \boldsymbol{E}'_m &= \frac{1}{\varepsilon_\perp}\left[\nabla_t \Phi'_m \times \mathbf{z}_0\right] \end{aligned} \quad \begin{cases} \nabla_t \cdot \frac{1}{\varepsilon_\perp}\nabla_t \Phi'_m + p_m \mu_\perp \Psi'_m = 0 & \frac{\partial}{\partial \mathbf{n}}\Psi'_m\big|_L = 0 \\ \nabla_t \cdot \mu_\perp \nabla_t \Psi'_m + p_m \mu_\perp \Phi'_m = 0 & \frac{\partial}{\partial \mathbf{n}}\Phi'_m\big|_L = 0 \end{cases} \tag{8}$$

$$\begin{aligned} \boldsymbol{E}''_n &= \nabla_t \Psi''_n \\ \boldsymbol{H}''_n &= \frac{1}{\mu_\perp}\left[\mathbf{z}_0 \times \nabla_t \Phi''_n\right] \end{aligned} \quad \begin{cases} \nabla_t \cdot \frac{1}{\mu_\perp}\nabla_t \Phi''_n + q_n \varepsilon_\perp \Psi''_n = 0 & \Psi''_n\big|_L = 0 \\ \nabla_t \cdot \varepsilon_\perp \nabla_t \Psi''_n + q_n \varepsilon_\perp \Phi''_n = 0 & \Phi''_n\big|_L = 0 \end{cases} \tag{9}$$

EVOLUTIONARY EQUATIONS

Projecting (2) on the basis obtained yields a system of governing equations for the modal amplitudes which are obtained as partial differential equations with ∂_t and ∂_z derivatives: i.e. they are *the Evolutionary Equations* (EE). We introduce the following notation for coupling coefficients and sums in EE describing intermodal transformation:

$$L_{mm'} = \frac{1}{S}\int_S \mathbf{z}_0 \cdot [\boldsymbol{E}_m \times \boldsymbol{H}_{m'}]dS; \quad K_{mm'} = \frac{1}{S}\int_S \varepsilon_\perp \mu_\perp \mathbf{z}_0 \cdot [\boldsymbol{E}_m \times \boldsymbol{H}_{m'}]dS \tag{10}$$

$$\sum_{m',n'} \begin{matrix} e'_{m'} \\ e''_{n'} \end{matrix} K_{\begin{matrix} m' \\ n' \end{matrix} \begin{matrix} m \\ m \end{matrix}} = \sum_{m'} e'_{m'} K_{m'm} + \sum_{n'} e''_{n'} K_{n'm} \quad \sum_{m',n'} \begin{matrix} h'_{m'} \\ h''_{n'} \end{matrix} L_{\begin{matrix} m \\ m' \end{matrix} \begin{matrix} m' \\ n' \end{matrix}} = \sum_{m'} h'_{m'} L_{mm'} + \sum_{n'} h''_{n'} L_{mn'} \quad \ldots \tag{11}$$

In this notation the EE look like:

$$\begin{cases} \partial_t \mu_\parallel \partial_t \varepsilon_\parallel \sum_{m',n'} \begin{matrix} e'_{m'} \\ e''_{n'} \end{matrix} K_{\begin{matrix} m' \\ n' \end{matrix} \begin{matrix} m \\ m \end{matrix}} + \partial_t \mu_\parallel \partial_z h'_m + p_m e'_m = \gamma_1; \quad \partial_t \varepsilon_\parallel \partial_t \mu_\parallel \sum_{m',n'} \begin{matrix} h'_{m'} \\ h''_{n'} \end{matrix} K_{\begin{matrix} m \\ n \end{matrix} \begin{matrix} m' \\ n' \end{matrix}} + \partial_t \varepsilon_\parallel \partial_z e''_n + q_n h''_n = \gamma_3; \\ \partial_z \mu_\parallel \partial_t \varepsilon_\parallel e'_m + \partial_z \mu_\parallel \partial_z \sum_{m',n'} \begin{matrix} h'_{m'} \\ h''_{n'} \end{matrix} L_{\begin{matrix} m \\ m' \end{matrix} \begin{matrix} m' \\ n' \end{matrix}} - \mu_\parallel p_m h'_m = \gamma_2; \partial_z \varepsilon_\parallel \partial_t \mu_\parallel h''_n + \partial_z \varepsilon_\parallel \partial_z \sum_{m',n'} \begin{matrix} e'_{m'} \\ e''_{n'} \end{matrix} L_{\begin{matrix} m' \\ n' \end{matrix} \begin{matrix} m \\ n \end{matrix}} - \varepsilon_\parallel q_n e''_n = \gamma_4. \end{cases} \tag{12}$$

where the RHS express via currents and charges (both given and conductivity ones):

$$\gamma_1 = -\partial_t \mu_{\|} \tfrac{1}{S} \int_S \mu_\perp \boldsymbol{j} \cdot [\boldsymbol{H}'_m \times \mathbf{z}_0] dS; \quad \gamma_3 = -\tfrac{1}{S} \int_S \varepsilon_\perp \left(\nabla_t \tfrac{1}{\varepsilon_\perp} j_z \right) \cdot \boldsymbol{E}''_n \, dS;$$
$$\gamma_2 = -\partial_z \mu_{\|} \tfrac{1}{S} \int_S \boldsymbol{j} \cdot \boldsymbol{E}'_m \, dS; \qquad \gamma_4 = -\tfrac{1}{S} \int_S \left(\nabla_t \tfrac{1}{\varepsilon_\perp} \rho \right) \cdot [\mathbf{z}_0 \times \boldsymbol{H}''_n] dS. \tag{13}$$

The coupling coefficients can be expressed via scalar potentials in a convenient form:

$$L_{mm'} / p_m = L_{m'm} / p_{m'} = \tfrac{1}{S} \int_S \mu_\perp \Psi'_m \Psi'_{m'} \, dS \quad L_{nn'} / q_{n'} = L_{n'n} / q_n = \tfrac{1}{S} \int_S \varepsilon_\perp \Psi''_n \Psi''_{n'} \, dS$$
$$K_{mm'} / p_{m'} = K_{m'm} / p_m = \tfrac{1}{S} \int_S \mu_\perp \Phi'_m \Phi'_{m'} \, dS \quad K_{nn'} / q_n = K_{n'n} / q_{n'} = \tfrac{1}{S} \int_S \varepsilon_\perp \Phi''_n \Phi''_{n'} \, dS \tag{14}$$

SOME CONCLUSIONS

1) The basis vector eigenfunctions (7) don't correspond to any of modes used in the Frequency Domain methods such as [3-4]. It can be easily checked on the simplest case of rectangular waveguide with slab. For this case after separating one variable: $D_x^2 \Psi'_{nm} = -\kappa_n^2 \Psi'_{nm}$, we obtain a fourth-order equation for every partial domain: $D_y^4 \Psi'_{nm} - 2\kappa_n^2 D_y^2 \Psi'_{nm} + \left(\kappa_n^4 - \varepsilon_i p_{nm}^2 \right) \Psi'_{nm} = 0$ with 4 boundary conditions on the interface: Ψ'_{nm}, $D_y \Psi'_{nm}$, $D_y^2 \Psi'_{nm}$, $\frac{1}{\varepsilon_\perp} \left(\kappa_n^2 D_y - D_y^3 \right) \Psi'_{nm}$ should be continuous.

2) It can be shown that for the case $\varepsilon_\perp \mu_\perp = \text{const}$ the equality $\Phi = \Psi$ holds and all the non-diagonal coupling coefficients vanish. It means that we have a single mode propagation case, i.e. the transversal configuration of the field remains the same while propagating along waveguide for arbitrary time dependence of the signal.

3) The method was verified on the harmonic signal propagation problem. Assuming harmonic dependence $\exp(i\omega t - i\beta z)$ of modal coefficients we obtain a SLAE instead of differential EE. ($\varepsilon_{\|} = 1 = \mu_{\|}$ should be assumed):

$$\begin{cases} -\omega^2 \varepsilon_0 \mu_0 \sum\limits_{m',n'} \dfrac{e'_{m'}}{e''_{n'}} K_{\substack{m'm \\ n'm}} + \omega\beta\mu_0 h'_m + p_m e'_m = 0; & -\omega^2 \varepsilon_0 \mu_0 \sum\limits_{m',n'} \dfrac{h'_{m'}}{h''_{n'}} K_{\substack{nm' \\ nm'}} + \omega\beta\varepsilon_0 e''_n + q_n h''_n = 0; \\ \omega\beta\varepsilon_0 e'_m - \beta^2 \sum\limits_{m',n'} \dfrac{h'_{m'}}{h''_{n'}} L_{\substack{m'm \\ m'n'}} - p_m h'_m = 0; & \omega\beta\mu_0 h''_n - \beta^2 \sum\limits_{m',n'} \dfrac{e'_{m'}}{e''_{n'}} L_{\substack{m'n \\ n'n}} - q_n e''_n = 0. \end{cases} \tag{15}$$

To obtain dispersion characteristics for the waveguide one have to solve this homogeneous system. Note that dispersion equation is a polynomial for any $\varepsilon_\perp$, its roots can be found easily with well-known techniques. It can be an alternative to methods [3,4]

4) Taking conductivity $\sigma(x, y)$ into consideration gives sums in RHS of (15) due to integrals from expansion series in (13). It doesn't complicate the problem.

REFERENCES

[1] O.A. Tretyakov *Evolutionary waveguide equations*, Radiotekhnika i Elektronika, vol.34, No.5, 1989 (in Russian). English translation in Soviet J. on Communication Technology and Electronics, 1989.

[2] O.A. Tretyakov, *The Evolutionary Approach to Analytical Study of Electromagnetic Phenomena in the Time Domain*, 2001 URSI International Symposium on Electromagnetic Theory, May 13-17, 2001, Victoria, Canada.

[3] P. Przybyszewski et al. *A New Class of Eigenfunction Expansion Methods for Fast Frequency-Domain Analysis of Waveguides*, IEEE Trans. on MTT, vol.50, No.2, February 2002.

[4] E. Silvestre et al. *Analysis of Inhomogeneously Filled Waveguides Using a Bi-Orthonormal-Basis Method*, IEEE Trans. on MTT, vol.48, No.4, April 2000.

ACCURATE "ABSORBING" CONDITIONS FOR NONSINUSOIDAL PROBLEMS OF DIFFRACTION FOR COMPACT OBJECTS

A.I. Vyazmitinova

Institute of Radiophysics and Electronics, Kharkov, Ukraine

vigor@ire.kharkov.ua

In the time domain the use of versatile finite-difference algorithms [1] allows one to solve efficiently the problems of analysis and model synthesis providing the following principle requirements are fulfilled. First, the analysis domain for the relevant original open boundary value problems should be restricted by exact "absorbing" conditions, which do not distort the physical processes simulated mathematically. Second, all mathematical constructions should be adequate for discretizing the problems (equations and all conditions) in rectangular coordinates with optimal and equal approximation error [2].

The paper reviews work on algorithmization of initial boundary value problems in the theory of periodic, waveguide; specifically, the case in point is simulation of transient processes in pulse radiators. In this paper we give formulations of the initial boundary value problems and basic results for class of antennas with gratings as dispersing elements.

The initial boundary value problem

$$\begin{cases} \left[-\varepsilon(g)\dfrac{\partial^2}{\partial t^2}-\sigma(g)\dfrac{\partial}{\partial t}+\dfrac{\partial^2}{\partial z^2}+\dfrac{\partial^2}{\partial y^2}\right]U(g,t)=F(g,t), \\ t>0, \quad g=\{y,z\}\in Q=R^2, \\ U(g,t)\big|_{t=0}=\varphi(g), \quad \dfrac{\partial}{\partial t}U(g,t)\Big|_{t=0}=\psi(g), \\ U(g,t)=E_x, \quad \dfrac{\partial}{\partial t}H_y=-\dfrac{1}{\eta_0}\dfrac{\partial}{\partial z}E_x, \quad \dfrac{\partial}{\partial t}H_z=\dfrac{1}{\eta_0}\dfrac{\partial}{\partial y}E_x, \quad E_y=E_z=H_x\equiv 0 \end{cases} \tag{1}$$

describes the radiation, propagation, and scattering processes of nonsinusoidal E-polarized waves in the space $R^2=\{g=\{y,z\}:|y|<\infty,|z|<\infty\}$. The inhomogeneities are given by the real finite functions $\sigma(g)=\sigma_0(g)\eta_0$ and $\varepsilon(g)$ ($\sigma_0(g)$ is the specific conductivity, $\eta_0=(\mu_0/\varepsilon_0)^{1/2}$ is the impedance of a free space, and $\varepsilon(g)$ is the relative permittivity). The time, t, in (1) has the dimensionality of length; it is the product of the actual time by the propagation velocity of the excitation in free space.

Let us assume that the functions F, φ, ψ, σ, and $\varepsilon-1$ are finite in Q and that their supports belong to domain $Q_L=\{g\in Q: L_4<y<L_3; L_2<y<L_1\}$ for all times considered ($0<t<T$). Then, above (below, to the right, to the left) the virtual

boundary $z = L_1$ ($z = L_2$, $y = L_3$, $y = L_4$) there are no sources and scatterers. Therefore in the domain ${}_L Q = Q \setminus \overline{Q_L}$ the function U corresponds to the outgoing wave, crossing the relevant boundary in one direction only, and satisfies the homogeneous problem (1) with $\varepsilon - 1 = \sigma = 0$. This fact makes possible to state (for each boundary) the radiation conditions for U, resulting immediately from (1), and then to use these conditions when narrowing the analysis domain down to half-space in problem (1). Using four conditions simultaneously and solving exactly the problem of corner points arising therewith (points of intersection of the lines $z = L_1$ and $y = L_3$, and $y = L_3$, $z = L_1$ and $y = L_4$, $z = L_2$ and $y = L_4$), we are led to the rectangular analysis domain Q_L. As result, we have

$$\begin{cases} \left[\dfrac{\partial}{\partial t} \pm \dfrac{\partial}{\partial z}\right] U(g,t) = \dfrac{2}{\pi} \displaystyle\int_0^{\pi/2} \dfrac{\partial V_1(g,t)}{\partial t} \sin^2 \varphi d\varphi, \quad z = \begin{cases} L_1 \\ L_2 \end{cases} \\ \left[\dfrac{\partial^2 V_1(g,t,\varphi)}{\partial t^2} - \dfrac{\partial W_1(g,t,\varphi)}{\partial y^2}\right] = 0, \quad \left.\dfrac{\partial V_1(g,t,\varphi)}{\partial t}\right|_{t=0} = V_1(g,t,\varphi)\big|_{t=0} = 0, \\ W_1(g,t,\varphi) = V_1(g,t,\varphi)\cos^2\varphi + U(g,t) \end{cases} \tag{2}$$

$$\begin{cases} \left[\dfrac{\partial}{\partial t} \pm \cos\varphi \dfrac{\partial}{\partial y}\right] W_1(g,t,\varphi) = \dfrac{2\cos\varphi}{\pi} \displaystyle\int_0^{\pi/2} \dfrac{\sin^2\gamma}{\cos^2\varphi + \sin^2\varphi\cos^2\varphi} \dfrac{\partial W_2(g,t,\gamma)}{\partial t} \sin^2 d\gamma, \\ z = \begin{cases} L_3 \\ L_4 \end{cases} \\ \left[\dfrac{\partial}{\partial t} \pm \cos\varphi \dfrac{\partial}{\partial z}\right] W_2(g,t,\varphi) = \dfrac{2\cos\varphi}{\pi} \displaystyle\int_0^{\pi/2} \dfrac{\sin^2\gamma}{\cos^2\varphi + \sin^2\varphi\cos^2\varphi} \dfrac{\partial W_1(g,t,\gamma)}{\partial t} \sin^2 d\gamma, \\ z = \begin{cases} L_1 \\ L_2 \end{cases} \end{cases} \tag{3}$$

$$\begin{cases} \left[\dfrac{\partial}{\partial t} \pm \dfrac{\partial}{\partial y}\right] U(g,t) = \dfrac{2}{\pi} \displaystyle\int_0^{\pi/2} \dfrac{\partial V_2(g,t,\varphi)}{\partial t} \sin^2 \varphi d\varphi, \quad z = \begin{cases} L_3 \\ L_4 \end{cases} \\ \left[\dfrac{\partial^2 V_2(g,t,\varphi)}{\partial t^2} - \dfrac{\partial W_2(g,t,\varphi)}{\partial z^2}\right] = 0, \quad \left.\dfrac{\partial V_2(g,t,\varphi)}{\partial t}\right|_{t=0} = V_2(g,t,\varphi)\big|_{t=0} = 0, \\ W_2(g,t,\varphi) = V_2(g,t,\varphi)\cos^2\varphi + U(g,t) \end{cases} \tag{4}$$

"Absorbing" conditions (2)-(4) are exact. When supplementing (1) by them, the class of correctness of the problem remains as before and the solution is not distorted. These conditions are local, the corresponding boundary, L, is piecewise coordinate one. Therefore the conditions discretization (2)-(4) and the incorporation of them into a standard finite-difference scheme is carried out in the framework of ordinary operations

[3]; their realization (solution of internal difference problems for the functions V_1 and V_2) does not require considerable additional computer resources. The resulting algorithms retain the efficiency of classical ones for closed problems in the rectangular grid. Replacing the polar grid with the rectangular one reduces the computation time by an order and over.

Examples of numerical implementation of algorithms based on the solution of equations (1)-(4) are presented in Figure 1.

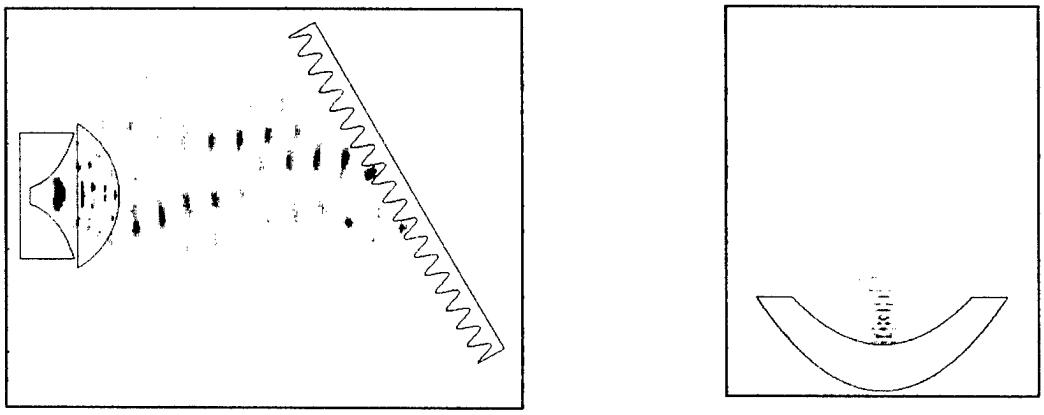


Fig. 1. Numerical solution of problem

REFERENCES

[1] Sirenko Y. K., Sukharevsky I.V., Sukharevsky O. I., Yashina N. P. Fundamental and applied problems in theory of electromagnetic wave scattering. – Kharkov: Krok, 2000.

[2] Sirenko Y. K., Perov A.O., and Yldiz E. Exact absorbing conditions for modeling of transients in open structures. // Telecommunications and Radio Engineering. – 2001.- V.55, №6-7. – P.80-90.

[3] Taflove A. Computational electrodynamics – the finite difference time domain method. – Massachusetts: Artech House, 1995.

MODELING OF VIDEOPULSE SCATTERING BY PLANE LAYERED DIELECTRIC STRUCTURES IN THE PRESENCE OF ERRORS

Olexander O. Puzanov

Usikov Institute for Radiophysics and Electronics of NASU
12 Proscura St., Kharkiv, 61085 Ukraine,
e-mail: puzanov@ire.kharkov.ua

It has been shown that existing experimental data on electric properties of media prove to be unsuitable for computation of fields of videopulse scattering by ground structures of large depth. Conditions of the "false" reflection emergence have been analyzed.

Experimental data on frequency dependences of relative permittivity $\varepsilon'(f)$ and specific conductivity $\sigma(f)$ prove often to be unsuitable for calculations of fields of nonsinusoidal radio wave scattering by ground structures. It is conditioned by violation of the interrelation between real and imaginary parts of complex permittivity. As it is known, this interrelation is established by Kramers-Kronig depressive relationships based on the causality principle [1-3]. The violation of this principle causes "false" reflections prior to information responses.

In view of what was told it is of interest to estimate the influence of distortions of frequency dependences of electric characteristics of a medium on calculation results. For that we will choose the Debye formula as a precise model of complex permittivity $\dot{\varepsilon} = \varepsilon_0 \varepsilon' - i\sigma/\omega$. Introducing the distortion in the precise model of $\dot{\varepsilon}$, by which we will describe electric properties of a homogeneous layer, we will analyze calculation results of the reflected electric field. Suppose the incident pulse with duration of 10 ns has the Gaussian time dependence. We form the layer of fresh water and a lower half-space (also homogeneous), bordering on the layer, of a material with permittivity $\varepsilon_3' = 5.2$ and specific conductivity $\sigma_3 = 2 \cdot 10^{-3}$ Sim/m for all frequencies. Analyze cases when the thickness d_2 of the water layer is 2 m, 5.5 m and 10 m. Let the height of the point of sight be $z_н$=2 m, and the angle of incidence be $\theta^{inc} = 0°$. Considering the structure of homogeneous areas one can isolate the "false" pulse effect itself by eliminating the influence of other reflections in an inhomogeneous dielectric.

According to Debye

$$\varepsilon'(\omega, \Theta) = \varepsilon'(\infty) + \frac{\varepsilon'(0,\Theta) - \varepsilon'(\infty)}{1 + [\omega\tau(\Theta)]^2}, \qquad \sigma(\omega, \Theta) = \omega^2 \tau(\Theta) \varepsilon_0 \frac{\varepsilon'(0,\Theta) - \varepsilon'(\infty)}{1 + [\omega\tau(\Theta)]^2}, \quad (1)$$

where $\varepsilon'(\infty)$ is the value of relative permittivity with $\omega \to \infty$, $\varepsilon'(0, \Theta)$ is the value of relative permittivity with $\omega \to 0$, ω — is the angular frequency [rad/s], Θ — is the temperature [°C], $\tau(\Theta)$ — is the relaxation time of molecules [s], $\varepsilon_0 = 8.85 \cdot 10^{-12}$ [F/m] — is the vacuum permittivity. For fresh water $\varepsilon'(\infty) \approx 4.9$, and the temperature dependences

of molecule relaxation time $\tau(\Theta)$ and the value $\varepsilon^r(0, \Theta)$ are represented by the following empirical equations:

$$\tau(\Theta) = 1.111 \cdot 10^{-10} - 3.824 \cdot 10^{-12}\Theta + 6.938 \cdot 10^{-14}\Theta^2 - 5.096 \cdot 10^{-16}\Theta^3,$$

$$\varepsilon^r(0,\Theta) = 88.045 - 0.415\Theta + 6.295 \cdot 10^{-4}\Theta^2 + 1.075 \cdot 10^{-5}\Theta^3.$$

The curves for $\varepsilon^r(f)$ and $\sigma(f)$ with Θ=10 °C calculated using the equations (1) are shown in Fig. 1 by heavy lines.

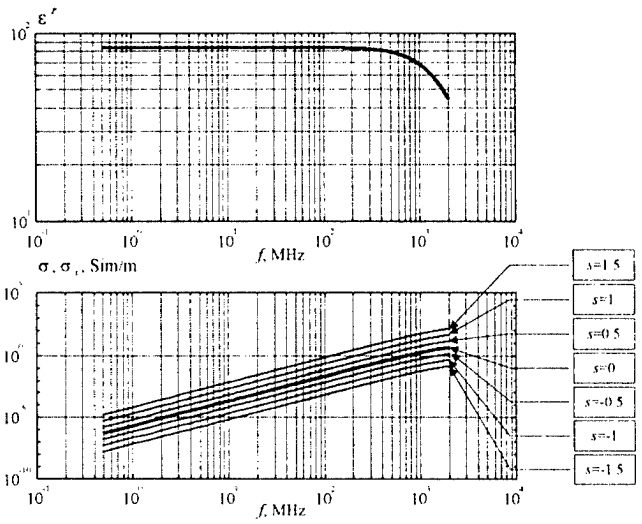


Fig.1. Dependences on the frequency of relative permittivity and specific conductivity (with s=0, heavy line) of fresh water at 10°C, calculated on the base of the Debye formula (1) and a set of functions $\sigma_s(f)$ (s=±0.5, ±1, ±1.5).

We form distortions for the plotted dependence of $\sigma(f)$ by a set of functions $\sigma_s(f)$ ($s = \pm 0.5, \pm 1, \pm 1.5$), which we will define by the expression $\lg\sigma_s(f) = s + \lg\sigma(f)$. When s=0 the distortions are absent and $\sigma_s(f)=\sigma(f)$. The functions $\sigma_s(f)$ (see Fig. 1) are plotted by thin lines. We will leave the dependence of $\varepsilon^r(f)$ without any alteration.

Illustrate the transient process transformation in the time domain conditioned by variations of the argument s by giving an example of calculation for the water layer of a thickness of 5.5 m (Fig. 2 and Fig. 3). It is possible to see that depending on the upward or downward distortion of the dependence of $\sigma(f)$ the "false" reflection effect is shown in *different* sections of the transient time dependence. So, the downward distortion (s<0) of the function $\sigma(f)$ causes the "false" reflection of negative polarity directly before the response from a lower boundary of the water layer. At the upward distortion (s>0) of the function $\sigma(f)$ the "false" reflection emerges in another representative place of the transient process and it is observed prior to the pulse from an upper water boundary. However now the ratio of the "false" pulse amplitude to the basic pulse amplitude is much less than in the previous case. At rather small distortions of the function $\sigma(f)$ (with s=±0.5, when $\sigma_s(f) = 10^{\pm 1/2}\sigma(f)$) the "false" reflection pulses do not emerge. Variations of the duration and amplitude of the pulse from the lower boundary is only observed.

The amplitude $A_в^s$ of reflections from the upper water boundary is weakly sensitive to distortions of the function $\sigma(f)$ and can increase approximately by 7%, what is characteristic of any thickness of the water layer (with s=1.5). A similar increase is conditioned by the growth of the reflection of lower frequencies from the upper boundary of a conductive dielectric with increasing its specific conductivity. The amplitude $A_н^s$ of reflections from the lower boundary is very sensitive to distortions. In comparison with the case when distortions are absent (s=0) it can increase by 292 % with s=-1.5 and d_2=10 m, or be diminished by 87.4 % with s=1.5 and d_2=10 m.

When $s<0$ and $s=0.5$ the "false" pulses do not arise before reflections from the upper boundary, and when $s=1$ these pulses appear. But their amplitude is rather small even for superior distortions. It can be only 2.49% of the basic reflection amplitude $A_в^s$ ($s=1.5$, $d_2=5.5$ m). At the same time the "false" pulses prior to reflections from the lower boundary are absent when $s=0$, and at negative values of s they can increase in amplitude up to 26.6% of the main reflection amplitude $A_н^s$ ($s=-1.5$, $d_2=10$ m). One should notice the fact that the more the thickness d_2 of the layer the more the value of the ratio of the "false" reflection amplitude from the lower boundary to the main pulse amplitude.

It is important to note that one cannot confuse the "false" reflection effect with signal distortion phenomena in the environment with dispersion. As it was shown above, the "false" pulses can also arise before a pulse reflected from the upper boundary of the dielectric layer bordering on air.

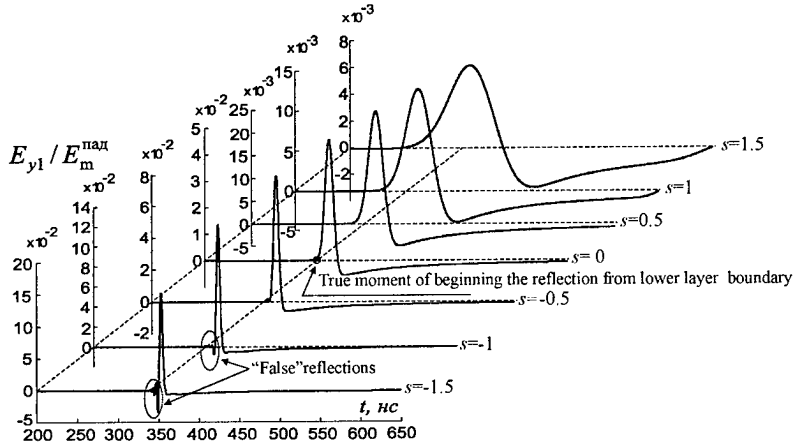


Fig.2. Dependences on time of a pulse reflected from the layer lower boundary at various distortions of frequency dependences of specific conductivity. The level of distortion is defined by values of the parameter $s=\pm1.5, \pm1, \pm0.5, 0$ (the water layer thickness is 5.5 m).

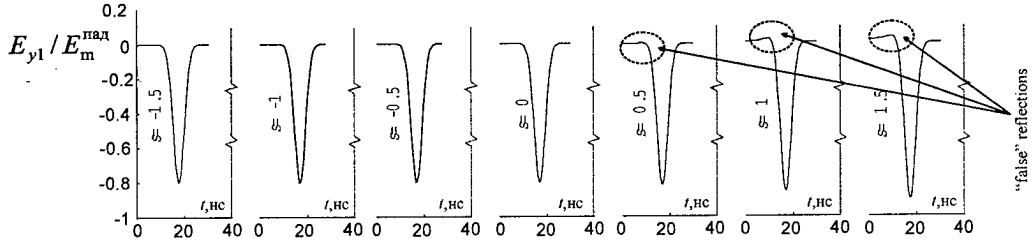


Fig.3 Dependences on time of a pulse reflected from the water upper boundary at various distortions of the frequency dependence of specific conductivity.

REFERENCES:

[1]. R. Hagedorn. Causality and Dispersion Interrelations // *Uspekhi fiz. nauk.* V.91, #1, January, 1967. –P. 151-160.

[2]. S.A.Masalov, O.O.Puzanov. Transient Radio Wave Scattering by Aeration Zones. *Proc. VIII Intern. Conf. on Mathem. Methods in Electrom. Theory.* (MMET'2000). — Kharkiv, Ukraine, September 12-15, 2000, —V. 1. — P. 262-264.

[3]. S.A Masalov., O.O.Puzanov. Ansatz to Correction of Experimental Electric Characteristics of Materials on the Bounded Frequency Interval // *MSMW'2001 Symposium Proceedings*, Kharkiv, Ukraine, June 4-9, 2001, —V.1. - P. 232-234.

TERMINATED TWO-WIRE TRANSMISSION LINE SUSPENDED IN AIR ILLUMINATED BY ELECTROMAGNETIC FIELD AND MEASUREMENT OF DIFFERENTIAL MODE CURRENT

İsa ARAZ[1,2], Osman ÇEREZCİ[2], Zafer DEMİR[2],

[1]TÜBİTAK-UEKAE EMC Lab. PO.Box:21 41470, Gebze, Kocaeli, TURKEY
[2] Sakarya University, Dept. Of Electric &Electronics, 54187 Esentepe, Sakarya, TURKEY
araz@uekae.tubitak.gov.tr

ABSTRACT - In this paper the terminated two-wire transmission line in air illuminated by continuous electromagnetic plane wave and the differential mode current flow over terminated elements measured by using monitoring current probe which is un susceptible with external field. The analytical solutions was obtained by using the earlier investigated the derivation of the two wire transmission line equation from Maxwell's equation. The comparison of measurement results with analytical results is represented.

INTRODUCTION: The effects of external electromagnetic fields on the conductors in the victim systems can be analyzed by using transmission line theory. The response of transmission line is illuminated by external electromagnetic fields has been reported by various investigators [1]-[4]. Taylor et al. [1] obtained firstly the analytical frequency domain solution for two-conductor line illuminated by electromagnetic field and later more convenient form by Smith [2].

In this paper, we measured differential mode current flows in terminating impedances at two-wire transmission line by using unsusceptible monitoring current probe. The current probe, which is used in the experiment, is commercial available probe but it is investigated by increasing susceptible level against external electromagnetic fields and it could be convenient for this kind of measurement. Transmission line model approach is used as a coupling model. In order to obtain analytical results, Smith's formulation is used. It is somewhat simple and easy to interpret physically and compact form of the complete solution for the transmission line mode currents in the terminations of two-wire transmission line illuminated by external electromagnetic fields [2]-[3].

MEASUREMENT OF CURRENT IN FREQUENCY DOMAIN: The model transmission line that used in the experiment is prepared with two-copper wires. The model transmission line is suspended in space in the chamber and illuminated by electromagnetic field between the frequency 200 - 1000 MHz. The line is terminated (loaded) with characteristic impedances at the both ends. The measurement was carried out in a fully anechoic chamber. The photograph of test setup is seen in figure 1. Before start the differential current measurement, the reference measurement was carried out.

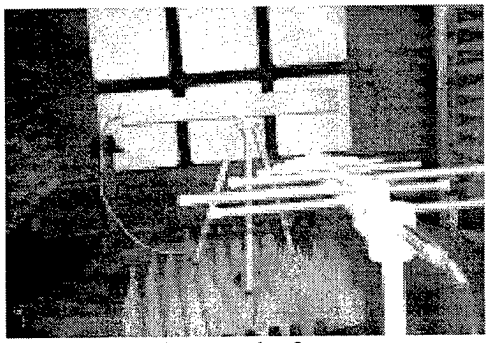


Figure 1 The photograph of test setup.

The measurement results are illustrated graphically in Figure 2 to 7. Figure 2 - 4 explain that the electric field of incident parallel to conductors and vertical to terminations case (case 1). Figure 5 - 7 explain that the electric field of incident vertical to conductors and parallel to terminations (case 2). The model line illuminated with under the broadside position (see in figure 3) and same condition of incident and polarization. In the figures of measurement results, curve one shows analytical result and curve two shows measured result.

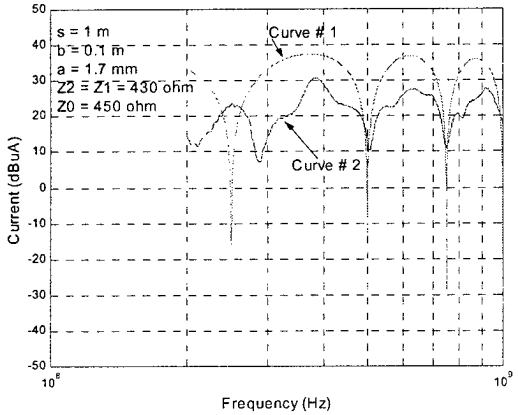


Figure 2 The comparison of measured differential current with spectrum of magnitude of the normalized current at the Z_2 termination. ($Z_1 = Z_2 = 430$ ohm in the case 1)

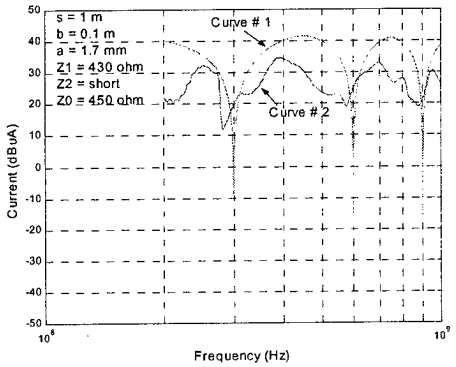


Figure 3 The comparison of measured differential current with spectrum of magnitude of the normalized current at the Z_2 termination. ($Z_1 = 430\ \Omega$, Z_2 = short circuit in the case 1)

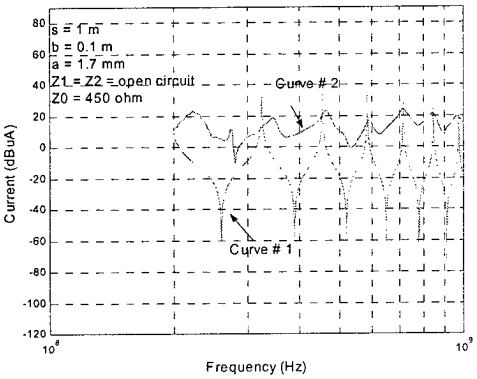


Figure 4 The comparison of measured differential current with spectrum of magnitude of the normalized current at the Z_2 termination. ($Z_1 = Z_2$ = open circuit in the case 1)

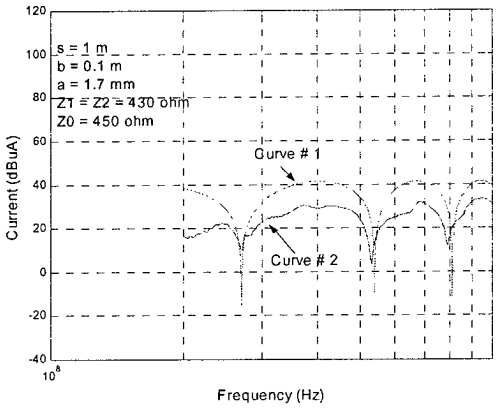


Figure 5 The comparison of measured differential current with spectrum of magnitude of the normalized current at the Z_2 termination. ($Z_1 = Z_2 = 430$ ohm in the case 2)

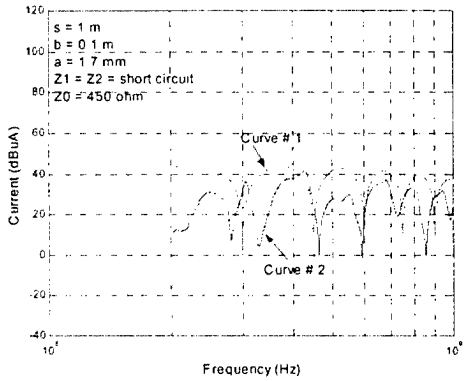


Figure 6 The comparison of measured differential current with spectrum of magnitude of the normalized current at the Z_2 termination. ($Z_1 = Z_2$ = short circuit in the case 2)

CONCLUSION: All figures represent that the measurement results similar with the analytical result except $Z_1 = Z_2$ = short circuit case in terms of resonance and minimum points of frequency in spectrum of magnitude of the current. In the practice In the resonance case the magnitude of current goes infinite (see in figures 4,5). A number of conclusions can be drawn from the measurement results:

1. In experiment the frequency response of the characteristic impedances of transmission line is not fix. So that, changing of impedance bring to slightly shift in frequency of minimum points.
2. In the figures minimum another call nulls points which crossing zero point of current means that there is no field to transmission line coupling in that frequency.
3. If the transmission line is terminated (at least one side) with similar characteristic impedance of line (matched case) no resonance is appear (see figure 2, 5) [5].
4. If the transmission line terminated at both side with high or low impedance (open and short circuit case) resonance occur in discrete frequency (see in figures 5, 6).
5. The frequency of resonance and minimum points dependence on the length of transmission line and termination impedance.

REFERENCES

[1] C.D. Taylor, R.S. Satterwhite, and C.W. Harrison, "The response of terminated two-wire transmission line excited by a non uniform electromagnetic field" IEEE Trans. Antennas Propagation., Vol. AP-13, pp. 987-989, Nov. 1965.

[2] A. A. Smith, "A more convenient form of the equations for the response of transmission line excited by non uniform fields, IEEE Trans. Electromag. Compat., Vol. EMC-15, pp. 151-152, Aug. 1973.

[3] Albert A. Smith, "Coupling Of External Electromagnetic Fields to Transmission Lines" John Wiley and Sons, 1977

[4] C.W. Harrison, "Bounds on the Load Currents Exposed One and Two Conductor Transmission Lines Electromagnetically coupled to a Rocket", IEEE Trans. Electromag. Compat., Vol. EMC-14, pp. 4-9, Feb. 1972.

[5] Niyazi Arı, Walter Blumer," The Response of a Terminated Uniform Two-Wire Transmission Line Excited By a Plane Electromagnetic Field" Electromagnetic Vol 8, pp.241-275, 1988.

[6] Frederic M. Tesche, "Plane Wave Coupling to Cables "Handbook of Electromagnetic Compatibility", Academic Press, Inc. 1995.

COMPUTATIONAL OPTOELECTRONICS

SINGLE-MODE FIBER WITH A REDUCED NON-ZERO DISPERTION IN WIDE RANGE OF WAVELENGTH

A.M. Gomilko, A.A.Gourjii, V.B. Katok, V.G.Levandovskyy, Y.D. Shchepkina

Scientific and Engineering Cable Lines Center of the Ukrainian Ministry of Communications,
7-a, Solomenskaya st., Kiev, 03110, Ukraine
Fax: + 380 44 248-0323; Tel: + 380 44 248-8596; E-mail: lvg_katok@ukrpack.net

ABSTRACT

With a method of synthesis of optic fibers [1] a profile of a refractive index in cross- section of a single-mode fiber with a non-zero displaced dispersion of a wavelength band at 1,55 – 1,625 μk, increased frequency band of a single-mode regime and increased effective area is obtained.

INTRODUCTION

Using the synthesis method based on the solution of a inverse scattering problem in non-relativistic quantum mechanics the profile of a refractive index in a cross section for a single mode gradient-type optical fiber with a reduced non-zero dispersion in a wide range of wavelength is obtained (1,55 - 1,625 μm). The synthesized fiber has a smooth curve describing the dependence of dispersion due to a wave length in diapason of 1310 nm, 1420 nm and 1665 nm. The small slope of the curve means that a minimum value of a dispersion is sufficient for compensation of a non-linear effect of interfusing of four waves. It helps to increase the capacity of a transmission system and allows to minimize the expenditures to compensate the dispersions.

Applying a synthesized fiber in a high-speed transmission lines allows to increase the lengths of transmission sections (DWDM), which do not contain regeneration devices or signal amplificators. Due to a broad band of wave lengths it is possible to apply cheaper lasers, multiplexers, demultiplexers and other devices for transmission lines with a wave compression (DWDM) and, therefore, to reduce the cost of transmission systems.

METHOD OF SYNTHESIS

The propagation of electromagnetic waves, the core of which has a gradient reflation index, for the linear-polarized modes in a normalized view is described with an equation

$$\frac{d^2\Phi(R)}{dR^2}+\left[u^2-v^2\left(g_1(R)+\frac{\left(l^2-1/4\right)}{v^2R^2}\right)\right]\Phi(R)=0, \qquad (1)$$

where $u^2=a^2\left(n_1^2k^2-\beta^2\right)$ is a normalized propagation coefficient; $v^2=a^2k^2n_1^2 2\Delta$ is a normalized frequency; a is a radius of a core; β is a longitudinal propagation coefficient; $\Delta=(n_1^2-n_2^2)\left(2n_1^2\right)^{-1}$; n_1 is a maximum value of refractive index in a core; n_2 is a value of refractive index in a cladding; l = 0,1,2,... is an azimuthally mode index; $k=\omega\sqrt{\varepsilon_0\mu_0}$ is a wave number in free space; ω is an angular frequency; ε_0 and μ_0 are dielectric and magnetic permeabilities of free space accordingly; $g_l(R)$ is an obscure function of a profile of refractive index; R is a dimensionless radial coordinate; Φ(R) is a proportional to cross-sectional amounting fields function, which contents to boundary conditions.

$$\Phi(R)\big|_{\rho\to 0}=0,\ \Phi(R)\big|_{\rho\to\infty}=\text{const},\ \Phi(R)\big|_{\rho=a+0}=\Phi(R)\big|_{\rho=a-0},\ \frac{d\Phi(R)}{dR}\bigg|_{\rho=a+0}=\frac{d\Phi(R)}{dR}\bigg|_{\rho=a-0} \qquad (2)$$

Snapping the frequency k and considering the problem for a specific azimuth index l results in receipt of a clone of the inverse scattering problem of a non-relativistic quantum mechanics. Therefore for synthesis SOF the mathematical methods of the solution of a inverse scattering problem a non-relativistic quantum mechanics will be used [2]. Gradient of refractive index in

cross section SOF and the cumulative distribution function of a fields of a mode, are determined on a known field pattern of a mode in SOF with a stepwise profile of refractive index [1]. The equation describing the properties of electromagnetic waves in such light guide is as follows

$$\frac{d^2\Phi_1(R)}{dR^2} + \left[u^2 - v^2\left(g_0(R) + \frac{\left(l^2 - 1/4\right)}{v^2R^2}\right)\right]\Phi_1(R) = 0.$$

$\Phi_1(R)$ – function proportional to a cross-sectional component of electrical fields; $g_0(R)$ is a function of a profile of refractive index in stepwise guide

$$g_0(R) = 0,\ R \in (0,1),\ g_0(R) = 1,\ R > 1.$$

The boundary condition is similarly to the equation (2).

Determination of a profile law of a dielectric permeability in a cross-section of synthesized SOF due to the method [1] is reduced to the solution of an integral Helfand-Levitan equation

$$K(R,t) = -\int_0^R K(R,y)G(y,t)dy - G(R,t) = 0,\quad (0 < y < t). \tag{3}$$

The core G(R,t) is entered with the help of an integral Stiltyess, where the integrating is carried out on change of spectrum functions of equations described wave processes in the initial $\xi_1(\rho)$ and and synthesized $\xi(\rho)$ SOF

$$d\xi_1(p) - d\xi(p) = \begin{cases} 0, & 0 < v^2 < p, \\ B\delta(p - p_0) - C\delta(p - p_1), & p \in (0, v^2), \\ 0, & p < 0 \end{cases}$$

where p is a spectral parameter, to be bound up with propagation coefficients by a ratio $p = u^2$, $\delta(p\text{-}p_i)$ – Dirac delta-function; $C = \left[\int_0^\infty \Phi_1^2(R, p_1)dR\right]^{-1}$ is a normalized coefficient. Here B is a normalized coefficient, it is subject to definition. In a considered case the equation (3) has the singular core, therefore its solution K(R,t) can be obtained in an analytical view. The law of change of refractive index in cross section of synthesized SOF is determined under the formula

$$g_1(R) = g_0(R) + 2\frac{d}{dR}K(R,R) \tag{4}$$

The function $\Phi(R)$ is calculated with the help of Povzner-Levitan transformation operator [1]

$$\Phi(R) = \Phi_1(R)\cdot\left[1 + B\int_0^R \Phi_1{}^2(t)dt\right]^{-1} \tag{5}$$

Normalized coefficient B, included in equations (4), (5) can be found from a ratio [3]

$$V_{gr}V_{ph} = c^2 \cdot \int_0^\infty R\Phi^2(R)dR \cdot \left[\int_0^\infty R\Phi^2(R)n^2(R)dR\right]^{-1},$$

which describes the distribution of an electromagnetic field in cross section of a fiber with phase velocity V_{ph} and group velocity V_{gr} of a distributing mode, c is velocity of light.

NUMERICAL CALCULATIONS

The obtained profile of refractive index in cross section of a SOF with a displaced dispersion in an effective range of frequencies is 1,55 – 1,625 mkm is shown in fig.1. The initial data for synthesis are: V = 3,2, V_{gr} =0,685, V_{ph} = 0,6925. Synthesized SOF has the same depth as the initial SOF with a stepwise profile of refractive index, for which two modes propagate on given frequency V= 3,2.

To check the accuracy of a synthesis method it was done the numerical experiment connected with a calculation of dispersion curves for synthesized SOF (fig. 2). The basic mode LP_{01} is given. The dotted line indicates a dispersion curve of an initial stepwise SOF. The circle marks a cut-off frequency of a following mode both in the synthesized and in the initial SOF accordingly. It is shown that the frequency band of an obtained SOF is wide than the band for the initial SOF with a stepwise profile of refractive index. The distributing field of propagated mode in order to frequency is shown in a fig. 3.

Figure 4 illustrates the curve of relation of a chromatic dispersion M [pc/(km nm)] in synthesized SOF due to a wavelength. Synthesized SOF has a non-zero displaced dispersion in a wave band λ = 1,55; λ= 1,625 mkm. Curves for a material dispersion M_{CMD}, profile dispersion M_{CPD} and wave guide dispersion M_W of the synthesized SOF are also plotted.

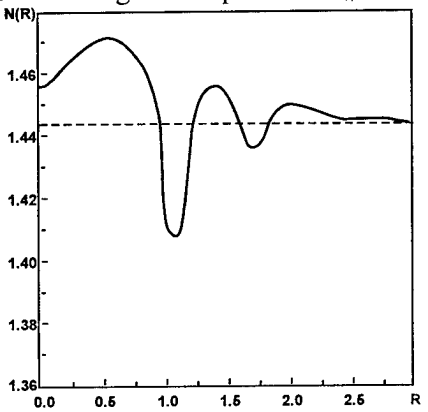


Fig.1 Profile of a refraction index for synthesized SOF. The dotted line indicates shows the refraction index in a cladding.

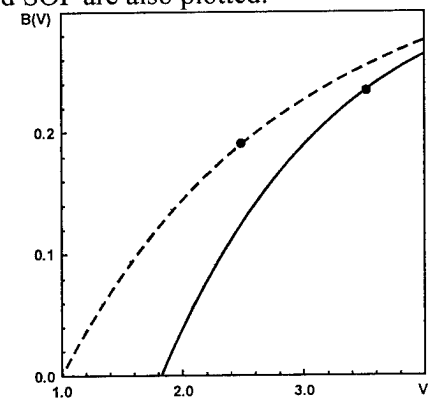


Fig.2 Dispersion curves for synthesized SOF.

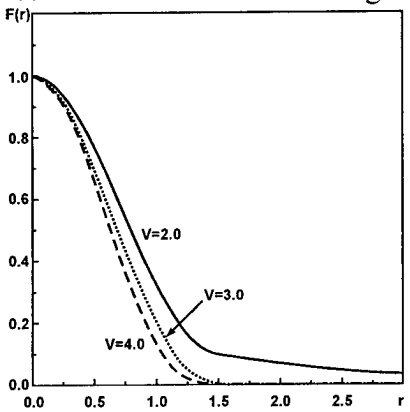


Fig.3 The distributing field of propagated mode for synthesized SOF.

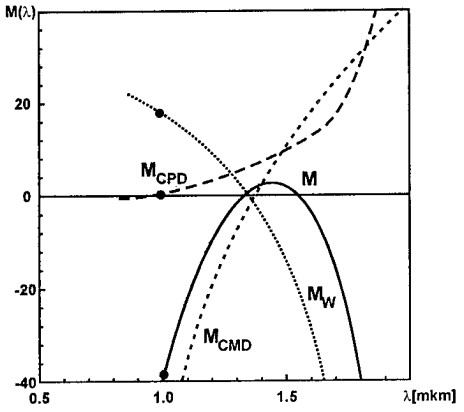


Fig.4. Dependence of chromatic dispersion M, [ps/(km nm)] in synthesized SOF due to wavelength.

REFERENCES

[1] A.Gomilko, A.Gourjii, E. Shchepkina /Syntheses of single-mode optical fibers with minmal dispersion/ICTON 2000 International conference on transparent optical networks Kielce. Poland. June 5-8, 2000

[2] I. I. Gelfand and B. M. Levitan About definition of differential operator by its spectral function // Izv. AN USSR, matematicheskie nauki, 1951, - N. 4 C. 309. (In Russian).

[3] Case K.M. On wave propagation in inhomogeneous media //J. Math. Phys.,1972. - V. 13, N 2360-387.

MATHEMATICAL ANALYSIS OF THE GUIDED MODES OF AN INTEGRATED OPTICAL GUIDE

Evgueni Kartchevski and George Hanson*

Department of Applied Mathematics, Kazan State University,
E-mail: Evgenii.Karchevskii@ksu.ru

*Department of Electrical Engineering, University of Wisconsin-Milwaukee,
E-mail: george@uwm.edu

ABSTRACT

The eigenvalue problem for guided modes of an integrated optical guide is reduced to a strongly-singular domain integral equation. It is proved that the operator of the domain integral equation is a Fredholm operator with zero index. It is also proved that the spectrum of the original problem can only be a set of isolated points.

INTRODUCTION

In this work we study the natural modes of an optical fiber integrated into a three-layer planar medium, which is representative of typical optical circuits. In the absence of a planar background, the basic properties of optical fibers are described in [1]. More recently, rigorous mathematical methods have been applied to the analysis of the modes of optical fibers, see, e.g., [2]-[4]. For the integrated optical guide, rigorous mathematical analysis has been presented for the guided modes in [5]-[7]. Due to the complexity of the integrated optical structure, domain integral equations utilizing appropriate Green's functions (to account for the background media) are a popular practical approach for computing the natural fiber modes [8]-[10]. In this work a rigorous mathematical analysis of the guided modes of an integrated optical fiber is presented based upon a strongly-singular domain integral equation.

STATEMENT OF THE PROBLEM

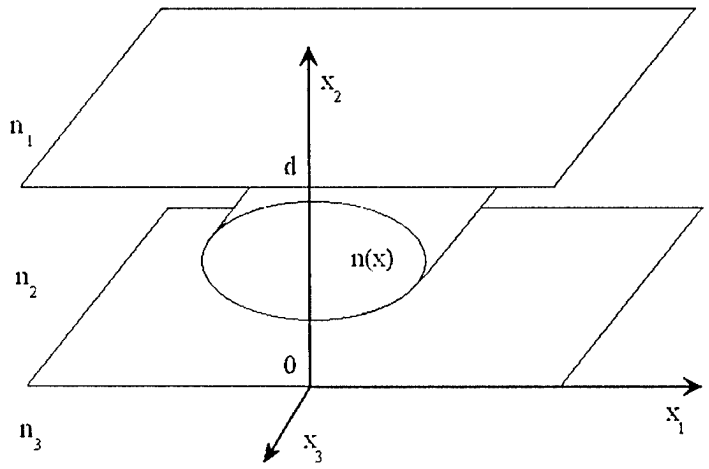


Fig.1. An integrated optical guide.

We consider the guided modes of the integrated optical guide (see Fig. 1). Let the three-dimensional space be occupied by an isotropic source-free medium, and let the refractive index

be prescribed as a positive real-valued function $n = n(x_1, x_2)$ independent of the longitudinal coordinate x_3. We assume that there exists a bounded domain Ω on the plane $R^2 = \{(x_1, x_2) : -\infty < x_1, x_2 < \infty\}$ such that $n = n_\infty(x_2)$, $x = (x_1, x_2) \in \Omega_\infty = R^2 \setminus \overline{\Omega}$, where $n_\infty(x_2)$ depends only on the x_2 variable. It is a piecewise-constant function represents the refractive index of so-called associated planar waveguide. For simplicity, we take $n_\infty(x_2) = \{n_1 \text{ if } x_2 > d,\ n_2 \text{ if } 0 < x_2 < d,\ n_3 \text{ if } x_2 < 0\}$. We assume without loss of generality that $n_2 \ge n_3 \ge n_1$. Denote by n_+ the maximum of the function n in the domain Ω. We assume that $\Omega \subset \Omega_2 = \{(x_1, x_2) : -\infty < x_1 < \infty, 0 < x_2 < d\}$, $n_+ > n_2$, and also that function n is a continuous function in Ω_2, i.e., that the guide does not have a sharp boundary.

The modal problem can be formulated as a vector eigenvalue problem for the set of differential equations (we use notations [2] for differential operators)

$$\mathrm{Rot}_\beta \mathbf{E} = i\omega\mu_0 \mathbf{H}, \quad \mathrm{Rot}_\beta \mathbf{H} = -i\omega\varepsilon_0 n^2 \mathbf{E}. \tag{1}$$

Here ε_0, μ_0 are the free-space dielectric and magnetic constants, respectively. We consider the propagation constant β as an unknown complex parameter and radian frequency $\omega > 0$ as a given parameter. We seek non-zero solutions $[\mathbf{E}, \mathbf{H}]$ of set (1) in the space $\left(L_2(R^2)\right)^6$.

Denote by $\Lambda^{(1)}$ the sheet of the Riemann surface of the function $\sqrt{k^2 n_2^2 - \beta^2}$, where $k^2 = \omega^2 \varepsilon_0 \mu_0$, which is specified by the condition $\mathrm{Im}\sqrt{k^2 n_2^2 - \beta^2} \ge 0$. Denote by β_j the propagation constants of TE and TM modes of the associated planar waveguide [1]. It is well known that there exist no more than a finite number of values β_j. All of the values β_j belong to domain $\{\beta \in \Lambda^{(1)} : \mathrm{Im}\,\beta = 0,\ kn_3 < |\beta| < kn_2\}$. In a similar way to [7] we can see that the domain $D = \{\beta \in \Lambda^{(1)} : \mathrm{Re}\,\beta = 0\} \cup \{\beta \in \Lambda^{(1)} : \mathrm{Im}\,\beta = 0, |\beta| < \gamma\}$, where $\gamma = \max_j \beta_j$, corresponds to the continuum of propagation constants of radiation modes that do not belong to $\left(L_2(R^2)\right)^6$. Therefore we do not investigate the values $\beta \in D$.

Definition 1. *A nonzero vector* $[\mathbf{E}, \mathbf{H}] \in \left(L_2(R^2)\right)^6$ *is referred to as an eigenvector of problem (1) corresponding to an eigenvalue* $\beta \in \Lambda = \Lambda^{(1)} \setminus D$ *if relation (1) is valid. The set of all eigenvalues of problem (1) is called the spectrum of this problem.*

MAIN RESULTS

Theorem 1. *The set* $\{\beta \in \Lambda^{(1)} : \mathrm{Im}\,\beta = 0, |\beta| \ge kn_+\}$ *is free of the eigenvalues of problem (1).*

This theorem was proved in [1] for the case $n_2 = n_3 = n_1$. For the general case the proof is analogous.

If $[\mathbf{E}, \mathbf{H}]$ is an eigenvector of problem (1) corresponding to an eigenvalue $\beta \in \Lambda$, then

$$\mathbf{E}(x) = \left(k^2 n_\infty^2 + \mathrm{Grad}_\beta \mathrm{Div}_\beta\right) \frac{1}{n_\infty^2} \int_\Omega \left(n^2(y) - n_\infty^2\right) G(\beta; x, y) \mathbf{E}(y) dy, \tag{2}$$

$$\mathbf{H}(x) = -i\omega\varepsilon_0 \operatorname{Rot}_\beta \int_\Omega \left(n^2(y) - n_\infty^2\right) G(\beta; x, y)\mathbf{E}(y)dy, \quad x \notin \partial\Omega_2, \tag{3}$$

where function G is the well known tensor Green function [9]. For any $(x, y) \in \Omega^2$ the function G is analytic for $\beta \in \Lambda$. Passing the operator $\operatorname{Grad}_\beta \operatorname{Div}_\beta$ under the integral in relation (2), and using the differentiation rule [11] for weakly singular integrals we obtain a nonlinear spectral problem for a strongly-singular domain integral equation

$$A(\beta)\mathbf{E} = 0, x \in \Omega; \quad A : \left(L_2(\Omega)\right)^3 \to \left(L_2(\Omega)\right)^3. \tag{4}$$

Theorem 2. *For all $\beta \in \Lambda$ the operator $A(\beta)$ is Fredholm with zero index.*
This theorem is proved by general results of the theory of singular integral operators.

Definition 2. *A nonzero vector $\mathbf{E} \in \left(L_2(\Omega)\right)^3$ is called an eigenvector of the operator-valued function $A(\beta)$ corresponding to an eigenvalue $\beta \in \Lambda$ if relation (4) is valid.*

Theorem 3. *Suppose $[\mathbf{E}, \mathbf{H}] \in \left(L_2(R^2)\right)^6$ is an eigenvector of the problem (1) corresponding to an eigenvalue $\beta \in \Lambda$. Then $\mathbf{E} \in \left(L_2(\Omega)\right)^3$ is the eigenvector of the operator-valued function $A(\beta)$ corresponding to the same eigenvalue β. Suppose $\mathbf{E} \in \left(L_2(\Omega)\right)^3$ is an eigenvector of the operator-valued function $A(\beta)$ corresponding to an eigenvalue $\beta \in \Lambda$ and also let vector $[\mathbf{E}, \mathbf{H}]$ is defined by (3), (4) on R^2 Then $[\mathbf{E}, \mathbf{H}] \in \left(L_2(R^2)\right)^6$ and $[\mathbf{E}, \mathbf{H}]$ is the eigenvector of the problem (1) corresponding to the same eigenvalue β.*
This theorem is proved by direct calculations.

Theorem 4. *The spectrum of problem (1) can be only a set of isolated points on Λ.*
This theorem is followed from theorems 1-3 and general results of the theory of operator-valued functions [12].

REFERENCES

[1] D. Marcuse, Theory of Dielectric Optical Waveguides, Academic Press, New York, 1974.
[2] A. Bamberger, A.-S. Bonnet, SIAM J. Math. Analysis, 21 (1990), pp. 1487-1510.
[3] H.P. Urbach, SIAM J. Math. Anal. 27(1996), pp. 204-220.
[4] E.M. Karchevskii, Differential Equations, 36(2000), pp. 1109-1111.
[5] A.S. Bonnet-BenDhia, G. Caloz, and F. Mahe, IMA J. App. Math., 60(1998), pp. 225-261.
[6] D.G. Pedreira and P. Joly, SIAM J. Numer. Analysis, 39(2001), pp. 596-623.
[7] A.S. Bonnet-BenDhia, P. Joly, Mathematical modeling in optical science, Frontiers Appl. Math., SIAM, Philadelphia, PA, 22 (2001), pp. 273-324
[8] J.S. Bagby, D.P. Nyquist, and B.C. IEEE Trans. Microwave Theory Tech., MTT-29(1985), pp. 906-915.
[9] J.S. Bagby, D.P. Nyquist, IEEE Trans. Microwave Theory Tech., MTT-35 (1987), pp. 206-210.
[10] E.W. Kolk, N.H.G. Baken, and H. Blok, IEEE Trans. Microwave Theory Tech., 38(1990), pp. 78-85.
[11] S.G. Mikhlin, S.P. Prossdorf, Singular integral operators, Springer-Verlag, Berlin, 1986.
[12] I.C. Gohberg, M.G. Krein, Introduction to the theory of linear nonselfadjoint operators, Providence, R.I., American Mathematical Society, 1969.

FULL VECTOR ANALYSIS OF OPTICAL FIBRE FACET

I.Vorgul, A.Vukovic, P.Sewell, T.Benson

School of Electrical and Electronic Engineering, University of Nottingham, University Park, Nottingham, NG7 2RD, e-mail: eeziv@gwmail.nottingham.ac.uk

ABSTRACT

The normal facet full vector problem is accurately solved for a vector circular optical fibre with a high efficient algorithm. The Free Space Radiation Mode (FSRM) method is used to investigate the facet reflectivity for a set of incident modes having all six components of electromagnetic field dependent on all three spatial coordinates. The analysis yields a simple integral for the reflection coefficient for each mode, which makes calculations fast and reliable. Vector results for the reflectivity of the fundamental EH_{11} mode are compared with the scalar ones showing significant quantitative differences between them (<40 dB).

INTRODUCTION

Accurate controlling and prediction of end facets reflectivities is significant for designing semiconductor travelling wave amplifiers, modern lasers and grating systems [1]. The most common requirement of such a design is low facet reflectivitiy in combination with additional requirements for the waveband and polarisation characteristics. Very low facet reflectivities are most commonly achieved using layered antifreflection coatings (AR) or angling the facet [2], [3].

The problem of design and optimisation of optical waveguide facets is now well elaborated for rectangular waveguides [4], [5], including scalar as well as vector analysis [6]. Optical fibre facets were modelled in scalar approximation considering only guided mode diffraction at the end of fibres [7], [8]. Although scalar approximation gives accurate results for the case of weakly guiding waveguides, the vector analysis is significant in polarisation-sensitive devices, as shown in [6] for a rectangular waveguide. Numerical methods directly applied to vector fibre facets lead to a high computation time, as well as losses of the result reliability. In this paper we present a full vectorial semi-analytical analysis of circular fibre facet reflectivity. The most general case of all six field components dependable on all three spatial co-ordinates for the guided modes is considered. The radiation field is approximated by assuming that it propagates in a region with a uniform refractive index, an approximation well suited for small refractive index difference in the transverse direction [9]. Numerical results are validated by their comparing with FSRM results for scalar analysis revealing lower reflectivity for vector coated facet.

THEORY

We consider a circular fibre incident on a normal plane at z=0. Fig.1 illustrates the side view of the structure and the adopted notations. The fibre core radius is equal to ρ and the refractive indices of the core and the cladding are n_{core} and n_{clad} respectively. The cladding is taken to be infinite, as its diameter is usually much greater than that of the core. As mentioned above, we assume small transverse variation of refractive index in the fibre, typically less than 10%.

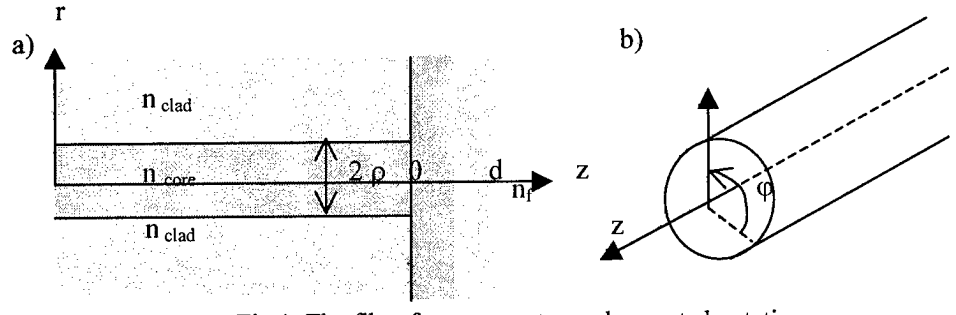


Fig.1. The fibre facet geometry and accepted notations

To make the analysis more general, we consider all six field components. All guided modes supported by the fibre are rigorously included in theory. Besides the finite number of the guided

modes, the fibre supports a continuous spectrum of radiation modes, which play a significant role in a presence of longitudinal discontinuities. The radiation field of the fibre is difficult to include into theory exactly. According to the FSRM approach, the small transverse refractive index step allows to interpret the radiation field as the radiation spectrum in a homogeneous medium. Such an approximation allows formulation of a semi-analytical solution of the vector problem, providing a good compromise between the description accuracy and the model simplicity.

The longitudinal field components of the modes (i.e., E_z, H_z), in cylindrical co-ordinates are proportional to a product of a cylindrical function with respect to the radial co-ordinate and $\sin n\varphi$ or $\cos n\varphi$, where φ is an angular co-ordinate and n is the mode number [10]. The transverse field components of these modes (i.e., $E_{r,\varphi}$, $H_{r,\varphi}$), can be expressed similarly, but as a combination of cylindrical functions of different orders instead of just one function in the case of longitudinal components. To make analytical integration of Fourier transform of the modes possible, the transverse Cartesian components of the guided modes (i.e., $E_{x,y}$, $H_{x,y}$) in dependence on cylindrical co-ordinates will be considered, expressed in terms of longitudinal components.

The fibre supports a finite number of guided modes and a spectrum of the radiation field. The total electric and magnetic fields in the fibre (for $z \le 0$) can be expressed as

$$E(r,\varphi,z) = \sum_{n=1}^{N} E_n^{+}(r,\varphi)\, e^{-j\beta_n z} + \sum_{n=1}^{N} R_n E_n^{-}(r,\varphi)\, e^{+j\beta_n z} + E_r(r,\varphi,z), \quad (1)$$

and $$H(r,\varphi,z) = \sum_{n=1}^{N} H_n^{+}(r,\varphi)\, e^{-j\beta_n z} + \sum_{n=1}^{N} R_n H_n^{-}(r,\varphi)\, e^{+j\beta_n z} + H_r(r,\varphi,z), \quad (2)$$

where $E_r, H_r(r,\theta,z)$ is the radiation field in the fibre, propagating away from the facet. The superscripts + and - indicate forward and backward going fields with respect to z-axis direction, respectively, and β_n and R_n are the propagation constant and the reflectivity of the corresponding guided mode, respectively. The radiation field in the fibre assumed to propagate in a uniform half-space with a refractive index can be expressed as

$$E_r(r,\varphi,z) = \int_0^{\infty} q\,dq \int_0^{2\pi} d\theta\; e^{i r\cos(\theta-\varphi)}\, e_r(q,\theta)\, e^{i\sqrt{n_{clad}^2 k_0^2 - q^2}\, z} \quad (3)$$

and $$H_r(r,\varphi,z) = \int_0^{\infty} q\,dq \int_0^{2\pi} d\theta\; e^{i r\cos(\theta-\varphi)}\, h_r(q,\theta)\, e^{i\sqrt{n_{clad}^2 k_0^2 - q^2}\, z}, \quad (4)$$

where $e_r(q,\theta)$ and $h_r(q,\theta)$ are Fourier transformed fields and q and θ are Fourier.

The forward going radiation field (for $z \ge 0$), $E_f, H_f(r,\theta,z)$ is exactly described by a similar representation to (3,4) but with the propagation constant equal to $\gamma(q,\theta) = \sqrt{n_f^2 k_0^2 - q^2}$.

Applying the boundary conditions at z=0 yields the following system of equations:

$$\left[\sum_{n=1}^{N} E_n^{+}(r,\varphi) + \sum_{n=1}^{N}\sum_{m=1}^{M} R_{nm} E^{-}{}_{nm}(r,\varphi) + E_r(r,\varphi,z)\right] \times \hat{z}\Big|_{z=0} = \left[E_f(r,\varphi,z)\right] \times \hat{z}\Big|_{z=0}, \quad (5)$$

$$\left[\sum_{n=1}^{N} H_n^{+}(r,\varphi) + \sum_{n=1}^{N}\sum_{m=1}^{M} R_{nm} H^{-}{}_{nm}(r,\varphi) + Y_r(r,\varphi) E_r(r,\varphi,z)\right] \times \hat{z}\Big|_{z=0} = \left[Y_f(r,\varphi) E_r(r,\varphi,z)\right] \times \hat{z}\Big|_{z=0}, \quad (6)$$

where the magnetic component of the radiation field is expressed after the electric one using the admittance operators Y_r and Y_f of the correspondent media, which are 2x2 matrices with the elements being differential operators or combinations of elementary functions in spatial or Fourier representations, respectively.

With the view to simplify the analysis, 2D Fourier transform is applied to all field components in equations (5,6). In order to solve the system (4)-(5) for the modal reflectivities R_n, the radiation field can be expressed as

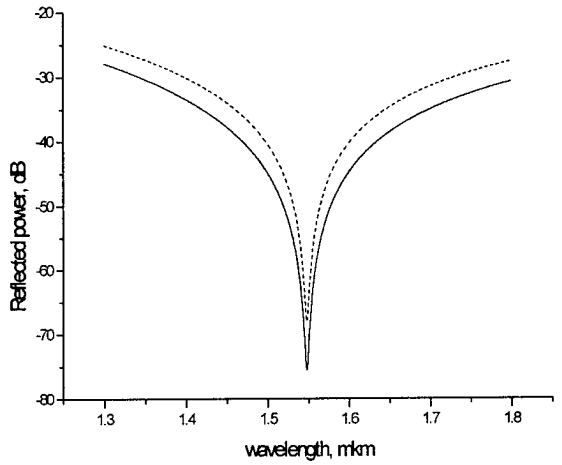
$$e_r(q,\theta) = \left(Y_f - Y_r\right)^{-1}\left[\sum_{n=1}^{N}\left(h_n^{+}(q,\theta) - Y_f\, e_n^{+}(q,\theta)\right) + \sum_{n=1}^{N} R_n\left(h_n^{-}(q,\theta) - Y_f\, e_n^{-}(q,\theta)\right)\right]. \quad (7)$$

The modes orthogonality condition

$$\int_0^{\infty} q\,dq \int_0^{2\pi} d\theta \left[e_r(q,\theta) \times (h_{nm}^{-}(q,\theta))^{*} + (h_{nm}^{-}(q,\theta))^{*} \times h_r(q,\theta)\right]\cdot \hat{z} = 0, \quad (8)$$

results in the algebraic system of equations for the guided modes reflectivities. The Fourier transforms of the guided modes used in (7) and (8) are found analytically for any order of the modes, after which the integral over θ can be solved exactly.

CALCULATION RESULTS



The results for fibre reflectivity are for fundamental EH_{11} mode incident on the facet coated with a quarter-wavelength layer are shown in Fig.2. The fibre parameters are n_{core} = 1.4516, n_{clad} = 1.4473, and 2ρ=8.7 μm. The solid line represents the vector results and the dash line stands for scalar analysis. The difference between the vector and the scalar results is within the limits expected from Fresnel formula

$$\left|R_{vector} - R_{scalar}\right| \approx \frac{\left|\beta_{vector} - \beta_{scalar}\right|}{2\,\beta_{vector}}.$$

Fig.2. Power reflectivity for a quarter wavelength coating on a fibre with ncore=1.4516, nclad=1.4473, and diameter=8.7, for vector (solid line) and scalar (dashed line)

REFERENCES

[1] T.Ikegami, "Reflectivity of mode of facet and oscillation mode in double heterostructure injection lasers", IEEE J. Quantum Electron., Vol. QE-8, pp. 470-476, 1976.

[2] C.Vassalo, "Reflectivity of multidielectric coatings deposited on the end of a weakly guiding dielectric slab waveguide", J. Opt.Soc. Amer., Vol. 5, pp.1818-1928, 1988.

[3] C. Zah, J. Osinsky, C. Caneau, S. Menocal, L. Reigh, F. Salzman, F. Shokoohi and T. Lee, "Fabrication and perfomance of 1.5 μm GaInAsP travelling-wave laser amplifiers with angled facets", Electron. Lett., Vol. 23, pp. 990-991, 1987.

[4] C. J. Smartt, T. M. Benson and P. C. Kendall, "Exact analysis of waveguide discontinuitoes: junctions and laser facets", Electronics Lett., Vol. 26, No. 15, pp. 1352-1353, 1993.

[5] M. Reed, T. M. Benson, P. C. Kendall and P. Sewell, "Antireflection-coated angled facet design", IEE Proc.-Optoelectron., Vol. 143, No. 4, pp. 214-220, 1996.

[6] P.Sewell,M.Reed,T.M.Benson, and P.C.Kendall, *Full vectorial analysis of two-dimensional angled and coated waveguide facets*, IEEE J.Quantum Electronics,V.33,N 12, Dec.1997, p.2311-2317.

[7] M.Imtaar, S.J. Al-Bader, L. Lightwave Technol., Vol. 13, p.137, 1995.

[8] A. B. Manenkov, T. M. Benson, P. C. Kendall, and P. Sewell, "Applicability of scalar theory for analysis of mode reflection from an optical dielectric waveguide end", J. Opt. Quantum Electronics, Vol. 20, No. 3, 2000.

[9] P. C. Kendall, D. A. Roberts, P. N. Robson, M. J. Adams, and M. J. Robertson, "New formula for semiconductor laser facet reflectivitiy", IEEE Photonics Technol. Lett., Vol. 5, No. 2, pp.148-149, 1993.

[10] A.W.Snyder and J.D.Love, Optical Waveguide Theory, Chapman and Hall, 734 p.

MATHEMATICAL MODELLING OF UNSYMMETRICAL OPTICAL MIRRORS FOR FEMTOSECOND IMPULSE GENERATION

I. A. Sukhoivanov, V. V. Lysak, A. Shulika

Kharkiv Technical University of Radio Electronics
Lenin av. 14, Kharkiv, 16166, Ukraine, Tel.: (0572)-40-94-84, Fax: (0572) 40-91-07,
Email: Sukhoivanov@kture.kharkov.ua

INTRODUCTION

Femtosecond ($\approx 10^{-15} s$) pulse laser systems open new applications of ultrafast processes investigation in physics, engineering, chemistry, biology and medicine.
Short – pulse generation has advanced to a degree where the bandwidth of standard Bragg mirrors limits the pulse width of ultrashort pulsed lasers [1].

In work [2] the double-chirped mirrors (DCM) are used for producing the sub – 10 fs pulses (Fig. 1). Physically the dispersion management with chirped mirrors can be explained as follows. Quasi-monochromatic wave-packets carried at different wavelengths penetrate to different depth before being reflected (Fig. 2), as a consequence of a modulation of the multilayer period across the layer stack. The increasing multilayer period with increasing distance from the mirror surface implies that radiation with increasing wavelength has to penetrate deeper before being reflected and experiences a longer delay. The result is a group delay that increases with increasing wavelength, giving rise to negative GDD. The further reduction of duration of the pulse is possible at reduction of the Bragg grating optical thickness. [3]

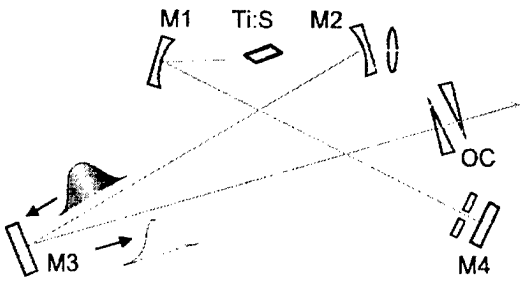


Fig. 1. Kerr-Lens Mode-Locked Mirror-Dispersion-Controlled Ti:Sapphire Oscillator. Double chirped mirrors (M1-M4) were employed as a means of dispersion control, OC-output cavity.

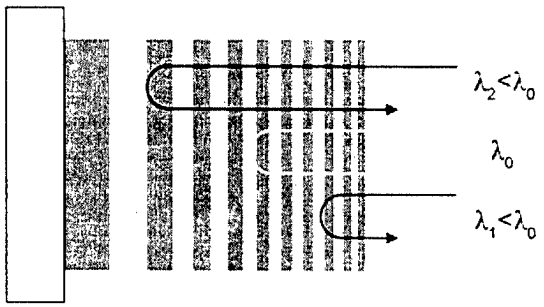


Fig. 2. Dispersion management with chirped mirrors

In papers [4, 5] the analytical design and theory of DCM are present. But in these works only thickness for high refractive index layers is changed. Further decrease of pulse duration is possible by decreasing of optical path of Bragg mirror. In this paper we investigate the dispersion characteristics of chirped mirrors (CM) with change both high and low refractive index layers with different chirping order.

THEORY

In our case we use a structure like [1]. Grating materials are TiO_2 with refractive index $n_h = 2.5$ and SiO_2 with $n_l = 1.5$ The Bragg wavelength $\lambda_B = 800$ nm.

For investigation we use the exact calculation of the transfer matrix M [5]:

$$\begin{pmatrix} A(0) \\ B(0) \end{pmatrix} = M(0,L)\begin{pmatrix} A(L) \\ B(L) \end{pmatrix} = \begin{pmatrix} M_{11} & M_{12} \\ M_{21} & M_{22} \end{pmatrix}\begin{pmatrix} A(L) \\ B(L) \end{pmatrix}, \tag{1}$$

where L is the length of the medium expressed by the number of layer pairs, A and B are the right – and leftward travelling waves respectively.

Transfer matrix M is the product of matrices for each period of layer

$$M(0,L) = \prod_{m=1}^{N-1} M(\Lambda_m, \Lambda_{m+1}), \tag{2}$$

$$M(\Lambda_m, \Lambda_{m+1}) = T_{l,m} \cdot S_u \cdot T_{h,m} \cdot S_d, \tag{3}$$

where Λ_m - high +low refraction index layer period, $T_{h,m}$ and $T_{l,m}$ - propagation wave matrices for high and low refraction index layer respectively, S_u и S_d - normalized up and down Fresnel matrices respectively.

$$T_{h,m} = \begin{pmatrix} e^{i\phi_{h,m}} & 0 \\ 0 & e^{-i\phi_{h,m}} \end{pmatrix} \qquad T_{l,m} = \begin{pmatrix} e^{i\phi_{l,m}} & 0 \\ 0 & e^{-i\phi_{l,m}} \end{pmatrix}$$

$$S_u = \frac{1}{2\sqrt{n_h n_l}}\begin{pmatrix} n_h + n_l & n_l - n_h \\ n_l - n_h & n_h + n_l \end{pmatrix} \quad S_d = \frac{1}{2\sqrt{n_h n_l}}\begin{pmatrix} n_h + n_l & n_h - n_l \\ n_h - n_l & n_h + n_l \end{pmatrix}. \tag{4}$$

$$\phi_{h,m} = kn_h d_{n,m},\ \phi_{l,m} = kn_l d_{l,m},\ d_{h,m} = (m/N)^{o_{ch}} \lambda_B / (4\pi n_h), \quad d_{l,m} = (m/N)^{o_{ch}} \lambda_B / (4\pi n_l), \tag{5}$$

where k is the wavevector; $\phi_{h,m}, \phi_{l,m}, d_{h,m}, d_{l,m}$ are phase and thickness of high and low refraction index layer for m - period respectively, N – number of chirped layer periods, o_{ch} is the chirping order.

The complex reflectivity r_m of the periodic structure for the wave incident from the left side is given by

$$r_m = \frac{A(0)}{B(0)} = \frac{M_{21}}{M_{11}} = \sqrt{R}e^{j\Phi}, \tag{6}$$

where R and Φ are the amplitude and phase of the reflectivity, respectively.

The group delay GD of the chirped mirror is generally given by $GD(\omega) = -\partial\Phi / \partial\omega$, where ω is the optical frequency. The group delay dispersion GDD is given by $GDD(\omega) = \partial GD(\omega) / \partial\omega$.

CALCULATION RESULTS

In our case the structure consists of 25 layers. First 12 layers are chirped with $d_h = (k/12)^{o_{ch}} \lambda_B / (4\pi n_h)$, $d_l = (k/12)^{o_{ch}} \lambda_B / (4\pi n_l)$, where o_{ch} is the chirping order. Next 13 layers compose the quarter–wave section with fixed Bragg wavelength. It is necessary to obtain high reflectance over a wavelength range as broad as possible. Fig. 3 shows the dependence of *GD* and *GDD* from the optical wavelength at various meanings o_{ch}. For the second - and third - order CM at the Bragg wavelength *GDD* equals zero and for fourth – order CM we have a negative and slightly constant *GDD* with an absolute value 16.7 fs^2.

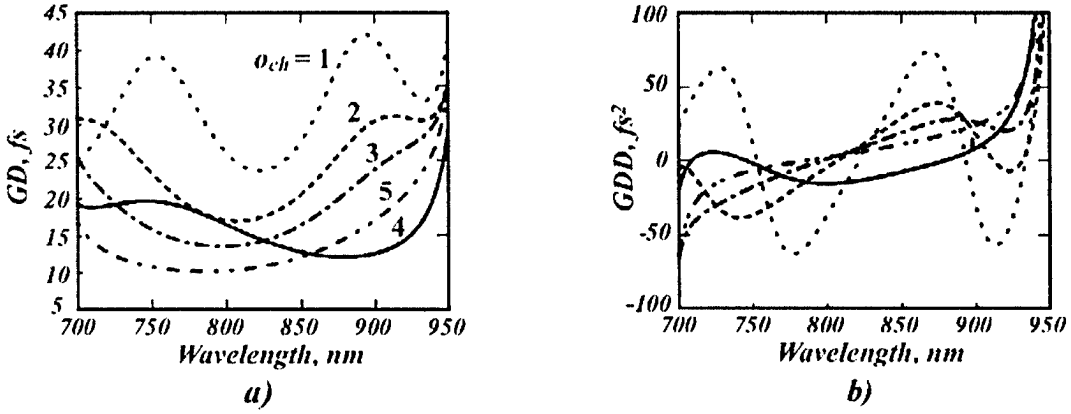


Fig. 3. Group delay (a) and group delay dispersion (b) versus optical wavelength at various meanings o_{ch}.Dotted line: o_{ch}=1, Dashed line: o_{ch}=2, Dash-dotted line: o_{ch}=3, Solid line: o_{ch}=4 Dash-two-dotted line: o_{ch}=5

CONCLUSIONS

The chirping mirrors with chirping both high and low refractive index layers are investigated using the transfer matrix method. The results show the negative and slightly constant group delay dispersion with an absolute value 16.7 fs^2 at the Bragg wavelength for the fourth – order chirping mirrors. These results allow further investigating the light propagation in asymmetrical periodical structures and pulse reflection from new type of mirrors.

REFERENCES

[1] F. X. Kaertner, N. Matuschek, T. R. Schibli, U. Keller, H.A. Haus, C. Heine, R. Morf, V. Scheuer, M. Tilsch, T. Tschudi, Design and fabrication of double-chirped mirrors // Opt. Lett. 22(11), pp. 831-833 (1997).

[2] U. Morgner, R. Ell, T.R. Schibli, P. Wagenblast, F. X. Kaertner, J.G. Fujimoto, E. P. Ippen, V. Scheuer, G. Angelow, T. Tschudi, Double-chirped mirror pairs covering one octave of bandwidth // Proc. CLEO'00, **CMB2** (2000).

[3] R. Szipöcs, K. Ferencz, Ch. Spielmann, F. Krausz, "Chirped multilayer coatings for broadband dispersion control in femtosecond lasers," Opt. Lett. **19**, p. 201 (1994).

[4] N. Matuschek, F. X. Kaertner and U. Keller, Theory of double-chirping mirrors // IEEE JSQE, 4(2), pp. 197 – 208 (1998).

[5] N. Matuschek, F. X. Kaertner and U. Keller, Analytical design of double-chirped mirrors with custom-tailored dispersion characteristics // IEEE JQE. 35(2), pp. 129 – 137 (1999)

MODELLING OF RADIATION FIELD EXCITED ON SHARP WAVEGUIDE DISCONTINUITIES BY NUMERICAL AND SEMI-ANALYTICAL METHODS

Elena A. Romanova[1], Szabolcs B. Gaal[2]

[1] Saratov State University, Astrakhanskaya 83, 410026, Saratov, Russia
[2] University of Twente, NL-7500 AE Enschede, Netherlands

ABSTRACT

Propagation of radiation field excited on a step-like discontinuity of dielectric slab waveguide is considered by using two different techniques: the Finite-Difference Beam Propagation Method and the Green's Function Method. Comparison of these techniques enables to evaluate approximations used in the FD-BPM as well as the truncation errors and influence of interface conditions.

INTRODUCTION

If radiation propagating along a waveguide axis occurs to be mismatched with modal field over some cross–section, spatial transient process being a result of light scattering from the irregularity occurs in longitudinally segmented devices: the radiation field excited at a step–like discontinuity by the incoming field leaks out of the fiber leaving merely the guided part of the total field behind [1,2].

The general approach to the diffraction problem solution based on the integral equations formalism and applied to the non-uniform part of the dielectric waveguide is presented in [3]. To solve the system of integral equations, the Galerkin method was applied that needs large computational time [4]. Another technique based on an iteration of the surface mode amplitudes was found to be more efficient. The method was used to calculate and analyse different types of discontinuities in planar dielectric waveguides [5]. Scattering from inhomogeneities immersed inside a dielectric slab waveguide was investigated analytically by solving initially a separate boundary-value problem to obtain a Green's function and then developing a procedure to solve a set of coupled equations for expansion coefficients of fields inside the inhomogeneity [6].

An alternative approach is to work with the total electric field. The most commonly used numerical method to solve the scalar wave equation is the Beam Propagation Method (BPM) [7] based conventionally on the Fast Fourier Transform (FFT-BPM). An alternate numerical scheme to solve the wave equation is to use a finite-difference approximation [8]. Following the Finite-Difference Beam Propagation Method (FD-BPM), the wave equation is replaced by a finite-difference scheme. Comparative analysis of the radiation field modelling by the FFT-BPM and the FD-BPM is presented in particular, in [9].

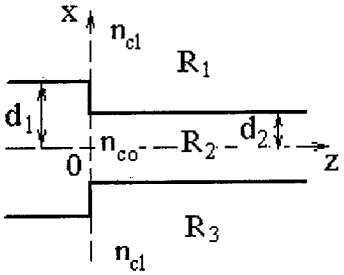


Fig.1

In this paper, we present an example of modelling of the radiation field propagation in a slab waveguide using the Green's Function Method (GFM) and the FD-BPM.

Instead of Gaussian beam excitation [9], we consider here a step-like discontinuity (Fig.1) consisting of two regular segments of slab waveguides with identical refractive index distributions and different core widths.

DESCRIPTION OF THE TECHNIQUES

Total field propagation through the step-like discontinuity can be simulated by the **FD-BPM** via solution of the paraxial wave equation:

$$\left(2i\beta\frac{\partial}{\partial z}+\frac{\partial^2}{\partial x^2}+\chi\right)E(x,z)=0 \tag{1}$$

for the slowly varying amplitude of the electrical field $E(x,z)$ with the longitudinal propagation constant β. Here z and x are longitudinal and transverse co-ordinates, respectively. The susceptibility is denoted by χ. Transverse distribution of the initial field is taken as:

$$E(x,0)=A\begin{cases}\cos(u_1 x/d_1)/\cos(u_1), x\le d_1\\ \exp(-w_1 x/d_1)/\exp(-w_1), x>d_1\end{cases} \tag{2}$$

that corresponds to the TE modal field of the first waveguide (u_1 and w_1 are transverse wavenumbers). This field in general is assumed to be unmatched with the TE modal field of the second waveguide ($d_1 \neq d_2$) that results in effective leakage of the power on the discontinuity.

This implementation of the FD-BPM enables to consider only the forward-travelling waves that is a reason to use the same approximation in the **GFM**. Following this technique, field distribution at any point z can be expressed by the integral:

$$E(x,z)=\int_{-\infty}^{\infty}dx'\left(E(x',0)\frac{\partial}{\partial z'}\Gamma(x,z\mid x',z')-\Gamma(x,z\mid x',z')\frac{\partial}{\partial z'}E(x',0)\right) \tag{3}$$

where the Green's function $\Gamma(x,z|x',z')$ is constructed so that it is zero on the interface $z=0$: $\Gamma(x,z|x',z')=G(x,z|x',z')-G(x,-z|x',z')$. Using the Fourier transform with respect to the z coordinate, we can obtain the following integral to be evaluated:

$$E(x,z)=-i\int_{-\infty}^{\infty}\beta\,d\beta\int_{-\infty}^{\infty}dx'\,E(x',0)G(x,z\mid x',\beta)\exp(-i\beta z') \tag{4}$$

With an assumed time dependence $exp(-i\omega t)$, the field of point sources in the core (region R_2) satisfies the non-homogeneous wave equation:

$$\left(\frac{d^2}{dx^2}+u_2^2\right)G^{(2)}=\delta(x-x')\exp(i\beta z)/(2\pi) \tag{5}$$

and consists of a superposition of homogeneous and non-homogeneous solutions:

$$G^{(2)}=a_2\cos(u_2x)+b_2\sin(u_2x)+i\exp(i\beta z-iu_2\mid x-x'\mid)/(4\pi u_2) \tag{6}$$

where $u_2=d_2\sqrt{k^2n_{co}^2-\beta^2}$. In the claddings (regions R_1, R_3), the field satisfies the wave equation:

$$\left(\frac{d^2}{dx^2}-w_2^2\right)G^{(1),(3)}=0 \tag{7}$$

and can be written in the form:

$$G^{(1)}=b_1\exp(-w_2x)\quad\text{and}\quad G^{(3)}=a_3\exp(w_2x) \tag{8}$$

with $w_2=d_2\sqrt{\beta^2-k^2n_{cl}^2}$.

The unknown coefficients b_1, a_2, b_2, a_3 can be obtained by using the boundary conditions on the surfaces $x=\pm 1$ (coordinates are normalised to d_2). Finally, the Green's function in the core region is found to be:

$$G^{(2)} = i\exp(i\beta z - iu_2 |x-x'|)/(2\pi u_2) -$$
$$-\exp(i\beta z - iu_2)\left(1+i\frac{w_2}{u_2}\right)\left(\frac{\cos(u_2x')\cos(u_2x)}{w_2\cos u_2 - u_2\sin u_2}+i\frac{\sin(u_2x')\sin(u_2x)}{w_2\sin u_2 + u_2\cos u_2}\right)/(4\pi) \quad (9)$$

Roots of the denominators in (9) determine the wavenumbers of the TE guided modes of the slab waveguide and are located inside the interval: $k^2n_{cl}^2 < \beta^2 < k^2n_{co}^2$.

Accuracy of the FD-BPM is well known to depend first, on the order of the transverse derivatives approximation [10] with special attention to interface conditions [11] and secondly, on parameters of a computational grid applied. A common way to evaluate the accuracy is to estimate numerical attenuation of the solution when the waveguide is assumed to be excited numerically by its proper modal field. If $E(x',0)$ corresponds to transverse distribution of the TE mode field given by (2), the second item of the sum in the lower part of (9) is zero and after some algebra one obtains:

$$E(x,z) = A\exp(i\beta z)\cos\left(\frac{d_2}{d_1}u_1x\right)/\cos(u_1) + \tilde{\Psi}(x,z) \quad (10)$$

with $\tilde{\Psi}(x,z) = \int_{-\infty}^{\infty} d\beta \frac{F(\beta)\exp(i\beta z)\cos(u_2x)}{w_2\cos u_2 - u_2\sin u_2}$. If $d_1=d_2$ (matched excitation), $F(\beta_0)=0$ when β coincides with a root of the denominator β_0 resulting in $\tilde{\Psi}(x,z)=0$. If $d_1 \neq d_2$ (unmatched excitation), $\tilde{\Psi}(x,z)\neq 0$ because of the guided mode poles. In order to calculate integrals in (10), an appropriate numerical technique should be used [6,12].

CONCLUSIONS

Two different techniques are applied to solve the same problem of radiation field propagation in a slab waveguide with a sharp discontinuity. In spite of the GFM is relatively complicated it is free from the truncation errors and errors of interface conditions modelling and can be used to evaluate these errors generated by the FD-BPM as well as feasibility of the paraxial approximation used by the FD-BPM.

REFERENCES

[1] D.Marcuse, *Bell. Syst. Tech. J.* 52 817-818, 1973.
[2] P.G.Suchoski, Jr., and V.Ramaswamy, *J. Opt. Soc. Am. A.* 3(2) 194-203, 1986.
[3] K.Tanaka, M.Tanaka and T.Omoya, *J.Opt.Soc.Am.A*, 15,101-105, 1998.
[4] E.N.Vasiliev, A.V.Polynkin, V.V.Soloduhov, *Radiotechniques and Electronics.* 25(9) 1862-1872, 1980.
[5] E.N.Vasiliev, A.V.Polynkin, V.V.Soloduhov, *Izv.VUZov "Radioelectronics".* 26(2) 72-76, 1983.
[6] N.K.Uzunoglu, J.G.Fikioris, *J.Opt.Soc.Am.*, 72(5) 628-637, 1982.
[7] M.D.Feit, J.A.Fleck, *Opt. Lett.* 14(13) 662-664, 1989.
[8] Y.Chung, N.Dagli, *J. of Quantum Electron.* 26(8) 1335-1339, 1990.
[9] E.A.Romanova, E.V.Bekker, M.Marciniak, *Opt. and Quantum Electron.* 34(5) 607-619, 2002.
[10] J.Yamauchi, J.Shibayama, H.Nakano, *Opt.and Quantum Electron.*, 31, 675-687,1999.
[11] X.P.Chiou, Y-C.Chiang, H-C Chang, *J. of Lightwave Technol.* 18 (2), 243-251, 2000.
[12] A.G.Yarovoy, *IEICE Trans.Electron.*, E 78-C (10), 1440-1446, 1995.

COUPLED OSCILLATIONS IN THE THEORY OF LAYERED DIELECTRIC

Mykola I. Ayzatsky, Katherina Yu. Kramarenko
National Scientific Center – Kharkov Institute of Physics and Technology
Akademicheskaya St.,1, Kharkiv 61108, Ukraine
e-mail: kramer@kipt.kharkiv.ua

ABSTRACT

The periodic dielectric layered structure is considered in the case when at the interface between layers with high and low value of refractive index the full internal reflection takes place. The possibility of using of the coupled oscillation model (circuit model) for the description of the layered structure is shown. The considered model gives the possibility to make an approximate analysis of various multilayered structures and develop new multilayer films.

INTRODUCTION

The methods of tuning of slow-wave structures, based on inhomogeneous disk-loaded waveguides, using the special cavity stacks was developed [1]. Such methods based on the various cavity stacks allow not only to tune the resonant structures, but to synthesize new regular non-periodic systems, which transmit RF power at the working frequency. These methods of tuning are the most effective in the case, when every resonator of the structure strongly interacts only with adjoining cells. The mathematical model of tuning procedure is based on the method of coupled oscillators. To use the developed method for creating new inhomogeneous multi-layered structures, it is necessary to have the similar method for calculation of layered structure characteristics. In this paper we represent a new method for description the characteristics of periodic dielectric structure.

EIGEN OSCILLATIONS OF THE DIELECTRIC LAYER

We consider the propagation of a TM polarized wave in periodic dielectric structure. The structure period consists of two layers with refractive index n_1 and n_2, layer thickness d_1 and d_2, correspondingly. Electromagnetic fields in the layers with high value of refractive index (n_1) we expand into Fourier–series with the set of functions, which have been obtained from the boundary problem with zero boundary conditions for the tangential component of the electric field ($E_m^{(k)}(0) = E_m^{(k)}(d_1) = 0$):

$$E_x^{(k)} = \sum_{m=0}^{\infty} A_m^{(k)} E_m^{(k)}(z); \tag{1.1}$$

$$H_y^{(k)} = \sum_{m=0}^{\infty} B_m^{(k)} H_m^{(k)}(z). \tag{1.2}$$

The eigen functions are as follows:

$$E_m^{(k)} = \sin(h_m(z - kD)); \tag{2.1}$$

$$H_m^{(k)} = \frac{\omega_m n_1^2 \varepsilon_0}{i h_m} \cos(h_m(z - kD)), \tag{2.2}$$

where $\omega_m = \frac{c}{n_1}\sqrt{\left(\frac{\pi}{d_1}m\right)^2 + k_\perp^2}$ are the resonant frequencies of the layer, $h_m = \frac{\pi}{d_1}m$, $m = 0, 1, 2 \ldots$, $k_\perp$ is the transverse component of the wave vector, $D = d_1 + d_2$ is the structure period, k is the number of the structure period.

As the eigen functions determine some resonant frequencies of the layer, some oscillator may be put in accordance with each function. So, the infinite number of oscillators correspond to each layer. Coefficients $A_m^{(k)}$, $B_m^{(k)}$ in eqs. (1.1, 1.2) can be found from the problem of layer excitation by surface electric fields. Electromagnetic field in the layer with low refractive index we represent as superposition of two waves.

MODEL OF COUPLED OSCILLATORS IN THE THEORY OF LAYERED DIELECTRIC

We choose one oscillator in each layer with high value of refractive index as a basic. Let's suppose that at the interface between layers with high and low (second layer) value of refractive index the full internal reflection takes place. The parameters of the second layer determine the coupling between the oscillators. With the help of the method of excitation of volumes by surface fields we obtain the set of coupled equations for the amplitudes of basic oscillators. These equations have the following form:

$$\left(\omega^2 - \omega_m^2\right)B_m^{(k)} = \omega_m^2\eta\sum_s B_m^{(s)}\tilde{\rho}^{|k-s|} + \omega_m^2\mu\sum_s\left(B_m^{(s-1)} + B_m^{(s+1)}\right)\tilde{\rho}^{|k-s|} \tag{3}$$

where $\eta = \frac{\tilde{\rho}}{1-\tilde{\rho}^2}\frac{4n_1^2 d_1\left((-1)^m s_1 - \alpha_1 - \alpha_2\right)}{\left((\pi m)^2 + k_\perp^2 d_1^2\right)\tilde{s}_1 s_2}$, $\mu = \frac{\tilde{\rho}}{1-\tilde{\rho}^2}\frac{(-1)^m 2n_1^2 d_1}{\left((\pi m)^2 + k_\perp^2 d_1^2\right)\tilde{s}_1}$,

$\tilde{\rho} = \tilde{Q} + (-1)^m\sqrt{\tilde{Q}^2 - 1}$, with $\tilde{Q} = \frac{(\tilde{\alpha}_1 + \alpha_2)^2 - \tilde{s}_1^2 - s_2^2}{\tilde{s}_1 s_2}$, $\alpha_1 = \frac{n_1^2\cos(h_1 d_1)}{h_1\sin(h_1 d_1)}$,

$\alpha_2 = \frac{n_2^2\cos(h_2 d_2)}{h_2\sin(h_2 d_2)}$, $s_1 = \frac{n_1^2}{h_1\sin(h_1 d_1)}$, $s_2 = \frac{n_2^2}{h_2\sin(h_2 d_2)}$, $\tilde{\alpha}_1 = \alpha_1 + \frac{2n_1^2 d_1}{(\pi m)^2 - (h_1 d_1)^2}$,

$\tilde{s}_1 = s_1 + \frac{(-1)^m 2n_1^2 d_1}{(\pi m)^2 - (h_1 d_1)^2}$, $h_1 = \sqrt{\frac{\omega^2}{c^2}n_1^2 - k_\perp^2}$, $h_2 = \sqrt{\frac{\omega^2}{c^2}n_2^2 - k_\perp^2}$. At that, $|\tilde{\rho}| < 1$.

The left part of equation (3) coincide the harmonic oscillator equation (ω_m is the resonant frequency, $B_m^{(k)}$ is the amplitude of the oscillation). The number of the components at the right part of equation (3) depends upon the degree of coupling between the oscillators. For "paired coupling" equation (3) will have the form:

$$\left(\omega^2 - \omega_m^2\right)B_m^{(k)} = B_m^{(k)}\omega_m^2(\eta + 2\mu\tilde{\rho}) + \left(B_m^{(k-1)} + B_m^{(k+1)}\right)\omega_m^2(\mu + \eta\tilde{\rho} + \mu\tilde{\rho}^2) \tag{4}$$

For "cross-cavity coupling" equation (3) will have the following form:

$$\left(\omega^2 - \omega_m^2\right)B_m^{(k)} = B_m^{(k)}\omega_m^2(\eta + 2\mu\tilde{\rho}) + \left(B_m^{(k-1)} + B_m^{(k+1)}\right)\omega_m^2(\mu + \eta\tilde{\rho} + \mu\tilde{\rho}^2) +$$
$$+ \left(B_m^{(k-2)} + B_m^{(k+2)}\right)\omega_m^2(\mu\tilde{\rho} + \eta\tilde{\rho}^2 + \mu\tilde{\rho}^3) \tag{5}$$

Dependence of dimensionless frequency (ω/ω_0) versus the phase shift per period (ϕ) inside the first passband of layered structure ($m = 0$) is shown on fig. 1. We compare the dispersion characteristics obtained from the equations for "paired coupling" (eq. 4) and

cross-cavity coupling" (eq. 5) with real dispersion curve of periodic dielectric structure for several values of the thickness of second layer. Results are given in Table 1.
One can see, that for sufficiently thick second layer the model of coupled oscillators can be used for description the layered structure.

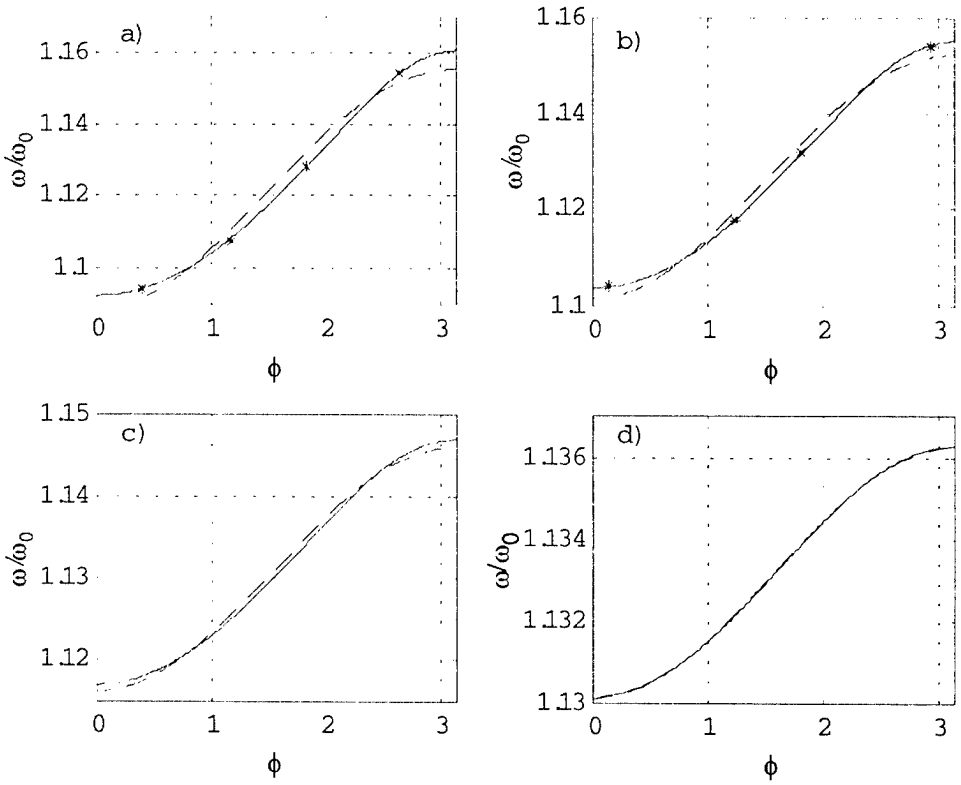


Fig. 1. Dispersion curve of periodic dielectric structure with $d_1 = \lambda_0 / n_1$ (solid line), dispersion curve from eq. 4 (dashed line), dispersion curve from eq. 5 (*) for the following values of second layer thickness: a) $d_2 = \lambda_0 / 8n_2$; b) $d_2 = \lambda_0 / 6n_2$; c) $d_2 = \lambda_0 / 4n_2$;d) $d_2 = \lambda_0 / 2n_2$, $\lambda_0 = 632.8\ nm$.

Table 1. Maximum deviation of ϕ determined from eqs. 4, 5 from the real value inside the first passband ($m = 0$) of periodic dielectric structure for different values of second layer thickness; $d_1 = \lambda_0 / n_1$, $\lambda_0 = 632.8\ nm$.

$d_1 = \lambda_0 / n_1$	$d_2 = \lambda_0 / 8n_2$	$d_2 = \lambda_0 / 6n_2$	$d_2 = \lambda_0 / 4n_2$	$d_2 = \lambda_0 / 2n_2$
"pared coupling"	25.25°	22.7°	18.02°	3.81°
"cross-element coupling"	10.56°	7.86°	4.22°	0.06°

REFERENCES

[1] Aizatsky M.I., Biller E.Z. "Development of inhomogeneous disk-loaded accelerating waveguides and RF-coupling". Proceedings of the XVIII Linear Accelerator Conference, Geneva. – 1996. – 1. – P.119-121.

STRATIFICATION METHOD FOR ANALYSIS OF THE RADIAL INHOMOGENEOUS DIELECTRIC WAVEGUIDE: A NEW APPROACH TOWARDS REALIZATION

Victor Katok, Michail Kotenko, Olena Ometsinska
State University of Informative and Communicative Technology.
Scientific and Engineering Cable Lines Center, Kyiv, Ukraine
E-mail: katok@ukrpak.net, michael_kot@mail.ru

ABSTRACT

In this article we proposed a new approach towards realization of the stratification method for analysis of electrodynamic characteristics of radial inhomogeneous dielectric waveguide. We also used exact solutions of the wave equations.

INTRODUCTION

The analysis of characteristics of a light-guide is based on a solution of a boundary value problem for wave equations, the latter ones resulting from the Maxwell equations. Among the other approximate methods of its solution, the method of stratification has a number of advantages. The traditional realization of the algorithm for exact wave equations is linked to the solution of a badly conditioned system of the high order linear algebraic equations [1], and becomes complicated because of the large volume of calculations. The approach offered hereby solves this problem.

Exact equations for propagated waves in radial inhomogeneous dielectric waveguide

Let electromagnetic field in a dielectric light-guide with round cross section, which is regular along an axis, vary according to the principle: $\mathbf{E} = (E_r, E_\theta, E_z) \exp[-i(\omega t - \beta z - \nu\theta)]$, $\mathbf{H} = (H_r, H_\theta, H_z) \exp[-i(\omega t - \beta z - \nu\theta)]$, where ω is an angular frequency, β is a longitudinal mode propagation constant, $\nu = 0, 1...$ is an azimuth mode number. The components of amplitudes depend on radial coordinate r.

The system of coupled differential equations regarding longitudinal components E_z, H_z electrical and magnetic field describe the wave processes in optical fiber with arbitrary radial allocation of a core permittivity $\varepsilon(r)$

$$\left[\frac{d^2}{dr^2}+\frac{1}{r}\frac{d}{dr}+\left(\kappa^2-\frac{\nu^2}{r^2}\right)\right]H_z-\frac{\mu_0\omega^2\varepsilon_a'}{\kappa^2}\frac{dH_z}{dr}=-\frac{i\nu\beta\omega\varepsilon_a'}{\kappa^2}\frac{E_z}{r}, \quad (1)$$

$$\left[\frac{d^2}{dr^2}+\frac{1}{r}\frac{d}{dr}+\left(\kappa^2-\frac{\nu^2}{r^2}\right)\right]E_z-\frac{\beta^2\varepsilon_a'}{\varepsilon_a\kappa^2}\frac{dE_z}{dr}=\frac{i\nu\beta\mu_0\omega\varepsilon_a'}{\kappa^2\varepsilon_a}\frac{H_z}{r}, \quad (2)$$

which corresponds to the boundary conditions at core/cladding boundary $r = a$. The boundary conditions express equality on boundary of component fields E_z, H_z, E_θ, H_θ, where

$$E_\vartheta=\frac{1}{\kappa^2(r)}\left[\frac{\nu\beta}{r}E_z+i\omega\mu_0\frac{dH_z}{dr}\right],\quad H_\vartheta=\frac{1}{\kappa^2(r)}\left[-\frac{\nu\beta}{r}H_z+i\omega\varepsilon_a\frac{dE_z}{dr}\right],$$

and $\kappa^2(r)=\omega^2\mu_0\varepsilon_a-\beta^2$ and $\varepsilon_a=\varepsilon_0\varepsilon(r)$ is the absolute permittivity in a core region.

THE METHOD OF STRATIFICATION OF AN APPROXIMATE SOLUTION OF WAVE EQUATIONS

Stratification method [2] consists of approximation of an actual light-guide comprising gradiental core, with the multi-layered structure with N of cylindrical strata; the cover equals stratum (N + 1). The permittivity $\varepsilon_j = (n_j)^2$ of the j-stratum, where j = 1, 2, ... N+1, is constant, and its value and thickness of a stratum $\rho_j=r_j/a$ are chosen in such a way that it is convenient to approximate an actual refractive index profile (RIP) (n_j – refractive index).

Within the boundaries of the j-stratum, (1) and (2) are the Bessel equations of ν-order, and they are linked by the boundary conditions. Therefore, allocation of longitudinal components within the fields in j-stratum (j = 2, 3 ... N) can be described by the linear combination of cylindrical functions

$$E_{zj} = i[A_j Z_{1\nu}(|\kappa_j|\rho) + B_j Z_{2\nu}(|\kappa_j|\rho)],\ H_{zj} = \sqrt{\varepsilon_0/\mu_0}\,[C_j Z_{1\nu}(|\kappa_j|\rho) + D_j Z_{2\nu}(|\kappa_j|\rho)], \qquad (3)$$

and the field in the first sphere and covering – with the help of the following expressions:

$$\begin{bmatrix} E_{z1} \\ H_{z1} \end{bmatrix} = Z_{1\nu}(|\kappa_1|\rho)\begin{bmatrix} iA_1 \\ \sqrt{\varepsilon_0/\mu_0}\,C_1 \end{bmatrix}, \qquad \begin{bmatrix} E_{z,N+1} \\ H_{z,N+1} \end{bmatrix} = K_\nu(W\rho)\begin{bmatrix} iB_{N+1} \\ \sqrt{\varepsilon_0/\mu_0}\,D_{N+1} \end{bmatrix}, \qquad (4)$$

Where $\kappa_j^2 = a^2(\varepsilon_j k^2 - \beta^2)$, $W^2 = a^2(\beta^2 - \varepsilon_{N+1}k^2) > 0$, $k=\omega/c$ is the wave number in a free space, and $Z_{1\nu}$, $Z_{2\nu}$ – Bessel functions of ν-order, belonging to the 1st and 2nd types respectively. Depending on whether the cross-wave number κ_j in the relevant stratum appears to be real or imaginary one, cylindrical functions are rendered as usual cylindrical functions J_ν, Y_ν and as modified – I_ν, K_ν.

Considering (3) and (4), the boundary conditions when $\rho = \rho_j$ between the j-stratum and (j + 1) stratum of a core, and with N = 1 on the boundary of a core /clading gain the following aspect

$$M_j(\rho_j)\begin{bmatrix} A_j \\ B_j \\ C_j \\ D_j \end{bmatrix} = M_{j+1}(\rho_j)\begin{bmatrix} A_{j+1} \\ B_{j+1} \\ C_{j+1} \\ D_{j+1} \end{bmatrix}, \qquad M_N(\rho_N)\begin{bmatrix} A_N \\ B_N \\ C_N \\ D_N \end{bmatrix} = K_\nu(W)\begin{bmatrix} B_{N+1} \\ D_{N+1} \\ -\nu\beta a B_{N+1}/W^2 - kaKD_{N+1} \\ -n_{N+1}^2 kaKB_{N+1} - \nu\beta a D_{N+1}/W^2 \end{bmatrix}, \qquad (5)$$

where $K=K_\nu'(W)/(K_\nu(W)W)$, a $M_p(\rho_j)$ ($p = j, j+1$) – matrix

$$M_p(\rho_j) = \begin{bmatrix} Z_{1\nu}(\rho_j|\kappa_p) & Z_{21\nu}(\rho_j|\kappa_p) & 0 & 0 \\ 0 & 0 & Z_{1\nu}(\rho_j\kappa_p) & Z_{2\nu}(\rho_j|\kappa_p) \\ \nu\beta a Z_{1\nu}(\rho_j\kappa_p) & \nu\beta a Z_{2\nu}(\rho_j|\kappa_p|) & kaZ_{1\nu}'(\rho_j\kappa_p|) & kaZ_{2\nu}'(\rho_j\kappa_p) \\ \rho_j\kappa_p^2 & \rho_j\kappa_p^2 & |\kappa_p|Sign(\kappa_p^2) & \kappa_p Sign(\kappa_p^2) \\ \dfrac{n_p^2 kaZ_{1\nu}'(\rho_j|\kappa_p)}{|\kappa_p|Sign(\kappa_p^2)} & \dfrac{n_p^2 kaZ_{2\nu}'(\rho_j\kappa_p|)}{|\kappa_p|Sign(\kappa_p^2)} & \dfrac{\nu\beta a Z_{1\nu}(\rho_j\kappa_p)}{\rho_j\kappa_p^2} & \dfrac{\nu\beta a Z_{2\nu}(\rho_j|\kappa_p)}{\rho_j\kappa_p^2} \end{bmatrix},$$

In which for the 1-st stratum (j = 1, p = 1) it is necessary to consider all the components of the 2 and 4-th columns zero. In the matrix of coefficients for allocation of fields it is necessary to consider B_1= D_1=0.

Within the traditional implementation of the method of stratification of realization of boundary conditions, (5) leads to homogeneous system $4N$ of the linear algebraic equations with regard to $4N$ of unknown coefficients in allocation of fields (3), (4). The requirement for existence of the nonzero solution for this system displays dispersion relation (secular equation) $\det S(k, \beta) = 0$, where S is matrix of coefficients of a system. For the calculated value of the radical β
of a secular equation (k – fixed value), the distribution coefficients of the fields can be determined from heterogeneous system $4N$-1 of the equations. With the known allocation of the fields, it is possible to make calculations concerning other electrodynamic characteristics of a light-guide. Not only is such an approach time-consuming and complicated, but also it might lead to the unreliable outcomes as a result of a poor conditionality in the systems of high order [1].

REALIZATION OF THE STRATIFICATION METHOD ON THE BASIS OF TRANSMISSION MATRIXES

Below we suggest the method that helps to eliminate the indicated complications. It is based on deriving transmission between the neighboring strata at the expense of analytical transformations of compact expression for a matrix. It allows obtaining a secular equation of a light-guide in a full-scale shape, which is convenient for the analysis.

Let us express from (5) the matrix of coefficients in j+1-th stratum, using the coefficients in j-th stratum

$$X_{j+1} = T(\rho_j)X_j, \qquad T(\rho_j) = [M_{j+1}(\rho_j)]^{-1} \cdot M_j(\rho_j), \qquad j = 1, 2, \ldots N-1, \tag{6}$$

where X_j is matrix-column of coefficients for allocation of the field (3) in j-th stratum. We shall name $T(\rho_j)$ a matrix of transmission from j to $(j+1)$ stratum of a core.

After volumetric analytical transformations (with the multiple usage of the value of Wronskian for cylindrical functions [1]), $T(\rho_j)$ gains its visual aspect

$$T(\rho_j) = \begin{bmatrix} m_{12,2}(j) & m_{22,2}(j) & f_{12}(j)/n_{j+1}^2 & f_{22}(j)/n_{j+1}^2 \\ -m_{11,2}(j) & -m_{21,2}(j) & -f_{11}(j)/n_{j+1}^2 & -f_{21}(j)/n_{j+1}^2 \\ f_{12}(j) & f_{22}(j) & m_{12,1}(j) & m_{22,1}(j) \\ -f_{11}(j) & -f_{21}(j) & -m_{11,1}(j) & -m_{21,1}(j) \end{bmatrix} \tag{7}$$

where $m_{rs,t}(j) = \rho_j|\kappa_{j+1}|e_{j+1}[Z_{rv}(\rho_j|\kappa_j|)\, Z'_{sv}(\rho_j|\kappa_{j+1}|) - \eta x(j) Z_{sv}(\rho_j|\kappa_{j+1}|) Z'_{rv}(\rho_j|\kappa_j|)]$;

$f_{rs}(j) = \nu\beta/k e_{j+1}(1-\kappa_{j+1}{}^2/\kappa_j{}^2) Z_{rv}(\rho_j|\kappa_j|) Z_{sv}(\rho_j|\kappa_{j+1}|)$; $x(j)=y_j y_{j+1}$; $r, s = 1,2$;

$$e_{j+1} = \begin{cases} \pi/2, & \text{if } \kappa_{j+1}^2 > 0, \\ -1, & \text{if } \kappa_{j+1}^2 < 0; \end{cases} \qquad \eta = \begin{cases} 1, & \text{if } i = 1, \\ \varepsilon_j/\varepsilon_{j+1}, & \text{if } i = 2; \end{cases} \qquad y_p = \begin{cases} 1, & \text{if } \kappa_p^2 > 0, \\ -1, & \text{if } \kappa_p^2 < 0, \end{cases}.$$

Sequentially satisfying boundary conditions (5) (starting from the interior boundary $\rho = \rho_1$ stratum of a core), we shall express a matrix of coefficients of N stratum through the matrix of the relevant coefficients of the 1st stratum. Let us replace the obtained matrix to the left part of the boundary condition (5), with $N = 1$. In the outcome we shall receive a homogeneous system comprising 4 linear algebraic equations regarding quantities A_1, $C1$, B_{N+1}, D_{N+1}.

$$M_N(\rho_N)T\begin{bmatrix} A_1 \\ 0 \\ C_1 \\ 0 \end{bmatrix} = K_v(W)\begin{bmatrix} B_{N+1} \\ D_{N+1} \\ -v\beta aB_{N+1}/W^2 - kaKD_{N+1}/W \\ -n_{N+1}^2 kaKB_{N+1}/W - v\beta aD_{N+1}/W^2 \end{bmatrix}, \quad T=T_{N-1}(\rho_{N-1})T_{N-2}(\rho_{N-2})\ldots T_1(\rho_1), \quad (8)$$

where T shall be named as **matrix of transmission** from the 1-st to N stratum of a core. The matrix of transmission (7) with $\varepsilon_j \rightarrow \varepsilon_{j+1}$ is transformed into the unitary matrix., which ensures the correctness obtained with the method of stratification of an approximate solution with the large N, as well as possibility of the analysis of a single-stage light-guide (N=1) on the basis of the common algorithm.

The requirement for existence of the non-zero set of equations (8) leads to the dispersion relation in its full-scale aspect, which can be fixed in a way convenient for our analysis

$$F_{TE}(V, B, v)F_{TH}(V, B, v)+v^{2(N-1)}F_1(V, B)+v^2F_2(V, B, v)+v^NF_3(V, B, v)=0, \quad (9)$$

where B and V – phase parameter of a light-guide and normalized frequency:

$B = (\beta^2/k^2-\varepsilon_{cl})/(\varepsilon_{max}-\varepsilon_{cl})$, $V = ak\sqrt{\varepsilon_{max}-\varepsilon_{cl}} \geq 0$, $B \in [0;1]$.

Because of the fact that the dependence of all functions within the number (9) on v is polynomial, with v =0 number (9) disintegrates into dispersion equations for TE- and TH- waves: F_{TE} (V, B, 0) =0 and F_{TH} (V, B, 0) =0. In case v≠0, (9) is a secular equation for the hybrid modes EH and HE, while with v=1 – for the basic mode HE_{11}. With B→0 for light-guides with the negative value of volume RIP [3], the third item in the left-hand part (9) is dominating, and equation $F_2(V, B, 1)=0$ provides good approximation for calculation of the non-zero frequency of intercepting of the basic mode (while applying the methods different from the one mentioned above, the procedure presents essential difficulties).

With calculated on fixed frequency V of a value of radical B of the equation (9), we can determine the relative values of coefficients on the basis of 3 random equations of a system (8). Afterwards, according to the formula (6), distribution coefficients of the fields can be calculated, starting from the 2nd stratum and finishing with N.

CONCLUSION

The offered approach to realization of the stratification method on the basis of the obtained full-scale expression for a matrix of transmission eliminates the problem of solution of the poorly stipulated set of equations of the high order. This problem used to be major part of the traditional approach. The secular equation that we obtained with the use of a transmission matrix, displays itself as being convenient for the analysis and calculation of a dispersion characteristics of modes of a light-guide. It allows for essential reducing of the volume of calculations dealing with the problems of analysis of light-guides with the composite RIP.

REFERENCES

[1] Belanov A. S., Krivenkov V. I., Kolomiytseva E. A. Dispersion calculation in light-guide with complicated refractive index profile (in Russian) // Radiotekhnika. – 1998. – No 3. – pp. 32–35.

[2] Clarricoats P.J.B., Chan K.B. Electromagnetic-wave propagation along radially inhomogeneous dielectric cylinders// Ell. Lett. – 1970. – Vol. 6, No. 22. – pp. 694–695.

[3] Kotenko M. Investigation of effect shifting normalized cutoff frequency of a round light guide with negative profile volume// ICTON 2002. - pp. 225 – 229.

PRINTED ANTENNAS AND CIRCUITS

DIFFRACTION OF ELECTROMAGNETIC WAVE BY AN ARRAY OF COMPLEX SHAPE MICROSTRIP REFLECTORS

Alexander M. Lerer, Gennady P. Sinyavsky and Dmitry E. Zelenchuk

Applied Electrodynamics and Computer Modelling Department
Rostov State University, Rostov-on-Don, Russia

E-mail: lerer@phys.rnd.runnet.ru, sinyavsky@phys.rnd.runnet.ru
zelenchuk@phys.rnd.runnet.ru

ABSTRACT

An approach for solving the problem of electromagnetic wave diffraction by an array of complex shape microstrip reflectors is proposed. The approach employs basis function taking into account the edge condition in all the points of complex shape microstrip reflectors except the corner ones. Several numerical results for polygon-shape microstrip reflector arrays are presented.

INTRODUCTION

At present microstrip reflector arrays are widely used to implement low-cost and low size antennas. Such arrays consist of a planar array of microstrip patches on a dielectric substrate. Usually the patches are of simple shape (rectangular or disk-like) [1]. Using the patches of complex shape can decrease size of the array and increase bandwidth. Fundamental problem for the arrays is the diffraction of electromagnetic wave by an array of complex shape microstrip reflectors. There are several papers employing FDTD or FEM technique to solve the problem. However, these techniques require significant

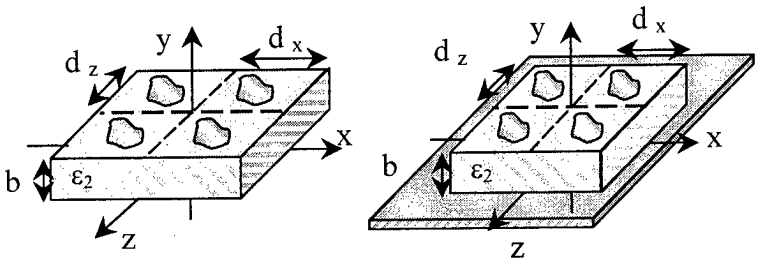


Fig. 1.Array of complex shape microstrip reflectors on dielectric layer (a), the same one with ground plane (b).

computational resources. The paper presents a fast method to solve the problem of electromagnetic wave diffraction by an array of complex shape microstrip reflectors placed on multilayered dielectric substrate.

FORMULATION

Structures to be considered are shown in Fig.1. Microstrip patches are supposed to be infinitely thin and perfectly conducting. Structure under consideration is excited by TM -polarized plane wave with electric field strength $\vec{E}^{inc}$; the proposed scheme, however, also is appropriate to TE-polarized excitation with minimal modifications.
Electromagnetic fields are expressed in the terms of electrical and magnetic Hertz vectors, which have only y-directed component. Having satisfied boundary conditions at the boundaries of dielectric layers and the plane y = b, the problem is reduced to following integral equations [2]:

$$-grad\iint_S \sigma(x',z')g_m(x-x',z-z')ds' - \iint_S \vec{J}(x',z')g_e(x-x',z-z')ds' = \frac{ik\vec{E}^{inc}}{Z_0}$$

where S means surface of microstrip reflector, $\vec{J}(x,z)$ – current density, $\sigma = \frac{\partial J_x}{\partial x} + \frac{\partial J_z}{\partial z}$ – quantity proportional to charge density, $g_{m,e}$ are written employing Floquet's theorem for the case of infinite array as follows:

$$g_{m,e}(x,z) = \frac{2\pi}{d_x d_z}\sum_{m=-\infty}^{\infty}\sum_{n=-\infty}^{\infty} f_{m,e}(\rho_{mn})\exp\left[-i(\alpha_m x+\beta_n z)\right],$$

where $f_m(\rho)=\left[1/\varphi_m(\rho)+k^2/\varphi_e(\rho)\right]/\rho^2$, $f_e(\rho)=k^2/\varphi_e(\rho)$, $\varphi_{e,m}$ are the known functions depending only on frequency, number of dielectric layers and their parameters and $\rho_{mn}^2=\alpha_m^2+\beta_n^2$. When $\rho\to\infty\ \varphi_m\approx(\varepsilon_1+\varepsilon_2)/\rho$, $\varphi_e\approx k^2/(2\rho)$, $\varepsilon_{1,2}$ are the permittivities of dielectric layers that contain the patch. To solve the integral equations, the Galerkin method has been employed. In order to obtain efficient solution the basis functions taking into account the edge condition in all the points of complex shape microstrip reflectors except the corner ones:

$$\sigma(x,z)=\frac{1}{l(z)L}\sum_{j,m=0}^{\infty} S_{j,m}T_j\left(\frac{x-a(z)}{l(z)}\right)T_m\left(\frac{z}{L}\right)=\sum_{j,m=0}^{\infty} S_{j,m}\sigma_{j,m}(x,z),$$

where $T_m(x)$ are the weighted Chebyshev polynomials of the 1st kind, $S_{j,m}$ are unknown coefficients, $a(z)=\left[l^+(z)+l^-(z)\right]/2$, $l(z)=\left[l^+(z)-l^-(z)\right]/2$. Expressions for the current components are more complicated and can be found in [2]. Functions $l^+(z)$ and $l^-(z)$ denote upper and lower boundaries of the patch. In turn vertical lines $|z|=L$ are left and right boundaries of it, moreover these vertical lines can be even of zero length. Transition to the coordinates

$$x = a(L\cos r) + l(L\cos r)\cos t,\ z = L\cos r$$

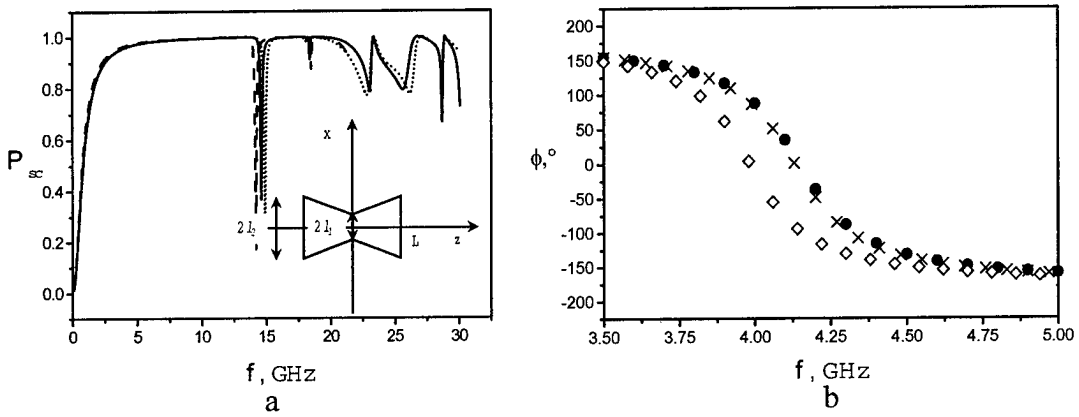


Fig.2. Normalized power scattered into the upper half-space by arrays without ground plane (a). Phase of electric field strength scattered by arrays with ground plane (b). Parameters of the arrays: dashed curve (a) or •(b) – l_1 = 1.2mm, l_2 = 1mm; solid (a) or ×(b) – l_1 = 1mm, l_2 = 1mm; dotted (a) or ◊(b) – l_1 = 1mm, l_2 = 1.2mm and ε_2 = 9.8, b_2 = 0.5mm, L=5mm,d_x = 3mm, d_z = 11mm, incidence angle is 45°.

helps decrease computational requirements for surface integrals calculations.
In addition there we have improved solution convergence by means of extracting the singular part of the integral equations kernel and transforming slowly convergent series into fast convergent ones. As the result a low-order system of linear algebraic equations has been obtained. The order of the system is shown not to exceed 10 and corresponding solution error is shown not to exceed 0.1 per cent.

NUMERICAL RESULTS AND CONCLUSION

Following the presented above method a computer program to study diffraction of electromagnetic wave by a two–dimensional array of complex-shape microstrip reflectors has been developed. By using this computer program we obtained numerical results shown in Fig. 2. Minima in Fig 2.a correspond to the first resonance (almost complete "blindness" effect) and surface waves excited in dielectric substrate. Fig. 2.b shows phase characteristics and one can see that the array of patches with narrowing in the center has got lower resonance in comparison with the others. This effect can be explained by the appearance of additional capacitance in narrowed patches.

REFERENCES

[1] J.A. Encinar, *IEEE Trans. Antennas Propagat.*, 2001, vol. AP-49, no 10, pp.1403-1410.
[2] A.M. Lerer, Y.A. Reisenkind, V.A. Sledkov, *Radiotekhnika i Elektronika*, 2000, vol.45, №3.

COMPARISON OF CAD FORMULAS, MOMENT METHOD AND EXPERIMENTS FOR RECTANGULAR MICROSTRIP ANTENNAS

Vladimír SCHEJBAL*, Zbynek RAIDA#, Zdenek NOVACEK#

* University of Pardubice, Studentska 95, 532 10 Pardubice, Czech Republic

Brno University of Technology, Purkynova 118, 612 00 Brno, Czech Republic

vladimir.schejbal@upce.cz, raida@urel.fee.vutbr.cz, novacek@urel.fee.vutbr.cz

ABSTRACT

Calculations of several cases for rectangular microstrip patch antennas using more accurate cavity model have been compared with the conventional cavity calculations, expressions generated by curve fitting to full wave solutions and method of moments. Calculated as well as experimental values have been studied for different thickness, patch sizes and substrate materials with different permitivities and losses.

INTRODUCTION

During the past twenty years, microstrip patch antennas experienced a great gain in popularity. They are well known for their highly desirable physical characteristics such as low profile, lightweight, low cost, ruggedness, and conformability. Numerous researchers have investigated their basic characteristics and extensive efforts have also been devoted to the design of "frequency agile," "polarization agile," or dual-band patch antennas. Although patch antennas appear simple and are easy to fabricate, obtaining electromagnetic fields, which satisfy all the boundary conditions, is a complicated task. For this reason, simplified approaches such as the transmission line model and the cavity model have been developed. The cavity model is particularly popular [1] - [3]. The basic idea of the cavity model is to treat the region between the patch and ground plane as a resonant leaky cavity. The simplified approaches allow the analysis as well as the design of rectangular microstrip patch antennas but the accuracy of those formulas is rather low. On the other hand, the more accurate full-wave analysis [3], [9] cannot be used for design because it is very time consuming. Therefore, new simple computer-aided design formulas for the rectangular microstrip patch antennas have been developed [4] (MSANCAD program), which use the cavity model but the more accurate models for open-end effect of microstrip lines and the effective permitivity are used.

One of the common methods of feeding a patch antenna is by means of a coaxial probe. The basic configuration is shown in Fig. 1, where a single metallic rectangular patch is printed on a grounded substrate. The patch is of length B, width A and substrate thickness h. The dielectric substrate has a relative permitivity ε_r. The feed-point coordinates of coaxial probe are $x_o = A/2$ and $y_o = L$. In this case, the linear polarization is radiated and the dominant mode is TM_{10}.

COMPARISON OF CAD FORMULAS AND EXPERIMENTS

The various rectangular patches have been calculated using MSANCAD program [4]. The results have been compared with the conventional cavity calculations using program MSANT [5], expressions generated by curve fitting to full wave solution (program PATCHD [6]) and method of moments (MoM) as well as experimental

values. A variety of different substrate thickness and patch sizes with various widths to length ratios and permitivities have been considered. Some of the comparison results have been already published ([4], [7] and [8]) and, therefore, they are not repeated here.

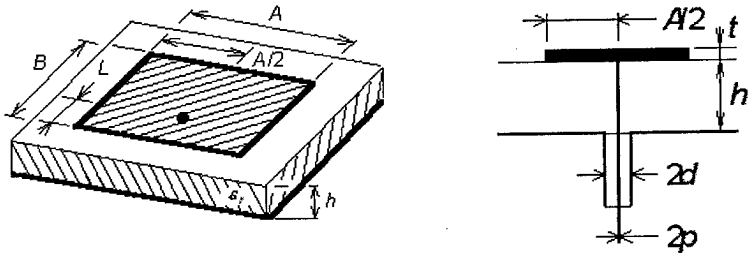


Fig. 1. Rectangular patch antenna fed by a coaxial probe

To perform the detailed comparison, several samples of patch antennas with various substrates have been completed [9]. In Fig. 2 and 3, the input impedance of antenna 1 and 2 are given. Antenna 1 uses the AR 600 substrate with measured $\varepsilon_r = 6.45$ and $\text{tg}\,\delta = 64\times10^{-4}$ (the producer declares values of $\varepsilon_r = 6.0 \pm 0.5$ and $\text{tg}\,\delta = 35\times10^{-4}$). The substrate dimensions are 90×90 mm. The patch dimensions are $A = B = 68$ mm. The 50Ω connector is placed at $L = 25$ mm, $p = 0.6$ mm. Antenna 2 uses the rather loss substrate with measured $\varepsilon_r = 4.24$ and $\text{tg}\,\delta = 266\times10^{-4}$. The substrate dimensions are 200×140 mm. The patch dimensions are $A = 100$ mm and $B = 80$ mm. The 50Ω connector is placed at $L = 5$ mm, $p = 0.6$ mm.

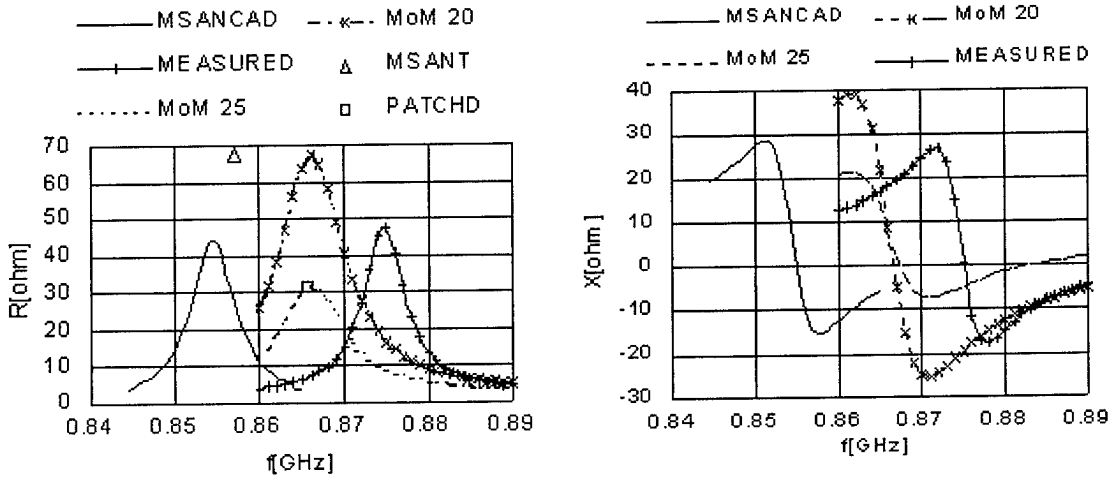


Fig. 2. Input resistance and reactance of probe-fed rectangular patch (antenna 1)

The input impedance has been measured using vector analyzer. The measured values have been corrected by means of directional coupler parameters. The MoM with two-dimensional model of coaxial probe feeding is employed. The input impedance is calculated using surface currents. It can be seen that the calculations and measured values are in agreement.

CONCLUSIONS

Various simple CAD formulas for a rectangular patch antenna have been presented (see [1] to [4]). The method [4] (code MSANCAD) uses the cavity model with the more

accurate models for open-end effect of microstrip lines and the effective permitivity. That allows increasing accuracy and reliability. Because of the relative simplicity of the model [4], the analysis as well as the design of rectangular microstrip patch antennas can be performed. Published comparisons ([4], [7] and [8]) are not repeated here.

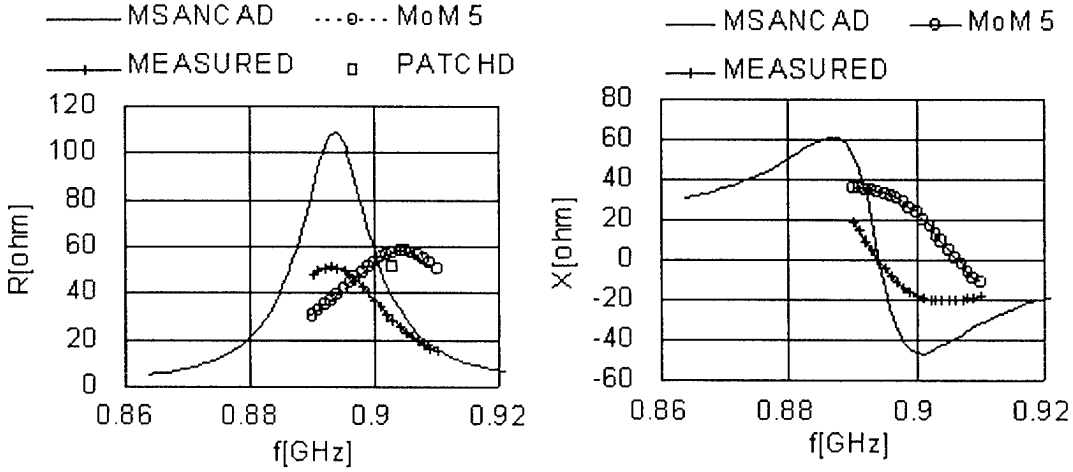


Fig. 3. Input resistance and reactance of probe-fed rectangular patch (antenna 2)

The MSANCAD [4] calculations have been compared with MSANT [5] and PATCHD [6] (resonant resistances are only calculated), the input impedance measurements and MoM computations (MoM 20 and MoM 25 use L = 20 and 25 mm, respectively). The differences between measurement and MSANCAD, PATCHD, MSAMT and MoM resonant frequencies are about 1%. Considering the impedance input characteristics bigger differences can be observed (the MSANT resonant resistance is 218 Ω for antenna 2 and it is not shown).

REFERENCES

[1] Carver, K.R. - Mink, J.W.: Microstrip antenna technology. *IEEE Trans.*, **AP-29**, 1981, no. 1, pp. 2 - 24.

[2] Collin, R.E.: *Antennas and radiowave propagation.* N.York, McGraw-Hill 1985, pp. 273-283.

[3] Lee, K. F. - Chen, W.: *Advances in microsptrip and printed antennas.* N. York J. Wiley 1997.

[4] Schejbal, V.: CAD of rectangular mircostrip antennas. *Radioengineering.* **8,** 1999, no. 3, pp. 17 - 20.

[5] Pozar, D.M.: *Antenna design using personal computers.* Dedham, Artech House 1985.

[6] Sainati, R.A.: *CAD of microstrip antennas for wireless applications.* Norwood, Artech House 1996.

[7] Schejbal, V.: Investigation of CAD for rectangular mircostrip antennas. *The 10th Conference on Microwave Techniques.* Pardubice, COMITE 1999, Oct. 12-13, 1999, pp. 135 - 138.

[8] Scheibal, V. Raida, Z. Novacek, Z.: CAD formulas and experiments for rectangular microstrip antennas. *MIKON – 2000,* Wroclaw, 2000, Volume 1, s. 159 - 162.

[9] Cernohorsky, D. Raida, Z. Skvor, Z. Novacek, Z.: *Analysis and optimization of microwave structures* (in Czech). Brno, Vutium 1999.

A LINE INTEGRAL REPRESENTATION OF THE PHYSICAL OPTICS FAR FIELD FROM PLANE PEC SCATTERERS ILLUMINATED BY ELECTRIC OR MAGNETIC HERTZIAN DIPOLES

Samel Arslanagić, Peter Meincke, Erik Jørgensen, and Olav Breinbjerg
Ørsted•DTU, Electromagnetic Systems, Technical University of Denmark,
Building 348, Ørsteds Plads, DK-2800 Kgs. Lyngby, Denmark,
Tel: +45 4588 1444, Fax: +45 4593 1634, E-mail: ob@oersted.dtu.dk

ABSTRACT We derive a line integral representation of the physical optics (PO) scattered far field that yields the exact same result as the conventional surface radiation integral. This representation applies to a perfectly electrically conducting plane scatterer illuminated by electric or magnetic Hertzian dipoles.

1. INTRODUCTION

Various line integral representations of the PO scattered field were reported in the literature (see [1]-[2] and previous works referenced therein). In [1]-[2] a line integral representation of the electric and magnetic PO field for arbitrary observation points scattered from a perfectly electrically conducting (PEC) planar plate illuminated by an electric as well as a magnetic Hertzian dipole (HD) was reported. In many applications it is sufficient to know the PO scattered far field. The expressions in [1]-[2] hold also for the case of a far-field observation point but are numerically inconvenient in this case, since they contain terms which do not contribute to the far field, and since they are subject to inaccuracies resulting from the use of a large but finite observation distance. In this paper we derive a line integral representation of the PO scattered far field that, in contrast to the general expressions, includes the distance-dependent part of the far field as an explicit factor. Throughout the paper the time factor exp(jωt) is suppressed.

2. THE LINE INTEGRAL DERIVATION

Consider the scattering configuration in Fig. 1. It consists of a plane, arbitrarily shaped, PEC plate A illuminated by either an electric or a magnetic HD with position vector $\mathbf{r}_S$. The observation point F and the image point I, with respect to the plane of the plate, are in the far-field region. Consequently, the truncated cones $V^{O,I}$ from [1],[2] are converted into the cylinders $C^{F,I}$ whose generators extend from the far-field observation and image points, respectively, to the edge Γ of the plate. The HD is located in the half space, including the plane of the plate, into which the unit normal vector $\hat{\mathbf{n}}$ of the plate is directed. However, the HD is not to be placed on the plate itself. In addition, $\hat{\mathbf{n}}$ is related to the edge unit tangent vector $\hat{\mathbf{t}}$ via the right-hand rule.

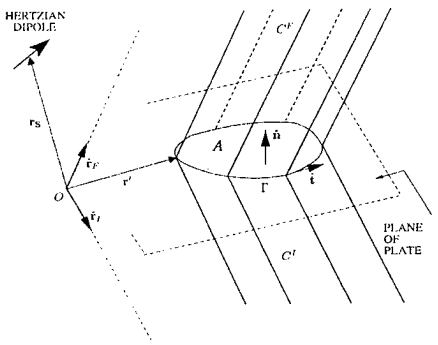


Fig. 1 Scattering configuration.

The observation point is, without loss of generality, assumed to be located in the same half-space as the HD, i.e., $\hat{\mathbf{r}}_F \cdot \hat{\mathbf{n}} \geq 0$. Finally, it is noted that the HD is not to be located on the surface of the cylinder C^F.

First, consider the illumination by an electric HD with the electric current density $\mathbf{J}_e = \boldsymbol{\alpha}_e \delta(\mathbf{r} - \mathbf{r}_S)$ where $\boldsymbol{\alpha}_e$ [Am] is the electric dipole moment and δ is the Dirac delta function. By evaluation of the analytical limit of [2, (11)] as the distance r_F to the far-field observation point tends to infinity, we find that the magnetic PO scattered far field, $\mathbf{H}^{PO}_{e,f}(\mathbf{r}_F)$ (subscripts e and f refer to the electric HD illumination and the far-field observation point, respectively), is

$$\mathbf{H}^{PO}_{e,f}(\mathbf{r}_F) = \frac{e^{-jkr_F}}{r_F} \int_\Gamma \Big[\hat{\mathbf{t}} \cdot \big(e^{jk\hat{\mathbf{r}}_F \cdot \mathbf{r}'} \, \overline{\mathbf{W}}_{e,f}(\mathbf{r}_F, \mathbf{r}') - e^{jk\hat{\mathbf{r}}_I \cdot \mathbf{r}'} \, \overline{\mathbf{W}}_{e,f}(\mathbf{r}_I, \mathbf{r}') \cdot (\overline{\mathbf{I}} - 2\hat{\mathbf{n}}\hat{\mathbf{n}}) \big) + \frac{1}{2\pi} e^{jk\hat{\mathbf{r}}_I \cdot \mathbf{r}'} \hat{\mathbf{n}}\hat{\mathbf{n}} \cdot (\hat{\mathbf{t}} \times \mathbf{H}^i_e(\mathbf{r}')) \Big] d\Gamma' - \mathbf{H}^i_e(\mathbf{r}_F) \chi(\mathbf{r}_F) \tag{1}$$

where the incident magnetic field $\mathbf{H}^i_e$ is given in [5, (12)], $\mathbf{r}'$ is the position vector of the integration point and k is the wave number. $\chi(\mathbf{r}_F) = 1$ if the HD is inside the cylinder C^F and zero otherwise. The dyad $\overline{\mathbf{W}}_{e,f}$ is the far-field version of [2, (13)] and reads

$$\overline{\mathbf{W}}_{e,f}(\mathbf{r}, \mathbf{r}') = \frac{e^{-jk\rho}}{(4\pi)^2} \big(K_{1,f}(\mathbf{A}_f \boldsymbol{\rho} \cdot (\overline{\mathbf{I}} - \hat{\mathbf{r}}\hat{\mathbf{r}}) \times \boldsymbol{\alpha}_e) + K_{2,f}(-\boldsymbol{\alpha}_e \hat{\mathbf{r}} + \overline{\mathbf{I}} \hat{\mathbf{r}} \cdot \boldsymbol{\alpha}_e + jk\mathbf{A}_f \mathbf{B}_f) + K_{3,f} \mathbf{A}_f \mathbf{B}_f \big) \tag{2}$$

with $\mathbf{A}_f = \hat{\mathbf{r}} \times \boldsymbol{\rho}$, $\mathbf{B}_f = \hat{\mathbf{r}} \times \boldsymbol{\alpha}_e$, $\boldsymbol{\rho} = \rho\hat{\boldsymbol{\rho}} = \mathbf{r}' - \mathbf{r}_S$ and $\hat{\mathbf{r}} = r^{-1}\mathbf{r}$. The functions $K_{1,f}$ - $K_{3,f}$ are

$$K_{1,f} = \frac{1}{\rho^2} \left(\frac{jk}{\rho - \hat{\mathbf{r}} \cdot \boldsymbol{\rho}} + \frac{2 - \hat{\mathbf{r}} \cdot \hat{\boldsymbol{\rho}}}{(\rho - \hat{\mathbf{r}} \cdot \boldsymbol{\rho})^2} \right) - e^{jk(\rho - \hat{\mathbf{r}} \cdot \boldsymbol{\rho})} \frac{4}{(\rho^2 - (\hat{\mathbf{r}} \cdot \boldsymbol{\rho})^2)^2} \tag{3}$$

$$K_{2,f} = \frac{1}{\rho} \frac{1}{\rho - \hat{\mathbf{r}} \cdot \boldsymbol{\rho}} - e^{jk(\rho - \hat{\mathbf{r}} \cdot \boldsymbol{\rho})} \frac{2}{\rho^2 - (\hat{\mathbf{r}} \cdot \boldsymbol{\rho})^2} \tag{4}$$

$$K_{3,f} = -\frac{1}{\rho^3}(1 + jk\rho) \tag{5}$$

Now the associated electric PO scattered far field is readily found as

$$\mathbf{E}^{PO}_{e,f}(\mathbf{r}_F) = -Z \, \hat{\mathbf{r}}_F \times \mathbf{H}^{PO}_{e,f}(\mathbf{r}_F) \tag{6}$$

with Z denoting the intrinsic impedance of the ambient medium.

Second, consider the illumination by a magnetic HD with the magnetic current density $\mathbf{J}_m = \boldsymbol{\alpha}_m \delta(\mathbf{r} - \mathbf{r}_S)$ where $\boldsymbol{\alpha}_m$ [Vm] is the magnetic dipole moment. By evaluating the analytical limit of the general expressions [1], [2], we find that the electric PO scattered far field, $\mathbf{E}^{PO}_{m,f}(\mathbf{r}_F)$ (the subscript m refers to the magnetic HD illumination), is given by (7). In (7) we use (2) to obtain $\overline{\mathbf{W}}_{m,f}$ as $\overline{\mathbf{W}}_{m,f} = -Z \, \overline{\mathbf{W}}_{e,f}$ with $\boldsymbol{\alpha}_e$ replaced by $Z^{-1}\boldsymbol{\alpha}_m$. The incident magnetic field $\mathbf{H}^i_m$ is given in [5, (21)] while the incident electric field is

$\mathbf{E}^{\mathrm{i}}_{\mathrm{m}}(\mathbf{r}') = -G(\mathbf{r}', \mathbf{r}_{\mathrm{S}})(jk + 1/\rho)\,\boldsymbol{\alpha}_{\mathrm{m}} \times \hat{\boldsymbol{\rho}}$ where $G(\mathbf{r}', \mathbf{r}_{\mathrm{S}})$ is the scalar Green's function.

$$\mathbf{E}^{\mathrm{PO}}_{\mathrm{m,f}}(\mathbf{r}_{\mathrm{F}}) = \frac{\mathrm{e}^{-jkr_{\mathrm{F}}}}{r_{\mathrm{F}}} \int_{\Gamma} [\hat{\mathbf{t}} \cdot (\mathrm{e}^{jk\hat{\mathbf{r}}_{\mathrm{F}} \cdot \mathbf{r}'}\, \bar{\mathbf{W}}_{\mathrm{m,f}}(\mathbf{r}_{\mathrm{F}}, \mathbf{r}') + \mathrm{e}^{jk\hat{\mathbf{r}}_{\mathrm{I}} \cdot \mathbf{r}'}\, \bar{\mathbf{W}}_{\mathrm{m,f}}(\mathbf{r}_{\mathrm{I}}, \mathbf{r}') \cdot (\bar{\mathbf{I}} - 2\hat{\mathbf{n}}\hat{\mathbf{n}})$$

$$- \frac{Z}{2\pi} \mathrm{e}^{jk\hat{\mathbf{r}}_{\mathrm{F}} \cdot \mathbf{r}'} \mathbf{H}^{\mathrm{i}}_{\mathrm{m}}(\mathbf{r}') \hat{\mathbf{r}}_{\mathrm{F}}) + \frac{1}{2\pi} \mathrm{e}^{jk\hat{\mathbf{r}}_{\mathrm{F}} \cdot \mathbf{r}'} (\bar{\mathbf{I}} - \hat{\mathbf{n}}\hat{\mathbf{n}}) \cdot (\hat{\mathbf{t}} \times \mathbf{E}^{\mathrm{i}}_{\mathrm{m}}(\mathbf{r}'))] \mathrm{d}\Gamma' - \mathbf{E}^{\mathrm{i}}_{\mathrm{m}}(\mathbf{r}_{\mathrm{F}}) \chi(\mathbf{r}_{\mathrm{F}}) \quad (7)$$

3. NUMERICAL RESULTS

The exactness of the new results is now illustrated through a comparison of the PO scattered far fields obtained by use of the conventional surface radiation integral and the new line integrals. Scattering by a rectangular plate with the dimensions 4λ by 3λ (λ being the wavelength) is considered. The plate is located in the *xy*-plane with one of its corners positioned at the origin of the Cartesian *xyz*-coordinate system (see Fig. 2). The HD is placed at (3λ, 1λ, 2λ) with the dipole moment $\boldsymbol{\alpha}_e$ = (1, 1, 1) Am for the electric HD and $\boldsymbol{\alpha}_m$ = (376, 376, 376) Vm for the magnetic HD. The observation points are located in the φ = 60° plane with θ∈ [0°, 90°]. For this configuration the dipole is inside the cylinder C^F for θ∈ [0°, 30°[and outside for θ∈]30°,90°]. In Fig. 3 the source is an electric HD and in Fig. 4 the source is a magnetic HD. The figures show the amplitudes of the θ- and φ-components of the electric PO scattered far-field pattern. Perfect agreement is found between the two methods of calculation. This was also found for the phase.

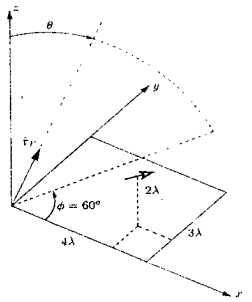


Fig. 2

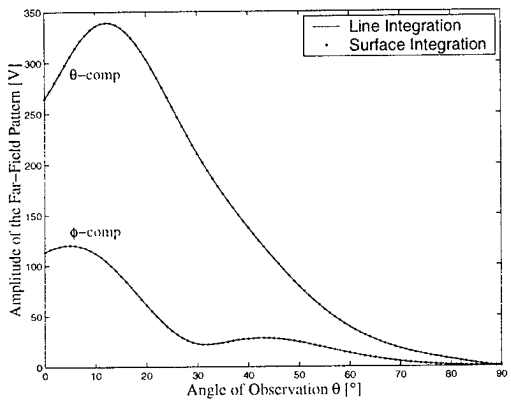


Fig. 3 Electric HD illumination.

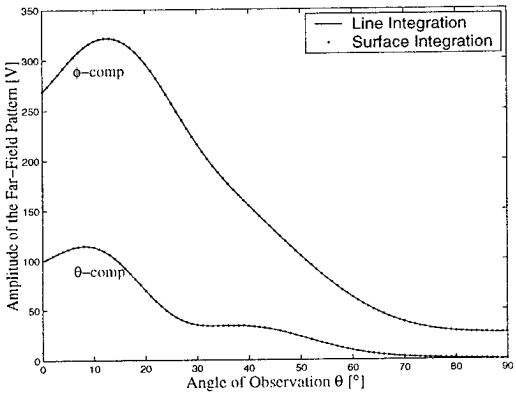


Fig. 4 Magnetic HD illumination.

REFERENCES

[1] P. Meincke Johansen and O. Breinbjerg, "An Exact Line Integral Representation of the Physical Optics Scattered Field: The Case of a Perfectly Conducting Polyhedral Structure Illuminated by Electric Hertzian Dipoles," *IEEE Trans. Antennas Propagat.*, vol. 43, no. 7, pp. 689-696, July 1995.

[2] P. Meincke, O. Breinbjerg and E. Jørgensen, "An Exact Line Integral Representation of the Magnetic Physical Optics Scattered Field," accepted for publication in *IEEE Trans. Antennas Propagat.*

CLOSED–FORM GREEN'S FUNCTION AND ITS USING FOR ANALYSIS OF MICROSTRIP ANTENNAS

L. M. Karpukov, S. N. Romanenko, R. D. Pulov
Zaporizhzhya National Technical University
Zhukovsky str., 64, Zaporizhzhya, 69063, Ukraine
Phone: 8 (0612) 643281, E-mail: sergeyr@pisem.net

ABSTRACT

A system of microstrip antenna modelling is presented. The modelling is accomplished on the base of the integral equation composed by means of vector electric potential Green's function. The integral equation is solved by method of moments in spatial domain. The calculation is effective due to usage of the closed-form of the Green's function. The process of spatial domain Green's function composing is formalized by using of microstrip structure decomposition model.

INTRODUCTION

Integral equations are widely used for microstrip circuits and antennas modelling. These equations are composed by using of Green's functions for vector and scalar electric potentials and are solved by method of moments [1].

Computational expenses for modeling at this approach are basically determined my method of Green's function calculation. Significant increase of modeling effectiveness can be provided using a closed-form Green's function as explicit dependencies of spatial coordinates [1].

The closed form can be derived as a result of approximation of spectral-domain Green's function representation as an exponential series with transformation to spatial domain through Sommerfeld identity [1-3]. The approximation is commonly realized by Prony techniques [2], based on the pencil-of-functions [3] and their modifications.

In the presented system there used a closed form on the basis of expansion on small parameter of Green's function spectral dependencies to exponential series. Computations formalizing is accomplished by introduction of substrate structure decomposition model. This model allows to form a set of auxiliary image-currents in an open space by method of repeated reflections, which determine the spectral-domain Green function.

THEORETICAL PART

In common, applying method of moments to the integral equation for surface currents gives the following system of equations:

$$\mathbf{Z}\cdot\mathbf{I}=\mathbf{V}\,. \tag{1}$$

The elements of impedance matrix Z and voltage vector V are determined in the following way:

$$Z_{mn} = \int_{S_m}\varphi_m(r)\int_{S_n}\phi_n(r_0)Z(r,r_0)\,dr\,dr_0\,, \tag{2}$$

$$V_m = \int_{S_m} \varphi_m(r)E(r)dr, \tag{3}$$

where φ_m, ϕ_n are sample and basis functions of the subregions, $Z(\mathbf{r},\mathbf{r}_0)$ is mutual impedance tensor which is connected with components of vector electric potential tensor $G(\mathbf{r},\mathbf{r}_0)$.

Suppose the z-axis of Cartesian coordinate system is perpendicular to the surfaces of microstrip media sections. Then the components of tensor in spectral domain can be presented as follows [4]:

$$\left.\begin{aligned} &\hat{G}_{\tau\tau} = \frac{\mu_0\hat{\delta}}{2k_{z0}}(1+\Gamma_\tau)e^{-k_{z0}(z-h)}, \quad \hat{G}_{zz} = \frac{\mu_0\hat{\delta}}{2k_{z0}}(1+\Gamma_z)e^{-k_{z0}(z-h)}, \\ &\partial\hat{G}_{z\tau}/\partial z = jk_\tau\alpha\cdot\frac{\mu_0\hat{\delta}}{2k_{z0}}(1+\Gamma_\tau)(1+\Gamma_z)e^{-k_{z0}(z-h)}, \end{aligned}\right\} \tag{4}$$

where $\Gamma_\tau = \dfrac{\Gamma_k - e^{-2k_{z1}h}}{1-\Gamma_k e^{-2k_{z1}h}}$, $\Gamma_z = \dfrac{\Gamma_\varepsilon + \Gamma_n}{1+\Gamma_\varepsilon\Gamma_n}$, $\Gamma_n = \dfrac{\Gamma_k + e^{-2k_{z1}h}}{1+\Gamma_k e^{-2k_{z1}h}}$, $\Gamma_\varepsilon = \dfrac{\varepsilon_r - 1}{\varepsilon_r - 1}$, $\Gamma_k = \dfrac{k_{z0}-k_{z1}}{k_{z0}+k_{z1}}$,

$\alpha = \dfrac{\Gamma_\varepsilon}{(1+\Gamma_\varepsilon)}$, $\hat{\delta} = \dfrac{e^{jk_x x_0 + jk_y y_0}}{(2\pi)^2}$, $k_{z0}^2 = \gamma^2 - k_0^2$, $k_{z1}^2 = \gamma^2 - k_0^2\varepsilon_r$, $\gamma^2 = k_x^2 + k_y^2$;

jk_τ is Fourier transformation variable on coordinate τ=x,y; h and ε_r are thickness and relative permittivity of a dielectric substrate.

Function Γ_τ can be approximated as given in [4] provided that $k_0h(\varepsilon r-1)^{1/2}<\pi/2$:

$$\Gamma_\tau = \frac{\Gamma_\delta - e^{-k_{z0}h}}{1-\Gamma_\delta e^{-k_{z0}h}}\cdot e^{-k_{z0}h}, \tag{5}$$

where $\Gamma_\delta = 1-\delta h\cdot ctg(\delta h)$, $\delta = k_0(\varepsilon_r-1)^{1/2}$.

The original of $\hat{G}_{\tau\tau}$ is composed according to (5):

$$G_{\tau\tau}(r) = \frac{\mu_0}{4\pi}\left(u_0^+ + u_0^-\right). \tag{6}$$

The computation of u_0^- is made by recurrent formula:

$$u_n^- = \Gamma_\delta u_{n+1}^+ - u_{n+2}^+ + \Gamma_\delta u_{n+1}^-, \tag{7}$$

where $u_n^+ = e^{-jk_0\sqrt{r^2+(nh)^2}} \Big/ \sqrt{r^2+(nh)^2}$, initial condition $u_{N+1}^- = 0$, $N \to \infty$.

The original of $\hat{G}_{zz}$ is approximated by the following expression:

$$G_{zz}(r) = \frac{\mu_0}{4\pi}\left(u_{I_{0,0}}^+ + S_{11}u_{I_{0,0}}^+ + S_{12}\,u_{2_{1,0}}^- - S_{13}\,u_{2_{0,1}}^-\right), \tag{8}$$

the parts of which are calculated by recurrent formula as follows:

$$\begin{bmatrix} u_{2_{n,m}}^- \\ u_{3_{n,m}}^- \end{bmatrix} = \begin{bmatrix} S_{22} & -S_{23} \\ S_{32} & -S_{33} \end{bmatrix}\cdot\begin{bmatrix} u_{2_{n+1,m}}^- \\ u_{3_{n,m+1}}^- \end{bmatrix} + \begin{bmatrix} S_{21}u_{I_{n,m}}^+ \\ S_{31}u_{I_{n,m}}^+ \end{bmatrix}. \tag{9}$$

where

$$u^{+}_{1_{n,m}} = e^{-jk_0\sqrt{r^2+(n2h+m2\Delta/(j\delta h_e))^2}} \Big/ \sqrt{r^2+(n2h+m2\Delta/(j\delta h_e))^2},$$

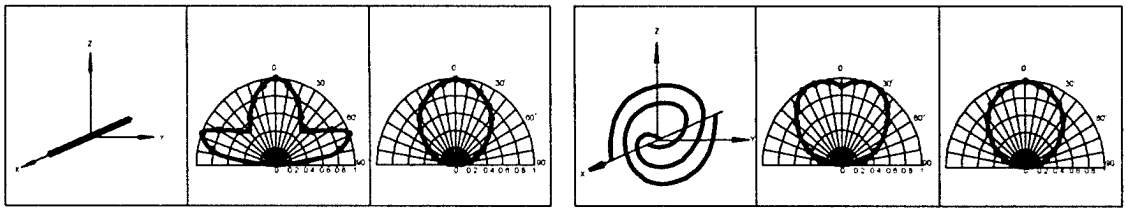
initial condition $u^{-}_{2_{N+1,M}} = 0, \quad u^{-}_{3_{N,M+1}} = 0, \quad N \to \infty, \quad M \to \infty$.

The formula for original of $\partial\hat{G}_{z\tau}/\partial z$ is composed in similar way.

MODELLING SYSTEM AND RESULTS OF COMPUTATION

The considered above method of Green's function calculation is realized in the system of wire antenna modeling [5] where used a precise basis for surface currents approximation and Pocklington integral equation. This approach provided a significant simplification of computation procedures as well as flexibility in respect of the form of radiating elements.

As an example figure 1 presents the modeling results of scattering pattern of a microstrip half-wave vibrator (a) and a spiral antenna (b) with conductor width d=0,8mm on frequency F=10GHz for a substrate with ε_r=9,3, h=2 mm. Spiral parameter a=9mm, gap between the spirals s=0,6 mm.



a) b)

Figure 1. The far-field pattern for λ/2 vibrator (a), and a spiral antenna (b).

The results of modeling in the system have good compliance with the known data at insignificant computational expenses.

REFERENCES

[1] M.J Tsai, F. De Flaviis, O. Fordham, N.G. Alexopoulus, "Modeling planar arbitrarily shaped microstrip elements in multilayered media", *IEEE Trans. Microwave Theory Tech.*, vol. MTT-45, No. 3, pp. 330 – 336, Mar., 1997.

[2] Y.L. Chow, D.G. Fang, J.J. Yang, G.E. Howard, "A closed-form spatial Green's functions for the thick microstrip substrate", *IEEE Trans. Microwave Theory Tech..*, vol. MTT-39, No. 3, pp. 588 – 592, Mar. 1991.

[3] Y. Hua, T.K. Sarkan, "Generalized pencil-of-function method for extracting poles of an EM system from transient response", *IEEE Trans. Antennas Propagat.*, vol. AP-37, No. 2, pp. 229 – 234, Feb. 1989.

[4] L.M. Karpukov, "Model of calculation of Green's function for microstrip structure in spatial domain", *Radio Electronics, Computer Science, Control*, No.2, pp. 28 – 33, 2001.

[5] S.N. Romanenko, L.M. Karpukov, R.D. Pulov, "Wire antenna computer modelling system", Proc. of the Int. Conf. TCSET'2002. Lviv-Slavsko, Ukraine, pp. 155-157, Feb. 2002.

ACCURATE ANALYSIS OF PBG STRUCTURES FOR HIGH EFFICIENCY POWER AMPLIFIER DESIGN

J.V. Rassokhina, A.N. Rudiakova, V.G. Krizhanovski

Donetsk National University, Radiophysics Dept.
ul. Universitetskaya 24, Donetsk 83055, Ukraine,
radio@dongu.donetsk.ua or anna@texnika.com.ua

ABSTRACT

The paper presents an accurate analysis of the periodical microstrip structure on the 2-D lattice of square holes at the ground plane and its application for circuit design of high-efficiency power amplifiers.

INTRODUCTION

The growing interest in photonic bandgap (PBG) materials has created a demand for efficient methods of analysis of periodic structures. Periodic structures have been the subject of numerous investigations due to their importance in slow-wave structures and corrugated antennas. Potonic bandgap microstrip structures have bin proposed as a novel way to accomplish the filtering providing a board reject band [1-6].

PBG STRUCTURE ANALYSIS

Due to the complexity of PBG structure, their characterization can be achieved only via a full-wave analysis such as plane wave expansion, integral equation method, finite element method, etc. Here, the accurate analysis of PBG microstrip structure on the 2-D lattice of square holes at the ground plane was performed using the mixed potential integral equations (MPIE).

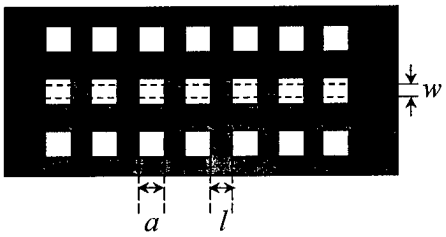


Fig. 1. Microstrip 2-D PBG line with etched squares in the ground plane.

A microstrip line (MSL) with etched squares in the ground plane is shown in Fig.1. Such a structure is equivalent to inclusions of high-impedance sections in original MSL. Using the partial regions' approach, this structure can be divided into homogeneous sections with and without etched squares in the ground plane as shown in Fig. 2. The eigenwaves problem needs to be solved for the each of sections, then diffraction integrals and quasi-TEM wave scattering characteristics on 2-D-lattice can be found. The level 3 (see Fig. 2) of screened MSL can be considered as evanescent waveguide that has to be taken into account for diffraction integrals' calculation.

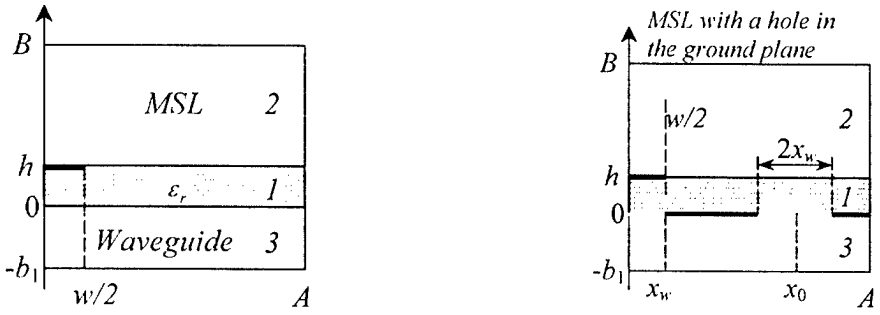


Fig. 2. Partial regions of microstrip PBG structure.

The microstrip line eigenwaves problem formulation is standard: z-components of electric and magnetic Hertz's vectors $\mathbf{\Pi}_{e,hj} = (0,0,\Pi_{e,hj})$ are satisfied to the Helmholtz's equation in the partial regions 1-3 (see Fig.2) and to the boundary conditions on screen's and strip's ideally-conductive metal surface. The wave equation solution for the partial regions 1-3 can be found as Fourier series. The Fourier coefficients can be expressed through the field components at the strips' plane at $y=h$ and $y=0$. The achieved integral equations are solved by the Galerkin's method with account of field behavior at an infinitely thin edges and symmetry of a problem relative to the $x=0$ plane. The detail description of an algorithm and its convergence can be found in [7]. In case of MSL with a holes in the ground plane, there are two solutions (accounting vacuous) for quasi-TEM eigen waves. Further, the eigen wave's solution of the central strip is considered.

The calculation of coupling coefficients between the quasi-TEM wave of MSL with a hole in the ground plane and waveguide in region 3 (see Fig. 2) showed that coupling is provided by the odd H-waves of waveguide. The one TEM-wave and 16 waveguide's modes were taken into account. Figure 3 shows an example of 2-D lattice line with etched squares in the ground plane design. Its contains of 5 unit sections. Base transmission line is MSL with the wave impedance $Z_0=50\Omega$ on dielectric substrate with $\varepsilon_{r1}=9.8$, $w=h=1$mm.

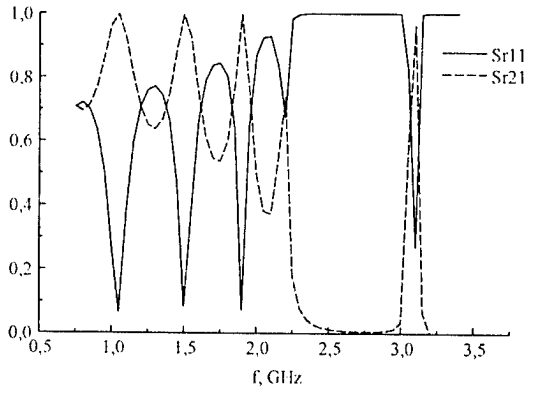


Fig. 3. S-parameter of 5-section PBG microstrip circuit with $a=x_w=5$ mm, $l=9.18$ mm, $x_0=7.0$ mm.

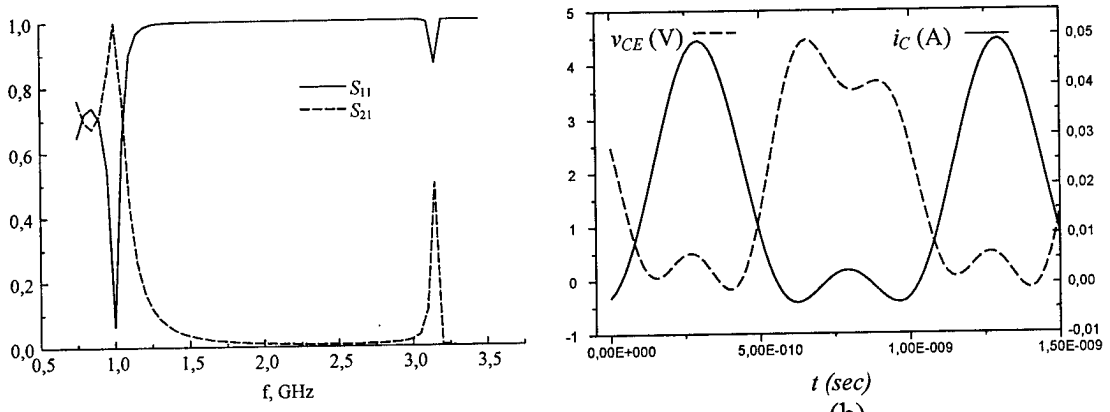


Fig. 4. S-parameters (a) of 3-section PBG microstrip circuit for class-F PA with x_{w1}=x_{w3}=2.065 mm, x_{w2}=2.8 mm, a_1=a_3=12.177 mm, a_2=12.18 mm, x_0=7.0 mm, l=10.97mm, and collector current and voltage waveforms (b).

Using described algorithm, a harmonic filter for 1GHz class-F power amplifier contains 3 unit sections of a PGB structure was designed. Here, x_{w1}=x_{w3}=2.065 mm, x_{w2}=2.8 mm, a_1=a_3=12.177 mm, a_2=12.18 mm, x_0=7.0 mm, l=10.97 mm. In order to tune phase characteristics, a length of input MSL was varied (as in [8]). The S-parameters of designed network along with collector current and voltage waveforms are shown in Fig. 4, (a) and (b), respectively. Collector efficiency of simulated power amplifier was as high as 74.7%.

REFERENCES

[1] V. Radisic, Y. Qian, and T. Itoh, "Broad-band Power Amplifier Using Dielectric Photonic Bandgap Structure", *IEEE Microwave Guided Wave Lett.*, vol. 8, pp. 13-14, Jan. 1998.

[2] I. Rumsey, M. Piket-May, and P. K. Kelly, "Photonic Bandgap Structures Used as Filters in Microstrip Circuit", *IEEE Microwave Guided Wave Lett.*, vol. 8, pp. 336-338, Oct. 1998.

[3] V. Radisic, Y. Qian, R. Coccioli, and T. Itoh, "Novel 2-D Photonic Bandgap Structures for Microstrip Lines", *IEEE Microwave Guided Wave Lett.*, vol. 8, pp. 69-71, Feb. 1998.

[4] F.-R. Yang, Y. Qian, R. Coccioli, and T. Itoh, "A Novel Low-loss Slow-wave Microstrip Structure", *IEEE Microwave Guided Wave Lett.*, vol. 8, pp. 372-374, Nov. 1998.

[5] T. Kim and C. Seo, "A Novel Photonic Bandgap Structure for Low-pass Filter of Wide Stopband", *IEEE Microwave Guided Wave Lett.*, vol. 10, pp. 13-15, Jan. 2000.

[6] D. Ahn, J.-S. Park, C.-S. Kim, J. Kim, Y. Qian, and T. Itoh, "A design of the low-pass filter using the novel microstrip defected ground structure", *IEEE Trans. on MTT*, vol. 49, pp. 86-92, Jan. 2001.

[7] V. G. Kryzhanovskii and Yu. V. Rassokhina, "A Microstrip Transmission Line with an Inverse Three-Layer *Dielectric* Filling for Microwave Filtering Circuits", *Journal of Communications Technology and Electronics*, № 10, pp. 1115, 2001.

[8] J.V. Rassokhina, A.N. Rudiakova, V.G. Krizhanovski, "Three-layered dielectric filling microstrip line filter for high-efficiency polyharmonic power amplifiers", MSMW*2001, The Fourth International Kharkov *Symposium* "Physics and Engineering of Millimeter and Sub-Millimeter Waves", Kharkov, Ukraine, June 4-9, 2001, V.2.-P. 693-695.

NUMERICAL SIMULATION OF THE MICROSTRIP PHASED ARRAY

A.O. Kasyanov, V.A. Obukhovets, V.I. Zagorovsky

Taganrog State University of Radio Engineering, Russia
Russia, 347928, Taganrog, GSP-17 A, Nekrasovsky str., 44
Phone (8634)37-18-83, Fax (86344) 6-50-19, E-mail: vao@tsure.ru

Full-wave solution of electromagnetic problem about lumped excitation of a microstrip phased array has been obtained. Microstrip antennas attract much attention due to their numerous advantages. However any single printed antenna has low directivity. Microstrip arrays overcome this demerit. However, experimentation and measuring of parameters of arrays are complex and expensive procedures. This causes significant interest to creation of mathematical and computational models of arrays. The purpose of the present work is the development of a mathematical model for a printed antenna array. This antenna consists of arbitrary-shape microstrip radiators excited by a periodic system of probes simulating coaxial waveguides or two-wire transmission lines. Rectangular grid nodes determine the placements of printed radiators. Presented mathematical model allows investigating the microstrip radiators, which contain controllable elements used to expand an antenna array angular scanning sector. A conducting probe with an impedance load simulates each controllable element. It is necessary to introduce an impedance distribution on the probe.

The mathematical model foundation for the microstrip is the concept of infinite periodic array. Such an approach is reasonable because of consideration of multielement arrays with rather complicated element structure. An alternative way of simulating can be based on so called "element by element method" with taking into account mutual couplings between array elements. This way can become very difficult because of necessity to solve large-size sets of integral equations (IE). Proposed mathematical model is based on the periodical structure conception and an IE solution. A set of IEs for the magnetic and electric currents on the surface of the array unit cell has been developed. These vector IEs are obtained from the Lorentz lemma:

$$\int_{S_{slot}} E\left[H_1^{(l)aux} + H_2^{(l)aux}\right] dS_q - \int_{S_{shunt}} \left[\vec{n}_2, \vec{H}_2(q)\right] \vec{E}_2^{(l)aux}(q,p)\, dS_q -$$

$$- \int_{S_{shunt}} \left[\vec{n}_2, \vec{E}_2(q)\right] \vec{H}_2^{(l)aux}(q,p)\, dS_q = \int_{S_{ring}} \left[\vec{n}_2, \vec{E}_2^{feed}(q)\right] \vec{H}_2^{(l)aux}(q,p)\, dS_q .$$

Application of the periodicity condition allows reducing the solution area to one Floquet channel. The magnetic current density on the array aperture and the electrical currents in controllable elements are determined from IE set obtained from the boundary conditions. The moment method is used for IE numerical solution. The subsection rooftop function set is used for magnetic current approximation. By solving these IEs, we determine magnetic and electric currents. Then we can determine input impedance of printed radiator, radiation fields and other important parameters of considered antenna array. Results of numerical simulation of the microstrip phased arrays will be presented. Comparison with known theoretical data allows to validate numerical solutions and confirm the adequacy of the mathematical model. Numerical analysis of the microstrip phased array radiation characteristics have been carried out. These numerical results can be used to develop antennas with optimal parameters.

THE PHOTONIC BANDGAP MICROSTRIP CLASS-E AMPLIFIER

A.N. Rudiakova, Ju.V. Rassokhina, V.G. Krizhanovski

Donetsk National University, Radiophysics Dept.
ul. Universitetskaya 24, Donetsk 83055, Ukraine,
e-mail: anna@texnika.com.ua or radio@dongu.donetsk.ua

ABSTRACT

The paper presents the design and simulation of microwave class-E power amplifier based on the photonic bandgap microstrip structure on the 2-D lattice of square holes at the ground plane.

INTRODUCTION

Switching class-E power amplifiers provide high-efficiency conversion of dc to ac via careful design of the transient waveforms of a resonant load network [1, 2]. Earlier class-E designs have concentrated on the development of lumped element load network topologies for RF applications operating in the megahertz range [1 – 3]. However, in the microwave region, lumped elements are not so easily fabricated and may depart from idealized components. Recent developments in the literature include a transmission line circuit utilizing a series line and single shunt stub to achieve class-E operation [4], and a power combining four transistor class-E amplifier [5] employing GaAs MESFETs to obtain an output power 2.95W at 935MHz, with a power-added efficiency of 67%. Transmission line topology and design methodologies of narrow-band microstrip class-E amplifier were considered also in [6].

Recently, photonic bandgap (PBG) microstrip structures have been proposed as a novel way to accomplish the filtering providing a board reject band [7 – 10]. Such a structures can be successfully used as the output networks of high-efficiency power amplifiers. Presented paper describes the design of microwave class-E power amplifier based on the microstrip structure on the 2-D lattice of square holes at the ground plane.

AMPLIFIER DESIGN

The low-order class-E circuit [1,2] is shown in Fig. 1(a).

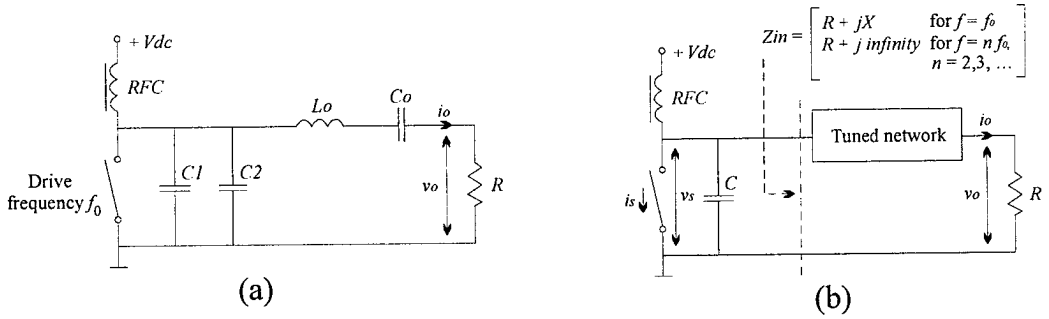


Fig. 1. (a) Class-E amplifier with the low-order network. (b) Equivalent circuit.

Design equations [2, 6] for an idealized class-E amplifier with a 50% duty cycle are reproduced below (component symbols are depicted in Fig 1(b)):

$$\left.\begin{array}{l}\text{Output power: } P_o = V_{dc}{}^2/R_{dc}\text{ ; Equivalent dc resistance: } R_{dc} = 1.7337R; \\ \text{Shunt susceptance: } B = \omega C = 1/5.4466R\text{ ; Load angle: } \varphi = 49.052^0; \\ \text{Load-network impedance: } Z = R + jX\text{ , where } X = 1.152R; \\ \text{Peak switch voltage: } v_{s\max} = 3.56V_{dc}\text{ ; Peak switch current: } i_{s\max} = 2.84I_{dc}.\end{array}\right\} \quad (1)$$

According to (1), needed input impedance of output network was calculated in order to provide 25mW output power into a 50Ω resistive load at 1GHz.

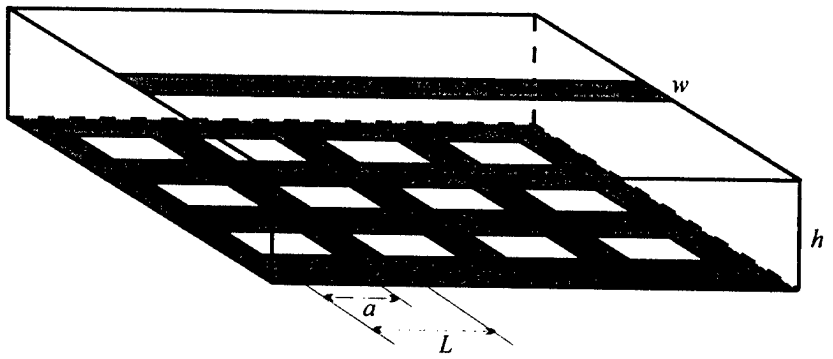


Fig. 2. Considered PBG structure.

The photonic bandgap microstrip structure on the 2-D lattice of square holes at the ground plane used for an output network design is shown in Fig. 2. Here, the sizes of a and L were equal 12.5mm and 30mm, respectively.

SIMULATION RESULTS

Collector efficiency of simulated class-E amplifier based on considering PGB structure was as high as 95.53% for 2V supply and 22mW output power.

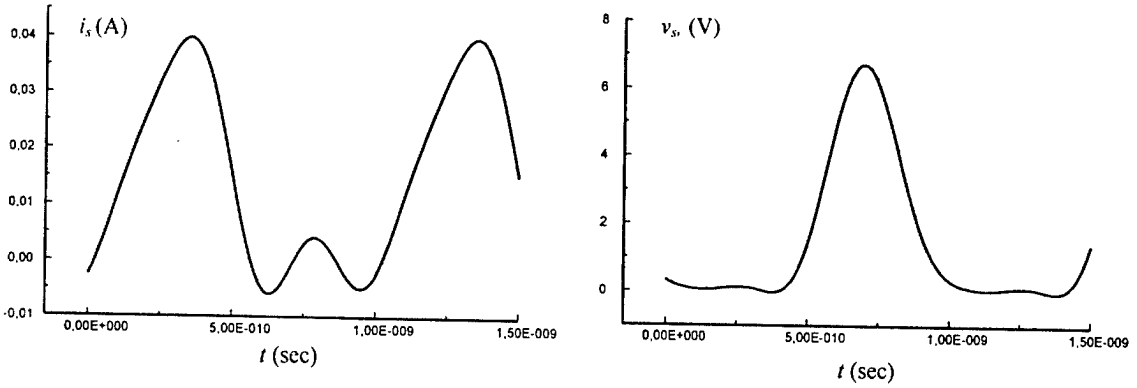


Fig. 3. Simulated waveforms of transistor output current (a) and voltage (b).

The simulated collector current and collector-emitter voltage waveforms of designed class-E amplifier are shown in Fig. 3(a) and 3(b), respectively. As can be seen from figures, these waveforms are in agreement with target waveforms of class-E amplifier [1, 6].

CONCLUSIONS

The class-E power amplifier using PBG microstrip structure on the 2-D lattice of square holes at the ground plane was designed and simulated. As high collector efficiency as 95.53% for 2V supply and 22mW output power at 1 GHz was achieved by proper tuning. The result shows the prospects of future using of such structures for high-efficiency amplifiers' networks design.

REFERENCES

[1] N. O. Sokal and A. D. Sokal, "Class E—A New Class of High-efficiency Tuned Single-ended Switching Power Amplifiers," *IEEE J. Solid-State Circuits*, vol. SC-10, pp. 168–176, June 1975.

[2] F. H. Raab, "Idealized Operation of the Class E Tuned Power Amplifier," *IEEE Trans. Circuits Syst.*, vol. CAS-25, pp. 725–735, Dec. 1977.

[3] M. K. Kazimierczuk, K. Puczko, "Exact Analysis of a Class E Tuned Amplifier at any Q and Switch Duty Cycle", *IEEE Transactions on Circuits and Systems*, vol. 34, pp. 149-159, February 1987.

[4] T. Mader and Z. Popovic, "The Transmission-line High-efficiency Class-E Amplifier," *IEEE Microwave Guided Wave Lett.*, vol. 5, pp. 290–292, Sept. 1995.

[5] A. L. Martin and A. Mortazawi, "A Class-E Power Amplifier Based on an Extended Resonance Technique," *IEEE Trans. Microwave Theory Tech.*, vol. 48, Jan. 2000.

[6] A. J. Wilkinson, J. K. A. Everard, "Transmission-Line Load-Network Topology for Class-E Power Amplifiers", *IEEE Trans. on MTT*, vol. 49, pp. 1202 – 1210, June 2001.

[7] I. Rumsey, M. Piket-May, and P. K. Kelly, "Photonic Bandgap Structures Used as Filters in Microstrip Circuit", *IEEE Microwave Guided Wave Lett.*, vol. 8, pp. 336-338, Oct. 1998.

[8] V. Radisic, Y. Qian, R. Coccioli, and T. Itoh, "Novel 2-D Photonic Bandgap Structures for Microstrip Lines", *IEEE Microwave Guided Wave Lett.*, vol. 8, pp. 69-71, Feb. 1998.

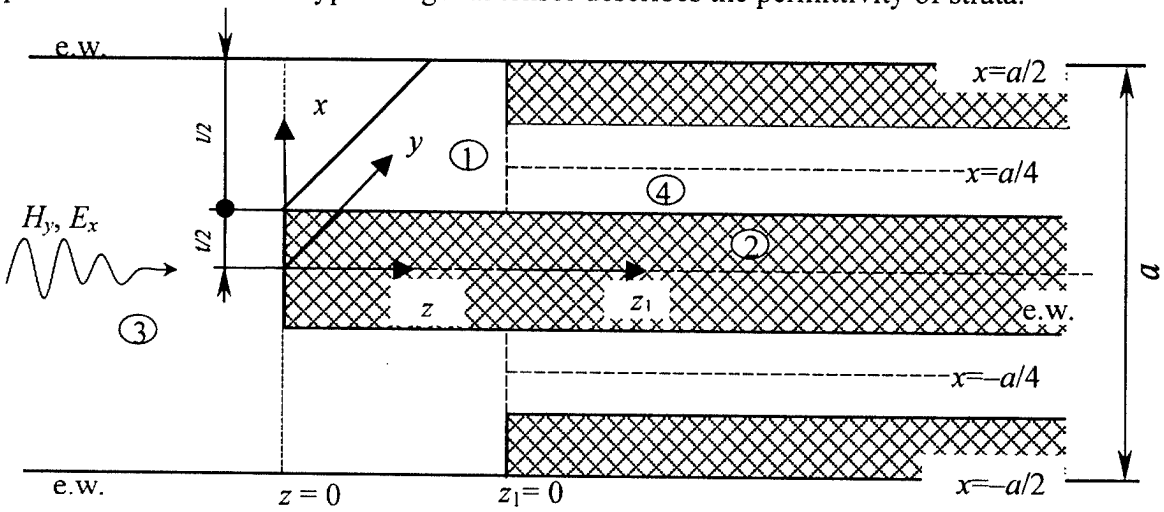
[9] F.-R. Yang, Y. Qian, R. Coccioli, and T. Itoh, "A Novel Low-loss Slow-wave Microstrip Structure", *IEEE Microwave Guided Wave Lett.*, vol. 8, pp. 372-374, Nov. 1998.

[10] D. Ahn, J.-S. Park, C.-S. Kim, J. Kim, Y. Qian, and T. Itoh, "A Design of the Low-pass Filter Using the Novel Microstrip Defected Ground Structure", *IEEE Trans. on MTT*, vol. 49, pp. 86-92, Jan. 2001.

DIFFRACTION OF A PLANE H-POLARISED ELECTROMAGNETIC WAVE BY TWO SEQUENTIALLY INCLUDED STRATIFIED PERIODIC DIELECTRIC STRUCTURES

Viktor Naidenko and Elena Guseva
National Technical University of Ukraine «Kyiv Polytechnic Institute»,
37 Prospect Peremogy, Kyiv, 03056, Ukraine
E-mail: v_naidenko@yahoo.com

The geometry of a problem considered is shown in the figure. A plane H-polarised electromagnetic wave drops on periodic in x-direction stratified dielectric structure with a period a. After dispersing by boundary $z = 0$ waves, passed in area 1 + 2, are dispersed by boundary $z = w$ ($z_1 = 0$), partially getting in area 2 + 4. A matching problem in [1] leads to problems of the similar type. Diagonal tensor describes the permittivity of strata.



It is proved in [2], that the planes of symmetry $x = 0$ and $x = a/2$ at excitation by a plane H-polarised electromagnetic wave must be electric walls. The structure to the right of the boundary $z_1 = 0$ ($z = w$) has a twice smaller period – $a/2$. The planes of symmetry $x = 0$ and $x = \pm a/2$ here are also electric walls. However, aside from these planes of symmetry there are some other planes of symmetry at $x = \pm a/4$. In these planes of symmetry there are not direct requirements on the field mode. But, as the planes of symmetry $x = 0$ and $x = \pm a/2$ are electric walls, the planes of symmetry $x = \pm a/4$ can be either electric walls, or magnetic ones. Therefore fields in region $z>w$ should be taken as the total of fields with electrical and magnetic walls in the plane of symmetry $x = \pm a/4$. Fields with electric walls in planes of symmetry $x = \pm a/4$ can be found from the same dispersion equations as in [3], after substitution $a \to a/2$. The dispersion equation for fields with magnetic walls in planes of symmetry $x = \pm a/4$ of region 2 + 4 is as follows

$$\frac{\varepsilon_{z2}}{\varepsilon_{z4}} \frac{2t}{l-t} u_m^M cthu_m^M = v_m^M tgv_m^M .$$

Here the superscript corresponds to the magnetic wall in planes of symmetry of type $x = \pm a/4$, and the subscript determines the number of the root,

$$v_m^v = h_m^M \frac{t}{2}, \quad u_m^v = q_m^M \frac{l-t}{4}, \quad (\gamma_m^M)^2 = (q_m^M)^2 \frac{\varepsilon_{x4}}{\varepsilon_{z4}} + k^2\varepsilon_{x4} = k^2\varepsilon_{x2} - (h_m^M)^2 \frac{\varepsilon_{x2}}{\varepsilon_{z2}} \quad C_m = D_m \frac{\cos v_m^M}{shu_m^M}.$$

The fields in region 3 can be written down as

$$H_{y3} = e^{-ikz} + R_0 \cdot e^{ikz} + \sum_{n=1}^{\infty} R_n e^{\Gamma_n z} \cos(2\pi n \frac{x}{a}), \quad \Gamma_n = \sqrt{\left(\frac{2\pi n}{a}\right)^2 - k^2}.$$

Here and further other components are derived from Maxwell's equations under the earlier specified conditions.

The fields in region 1 + 2 can be given as

$$H_{y1} = \sum_{m=1}^{\infty} \left(A_m e^{-i\gamma_m z} + A_m^- e^{i\gamma_m z}\right) \mathrm{ch}(q_m(x - \frac{a}{2})), \quad H_{y2} = \sum_{m=1}^{\infty} \left(B_m e^{-i\gamma_m z} + B_m^- e^{i\gamma_m z}\right) \cos(h_m x), \quad \gamma_m = \sqrt{k^2\varepsilon_{x2} - h_m^2 \frac{\varepsilon_{x2}}{\varepsilon_{z2}}}.$$

Link between A_m^- and B_m^- is the same as between A_m and B_m in [3].

Fields in region 2 + 4 with electric and magnetic walls in planes $x = \pm a/4$ are

$$H_y^e = \sum_{p=1}^{\infty} \begin{Bmatrix} N_p \cos(h_p^e(x - \frac{a}{2})) \\ L_p ch(q_p^e(x - \frac{a}{4})) \\ N_p \cos(h_p^e x) \end{Bmatrix} e^{-i\gamma_{ep} z_1}, \quad H_y^M = \sum_{p=1}^{\infty} \begin{Bmatrix} -D_p \cos(h_p^M(x - \frac{a}{2})) \\ C_p sh(q_p^M(x - \frac{a}{4})) \\ D_p \cos(h_p^M x) \end{Bmatrix} e^{-i\gamma_m^M z_1} \quad npu \quad \begin{matrix} \frac{a-t}{2} < x < \frac{a}{2}, \\ \frac{t}{2} < x < \frac{a-t}{2}, \\ 0 < x < \frac{t}{2}. \end{matrix}$$

Subordinating fields to boundary conditions, using a system of trial functions $\left\{\cos(2\pi n \frac{x}{a})\right\}_{n=0}^{\infty}$ and applying the moment method we'll receive a system of linear algebraic equations (SLAE) of a solved problem.

At actual limitations on number of waves taken into account, the order of the obtained SLAE is high. However, coefficients R_n in the sub-SLAE, taken as a result of satisfying boundary conditions at $z = 0$, are simply expressed through A_m, A_m^-, B_m, B_m^-. Let's eliminate R_n and therefore reduce the SLAE order. We'll have:

$$\sum_{m=1}^{\infty} A_m \left[\left(\frac{\Gamma_n}{k} + i\frac{\gamma_m}{k}\frac{\varepsilon_{x3}}{\varepsilon_{x1}}\right)\varphi_{mn} + \frac{chu_m}{\cos v_m}\left(\frac{\Gamma_n}{k} + i\frac{\gamma_m}{k}\frac{\varepsilon_{x3}}{\varepsilon_{x2}}\right)F_{mn} \right] +$$

$$+ \sum_{m=1}^{\infty} A_m^- \left[\left(\frac{\Gamma_n}{k} - i\frac{\gamma_m}{k}\frac{\varepsilon_{x3}}{\varepsilon_{x1}}\right)\varphi_{mn} + \frac{chu_m}{\cos v_m}\left(\frac{\Gamma_n}{k} - i\frac{\gamma_m}{k}\frac{\varepsilon_{x3}}{\varepsilon_{x2}}\right)F_{mn} \right] = 4\delta_{n0}, \quad n = 0,1,2,\ldots,$$

$$\sum_{m=1}^{\infty} A_m e^{-i\gamma_m W}\left(\varphi_{mn} + \frac{chu_m}{\cos v_m}F_{mn}\right) + \sum_{m=1}^{M} A_m^- e^{i\gamma_m W}\left(\varphi_{mn} + \frac{chu_m}{\cos v_m}F_{mn}\right) = \begin{cases} \sum_{p=1}^{\infty} L_p\left(\Phi_{pn}^{eh} + 2\frac{chu_p^e}{\cos v_p^e}F_{pn}^e\right), & n = 0,2,\ldots \\ \sum_{p=1}^{\infty} C_p\left(\Phi_{pn}^{mh} - 2\frac{shu_p^M}{\cos v_p^M}F_{pn}^M\right) & n = 1,3,\ldots, \end{cases}$$

$$\sum_{m=1}^{\infty} A_m e^{-i\gamma_m w}\frac{\gamma_m}{k}\left(\frac{\varphi_{mn}}{\varepsilon_{x1}}+\frac{chu_m}{\cos v_m}\frac{F_{mn}}{\varepsilon_{x2}}\right)-\sum_{m=1}^{\infty} A_m^{-} e^{i\gamma_m w}\frac{\gamma_m}{k}\left(\frac{\varphi_{mn}}{\varepsilon_{x1}}+\frac{chu_m}{\cos v_m}\frac{F_{mn}}{\varepsilon_{x2}}\right)=$$

$$=\left\{\begin{array}{l}\sum_{p=1}^{\infty} L_p\frac{\gamma_p^e}{k}\left(\frac{\Phi_{pn}^{eh}}{\varepsilon_{x4}}+\frac{2}{\varepsilon_{x2}}\frac{chu_p^e}{\cos v_p^e}F_{pn}^e\right),\quad n=0,2,\ldots\\ \sum_{p=1}^{\infty} C_p\frac{\gamma_p^M}{k}\left(\frac{\Phi_{pn}^{Mh}}{\varepsilon_{x4}}-\frac{2}{\varepsilon_{x2}}\frac{shu^M}{\cos v^M}F_{pn}^M\right),\quad n=1,3,\ldots\end{array}\right\},\quad n=0,1,\ldots\ ,$$

where δ_{n0} is equal to 1 at n=0 and 0 at $n\neq 0$, the formulae for φ_{mn}, F_{mn} are listed in [3], and

$$F_{pn}^e=\frac{4}{a}\int_0^{\frac{t}{2}}\cos(h_p^e x)\cos(2\pi n\frac{x}{a})dx,\quad F_{pn}^M=\frac{4}{a}\int_0^{\frac{t}{2}}\cos(h_p^M x)\cos(2\pi n\frac{x}{a})dx,$$

$$\Phi_{pn}^{eh}=\frac{4}{a}\int_{\frac{t}{2}}^{\frac{a-t}{2}} ch(q_p^e(x-\frac{a}{4}))\cos(2\pi n\frac{x}{a})dx,\quad \Phi_{pn}^{Mh}=\frac{4}{a}\int_{\frac{t}{2}}^{\frac{a-t}{2}} sh(q_p^M(x-\frac{a}{4}))\cos(2\pi n\frac{x}{a})dx$$

The calculated magnitude and phase of a reflectivity coefficient R_0 as a function of w at constant a, t, ε are shown in the table.

w, mm			0	25	50	75	100	125	150	175	200	225
a=160 mm, t=20 mm	ε′=2	|R|	0.03397	0.02995	0.01862	0.00282	0.01370	0.02689	0.03359	0.03221	0.02308	0.00837
		argR°	4.79799	-23.160	-51.802	-86.95	74.4423	45.3817	16.3825	-12.275	-40.907	-70.888
	ε′=5	|R|	0.05715	0.05078	0.03050	0.00277	0.02623	0.04819	0.05797	0.05312	0.03485	0.00777
		argR°	10.3886	-17.102	-46.906	-101.42	80.3676	49.8499	20.0037	-9.6216	-39.510	-74.796
	ε′=10	|R|	0.06350	0.05771	0.03404	0.00261	0.03158	0.05622	0.06628	0.05921	0.03680	0.00503
		argR°	14.6052	-11.635	-41.968	-125.25	6.3579	54.7741	24.3151	-6.0008	-36.965	-84.784
a=240 mm, t=100 mm	ε′=2	|R|	0.13577	0.11542	0.06038	0.01392	0.08172	0.12475	0.13022	0.09672	0.03475	0.04317
		argR°	1.93685	-26.075	-53.382	71.1760	58.1038	29.2369	0.01373	-28.145	-45.647	66.3780
	ε′=5	|R|	0.29837	0.26045	0.16118	0.06132	0.10042	0.14946	0.13864	0.12386	0.16752	0.22795
		argR°	7.40310	-19.465	-40.354	-21.424	31.2138	20.9081	10.8797	22.9391	33.1451	24.7836
	ε′=10	|R|	0.39346	0.34496	0.18954	0.08134	0.23437	0.32585	0.37896	0.38937	0.31749	0.14239
		argR°	2.97062	-28.154	-71.513	140.458	72.7125	45.4853	23.0286	-2.2198	-35.076	-87.438

Comparing results from [3] and calculated ones shows essential decrease of the magnitude of the reflectivity coefficient. So, the method offered in [1], is effective.

REFERENCES

[1] V. I. Naidenko. Pat. of Ukraine. № 28741A. Bul. № 5 – 11. Publicat. 29. 12. 1999.

[2] Axial-symmetric Periodic Structures and Resonators/ V. I. Naidenko, F. F. Dubrovka – Kyiv, Vyshcha shkola, 1985. – 224 c. (in Russian).

[3] V. I. Naidenko, E. V. Guseva. Matching of the Normally Incident H-Polarized Plane Wave with a Layered Half-space. Proc. of Conf. MMET-2000. p. 595 – 597.

GEORADAR AND REMOTE SENSING

WIND FLIGHT CONDITIONS MODEL

Yu.A. Averyanova, A.A. Averyanov, F. J. Yanovsky

National Aviation University1, Cosmonavta Komarova ave., Kiev, 03058, Ukraine
E-mail: markovski@svitonline.com

ABSTRACT Possible mathematical models of atmospheric process as a result of superposition of random and deterministic components of wind shear vector in the air space under study are considered. The canonical decompositions are used. The methods of necessary measurable data obtaining and the way of measurable parameter estimating as well as their separation are discussed. Method of state space and optimal stationary measuring system are suggested to be studied for data processing.

Meteorological conditions (special weather conditions) are known to be a factor which affects essentially on safety and quality of flights [1]. Wind phenomena which make aerodynamic influence on aircraft directly are the most dangerous.
Character and rate of danger of special weather conditions, which effect aircraft, depend on type and intensity of the phenomenon, sizes and mass of aircraft, aerodynamic characteristics and operation phase. The most negative is combination of mentioned factors during the takeoff or landing in the presence of wind shear and turbulence near the ground surface. In this case regimes of flight are close to critical: maneuver time and space of aircraft are limited.
By definition [2], wind shear is a change of wind vector from one space point to another, and it can be evaluated as difference between wind vectors in two points, which are vectors as well because they have velocity and direction.
As wind shear can appears in combination with turbulence, mathematical model of wind conditions includes constant and variable components. Constant component represents wind shear and variable one represents turbulence. So, on the whole, mathematical model of wind conditions can be represented as random process which includes constant and variable components. Momentary value of vector in some space point will be determined as the sum of constant and variable components. Wind shear determination problem leads to finding of wind vector over the elementary volumes and corresponding wind shear calculating.

Considering temporal and spatial changes of wind vector X(t) as random time-dependent process it can be represented as superposition of random and determinate components in 3-dimensional space. This process depends on time and space coordinates. It can be described by mathematical model in the form of canonical decomposition [3]:

$$X(t,x,y,z) = m_x(t,x,y,z) + \sum_v V_{v(x,y,z)} X_v(t,x,y,z) \qquad (1)$$

where $m_x(t,x,y,z)$ is mean of observed random process; V_v are uncorrelated random variables with mean equals zero; $X_v(t)$ are some (nonrandom) functions of time.

Representation as canonical decomposition will allow to separate constant and variable components (wind shear and turbulence) at signal processing.

Practically it is impossible to realize the general model (1) because measuring equipment, which is used in reality (anemometers, Doppler radar sets), allow to take measurements of wind vector only discretely in space or (and) time. Therefore, it is rationally to use a discrete model of the evaluated space parameters:

$$X(t_k, x_i, y_j, z_r) = m_x(t_k, x_i, y_j, z_r) + \sum_{\nu} V_{\nu(x_i, y_j, z_r)} X_{\nu}(t_k, x_i, y_j, z_r), \qquad (2)$$

where t_k are reading moments of observed value; x_i, y_j, z_r are the numbers of coordinates in corresponding axis of the some elementary volume center of the space. Evaluating of measuring parameters averaged over this volume is made over the limits of elementary volume.

Corresponding averaged discrete readings related to geometrical sizes of the space elementary volumes are determined by scanning beam aperture on corresponding distance from radar antenna at using of Doppler radar. And only radial component of velocity is measured. So, equation (1) is simplified:

$$X(t_k, z_r) = m_x(t_k, z_r) + \sum V_{v_{z_r}} X_{\nu}(t_k, z_r), \qquad (3)$$

where z_r is coordinate axis which corresponds to axis of symmetry of scanning beam aperture; r is a number of elementary volume which defines the distance between the center of the volume and antenna.

Therefore, the problem of wind vector determination in the given point of the space with Doppler radar leads to evaluating velocity vector component according to the equation (3) for corresponding axis of some orthogonal system. It is convenient for practical using at air navigation, especially, for the systems which deal with runway, construction line of airplane or routing line of flight.

In this case vector X(t) is considered as useful signal which characterizes studied space. It is supplied on the input of measuring instrument (input of radar set). Evaluating of signal X(t) is made according to the signal observed on the output of radar Y(t). It is represented as n-dimensional real-valued vector-function. It is defined by the following expression:

$$Y(t) = G[X(t), H(t)], \qquad (4)$$

where H(t) is n-dimensional real-valued vector-function which defines measurement error; G is arbitrary real-valued abstract function.

Abstract function G is represented as necessary linear operator:

$$G[\overline{Y}] = G_0[\overline{Y}] + \overline{X}_n,$$

with G_0 as arbitrary homogeneous abstract function and $\overline{X}_n$ as given nonrandom nonzero s-dimensional vector.

Determination of optimal weighting functions $G_0^*(t,\tau)$ and $\overline{X}_n$ are made with Wiener-Hopf integral equation:

$$\int_{t-T}^{t} G_0^*(t_1,\tau_1)K_Y(\tau_1,\tau_2)d\tau_1 = K_{XY}(t,\tau_2) \ . \tag{5}$$

Vector-function $\overline{X}_n(t)$, which provides non-bias estimate, is defined by the following equation:

$$\overline{X}_n(t) = m_x(t) - \int_{t-T}^{t} G_0^*(t_1,\tau_1)m_x(\tau_1)d\tau_1 \ . \tag{6}$$

Integration in formulas (5), (6) is made over the limits which define boundaries of elementary volume of space.

Optimal invariant estimate of signal is found by using Lagrange functions of function and undetermined multipliers.

Suggested model of estimation (5) allows to minimize the time of signal processing.

A model of measurements with one Doppler radar gives a possibility to determine only a projection of total wind on the axis of radar beam. It is necessary to use 3-positional radar system with interorthogonal scanning beam orientations to determine wind vectors. As it is impossible to realize a 3-positional system onboard, it is necessary to make out methods of obtaining and use of additional information for total wind vector estimation.

REFERENCES

[1] The third enclosure to International Civil Aviation Convention (ICAO). Meteorological support of international aviation.

[2] ICAO circular 186-AN/122. Wind shear.

[3] Ivanov YU.P and others. "Complexation of data-measurement devices of aircrafts"L.: Mashinostroenie, 1981.207 p.

[4] Rosin and others." Statistical dynamic ant control system efficiency theory".M: Mashinostroenie, 1981.312 p.

[5] Sage E., Mils G. "Estimation theory and its application for connection and measurement". M.: Svyazy, 1976.496 p.

[6] Afanasyeva L.A. and others. "Predictive Windshear System". Flight safety problems. VINITI. 2001 №2, p.31-44, 6 fig.

NONPARAMETRIC ALGORITHM FOR A DETECTION OF RANDOM PROCESS DISORDER IN THE SIGNALS OF RADAR REMOTE SENSING

I. Prokopenko*, K. Prokopenko*

*National Aviation University; Addres for communication: Grazdanskaja 41, Irpen, Kiev region,Ukraine,08200;tel .+380-044-9755-640

E-mail: kostya@home.hau.org.ua

ABSTRACT

The new nonparametric algorithm of radar signal disorder detection task has been considered. The algorithm is based on spectral estimating of a few signal samples of a few close windows and nonparametric Wilkockson's test application to compare them. The algorithm can be used for radar signal detection specifically in the tasks of turbulence detection in clouds and precipitation as well as for moving target detection. The efficiency of the new algorithm is analyzed.

INTRODUCTION

The determination of position where radar cross-section becomes different appreciably in comparison with previous one is an important problem of signal analysis. Radar signal is an unsteady random process. The difficulty of determining the moment when the signal characteristics change is associated with the fact that radar signal statistical characteristics haven't been defined a priori.

This paper considers the nonparametric rank algorithm synthesis for random process disorder detection that is used for evaluating statistical characteristics of the point of time when the change occurred. The effectiveness of the algorithm is researched by means of statistical modeling.

THE SYNTHESIS OF ALGORITHM

We define the row of radar signal samples as **S(kT), k=0,1,...,** where T is the time sampling interval.

Let us consider a radar signal to be a segment of random process realization, whose length is $\mathbf{M_l*T=Q*N*T}$, where N is the fixed number, whose name is the size of the analysis window, **Q** is the number of windows.

Let us consider, that in the time interval equal to the length of the analysis window, a radar signal is a stationary random process. The row of signal samples, that correspond to the l-th window , can be presented in the decomposition into the harmonic functions:

$$S_l(kT) = \sum_{i=0}^{N-1} a_{li} e^{jw\frac{2\pi}{N}ik}, \quad k = 0,...,N-1, \quad l = 1,...,Q \ , \tag{1}$$

where the coefficients of decomposition are determined by the formula

$$a_{li} = \frac{1}{N}\sum_{k=0}^{N-1} S_l(kT) e^{-jw\frac{2\pi}{N}ik}, \quad l = 1,...,Q \ . \tag{2}$$

The decomposition coefficients (2) will be the co-ordinates of the signal segments in the criteria-space. For signal segments which differ from each other in the form of spectral characteristics independent of signal power , for each signal segment we determine

normalized spectral coefficients of Fourier series decomposition. The decomposition coefficients a_{ij} are complex numbers and contain the information about the amplitude and phase of the i-th harmonic of the j-th signal. To reduce the dimensions of the vector representing the signal we can use normalized amplitude spectral coefficients

$$a'_{li} = \frac{|a_{li}|}{\sqrt{\sum_{i=0}^{N-1} |a_{li}|^2}}, \quad l = 1,..., Q, \quad i = 0,..., N/2 \tag{3}$$

In the same way each of the signal segments can be characterized by probability density distribution of normalized amplitude spectral coefficients (3) $f_l(a'_{l,0},...,a'_{l,N/2})$, $l = 1,...,Q$.

In general case the probability density distributions of normalized amplitude spectral coefficients are unknown and for synthesizing the algorithm for random process disorder detection (the moment when the characteristics of the signal change) the methods of nonparametric statistics should be applied.

The random process disorder detection task is to check nonparametric hypotheses about the probability density distribution of normalized spectral coefficients of Fourier series decomposition of neighboring signal segments (neighboring windows).

For the synthesis of the nonparametric test (Q+1) windows are created. In each window the amplitude spectrum is calculated. The results of spectrum calculation using the i-th realization of random process can be presented in the form of the following matrix

$$A_i = \begin{pmatrix} a'_{k,0},....., a'_{k,N/2} \\ ..... \\ a'_{k-Q,0},..., a'_{k-Q,N/2} \end{pmatrix}.$$

The first index of matrix cell indicates the harmonic number. The second index denotes the window number. The hypothesis H_0 implies that the probability density distributions of normalized spectral coefficients of the k-th and (k-1),...,(k-Q)-th windows are equal

$$f(a'_{k,0},...a'_{k,N/2}) = f(a'_{k-l,0},...a'_{k-l,N/2}) \quad , \quad l = 1,.Q.$$

The hypothesis H_1 implies that the probabilities density distributions of normalized spectral coefficients of the k-th and (k-1),...,(k-Q)-th windows are different

$$f(a'_{k,0},...a'_{k,N/2}) \neq f(a'_{k-l,0},...a'_{k-l,N/2}) \quad , \quad l = 1,.Q.$$

For checking the nonparametric hypotheses H_0 and H_1 concerning the distribution function of A-matrix cells the modification of Wilkockson's statisic [1] is used.

$$L(A_1,..,A_M) = \sum_{m=1}^{M} \max_{i,j} \sum_{i=0}^{\frac{N}{2}} \sum_{j=0}^{\frac{N}{2}} |R_{i,m} - R_{j,m}|, \tag{4}$$

where $R_{i,m}$ is the rank of the i-th harmonic amplitude estimation using the m-th realization of random process , which is obtained in the k-th window $a'_{i,k}$, comparing amplitude estimations of the same harmonic $a'_{k-l,i}, l = 1,...,Q$ in the preceding p windows, M is the number of random process realization .

The random process disorder detection algorithm consists of calculating $L(A_1,..,A_M)$ statisic and comparing it with the threshold of decision V_d. If statistic $L(A_1,..,A_M)$ exceeds the threshold V_d, then the detection algorithm generates one, that determines acceptance of hypothesis H_1. Otherwise hypothesis H_0 will be accepted.
The threshold of decision V_d is calculated with regard to the given probability of disorder false alarm-α.

ANALYSIS OF EFFICIENCY

The evaluation of the detection characteristics was done by the Monte-Carlo method. Random process realizations are modeled as a mix of harmonics signal with amplitude U , frequency ω_1 and Gaussian noise with variance σ_n^2.

$$S_i(lT) = U\cos(\omega_{g_l} lT + \varphi_i) + \eta(lT),\ l = 0,...,N(Q+1)-1,\quad i = 1,M$$

where $$g_l = \begin{cases} 1, l = 0,...,(N-1); \\ 2, l = N,...,N(Q+1)-1; \end{cases}$$

φ_i – *random phase.*

Random process disorder consists in changing the frequency of harmonic signals that reaches the value of ω_2. The amplitude of harmonic signal and the variance of noise are not changed. The changing of frequency is $\Delta\omega = \omega_2 - \omega_1 = 2\pi / NT$, where N is the size of windows created for rank statisic calculating, T-is the time sampling interval.
The signal to noise ratio b is calculated according to the formula $b = U^2 / 2q$. The characteristics of the random process disorder detection D are shown in Figure 1.

The reliability of the random process disorder detection was calculated for different numbers of samples N and number of windows Q. The following sample sizes have been adopted: M=16; N = 16; Q=2,3,8. The detection threshold was set to provide the given value of the false alarm probability $\alpha = 0.05$.

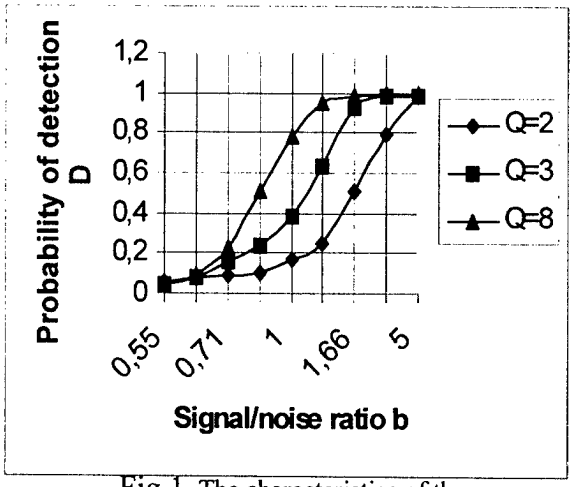


Fig.1. The characteristics of the random process disorder detection

REFERENCES

[1] Kendall, M.G. and Stuart, A. (1967). The Advanced Theory of Statistics. Vol. 2, Inference and relationship, 2nd edition, London, *Charles Griffin Publ.*, 1967.

DOPPLER-POLARIMETRIC RETRIEVAL OF RAIN RATE AND TURBULENCE INTENSITY IN PRECIPITATION

F.J. Yanovsky
National Aviation University
Faculty of Electronics and Telecommunications
1 Prospect Komarova, Kiev, 03680, Ukraine
e-mail: yanovsky@i.com.ua

ABSTRACT

This paper deals with mathematical modeling and simulation of echo-signals of microwave remote sensing of precipitation in both frequency and time domains. It establishes some important relationships between Doppler-Polarimetric observables and weather object under observation.

INTRODUCTION

Determination of the relationships between radar echo-signal characteristics and intensity of rain is the oldest problem of radar meteorology. Later more sophisticated parameters of rain microstructure and turbulence in rain became available for the deriving from radar returns. The implementation of Doppler-polarimetric radars opens new possibilities to improve the quality of radar measuring intensity and other parameters of rain.

In order to analyze different algorithms of weather signal processing comparing them between themselves at various meteorological conditions, it is necessary to have in possession some controllable radar signal models. These models must use some critical meteorological characteristics (rain rate, turbulence intensity, etc.) as initial parameters and provide samples of simulated radar signals on the output.

A complex of mathematical models of Doppler-polarimetric spectra of radar signals from rain is described. Some of the models were developed [1] as a part of joint project of the International Research Centre for Telecommunications and Radar (IRCTR) at the Delft University of Technology (The Netherlands) and the National Aviation University (Kiev, Ukraine). These models are very useful for data analysis and interpretation especially for CW FM atmospheric radars like DARR and TARA [2]. However impulse radars are also widely used for weather observations.

In this paper we consider approaches to the modeling Doppler-polarimetric temporal signal samples and spectral realizations. The purpose is to relate Doppler-Polarimetric observables with weather object parameters for data interpretation.

INITIAL MODELS OF RAIN AND TURBULENCE

The microstructure of rain is described by statistical distributions of the size, shape, fall speed, orientation, and concentration of raindrops. The fall speed of raindrops in stagnant air is related to their size. The shape of a falling raindrop is not exactly spherical: it is flattened at the base. In quiet air the horizontal axis of a spheroid droplet is horizontal. Local disturbances of the air density and wind variations may force the raindrop

to cant. The canting angle of drop is a random value assumed to be subjected to Gaussian distribution. The gamma-distribution is used as a model of dropsize distribution:

$$N(D) = N_0 D^{\mu} e^{-\frac{3.67+\mu}{D_0} D} \tag{1}$$

with μ as spread parameter, and D_0 as median drop diameter. The dropsize distribution plays an important role in the development of the model because it effects on both Doppler and polarization characteristics. The inertia of raindrops in a turbulent environment is taken into account in accordance with [2].

The turbulence energetic spectrum $S(\Omega)$ is a decomposition of the kinetic energy of turbulence in Fourier series on the wave numbers $\Omega = 2\pi / L$ (spatial frequency). In the inertial subrange, if the conditions of homogeneity and local isotropy of turbulence are valid, the analytical expression of turbulence spectrum is:

$$S(\Omega) = C\,\varepsilon^{2/3}\Omega^{-5/3} \tag{2}$$

where C is a dimensionless constant, and ε is the eddy dissipation rate. Ω is defined as $\Omega = \left|\vec{\Omega}\right| = 2\pi / L$ with $\vec{\Omega}$ as three-dimensional turbulence wave-vector. The kinetic energy of turbulence passes on consecutively from large scales to small ones, and then it is dissipated at the scale $l \le l_{min}$. The latter process is quantified by the eddy dissipation rate ε , which is a fundamental parameter of turbulence that characterizes the turbulence intensity. It does not depend on scale of turbulence within the inertial subrange, which makes ε convenient as an initial parameter for the modeling.

SIMULATION OF DOPPLER-POLARIMETRIC SPECTRA

The Doppler measurements give the information about the dynamic properties of the process (for example, wind, speed of drops falling), and the polarimetry is connected to the shape and orientation of the hydrometeors. For researching the relationship between the intensity of precipitation and radar echo the model [1] was used. It takes into consideration the polarization properties of radar signal, reflected from the ensemble of raindrops as a function of their speed. The model takes into account polarization features caused by the shape and spatial orientation of drops and the influence of turbulence on radar scatteres. It allows calculating the power spectra of radar signals from rain $S_{mn}(v)$, where v – is the radial component of Doppler speed, at different combinations of polarization on transmitting (first index) and receiving (second index). The indexes may have the following meanings: m=x; y, n=x; y, x-y - linear orthogonal polarization base. If the basis is "horizontal - vertical" (x=h; y=v), the model provides spectra $S_{hh}(v)$, $S_{vv}(v)$, which correspond to the two main polarization components on orthogonal polarizations. The model takes into account parameters of atmospheric turbulence - eddy dissipation rate ε and the range of turbulence scales L_{max}, parameters of radar and

the characteristic of a microstructure of rain - dropsize distribution, which allows to calculate the rain intensity.
On the basis of the developed models, the application package is developed and implemented as software for radar data interpretation.
In frequency domain the model gives Doppler energy spectra at different combinations of linear polarization of transmitted and received waves. Polarization observables such as differential reflectivity and linear depolarization ratio are calculated as functions of the Doppler velocity.

SIMULATION OF TEMPORAL SAMPLES

From power spectra we can easily calculate the power or amplitude of the signal. However, complex spectra are necessary to retrieve the appropriate temporal realizations by the Fourier inversion. That is why we simulated temporal samples according to general equation $V(t) = I(t) + jQ(t)$, where $I(t)$ and $Q(t)$ are random functions depending on the Rayleigh distributed amplitudes [3]. The mean amplitude was determined by the corresponding power spectra $S_{hh}(v)$, $S_{vv}(v)$, and $S_{hv}(v)$.
In time domain the model enables simulating the complex signal, which corresponds to Doppler-polarimetric radar with quadrature channels. In other respects the simulation in time domain was done independently on the calculated Doppler spectra.
Verification of the model has been done in frequency domain using the Delft Atmospheric Research Radar DARR [2], which is widely used for the research of the microstructure of precipitation.

MEASURABLE VARIABLES

In this paper we calculated such Doppler-polarimetric parameters in frequency domain: mean Doppler velocity at orthogonal polarizations $\overline{V}_{hh}$, $\overline{V}_{vv}$, $\overline{V}_{hv}$, Doppler spectrum width at different polarizations ΔV_{hh}, ΔV_{vv}, ΔV_{hv}, the difference between mean Doppler velocity at orthogonal polarizations $DDV = \overline{V}_{hh} - \overline{V}_{vv}$, and the slope of the regression line *SlpZdr* of a spectral differential reflectivity $Zdr(v) = 10\lg[S_{hh}(v)/S_{vv}(v)]$. In time domain the correlation window τ_k was calculated.

RESULTS OF MODELING AND COMPARISON WITH DATA

We will show that mentioned parameters could be related with microstructure and turbulence in rain. Finally, eddy dissipation rate and rain rate will be retrieved.
Comparison between Doppler spectrum width σ_f calculated from spectral samples and correlation window calculated from temporal samples is shown in Fig. 1. One of the results, which displays the relation between parameter ΔV and median diameter D_0 of the raindrops at constant μ and different ε is shown in Fig. 2.
Median drop diameter D_0 of raindrops is connected with rain intensity by the following equation:

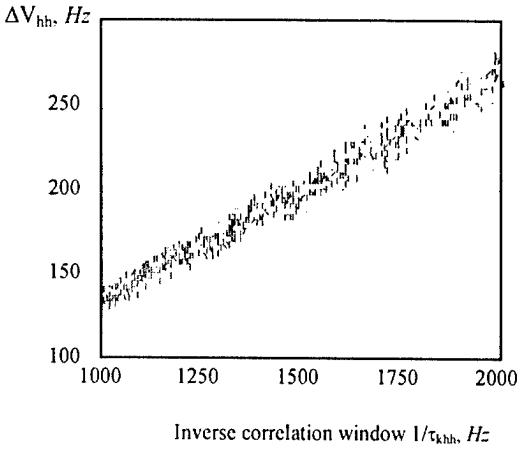


Fig. 1. Comparison of spectral and temporal modeled parameters.

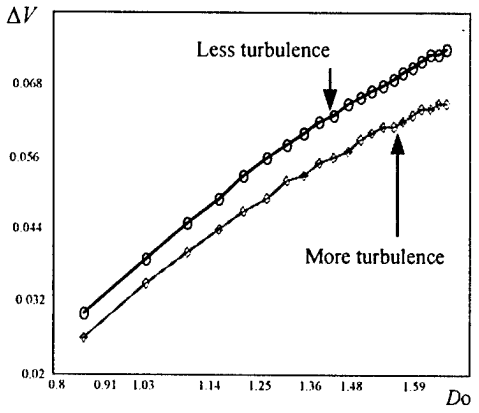


Fig. 2. Doppler spectrum width versus median drop

$$R(D_0) = \int_0^\infty N(D, D_0) v(D) V(D) dD, \qquad (3)$$

where $N(D, D_0)$ is given by formula (1), $v(D)$ is a fall speed of the drop of size D, $V(D)$ is the volume of drop with equivalent diameter D.

It is seen that DDV is more if the rain rate is more. It is because of the big drops are more oblate and fall faster than small ones. Having big axis horizontal they give more signal at *hh* polarization in comparison with *vv* polarization. Turbulence disturbs the velocities of drops and drop normal orientation. That is why turbulence decreases the degree of the connection between ΔV and D_0. It is clearly displayed in figure 2.

The relationship in logarithmic scale between the parameter of intensity of turbulence ε [cm^2/s^3] and the Doppler spectrum width ΔV_{hh} [m\s], appointed at -3dB level is shown in figure 3 at three values of spread μ of the dropsize gamma-distribution (1).

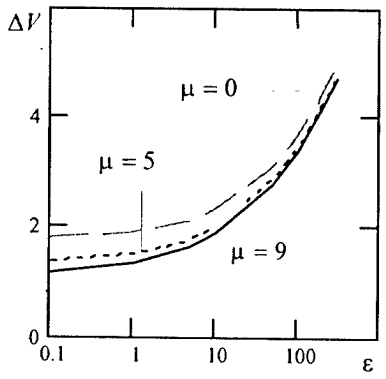


Fig. 3. The relationship between the intensity of turbulence and Doppler spectrum width.

Figure 4 displays the relationship between turbulence eddy dissipation rate ε [cm^2/s^3] and the slope of linear regression line of the spectral differential reflectivity *SlpZdr*.

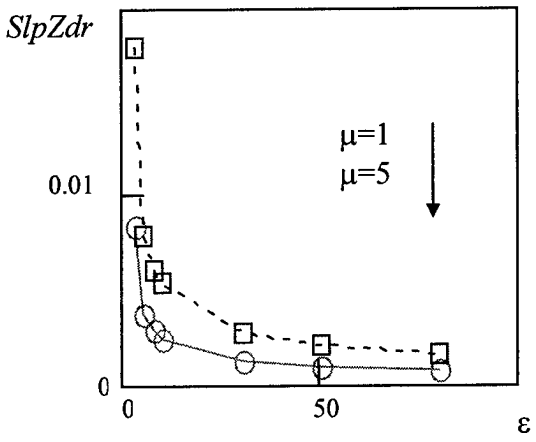


Fig. 4. Relationship between spectral differential reflectivity and turbulence

The adequacy of the model has been justified by the comparison of modeled and measured data, which were done with Delft Atmospheric Research Radar (DARR). As an example, in figure 5 one can see the relation *SlpZdr* versus Doppler spectrum width using the results of the calculation with the model (solid line) and measured data (circles). Good coincidence can be seen.

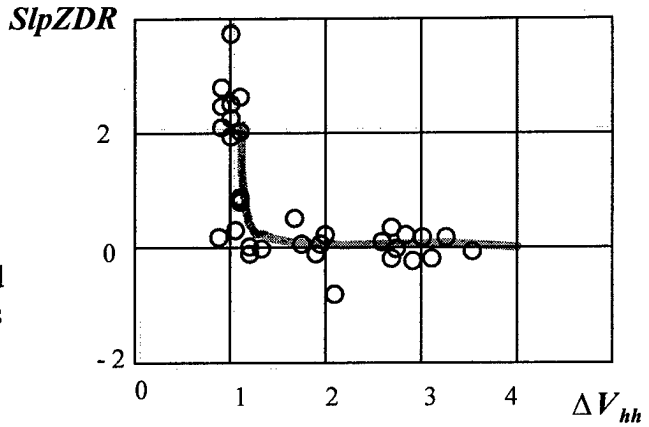


Fig.5. Comparison of measured and modeled slope of Zdr(v) vs Doppler spectrum width

CONCLUSION

The study has shown that considered Doppler and polarization parameters of radar signal contain information on rain microstructure and turbulence intensity in weather object. The connection between the parameters of a signal of the Doppler-polarimetric

radar (Doppler spectrum width, differential Doppler velocity and slope of the regression line of the spectral Zdr) and the intensity of turbulence hes been established.
The combination of Doppler and polarization diversity in weather radars enables a detailed study of microphysical phenomena in weather objects. An important application of modeled signals is to compare different signal processing algorithms of turbulence detection in clouds and precipitation and measuring the intensity of turbulence and other meteorological parameters.
Fourier analysis shows the correspondence between the calculated Doppler spectra and the simulated independently time samplings of radar signal from rain.
The model of temporal samples of radar signal reflected from rain can be used for the analysis of different signal processing algorithms of the extracting meteorological information.
All the data and results where received on the computer, using the developed mathematical models, which were previously validated using the comparison with the real experimental data.
The differential Doppler velocity of raindrops carries the important information on microstructure of rain and can be used in order to measure the rain intensity. However turbulence decreases this effect and should be taken into consideration as well. Actually simultaneous measuring turbulence intensity and rain rate help to increase accuracy of the estimation of both parameters.
The quantitative results need for more extensive experimental confirmation.
The method based on these researches can be practically used for study turbulence in precipitation, as well as for measuring rate rain and study rain microstructure, and it is difficult to say which of this two applications is more important to the practice. The obvious applications of these results are: detection of turbulent zones dangerous for flight, meteorological and hydrological observations and prognoses, climatic research and others.

ACKNOWLEDGEMENT

This research was supported by the International Research Centre for Telecommunications and Radar at the Delft University of Technology (TU-Delft). The author would like to thank Leo Ligthart and Herman Russchenberg for the great experience obtained during the joint work in TU-Delft and numerous useful discussions on the microwave remote sensing of rain. He wishes to express special thanks to Christine Unal who made important experiments with DARR.

REFERENCES

1. F.J.Yanovsky, H.W.J. Russchenberg, L.P. Ligthart, and V.S. Fomichev, "Microwave Doppler-Polarimetric Technique for Study of Turbulence in Precipitation," *IEEE IGARSS 2000, Honolulu, Hawaii*, Vol. V, pp. 2296-2298.
2. H.W.J. Russchenberg, L.P. Ligthart, J.P.V. Poiares Baptista, and G. Brussard, "Remote sensing of precipitation with a multi-polarized Doppler (FM-CW) research radar: applications to propagation studies", *ESA Journal*, Vol. 14, 1990.
3. R.J. Doviak and D.S. Zrnic, Doppler Radar and Weather Observations. London: Academic Press, Inc., 1993.

RELATIONSHIP BETWEEN AN INTERVAL OF CORRELATION OF ECHO-SIGNAL ENVELOPE AND TURBULENE INTENSITY IN RADAR REFLECTING VOLUME OF CLOUD OR PRECIPITATION

Yahya Salameh Khraisat

Al-Balga Applied University Jordan and Al-Huson Polytechnic University
P.O. 1375 , Irbid 21110, Jordan
Yayha114@hotmail.com

ABSTRACT

The width of Autocorrelation Function (ACF) is characterized by the interval of correlation at the 0.5 level, $\tau_{0.5}$. The eddy dissipation rate (ε) is a fundamental parameter that describes the intensity of turbulence. We use the data of simulation and build a model of relationship between the characteristics of a radar echo-signal and parameters of reflecting objects given in [4] at sample size n=30. The results of calculation after formula (6) with K as level of a reference of an interval of correlation (K=0.5, λ=3.2cm) are presented. We can see rather good agreement of the interval of correlation with the intensity of turbulence (ε).

The simulation results enable us to consider that sample size n=15 is insufficient for deriving a measuring information by using the classical algorithms for ACF calculation.

MAIN CONTAINS OF THE PAPER

If S(f) is a gaussian Doppler spectrum with the middle frequency f_0 and frequency dispersion $\sigma^2 f$, then the spectrum fluctuation Sp (F) after amplitude detection (see [1]), is given by:

$$Sp(F) = \int_{-\infty}^{\infty} S(f)S(f+F)df = \frac{1}{\sqrt{2\Pi\sigma_f}} \exp(-\frac{F^2}{2\sigma_F{}^2}) \ , \qquad (1)$$

Here $\sigma^2 F = 2\sigma f^2$ is the normalized ACF determined after the formula

$$R(\tau) = \exp(-2\Pi^2\sigma_F{}^2\tau^2) = \exp(-4\Pi^2\sigma_f{}^2\tau^2) = \exp(\mathrm{Ln}K\frac{\tau^2}{\tau_k^2}), \qquad (2)$$

where τ_k is the interval of correlation calculated at the level K<1.

Doppler relation $f = 2v/\lambda$ enables us to consider the spectrum S(f) as a distribution of radial velocities of scatters. On taking into account (2), the radial velocities dispersion σ_v^2 can be obtained by the following relation:

$$\sigma_v^2 = \frac{\lambda^2}{4}\sigma_f^2 = \frac{\lambda^2}{8}\sigma_F^2 = \frac{\lambda^2 \mid \mathrm{Lnk} \mid}{(4\Pi\tau_K)^2} \tag{3}$$

It is known that σ_v^2 is determined by plenty of factors:

$$\sigma_v^2 = \sigma_s^2 + \sigma_a^2 + \sigma_d^2 + \sigma_o^2 + \sigma_t^2, \tag{4}$$

where σ_s^2 is the wind motion contribution, σ_a^2 is the antenna motion contribution, σ_d^2 is from the different velocities of falling droplets, σ_t^2 is the contribution of turbulence, σ_o^2 is contribution of vibration and orientation of weather observers.

With taking into account (4) in horizontal sensing of clouds and precipitation, we consider the shape of scatters to be cylindrical with the length $C\tau s/2$ (where τ_s is duration of radiated pulse) and radius $r = R\theta/2$ (where θ is antenna pattern width, and R is the distance to reflecting object). Then frequency dispersion is related to (ε) as follows:

$$\sigma_F^2 \approx 0.206(\frac{2}{\lambda})^2 \xi \varepsilon^{2/3} h^{2/3} \frac{11-\alpha^{5/3}}{3-\alpha}, \tag{5}$$

where $\alpha = 2r/h$, ξ is a numerical factor around unity (from the Kolmogorov – Obuknov Law). If $\alpha \approx 1$, then from (5) we accept:

$$\varepsilon = \frac{0.042 \mid \mathrm{Lnk} \mid^{3/2} \lambda^3}{\Pi^5 h \tau_k^3} \tag{6}$$

The width of ACF is characterized by the interval of correlation $\tau_{0,5}$ at the level of 0.5. A relationship between $\tau_{0.5}$ and (ε) calculated by using the data of simulation with the sample size n=30 is shown by dots in Fig.1. We observe rather good agreement of the interval of correlation with the intensity of turbulence. (ε).

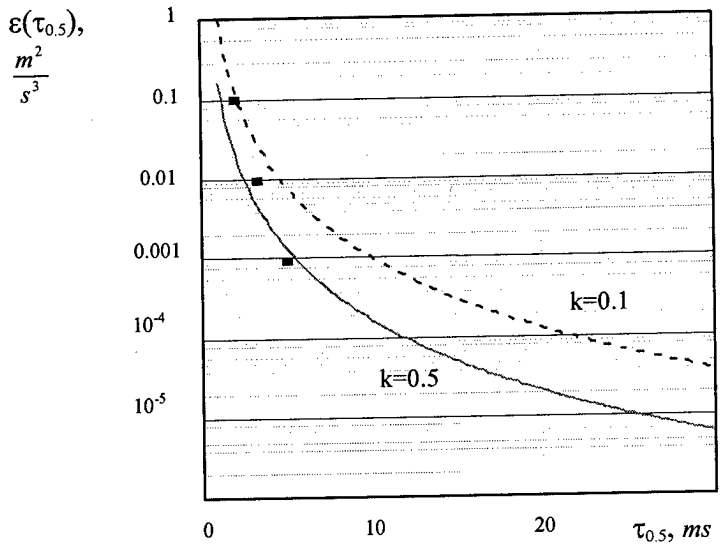


Fig. 1. Relationship between the interval of correlation and eddy dissipation rate.

The solid line in Fig.1 shows results calculated after the formula (6) with K as a level of reference of the interval of correlation ($K=0.5, \lambda=3.2\times10^{-2}$m). These results of simulation give a foundation to consider that the sample size n=15 is insufficient for deriving a measuring information by using the classical algorithms for calculation ACF.

REFERENCES

[1] Yanovsky F.J. Dispersion evaluation turbulence pulsation velocities of wind in storm by interval of correlation echo- signal non-coherent airborne weather radar (AWR) N 7213 – 73 dep 1973, p.11.

[2] Yanovsky F.J. About using AWR for evaluation turbulence parameters in clouds, "Radio technica and Electronica", Tom 19, N8, 1974, pp. 1963-1965.

[3] Gorelik A.G., Milnickuk U.V, Chernikov A.A., Relationship between statistical characteristic of radar signal and dynamic parameters and microstructure of meteorological objects, Trudy TsAO, no 48, 1963, pp. 3-55 (in Russian).

[4] Khraisat Y.S. Some results of simulation of processes of an inverse scattering from turbulized meteorological objects, Problems of Automation and Control, KIUCA Press, 1998, pp. 13-22.

METHODS OF IMPROVING OF THE SUBSURFACE OBJECTS IMAGES RECONSTRUCTED BY THE TOMOGRAPHY PROCESS

A. Vertiy* (1), (2), S. Gavrilov (1)

(1) TUBITAK– MRC, TUJRL, Gebze–Kocaeli, Turkey
(2) IRE NASU, Kharkov, Ukraine
Mailing address: TUBITAK-MRC, TUJRL, P.O. Box 21, 41470 Gebze – Kocaeli, Turkey
Telephone: +90 262 641 23 00/4786 (A. Vertiy), 4790 (S. Gavrilov)
Fax: +90 262 643 04 67
E-mail: Alex.Vertii@posta.mam.gov.tr Sergiy.Gavrilov@posta.mam.gov.tr

ABSTRACT

A possibility of an application of the tomography method and spectrum filtering for the images reconstruction of the cross-sections of different inhomogeneities, which are taking place under plane surface of a medium, has been studied. The spectral approach, use of the information containing in near field of scattering object, opportunity of use of the tomography algorithm in a case of strongly absorbing environments have allowed essentially to improve quality of the restored images and have expanded the application area of the subsurface tomography. Obtained results can find application in practice at designing of the tomography systems used for visualisation of the subsurface targets.

ALGORITHMS CONSIDERATION

Modeling and the experiments on restoration of the cross sections images of various objects embedded in an environment by using the subsurface tomography method can be based on the tomography integral equation [1]

$$\frac{\hat{\psi}(\nu, y_1)\exp(i\gamma_1 y_1)}{c_1(\nu)} = \iint_S K(x', y')\exp[-2\pi i(\alpha x' + \beta y')]dx'dy' \qquad (1)$$

where $\hat{\psi}(\nu, y_1)$ is Fourier image of complex scattered field $\psi(x, y_1)$, which should be measured above surface of probed medium at line $y = y_1$; variable ν is the space frequency; $c_1[\gamma_1(\nu), \gamma_2(\nu)]$ is complex function of ν; γ_1, γ_2 and β are complex functions of ν in general case; α is real function of ν; function $K(x', y')$ represents the normalized polarization current in the subsurface region S (cross-section of an investigated cylindrical subsurface object), which is sought for and which is source of scattered field $\psi(x, y_1)$. Investigated region S is limited, so integral in equation (1) can be considered in infinite limits. It is supposed here that the Fourier transform of the scattered field exists, as this field is located in space. In practice measured field is mostly total field and represents the sum of three fields. They are incident, reflected by the plane surface of environment and scattered by region S fields. The probing

(incident) field in considered algorithm has a kind of a plane wave. In this case incident and reflected fields in probing line can be calculated theoretically and then deducted from total field. However, in practice this operation is unrealizable as the probing field is not plane wave. Incident and reflected fields are unknown generally. Experiments on restoration of the cross-sections images of various objects at use in the equation (1) of total field measured on the limited line (line of scanning) have shown that the surface image presenting in the restored cross-section of the subsurface region can not be completely removed by subtraction of known plane wave incident and reflected fields. Such operation essentially does not improve the image quality of the required scattering object, and the weakly scattering objects located near to the medium surface poorly come to light. Thus there is a problem of use in the reconstruction algorithm of the equation (1) and measured total field. It is considered below an algorithm allowing to allocate a scattered field from a total field and by that essentially to improve quality of the image.

Let we consider equation (1) and suppose that in inversion the data about total field at line $y = y_1$ ($y_1 < 0$) are used. The equation (1) can be written then in the form

$$\left\{\hat{\psi}(\nu, y_1) + [\exp(ik_1 y_1 \cos\theta_1) + R\exp(-ik_1 y_1 \cos\theta_1)]\int_{x_2}^{x_3} \exp[-2\pi i(\nu - \nu_0)x]dx\right\}\frac{\exp(i\gamma_1 y_1)}{c_1(\nu)} =$$

$$= \int_{x_2}^{x_3}\int_{0}^{y_b} K(x,y)\exp[-2\pi i(\alpha x + \beta y)]dxdy, \quad \text{where } \nu_0 = \frac{k_1 \sin\theta_1}{2\pi} \tag{2}$$

and second term from left side of equation (2) is the Fourier transform of incident and reflected fields. The reflection coefficient is denoted by R. The borders of the scanning area are designated by x_2, x_3 ($x_3 > x_2$) and integral is taken in this limits. It is supposed that the image function is reconstructed in the rectangular region $x_2 < x < x_3$, $0 < y < y_b$. Values k_1, y_1, θ_1, x_2, x_3 and R are parameters which can be changed.

One can see from (2) that reconstructed function $K(x,y)$ can be presented as follows $K(x,y) = K^s(x,y) + K^r(x,y)$. First term $K^s(x,y)$ is required function defining distribution of polarization current in the region S. Another term $K^r(x,y)$ is defined by integral equation

$$\frac{[\exp(ik_1 y_1 \cos\theta_1) + R\exp(-ik_1 y_1 \cos\theta_1)]\exp(i\gamma_1 y_1)}{c_1(\nu)}\int_{x_2}^{x_3}\exp[-2\pi i(\nu - \nu_0)x]dx =$$

$$= \int_{x_2}^{x_3}\int_{0}^{y_b} K^r(x,y)\exp[-2\pi i(\alpha x + \beta y)]dxdy. \tag{3}$$

The function $K^r(x,y)$ is imposed on function $K^s(x,y)$. Therefore the scattering region S can be poorly observed in the reconstructed image of the probed subsurface region.

Hence the function $K^r(x,y)$ should be removed at a stage of the image reconstruction. In general case the function $K^r(x,y)$ can be removed from reconstruction process by filtering of spectrum of the measured field in the Fourier space. The process of the filtering consists in following. One can see from (3) that integral in it left part is $\delta(\nu-\nu_0)$ if x_2 and x_3 are tended to $-\infty$ and ∞, respectively. So, if only one component at the space frequency $\nu=\nu_0$ is deleted from spectrum of measured field, left part of (3) will be equal to zero and $K^r(x,y)\equiv 0$. In this case also will be deleted one component at $\nu=\nu_0$ from spectrum $\hat{\psi}$. Bat spectrum $\hat{\psi}$ is usually determined in a wide frequency band and deleting only one component from this spectrum cannot essential change the image of the subsurface object. Let the complex numbers F_2, F_3 are complex amplitudes of measured field at final points of scanning x_2, x_3, respectively. If field scattered by a subsurface object is equal to zero in intervals $(-\infty, x_2]$, $[x_3, \infty)$ (that is supposed), the complex numbers F_2, F_3 are complex amplitudes of field created by incident and reflected from the mediums interface waves. This field does not depend on x and it will be used only one number $F=(F_1+F_2)/2$ as its complex amplitude. Let coordinate points x_1, x_4 such, that $x_1 \ll x_2$ and $x_4 \gg x_3$, then two new functions $I_1(\nu-\nu_0)$ and $I_2(\nu-\nu_0)$ can be defined by integrals

$$I_1(\nu-\nu_0)=F\int_{x_1}^{x_2}\exp[-2\pi i(\nu-\nu_0)x]dx \text{ and } I_2(\nu-\nu_0)=F\int_{x_3}^{x_4}\exp[-2\pi i(\nu-\nu_0)x]dx \quad (4)$$

where x_1, x_2, x_3, x_4 are parameters and x_2, x_3 are specified by size of the scanning region. The functions $I_1(\nu)$ and $I_2(\nu)$ can be added to spectrum of measured field. After this operation, the new spectrum is sum of two functions: $\hat{\psi}(\nu)$ and $\hat{\psi}_\delta(\nu-\nu_0)$. If $x_1=-A$ and $x_4=B$ where A and B sufficiently large numbers, the function $\hat{\psi}_\delta(\nu-\nu_0)$ approaches to delta-function $\delta(\nu-\nu_0)$ and can be deleted from spectrum by a filter. After filtering the function $K^s(x,y)$ is calculated from equation (2) using its inverse. Inversion of (1) was considered in [1]. It was determined using results of this work that polarization currents are good reconstructed around borders of an inhomogeneity buried in lossy medium if complex values of functions $\gamma_1(\nu)$, $\gamma_2(\nu)$ and $\beta(\nu)$ are taken in account in the inverse of the tomography integral equation (1). Reconstruction in this case gives enables to receive the image of object, which is taking place under the surface of environment, in such form, as though lossy in this environment connected with it conductivity were absent.

REFERENCES

[1] A. A. Vertiy, S. P. Gavrilov, S. Aksoy, I.V. Voynovskyy, A. M. Kudelya, V. N. Stepanyuk, "Reconstruction of Microwave Images of the Subsurface Objects by Diffraction Tomography and Stepped-Frequency Radar Methods", Zarubejnaya Radioelektronika. Uspehi Sovremennoy Radioelektroniki (Russia), № 7, 2001, pp. 17-52.

AN ART ALGORITHM FOR IMAGING OF BURIED CYLINDRICAL BODIES ILLUMINATED BY GAUSSIAN BEAMS

Fatih DiKMEN [1], Ali ALKUMRU [1], Osman YILDIRIM [2]

Gebze Institute of Technology, Department of electronics Engeneering, 41400 Gebze, Kocaeli, TURKEY

Air Force Academy, Department jf Research & Development, 34807 Yesilyurt, Istanbul, TURKEY.

INTRODUCTION

In the past three decades, several exact and numerical techniques have been established in order to solve the inverse scattering problems in connection with cylindrical bodies. These methods can also be divided into two categories: (a) non-iterative methods and (b) iterative methods. The iterative methods include the Algebraic Reconstruction Technique (ART) [1] and Simultaneous Iterative Reconstruction Technique (SIRT). These methods generate reconstruction via an iterative process, which begins with an initial estimate of the object being constructed and then improves on this initial estimate via a sequence of estimates that presumably converge to an optimum reconstruction after some large number of iterations. The ART algorithm was first employed in Computerized Tomography (CT). Ladas and Devaney [2] developed an iterative algorithm of the ART type for Diffraction Tomography (DT) using the Rytov approximation. And also this algorithm has been successfully used in the case of buried bodies by Akduman and Alkumru [3].

The purpose of this work is to develop an ART algorithm to solve the electromagnetic inverse scattering problem whose aim is to recover the electromagnetic properties as well as the geometry of the infinitely long cylindrical bodies buried in a half space. The problem then consists of finding the constitutive parameters of the buried body by using the data collected throughout the measurements along a line in the half space not containing the body. The buried body will be illuminated by a Gaussian Beam which is excited in the same region where the data will be collected. The problem considered here can also be interpreted as the use of an iterative algorithm of the ART type which basically consists of an application of the Kaczmarz method [4] to solve an inverse scattering problem related to buried cylindrical bodies illuminated by Gaussian Beams where a method constituted on a complex manifold technique was previously used [5].

FORMULATION OF PROBLEM

Assume that the regions $x_2>0$ and $x_2<0$ are filled with the materials having electromagnetic constitutive parameters ε_0, μ_0, $\sigma=0$ and ε_1, μ_0, $\sigma=0$, respectively (Fig. 1). An infinitely long cylindrical body D, which is composed by a non-magnetic simple material is located in the region $x_2<0$ parallel to Ox_3 axis. The dielectric permittivity $\varepsilon(x)$ and conductivity $\sigma(x)$ of the body D are scalar functions of the space coordinates in R^2. The cylindrical body D can be composed of several finite number of disjoint parts.

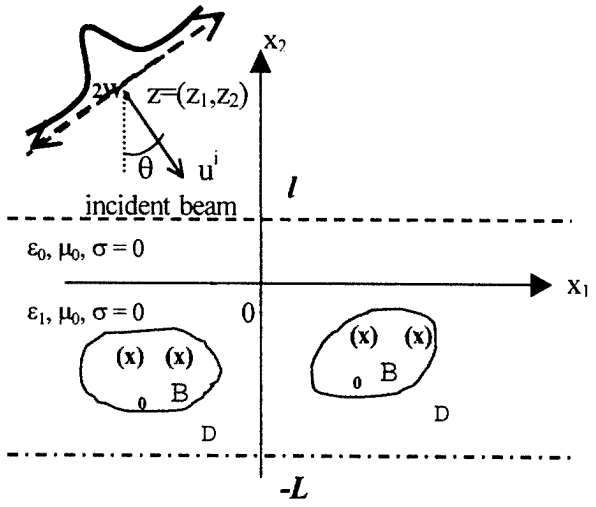


Figure 1

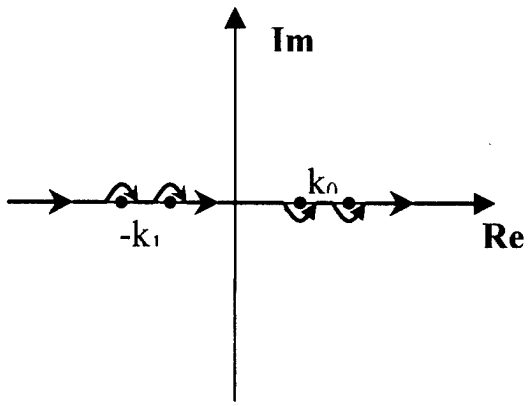


Figure 2

The aim of this work is to find a method for determining the geometry (location and shape) and physical parameters (ε(x) and σ(x)) of the body D by observing its effect on the illumination of a Gaussian beam excited in the region $x_2 > 0$. In the following analysis it is assumed that the incident wave is a Gaussian beam whose electric field $\vec{E}^i$ is parallel to the Ox_3 axis, namely;

$$\vec{E}^i = \left(0,0,u^i(x;z)\right) \tag{1}$$

$$u^i(x;z) = \frac{1}{2\pi}\int_{C_1} \frac{\exp\left[P(\lambda)\right]}{\cos\theta} \exp\left\{i\lambda x_1 + \gamma_0(\lambda)x_2\right\} d\lambda \qquad x_2 > 0,\ \lambda \in C_1 \tag{2}$$

with $P(\lambda) = -\left[W_0(\lambda - k_0\sin\theta)/(2\cos\theta)\right]^2 - i\lambda z_1 - \gamma_0(\lambda)z_2$, where W_0, z and θ are depicted in Figure 1 and C_1 is the line shown in Figure 2 while the function γ_0 stands for the square root $\gamma_0(\lambda) = \sqrt{\lambda^2 - k_0^2}$ defined in the complex λ-plane cut as shown in Figure 2 with the condition $\gamma_0(0) = -ik_0$ with k_0 the wavenumber of the region $x_2>0$.

The integral representation of the scattered field $u_D(x)$ by means of the Green's function of the two part space and using the well-known Born approximation, the Fourier transform of the scattered field $u_D(x)$ with respect to x_1 at the line $x_2=l>0$ gives

$$\hat{u}_D(\nu,l) = \frac{k_1^2 \exp\left(-\gamma_0(\nu)l\right)}{\pi\cos\theta\left[\gamma_0(\nu)+\gamma_1(\nu)\right]} \int_{C_1} \frac{\gamma_0(\lambda)}{\left[\gamma_0(\lambda)+\gamma_1(\lambda)\right]} \hat{v}\left(\nu-\lambda, i\left[\gamma_1(\nu)+\gamma_1(\lambda)\right]\right)\exp\left[P(\lambda)\right] d\lambda \tag{3}$$

where $\gamma_1(\lambda) = \sqrt{\lambda^2 - k_1^2}$ is the square root function defined by $\gamma_1(0) = -ik_1$ and $\hat{v}$ is the two dimensional Fourier transform of the object function given by $v(x) = \left[\left(\varepsilon(x) + i\sigma(x)/\omega\right)/\varepsilon_1\right] - 1$.

Our purpose is now to solve $v(x)$ from (3) by using the generalized ART algorithm. To this end the asymptotic evaluation of the integral in (3) by saddle-point technique provides

$$\hat{u}_D(\nu,l) \cong \frac{k_1^2 \exp\left(-\gamma_0(\nu)l\right)}{\pi\cos\theta\left[\gamma_0(\nu)+\gamma_1(\nu)\right]} \frac{\gamma_0(\lambda_s)}{\left[\gamma_0(\lambda_s)+\gamma_1(\lambda_s)\right]} M\hat{v}\left(\nu-\lambda_s, i\left[\gamma_1(\nu)+\gamma_1(\lambda_s)\right]\right)\exp\left[P(\lambda_s)\right] \tag{4}$$

$$\lambda_s = k_0 \sin\theta + \left[k_0(z_1\cos\theta + z_2\sin\theta)\right] \Big/ \left[\left(iW_0^2 k_0 \Big/ 2\cos\theta\right) - z_2 + \left(i\sin^2\theta \Big/ k_0\cos^3\theta\right)\right] \tag{5}$$

In (4) $M\hat{v}$ is the two dimensional Fourier transform of the masking operator on $v(x)$:

$$Mv(x) = \begin{cases} v(x) & , -L < x_2 < 0 \\ 0 & , \textit{otherwise} \end{cases} \tag{6}$$

By multiplying both sides of (4) by $e^{-iv\,x_1}/2\pi$ and integrating over the interval $v\in(-k_1, k_1)$ for certain fixed values of θ_n for n=1,2,...,N , one gets a system of linear operator equations:

$$A_n v(x_1) = a_n(x_1), \qquad n = 1,\ldots,N \tag{7 a}$$

$$A_n v(x_1) = \frac{k_1^2 \gamma_0(\lambda_s^n) exp\left[P(\lambda_s^n)\right]}{2\pi^2 \cos\theta_n \left[\gamma_0(\lambda_s^n) + \gamma_1(\lambda_s^n)\right]} \int_{-k_1}^{k_1} \frac{exp\left(-\gamma_0(v)l\right)}{\left[\gamma_0(v) + \gamma_1(v)\right]} M\hat{v}\left(v - \lambda_s^n, i\left[\gamma_1(v) + \gamma_1(\lambda_s^n)\right]\right) e^{ivx_1} dv \tag{7 b}$$

with θ_n=arctan(-z_1^n/ z_2^n) and $\lambda_s^n = k_0\sin\theta_n$. Thus the problem is to obtain $v(x)$ from the method which is based on the iterative solution of the operator equation system given in (7 a). The right-hand side of (7 a) is known from scattering field measurements performed along the line $x_2=l$ >0 for the incidence angles θ_n , n=1,2,...,N. Then the system of operator equations (7 a) can be solved by using the method proposed by Kaczmarz [6] in the following form

$$v_0 = v^j \quad , \quad v_n = v_{n-1} + A_n^*\left(A_n A_n^*\right)^{-1}\left(a_n - A_n v_{n-1}\right), \quad n = 1,\ldots,N, \quad v^{j+1} = v_N \tag{8}$$

Here j is the iteration number and v_0 is the initial estimate value of the unknown function $v(x)$ while A_n^* denotes the adjoint of A_n defined by the inner products in the related Hilbert spaces. Namely ;

$$\left(A_n v(x_1), a_n(x_1)\right)_H = \left(v(x), A_n^* a_n(x)\right)_{H_n} \tag{9 a}$$

After some straightforward manipulations one can easily obtain the adjoint and composite operator appearing in (8) and gets

$$A_n^*\left(A_n A_n^*\right)^{-1}\left(a_n - A_n v_{n-1}\right) = \frac{1}{2k_1^2 L} exp\left(-ik_0 z_2^n / \cos\theta_n\right)\left[\cos\theta_n + \sqrt{(k_1/k_1)^2 - \sin^2\theta_n}\right] \times \tag{10}$$

$$M\int_{-k_1}^{k_1}\left[\gamma_0(v)+\gamma_1(v)\right] e^{\gamma_0(v)l}\left[\hat{a}_n(v) - A_n\hat{v}_{n-1}(v)\right] exp\left(i\left(v - k_0\sin\theta_n\right)x_1 - \left[\gamma_1(v) - i\sqrt{k_1^2 - k_0^2\sin^2\theta_n}\right]x_2\right)dv \ , \ n = 1,\ldots,N$$

REFERENCES

[1] Gordon, R., "A tutorial on ART", IEEE Trans. Nuclear Science, NS-21, pp:78-93, 1974.

[2] Ladas, K.T. and Devaney, A.J., "Generalized ART algorithm for diffraction tomography", Inverse Problems, 7, ppp: 109-125, 1991.

[3] Akduman I. And Alkumru A, "A generalized ART algorithm for inverse scattering problems related to buried cylindrical bodies", Inverse Problems 11, pp:1125-1135, 1995.

[4] Natterer F., "The Mathematics of Computerized Tomography", Wiley, New York, 1986.

[5] Akduman I., "An Inverse Scattering Problem Related to buried cylindrical bodies illuminated by Gaussian Beams", Inverse Problems, 10, 213-226, 1994.

[6] S. Kaczmarz, "Angemaemrte Auflaesung von systemen linearer Gleichungen", Bull. Int. Acad. Pol. Sci. Lett. A 335-37,1937.

ESTIMATION OF GEOMETRICAL PARAMETERS OF PERFECTLY CONDUCTING CYLINDRICAL OBJECT BURIED IN DIELECTRIC HALF-SPACE BY ITS SCATTERING CHARACTERISTICS

A.V. Muzychenko, A.Z. Sazonov, O.I. Sukharevsky

Kharkov Military University, Kharkov, Ukraine
E-mail: sukharevsky@euro.dinos.net

ABSTRACT

The possibility of geometrical parameters determination of perfectly conducting infinite cylinder (radius of surface curvature in a neighborhood of a line of mirror reflection and orientation) located in a dielectric half-space (in particular with parameters of a ground) is justified. The proposed technique is based on asymptotic relations characterizing a field scattered by such an object when a plane monochromatic electromagnetic wave is incident on its surface.

INTRODUCTION

In a number of applications there is a necessity of determination of geometrical parameters of a cylindrical scatterer located in a dielectric lossy half-space. One of such applications is diagnostics of various-purpose pipelines (for example oil or gas). In the paper, a possibility of this problem solution for an infinite perfectly conducting circular cylinder is justified. Cylinder's radius is greater than the length of the incident electromagnetic wave. The technique is based on relations characterizing solution of direct problem for such a scatterer. These relations are obtained by deriving a number of asymptotic estimations of integrals for

- currents on the scatterer surface in a small neighborhood of the stationary phase point;
- electromagnetic field scattered by the object in the far-field region.

ASYMPTOTIC SOLUTION OF THE PROBLEM OF ELECTROMAGNETIC WAVE SCATTERING BY A PERFECTLY CONDUCTING CYLINDRICAL OBJECT BURRIED IN A DISPERSIVE LOSSY DIELECTRIC HALF-SPACE

An infinite perfectly conducting cylindrical scatterer with the surface L located at the depth d in a homogeneous half-space G_2 with parameters ε_2, μ_2, characterized by the wave number k_2 (generally complex-valued) is considered (Fig. 1). The origin of a coordinate system $OXYZ$ is placed above the center of the object on its surface. The axis OZ is directed along the generator of the cylinder. The interface between the half-space G_1 with parameters of free space and half-space G_2 is the plane L_1. A plane monochromatic electromagnetic wave of unit amplitude normally incidents from the half-space G_1 on the media interface. Its wavelength is assumed much smaller than characteristic radius of curvature and geometrical size of the scatterer. It is required to

determine the field scattered by this cylinder at a point above its center in area G_1 high above the plane L_1.

For solution of this problem we shall take advantage of integral representation of total electromagnetic field in the presence of cylindrical object buried in the half-space G_2:

$$u(\vec{\psi}) = u_0(\vec{\psi}) + \int_L \left[u(\vec{\xi}) \frac{\partial F(\vec{\psi},\vec{\xi})}{\partial n} - F(\vec{\psi},\vec{\xi}) \frac{\partial u(\vec{\xi})}{\partial n} \right] dl \qquad (1)$$

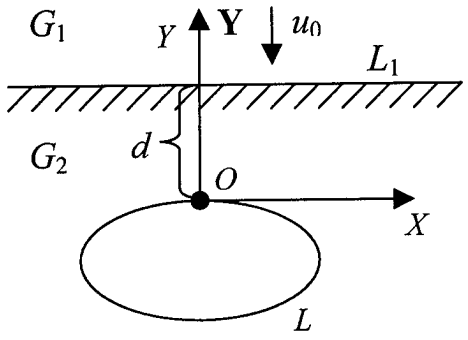


Fig. 1

where functions u, u_0 are the z - components of the vector of electric (in the case of the E-polarization) or magnetic (H-polarization) total and incident field, respectively; the function $F(\vec{\psi},\vec{\xi})$ is the field of a current line in the presence of half-space G_2; $\vec{\psi}$ is the position vector of observation point with coordinates x_0, y_0; $\vec{\xi}$ is the position vector of the point of integration along line L with coordinates x, y. By the E (H-)- polarization we imply the case of the vector of electric (magnetic) field of the incident electromagnetic wave parallel to the generator of cylinder.

One can derive the formulas characterizing electromagnetic field scattered by the cylinder by following [1]. The final expressions are given by:

- for the E- polarization case

$$u_p(\vec{\psi}) = \frac{-e^{ik_1(y_0+d)}}{\sqrt{y_0+d}} \frac{e^{i2k_2d}\sqrt{2k_1k_2R}\,p}{k_1+k_2} \left(1 + \frac{5i}{16k_2R} + \frac{k_1-k_2}{k_1+k_2}\sqrt{\frac{R}{R+4d}}\, e^{i2k_2d}\left(\frac{3i}{16k_2R}-1\right)\right), \qquad (2)$$

- for the H- polarization case

$$u_p(\vec{\psi}) = \frac{e^{ik_1(y_0+d)}}{\sqrt{y_0+d}} \frac{e^{i2k_2d}\sqrt{2k_1k_2R}\,p}{k_1+k_2} \left(1 + \frac{5i}{16k_2R} - \frac{k_1-k_2}{k_1+k_2}\sqrt{\frac{R}{R+4d}}\, e^{i2k_2d}\left(\frac{3i}{16k_2R}-1\right)\right). \qquad (3)$$

The adequacy of the obtained relations was tested by comparing the results of calculations with simulation of the scattering characteristics based on the method of integral equations [2]. This comparison has shown that the error of results of calculation after the formulas (2), (3) decreases if the frequency of sounding wave increases, and at $|k_2R| = 8$ ($\lambda_2 \approx 0{,}75R$) it already becomes 8 %. It is evident that the use of presented technique is possible for engineering estimations.

DETERMINATION OF PARAMETERS OF CYLINDER BURRIED IN DIELECTRIC HALF-SPACE

Thus formulas (2), (3) yield the relationships between the field scattered by the cylinder and its radius and burial depth. They allow to construct an algorithm of inverse problem solution – determination of parameters of unknown cylindrical object by its scattering characteristics measured in far-field zone.

Let antenna system of monostatic radar be located at the point $\vec{x}$ at large height from the ground surface (for example, it can be an airborne radar). Assume that location of

underground object is determined and besides it is known that it has cylindrical form. It is required to carry out the sounding with two orthogonal polarizations whose directions are characterized by the unit vectors $\vec{u}_1^0$ and $\vec{u}_2^0$. At the observation point, the measurement of scattered field characteristics is carried out with the same polarizations. As a result, amplitudes of the fields $\vec{u}_1$ and $\vec{u}_2$ are determined. Let the cylinder axis form an angle φ with the vector $\vec{u}_1$. Denote by $\vec{u}_{\parallel}$ and $\vec{u}_{\perp}$ the vectors of the scattered field corresponding to the case when polarization vector is parallel or perpendicular to cylinder's axis, respectively. Then we can write

$$|\vec{u}_1|^2 = |\vec{u}_{\parallel}|^2 \cos^2\varphi + |\vec{u}_{\perp}|^2 \sin^2\varphi,$$

$$|\vec{u}_2|^2 = |\vec{u}_{\parallel}|^2 \sin^2\varphi + |\vec{u}_{\perp}|^2 \cos^2\varphi,$$

therefore

$$|\vec{u}_1|^2 + |\vec{u}_2|^2 = |\vec{u}_{\parallel}|^2 + |\vec{u}_{\perp}|^2 \tag{4}$$

$$|\vec{u}_1|^2 - |\vec{u}_2|^2 = \left(|\vec{u}_{\parallel}|^2 - |\vec{u}_{\perp}|^2\right)\cos 2\varphi\,. \tag{5}$$

Suppose now that the left hand parts of both expressions are known from measurements. Right hand parts are functions of unknown parameters. Analytical form of these functions is given by formulas (2), (3). The orientation angle does not appear in equation (4). Further operations depend on availability and structure of a priori information. In the case when the burial depth is known (for example it has been measured), one can determine the cylinder radius from equation (4). Then the cylinder axis orientation is determined from equation (5).

Denote that carrying out the measuremens even with a single additional sounding frequency brings additional information that allows solving the problem without a priori data.

It is needed to note that for application of the presented algorithm an information about the electrical parameters of the ground is required. This information can be obtained from the digitalized maps or from the data of radar measurements.

REFERENCES

[1] Sukharevsky O.I., Muzychenko A.V., Sazonov A.Z. Asymptotic Solution of Problem of Electromagnetic Wave Scattering by Perfectly Conducting Cylindrical Object Embedded in a Dielectric Half-Space, *Radiofizika i Radioastronomiya*. – 2002. – Vol. 7, no 1 –pp. 28 – 36 (in Russian).

[2] Sukharevsky O.I., Zalevsky G.S. Muzychenko A.V. Frequency and Pulse Responses of Subsurface Objects, *Radiotekhnika*. – 2001. – no 6 – pp. 6 – 13 (in Russian).

APPLICATION OF WAVELET ANALYSIS FOR DETECTION OF CYLINDRICAL OBJECTS IN DIELECTRIC LAYER USING CHARACTERISTIC OF REFLECTION

M. V. Andreev, O. O. Drobakhin, D. Yu. Saltykov

Department of Radiophysics, Dniepropetrovsk National University
13 Nauchny pereulok, Dniepropetrovsk, 49050, Ukraine
E-mail: microwave@mail.dsu.dp.ua

ABSTRACT

The problem of detection and estimation of parameters of cylindrical objects in a dielectric layer using a reflection characteristic has been considered. A reflection characteristic for fixed frequency was obtained by scanning the interface of dielectric structure by measuring antenna probe. Use of the multiscale discrete wavelet analysis has allowed one to select the peculiarities of the reflection characteristic which have been caused by the presence of objects. Thus their localization on the background of noise have been completely successful. The approximating properties of different wavelet bases for the given class of physical data using different types of measuring probes at different frequencies and for different depth of object dispositions have been explored.

INTRODUCTION

At present the wavelet analysis has become the powerful mathematical instrument in many investigations [1-3]. In basic it is used for processing non-stationary or non-uniform signals of different types. Wavelets are capable to detect the difference in characteristics at different resolutions by scale change and to analyze the signal properties in different points of observation interval using translation. It determines preferability of wavelets using for the analysis of characteristics of reflection with local discontinuities containing the information on explored objects. Possibility of use of the wavelet analysis for detection of objects in dielectric layer using a reflection characteristic from explored structure has been considered in this paper.

BASIC CONCEPTION

The problem of detection and estimation of parameters of cylindrical objects in a dielectric layer using a reflection characteristic has been considered. The reflection characteristic at fixed frequency has been obtained by scanning the frontier interface of dielectric structure by measuring antenna probe. Pyramidal horn, H- and E- sectorial horns, open-ended waveguide have been used as measuring probe. The reflection characteristic has been measured by reflectometer. The sizes of cylindrical objects in the form of cylindrical holes in the dielectric layer were approximately equal to wavelength of radiation. The parameters of objects $\vec{p}$ (hole center locations and sizes) have been estimated using the data of intensity of reflected wave R_Σ as function of the cross coordinate x. For description of this dependence the expression has been used:

$$R_\Sigma(x,\vec{p}) = R_0 + \sum_{m=1}^{M} R(x,p_m), \qquad (1)$$

where $R(x,p_m)=\iint_D E(x,p_m,\xi,\zeta)d\xi\,d\zeta$ is integral from allocation of reflected field E from m-th object on the aperture D of measuring probe, p_m are parameters of m-th object and $\vec{p}=\{p_1,p_2,\ldots,p_M\}$. An experience of practical use has shown that for estimation of centers c_m and cross sizes (radiuses) r_m of cylindrical holes enough even of unrigorous model in next form

$$R(x,c_m,r_m)=\frac{a}{\pi}\left\{\mathrm{f}\left[\frac{\pi(x-c_m-r_m)}{a}\right]-\mathrm{f}\left[\frac{\pi(x-c_m+r_m)}{a}\right]\right\}, \qquad (2)$$

where a is cross size on the aperture of measuring probe along x, also function is used

$$\mathrm{f}(x)=\begin{cases}\sin x, & |x|\le\pi/2\\ x/|x|, & |x|>\pi/2\end{cases}. \qquad (3)$$

The experimentally obtained reflection characteristics $\mathbf{R}_\Sigma\subset V_0\in R^N$ have strong distortions (see fig. 1a and 2a), stipulated by the different reasons and having different character (low-frequency trend, high-frequency oscillations with separate pulsing outlets). They do not allow one to select the indicated reflections from objects (especially with small sizes) on background of noise.

As the peaks of reflections from objects $R(x,c_m,r_m)$ are well enough localized in x at intervals $[c_m-(r_m+a/2);\ c_m+(r_m+a/2)]$, for overcoming this problem the multiscale wavelet decomposition of the reflection characteristic has been used $\mathbf{R}_\Sigma=\mathbf{A}_J+\sum_{j=1}^{J}\mathbf{D}_j$, where $\mathbf{A}_j=\sum_{k=0}^{N_j-1}a_{j,k}\varphi_{j,k}$ and $\mathbf{D}_j=\sum_{k=0}^{N_j-1}d_{j,k}\psi_{j,k}$ are representations of coefficients of approximations $\mathbf{a}_j=\{a_{j,k}\}_{k=\overline{1,N_j}}$ and details $\mathbf{d}_j=\{d_{j,k}\}_{k=\overline{1,N_j}}$ in subspace of a signal V_0. $\{\varphi_{j,k}\}_{k=\overline{1,N_j}}$ and $\{\psi_{j,k}\}_{k=\overline{1,N_j}}$ are orthonormal wavelet basis for subspace of approximation $V_j\subset V_0$ and subspace of details $W_j\perp V_j$; N_j is the number of coefficients on j-th decomposition level; J is the number of decomposition levels. Thresholding (threshold zerofilling) of small coefficients of expansion $d_j<t_j$ in subspace of details W_j and complete zerofilling of coefficients of expansion in subspace of approximation V_J ($a_J=0$) has been used for the reconstruction of reflections from objects. The entropy approach has been used for a choice of the value of the threshold: $t_j=E(\mathbf{d}_j)/N_j$.

NUMERICAL AND EXPERIMENTAL RESULTS

The analysis has shown the greater efficiency of special form of entropy criteria. The entropy has been calculated in form of concentration of expansion coefficients in norm L_1: $E(\mathbf{d}_j)=\sum_{k=0}^{N_j-1}d_{j,k}$. The additional threshold zerofilling was used in reconstructed signal space for removing the negative values of reconstructed reflection characteristic.

The approximating properties of different wavelet bases for the given class of physical data have been explored. The influence of types of scaling and wavelet functions on quality of expansion is analyzed. For a solution of the problem considered, advantages of Daubechies wavelets of the seventh order and coiflets of the third order have been determined. The influence of measuring probe (pyramidal horn, H- and E- sectorial horns, open-ended waveguide), influence of measuring frequency and depth of position of cylindrical holes on obtained results has been explored additionally. As an example the results of use of developed technique for typical cases are presented. The reflection data of scanning at frequency 24 GHz by E-sectorial horn of two-layer dielectric structure are presented in fig. 1. The structure has contained continuous layer with thickness of 10 mm and layer with thickness of 5 mm with three holes of diameter 12 mm (hole 1), 3 mm (hole 2), 6 mm (hole 3) and distance 110 mm between them. The data of scanning on frequency 19.6 GHz by H-sectorial horn of three-layer dielectric structure are depicted in fig. 2. The indicated layer with holes has been disposed between two dielectric layers by width of 5 mm.

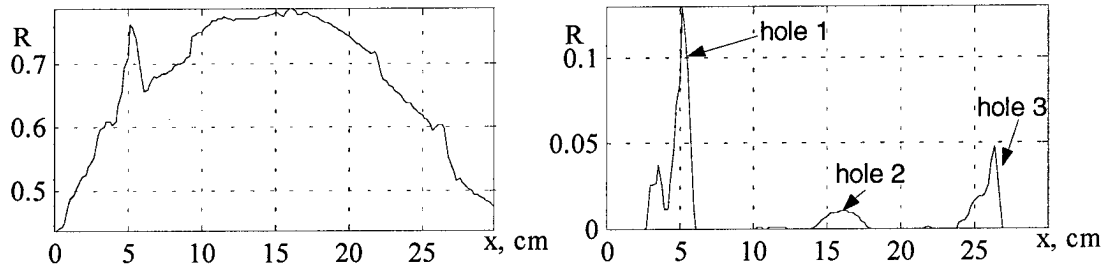


Fig. 1. Measured with using of E-sectorial horn (a) and reconstructed with using of Daubechies wavelet of 7 order (b) reflection characteristics

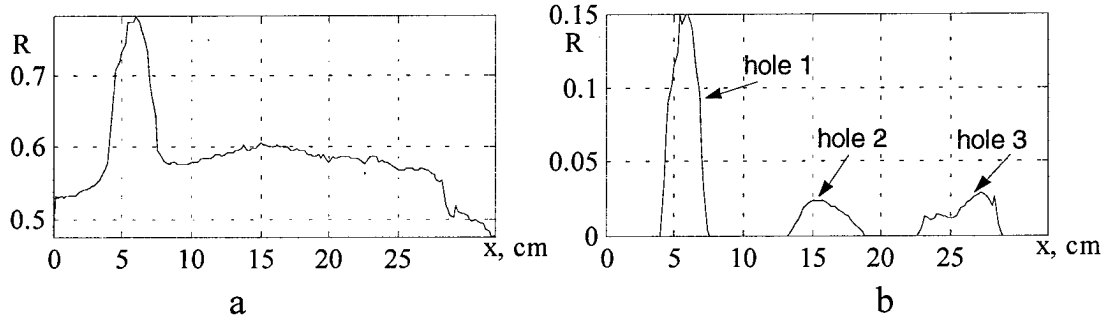


Fig. 2. Measured with using of H-sectorial horn (a) and reconstructed with using of coiflets of 3 order (b) reflection characteristics

REFERENCES

[1] Daubechies I., "The wavelet transform, time-frequency localization and signal analysis", *IEEE Trans. Inf. Theory*, 1990, vol. 36, pp. 961-1005.

[2] Wavelets and Their Application. Ed. R. Coifman. – Boston: Jones and Barlett Publ., 1992.

[3] Erlebacher G., Hussaini M. Y., Jameson L. M. Wavelets: Theory and Application. – New York: Oxford Univ. Press, 1996.

PARAMETERS OPTIMIZATION FOR SYNTHESIZING APERTURE METHOD AT PRACTICAL USE OF CONTINUOUS RADIATION UNDERGROUND RADAR

A.A. Palto
Institute of Applied Physics
National Academy of Sciences of Belarus, Minsk, Belarus
E-mail: palto@iaph.bas-net.by

ABSTRACT

A modification of the aperture synthesizing method aimed at improving resolution of the subsurface radar is proposed. The results of the data processing by this method are presented. The input data had been obtained with the use of a prototype of the step-frequency subsurface radar developed in the Institute of Applied Physics.

INTRODUCTION

The area of practical application of underground radar constantly extends during recent years. They are used for detection and classification of objects and structures of both artificial and natural origin that are located inside a dielectric medium (soil, rocky breeds, wall of building constructions etc.). The underground exploration is applied at evaluation of state of roads and railway cloth, search of the buried organic bodies, unexploded shells [1] and other ammunitions, localization of sewer pipes and underground utilities etc. [2]. Thus, the problem of determination of the sizes and form of hidden objects is doubtless actual. Many authors investigated the aperture synthesizing method to improve the radar resolution [3-4].

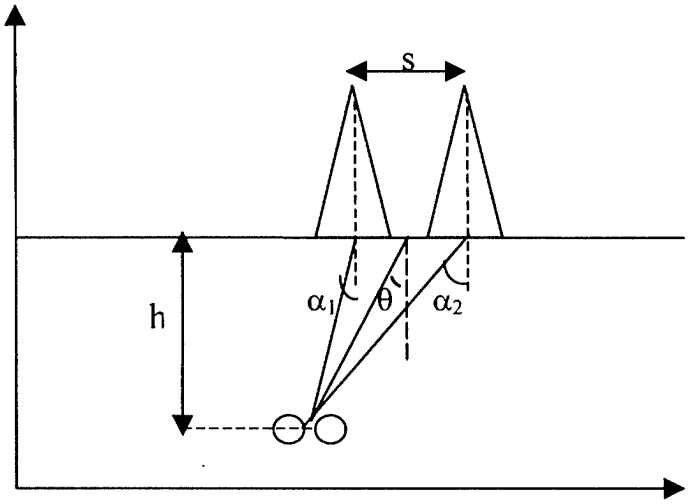


Fig. 1

The paper is devoted to the analysis and determination of optimal parameters of mathematical data processing obtained with use of the step-frequency underground radar, intended for detection of underground objects.

EXPERIMENT

The scheme of experiment is shown on Fig. 1. The radar includes receiving and transmitting horn antennas separated by 40 cm from each other. The scanning was carried out in steps of 10 cm along ground surface and across two pipes buried at a

depth of about 60 cm. The frequency range of 0.5 GHz to 1.4 GHz has been selected as a compromise between the penetration depth depending on conductivity and permittivity of the soil, and the resolution. The radar measures the reflection coefficient in the frequency band of operation for a number of points on the ground surface. Then the collected data with use of Fourier transform are converted into a time domain. Buried objects of different reflectivity produce peaks of corresponding amplitudes P that are delayed in accordance with their depths. Since the antenna radiation pattern $F(\alpha)$ has some width, the aperture synthesizing can be carried out using several nearest surface points, instead of whole route of scanning.

SYNTHESIZING

In the experiment the horn antennas had been used. Their radiation pattern as a function of angle α is determined by the expression [5]:

$$F(\alpha) = \cos(\alpha) * \frac{\cos(k * b/2 * \sin(\alpha))}{1 - (2 * c/\lambda * \sin(\alpha))^2}, \quad (1)$$

where c and b denote aperture dimensions, λ is wavelength in the ground, $k = 2\pi / \lambda$ - propagation constant. The expression for the pattern of the system from two antennas is as follows:

$$F(\theta) = F(\alpha_1) * F(\alpha_2), \quad (2)$$

where α_1, α_2 are angles between line to point of observation and normal to antennas A1 and A2. Let coordinates of the point are (x_i, y_j) and for aperture synthesizing t nearest points are used. Then synthetic aperture method proposed here is principally based on [4]:

$$Q(x_i, y_j) = \sum_{m=-t}^{t} D_m \cdot P(x_{i+m}, y_m), \quad (3)$$

where $y_m = \sqrt{(x_{i+m} - x_i)^2 + y_j^2}$ and D_m is a weighting function. Obviously, the amplitude of each response from the object illuminated at the angle α will be less in $F(\alpha)$ times. Then, the weighting function can be defined as:

$$D_m = 1 / F(\theta). \quad (4)$$

The equation (3) together with (4) allows taking into account the antenna radiation pattern and using the additional information from nearest responses.

RESULTS

The results of the data processing are shown in Fig. 2 and Fig. 3 that present obtained image without and with aperture synthesizing with optimal parameters, respectively. In the aperture synthesis only data from three nearest points had been utilized.

In Fig. 2 one can see that the two pipes are not resolved. Aperture synthesis allows observing two pipes as separated objects (Fig. 3). Thus, such choice of the aperture

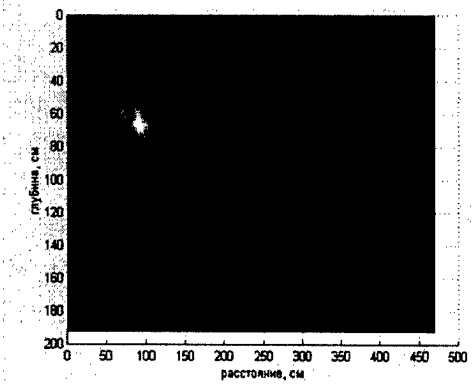


Fig.2

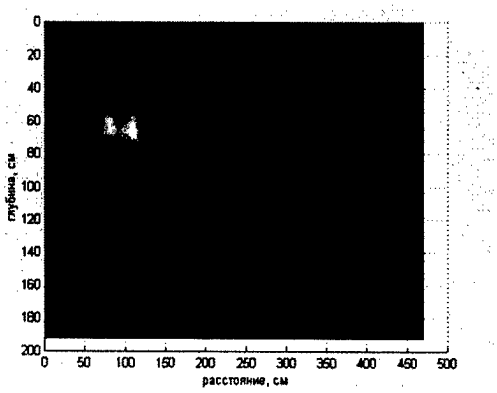


Fig.3

synthesizing parameters allows resolving near objects. Parameters of synthesis can be determined from conditions of practical use of the radar in a particular application. So, insufficient number of points used for synthesizing leads to restricted quality of image. Too large number of points just adds a noise. For the given antennas and soil the optimal synthesizing implies use of three nearest points before and three after the central point.

The proposed method can be applied for any type of radars. So, for pulsed radar the received echo should be merely substituted into (3) as P. For other type of antennas an expression (1) will change. Separation of antennas is taken into account by angles α_1 and α_2 in the formula (2).

REFERENCES

[1] Jacqueline M.Bourgeois, Glenn S.Smith "A complete Electromagnetic Simulation of the Separated-Aperture Sensor for Detecting Buried Land Mines" IEEE Transactions On Antennas and Propagation, Vol.46, No.10 October 1998.

[2] Leon Peters Jr., Jeffrey J.Daniels, Jonathan D. Young "Ground Penetrating Radar as a Subsurface Environmental Sensing Tool". Proceedings of the IEEE, Vol.82, NO.12, December 1994.

[3] Kovalenko.V.O., Masalov.S.A. "Modification of the aperture synthesizing method for underground sounding data processing" Ultra-Wideband, Short-Pulse Electromagnetics 4,Edited by Heyman et al., Kluwer Academic/Plenum Publishers, New York, 1999.

[4]Arai I., Suzuki T. "Experimental Results on Subsurface Radar with Improved Resolution" Journal of Electromagnetic Waves and Applications, vol.7, No.11, 1479-1495, 1993.

[5] D.M. Sazonov "Antennas and UHF-devises". Moscow, 1988. (in Russian)

WIRE AND WAVEGUIDE ANTENNAS

CURVED-WIRE ANTENNAS SOLUTION TECHNIQUE

Mikhail B. Protsenko

Sevastopol National Technical University
Studgorodok, Sevastopol-99053, Ukraine
E-mail: sevgtu@stel.sebastopol.ua

ABSTRACT

The algorithm and analysis program for spiral antennas with using of curvilinear segmentation are developed on the basis of generalized induced EMF Method (Galerkin's method) in conformity with Harrington equation. Comparison with well-known results is carried out.

INTRODUCTION

Recently, more and more attention is gave to the antenna systems consisting of any type of curvilinear radiators, particularly spiral form radiators. Because of large diversity of such radiators the development of suitable numerical analysis algorithms is actual. Such algorithms are the basis to solve the problems of antenna optimization and constructive synthesis.

Today, there are many algorithms for thin-wire antenna numerical analysis (e,g,., [1]-[4]) used for designing of antenna-feeder devices. Such mathematical models, as a rule, are directed to calculation of radiators with divers configuration approximated by linear segments [1,2]. The choice of linear segments is stipulated for presence of corresponding analytic expressions, to a greater extent. However, there are problems related to attainment of acceptable tolerance, computational stability and computational burdens. Given problems substantially reduces efficiency of numerical investigations of curvilinear radiators. Therefore it is advisable to approximate radiator by the curvilinear segments. It is allow to obtain more accurate results on the one hand and to reduce the segment number of curvilinear radiator on the other.

In the paper the technique of Harrington equation solving used Galerkin's method is presented. The curvilinear segments are used for the analysis of spiral antennas.

GENERAL FORMULATION

The integro-differential Harrington equation [3] governing the electric current on general three-dimensional curved wires was applied. The wire is assumed to be a perfect electrical conductor and to be thin, which means that the radius is must smaller than the wavelength and the length of wire. Under these thin-wire conditions, the current is taken to be axially directed, circumferentially invariant. The equation governing the total axial current $I(s)\cdot\vec{s}$ on the thin curved wire is

$$-j30k\int_S I(s')\cdot\vec{s}'\cdot\vec{s}\cdot G(s,s')+\frac{dI(s')}{ds'}\cdot\frac{dG(s,s')}{ds}ds'=-E(s),$$
$$s,s'\in S, \qquad (1)$$

in which S is the wire axis contour, s denotes the arc displacement along S from a reference to a point on the wire axis, $\vec{s}$ is the unit vector tangent to S at this point, and k is the free space wave number. $G(s,s')$ is the kernel or Green's function

$$G(s,s')=\frac{1}{2\pi}\int_{-\pi}^{\pi}\frac{\exp(-jkR)}{R}\cdot d\phi', \qquad (2)$$

in which R is the distance between the source and observation point on the wire surface and $E(s)$ is the incident electric field, which illuminates the wire, evaluated in Eq.1 on the wire surface at arc displacement s.
The generalized induced EMF Method (Galerkin's method) was used to solve the Eq.1. It is equivalent to the method of moments with sinusoidal basis and weight functions.

CALCULATION ALGORITHM OF CURRENT DISTRIBUTION FUNCTION FOR SPIRAL ANTENNAS

1. Spiral antenna geometry assignment.
1.1 Assignment of parametric dependencies, describing the spiral arms geometry in Cartesian coordinate system.
1.2 Partial derivation of length element coordinates with given parameter and calculation of radiator lengths.
2.1 Calculation of number of segments for each radiator.
2.2 Calculation of parametric angles corresponding to segment connection points.
3 Redefinition of parametric dependencies, describing the cross segments geometry in Cartesian coordinate system.
3.1 Calculation of number of dipole segments along the radiator.
3.2 Redefinition of parametric angles corresponding to the ends of lower and upper arms of the dipole segments.
3.3 Redefinition of parametric dependencies to define the geometry of lower and upper arms of the dipole segments.
3.4 Derivation of length element coordinates and current length of lower and upper arms of the dipole segments with respect to given parameter.
3.5 Approximation of dipole segments current distribution and its derivation with length of dipole segment arms.
4 Integral and matrix equations compiling.
4.1 Calculation of distance between the observation and integration points and also increment calculation depending on parametric angle in observation point.
4.2 Calculation of Green's function and its increment depending on distance between the observation and integration points.
4.3 Calculation of scalar product of the unit tangential vectors in the observation and integration points.
4.4 Calculation of tangential component of radiation field in observation point.
4.5 Calculation of matrix of proper and mutual radiation impedance of dipole segments.
5 Assignment of column-matrix with exciting EMF, which are defined with the given incident electric field distribution $E(s)$. Equations system solution with respect to complex current amplitude of segments.

6 Recovery of distribution current dependence along the curvilinear wire radiator and antenna radiation characteristics calculation.

RESULTS

The program package for spiral antenna numerical analysis is developed on the basis of presented technique. The programs are made on MathCAD package and Borland Delphi. The only subprograms describing the parametric dependencies of radiators Cartesian coordinates are changed for antennas with divers configurations.

Calculation of input impedance of helix antenna located on flat reflector was carried out. The helix has the dimensions: circumference of helical cylinder equals the wavelength, pitch angle 12.5^{o}.

Fig.1 shows the configuration of balanced helical antenna and the change in the input impedance with increase in the number of turns. Here, there are the similar results presented for helical antenna input impedance computed in [4].

REFERENCES

[1] T. J. Cui and W. C. Chew "Accurate Model of Arbitrary Wire Antennas in Free Space, Above or Inside Ground", *IEEE Trans. Antennas and Propagation,* vol.48, №4, Apr, pp. 482 – 493, 2000.

[2] S. D. Rogers and C. M. Butler "An Efficient Curved-Wire Integral Equation Solution Technique", *IEEE Trans. Antennas and Propagation,* vol.49,№1, Jan, pp. 70 – 79, 2001.

[3] R.F. Harrington, *Field Computation by Moment Methods,* Malabar, FL: Krieger, 1968.

[4] Nakano H. *Helical and Spiral Antennas: A Numerical Approach,* Letchworth; New York etc. Rec. Stud. Press. John Wiley and Sons, 1987.

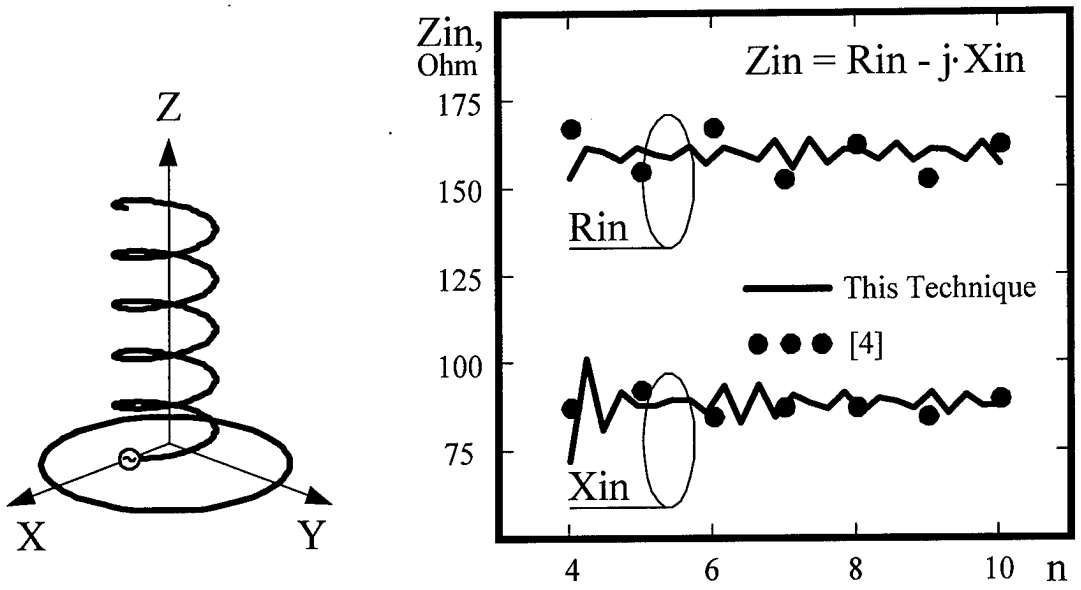


Fig. 1 Configuration of balanced helical antenna and its input impedance

THE PROPERTIES OF THE FRACTAL WIRE ANTENNAS

L. M. Karpukov, V.M. Onufrienko, S. N. Romanenko

Zaporizhzhya National Technical University
Zhukovsky str., 64, Zaporizhzhya, 69063, Ukraine
Phone: 8 (0612) 646575, E-mail: onufr@zstu.edu.ua

ABSTRACT

The results of modelling of wire antenna with fractal configuration of radiating elements are presented. For analysis the fractional differintegration calculus is used. Antenna diagrams depending on index of fractality of consisting vibrators are compared.

INTRODUCTION

The necessity of perfection of mobil communication makes it actual designing and studying of properties of nonsymmetrical antennas with very little electrical length of vertical parts of vibrators. It is interesting to use inhomogenious artificial mediums with vertical and inclined vibrator elements placed near to each other and weakly radiate because of odd currents. Antennas with such properties my be realised on the base of designing of fractal radiating elements.

As a result of covering of fractal part of vibrator by regular compacts the problem of analysis is reduced to construction of the Housdorff's smoothing measure on the physically prefractal layer with differintegration of equilibrational current density over the projection of fractal set on smooth segment.

Proceeding from the fractal representations about the current structure in a conductor and the field induced in an artificial metal-dielectric medium, using of the concept of fractional differintegration calculus the proved fact [1] is used in this paper that the behaviour of the field component u(r) in the medium with fractal properties of conductivity, permittivity etc. may be described by fractional integrodifferential (α-characteristic):

$$u^{(\alpha)}(r)={}_aI_r^{\alpha}({}_aD_r^{\alpha}u^{(\alpha)})(r)=\frac{1}{\Gamma(\alpha)}\int_a^r\frac{({}_aD_{r'}^{\alpha}u^{(\alpha)})(r')}{(r-r')^{1-\alpha}}dr' \ , \qquad (1)$$

where $\Gamma(\alpha)$ - Euler's gamma-function, $0<\alpha<1$ - scaling index, $({}_aD_r^{\alpha}u^{(\alpha)})(r)$ - satisfies the Helmholz equation with corresponding boundary conditions.

MAIN PART

The basis of the analysis of the fractal element of wire vibrator is the assumption that α-characteristic of a current has a direction along the axis of cylinder and is symmetrical in azimuth. This allows consideration the average fractal distributions of current only along the axis of conductor and the description of ideal fractal conductivity may be accomplished by introducing the constant scaling index α. In this case the edge effects are taken into account because α-characteristic of the field on the butt-end of a vibrator corresponds to the exponential behaviour of the field near the edge. Such behaviour corresponds to the model of so-called 2^{α}-fields [2].

Using the solution of the Maxwell's equations in the view of α-potential for conducting cylinder of length L and radius a, the approximation of the longitudinal component of vector potential may be received:

$$A_z^{(\alpha)}(z) = \int_{-L/2}^{L/2} I^{(\alpha)}(z')G(r)d^{\alpha}z', \tag{2}$$

where $r = \sqrt{a^2 + (z-z')^2}$, G(r) – free space Green's function, $d^{\alpha}z' = \delta^{\alpha}(z-z')dz'$ - differintegrational element of length, α-dimensional Dirac function

$$\delta^{\alpha}(z-z') = \frac{1}{\Gamma(\alpha)}\frac{1}{(z-z')^{1-\alpha}}. \tag{3}$$

Here α - scaling index.

Taking into account the relationship of $A_z^{(\alpha)}(z)$ with α-characteristic of the electric field component $E_z^{(\alpha)}$, the Pocklingtone integral equation may be derived

$$-j\omega\varepsilon E_z^{(\alpha)}(z) = \frac{1}{\Gamma(\alpha)}\int_{-L/2}^{L/2} I^{(\alpha)}(z')\left(\frac{\partial^2}{\partial z^2} + k^2\right)G(r)\frac{dz'}{(z-z')^{1-\alpha}}, \tag{4}$$

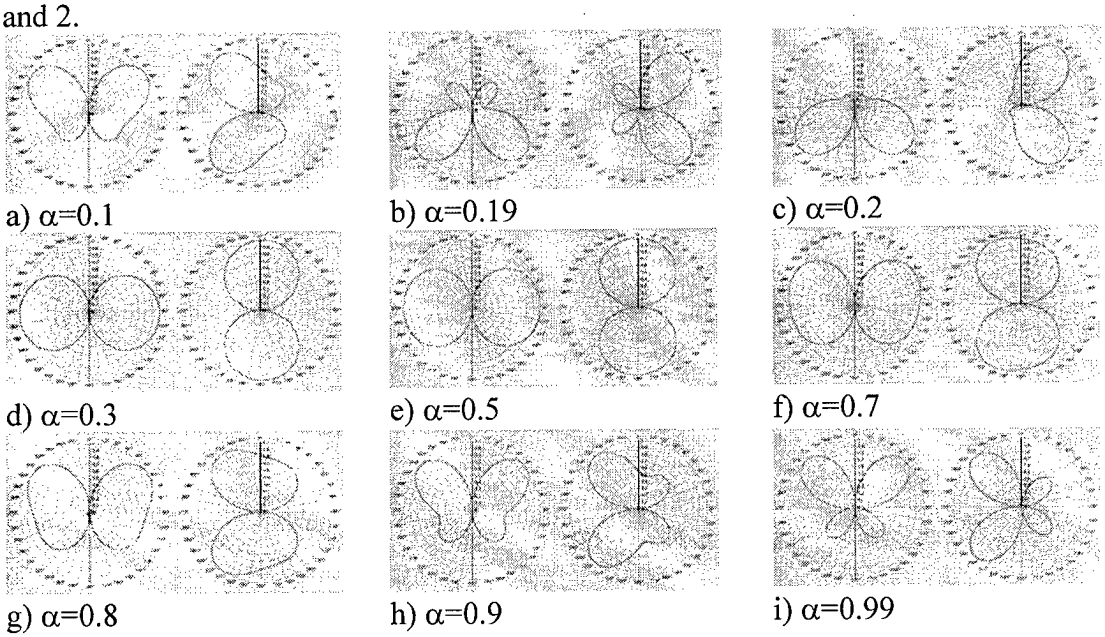
which is analogous to the Abel integral equation.

As a result, α-characteristics of longitudinal $E_z^{(\alpha)}$ and radial $E_\rho^{(\alpha)}$ components of the electric field of fractal vibrator may be obtained in the view:

$$E_z^{(\alpha)}(z) = \frac{I_0}{j\omega\varepsilon\Gamma(\alpha)}\int_{-L/2}^{L/2}\left(\frac{\partial^2}{\partial z^2} + k^2\right)G(r)\frac{dz'}{(z-z')^{1-\alpha}}, \tag{5}$$

$$E_\rho^{(\alpha)}(z) = \frac{I_0}{j\omega\varepsilon\Gamma(\alpha)}\int_{-L/2}^{L/2}\frac{\partial^2 G(r)}{\partial z^2}\frac{dz'}{(z-z')^{1-\alpha}}. \tag{6}$$

Some results of modelling [3] of the fractal wire antennas are shown below in figures 1 and 2.

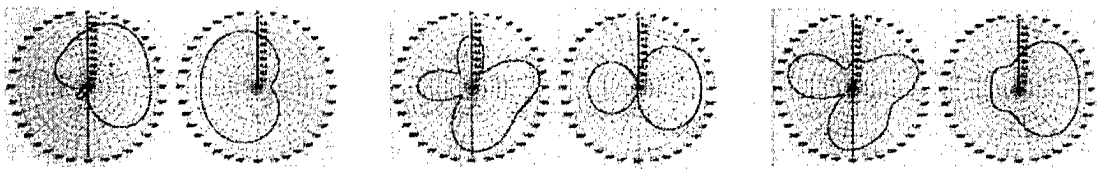


a) α=0.1 b) α=0.19 c) α=0.2

d) α=0.3 e) α=0.5 f) α=0.7

g) α=0.8 h) α=0.9 i) α=0.99

Figure 1. Changing of the far-field pattern for λ/2 fractal vibrator.



a) α=0.1 b) α=0.3 c) α=0.9

Figure 2. Changing of the far-field pattern of the corner-fed square loop fractal antenna.

Figure 1 demonstrates how the far-field pattern of the $\lambda/2$-vibrator is changed in the process of variation of the scaling index α, and figure 2 shows the same for the corner-fed square loop fractal antenna.

CONCLUSIONS

Presented results show that variation of the scaling index α allow changing the far-field pattern of the fractal wire antennas in very wide limits. Theoretical results are comparable with experimental [4].

REFERENCES

[1] Onufrienko V. M. "Physical and Geometric Interpretation of Electromagnetic Field's α-Characteristics", *Telecommunications and Radio Engineering*, Vol.53, №4-5, 1999, pp.136-139.

[2] Engheta N. "On Fractional Calculus and Fractional Multipoles in Electromagnetism", *IEEE Trans. On Antenna and Prop.*, 44, 4, 1996, pp.554-566.

[3] Romanenko S., Karpukov L., Pulov R. "Wire Antenna Computer Modelling System", Proceedings of the International Conference TCSET'2002, Lviv-Slavsko, 2002, pp.155-157.

[4] John P. Gianvittirio and Yahya Rahmat-Samii, "Fractal Antennas: A Novel Antenna Miniaturization Technique, and Applications", *IEEE Antennas and Propagation Magazine*, 44, 1, February 2002, pp. 20-36.

RADIATION RESISTANCE OF AN ELECTRIC DIPOLE HAVING DIFFERENT ORIENTATIONS WHEN CHANGING THE POSITION OF A PLANE SCREEN

Nadezhda P.Yeliseyeva, Nikolay N. Gorobets

V. Karazin National University of Kharkov, 4 Svobody Sq., Kharkov, 61077, Ukraine,
Email: Nadezhda.P.Yeliseyeva @ univer. kharkov. ua

ABSTRACT

3-D radiation problem solution in a far zone of an ideally conducting rectangular plane screen excited by an arbitrarily oriented electric dipole when changing the position of a screen has been obtained by the uniform geometrical theory of diffraction method. Numerical comparative analysis of the radiation resistance of an dipole having different orientations depending on the screen displacement is carried out.

INTRODUCTION

The asymptotic solution of the 3-D diffraction problem of radiation of an arbitrarily oriented electric dipole from an ideally conducting infinitely thin rectangular screen in the far field zone was obtained in paper [1] using the uniform geometrical diffraction theory (UGTD) method. On the base of the algorithms developed for solving such problems in the case, when the dipole was placed above the screen midpoint, the radiation resistance **R** of the screen-and-dipole system was calculated and analyzed in [2] depending on the dipole orientation, its distance from the screen, and the screen dimensions. Now the algorithms and computer codes for calculation of the dependencies **R** on the varying the screen position were worked out.

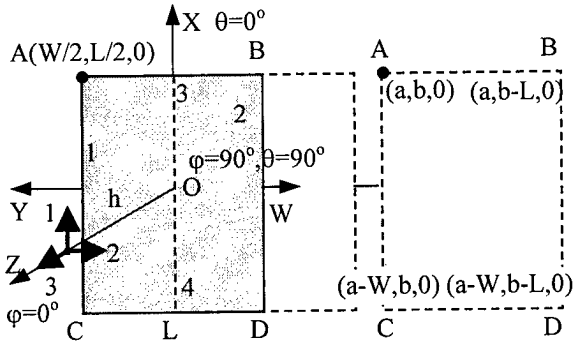


Figure 1

STATEMENT OF THE PROBLEM

In the rectangular co-ordinate system XYZ (Figure1) the electric dipole location is indicated by the co-ordinates (0,0,**h**), the metallic infinitely thin rectangular screen ABCD with its sizes **L** and **W** is situated in the XY - plane being defined by the co-ordinates of the apex **A(a,b,0)**. Consider three cases of the dipole orientation: dipoles 1,2,3, oriented along the X,Y,Z-axes. For each of the dipoles the full radiation field is determined as the sum of geometrical optics (GO) fields and the fields of the waves excited by GO field on each of the four screen edges.The GO field light-and-shadow boundaries are defined on an infinitely distant observation sphere by equations of the curvilinear quadrangle, whose sides, in the θ, φ spherical co-ordinate system (Figure1) are the arcs of circles. According to the GTD postulates, the edge waves terminate in space at the light-and-shadow boundary surfaces in the Keller form cones due to the finite screen dimensions. The cones are formed by the extreme GO rays passing through the screen corner points A,B,C,D. The congruences of the AC and BD edge waves terminate at the surfaces of shadow cones with cone angles

$$\beta_{1A} = \arctan|(h^2+b^2)^{1/2}/a|, \qquad \beta_{1C} = \arctan|(h^2+b^2)^{1/2}/(a-W)|, \tag{1}$$
$$\beta_{2B} = \arctan|(h^2+(b-L)^2)^{1/2}/a|, \quad \beta_{2D} = \arctan|(h^2+(b-L)^2)^{1/2}/(a-W)|$$

and those of AB and CD edge waves terminate at shadow cones with cone angles

$$\beta_{3A} = \arctan|(h^2+a^2)^{1/2}/b|, \quad \beta_{3B} = \arctan|(h^2+a^2)^{1/2}/(b-L)|, \quad (2)$$
$$\beta_{4C} = \arctan|(h^2+(a-W)^2)^{1/2}/b|, \quad \beta_{4D} = \arctan|(h^2+(a-W)^2)^{1/2}/(b-L)|.$$

The equations of the lines of intersection of the shadow cones of the AB and CD edge waves with the observation sphere are the equations of circles

$$\theta_{3A,B}=\arctan(\sin\varphi(\tan^2\beta_{3A,B} - \cot an^2\varphi))^{-1}, \ \theta_{4C,D}=\arctan(\sin\varphi(\tan^2\beta_{4C,D} - \cot an^2\varphi))^{-1} \quad (3),$$

the equations of circles for the AC and BD edge waves are

$$\theta_{1A} = \beta_{1A}, \ \theta_{1C} = \beta_{1C}, \ \theta_{2B} = \beta_{2B}, \ \theta_{2D} = \beta_{2D}. \quad (4)$$

One can see from (1) - (4) that the boundary angles θ_b, φ_b, at which the edge waves give the contribution to the far field, are varying when changing the position of the screen. We defined the light-and-shadow regions of GO and edge waves for three characteristic cases of the screen position on the Y-axes: **b > L** - the dipole is located to the right of the screen, **b < 0** - the dipole is located to the left of the screen, **b = L...0** - the dipole is located above the screen, the co-ordinate $\mathbf{x_A}$ being in the interval **a = 0 ... W**, $\mathbf{z_A = 0}$.

The total radiation resistance **R** is calculated through the mean radiated power of the antenna as **R =AI**, where $I_\Sigma = \int_0^{2\pi} d\varphi \int_0^{\pi} f^2(\theta,\varphi)\sin\theta d\theta$, $f^2(\theta,\varphi)= |f_\theta(\theta,\varphi)|^2+|f_\varphi(\theta,\varphi)|^2$.

$A=30\pi(l/\lambda)^2$ is the numerical factor proportional to the dipole electric length, l/λ; $f_\theta(\theta,\varphi)$, $f_\varphi(\theta,\varphi)$ - the directive patterns of the antenna. To study the physical peculiarities of the radiation resistance formation on depending of the dipole orientation we are calculated separately the radiation resistance of the GO field $\mathbf{R}_{go}$, the ones of the edge waves fields at the lateral (1,2) $\mathbf{R}_{lat}$ and at the transversal (3,4) $\mathbf{R}_{tr}$ screen edges too.

NUMERICAL RESULTS

The dependencies of the radiation resistance of the dipole having different orientations on the varying co-ordinates of the screen apex **A(a,b,0)** have been investigated. Some dependencies of the normalised radiation resistance on **b/** are shown in Fig.2 when the dipole is placed at **h=0.25** : the separate radiation resistance $\mathbf{R}_{go}$(a), $\mathbf{R}_{lat}$ (b), $\mathbf{R}_{tr}$ (c) under exciting the screen with its sizes **L=3** , **W=3** and **a=1.5** by the dipoles 1,2,3; the total radiation resistance $\mathbf{R}_1$, $\mathbf{R}_2$, $\mathbf{R}_3$ of the dipole 1(d),2(e),3(e) exciting the same screen under different co-ordinate **a**; the total radiation resistance **R** under **a=0.5** (f), when the screen dimensions are equal to **L=3** , **W= ; 3** . Here the curves 1,2,3 are determined by the **R** of the dipoles 1,2,3 respectively under **W=** ; the curves 4,5,6 are determined by the **R** for the same dipoles respectively under **W=3** . The dipole is located above the screen when **b/** are changing from **0** to **3** , being out of this interval the dipole is located by the side of the screen. The **R** values of the curves 1, 2, 4, 5 are near to **R =9.647A**, the **R** of the curves 3, 6 exceed **R =11.363A**(**R** , **R** are the radiation resistance of the dipole, with an infinite screen). From the analyses of the dependencies **R** on **b/** for the screens with different **L** and **W** (f), it follows that in the case when the dipole is oriented perpendicular to the screen and placed above the screen, the **R** values are higher for the smaller **W** values (3); when the dipole is placed by side of the screen, the curve of the **R** (3) falls steeper with regard to $\mathbf{R}_o$**=8.37A** of a dipole in free space under the smaller **W** values.

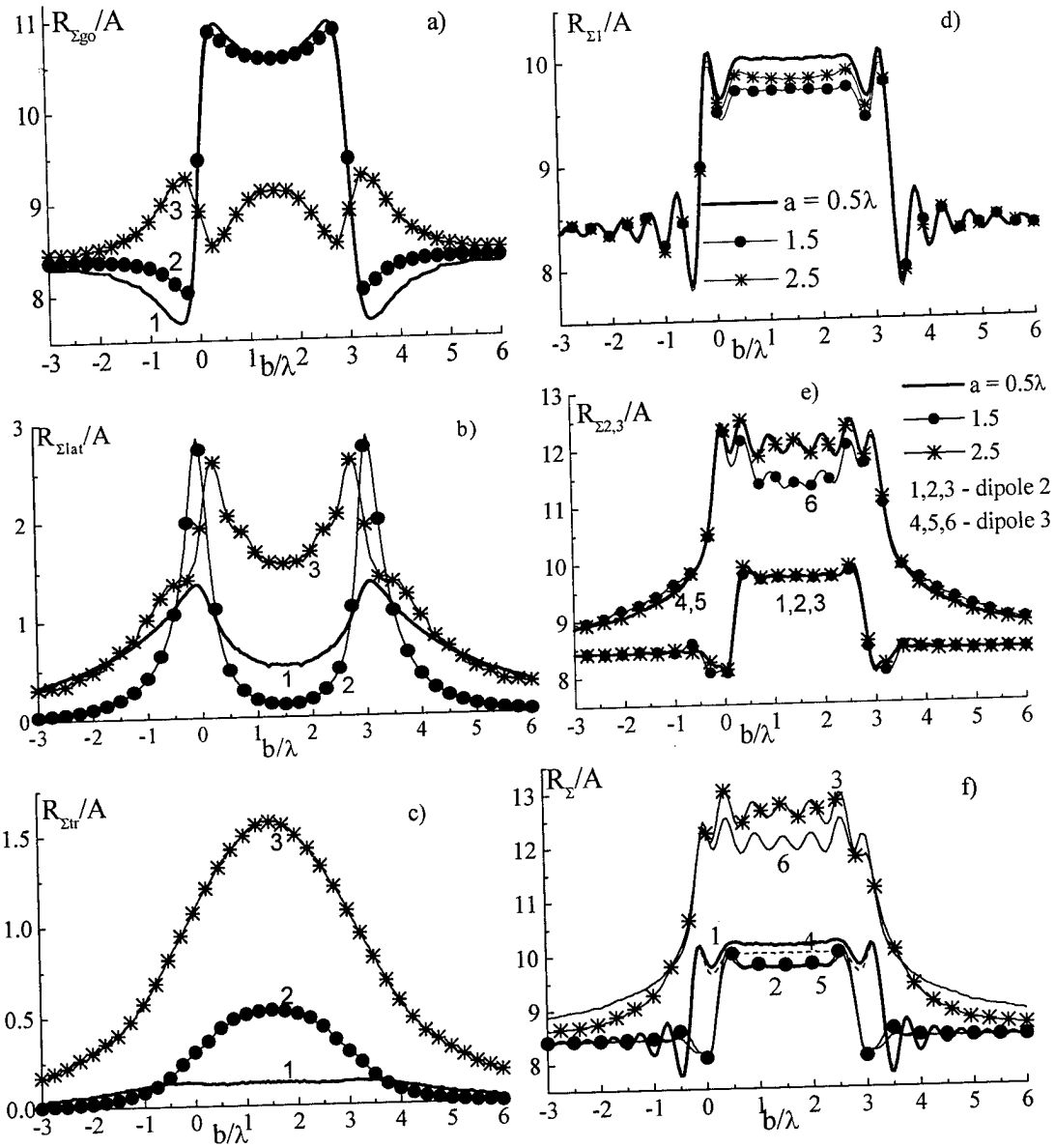


Figure 2

CONCLUSIONS

Using the uniform geometric diffraction theory method, algorithms and computer codes for calculating the radiation field intensity of the electric dipole in presence of infinitely thin perfectly conducting rectangular screen arbitrarily placed and oriented in space have been worked out. On this base, the radiation resistance of the screen-and-dipole radiating system are computed and analyzed in relation to the dipole orientation and the screen dimensions when changing the position of the plane screen.

REFERENCES

[1].Yeliseyeva N.P. Pattern Analysis of an Arbitrarily Oriented Oscillator Placed above a Flat Screen // Telecommunications and Radio Engineering . - 1999.- Vol. 53, № 1. - P. 43-53.

[2].Yeliseyeva N.P. Radiation Resistance of an Electric Dipole Oriented Arbitrarily above a Plane Screen // Telecommunications and Radio Engineering .- 1997.- Vol. 51 (2-3). - P. 195-201.

ANALYSIS OF VERTICAL WIRE ANTENNA ABOVE IMPERFECT GROUND USING DISCRETE COMPLEX IMAGE METHOD

Mohammad Hakkak [*,**], Bijan Abbasi Arand [*,**]
[*] Tarbiat Modarres University, P.O.B. 14115-143, Tehran, Iran
[**] Iran Telecom Research Center (ITRC), P.O.B.14399, Tehran, Iran

m.hakkak@itrc.ac.ir abbasib@modares.ac.ir

ABSTRACT

A simple and almost exact image method is proposed for the analysis of vertical thin-wire antennas above lossy ground. This method is based on the replacement of the lossy half-space by a few complex images. The GPOF technique and Sommerfeld integral equation are used to find the location and intensity of the current images. Similar to dipole sources, a few proper image line sources are obtained for an original line source. The results obtained for the radiation pattern of this equivalent structure are found to practically coincide with the exact results (i.e. those obtained from the Sommerfeld theory). Compared to other methods of solution, this method is conceptually much simpler and requires less computing time

THEORETICAL BACKGROUND

The geometry of the vertical wire antenna of length L, located at a height h above an imperfect conducting half-space as shown in Fig. 1.
According to the thin-wire approximation and Sommerfeld theory [1, 2], the z-component of the radiated electric field can be expressed as

$$E_Z = \frac{1}{j4\pi\omega\varepsilon_0}\int_L [\frac{\partial^2}{\partial z^2} + k_0^2][g_0(z,z') + \frac{n^2-1}{n^2+1}g_1(z,z') + \frac{2n^2}{n^2+1}U_2]\times I(z')d(z') \qquad (1)$$

Where $I(z')$ is current distribution along the antenna, $g_0(z,z')$ denotes the free-space Green function of the form

$$g_0(z,z') = \frac{e^{-jk_0R_1}}{R_1} \qquad (2)$$

While $g_1(z,z')$ follows from image theory:

$$g_1(z,z') = \frac{e^{-jk_0R_2}}{R_2} \qquad (3)$$

In which k_0 and k_1 are the phase constant of free space and lossy ground, respectively, and R_1 and R_2 are the distances from the antenna and from its image to the observation point. The medium of lower half-space is taken to be lossy ground characterized by

$(n^2\varepsilon_0, \mu_0)$, with $n^2 = \varepsilon_r - j\sigma/\omega\varepsilon_0$, where ε_r is the relative dielectric constant, and σ is the conductivity of the medium. Sommerfeld integral U_2 is defined as follows:

$$U_2 = k_0 \int_0^\infty \frac{1}{u_0} \frac{u_0 - u_1}{n^2 u_0 + u_1} e^{-k_0 u_0 (z+h)} J_0(k_0 \lambda \rho) \lambda d\lambda \tag{4}$$

Where $u_0 = \sqrt{\lambda^2 - 1}$, $u_1 = \sqrt{\lambda^2 - n^2}$, $\rho = [(x-x')^2 + (y-y')^2]^{1/2}$, $J_0(k_0\lambda\rho)$ is a zero-order Bessel function, while h is the distance from the interface to the antenna.

NUMERICAL EVALUATION

The integrand in the Sommerfeld integral U_2 is a weakly damped quasioscillatory complex function, which greatly complicates accurate numerical evaluation of the integral and makes it quite lengthy. By using the DCIM [2] method and GPOF [5] technique, the $(u_0 - u_1)/(n^2 u_0 + u_1)$ term in U_2 can be approximated by

$$\frac{u_0 - u_1}{n^2 u_0 + u_1} = \sum_{i=1}^{N} a_i e^{b_i u_0} \tag{5}$$

Therefore U_2 becomes

$$U_2 = \sum_{i=1}^{N} a_i \frac{e^{-jk_0 r_i}}{r_i} \tag{6}$$

Where $r_i = \sqrt{(\rho^2 + (z + h - b_i/k_0)^2}$, $z \geq 0$

Based on the above complex images and superposition principle, the dipole images are extended to wire line sources. Therefore the equivalent image line sources can be defined by

$$I_1(z') = \frac{n^2 - 1}{n^2 + 1} I_0(z') \qquad -(h+l) \leq z' \leq -h \qquad \text{Quasistatic image} \tag{7}$$

$$I_i(z') = \frac{2n^2}{n^2 + 1} a_i I_0(z') \qquad -(h+l) + \frac{b_i}{k_0} \leq z' \leq -h + \frac{b_i}{k_0} \quad \text{i=2,..., N Complex images} \tag{8}$$

a_i , b_i, and N are determined from the GPOF technique and required accuracy.

NUMERICAL RESULTS

Considering the original source and N discrete images, we have $N+1$ element collinear arrays. Therefore, the radiated electric field is obtained as

$$E_\theta = j\omega\mu \frac{e^{-jk_0 r}}{4\pi r} \{\sin\theta \int_{-1/2}^{1/2} i(z') e^{jk_0 z' \cos\theta} dz'\} . \{\sum_{n=0}^{N+1} I_n e^{jk_0 z_n \cos\theta}\} \tag{9}$$

The current distribution of vertical wire antenna is assumed sinusoidal and can be written as

$$I_0(z') = I_0 \sin[k_0(\frac{l}{2} - |z|)] \qquad h \le z \le h + l \tag{10}$$

The radiation electric fields of this line source above lossy ground and also above perfect electric conductor are computed and shown in Fig. 2.

CONCLUSION

The DCIM with proper number of images is practically as accurate as the exact Sommerfeld-based method for analysis of vertical wire antenna. However, it is much simpler and significantly faster. The radiation pattern of wire can be considered as exact for all regions.

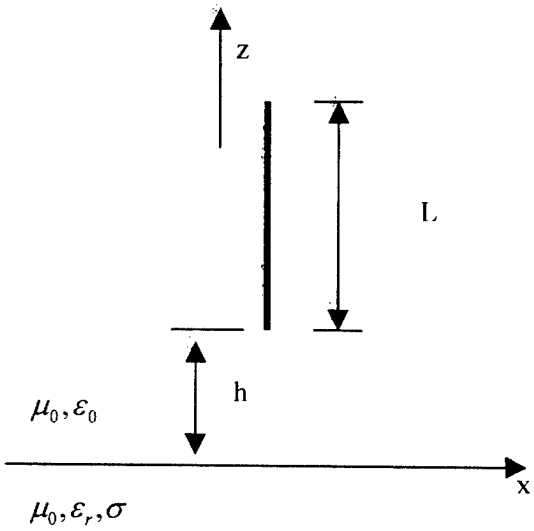


Fig.1 Vertical wire antenna over imperfect conducting half-space

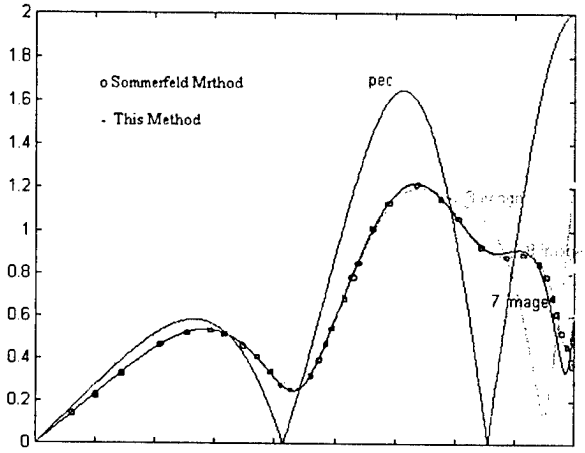


Fig. 2 Radiated electric field of half-wave dipole above ground with $\varepsilon_{r=10}$ and $\sigma = 10ms/m$

REFERENCES

[1] BANOS, A: Dipole radiation in the presence of a conducting half-space, Pergamon, New York, 1966.

[2] YANG, J. J., CHOW, Y.L., and FANG, D. G.: "Discrete complex images of a three-dimensional dipole above and within a lossy ground," IEE PROCEEDINGS-H, Vol.138, No.4, 1991.

[3] Y. L. Chow, J. J. Yang, D. G. Fang, and, G. E. Howard " A Closed Form Spatial Green's Function for the Thick Microstrip Substrate," IEEE Trans. MTT, Vol 39, No.3,pp. 588-592, Mar. 1991.

[4] T. K. SARKAR and O. PEREIRA "Using the Matrix Pencil Method to Estimate the Parameters of a Sum of Complex Exponentials," IEEE AP Magazine, Vol.37, No.1, pp.48-55, Feb.1995.

[5] Y. HUE and T. K. SARKAR, "Generalized Pencil-Of–Function Method for Extracting Poles of an EM System from Its Transient Response," IEEE Trans. AP ,Vol.37,pp.229-234, Feb.1989

RADIATION FROM A PLANAR WAVEGUIDE WITH SYMMETRICAL FLANGE

Sergei G. Vashtalov

Department of Radiophysics, Tomsk State University,
36, Lenin Ave, Tomsk, 634050, Russia
E-mail: vsg@elefot.tsu.ru

ABSTRACT

The problem of radiation from a planar waveguide with symmetrical flange is studied. This is one of the model problems of the diffraction theory. The method of partial regions is used. In the first and second subregions the fields are presented in terms of Fourier integrals, and in the third subregion – in terms of Sommerfeld-Maliuzhinets integral. After binding the fields on common subregion boundaries, the calculation reduces to the set of inhomogenious functional Maliuzhinets equations, which are solved by Tuzhilin S-integrals. This allows for the initial problem to be formulated as the infinite set of algebraic linear equations relative to transformation coefficients of waveguide waves

PROBLEM FORMULATION AND METHOD OF SOLUTION

One of the model problem of diffraction theory is a problem of radiation from the waveguide with symmetrical flange. Planar half-infinite waveguide with $2a$ height and with symmetrical flange is excited by the base wave of the *TEM* type with the amplitude equal to one:

$$H_y^i(x,z)=\exp(ikz), \qquad |x|<a, \quad -\infty<z\le 0, \qquad \left(\exp(-i\omega t)\right), \quad (1)$$

where $k=2\pi/\lambda$ is a wavenumber.

The problem is worked out by the method of partial regions. Taking into account the symmetry of the incident field and the symmetry of the structure related to plane $x=0$, let us study the fields in the following three subregions:

$$1.\,0\le x\le a, \quad z\le 0; \qquad 2.\,0\le x\le a, \quad z\ge 0; \qquad 3.\,r\ge 0, \quad 0\le\varphi\le\Phi\ , \qquad (2)$$

where the Cartesian and polar coordinates are connected by the equations $x-a=r\sin\varphi$, $z=r\cos\varphi$.

Let us represent the total field in the waveguide as superposition of eigenwaves of $E_{0,2n}$ type with unknown amplitudes of the excited waves A_n

$$H_y^1(x,z)=\exp(ikz)+\sum_{n=0}^{\infty}A_n\cos\frac{n\pi x}{a}\exp(-i\alpha_n z), \qquad (3)$$

where $\alpha_n=\sqrt{k^2-(n\pi/a)^2}$ are constants of propagation.

The field in region 2 is presented as Fourier integral

$$H_y^2(x,z)=\frac{1}{2\pi}\int_{-\infty}^{\infty}\Psi_+(x,\alpha)\exp(-i\alpha z)d\alpha\ , \tag{4}$$

$$\Psi_+(x,\alpha)=\frac{C_+(\alpha)}{\gamma\sinh\gamma a}\cosh\gamma x+\frac{i}{\alpha+k}+i\sum_{n=0}^{\infty}\frac{A_n}{\alpha-\alpha_n}\cos\frac{n\pi x}{a}, \tag{5}$$

$$C_+(\alpha_n)=-i(-1)^n\varepsilon_n\alpha_n aA_n\ , \qquad \varepsilon_n=\begin{cases}1\\2\end{cases}\begin{matrix}when & n\geq 1\\ when & n=0\end{matrix}, \tag{6}$$

where $\gamma=\sqrt{\alpha^2-k^2}$, $\mathrm{Re}\,\gamma>0$.

The field in region 3 is presented as Sommerfeld-Maliuzhinets integral [1] with transform $S_\Phi(p)$

$$H_y^3(r,\varphi)=\frac{1}{2\pi i}\int_\gamma\exp(-ik\cos p)S_\Phi(p+\varphi)dp, \tag{7}$$

The set of integral equations is obtained using the condition of vanishing of the tangential component of the electric field on the flange and the conditions of continuity of the tangential components of the field on the boundary of regions 2 and 3.

$$\frac{1}{2\pi i}\int_\gamma\exp(-ikr\cos p)S_\Phi(p+\Phi)\sin p dp=0, \tag{8}$$

$$\frac{1}{2\pi i}\int_\gamma\exp(-ikr\cos p)S_\Phi(p)dp=\frac{1}{2\pi}\int_{-\infty}^{\infty}\Psi_+(a,\alpha)\exp(-i\alpha r)d\alpha, \tag{9}$$

$$\frac{1}{2\pi i}\int_\gamma\exp(-ikr\cos p)S_\Phi(p)\sin p dp=-\frac{1}{2\pi ik}\int_{-\infty}^{\infty}C_+(\alpha)\exp(-i\alpha r)d\alpha, \tag{10}$$

Then the inhomogenious functional equation for function $S_\Phi(p)$ is obtained by the inversion formula for Sommerfeld-Maliuzhinets integral [1]

$$S_\Phi(p)-S_\Phi(p+2\Phi)\exp(-2ika\sin p)=-\big(1-\exp(-2ika\sin p)\big)F(p)/2, \tag{11}$$

where

$$F(p)=\sin p\left(\frac{1}{\cos p+1}+\sum_{n=0}^{\infty}\frac{(-1)^nA_n}{\cos p-\cos\theta_n}\right), \tag{12}$$

$$\sin\theta_n=\frac{n\pi}{ka}, \qquad \cos\theta_n=\frac{\alpha_n}{k}, \qquad 0\leq\mathrm{Re}\,\theta_n\leq\frac{\pi}{2}\ . \tag{13}$$

The solution of equation (11) by Tuzhilin S integrals [2] is presented

$$S_\Phi(p)=\exp\big(w_\Phi(p)\big)\left(T(p,\pi)+\sum_{n=0}^{\infty}(-1)^nA_nT(p,\theta_n)\right), \tag{14}$$

where

$$w_\Phi(p)=-ika\Big(\big(\cos(p-\Phi)-\cos\Phi\big)/\sin\Phi+2\Phi\big(\cos(\pi p/\Phi)-1\big)/\big(\pi^2-\Phi^2\big)\Big), \tag{15}$$

$$T(p,\beta) = -\frac{\sin(\pi p/\Phi)}{4\Phi i}\int_{-i\infty}^{i\infty}\frac{f(\tau,\beta)d\tau}{\cos(\pi\tau/\Phi)-\cos(\pi p/\Phi)}\,, \tag{16}$$

$$f(p,\beta) = -\frac{\sin p}{2(\cos p-\cos\beta)}\left(1-\exp(-2ika\sin p)\right)\exp\left(-w_\Phi(p)\right)\,. \tag{17}$$

The infinite set of algebraic linear equations is obtained for unknown amplitudes A_n

$$-i(-1)^m\varepsilon_m ka\cos\theta_m A_m + \sum_{n=0}^{\infty}(-1)^n\Psi(\theta_m,\theta_n)A_n = -\Psi(\theta_m,\pi), \qquad m=0,1,2,\ldots, \tag{18}$$

where

$$\Psi(p,\beta) = \exp\left(w_\Phi(p)\right)\left(T(p,\beta)-T(p-2\Phi,\beta)\right)\,. \tag{19}$$

The solution of equation (11) was constructed for two particular cases: 1) $\Phi=\pi$ and 2) $\Phi=\pi/2$ in quite another way. In both cases the solution is as follows

$$S_\Phi(p) = \frac{\exp(-ika\sin p)}{2\sinh(ika\sin p)}C_\Phi(p) - \frac{1}{2}F(p)\,. \tag{20}$$

1) Homogenious Maliuzhinets equations are obtained for function $C_\pi(p)$. This function and unknown amplitudes are explicitly determined from these equations. The constructed solution totally coincides with the solution obtained by the factorization method [3].
2) In this case inhomogenious Maliuzhinets equations are obtained for function $C_{\pi/2}(p)$. Their solution can be written by Tuzhilin S-integrals [2]. The infinite set of algebraic linear equations is obtained for unknown amplitudes. This set of equations and its coefficients coincide with the obtained factorization method [4].

REFERENCES

[1] Maliuzhinets, G.D., "Das Sommerfeldische Integral und die Losung von Beugungsaufgaben in inkelgebieten," *Annalen der Physik*, Vol. 6, pp.107-112, 1960.

[2] Tuzhilin, A.A., "On the theory of inhomogeneous Maliuzhinets' functional equations," *Diff. Uravn.*, Vol. 9, pp.2058-2064, 1973.

[3] Weinstein, L.A., The Theory of Diffraction and the Factorization Method. Moscow: Sov. Radio, 1966.

[4] Voskresensky, G.V., and Zhurav, S.M., "Radiation from a parallel-plate flanged waveguide," Radiotekhnika i Elektronika, Vol. 21, pp.1390-1395, 1976.

RIGOROUS THEORY OF RECTANGULAR WAVEGUIDE ARRAYS WITH FINITE FLUSH MOUNTED DIELECTRIC COVER

M.B. Manuilov
Rostov State University, Physical faculty,
5 Sorge St., 344104, Rostov-on-Don, RUSSIA
E-mail: manuilov@phys.rnd.runnet.ru

ABSTRACT

Rigorous numerical-analytical field-theory technique for analysis of rectangular waveguide arrays with finite flush mounted dielectric cover is presented. The method is based on the dyadic Green function technique and Galerkin's method with taking into account the edge condition. The comparison of the presented theory with experimental and theoretical results of other works shows good agreement.

INTRODUCTION

The waveguide phased arrays flush mounted in flat or conform conducting surfaces find wide use in both radar and communications application. These array antennas are sometimes dielectrically loaded and usually covered with some dielectric material for environmental protection and for wide-angle impedance matching. There are no the simple methods based on the classical antenna theory to analyze the influence of the dielectric cover on the arrays performances. On the other hand, it is well known that both the high-order mode coupling as well as dielectric cover can individually produce scan blindness in waveguide phased arrays [1]. These reasons call for the rigorous field theory analysis of such arrays.

There is a number of 2D and 3D models to study rectangular waveguide arrays both with and without dielectric sheets. But only a few papers consider 3D models of finite rectangular waveguide arrays with dielectric sheets [2, 3] and only paper [2] takes into account the finite size of dielectric cover.

THEORY

In this paper a novel Galerkin's method based numerical-analytical approach to analysis of rectangular waveguide arrays with finite dielectric cover is presented. The array under consideration is covered with rectangular dielectric sheet flush mounted in perfectly conducting ground plane (Fig. 1). In general case array includes arbitrary number M of rectangular waveguides of differing size. All waveguides are arbitrary positioned under dielectric cover. Such a problem formulation gives the opportunity to study arrays with rectangular or hexagonal grid and arrays with non-equidistant grid or different-sized waveguide arrays. A major reason for employing different-sized elements and non-equidistant grid is a design flexibility in beam shaping and side lobe level control.

Rigorous field theory solution of the problem is based on the dyadic Green's function technique and Galerkin's method. The straightforward application of the equivalence principle and the continuity conditions on the common interfaces leads to the system of integral equations (SIE) for magnetic currents on the apertures of waveguides and dielectric cover. The components of dyadic Green's functions in SIE are written in the

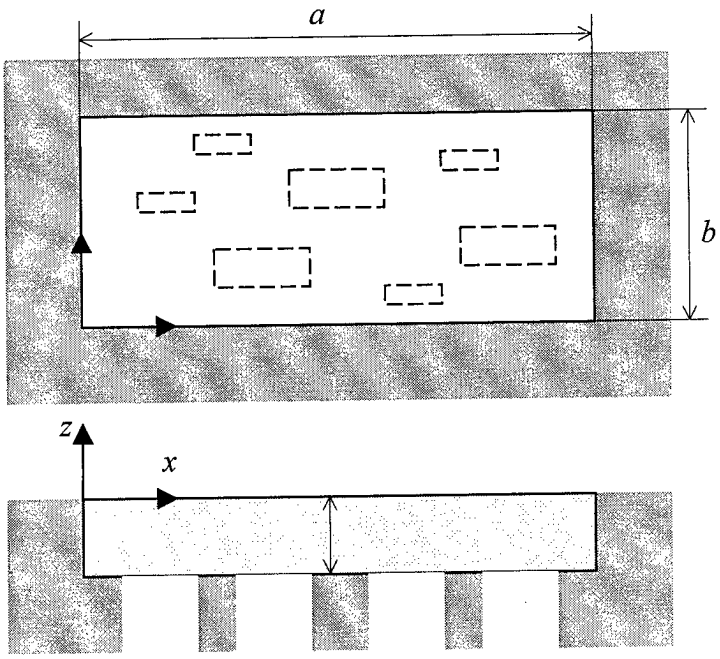


Fig.1. Rectangular waveguide array with finite flush mounted dielectric cover in an infinite perfectly conducting ground plane.

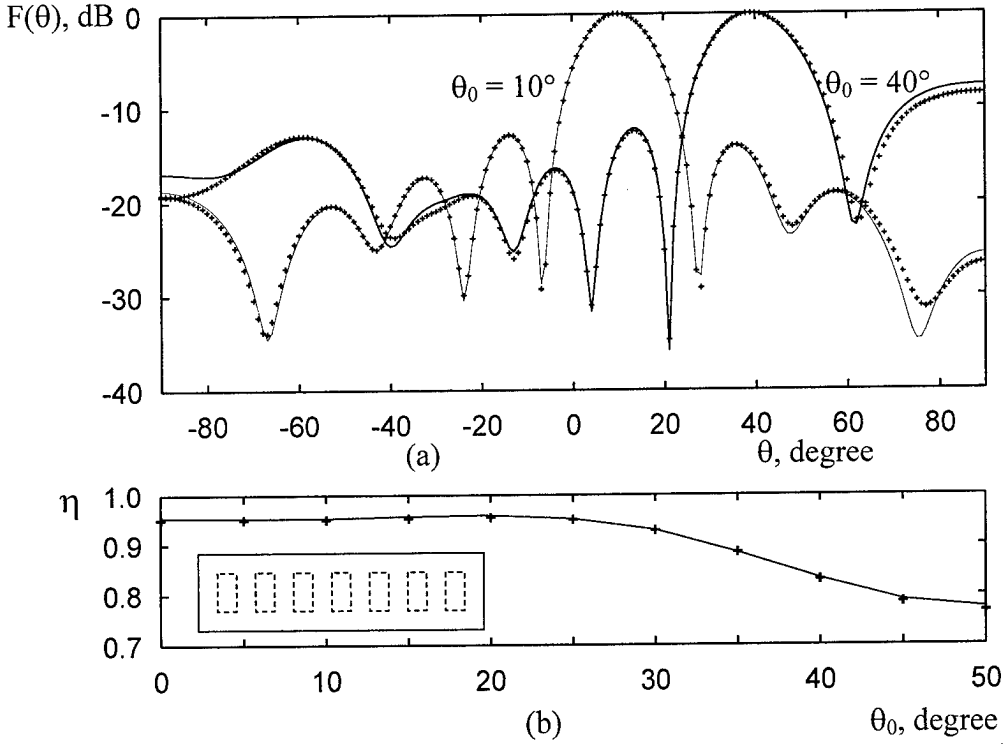


Fig. 2. E-plane radiation pattern (a) and efficiency (b) of 7-element array by uniform excitation and different scan angles θ_0. Presented theory ——— , theory of [2] +++ . ($\varepsilon_1 = 2.56$, $\varepsilon = 1$, $a = 0.73\lambda$, $b = 3.4\lambda$, $a_1 = 0.72\lambda$, $b_1 = 0.3\lambda$, $\Delta = 0.312\lambda$, $d_y = 0.5\lambda$.).

form of full wave modal expansions for rectangular waveguides and cavity (i.e. dielectric sheet). Free-space Green's function components are expressed as their Fourier transform representations.

The first key point of this theory is a special choice of the basis finctions for solving SIE. The weighted Chebyshev and Gegenbauer polynomials were used as basis functions taking into account the edge condition in explicit form. For example, equivalent magnetic current components on the νth waveguide aperture (ν=1, 2, ..., M) were written in the form of expansions

$$J^m_{\nu,x}(x,y) = \sum_{i=0}^{N_x'} \sum_{k=0}^{N_y'} u^{\nu,x}_{ik} \cdot X^{\nu,x}_i(x) \cdot Y^{\nu,x}_k(y) ,$$

$$X^{\nu,x}_i(x) = \left(1-(2(x-x_\nu)/a_\nu)^2\right)^{\tau+1/2} \cdot C^{\tau+1}_i\left(2(x-x_\nu)/a_\nu\right) ,$$

$$Y^{\nu,x}_k(y) = \left(1-(2(y-y_\nu)/b_\nu)^2\right)^{\tau-1/2} \cdot C^{\tau}_k\left(2(y-y_\nu)/b_\nu\right) ,$$

$$J^m_{\nu,y}(x,y) = \sum_{i=0}^{N_x'} \sum_{k=0}^{N_y'} u^{\nu,y}_{ik} \cdot X^{\nu,y}_i(x) \cdot Y^{\nu,y}_k(y) ,$$

$$X^{\nu,y}_i(x) = \left(1-(2(x-x_\nu)/a_\nu)^2\right)^{\tau-1/2} \cdot C^{\tau}_i\left(2(x-x_\nu)/a_\nu\right) ,$$

$$Y^{\nu,y}_k(y) = \left(1-(2(y-y_\nu)/b_\nu)^2\right)^{\tau+1/2} \cdot C^{\tau+1}_k\left(2(y-y_\nu)/b_\nu\right) .$$

where u_{ik} are unknown coefficients, $C^\tau_i(x)$ are Gegenbauer polynomials ($0 \le \tau \le 1/6$), (x_ν, y_ν) are coordinates of the central point of the νth waveguide aperture.

By implementation of the standard Galerkin's method procedure the SIE is reduced to the system of linear algebraic equations (SLAE). Therefore the second basic point of the theory is both analytical and numerical techniques of evaluation of double infinite integrals included into some matrix elements of SLAE.

RESULTS

Numerical results given in the paper demonstrate good numerical convergence and accuracy of this theory by comparison with the both theoretical and experimental results of other works for some particular cases [2, 4] (Fig. 2). Some examples of radiation patterns for arrays with number of waveguides up to 100 were considered.

REFERENCES

[1] A. Amitey, V. Galindo, C.P. Wu, Theory and Analysis of Phased Array Antennas, New York: Wiley, 1972.

[2] B. D. Manuilov, B.G. Borisov, K.E. Sariev, V.M. Shablovsky // Radiotekhnika (in Russian), 1991, № 4, pp. 60-62.

[3] P.D. Patel, M.C. Bailey // IEEE Trans. on Antennas and Propag., 1997, vol. AP-45, № 12, pp.1749-1757.

[4] R. J. Mailloux // IEEE Trans. on Antennas and Prop., 1969, vol. AP-17, N. 1, pp. 49-55.

SOLUTION OF THREE-DIMENTIONAL ELECTROMAGNETIC PROBLEMS

V.M. Morozov, V.I. Magro, M. Guarab

Dniepropetrovsk National University,
13 Nauchnij pereulok, 49050 Dniepropetrovsk, UKRAINE
Phone: (38) 0562-467995, e-mail: morozovvmd@hotmail.com

ABSTRACT

Solution of three-dimensional problem of radiation from an infinite waveguide antenna array is considered. Investigated is an antenna array with subarray of matching elements. Antenna system has triangular cells of radiation elements location. The study method is based on using an integral equation with separation of piercing domain.

INTRODUCTION

The method of integral equation is an efficient tool for solving three-dimensional problems. The paper subject is application of the method of integral equation to the analysis of a waveguide antenna array with triangular spacing of radiation elements. The whole domain of the field determination is subdivided into a piercing domain and partial domains (Fig. 1). The theorem of the vector theory of diffraction is used for obtaining the total field in the piercing domain. Theoretical investigation of antenna array composed of open-ended rectangular waveguides and finite subarray for obtaining the impedance matching with free space is presented.

METHOD OF SOLUTION

The vector theory of diffraction is a theory of diffraction of electromagnetic field in three-dimensional space. Maxwell's equations lead to an equation for $\vec{E}$ field:

$$[\vec{\nabla}[\vec{\nabla}\vec{E}]] - k^2\vec{E} = -j\omega\mu\,\vec{J}_{exc}, \tag{1}$$

where $\vec{J}_{exc}$ is a given current.

Consider the Green's tensor of electric type, which satisfies the equation

$$[\vec{\nabla}[\vec{\nabla}\vec{G}^e(\vec{r},\vec{r}')]] - k^2\vec{G}^e(\vec{r},\vec{r}') = \vec{I}\delta(\vec{r}-\vec{r}'). \tag{2}$$

In (2), $\vec{I}$ is a unit tensor of the second rank with components $(\vec{I})_{\alpha\beta} = \delta_{\alpha\beta}$; α and β in three-dimensional space are 1,2,3. Multiply the equation (1) from the right with $\vec{G}^e(\vec{r},\vec{r}')$ and multiply the equation (2) from the left with $\vec{E}$. Subtract the second from the first and obtain

$$[\vec{\nabla}[\vec{\nabla}\vec{E}]]\vec{G}^e - \vec{E}[\vec{\nabla}[\vec{\nabla}\vec{G}^e]] = -j\omega\vec{J}_{exc}\vec{G}^e - \vec{E}\delta(\vec{r}-\vec{r}'). \tag{3}$$

Here $\vec{E}\bullet\vec{I} = \vec{E}$. Traditional method of solution of the equation (3) is spatial integration of both sides of equation and application of the Green's theorem. Besides, the solution of equation (3) can be obtained by using the Gauss theorem. For the left hand side of equation (3), by using the relations

$$[\vec{\nabla}[\vec{\nabla}\vec{E}]]\vec{G}^e - \vec{E}[\vec{\nabla}[\vec{\nabla}\vec{G}^e]] = \vec{\nabla}[[[\vec{\nabla}\vec{E}]\vec{G}^e] + [\vec{E}[\vec{\nabla}\vec{G}^e]]],$$

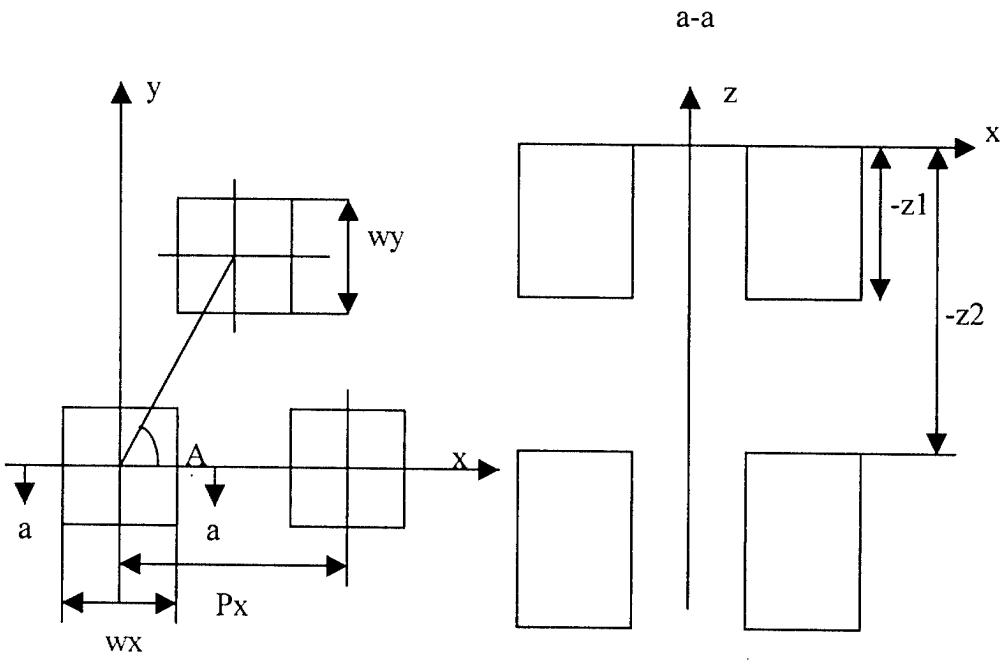


Fig. 1. Antenna array geometry

equation (3) can be written in the form

$$\vec{E}(\vec{r})\delta(\vec{r}-\vec{r}') = -j\omega\mu\,\vec{J}_{exc}(\vec{r})\vec{G}^{e}(\vec{r},\vec{r}') - \nabla\{[[\vec{\nabla}\vec{E}(\vec{r})]\vec{G}^{e}(\vec{r},\vec{r}')] + \vec{E}(\vec{r})[\vec{\nabla}\vec{G}^{e}(\vec{r},\vec{r}')]]\}, \tag{4}$$

where $\vec{r}$ is the variable of integration and $\vec{r}'$ is the point of observation which is inside V. The surface of integration S is the boundary of V. After spatial integration over V and application of the Gauss theorem, a general theorem (formula) of the vector theory of diffraction is obtained:

$$\vec{E}(\vec{r}) = -j\omega\mu \int_{V_{exc}} J_{exc}(\vec{r})\vec{G}^{e}(\vec{r},\vec{r}')dV - \oint_{S}\vec{n}([\vec{E}(\vec{r})[\vec{\nabla}\vec{G}^{e}(\vec{r},\vec{r}')]] + [[\vec{\nabla}\,\vec{E}(\vec{r})]\vec{G}^{e}(\vec{r},\vec{r}')])dS. \tag{5}$$

Here $\vec{n}$ is external normal to surface S. Equation (5) represents the electric intensity $\vec{E}$ at the point of observation as a sum of fields. They are formed by the current in volume V_{exc}, and the fields $\vec{E}(\vec{r})$ and $[\vec{\nabla}\vec{E}(\vec{r})]$ on surface S. Analogous result for determination of $\vec{H}(\vec{r}')$ can be obtained as

$$\vec{H}(\vec{r}') = \int_{V_{exc}} [\vec{\nabla}\vec{J}_{exc}(\vec{r})]\vec{G}^{e}(\vec{r},\vec{r}')\,dV - \oint_{S}\vec{n}\{[\vec{H}(\vec{r})[\vec{\nabla}\vec{G}^{e}(\vec{r},\vec{r}')]] + [[\vec{\nabla}\vec{H}(\vec{r})]\vec{G}^{e}(\vec{r},\vec{r}')]\}dS \tag{6}$$

In equations (5) and (6), the boundary conditions for tensor $\vec{G}^{e}(\vec{r},\vec{r}')$ are not concrete. Consider a combined surface S containing a conducting surface and a hole. The hole domain is denoted as $\sum$. Then boundary conditions yield the following formula of the vector theory of diffraction

$$\vec{E}(\vec{r}') = -j\omega\mu \int_{V_{exc}} \vec{J}_{exc}(\vec{r})\vec{G}_1^e(\vec{r},\vec{r}')dV - [\vec{\nabla}' \int_{\Sigma} \vec{G}_2^e(\vec{r},\vec{r}')[\vec{n}\vec{E}(\vec{r})]dS].$$

This representation is convenient in computations.

PROBLEM FORMULATION

For a unit cell the whole domain of the field determination is subdivided into three domains:

I – waveguide extended to infinity (piercing domain)

$-wx/2 \le x \le wx/2$; $-wy/2 \le y \le wy/2$; $-\infty \le z \le \infty$;

II – Floquet channel

$-Px/2 \le x \le Px/2$; $-\frac{PA\sin(A)}{2} \le y \le \frac{PA\sin(A)}{2}$; $-z2 \le z \le -z1$;

III – semi-infinite Floquet channel

$-Px/2 \le x \le Px/2$; $-\frac{PA\sin(A)}{2} \le y \le \frac{PA\sin(A)}{2}$; $0 \le z \le \infty$;

Thanks to the theorem of the vector theory of diffraction, one can write integral representation for the total field in the piercing domain, $0 \le z \le \infty$, as

$$\vec{E}^1(x,y,z) = \vec{E}^1_{exc} + [\vec{\nabla} \int_{S^1} \vec{G}^1(x,y,z;x'y'z')[\vec{n}\,\vec{E}^1(x',y',z')]dS].$$

Here $\vec{n}$ is the inner unit normal to the boundary S^1; $\vec{G}^1(\vec{r},\vec{r}')$ is the dyadic Green's function of potential type of the second kind which satisfies the Helmholts equation

$$\Delta\vec{G}^1(\vec{r},\vec{r}') + k^2\,\vec{G}^1(\vec{r},\vec{r}') = -\vec{I}\,\delta(\vec{r}-\vec{r}')$$

and the boundary conditions on conductor surface S'

$$[\vec{n}[\vec{\nabla}\vec{G}^1(\vec{r},\vec{r}')]] = 0;$$

$$(\vec{n}\vec{G}^1(\vec{r},\vec{r}')) = 0, \quad \vec{r},\vec{r}' \in S'.$$

Place the observation point at z=-z2, -z1, 0 and take into consideration the boundary condition for the tangential component of the vector of electric field. Then we obtain a system of the Fredholm integral equations of the second kind. Application of the Galerkin method finally yields a system of linear algebraic equations, which can be solved by the use of the truncation.

Numerical results obtained agree well with other available data. The influence of geometrical parameters on the reflectivity in the waveguide is investigated. It is shown that the presence of a matching inner resonator makes it possible to improve the characteristics of antenna array.

BASIS FUNCTIONS IN THE ANALYSIS OF ELECTRICALLY LONG SLOTS IN RECTANGULAR WAVEGUIDE WITH THE INDUCED MAGNETOMOTIVE FORCES METHOD

V.A. Katrich, V.I. Kiyko, M.V. Nesterenko, L.P.Yatsuk
V.N.Karazin Kharkov National University, 61077, Svobody Sq.,4, Kharkov, Ukraine
E-mail: Mikhail.V.Nesterenko@univer.kharkov.ua

INTRODUCTION

In the super-high frequency technique narrow slots are widely used as independent radiators or elements of waveguide antenna arrays. The foundations of slot theory and calculation algorithms have been developed mainly for comparatively short slots of length $2L \le \lambda$, where λ is an operating wavelength. But in some cases (for example when an antenna must have a pattern of special form, a pattern with a narrow main beam and low sidelobes or by producing multi-frequency, multi-channel antennas, ones with complex apertures) it is necessary to use slots with $2L > \lambda$.

Among the most effective methods of analysis of such radiators (for example a longitudinal slot in a broad wall of a rectangular waveguide) one can name moments method [1], Galyorkin's method [1,2]. The last one reduces to the same system of linear algebraic equations (SLAE) as the Ritz method applied to the solving the variation problem, equivalent to the initial integral equation concerning the magnetic current in a slot. During realization of these methods various basis functions and weight ones may be used: piecewise constant [3], piecewise linear and piecewise sinusoidal [4], even Gegenbauer polynomials [5], trigonometric functions [6]. Using these methods one must solve N-order SLAE, where N is a number of linearly independent basis functions. Matrix elements of such system (their number is N^2) very often cannot be found analytically. As a rule half of them result from single or double numerical integration which is not very simple.

For more then one slot the order of SLAE increases proportionally to their number. In order to make easier solving the problem it is necessary to diminish a number of approximating functions – to use one or two functions (depending on an excitation character) for a slot as it was done in [7-9]. In a special case when only one approximation function is used for every slot in the multielement system Galyorkin's method gets a name «induced magnetomotive forces method (IMMFM)» [2]. The solution in this case is the more correct the more correctly approximating function describes distribution of the magnetic current in the slot. In [7-9] the half-wave and one-wave sinusoidal functions were used for slots of length $2L \le \lambda$. For the longer slots it is necessary to use a greater number of approximating functions. We suggest here the more perfect functions for the IMMFM, which provide a good current approximation for the more long slots. These functions were obtained by solving the integral equation for the magnetic current in a slot with the asymptotic method of averaging [10]. In this paper the results of investigation of electrically long slots electrodynamic characteristics using these functions are presented. The slots are supposed to be cut in a broad wall of a rectangular waveguide. The numerical results are compared with ones of other authors and with the experimental data.

MAIN PART

In a general case a projection of an original field $H_{0s}(s)$ on the slot axis and a magnetic current in it $J(s)$ can be presented using two components: symmetrical and antisymmetrical one along a slot with respect to its center. Let s be the local coordinate connected to the slot. Then $H_{0s}(s) = H^s_{0s}(s) + H^a_{0s}(s)$, $J(s) = J^s(s) + J^a(s)$. Accounting this the integral-differential equation for the current in the narrow linear slot ($d/2L << 1$, $d/\lambda << 1$, where d is a width of the slot), may be written as [10]:

$$\left(\frac{d^2}{ds^2} + k^2\right)\int_{-L}^{L} J(s')[G^e_s(s,s') + G^i_s(s,s')]ds' = -i\omega[H^s_{0s}(s) + H^a_{0s}(s)]. \quad (1)$$

Here $G^e_s(s,s')$ and $G^i_s(s,s')$ are quasi-one-dimensional Green's functions for the vector potential respectively in the external ("e") and internal ("i") coupled volumes, $k = 2\pi/\lambda$, ω - cyclic frequency (time dependence $e^{i\omega t}$). Let us represent the current as a product of unknown amplitudes and known distribution functions

$$J(s) = J^s_0 f^s(s) + J^a_0 f^a(s), \quad (2)$$

where the functions $f^s(s)$ and $f^a(s)$ must satisfy the following boundary conditions $f^s(\pm L) = 0$, $f^a(\pm L) = 0$. For the longitudinal slot in a broad wall of the rectangular waveguide with the cross section $a \times b$ the magnetic field of the incident wave can be written as $H_{0s}(s) = H_0 \cos\frac{\pi x_0}{a}(\cos k_g s - i \sin k_g s)$, where H_0 is an amplitude of the wave, x_0 is a distance from the narrow wall to the slot axis, $k_g = \sqrt{k^2 - (\pi/a)^2} = 2\pi/\lambda_g$, λ_g is the wave length in a waveguide. Basis functions $f^s(s)$ and $f^a(s)$ can be chosen in the following form [10]:

$$f^s(s) = \cos ks \cos k_g L - \cos kL \cos k_g s, \quad f^a(s) = \sin ks \sin k_g L - \sin kL \sin k_g s. \quad (3)$$

Then according to the IMMFM [2] we transform (1) using (3) into the system of two independent algebraic equations concerning unknown amplitudes J^s_0 and J^a_0

$$J^s_0[Y^e_s(kd,kL) + Y^i_s(kd,kL)] = M_s(kL), \quad J^a_0[Y^e_a(kd,kL) + Y^i_a(kd,kL)] = M_a(kL), \quad (4)$$

where

$$Y^{e,i}_{s,a} = \int_{-L}^{L} f^{s,a}(s)\left[\left(\frac{d^2}{ds^2} + k^2\right)\int_{-L}^{L} f^{s,a}(s')G^{e,i}_{s,a}(s,s')ds'\right]ds, \quad M_{s,a} = -i\omega\int_{-L}^{L} f^{s,a}(s)H^{s,a}_{0s}(s)ds. \quad (5)$$

The solution of (4) with the account of (2,3,5) gives us the desired expression for the current. The results of calculations (Figure 1-3, $|S_\Sigma|^2$ – normalized radiated power, h – wall thickness) show a good agreement up to the electric length of slots $2L/\lambda \le 2.75$ of our results obtained by using only two functions (3), experimental data and results

obtained in with Galyorkin's method [6]: $J(s) = \sum_{n=1}^{N} J_n \sin\frac{n\pi(L+s)}{2L}$ and moment method [3]. The last two methods demand not less then 12 basis functions for the longest slots.

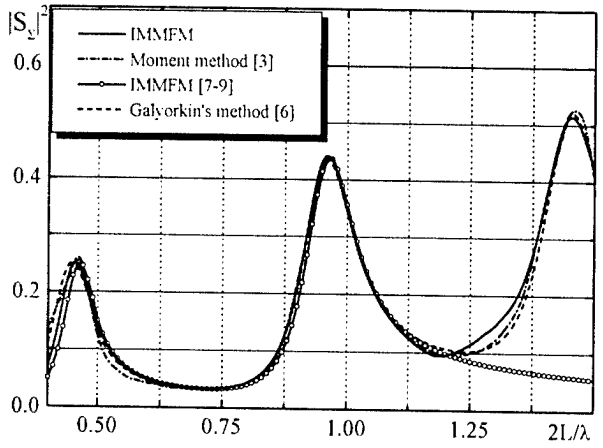


Figure1: a=22.86mm, b=10.16mm, λ=32mm, d=1.5875mm, x_0=7.43mm, h=0mm.

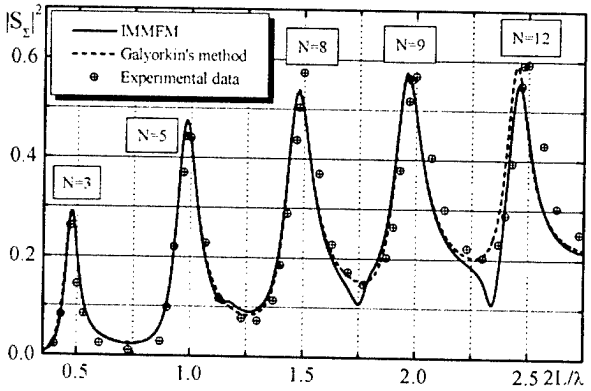


Figure 2: a=23mm, b=10mm, d=1.5mm, λ=30mm, x_0=a/4, h=1mm.

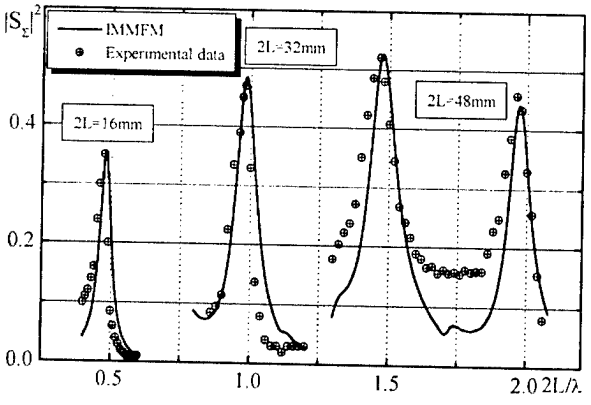


Figure 3: a=23mm, b=10mm, d=1mm, x_0=6.5mm, h=1mm.

CONCLUSION

As a result of investigations performed we can affirm that the proposed mathematical model is adequate to the real electromagnetic process. The results obtained can be used at designing waveguide-antenna devices having electrically long slots or their systems as coupling elements.

REFERENCES

[1] Calculating Methods in Electrodynamics / By edit. R. Mittra. Moscow, Mir, 1977, 485p.

[2] Feld Ya.N., Benenson S.L. Antenna-and-feeder devices.Moscow, Zhukovsky VVIA, 1959, ch.2, 551p.

[3] Khac T.V, Carson C.T. IEEE Trans.1973,v.AP-21,№ 9,pp.708-710.

[4] Whetten F.L., Balanis C.A. IEEE Trans. 1991, v.AP-39, №11, pp.1553-1560.

[5] Plotnikov V.N., Radcig Yu.Yu., Eminov S.I. JCMMP (Russia). 1994, v.34, №1, pp.68-77.

[6] Katrich V.A., Lyaschenko V.A., Poluyanenko N.A. Zarubezhnaya Radioelectronica (Russia). 2001, №6, pp.72-79.

[7] Yatsuk L.P., Smirnova I.V. Izvestiya Vuzov. Radioelectronika (Ukraine). 1967,v.10,№4,pp.359-369.

[8] Das D.N., Sanyal G.S. Proc. IEE. 1970, v.117, pp.41-44.

[9] Fridberg P.Sh. Radiotechnika and Electronica (Russia). 1977, v.22, №6, pp.1270-1273.

[10] Katrich V.A., Nesterenko M.V., Khizhnyak N.A. Radiophysics & Radioastronomy. 2001, v.6, №3, pp.230-240.

A WAVEGUIDE-BASED ANTENNA ARRAY EXITED BY A SURFACE WAVE

A.V. Gribovsky

Institute of Radio Astronomy, National Academy of Sciences of Ukraine
4, Chervonopraporna St., Kharkov 61002, Ukraine
E-mail: grib@rian.kharkov.ua

In this paper, we present and analyze a model phased antenna array of rectangular waveguides that employs a new mode of excitation and a new approach to the antenna pattern scanning. The phased antenna array is excited by a surface wave of a planar dielectric waveguide lying on a metal substrate.

Phased antenna arrays composed of open ends of waveguides are widely and effectively used in radar, communication and other areas where enhanced levels of the radiated power and fast control of the antenna pattern are required. Such antennas have shown a particularly good performance at shorter wavelengths of the UHF and SHF bands. At shorter centimeter wavelengths and especially at millimeter waves problems arise associated with the construction of feed systems for phased antenna array elements and antenna pattern control units. The difficulties result from the increased dimensions of both structural elements of waveguide channel feed systems and those of antenna pattern control units (phase shifters) as compared with the transverse sizes of the waveguide channels. As a result, a satisfactory matching of a generator (receiver) with the antenna array is impeded.

The phased antenna array is excited by a surface wave of a planar dielectric waveguide lying on a metal substrate. Waveguiding elements in the antenna are fed through the conversion of the surface wave of the planar dielectric waveguide into propagating modes of the waveguide channels. Such mode of the waveguide channel driving removes the problem of matching the antenna feed line with the waveguiding channels. The new mode of antenna pattern scanning of the waveguide-based phased antenna array consists in changing the surface wave propagation direction across the plane of the antenna array aperture. The change of the propagation direction of the surface wave with a plane phase front results in changing the phase distribution of the electromagnetic field over the waveguiding channel aperture, and thus in changing the radiation direction of the phased antenna array [1]. This approach to the control of the phased antenna array radiation would relieve from the necessity of employing expensive phase-shifters of the millimeter wave band.

The model phased antenna array under analysis is shown in Fig.1. The structure consists of an infinite perfectly conducting screen of a finite thickness h_d with waveguiding channels of rectangular cross-section (Fig.1a). The screen lies within the plane $x0y$. Centers of the waveguiding channels are allocated periodically along two non-orthogonal directions making an angle χ. The value of χ equal 90° corresponds to an array with the rectangular mesh. The waveguide cross-sections, $a \times b$, are selected

such that the only propagational mode in the waveguides is the fundamental TE_{10} -

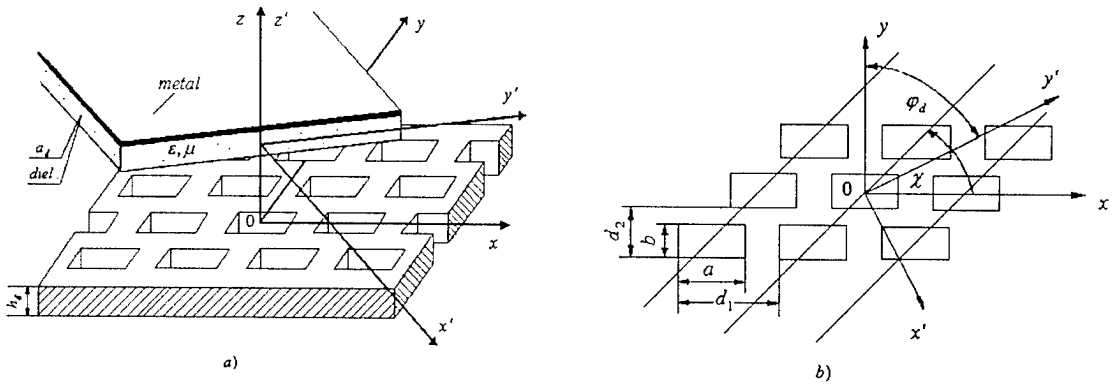


Fig.1

mode. The antenna array under consideration is characterized by a waveguide cell of $d_1 \times d_2$ in size (Fig.1b). A dielectric plate (diel.) of thickness a_d backed by a metal substrate (metal) is placed at a distance b_d from the screen within the plane parallel to the aperture plane of the phased antenna array. The coordinate frame $x'y'z'$ is tied to the plate. The dielectric constant of the plate is ε, while its permeability is equal to one. The E_{00} surface wave of amplitude q_d propagates through the dielectric plate along the $0y'$ axis at an angle φ_d with respect to the $0y$ axis.

The transverse electric field component $\bar{E}_t$ can be represented with the range behind the screen ($z < -h_d$) as a complete set of spatial vectorial TE – and TM – modes, viz. [1]:

$$\bar{E}_t(x,y,z) = \sum_{q=-\infty}^{\infty}\sum_{s=-\infty}^{\infty} d_{qs}^{(1)} \bar{\Psi}_{qs}^{(1)} e^{-i\Gamma_{qs} z} + \sum_{q=-\infty}^{\infty}\sum_{s=-\infty}^{\infty} d_{qs}^{(2)} \bar{\Psi}_{qs}^{(2)} e^{-i\Gamma_{qs} z} . \qquad (1)$$

Here $d_{qs}^{(1)}$ and $d_{qs}^{(2)}$ are unknown amplitudes of the spatial TE – and TM – modes, respectively.

The algorithm developed to compute electromagnetic field amplitudes makes it possible to analyze the antenna performance in the multiwave operation mode. In addition, the multi-wave mode allows modeling the antenna array capable of simultaneous reception or transmission at several directions.

It is known from the antenna array theory [1] that if the electromagnetic field in waveguiding channels is varied between waveguiding cells as

$$\bar{E}_{mn}(\bar{H}_{mn}) = \bar{E}_{00}(\bar{H}_{00}) \exp\{i(m\psi_x + n\psi_y)\}, \qquad (2)$$

where $\bar{E}_{mn}(x,y)$ and $\bar{H}_{mn}(x,y)$ is the electromagnetic field in the waveguiding channel labeled by m,n; $\bar{E}_{00}(x,y)$ and $\bar{H}_{00}(x,y)$ is the electromagnetic field in waveguide 0,0; and ψ_x and ψ_y are fixed phase shifts along the axes $0x$ and $0y$, respectively, then the linear phase distribution Eq.(2) will produce radiation toward the direction given by the angles ϑ and φ determined from the relations

$$\psi_x = kd_x \sin\vartheta\cos\varphi; \qquad \psi_y = kd_y \sin\vartheta\sin\varphi. \tag{3}$$

Here $k = 2\pi/\lambda$; d_x and d_y are the waveguiding cell dimensions along the axes $0x$ and $0y$, respectively; and ϑ and φ are angles in the polar spherical coordinate system. The surface wave propagating through the dielectric plate is characterized by a plane phase front. Hence, the electromagnetic field excited in the waveguiding channels with a fixed propagation direction of the surface wave follows a law similar to that given by Eq.(2). Changing the surface wave propagation direction (changing the angle φ_d) results in changing the electromagnetic field distribution over the waveguiding channels, and hence, according to Eq.(3), in changing the radiation direction of the phased antenna array.

Fig.2 show absolute values of the spatial mode complex amplitudes in dependence on the propagation direction of the surface wave through the dielectric plate.

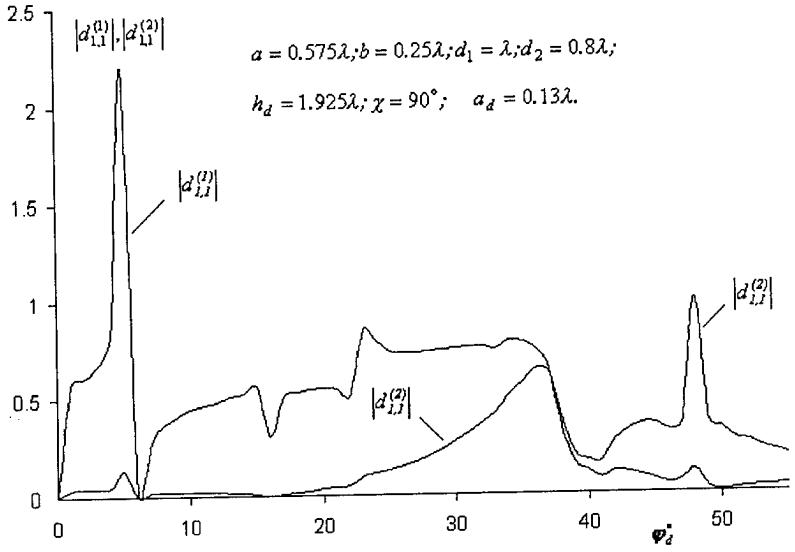


Fig.2

If the angle φ_d is varied within the range $\varphi_d = 0° \div 47°$, then the beam produced by the mode with q 1and s 1 changes its orientation within the angular range $\vartheta_{11} = 78° \div 17.5°$ and $\varphi_{11} = 89° \div -74.4°$. Thus, the paper suggests a new mode of excitation and control of radiation from a phased antenna array of open ends of waveguides that is based on the use of a surface wave. The design simplicity of the phased antenna array and the simple technique of the radiation excitation and control allow us to claim that the model suggested for the phased antenna array of open ends of waveguides is promising for millimeter wave applications.

REFERENCES

[1] N.Amitay, V.Galindo and C.P.Wu. Theory and Analysis of Phased Array Antennas. 1972, New York, 400p.

HISTORY OF THE INTERNATIONAL CONFERENCE ON MATHEMATICAL METHODS IN ELECTROMAGNETIC THEORY

MMET*02

MMET series of conferences was started in 1988 and since 1990 it has been the only regular symposium in the Former Soviet Union on electromagnetics that has English as medium of presentation and discussion. Information on the previous MMET meetings can be found in the Antennas and Propagation Magazine:

1. **Edward V. Jull** . Report on the Fourth International Seminar on Mathematical Methods in Electromagnetic Theory (MMET*91), *IEEE Antennas and Propagation Magazine*, Vol. 34, No 2, April 1992, pp.79-80.

2. **Donald R. Wilton** and **Prabhakar H. Pathak** , Highlights of MMET*94, the Mathematical Methods in Electromagnetic Theory Conference, *IEEE Antennas and Propagation Magazine*, Vol. 37, No 5, October 1995, pp.108-112.

3. **Fred Gardiol**, Report on the 6-th International Seminar on Mathematical Methods in Electromagnetic Theory (MMET*96), Lviv, Ukraine, *IEEE Antennas and Propagation Magazine*, Vol. 38, No 6, December 1996, pp.79-80.

4. **Radovan Zentner,** Report on MMET*98, *IEEE Antennas and Propagation Magazine*, Vol. 40, No 3, June 1998, pp. 67-69.

4. **Richard L. Dowden** and **Craig J. Rodger**, Report on MMET*98, *IEEE Antennas and Propagation Magazine,* Vol. 40, No 5, August 1998, pp. 61-64.

5. **Nader Engheta**, Report on MMET*2000: International Conference on Mathematical Methods in Electromagnetic Theory, Kharkov, Ukraine, September 12-15, 2000, *IEEE Antennas and Propagation Magazine*, Vol. 43, No 3, June 2001, pp. 102-106.

or on our web-page:

www.kharkov.ukrtel.net/mmet02

AUTHORS LIST

A

Alkumru A. 293
Altintas A. 586
Anastassiu H. T. 505
Andreev M. V. 299
Andrenko A. 21
Andriychuk M 79
Antyufeyeva M. S. 186
Arand B.A. 316
Araz.I. 222, 455, 473
Ari N. 463, 466
Arriaga J. 124
Arslanagic S. 257
Averkov Yu.O. 653
Averyanov A.A. 275
Averyanova Y.A. 275
Ayzatsky M.I. 242

B

Baghai-Wadji A. 27
Barkhudaryan N.V. 493
Bartuli E.R. 683
Bartolic J. 560
Batrakov D.O. 376
Baudrand H. 100
Beletskii N. N. 629
Benson T. 198, 233
Bijamov A. 407, 485
Bludov Y. V. 632
Bolshakov Y. P. 210
Bondarev V. 677
Borsch H. A. 686
Borysenko S. A. 629
Borulko V. F. 367. 551
Breinbjerg O. 257, 476, 499
Brovenko A. V. 573
Bugrova T. 432
Buharov S. V. 443
Butrym A. Y. 213
Bychkov A. 608
Bychkov A. 608

C

Carlemalm-Logothetis C. 602
Cerezci O. 222, 463, 466 473
Chandezon J. 416
Cheremisin A.A. 570
Chikichev I.S. 659
Chumachenko V.P. 529
Churyumov G.I. 201
Colak B. 473

D

Damienne B. 100
Daniel J.-P. 594
Daniele V. 87, 130
Demidtchik V. I. 420, 577
Demir Z. 222, 473
Derbov V. L. 67

De Vito P. 48
Dikmen F. 293, 576
Doroshenko V. A. 192, 589
Drize M. A. 210
Drobakhin O. O. 299, 599
Dubrovka F. 195
Dumin A. N. 189

E

Edenhofer P. 195
Engheta N. 175
Elschner G. 398

F

Fedorenko A.I. 508
Felbacq D. 118
Fikioris G. 73
Filipov Yu. F. 662
Freni A. 48

G

Gaal S. B. 239
Gaikovich K. P. 183
Gandel Y. V. 429
Gavrilov S. 290
Georgiev G. N. 674
Georgieva-Grosse M. 674
Gevorkyan E.A. 373
Ghvedashvili G. 485
Goblyk V. 569
Golovin D.V. 376
Gomilko A. M. 227
Goncharenko Y. 620
Gordienko A. N. 638
Gorelyshev S. A. 514
Gorobets N. N. 361, 313, 458
Goryashko V. A. 647
Goryushko D. N. 566
Gourjii A. A. 227
Gousenkova A. A. 496
Gribovsky A. V. 331
Guarab M. 325
Guseva E. 270

H

Hakkak M. 316
Halevi P. 124
Hanson G. 230
Hasanov E. 112
Hekim M. 455
Himdi M. 594
Hinata T. 404
Hoorfar A. 54
Hosono T. 404
Hrabar S. 560

I

Illyashenko L. N. 592
Ilyenko K. V. 647
Ivanchenko E. V. 452
Ivanov A. I. 517
Ivanov S. A. 469
Ivanov V. B. 611
Ivanov V. K. 623
Ivleeva S. N. 33

J

Jablonski T. 141
Jacob A. 163
Jorgensen E. 257, 476

K

Kalinchenko G. A. 387
Kamichev T. V. 469
Karamehmedovic M. 499
Karpukov L. M. 260, 310
Kartchevski E. 230
Kasyanov A. O. 266, 390

Katok V. 227, 245
Katrich V. A. 189, 328
Kazanskiy V. B. 523
Khakhinov V. V. 617
Khardikov V. V. 523
Khoroshun V. V. 429
Khraisat Y. S. 287
Kim O.S. 361, 476
Kirilenko A. 99, 482, 532, 535, 540
Kisel V. N. 508
Kivva F. 620
Kiyko V. I. 328
Klimov K. N. 210, 469
Kobayashi K. 152, 370
Komyachko A. A. 680
Kondratenko D. A. 157
Kondratyev Y. V. 599
Kornev R.V. 577
Koshikawa S. 152, 370
Kotenko M. 245
Kramarenko K. Y. 242
Krokhin A. 124
Krizhanovski V. G. 263, 267
Kulik D. Y. 535
Kulishenko S. F. 540
Kulynych Y. P. 364
Kurkin V. I. 614
Kurt M. B. 463
Kuryliak D. B. 370
Kyriacou G. 105

L

Lebedev A. M. 511
Le Maguer S. 136
Lerer A. M. 251, 387
Levandovskyy V. G. 227
Lewykin V. M. 379
Linnik V. V. 665
Logacheva L. 677
Lysak V. V. 236

M

Magath T. 42
Makarov A. I. 668
Maksymov I. S. 201
Malyuskin A. V. 566
Manuilov M. B. 322
Magro V.I. 325
Martynyuk S. 195
Matsuda T. 410
Matsushima A. 410
Meincke P. 257, 476
Melezhik P. N. 573
Minakova L. 543
Miroshnichenko V. I. 635
Mladyonov P. L. 395
Molinet F. 38
Mori A. 48
Morozov V. M. 325
Mospan L. 532
Muzychenko A. V. 296

N

Naidenko V. I. 270, 686
Nazarchuk Z. T. 364, 370
Nechitaylo S. V. 437
Nerukh A. G. 198, 204, 207
Nerukh D. A. 204
Nesterenko M. N. 328
Ney M. 136
Nosenko O. N. 458
Nosich A. 150, 413, 586, 594
Novacek Z. 254

O

Obukhovets V. A. 266, 390

Oguzer T. 586
Oinats A. V. 614
Okuno Y. 410
Oleynik M. P. 452
Ometsinska O. 245
Onufriyenko V. M. 310, 379, 382
Opanasenko A. N. 641
Ostroushko V. M. 635
Ovsyanikov V. V. 446, 638
Ozkan E. 576

P

Palto A. A. 302
Panin S. B. 579
Petrusenko I. V. 529
Pivnenko S. N. 361
Plastun S. V. 67
Pleshchinskii I. N. 546
Pleshchinskii N. B. 546, 665
Podlevskii B. M. 79
Ponomarchuk S. N. 614
Poyedinchuk A. Y. 416, 482, 573 579
Prokopenko I. 278
Prokopenko K. 278
Prokopenko Yu. V. 662
Prosvirnin S. L. 401, 426
Protsenko M. B. 307
Pulov R. D. 260
Puzanov O. 219

R

Raida Z. 254
Rassokhina J. V. 263, 267
Rathsfeld A. 398
Romanenko M. V. 449
Romanenko S. N. 260, 310
Romanova E. A. 239
Rondineau S. 594
Ruchenkov V. A. 210
Rud L. 543
Rudiakova A. N. 263, 267
Rusanov A. F. 644
Ruzhytska N. N. 204
Rydberg A. 602

S

Sakhnenko N. 207
Saltykov D.Y. 299
Samokhin A. 169
San E. 455
Saparishvili G. 485
Savelyev V. V. 452
Savenko P. O. 79
Sazonov A. Z. 296, 437, 493
Schejbal V. 254
Schmidt G. 398
Schneider G. 163
Schuenemann K. 42
Seker S. S. 466
Semenova E. K. 589
Senkevich S. I. 540
Serov V. V. 67
Sestroretsky B. V. 210, 469
Sewell P. 233
Shchepkina Y. D. 227
Shigesawa H. 93
Shilov S. V. 67
Shishkova A. V. 361
Shlepnev Y. O. 488
Shmat'ko A. A. 566
Shulga S. N. 566
Shulika A. 236
Shvets A. V. 623
Sidina W. 100
Sidorchuk N. V. 401
Sinyavsky G. P. 251
Sitsko M. U. 420

Smirnov Y.G. 33, 502
Sorkin A. R. 526
Sorokin S. N. 452
Sukharevsky O.I. 296, 437, 493
Sukhinin S. V. 157
Sukhoivanov I.A. 236
Sulima A.V. 582

T

Tabatadze V. 407
Tarapov S.I. 576
Tavzarashvili K. 407, 485
Tesneli A. 466
Tkach M. D. 79
Tkachenko V. 532
Tkachuk K. I. 514
Tolstikov M. V. 611
Tretyakov O. A. 186, 213
Trifonov T. 479
Tsuji M. 93
Tsupak A. A. 502
Tuchkin Y. 576
Turetken B. 455, 473
Tveretina O. 605
Tyrnov D.O. 426

U

Urazghildiiev I. 602

V

Van Thielen B. 61
Vandenbosch G. 61
Varavin A. V. 623
Vashtalov S. G. 319
Vasilets V. A. 514
Vassilyev Yu.V. 570
Vertiy A. 290
Vorgul I. 233
Vrancken M. 61
Vukovic A. 233
Vyazmitinova A. I.. 216
Vytovtov K. A. 554, 563

W

Wallin K. 602
Watanabe K. 423

Y

Yachin V.V. 401
Yachmenov A. A. 387
Yakovenko I.V. 650
Yakovenko V.M. 644, 650, 653
Yakovenko Y. 569
Yamasaki T. 404
Yanovsky F. J. 275, 281
Yatsenko T. Yu. 647
Yatsuk L. P. 328, 680
Yashina N. 416, 482
Yazici M. 455, 473
Yefimov B. P. 647
Yeliseyeva N. P. 313
Yermakov G. V. 440
Yildirim O. 293
Yoshimoto K. 410
Yumov I. B. 671
Yurekli A. I. 455

Z

Zagorovsky V. I. 266
Zantema H. 605
Zaridze R. 407, 485
Zelenchuk D. E. 251
Zhironkin Y. V. 680
Zhou D.-Q. 410
Zich R. 130
Zinenko T. L. 413
Zolla F. 118
Zvyagintsev A. A. 517